frontiers | Research Topics

Multimodality imaging in cardiomyopathy

Edited by
Monica Mukherjee, Allison G. Hays Juan Carlos Lopez-Mattei and Andrew D. Choi

Published in
Frontiers in Cardiovascular Medicine

ISSN 1664-8714
ISBN 978-2-83251-441-2
DOI 10.3389/978-2-83251-441-2

About Frontiers

Frontiers is more than just an open access publisher of scholarly articles: it is a pioneering approach to the world of academia, radically improving the way scholarly research is managed. The grand vision of Frontiers is a world where all people have an equal opportunity to seek, share and generate knowledge. Frontiers provides immediate and permanent online open access to all its publications, but this alone is not enough to realize our grand goals.

Frontiers journal series

The Frontiers journal series is a multi-tier and interdisciplinary set of open-access, online journals, promising a paradigm shift from the current review, selection and dissemination processes in academic publishing. All Frontiers journals are driven by researchers for researchers; therefore, they constitute a service to the scholarly community. At the same time, the *Frontiers journal series* operates on a revolutionary invention, the tiered publishing system, initially addressing specific communities of scholars, and gradually climbing up to broader public understanding, thus serving the interests of the lay society, too.

Dedication to quality

Each Frontiers article is a landmark of the highest quality, thanks to genuinely collaborative interactions between authors and review editors, who include some of the world's best academicians. Research must be certified by peers before entering a stream of knowledge that may eventually reach the public - and shape society; therefore, Frontiers only applies the most rigorous and unbiased reviews. Frontiers revolutionizes research publishing by freely delivering the most outstanding research, evaluated with no bias from both the academic and social point of view. By applying the most advanced information technologies, Frontiers is catapulting scholarly publishing into a new generation.

What are Frontiers Research Topics?

Frontiers Research Topics are very popular trademarks of the *Frontiers journals series*: they are collections of at least ten articles, all centered on a particular subject. With their unique mix of varied contributions from Original Research to Review Articles, Frontiers Research Topics unify the most influential researchers, the latest key findings and historical advances in a hot research area.

Find out more on how to host your own Frontiers Research Topic or contribute to one as an author by contacting the Frontiers editorial office: frontiersin.org/about/contact

Multimodality imaging in cardiomyopathy

Topic editors

Monica Mukherjee — The Johns Hopkins Hospital, Johns Hopkins Medicine, United States

Allison G. Hays — Johns Hopkins University, United States

Juan Carlos Lopez-Mattei — University of Texas MD Anderson Cancer Center, United States

Andrew D. Choi — George Washington University, United States

Citation

Mukherjee, M., Hays, A. G., Lopez-Mattei, J. C., Choi, A. D., eds. (2023). *Multimodality imaging in cardiomyopathy*. Lausanne: Frontiers Media SA. doi: 10.3389/978-2-83251-441-2

Table of contents

frontiers | Frontiers in Cardiovascular Medicine

TYPE Editorial
PUBLISHED 11 January 2023
DOI 10.3389/fcvm.2022.1082023

OPEN ACCESS

EDITED BY
Sebastian Kelle,
Deutsches Herzzentrum Berlin, Germany

REVIEWED BY
Victor Ferrari,
Hospital of the University of Pennsylvania, United States
Matthias Schneider,
Charité Universitätsmedizin Berlin, Germany

*CORRESPONDENCE
Monica Mukherjee
✉ mmukher2@jh.edu

SPECIALTY SECTION
This article was submitted to Cardiovascular Imaging, a section of the journal Frontiers in Cardiovascular Medicine

RECEIVED 27 October 2022
ACCEPTED 28 December 2022
PUBLISHED 11 January 2023

CITATION
Hays AG, Choi AD, Lopez-Mattei J and Mukherjee M (2023) Editorial: Multimodality imaging in cardiomyopathy. *Front. Cardiovasc. Med.* 9:1082023. doi: 10.3389/fcvm.2022.1082023

Editorial: Multimodality imaging in cardiomyopathy

Allison G. Hays[1], Andrew D. Choi[2], Juan Lopez-Mattei[3] and Monica Mukherjee[1]*

[1]Division of Cardiology, Johns Hopkins University School of Medicine, Baltimore, MD, United States, [2]Division of Cardiology, Department of Radiology, The George Washington University School of Medicine, Washington, DC, United States, [3]Heart and Vascular Institute, Lee Health Hospital, Fort Myers, FL, United States

KEYWORDS

echocardiography, cardiac magnetic resonance (CMR) imaging, cardiac computed tomographic (CT) imaging, positron emission tomography (PET), multimodality imaging

Editorial on the Research Topic
Multimodality imaging in cardiomyopathy

To the Editor,

Ad astra per aspera ("Through adversity, to the stars")—Adapted from Virgil

The recent coronavirus-19 (COVID-19) pandemic brought global society to a standstill, leading to a transformation across medicine and the retooling of cardiovascular medicine to adopt evidence based best practices that prioritize safety, efficacy and outcomes (1). The practice of cardiovascular imaging was truly transformed in a multitude of ways across North America and the world, especially when stratified by modality (2, 3). Through this adversity, multimodality cardiovascular imaging remained at the forefront of cardiovascular care by allowing for new approaches in the assessment of cardiac structure and function, providing mechanistic insights into pathobiology of disease. Cardiomyopathies vary widely in phenotype and clinical expression, as well as variable genetic underpinnings vs. those resulting from acquired states. Non-invasive imaging modalities such as echocardiography, cardiac CT (CCT), cardiac MRI (CMR), and nuclear techniques including positron emission tomography (PET) and SPECT imaging allow for delineation of cardiomyopathy phenotype as well as facilitating earlier diagnosis, risk stratification, and guidance of therapeutic decisions in cardiomyopathic states.

Given the broad range of techniques available, variability in utilization, and a range of expertise, the focus of this topic through state-of-the-art review articles (Covas et al.; Farrell et al.; Gambahaya et al.; Glynn et al.; Heidari-Bateni et al.; Ismail et al.; Scheel et al.; Wand et al.; Zghyer et al.) and selected original research (4) (Bi et al.; Sperry et al.; Tian et al.) was to survey contemporary clinical application of multimodality imaging techniques in advancing early diagnosis and management of patients with cardiomyopathies. We presented several review articles discussing common cardiomyopathies, specifically addressing the utility of multimodality imaging methods in early diagnosis, serial monitoring of therapeutic efficacy, and longitudinal follow-up. We also focused on the histopathology of each cardiomyopathic state and how imaging can unmask mechanism. In addition, this Research Topic highlighted the role and clinical utility of measuring more subtle indices of myocardial function including speckle tracking strain with echocardiography and feature tracking techniques using CMR (Tian et al.). Several reviews also described the emerging role of myocardial mapping using CMR to quantify left ventricular fibrosis, inflammation and edema and nuclear PET, which can yield important information in the workup of inflammatory cardiomyopathies. We also included original work about the value of CMR in cancer patients with presumed cardiomyopathy (Heidari-Bateni et al.). As clinical research has rapidly evolved in the diagnosis and workup of stress (Zghyer et al.) and infiltrative cardiomyopathy such as cardiac sarcoidosis (Wand et al.) and cardiac amyloidosis (Scheel et al.), and cardiac manifestations from cancer (Heidari-Bateni et al.), pulmonary hypertension (Farrell et al.), HIV

(Gambahaya et al.), pregnancy (Ismail et al.), and systemic diseases such as scleroderma (Glynn et al.) these state-of the-art reviews provide clinically applicable approaches to the diagnostic workup as well as the clinical value of each imaging modality. Further, artificial intelligence has erupted over the past decade through the use of machine learning algorithms (5). To address this, also included in this series, Covas et al. presented a review of recent advances in artificial intelligence in coronary artery disease imaging through algorithms that mimic human neural networks to improve cardiovascular risk prediction, accuracy identify coronary artery stenosis and allow for rapid evaluation of ischemia, flow and atherosclerosis quantification. These reviews present new frontiers in prevention, precision and monitoring of disease activity across many clinically relevant cardiomyopathic states, thereby providing practical guidance to clinicians across these conditions. Finally, these reviews provide a critical, balanced approach to the workup of cardiomyopathy, discussing the relative merits and weaknesses of each imaging technique.

Our series also included several important original research articles. In a pilotstudy by Sperry et al. evaluated the performance of F18-florbetapir as a novel tracer to identify ATTR cardiac amyloidosis. While data was limited by small sample size, it presents the tip of the iceberg in new frontiers in molecular PET imaging of amyloidosis. In a separate study, Tian et al. demonstrated the superiority of 3D right ventricular free wall strain over 2D free wall strain and conventional echocardiographic functional parameters in identifying the ischemic and non-ischemic etiologies of end-stage heart failure. This study importantly identifies the role of non-invasive imaging as a diagnostic tool to differentiate underlying cardiomyopathic etiologies.

To that end, these novel multimodality technologies hold promise for earlier diagnosis and non-invasive monitoring of cardiac involvement in systemic inflammatory diseases that will aid in preclinical studies, enhance patient selection, and provide surrogate end points in clinical trials, and improve clinical outcomes. In this post-pandemic era, *ad astra per aspera,* we hope this Research Topic provides new insights into clinical practice and allows practicing clinicians, trainees, and the global cardiovascular community to apply these advances in cardiovascular multimodality imaging practice.

Author contributions

All authors listed have made a substantial, direct, and intellectual contribution to the work and approved it for publication.

Conflict of interest

The authors declare that the research was conducted in the absence of any commercial or financial relationships that could be construed as a potential conflict of interest.

Publisher's note

References

1. Zoghbi WA, DiCarli MF, Blankstein R, Choi AD, Dilsizian V, Flachskampf FA, et al. Multimodality cardiovascular imaging in the midst of the COVID-19 pandemic: ramping up safely to a new normal. *JACC Cardiovasc Imaging.* (2020) 13:1615–26. doi: 10.1016/j.jcmg.2020.06.001

2. Hirschfeld CB, Shaw LJ, Williams MC, Lahey R, Villines TC, Dorbala S, et al. Impact of COVID-19 on cardiovascular testing in the united states versus the rest of the world. *JACC Cardiovasc Imaging.* (2021) 14:1787–99. doi: 10.1016/j.jcmg.2021.03.007

3. Singh V, Choi AD, Leipsic J, Aghayev A, Earls JP, Blanke P, et al. Use of cardiac CT amidst the COVID-19 pandemic and beyond: North American perspective.*J Cardiovasc Comput Tomogr.* (2021) 15:16–26. doi: 10.1016/j.jcct.2020.11.004

4. Han J, Saraf SL, Kavoliunaite L, Jain S, Hassan J, Hsu LL, et al. Program expansion of a day hospital dedicated to manage sickle cell pain. *Am J Hematol.* (2018) 93:E20–1. doi: 10.1002/ajh.24938

5. Griffin WF, Choi AD, Riess JS, Marques H, Chang HJ, Choi JH, et al. AI evaluation of stenosis on coronary CT angiography, comparison with quantitative coronary angiography and fractional flow reserve: a CREDENCE trial substudy. *JACC Cardiovasc Imaging.* (2022). doi: 10.1016/j.jcmg.2021.10.020. [Epub ahead of print].

frontiers in Cardiovascular Medicine

ORIGINAL RESEARCH
published: 25 June 2021
doi: 10.3389/fcvm.2021.693194

Pilot Study of F18-Florbetapir in the Early Evaluation of Cardiac Amyloidosis

Brett W. Sperry[1,2,3], *Ashley Bock*[1], *Frank P. DiFilippo*[1], *Joseph P. Donnelly*[1], *Mazen Hanna*[1]* *and Wael A. Jaber*[1]

[1] Cleveland Clinic Foundation, Kansas City, MO, United States, [2] Saint Luke's Mid America Heart Institute, Kansas City, MO, United States, [3] University of Missouri-Kansas City, Kansas City, MO, United States

OPEN ACCESS

Edited by:
Juan Carlos Lopez-Mattei, University of Texas MD Anderson Cancer Center, United States

Reviewed by:
Marcus R. Makowski, Technical University of Munich, Germany
Fabien Hyafil, Assistance Publique Hopitaux De Paris, France

***Correspondence:**
Mazen Hanna
hannam@ccf.org

Specialty section:
This article was submitted to Cardiovascular Imaging, a section of the journal Frontiers in Cardiovascular Medicine

Received: 10 April 2021
Accepted: 28 May 2021
Published: 25 June 2021

Citation:
Sperry BW, Bock A, DiFilippo FP, Donnelly JP, Hanna M and Jaber WA (2021) Pilot Study of F18-Florbetapir in the Early Evaluation of Cardiac Amyloidosis. Front. Cardiovasc. Med. 8:693194. doi: 10.3389/fcvm.2021.693194

Background: Cardiac amyloidosis is an increasingly recognized etiology of heart failure, in part due to the rise of non-invasive nuclear bone scintigraphy. Molecular imaging using positron emission tomography (PET) has promised the direct visualization of cardiac amyloid fibrils. We sought to assess the performance of F18-florbetapir PET in patients with a potential for cardiac amyloidosis in order to identify early disease.

Methods: We performed a pilot study of 12 patients: one with asymptomatic transthyretin cardiac amyloidosis, seven with a potential for developing cardiac amyloidosis (two smoldering myeloma and five with extracardiac biopsy demonstrating transthyretin amyloid deposits and negative technetium pyrophosphate scans), and four controls. Patients were imaged with PET/CT in listmode 10–20 min after receiving F18-florbetapir. Static images were created from this acquisition, and mean standardized uptake values (SUVs) of the left ventricular myocardium, blood pool, paraspinal muscles, and liver were calculated.

Results: All 12 patients demonstrated radiotracer uptake in the myocardium with mean SUV of 2.3 ± 0.4 and blood pool SUV of 0.8 ± 0.1. The patient with cardiac amyloidosis had SUV of 3.3, while mean SUV for patients at risk was 2.3 ± 0.4 and for controls was 2.2 ± 0.3. After 3 years of follow-up, one patient with SUV below the mean was subsequently diagnosed with ATTR cardiac amyloidosis.

Conclusion: In this cohort, PET with F18-florbetapir demonstrated non-specific radiotracer uptake in the myocardium in all patients using a static image protocol; though, the highest values were noted in a patient with ATTR cardiac amyloidosis. There was no difference in the intensity of F18-florbetapir uptake in at-risk patients and controls. Future studies should continue to investigate metabolic PET tracers and protocols in cardiac amyloidosis, including in early disease.

Keywords: light chain amyloidosis, florbetaben, cardiomyopathy, technetium pyrophosphate, positron emision tomography, ATTR

INTRODUCTION

Cardiac amyloidosis is an increasingly recognized etiology of heart failure (1), in part due to the rise of non-invasive cardiac imaging such as echocardiography with longitudinal strain, nuclear bone scintigraphy, and cardiac magnetic resonance imaging. Echocardiography with longitudinal strain and cardiac magnetic resonance imaging may demonstrate findings consistent with cardiac amyloidosis and improve prognostication, while bone scintigraphy with technetium-based agent [pyrophosphate (PYP), 3,3-diphosphono-1,2-propanodicarboxylic acid (DPD), and hydroxymethylene diphosphonate (HMDP)] are highly specific for transthyretin cardiac amyloidosis in the setting of negative blood and urine testing for a plasma cell disorder (2). These modalities have typically been studied in symptomatic patients, though there is evidence that pre-symptomatic/early disease may be detected (3). Data for direct visualization of amyloid fibrils with amyloid-binding PET agents are emerging. Thioflavin analogs such as F18-florbetapir have shown good discrimination of quantitative uptake between symptomatic cardiac amyloidosis as compared to healthy controls (3). Additional studies have demonstrated non-cardiac uptake in patients with light chain (AL) amyloidosis, highlighting the systemic nature of that disease (4, 5). Though, differentiation between light chain (AL) and transthyretin (ATTR) cardiac uptake may not be possible (6).

F18-florbetapir is FDA approved and indicated for β amyloid imaging of the brain to estimate plaque density in adults with cognitive impairment who are being evaluated for Alzheimer's Disease. As this radiotracer has demonstrated high sensitivity in early disease, this pilot study sought to test F18-florbetapir for early detection of cardiac amyloid deposits in asymptomatic patients.

METHODS

A total of 12 patients were prospectively enrolled in this pilot study and followed for 3 years. One patient was considered to have ATTR cardiac amyloidosis, seven patients had a potential for development of cardiac amyloidosis (two smoldering myeloma and five with extracardiac biopsy demonstrating transthyretin amyloid deposits and negative technetium pyrophosphate scans), and there were four control patients. Control patients were selected as they had negative biopsies for amyloidosis during routine carpal tunnel release surgery without signs or symptoms of the disease (7). This study was approved by the Institutional Review Board and Ethics Committee at the Cleveland Clinic, and all patients signed informed consent.

Patients were imaged using F18-florbetapir (10mCi) using a Biograph mCT 128 (Siemens Healthineers, Malvern, PA) PET/CT scanner with lutetium oxyorthosilicate crystals, time-of-flight capable photomultiplier tubes with coincidence timing resolution of 550 ps, and PET detectors covering an axial field of view of 21.4 cm. Images were acquired in listmode from 10 to 20 min after radiotracer injection, and static images were reconstructed by summing data including 3D iterative time-of-flight with resolution modeling. This post-injection time was chosen based upon prior study showing a large differential in standardized uptake values (SUVs) between patients and controls (8). Images were interpreted by identifying myocardial radiotracer uptake qualitatively (present or absent) and quantitatively using Corridor4DM software (Invia, Ann Arbor, MI). For quantitative measures, PET images were reoriented along the standard cardiac axes and the mean and standard deviation of cardiac uptake in the entire myocardium was quantified using SUVs. Regions of interest were also drawn in the blood pool (left atrium), paraspinal muscles, and liver and mean SUVs were calculated.

PYP scintigraphy was performed using SPECT/CT with Siemens Symbia T6 cameras, and patients were imaged 3 h after infusion of 20 mCi+/– 10% of technetium PYP intravenously as previously described (9). A semiquantitative score and heart-to-contralateral lung ratios were obtained, and studies were considered positive if there was radiotracer uptake localized to the myocardium on SPECT/CT images (9).

RESULTS

F18-florbetapir imaging showed visible radiotracer uptake in the myocardium in all patients (**Figure 1**) with mean SUV 2.3 ± 0.4. Patient 7 was asymptomatic from a cardiac perspective with normal levels of troponin T and NTproBNP, but had a positive PYP study (**Table 1**) in the setting of negative testing for a monoclonal protein and was considered to have cardiac amyloidosis at the time of enrollment. This patient had the highest myocardial SUV value of 3.3. Mean SUV for patients at risk was 2.3 ± 0.4, and for controls was 2.2 ± 0.3. All patients had myocardial SUV values above previously described healthy controls (SUV 1.4-1.7), and all patients had mean myocardial counts more than 2x blood pool counts (8). Blood pool, liver, and paraspinal muscle SUV values are also shown in the **Table 1**.

Of the seven patients with a potential for cardiac involvement, two had smoldering myeloma (1 IgG lambda with free light chain difference 873 mg/L, 1 IgG kappa with free light chain difference 339 mg/L), and five had ATTR with negative PYP scans (four with TTR deposits in the tenosynovium (7) and one with hereditary ATTR polyneuropathy). Patient 1 was asymptomatic from a cardiac perspective but had an abnormal cardiac MRI with native T1 time 1,300 msec (but without late gadolinium enhancement), an NTproBNP above reference range (607 pg/mL), but no fat pad or bone marrow biopsy evidence of amyloid deposits.

Patients were followed clinically for 3 years, and none developed new symptomatic cardiac amyloidosis. Two patients had follow-up PYP scans (**Figure 1**); patient 6 had Ala81Thr mutation and developed asymptomatic PYP conversion to Grade 3 uptake 3 years after enrollment despite initial low F18-florbetapir myocardial retention. Interestingly, F18-florbetapir muscle uptake in the cohort was highest in this patient.

DISCUSSION

In this prospective pilot study, F18-florbetapir identified qualitative and quantitative radiotracer uptake above previously

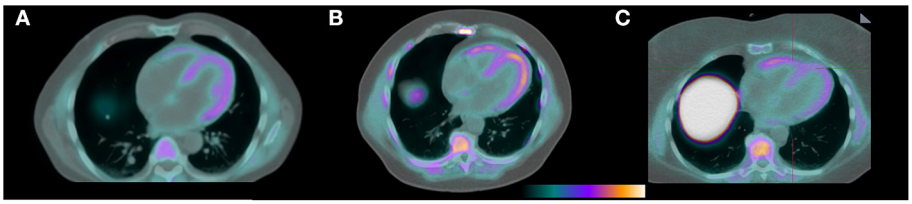

FIGURE 1 | F18-florbetapir PET/CT images demonstrating identifiable myocardial uptake of radiotracer in the patient with confirmed cardiac amyloidosis by technetium PYP (**A**, mean myocardial SUV 3.3), a patient with light chain MGUS and a potential for having cardiac AL amyloidosis (**B**, mean myocardial SUV 2.7), and a control patient with a negative tenosynovial biopsy for amyloidosis at the time of carpal tunnel release surgery (**C**, mean myocardial SUV 2.0).

TABLE 1 | Summary of patients and imaging results.

Patient	Age	Sex	History	F18-Florbetapir						
				Visual LV uptake	Mean SUV				Heart/BP ratio	Echo IVS	Additional Imaging
					LV	Blood pool	Paraspinal	Liver			
1	77	F	Smoldering myeloma	Yes	1.9	0.7	2.0	10.8	2.7	1.4 cm	CMR abnormal
2	70	M	Smoldering myeloma	Yes	2.7	0.7	2.2	10.9	3.9	1.6 cm	CMR normal
3	75	M	ATTRv - Val30Met	Yes	2.9	0.9	2.1	17.0	3.2	1.6 cm	PYP negative
4	80	M	ATTRwt	Yes	2.2	0.8	1.7	15.0	2.8	0.9 cm	PYP negative
5	72	F	ATTRwt	Yes	2.0	0.7	1.3	12.1	2.9	1.2 cm	PYP negative
6	73	F	ATTRv - Ala81Thr	Yes	1.9	0.9	3.0	15.3	2.1	0.9 cm	PYP negative*
7	67	M	ATTRwt	Yes	3.3	0.6	1.5	10.0	5.5	1.4 cm	PYP positive
8	65	M	ATTRwt	Yes	2.4	0.6	2.1	10.9	4.0	1.3 cm	PYP negative
9	83	M	CTS negative	Yes	2.5	0.9	0.8	14.4	2.8	N/a	N/a
10	67	M	CTS negative	Yes	2.3	0.7	1.6	14.8	3.3	N/a	N/a
11	66	F	CTS negative	Yes	1.8	0.8	1.3	8.3	2.3	N/a	N/a
12	69	F	CTS negative	Yes	2.0	1.0	1.2	10.4	2.0	N/a	N/a

*ATTRv, hereditary transthyretin amyloidosis; ATTRwt, wild-type transthyretin amyloidosis; BP, blood pool; CA, cardiac amyloidosis; CTS, carpal tunnel surgery biopsy; IVS, interventricular septum; LV, left ventricle; PYP, technetium pyrophosphate; SUV, standardized uptake value. *Developed Grade 3 uptake of PYP scan 3 years later.*

described control levels in all 12 patients. The one patient with technetium PYP evidence of cardiac amyloidosis did have the highest quantified myocardial SUV values. No patients developed clinical evidence of cardiac amyloidosis over 3 years, but one patient had asymptomatic conversion to a positive PYP scan despite low F18-florbetapir uptake at baseline.

This pilot study raises several important questions about cardiac amyloidosis, progression, and the utility of molecular PET imaging for this disease. One of the most important points to make relates to the comparison of F18-florbetapir with SPECT-based PYP and other bone scintigraphy. PYP has the benefit of being interpreted qualitatively on reconstructed tomographic images, while F18-florbetapir does not. That is to say, if SPECT PYP images demonstrate any radiotracer localized to the myocardium, i.e., highly specific for cardiac amyloidosis (and most likely ATTR). Yet, all patients undergoing F18-florbetapir PET have identifiable radiotracer localized to the myocardium that is significantly above blood pool values. Thus, specific thresholds are needed to separate positive from negative cases. Other protocols using a retention index could be examined in early disease, though these protocols involve up to a 60-min scan duration (6, 10) which may be difficult for some patients and inefficient for lab throughput. Our protocol utilized SUV calculation at a fixed time point 10–20 min after radiotracer injection which was based off of an analysis demonstrating good correlation between retention index and SUV measurements (8), and is in line with other PET protocols which generate static images for infection and inflammation. As only small differences were noted in F18-florbetapir myocardial SUV values, the utility of this protocol in the detection of early cardiac amyloidosis using this protocol appears limited.

Additionally, the speed of progression of myocardial amyloid deposits is currently unknown. AL amyloidosis has been thought to progress much more rapidly than ATTR amyloidosis; however, patient 6 had progression of ATTR cardiac amyloidosis on PYP nuclear scintigraphy over 3–4 years which was not preempted by significant F18-florbetapir uptake. As both patients during the study period with positive PYP scans were asymptomatic, this confirms the high sensitivity of PYP in early asymptomatic disease (11).

At this time, PET imaging with F18-florbetapir in cardiac amyloidosis remains an imaging modality best used in clinical research until more data accumulates regarding the best protocol to maximize sensitivity, specificity, differentiation

among amyloid subtypes, and ease of interpretation. Other PET radiotracers such as the thioflavin analogs F18-florbetaben, F18-flutemetamol, and C11-Pittsburgh compound B, and bone-seeking agents targeting microcalcifications like F18-NaF are similarly under investigation (12).

This pilot study is limited by an insufficient sample size to make broad conclusions about the utility of molecular PET imaging in cardiac amyloidosis. Further study is needed in asymptomatic patients or those with early disease, in both the AL and ATTR subtypes, to expand upon these findings. Repeat imaging could shed light on subclinical progression of disease and is an area of future research. At this time, PET imagings is not ubiquitously available and is more costly than technetium-based SPECT bone scintigraphy. In addition, this study also raises additional questions regarding the potential false negative rate of tenosynovial biopsy in our "control" patients. While these patients had negative tenosynovial biopsies and no signs or symptoms of amyloidosis, though unlikely, low level amyloid infiltration could have existed in the myocardium.

CONCLUSION

In this prospective pilot study, F18-florbetapir identified radiotracer uptake in the myocardium in early cardiac amyloidosis, patients with a potential for developing cardiac involvement of amyloidosis, and controls. F18-florbetapir uptake was qualitatively noted in the myocardium above blood pool in all patients, and there was significant overlap among quantitative uptake. There was no difference in the intensity of F18-florbetapir uptake in at-risk patients and controls. Future studies should investigate metabolic PET tracers and protocols for early detection of cardiac amyloidosis.

DATA AVAILABILITY STATEMENT

The raw data supporting the conclusions of this article will be made available by the authors, without undue reservation.

ETHICS STATEMENT

The studies involving human participants were reviewed and approved by Cleveland Clinic. The patients/participants provided their written informed consent to participate in this study.

AUTHOR CONTRIBUTIONS

BS and WJ conceived of the idea. BS, MH, WJ, and FD created the study design and planned the research. BS, AB, and JD carried out the research experiments. BS wrote the first draft of the manuscript. All authors critically reviewed the manuscript.

FUNDING

Funding was obtained from Avid Radiopharmaceuticals to supply doses of the radiotracer.

REFERENCES

1. Sperry BW, Saeed IM, Raza S, Kennedy KF, Hanna M, Spertus JA. Increasing rate of hospital admissions in patients with amyloidosis (from the National Inpatient Sample). *Am J Cardiol.* (2019) 124:1765–9. doi: 10.1016/j.amjcard.2019.08.045
2. Gillmore JD, Maurer MS, Falk RH, Merlini G, Damy T, Dispenzieri A, et al. Non-biopsy diagnosis of cardiac transthyretin amyloidosis. *Circulation.* (2016) 133:2404–12. doi: 10.1161/CIRCULATIONAHA.116.021612
3. Dorbala S, Cuddy S, Falk RH. How to image cardiac amyloidosis. *JACC Cardiovasc Imaging.* (2020) 13:1368–83. doi: 10.1016/j.jcmg.2019.07.015
4. Khor YM, Cuddy S, Harms HJ, Kijewski MF, Park MA, Robertson M, et al. Quantitative [18F]florbetapir PET/CT may identify lung involvement in patients with systemic AL amyloidosis. *Eur J Nucl Med Mol Imaging.* (2020) 47:1998–2009. doi: 10.1007/s00259-019-04627-7
5. Wagner T, Page J, Burniston M, Skillen A, Ross JC, Manwani R, et al. Extracardiac 18F-florbetapir imaging in patients with systemic amyloidosis: more than hearts and minds. *Eur J Nucl Med Mol Imaging.* (2018) 45:1129–38. doi: 10.1007/s00259-018-3995-2
6. Dorbala S, Vangala D, Semer J, Strader C, Bruyere JR Jr, Di Carli MF, et al. Imaging cardiac amyloidosis: a pilot study using ^{18}F-florbetapir positron emission tomography. *Eur J Nucl Med Mol Imaging.* (2014) 41:1652–62. doi: 10.1007/s00259-014-2787-6
7. Sperry BW, Reyes BA, Ikram A, Donnelly JP, Phelan D, Jaber WA, et al. Tenosynovial and cardiac amyloidosis in patients undergoing carpal tunnel release. *J Am Coll Cardiol.* (2018) 72:2040–50. doi: 10.1016/j.jacc.2018.07.092
8. Osborne DR, Acuff SN, Stuckey A, Wall JS. A routine PET/CT protocol with streamlined calculations for assessing cardiac amyloidosis using (18)F-Florbetapir. *Front Cardiovasc Med.* (2015) 2:23. doi: 10.3389/fcvm.2015.00023
9. Sperry BW, Vranian MN, Tower-Rader A, Hachamovitch R, Hanna M, Brunken R, et al. Regional variation in technetium pyrophosphate uptake in transthyretin cardiac amyloidosis and impact on mortality. *JACC Cardiovasc Imaging.* (2018) 11:234–42. doi: 10.1016/j.jcmg.2017.06.020
10. Genovesi D, Vergaro G, Giorgetti A, Marzullo P, Scipioni M, Santarelli MF, et al. [18F]-Florbetaben PET/CT for differential diagnosis among cardiac immunoglobulin light chain, transthyretin amyloidosis, and mimicking conditions. *JACC Cardiovasc Imaging.* (2021) 14:246–55. doi: 10.1016/j.jcmg.2020.05.031
11. Haq M, Pawar S, Berk JL, Miller EJ, Ruberg FL. Can 99mTc-Pyrophosphate aid in early detection of cardiac involvement in asymptomatic variant ttr amyloidosis? *JACC Cardiovasc Imaging.* (2017) 10:713–4. doi: 10.1016/j.jcmg.2016.06.003
12. Masri A, Bukhari S, Eisele YS, Soman P. Molecular imaging of cardiac amyloidosis. *J Nucl Med.* (2020) 61:965–70. doi: 10.2967/jnumed.120.245381

Conflict of Interest: BS is a consultant for Alnylam and Pfizer and has received research funding from Pfizer. MH has served on advisory boards for Alnylam, Eidos, AKCEA, and Pfizer.

The remaining authors declare that the research was conducted in the absence of any commercial or financial relationships that could be construed as a potential conflict of interest.

frontiers in Cardiovascular Medicine

ORIGINAL RESEARCH
published: 26 October 2021
doi: 10.3389/fcvm.2021.734820

Clinical Impact of Cardiovascular Magnetic Resonance in Cancer Patients With Suspected Cardiomyopathy

*Giv Heidari-Bateni[1], Jean-Bernard Durand[2], Cezar Iliescu[2], Greg Gladish[3], Anita Deswal[2], Amit R. Patel[4], Peter Kim[2], Juhee Song[5], Saamir Hassan[2], Nicolas Palaskas[2], Lauren A. Baldassarre[6], Chiara Bucciarelli-Ducci[7] and Juan Lopez-Mattei[2,3]**

[1] Department of Cardiology, Loma Linda University Medical Center, Loma Linda, CA, United States, [2] Department of Cardiology, MD Anderson Cancer Center, Houston, TX, United States, [3] Department of Thoracic Imaging, MD Anderson Cancer Center, Houston, TX, United States, [4] Cardiology Division, Department of Medicine, University of Chicago, Chicago, IL, United States, [5] Department of Biostatistics, The University of Texas MD Anderson Cancer Center, Houston, TX, United States, [6] Cardiovascular Medicine, Yale School of Medicine, New Haven, CT, United States, [7] Royal Brompton and Harefield Hospitals, Guy's and St Thomas' NHS Foundation Trust, King's College London, London, United Kingdom

OPEN ACCESS

Edited by:
Reza Nezafat,
Harvard University, United States

Reviewed by:
Otávio R. Coelho-Filho,
State University of Campinas, Brazil
Ian Paterson,
University of Alberta, Canada

***Correspondence:**
Juan Lopez-Mattei
jlopez9@mdanderson.org

Specialty section:
This article was submitted to Cardiovascular Imaging, a section of the journal Frontiers in Cardiovascular Medicine

Received: 01 July 2021
Accepted: 27 September 2021
Published: 26 October 2021

Citation:
Heidari-Bateni G, Durand J-B, Iliescu C, Gladish G, Deswal A, Patel AR, Kim P, Song J, Hassan S, Palaskas N, Baldassarre LA, Bucciarelli-Ducci C and Lopez-Mattei J (2021) Clinical Impact of Cardiovascular Magnetic Resonance in Cancer Patients With Suspected Cardiomyopathy. Front. Cardiovasc. Med. 8:734820. doi: 10.3389/fcvm.2021.734820

Objectives: To assess the clinical impact of Cardiovascular Magnetic Resonance (CMR) in clinical decision making of cancer patients with a suspected cardiomyopathy in a tertiary cancer center.

Background: Cardiomyopathies of diverse etiologies are frequently encountered in a Cardio-Oncology practice. The clinical impact of CMR after a presumptive diagnosis of cardiomyopathy has not been studied in cancer patients.

Methods: We reviewed data on cancer patients with presumptive diagnosis of cardiomyopathy who underwent CMR in a tertiary cancer center. The clinical impact of CMR was defined as either change in clinical diagnosis or management post CMR results. Univariate and multivariate logistic regression models were used to assess whether any of the baseline characteristics were predictive of the clinical impact of CMR.

Results: A total of 110 consecutive patients were identified. Clinical impact of CMR was seen in 68 (62%) patients. Change in the clinical diagnosis and management was seen in 56 (51%) and 41 (37%) of patients, respectively. The most common change was prevention of endomyocardial biopsy in 26 patients (24%). Overall, patients with higher left ventricular ejection fraction (LVEF) by echocardiography (echo), clinical impact was influenced more by CMR (LVEF of 37.2 ± 12.3% vs. 51.5 ± 11.6%, $p < 0.001$). Cancer diagnosis of multiple myeloma was associated with change in the management post CMR (adjusted OR of 25.6, 95% CI 4.0–162.4, $p = 0.001$). Suspicion of infiltrative cardiomyopathy was associated with a higher likelihood of change in diagnosis. Having an LVEF≥40 by echo was associated with change in diagnosis and management by CMR.

Conclusions: Utilization of CMR has a significant clinical impact in cancer patients with suspected cardiomyopathy. Patients with cancer diagnosis of multiple myeloma, suspicion of infiltrative cardiomyopathy and those with higher LVEF by echo seem to benefit more from CMR.

Keywords: cardiovascular magnetic resonance, cardiomyopathy, Cardio-Oncology, clinical impact, echocardiography

INTRODUCTION

The diagnosis and management of cardiomyopathies are important components of a Cardio-Oncology practice, given cancer patients are at an increased risk of heart failure (HF) (1) due to co-existing risk factors as well as cardiotoxic cancer therapeutics. The advancement of newer cancer therapies and improvement of survival rates, has led to an increase of the number of patients with cancer related cardiomyopathy (2, 3). In survivors of breast cancer, for instance, the adjusted 3-year cumulative incidence of anthracycline associated cardiomyopathy was calculated at 20.2 per 100 patients with an estimated increase by 21.7 per 100 patients with addition of trastuzumab (4).

Cardiovascular magnetic resonance (CMR) has been deemed appropriate for initial and sequential evaluation of patients with cardiomyopathies (specifically infiltrative, hypertrophic, and any cardiomyopathies of unclear etiology) based on appropriateness criteria from multimodality imaging scientific societies (5, 6). Moreover, CMR has an emergent role in detecting cardiotoxicity-related cardiomyopathy and other cardiovascular effects in patients undergoing anti-cancer therapy. Data from EuroCMR has shown that CMR has a strong impact on patient management, showing 62% of its findings impacting patient management (7). However, no data in cancer patients has been published in this regard.

In the current study, we aim to assess the clinical impact of CMR in clinical decision making for cancer patients with suspected cardiomyopathy in a large tertiary cancer center.

METHODS

We designed a retrospective cohort study of patients treated at the MD Anderson Cancer Center in Houston, TX, United States. We queried a CMR imaging database from May 2015 to September 2017 to identify consecutive patients who underwent CMR for clinically suspected cardiomyopathy. All patients included were receiving cancer treatment at our institution. The study protocol was approved by the institutional review board of MD Anderson Cancer Center. We included 110 consecutive patients that underwent CMR in either inpatient or outpatient settings. The diagnosis of cardiomyopathy was pre-established clinically by chart review and available echocardiographic findings in all inpatient cases and in the majority of outpatient cases. For a minority of cases referred from outside centers, a recent outside hospital echocardiography record was used. **Figure 1** illustrates a summary of study design algorithm. Given the diversity of cancer diagnosis in our cohort, we separated them into the following groups by cancer: solid tumors (most common was breast cancer, constituting 31% of the group), leukemia, lymphoma, myeloma and miscellaneous (more rare hematologic cancers).

All CMR images were acquired using a 1.5-T MRI scanner which was either Siemens Avanto (Siemens, Erlangen, Germany) or a 1.5-T GE AW (GE, Milwaukee, WI). All CMR exams were protocolled for cardiomyopathy, and included the following sequences: SSFP cines (real time cines if suspicion of constrictive pericarditis), T1 and T2 weighted double inversion recovery (IR) sequences, some included T2*, T1 (native and post contrast) and T2 mapping (Modified Look-Locker IR). Late gadolinium enhancement (LGE) was performed for tissue characterization using a segmented inversion-recovery sequence (in-plane spatial resolution, 1.8 × 1.3 mm; slice thickness, 8 mm; temporal resolution, 160–200 ms) 10–15 min after intravenous contrast administration (gadopentetate dimeglumine, 0.125 mmol/kg).

CMR images were interpreted independently by either a level 3 CMR board-certified cardiologist or a radiologist with level 3 equivalent training. Studies were reviewed to assess for image quality. Cases with poor quality studies, including those where gadolinium-based contrast was not administered, were excluded. For all patients, demographic and clinical variables including age, sex, type of malignancy, comorbidities, history of previous chemotherapy, and echocardiographic parameters were collected by electronic chart review. Patients with insufficient clinical data were excluded. The clinical impact of CMR was then assessed independently and determined upon consensus by two investigators (J.C.L., G.HB). We adopted the definitions per Abbasi et al. (8) where they defined significant clinical impact of CMR as either finding an entirely new diagnosis or if a change in clinical management occurred after CMR results. Change in diagnosis was defined as a diagnosis resulting from CMR that was previously unconfirmed or unsuspected. Change in management was defined as CMR results preventing or resulting in a procedure (invasive or medical), or admission or discharge from hospital (**Figure 1**). Changes in medical management that we considered as significant was either starting guideline directed medical treatment for heart failure or stopping it, starting or stopping anticoagulation, but no changes in cancer treatment were seen caused from CMR findings. Our outcomes were predefined as either clinical impact of CMR, depending on changes in diagnosis and changes in management. No survival

Abbreviations: CMR, Cardiovascular Magnetic Resonance; TTE, Transthoracic echocardiogram; LVEF, Left ventricular ejection fraction; LGE, Late Gadolinium enhancement.

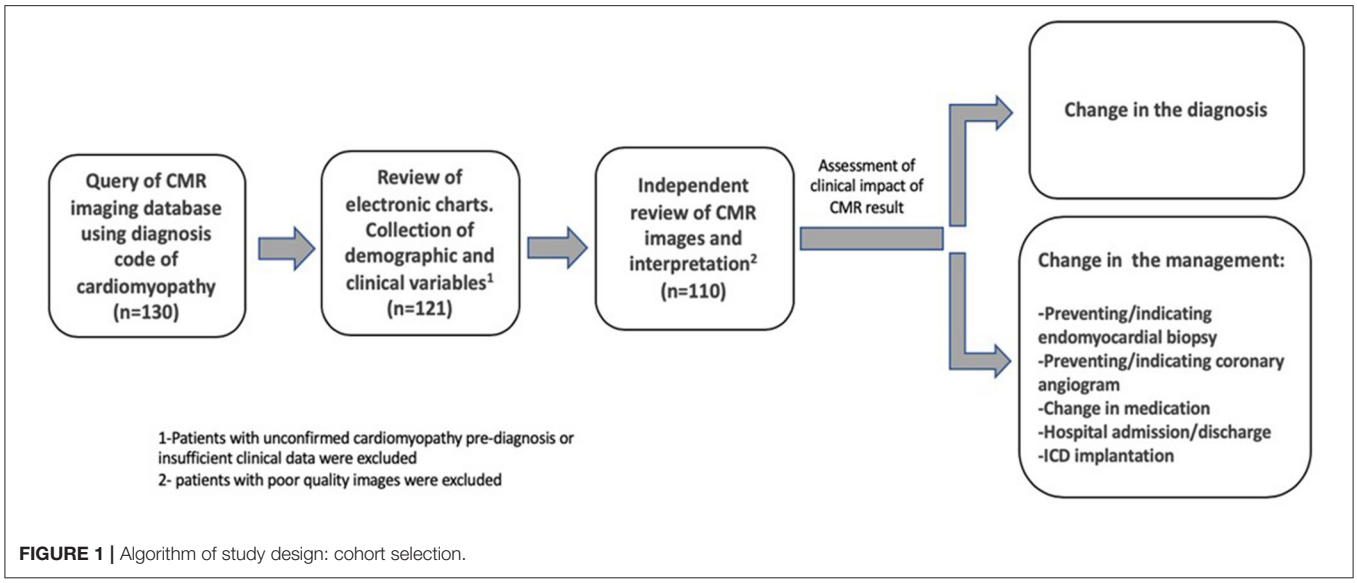

FIGURE 1 | Algorithm of study design: cohort selection.

analyses or hard endpoints were evaluated, just utilization endpoints as previously defined.

We evaluated patients' baseline clinical characteristics to assess if the clinical impact of CMR can be predicted by these characteristics. Univariate and multivariate logistic regression models were used to identify variables that were significantly associated with diagnosis change (change in diagnosis vs. no change), management change (change in management vs. no change), or either of them (any change vs. no change). Only variables with significant *p*-value in univariable analyses, or those with a trend toward a significant *p* value, were used in the multivariable analysis. Hosmer-Lemeshow test was used to check the model adequacy. A *p*-value less than 0.05 indicated a statistical significance. All statistical analyses were performed in SAS® Version 9.4 (SAS Institute, Cary, NC).

RESULTS

A total of 110 patients with clinical suspicion of cardiomyopathy were identified; of those 58 (53%) were female. The average age was 59 ± 15 years. Solid tumors were the most prevalent malignancies (40%), followed by myeloma (19%), and lymphoma (18%). **Table 1** summarizes baseline demographic and clinical characteristics of the patients. Indications for CMR with respective percentage frequencies were the following: Routine CMR for cardiomyopathy (64%), suspected infiltrative cardiomyopathy (25%), hypertrophic cardiomyopathy (6%), viability (3%), suspected arrhythmogenic right ventricular dysplasia (2%) and carcinoid heart disease (1%) (see **Table 2**). Following CMR, cardiomyopathies were categorized into six different diagnostic groups as summarized in **Table 3**. In 27 (25%) patients with suspected iron overload cardiomyopathy, amyloidosis, or suspected myocarditis, CMR showed no evidence of cardiomyopathy (normal ejection fraction, normal T2* and absence of late gadolinium enhancement) despite clinical suspicion and suggestive echocardiographic findings.

TABLE 1 | Baseline demographic and clinical characteristics of the patients.

Variable	Result[a]
Age (years)[b]	59 ± 15
Sex	
Male	52 (47%)
Female	58 (53%)
Type of malignancy	
Solid tumors	45 (41%)
Leukemia	14 (13%)
Lymphoma	20 (18%)
Multiple Myeloma	21 (19%)
Miscellaneous	10 (9%)
Ejection fraction by echocardiography (%)[b]	42± 13
Ejection fraction < 40%	32 (29%)
Diabetes	35 (32%)
Hypertension	65 (59%)
Atrial fibrillation	24 (22%)
History of chest radiotherapy	22 (21%)
History of coronary artery disease	27 (25%)
History of treatment with anthracycline	39 (36%)

[a]*Data are expressed as the number of cases (percentage of total) unless indicated otherwise.*
[b]*Data are expressed as the mean ± standard deviation.*

Overall, the clinical impact of CMR was seen in 68 (62%) patients. Results of CMR changed the diagnosis in 56 (51%), the management in 41 (37%), and both management and diagnosis in 29 (26%) patients. The most common clinical impact of CMR was prevention of endomyocardial biopsy in 26 (24%) patients by ruling out the working diagnosis of suspected infiltrative cardiomyopathy. One noticeable finding was that in 42 patients (38%) there was no change in diagnosis or management, and the mean LVEF in this group by TTE was 37 ± 12% in contrast to the 29 patients that had changes in both diagnosis and

TABLE 2 | CMR indications.

Variable	Frequency (%)
Routine CMR for cardiomyopathy	70 (64%)
Suspected infiltrative cardiomyopathy	27 (25%)
*Suspected hypertrophic cardiomyopathy	7 (6%)
*Viability	3 (3%)
*Suspected arrhythmogenic right ventricular dysplasia	2 (2%)
*Carcinoid heart disease	1 (1%)

*For further analysis these categories were included in Other CM in **Table 3**.

TABLE 3 | Final CMR diagnosis.

Diagnosis	Frequency[a]
NICM	49 (45%)
ICM	8 (7%)
Cardiac amyloidosis	6 (5%)
HCM	6 (5%)
Other CM	14 (13%)
Non compaction	1 (1%)
Takotsubo	1 (1%)
Myocarditis	4 (4%)
Chagas	1 (1%)
Iron overload	1 (1%)
RV failure [PH]	3 (3%)
Constrictive pericarditis	1 (1%)
Eosinophilic CM	1 (1%)
No cardiomyopathy	27 (25%)

[a]*Data are expressed as the number of cases (percentage of total). CMR, cardiac magnetic resonance imaging; NICM, non ischemic cardiomyopathy; ICM, Ischemic cardiomyopathy, HCM, hypertrophic cardiomyopathy; CM, cardiomyopathy; RV, right ventricle; PH, pulmonary hypertension.*

management, whose corresponding mean LVEF by TTE was 51 ± 11% ($p < 0.001$ by Chi-square test).

Table 4 summarizes all the management changes post CMR. Examples of patients with change in both diagnosis and management are summarized in **Table 5**. The clinical impact of CMR is illustrated in **Figure 2**. To assess whether any of the baseline characteristics can predict the clinical impact of CMR, univariate and multivariate logistic regression models were fitted, and they are summarized in **Tables 6**, **7**. All analyses demonstrated that a higher ejection fraction by echocardiography (LVEF ≥ 40) predicts a greater clinical impact of CMR, adjusting for type of malignancy (adjusted OR 7.09, 95% CI, 2.09–24.11, p value = 0.002 and 6.16 with 95% CI 1.47–25.77, p value = 0.013 for change in diagnosis and management respectively). For change in diagnosis, a suspicion of infiltrative cardiomyopathy, when compared with routine indication of CMR for cardiomyopathy had a higher likelihood of change in diagnosis in the multivariate analysis for change in diagnosis (adjusted OR: 10.03, 95% CI, 1.91–52.69, p value = 0.006), but not in multivariate analysis for change in management.

TABLE 4 | Summary of change in management followed by CMR results ($n = 110$).

Change in management	Frequency[a]
Prevented endomyocardial biopsy	26 (24%)
Change in medications	14 (13%)
Prevented coronary angiogram or PCI	11 (10%)
Resulted in endomyocardial biopsy	6 (5%)
Resulted in LHC	4 (4%)
Hospital admission	2 (2%)
Hospital discharge	1 (1%)
Resulted in ICD implantation	1 (1%)

[a]*Data are expressed as the number of cases (percentage of total). Some patients had change in more than one management category. CMR, cardiac magnetic resonance imaging; PCI, percutaneous coronary intervention; LHC, left heart catheterization; ICD, implantable cardioverter-defibrillator.*

We also found that "type of malignancy" predicted change in management post CMR. As shown in **Table 7**, multiple myeloma was the cancer group associated with significant change in the management post CMR (adjusted OR of 25.56 with 95% CI 4.02–162.44, p value = 0.001).

DISCUSSION

This study demonstrates a valuable role for CMR as part of the assessment for suspected or known cardiomyopathy in patients with cancer. In 62% of our patients there was a benefit from the addition of CMR imaging in their diagnostic work up, by achieving either a change in diagnosis or change in management. Furthermore, we identified baseline clinical characteristics that could predict the clinical impact of CMR. In particular, we showed that patients with higher left ventricular ejection fraction by echocardiography, patients with a diagnosis of multiple myeloma as the primary malignancy and those with suspicion of infiltrative cardiomyopathy were those in which CMR had the most clinical impact.

CMR has proven to have an additive role in diagnosis and management of patients with cardiomyopathy (8–10). However, in patients with non-ischemic cardiomyopathy, its value on routine use may be limited, given it may not yield more specific etiologies in majority of cases (11). Which was consistent with our findings, given routine CMR for cardiomyopathy didn't yield as much clinical impact as suspicion of infiltrative cardiomyopathy. Compared to echocardiography, CMR has a higher spatial resolution, larger field of view, highly reproducible ventricular volumes and ejection fraction quantification (12) with the ability for functional assessment and ability to perform tissue phenotyping using tissue characterization sequences such T1 weighted imaging with late gadolinium enhancement (LGE) (13), T2 weighted imaging and parametric mapping (14).

With the advancement of CMR techniques, recent multi-society expert consensus recommendations for multimodality imaging in cardiac amyloidosis have considered a central role for CMR in the non-invasive diagnosis of cardiac amyloidosis (15).

TABLE 5 | Examples of patients with (green) and without (red) changes in both diagnosis and management after CMR.

Patient description	Indication for CMR	CMR findings	Clinical impact
68 y/o F with infiltrative ductal carcinoma, PMHx of HLP and HTN. LVEF of 40-45% in echo with poor acoustic windows	Work up on etiology of cardiomyopathy and better assessment of EF prior to next round of chemotherapy	Inferior wall subendocardial infarction with partial viability in the RCA territory	Incidental finding of ischemic cardiomyopathy; underwent left heart catheterization
66 y/o M with Smoldering multiple myeloma, PMHx of diabetes. Echo finding of LVH and diastolic dysfunction.	Suspicion of infiltrative cardiomyopathy based on the echocardiogram findings	Hypertrophic cardiomyopathy; cardiac amyloidosis ruled out	Hypertrophic cardiomyopathy: no endomyocardial biopsy pursued
57 y/o with HTN, CLL and bladder cancer that had an LVEF of 40-45% by Echo	Work up on etiology of cardiomyopathy	Mid myocardial hyperenhancement in basal septum. LVEF: 52%. Diagnosis of NICM	No change in management as GDMT for HF was started with echo results. No change in diagnosis as echo findings and clinical presentation suggested NICM
62 y/o F with breast cancer and prior treatment with anthracycline, her Echo showed an LVEF of 39%	Work up on etiology of cardiomyopathy	Findings suggestive of non-ischemic cardiomyopathy. CMR LVEF of 37%.	No change in management as GDMT for HF was started with echo results. Echo identified correctly the clinical diagnosis.

CMR, cardiac magnetic resonance imaging; y/o, years old; F, female; M, male; PMHx, past medical history; HLP, hyperlipidemia; HTN, hypertension; EF, ejection fraction; RCA, right coronary artery; MGUS, monoclonal gamopathy of unknown significance; LV, left ventricle; NICM, non-ischemic cardiomyopathy; GDMT, guideline directed medical therapy; HF, Heart Failure.

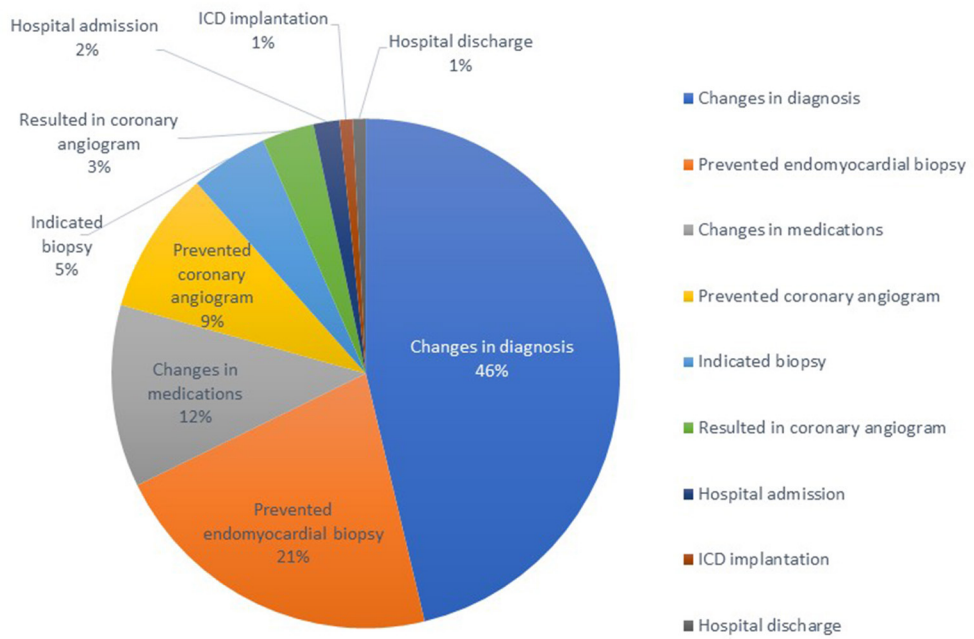

FIGURE 2 | Clinical impact of utilization of cardiac magnetic resonance in a tertiary cancer center: 121 events in total of 66 patients.

CMR is a cornerstone test in the evaluation of patients with left ventricular hypertrophy (LVH) phenotype on echocardiography and suspected infiltrative cardiomyopathies, explaining why there was a significant clinical impact in cancer patients with suspected infiltrative cardiomyopathy particularly those with primary multiple myeloma, given the risk to develop cardiac amyloidosis. This might in part explain our findings of baseline multiple myeloma predicting the clinical impact of CMR.

Multivariate analyses also revealed that the clinical impact of CMR in both diagnosis and management is more appreciated in patients' groups with an echo LVEF of 40% or higher and changes in diagnosis more likely with suspicion of infiltrative cardiomyopathy (adjusted OR 10.03, $p = 0.006$). This could be explained due to the high proportion of cases (25%) that CMR showed no evidence of cardiomyopathy despite clinical suspicion by TTE. This finding changes the

TABLE 6 | Selected univariate and multivariate analysis of factors predicting diagnosis change following CMR.

Variable	Univariate logistic regression model			Multivariate logistic regression model[c]		
	OR	95% CI	*P*-value	aOR	95% CI	*P*-value
Age	1.03	0.99–1.05	0.079	1.05	1.005–1.09	0.031
Female sex	0.77	0.35–1.72	0.521			
Type of malignancy[a]						
Lymphoma	0.73	0.22–2.37	0.596			
Leukemia	1.94	0.54–6.91	0.308			
MM	9.68	1.97–47.52	0.005			
Miscellaneous	4.24	0.79–22.84	0.093			
CMR indication[b]						
Infiltrative CM	12.29	2.66–56.83	0.001	10.03	1.91–52.69	0.006
Other	0.48	0.13–1.71	0.255	0.31	0.06–1.54	0.153
Diabetes	2.56	1.03–6.34	0.043			
Hypertension	1.05	0.46–2.38	0.905			
Atrial fibrillation	3.41	1.15–10.15	0.028			
Echocardiographic EF	1.08	1.04–1.13	<0.001			
EF≥40	5.35	1.99–14.38	0.001	7.09	2.09–24.11	0.002
EF≥50	7.21	2.60–19.98	<0.001			
History of treatment with anthracycline	0.33	0.14–0.80	0.014			

CMR, cardiac magnetic resonance imaging; OR, Odds Ratio; CI, confidence interval; aOR, adjusted odds ratio; EF, ejection fraction; N/A, not applicable (variable not included in the multivariate logistic regression model); CM, cardiomyopathy. [a]"Solid tumor" malignancy as reference group. [b]"Routine CMR for cardiomyopathy" as reference group. [c]The multivariate model initiated with the following variables: age, type of malignancy, diabetes, atrial fibrillation, EF, CMR indication, and history of anthracycline use. It reduced by stepwise selection to age, CMR indication, and EF as shown here. Same results obtained when using of EF ≥ 50% in lieu of ≥ 40% (adjusted OR of 7.57 with 95% CI 1.42–40.24, p value = 0.018 and adjusted OR of 9.13 with 95% CI 2.23–37.45, p value = 0.002 for CM infiltrative and EF≥50, respectively).

TABLE 7 | Selected univariate and multivariate analysis of factors predicting management change following CMR.

Variable	Univariate logistic regression model			Multivariate logistic regression model [c]		
	OR	95 % CI	*P*-value	aOR	95% CI	*P*-value
Age	1.01	0.98–1.04	0.443			
Female sex	1.43	0.59– 3.45	0.424			
Type of malignancy[a]						
Lymphoma	1.61	0.48–5.44	0.444	0.86	0.18–4.04	0.845
Leukemia	1.84	0.41–8.33	0.429	1.25	0.23–6.73	0.799
MM	18.40	3.55–95.50	0.001	25.56	4.02–162.44	0.001
Miscellaneous	4.60	0.72–29.33	0.106	3.99	0.33–48.36	0.277
CMR indication[b]						
Infiltrative CM	12.68	2.67–60.33	0.001			
Other	0.16	0.02–1.33	0.089			
Diabetes	1.90	0.71–5.06	0.199			
Hypertension	1.18	0.49–2.86	0.716			
Atrial fibrillation	2.03	0.62–6.67	0.246			
Echocardiographic EF	1.07	1.03–1.04	0.001			
EF≥40	4.54	1.60–12.86	0.004	6.16	1.47–25.77	0.013
EF≥50	5.01	1.73–14.51	0.003			
History anthracycline use	0.44	0.18–1.11	0.084			

CMR, cardiac magnetic resonance imaging; OR, Odds Ratio; CI, confidence interval; aOR, adjusted odds ratio; EF, ejection fraction; N/A, not applicable (variable not included in the multivariate logistic regression model); CM, cardiomyopathy. [a]"Solid tumor" malignancy as reference group. [b]"Routine CMR for cardiomyopathy" as reference group. [c]The multivariate model initiated with the following variables: type of malignancy, CMR indication, diabetes, EF, and history of anthracycline use. It reduced by stepwise selection to type of malignancy and EF as shown here. Same results obtained when using of EF ≥ 50% in lieu of ≥40% (adjusted OR of 16.92 with 95% CI 2.94–97.38, p value = 0.002 and adjusted OR of 3.85 with 95% CI 1.11–13.34, p value = 0.034 for MM and EF ≥ 50, respectively).

management dramatically, as patients could be able to resume chemotherapy promptly and without the need for treatment of Heart failure. Conversely, the patients that did not have significant change in diagnosis and management had lower mean LVEF by TTE, which could suggest that in most of these cases LV systolic dysfunction was identified appropriately by TTE. In other words, in the context of a significant decrease in LVEF that could be detected by TTE, CMR might not add to the diagnosis or management. Anthracycline and trastuzumab cardiotoxicity and related cardiomyopathies are not well characterized in CMR by a specific patterns of LGE or specific findings in parametric mapping (16). Conversely, if an LVEF measurement by TTE is borderline low or in the realm of 40%, CMR accurately differentiates true decreases from cases of preserved LV systolic function because of its robustness in reproducibility and less interobserver variability in ventricular volumes and LVEF quantification. This suggest that routine utilization of CMR for cardiomyopathy evaluation based on echo findings might not offer clinical benefit if echo identifies well possible etiologies such as decreased LVEF from anthracyclines. Also suspicion of infiltrative cardiomyopathy was associated with increased of change in diagnosis related with CMR. Which suggests that clinical impact by CMR is higher in patients for which iron overload cardiomyopathy or cardiac amyloidosis must be evaluated. CMR ruled out cardiomyopathy in 25% of patients. This has an impact for patients' mental wellbeing, withdrawal of heart failure medications and resumption of lifesaving cancer therapies. In our study, prevention of endomyocardial biopsy was found to be the most common clinical impact of CMR comprising 24% of patients. Prevention of endomyocardial biopsy is important in the setting of cancer particularly for those actively receiving chemotherapy given the increased risk of complications, mainly vascular complications and bleeding in this vulnerable group. A cost effectiveness analysis may also enlighten the economic benefit of using CMR as a gatekeeper for myocardial biopsy.

In conclusion, application of CMR in Cardio-Oncology appears to have frequent clinical impact (62% patients) on the evaluation of confirmed or suspected cases of cardiomyopathy in a cohort of cancer patients. Baseline systolic function from TTE, suspicion of infiltrative cardiomyopathy and primary malignancy type increase the likelihood of clinical impact of the addition of CMR to the diagnostic approach. Our findings support an important role of CMR in a Cardio-Oncology practice. Further larger and multi-center studies looking at hard clinical endpoints and cost-effectiveness analyses are needed to quantify better the benefits of CMR in these patients.

LIMITATIONS

We cannot exclude the role of selection and referral bias of the primary cardiologist when choosing the appropriate patient for CMR assessment; however, the studied patients represents a heterogeneous group either referred by outpatient centers or seen as an inpatient consult in a tertiary cardio-oncology practice.

Our study has some additional limitations. First, this is a retrospective study which can be skewed by limitations of medical documentation and the absence of a control group. Second, there are some known limitations in application of CMR such as patients with claustrophobia, prosthetic devices or foreign bodies. Also, 11 out of 121 (9%) of scans were excluded due to poor image quality or lack of contrast (see **Figure 1**), and therefore our results may overestimate the benefit of performing CMR.

Moreover, the economic value of CMR for all patients with suspected cardiomyopathy is uncertain. Similarly, there is no outcome data on survival benefit of using CMR in the management of cardiomyopathy in cancer patients. Undoubtedly a cost-effective analytical study or a comparative effectiveness study with focus on survival benefit can better highlight the value of this approach.

Clinical Perspectives

In patients with cancer and suspected cardiomyopathy, CMR may result in change in diagnosis and management in certain clinical scenarios. Patients with LVEF of 40% or more, those with suspicion of infiltrative cardiomyopathy and those with cancer diagnosis of multiple myeloma, have a higher likelihood to benefit from the use of CMR.

Further prospective research is needed to identify the value, including the economic burden, of the use of CMR for cancer patients with suspected cardiomyopathy.

DATA AVAILABILITY STATEMENT

The raw data supporting the conclusions of this article will be made available by the authors, without undue reservation.

ETHICS STATEMENT

The studies involving human participants were reviewed and approved by MD Anderson IRB provided exemption due to retrospective review. Written informed consent for participation was not required for this study in accordance with the national legislation and the institutional requirements.

AUTHOR CONTRIBUTIONS

GH-B and JL-M planned and wrote the manuscript. All other authors edited the manuscript.

FUNDING

The statistical analysis work was supported in part by the Cancer Center Support Grant (NCI Grant P30 CA016672). CB-D was supported by the NIHR Biomedical Research Centre at University Hospitals Bristol NHS Foundation Trust and the University of Bristol.

REFERENCES

1. Meijers WC, de Boer RA. Common risk factors for heart failure and cancer. *Cardiovasc Res.* (2019) 115:844–53. doi: 10.1093/cvr/cvz035
2. Curigliano G, Cardinale D, Dent S, Criscitiello C, Aseyev O, Lenihan D, et al. Cardiotoxicity of anticancer treatments: epidemiology, detection, and management. *CA Cancer J Clin.* (2016) 66:309–25. doi: 10.3322/caac.21341
3. Araujo-Gutierrez R, Ibarra-Cortez SH, Estep JD, Bhimaraj A, Guha A, Hussain I, et al. Incidence and outcomes of cancer treatment-related cardiomyopathy among referrals for advanced heart failure. *Cardio-Oncol* . (2018) 4:3. doi: 10.1186/s40959-018-0029-y
4. Chen J, Long JB, Hurria A, Owusu C, Steingart RM, Gross CP. Incidence of heart failure or cardiomyopathy after adjuvant trastuzumab therapy for breast cancer. *J Am Coll Cardiol.* (2012) 60:2504–12. doi: 10.1016/j.jacc.2012.07.068
5. Patel MR, Hendel RC, Carr JC, Gerstad NA, Gillam LD, Hodgson FJ, et al. ACCF/ACR/SCCT/SCMR/ASNC/NASCI/SCAI/SIR 2006 appropriateness criteria for cardiac computed tomography and cardiac magnetic resonance imaging: a report of the American College of Cardiology Foundation Quality Strategic Directions Committee Appropriateness Criteria Working Group, American College of Radiology, Society of Cardiovascular Computed Tomography, Society for Cardiovascular Magnetic Resonance, American Society of Nuclear Cardiology, North American Society for Cardiac Imaging, Society for Cardiovascular Angiography and Interventions, and Society of Interventional Radiology. *J Am Coll Cardiol.* (2006) 48:1475–97. doi: 10.1016/j.jacc.2006.07.003
6. Doherty JU, Kort S, Mehran R, Schoenhagen P, Soman P, Dehmer GJ, et al. ACC/AATS/AHA/ASE/ASNC/HRS/SCAI/SCCT/SCMR/STS 2019 appropriate use criteria for multimodality imaging in the assessment of cardiac structure and function in nonvalvular heart disease: a report of the American College of Cardiology Appropriate Use Criteria Task Force, American Association for Thoracic Surgery, American Heart Association, American Society of Echocardiography, American Society of Nuclear Cardiology, Heart Rhythm Society, Society for Cardiovascular Angiography and Interventions, Society of Cardiovascular Computed Tomography, Society for Cardiovascular Magnetic Resonance, and the Society of Thoracic Surgeons. *J Am Soc Echocard.* (2019) 32:553–79. doi: 10.1016/j.echo.2019.01.008
7. Bruder O, Wagner A, Lombardi M, Schwitter J, van Rossum A, Pilz G, et al. European Cardiovascular Magnetic Resonance (EuroCMR) registry–multi national results from 57 centers in 15 countries. *J Cardiovasc Mag Resonan.* (2013) 15:9. doi: 10.1186/1532-429X-15-S1-O96
8. Abbasi SA, Ertel A, Shah RV, Dandekar V, Chung J, Bhat G, et al. Impact of cardiovascular magnetic resonance on management and clinical decision-making in heart failure patients. *J Cardiovasc Mag Resonan.* (2013) 15:89. doi: 10.1186/1532-429X-15-89
9. Patel AR, Kramer CM. Role of cardiac magnetic resonance in the diagnosis and prognosis of nonischemic cardiomyopathy. *JACC Cardiovasc Imaging.* (2017) 10:1180–93. doi: 10.1016/j.jcmg.2017.08.005
10. Kramer CM. Role of cardiac MR imaging in cardiomyopathies. *J Nucl Med.* (2015) 56:39s–45s. doi: 10.2967/jnumed.114.142729
11. Paterson DI, Wells G, Erthal F, Mielniczuk L, O'Meara E, White J, et al. OUTSMART HF: a randomized controlled trial of routine versus selective cardiac magnetic resonance for patients with nonischemic heart failure (IMAGE-HF 1B). *Circulation.* (2020) 141:818–27. doi: 10.1161/CIRCULATIONAHA.119.043964
12. Bellenger NG, Davies LC, Francis JM, Coats AJ, Pennell DJ. Reduction in sample size for studies of remodeling in heart failure by the use of cardiovascular magnetic resonance. *J Cardiovasc Mag Reson.* (2000) 2:271–8. doi: 10.3109/10976640009148691
13. Shah DJ, Judd RM, Kim RJ. Technology insight: MRI of the myocardium. *Nat Clin Pract Cardiov Med.* (2005) 2:597–605. doi: 10.1038/ncpcardio0352
14. Salerno M, Kramer CM. Advances in parametric mapping with CMR imaging. *JACC Cardiov Imag.* (2013) 6:806–22. doi: 10.1016/j.jcmg.2013.05.005
15. Dorbala S, Ando Y, Bokhari S, Dispenzieri A, Falk RH, Ferrari VA, et al. ASNC/AHA/ASE/EANM/HFSA/ISA/SCMR/SNMMI expert consensus recommendations for multimodality imaging in cardiac amyloidosis: Part 1 of 2-evidence base and standardized methods of imaging. *J Nucl Cardiol.* (2019) 26:2065–123. doi: 10.1007/s12350-019-01760-6
16. Jordan JH, Todd RM, Vasu S, Hundley WG. Cardiovascular magnetic resonance in the oncology patient. *JACC Cardiov Imag.* (2018) 11:1150–72. doi: 10.1016/j.jcmg.2018.06.004

Author Disclaimer: The views expressed in this publication are those of the author(s) and not necessarily those of the NHS, the National Institute for Health Research or the Department of Health and Social Care.

Conflict of Interest: The authors declare that the research was conducted in the absence of any commercial or financial relationships that could be construed as a potential conflict of interest.

Publisher's Note: All claims expressed in this article are solely those of the authors and do not necessarily represent those of their affiliated organizations, or those of the publisher, the editors and the reviewers. Any product that may be evaluated in this article, or claim that may be made by its manufacturer, is not guaranteed or endorsed by the publisher.

frontiers in Cardiovascular Medicine

REVIEW
published: 18 January 2022
doi: 10.3389/fcvm.2021.794706

A Clinical Approach to Multimodality Imaging in Pulmonary Hypertension

Christine Farrell[1†], *Aparna Balasubramanian*[2†], *Allison G. Hays*[3], *Steven Hsu*[3], *Steven Rowe*[4], *Stefan L. Zimmerman*[4], *Paul M. Hassoun*[1], *Stephen C. Mathai*[2] *and Monica Mukherjee*[3*]

[1] Division of Medicine, Johns Hopkins University, Baltimore, MD, United States, [2] Division of Pulmonary and Critical Care Medicine, Johns Hopkins University, Baltimore, MD, United States, [3] Division of Cardiology, Johns Hopkins University, Baltimore, MD, United States, [4] Division of Radiology, Johns Hopkins University, Baltimore, MD, United States

Pulmonary hypertension (PH) is a clinical condition characterized by progressive elevations in mean pulmonary artery pressures and right ventricular dysfunction, associated with significant morbidity and mortality. For resting PH to develop, ∼50–70% of the pulmonary vasculature must be affected, suggesting that even mild hemodynamic abnormalities are representative of advanced pulmonary vascular disease. The definitive diagnosis of PH is based upon hemodynamics measured by right heart catheterization; however this is an invasive and resource intense study. Early identification of pulmonary vascular disease offers the opportunity to improve outcomes by instituting therapies that slow, reverse, or potentially prevent this devastating disease. Multimodality imaging, including non-invasive modalities such as echocardiography, computed tomography, ventilation perfusion scans, and cardiac magnetic resonance imaging, has emerged as an integral tool for screening, classifying, prognosticating, and monitoring response to therapy in PH. Additionally, novel imaging modalities such as echocardiographic strain imaging, 3D echocardiography, dual energy CT, FDG-PET, and 4D flow MRI are actively being investigated to assess the severity of right ventricular dysfunction in PH. In this review, we will describe the utility and clinical application of multimodality imaging techniques across PH subtypes as it pertains to screening and monitoring of PH.

Keywords: pulmonary hypertension, echocardiography, computed tomography, scintigraphy, magnetic resonance imaging

OPEN ACCESS

Edited by:
Erhan Tenekecioglu,
University of Health Sciences, Turkey

Reviewed by:
Francesco Sturla,
IRCCS Policlinico San Donato, Italy
Keiichi Hirono,
University of Toyama, Japan

***Correspondence:**
Monica Mukherjee
mmukher2@jhu.edu

[†] These authors share first authorship

Specialty section:
This article was submitted to Cardiovascular Imaging, a section of the journal Frontiers in Cardiovascular Medicine

Received: *14 October 2021*
Accepted: *22 November 2021*
Published: *18 January 2022*

Citation:
Farrell C, Balasubramanian A, Hays AG, Hsu S, Rowe S, Zimmerman SL, Hassoun PM, Mathai SC and Mukherjee M (2022) A Clinical Approach to Multimodality Imaging in Pulmonary Hypertension. Front. Cardiovasc. Med. 8:794706. doi: 10.3389/fcvm.2021.794706

KEY POINTS

- Pulmonary hypertension is a devastating disease and early detection improves morbidity and mortality.
- Echocardiography, computed tomography, nuclear imaging, and magnetic resonance imaging are non-invasive imaging studies for screening, classification, prognostication, and monitoring of pulmonary hypertension.
- New non-invasive imaging techniques such as strain imaging, 3D echocardiography, dual energy CT, and 4D flow MRI are emerging techniques that can assist in the diagnosis and monitoring of pulmonary hypertension.

INTRODUCTION

Pulmonary hypertension (PH) is an insidious, highly morbid, and heterogeneous disease that is characterized by elevations in pulmonary arterial pressures and is classified into five groups based on etiology (1–3). Early diagnosis and referral are associated with better clinical outcomes, however the time from symptom onset to diagnosis is often greater than 2 years (4–6). PH is exclusively diagnosed using confirmatory invasive right heart catheterization (RHC) to measure mean pulmonary artery pressure (mPAP), pulmonary capillary wedge pressure (PCWP), and pulmonary vascular resistance (PVR) (7). Currently, PH is defined by a mPAP >20 mmHg, a threshold which was recently decreased from ≥25 mmHg based on epidemiologic data demonstrating the distribution of mPAP among healthy individuals and the significant impact of mildly elevated pulmonary pressures on morbidity and mortality (8).

While RHC is the only method to directly measure pulmonary and right heart pressures, it is invasive, resource intensive, and carries procedural risk (9). As a result, in 2015, the European Society of Cardiology/European Respiratory Society guidelines recommended the use of a variety of non-invasive imaging modalities to screen and risk stratify patients (10). The standard of care for screening and classifying PH includes transthoracic echocardiogram (TTE), chest computed tomography (CT), ventilation perfusion (VQ) scan, RHC, and increasingly cardiac magnetic resonance imaging (CMR). Multimodality imaging is useful for screening, classifying, prognosticating, and monitoring effectiveness of therapy in PH. This review seeks to describe the current imaging modalities used in diagnosing and monitoring the various forms of PH along with several novel imaging modalities that may soon be incorporated into clinical practice.

METHODOLOGY

We conducted a search utilizing Medline/PubMed from November 1989 to June 2021 to identify relevant articles. Search terms included: pulmonary hypertension AND echocardiography OR magnetic resonance OR computed tomography OR nuclear OR cardiovascular imaging. Identified articles were then evaluated, including screening of references. Review articles, meta-analyses, and major medical society guideline documents were also assessed. Finally, selected articles were included if felt to be relevant in the authors' opinion. Data from these articles were abstracted and guided this narrative review.

RESULTS

We identified 46 articles on echocardiography, 19 on computerized tomography, 7 on nuclear medicine techniques including scintigraphy, and 45 on magnetic resonance imaging in PH.

Echocardiography

TTE is the most common imaging modality used to screen for PH and is the mainstay for screening, monitoring of therapeutic response, and prognostication (11). As most deaths from PH are from right heart failure, recognizing the presence, and quantifying the degree of right heart dysfunction, is helpful in monitoring disease progression and prognostication. In addition to conventional two-dimensional (2D) TTE, speckle-tracking strain imaging and three-dimensional (3D) echocardiography are more specialized techniques that are increasingly becoming part of the standard of care in monitoring right heart structure and function. Representative echocardiographic images are shown in **Figure 1**.

Screening for Pulmonary Hypertension

Screening for PH using conventional TTE primarily relies upon assessment of the right ventricular systolic pressure (RVSP), which is measured from the tricuspid regurgitant (TR) jet velocity and size/collapsibility of the inferior vena cava (IVC) to estimate right atrial pressure (RAP) (12). Using the modified Bernoulli equation, $RVSP = 4V^2 + RAP$ with V equaling the maximum TR jet velocity (13). For RVSP measurements > 40 mmHg, a right heart catherization is recommended (14). However, RVSP has been shown in numerous studies across various PH subgroups to poorly correlate with systolic pulmonary artery pressure (sPAP) measured by RHC. These studies have routinely shown that RVSP is ± 10 mmHg different to the true sPAP in approximately 50% of cases (15–18). Additionally, the ability to capture and quantify the TR jet velocity can be technically challenging and is estimated to be feasible in only 75% of cases (19). RVSP can be combined with other non-invasive measures to evaluate the need for a RHC in suspected PH (20). Additional RV hemodynamics can also be obtained including PA end-diastolic pressure using end-diastolic pulmonic regurgitation peak velocity, mean PA pressure, and pulmonary vascular resistance. Lastly, early closure of the pulmonic valve due to rapid pressure equilibration of the RV and PA in midsystole can be detected using both M-mode or pulse waved Doppler signal, known as the "flying W" sign (21).

Assessment of the Right Heart

The American Society of Echocardiography has standardized measurements of right-sided cardiac structure and function (13). Measurements include the right atrial and ventricular area, fractional area change (FAC) as a surrogate of right ventricular ejection fraction (RVEF), tricuspid annular plane systolic excursion (TAPSE), RVSP, and the presence of a pericardial effusion. A right atrial area measured at the end of systole >18 cm^2 has been independently associated with elevated right ventricular (RV) end-diastolic pressure (RVEDP) and mean RAP with a sensitivity of 89% and specificity of 82% (13, 22). The RV diameter at the base is considered enlarged when it is >42 mm. However, this measure only weakly correlates with the gold standard RV volume assessment *via* CMR (23, 24). Measurements based off estimations of the 2D RV area or volume, such as FAC or RVEF, are similarly flawed when compared to CMR techniques (25, 26) due to the complex shape of the right ventricle (27). Eccentricity index, or interventricular septal morphology, is a useful echocardiographic tool and assesses the interventricular dependency of the RV:LV from the parasternal short-axis view and is an important component of the

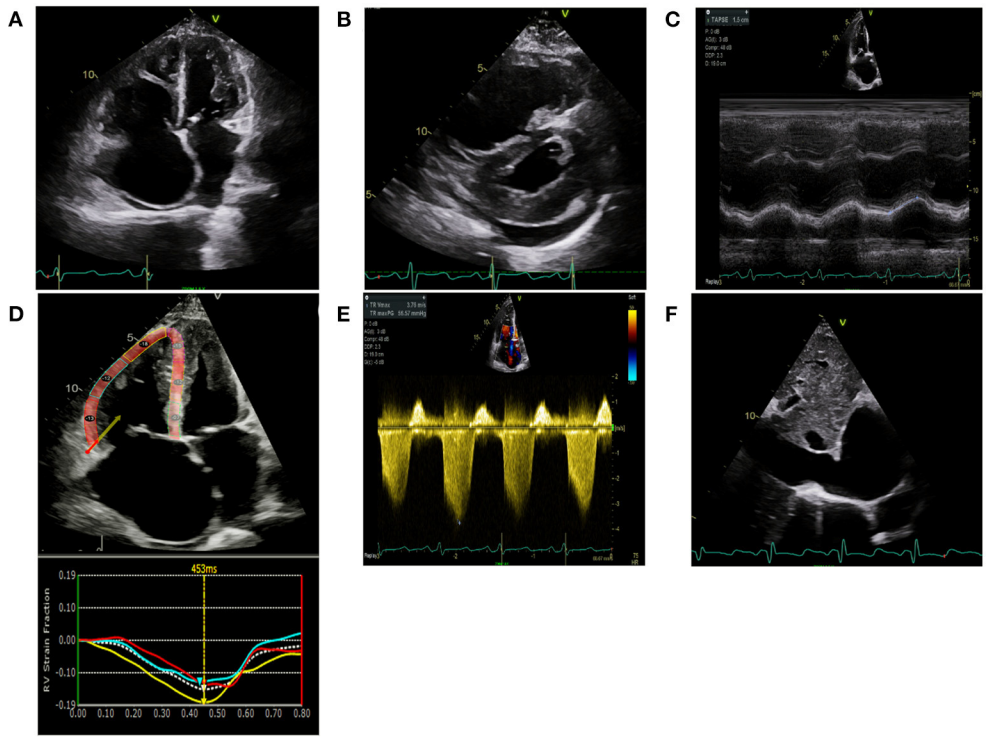

FIGURE 1 | Echocardiographic images are shown in a scleroderma patient with severe pulmonary hypertension on stable therapies. **(A)** Apical 4 chamber view demonstrates severe right atrial enlargement with bowing of the interatrial septum from right to left suggestive of elevated right atrial pressures. The right ventricle is severely dilated and hypertrophied with a prominent moderator band. The left ventricle is hypertrophied and small. **(B)** Parasternal short-axis is shown in the same patient with marked RV enlargement and evidence of RV pressure overload distorting the normal circular short-axis geometry of the LV. There is a small posterior pericardial effusion present. **(C)** Tricuspid annular plane systolic excursion (TAPSE) utilizes M-mode techniques to measure the longitudinal motion of the basal right ventricular wall segment during systole as an estimate of right ventricular systolic function. TAPSE is mildly reduced at 1.5 cm (normal >1.6 cm) however fractional area change was 24% (moderate-severely reduced). **(D)** Right Ventricular Longitudinal Systolic Strain (RVLSS) is a recent echocardiographic advancement based on ultrasound-myocardial tissue interactions. Each segment of the RV in this example corresponds with a strain curve with the white dotted line representing an average of the segmental strain for the regional curves in this view. Regional RV free wall strain is reduced in the basal and midventricular wall segments with less reduction in the apical segment. Global strain is an average of the three RV free wall segments and is −14.3%. **(E)** Right Ventricular Systolic Pressure utilizes the peak tricuspid velocity to calculate the peak right ventricular systolic pressure using the modified Bernoulli equation. RVSP= [peak gradient (mmHg) = right atrial pressure + (4 × Peak velocity 2)]. In this example, RVSP = 57 mmHg + 15 mmHg = 72 mmHg. **(F)** Right atrial pressures are estimated from the IVC diameter made in subcostal view at end-expiration. In this example, the IVC is severely dilated at 3.2 cm with minimal respiratory variation suggestive of markedly elevated right atrial pressure of 15 mmHg.

ESC/ERS recommendations for PH screening (11). The presence of RV hypertrophy may also be seen in chronic pressure/volume overload states.

Due to the inaccuracy of RV area and volume assessments using 2D echocardiographic techniques, other measurements are used to estimate RV function. Tricuspid annular plane systolic excursion (TAPSE) measures the movement of the tricuspid annulus toward the apex between diastole and systole in M-mode. A measurement ≤1.7 cm is considered abnormal (28). TAPSE has been shown to closely correlate with RVEF on CMR and RHC (29). However, TAPSE measurements should be interpreted with caution in patients with severe TR as they have been shown to be less accurate in that setting (30). The Tei index, or myocardial performance index (MPI) of the RV, is measured using either color or tissue Doppler imaging and is a ratio of isovolumic time, both in contraction and relaxation, to ejection time (31, 32). Systolic wave velocity (S′) is another measure of myocardial contraction measured from tissue Doppler imaging and has been validated in an epidemiologic study of healthy individuals to define normal values (33). Abnormal tissue Doppler S′ velocity is defined as <9.5 cm/s.

Prognostication

As right heart failure is the primary cause of death among individuals with PH, assessment of abnormalities in the right ventricle by echocardiogram offers significant prognostic information. RA area and estimation of right atrial pressure have been demonstrated to be associated with mortality secondary to right heart failure (34). RVSP has been found to be an independent predictor of mortality in PH (35, 36) and while neither sensitive nor specific, the presence of a pericardial effusion has been shown to predict mortality in PH patients (34, 37, 38).

Recently, the REVEAL registry has included echocardiographic assessment of pericardial effusion in prognostic risk assessment of PAH (REVEAL risk score). Regarding RV functional assessments in individuals with known PH, reduced TAPSE has been shown to have a nearly four-fold increased risk of death (39) with every 1 mm decrease in TAPSE increasing the unadjusted risk of death by 17% (40). Myocardial performance index is associated with clinical status and mortality, as well as change in clinical status over time in response to therapy (31, 41).

Speckle-Tracking Echocardiography (Echo Strain Imaging)

Strain imaging is being increasingly incorporated into clinical practice as a measurement of RV systolic function (42). Strain (ε) is the deformation of cardiac tissue from an applied force with $\varepsilon = (L_{systole}\text{-}L_{diastole})/L_{diastole}$ with L being length (42) and multiplied by 100 resulting in a percentage of myocardial deformation across the cardiac cycle. A positive number indicates lengthening, and a negative number indicates shortening. Strain imaging provides a feasible non-invasive technique to assess cardiac mechanics for the detection of subclinical ventricular dysfunction.

Using 2D echocardiographic techniques, there are two methods by which strain can be calculated: tissue Doppler imaging (TDI) and speckle tracking echocardiography (STE). TDI-derived strain calculates the rate at which a particular segment of the myocardium moves toward or away from the transducer (43). TDI is less commonly used since it is highly angle dependent and requires high frame rates. In contrast, STE is angle-independent and performed by measuring the movement, or deformation, of ultrasound pixels over the cardiac cycle. It is particularly helpful in the right heart as it tends to preferentially measure speckles at the endocardial border whose longitudinal fibers account for 80% of RV contraction. STE-derived strain can be reported across the RV free wall regions or as an average of visualized segments known as global longitudinal strain (GLS) and is expressed as a percentage and a more negative number signifies a more shortening of the myocardial segment during systole. Worsening strain refers to a less negative number (a lower absolute value) than expected or diminished deformation along the longitudinal axis. GLS typically represents the basal, midventricular, and apical RV free segments however it may also include the basal, midventricular, and apical segments of the interventricular septum. The latter approach, however, is less favored due to inability to isolate RV and LV contributions (42). The most common measurement of strain in the RV is GLS, however individual longitudinal segmental strain is also being investigated in PH (44).

Reduced RV function using STE GLS imaging predicts worse clinical outcomes such as right heart failure and death in PH across various subgroups (45–47). Additionally, a reduction in RV free wall strain has also been shown to predict worse outcomes in PH (48). Reduced strain is one of the earliest signs of RV dysfunction as patients with less longitudinal deformation had worse outcomes than matched controls with equivalent right heart dimensions and TAPSE (49, 50).

For a strain analysis to be done, 2D echo image quality must also be adequate at a frame rate of at least 70–90 frames per second. Strain imaging requires post processing using dedicated software and can be performed utilizing CMR-based techniques as well. Echo-derived strain requires specialized software and ultrasound machines, which may result in increased cost, however can typically be performed during real-time image acquisition with minimal increase in patient exam time or retrospectively on previously acquired images. There is also a significant learning curve in strain analysis as automated endocardial border definition must be verified manually by experienced operators (51). Additionally, there is well-described vendor-specific variability in strain measures (52) and the cutoff values for normal and abnormal strain also depend on the analytic software and modality, i.e., CMR vs. echo-derived strain, being used. Longitudinal strain monitoring must therefore ensure that patients' images are analyzed using the same software across time and should be performed by experienced operators.

Three-Dimensional Echocardiography

3D echocardiography is a state-of-the-art imaging strategy increasingly being used in clinical practice (53). Estimations of the RVEF have been found to be more closely correlated to those measured by CMR (54–57). However, 3D echo tends to underestimate the true RVEF (58). Despite this, the accessibility of 3D echo is greater than CMR which makes this an attractive alternative. In addition, strain imaging has been combined with 3D echo to accurately predict RVEF (59). 3D imaging can be performed during both 2D and transesophageal echocardiography and is recommended in the assessment of severe TR (60) for grading and determining suitability for intervention.

Chest Computed Tomography Imaging

Acquiring a non-contrast chest CT scan is part of the standard workup for the diagnosis of PH (10). The presence of lung disease on a chest CT along with abnormalities on pulmonary function tests can indicate PH secondary to lung disease (Group 3 PH). Along with its evaluation of the pulmonary parenchyma, there are several findings that can screen for PH on CT. These include the absolute size of the main pulmonary artery and its relative size compared to the aorta. Chest CT with contrast is also essential if acute pulmonary embolism is suspected as an etiology of PH. New CT techniques such as dual energy CT are also being investigated to measure lung perfusion qualitatively and quantitatively. A representative image from a patient with connective tissue disease- associated interstitial lung disease and mixed PH is shown in **Figure 2**.

Pulmonary Artery Size

The diameter of the main pulmonary artery (mPA) and its size in comparison to the ascending aorta correlate to mPAP on RHC. In the Framingham Heart Study, the 90th percentile for mPA diameter measured by CT was >29 mm in men and >27 mm in women (61). Subsequent work has shown that a mPA > 29 mm is correlated with elevated mPAP with a sensitivity and a specificity of ∼80% and an r of 0.6 (62–66). A ratio of the

mPA/ascending aorta >1 also correlated with elevated mPAP with ∼70% specificity and sensitivity. The mPA size can be enlarged in fibrotic lung disease which can confound its use as a screen for PH in patients with these disorders. CT has not been shown to predict PH as accurately as echo or CMR (67, 68) but its sensitivity and specificity increase when it is combined with these modalities for screening (69).

Dual Energy CT

Dual energy CT (DECT) is a technique that acquires CT angiographic (CTA) images of the pulmonary vasculature at two different energy levels after the administration of intravenous iodine-based contrast. Due to the different attenuation properties of iodine contrast at these two different energy levels, the quantity of iodine inside the pulmonary vasculature, which can serve as a surrogate for pulmonary perfusion, can be isolated and measured. As CT scans are commonly used in the work up of PH, DECT has the capability to be built into the screening chest CT without extra radiation (70). DECT is primarily used as a replacement for the V/Q scan in diagnosis of CTEPH, but has also been investigated as a screening tool for PH and a tool to assess the degree of PH. DECT has been shown to have an 80% sensitivity in the diagnosis of CTEPH compared to VQ scintigraphy (71–74) which is much improved compared to standard CTAs (75). While this is the most useful and well-understood utility of DECT, additional assessment of pulmonary perfused blood volumes (PBV), representing the total amount of iodine inside the pulmonary vasculature at a certain timepoint, can be qualitatively and quantitatively used to screen for PH. Patients with PH have a mosaic attenuation pattern on DECT given the dysregulation of the pulmonary vasculature inherent to the disease (76). Additionally, the total degree of PBV has been shown to correlate with mPAP (77) along with the ratio of PBV to the attenuation of the pulmonary artery (78, 79). However, many of these findings are non-specific.

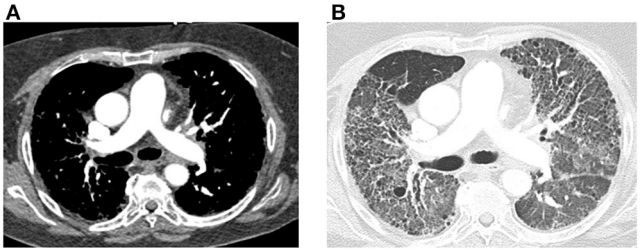

FIGURE 2 | Computed tomography (CT) images of the chest with and without contrast are shown from a 64-year-old female with connective tissue disease, severe interstitial lung disease, and mixed severe pulmonary hypertension are shown. **(A)** Transaxial images are shown demonstrating an enlarged main pulmonary arterial size at 3.2 cm when compared to ascending aorta size of 2.9 cm at the same level suggestive of pulmonary hypertension. There is no evidence of pulmonary embolism with optimal contrast opacification. **(B)** Transaxial images in the lung window demonstrate extensive bilateral diffuse groundglass opacities and honeycombing. There is associated intralobular and interstitial thickening and bronchiectasis consistent with patient's known history of connective tissue disease associated non-specific interstitial pneumonitis.

Scintigraphy and Nuclear Imaging

Ventilation-Perfusion (V/Q) Scans

V/Q Scintigraphy is part of the standardized diagnostic workup of PH, specifically for diagnosis of WHO Group 4 chronic thromboembolic pulmonary hypertension (CTEPH) (10). CTEPH is defined as PH in the presence of mismatched perfusion defects by V/Q scan as well as signs of thromboembolism on CT and/or pulmonary angiography following 3 months of therapeutic anticoagulation (10). This modality is considered to be the standard of care in the initial evaluation for PH etiologies due to high sensitivity and specificity in the diagnosis of CTEPH, outperforming CTA alone (80–82).

Nuclear Medicine Techniques

Increased stress on the right heart in PH results in an increase in myocyte glycolysis and can be measured with a radioactively tagged glucose analog and measured by PET. Increased 2-deoxy-2-[18F]fluoro-D-glucose (FDG) uptake in the RV is observed in patients with PH and correlated with mPAP (83–85). Increased FDG uptake has been found to be associated with clinical worsening and death, and patients who respond to therapy show decreased FDG uptake over time (86, 87). In addition, alternatives to FDG, such as a radiotracer targeting mannose receptors on macrophages, have been similarly observed to detect PAH and respond to pulmonary vasodilator therapy (88). Further, hybrid PET/MRI imaging has demonstrated that a combination of RV ejection fraction and tracer uptake was associated with clinical deterioration or death in PAH patients

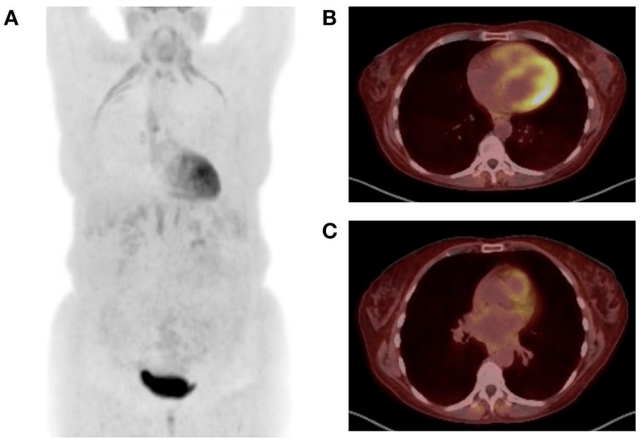

FIGURE 3 | Positron emission tomography (PET) images are shown from a 52-year-old woman with emphysema and associated Group 3 pulmonary hypertension presenting with acute exacerbation. 9.78 mCi ^{18}F-FDG injected at 119 mg/dl blood glucose level. Image acquisition 57 mins post injection. **(A)** Maximum intensity projection image demonstrates FDG uptake in the diaphragm, infrahyoid muscles, and intercostal muscles consistent with increased work of breathing noted during examination. There is also diffuse subcutaneous uptake, reflecting treatment with corticosteroids during the exacerbation. **(B)** Transaxial images at the midventricular level demonstrate abnormal uptake in the right ventricle. **(C)** Transaxial images at the level of the main pulmonary artery (mPA) demonstrate enlarged mPA and abnormal FDG uptake in the right ventricular outflow track.

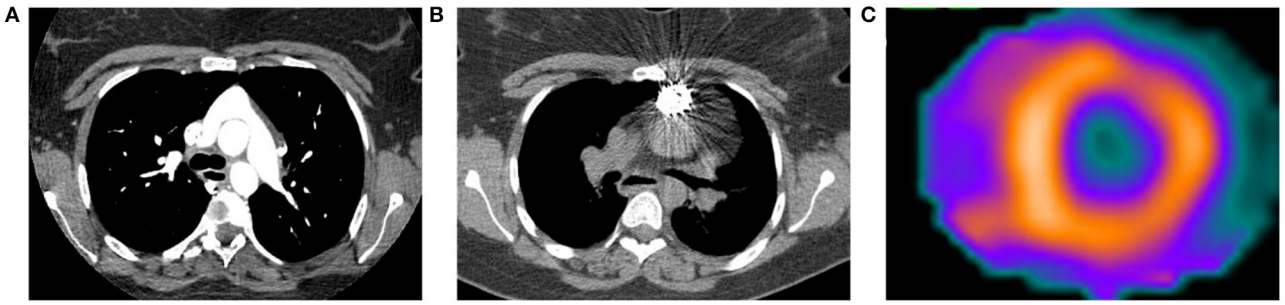

FIGURE 4 | Computed tomography (CT) and ^{99m}Tc-sestamibi single-photon emission computed tomography (SPECT) images from a 23-year-old woman with history of D-transposition of the great arteries (D-TGA) status-post repair. **(A)** Transaxial CT angiogram image demonstrating the characteristic appearance of the pulmonary artery and aorta after repair of D-TGA. **(B)** Non-contrast CT acquired at time of SPECT shows a stent in the pulmonary artery that was placed after the patient developed severe pulmonary artery stenosis. **(C)** Short axis SPECT image shows normal radiotracer distribution in the left ventricle with extension of uptake into the visualized portion of the right ventricle, consistent with pulmonary hypertension.

(89). **Figure 3** demonstrates representative FDG-PET imaging from a PH patient with emphysema.

Single-photon emission computed tomography (SPECT) utilizes multiple different radiotracers to evaluate cardiac perfusion and function. Analogous to PET, patients with PH will have evidence of thickening, enlargement, and metabolic derangement in the RV. The most commonly used radiotracers in modern cardiac SPECT are mitochondrial imaging agents (e.g., ^{99m}Tc-sestamibi), and their increased uptake in the RV is reflective of both increased RV mass and increased energy production and use (90). **Figure 4** is from a patient with a pulmonary artery stenosis and increased ^{99m}Tc-sestamibi uptake in the RV.

Cardiac Magnetic Resonance Imaging

CMR Quantitative Assessment of Structure and Function

CMR is a non-invasive, non-radiating imaging technique that allows for highly reproducible tissue characterization (90), permits assessment of radial and circumferential RV strain, and can distinguish ischemic-perfusion vs. fibrotic processes. CMR provides the best three-dimensional characterization of the RV and its dynamic relationship with the LV with high interstudy reproducibility (91). CMR also generates accurate 3D measurements of the RV throughout the cardiac cycle (92). Right ventricular mass, volume, and function can be accurately assessed and quantified on CMR. Additionally, evaluation of infiltrative disease processes relevant to development of cardiomyopathy is possible. Reduced RV ejection fraction, and RV end-systolic volume have been shown to be independent predictors of mortality (93–95). Reduced stroke volume has also been correlated with mortality (96), and improvements in stroke volume are seen in response to therapy (97, 98). Representative CMR images are demonstrated in **Figure 5**.

CMR Tissue Characterization and Perfusion Imaging

In the assessment of PH, CMR can be of particular value in patients with rheumatologic etiologies allowing for identification of occult lesions such as myocarditis, interstitial edema, myocardial infarction, and diffuse endocardial fibrosis (99). Assessment of native T1 and post-contrast T1 mapping allows for the accurate differentiation between the acute and chronic phases in many rheumatologic disorders. Understanding to what extent either ischemic injury or inflammation contributes to myocardial damage and fibrosis is also important in therapeutic interventions (100).

Late gadolinium enhancement (LGE) is a well validated approach for the evaluation of focal myocardial scarring and is the gold standard for *in vivo* assessment of replacement

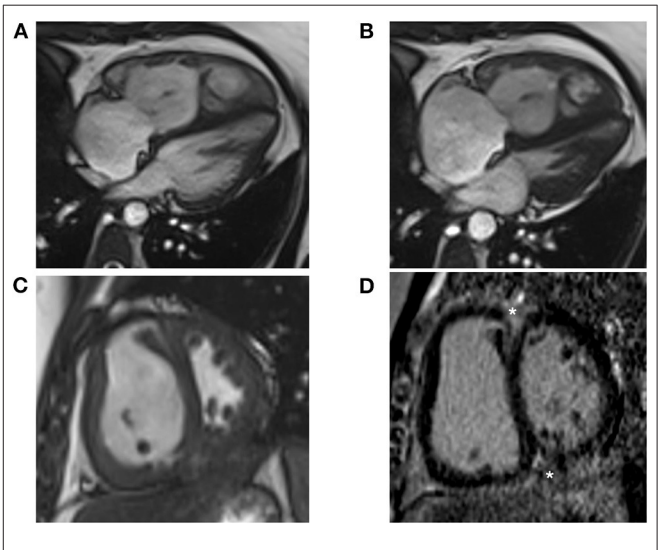

FIGURE 5 | Cardiac Magnetic Resonance (CMR) images are shown from a 38-year-old female with idiopathic pulmonary arterial hypertension. **(A)** Four-chamber bright blood CMR image from end diastole shows a dilated and hypertrophied right ventricle at a mean pulmonary pressure of 47 mmHg. End systolic images show leftward bowing of the interventricular septum from elevated right ventricular pressure. **(B)** Late systolic images show leftward bowing of the interventricular septum from elevated RV pressure. **(C)** Short axis CMR image shows marked hypertrophy of the right ventricular free wall and septal bowing. **(D)** Short axis LGE image shows prominent enhancement at the anterior and inferior RV insertion points (asterisks).

macroscopic fibrosis (99). CMR techniques can detect fibrosis in as little as 1 cm^3 of tissue with excellent agreement with histologic studies (99, 101). Native T1 mapping and extracellular volume (ECV) quantification may be more sensitive than LGE techniques at detecting low-grade inflammation and diffuse myocardial fibrosis (102). In fact, in a recent study, rheumatologic patients were found to have higher T1 and T2 values, as well as expanded ECV compared with control subjects, with the most significant differences between native T1 and T2, independent of the presence of LGE (103). The extent and location of LGE in the RV can also indicate presence of RV stress. Delayed enhancement from gadolinium (10–20 mins after injection) is associated with cardiac fibrosis (104). Delayed enhancement mass at the insertion points of the RV is a sensitive and specific marker for PH (105–108). The extent of delayed enhancement mass into the interventricular septum is associated with worse RV function and clinical outcomes (109–111).

Quantification of myocardial perfusion utilizing CMR is observer-independent and highly reproducible (112). CMR perfusion imaging may allow for the investigation of characteristic disease-specific findings beyond the hemodynamic derangements in loading conditions in PH. In a study of CMR perfusion imaging in PAH patients associated with the autoimmune disorder systemic sclerosis (SSc-PAH) vs. those with idiopathic PAH (IPAH), RV and LV perfusion was significantly reduced and inversely correlated with RV workload and ejection fraction (113). Reduction in RV myocardial perfusion reserve was significantly correlated with worse hemodynamic profile and decreased RV function suggesting that reduced myocardial perfusion reserve may contribute to RV dysfunction in patients with PAH (113). CMR markers of RV remodeling and fibrosis, including RV and LV ventricular mass index, LGE and RV myocardial perfusion index, were also predictive of survival and improved with PAH-specific therapies.

CMR Strain Imaging

With high spatial and temporal resolution, CMR allows for quantification of global RV function across three coordinate directions (circumferential, radial, and longitudinal), as well as precise analysis of RV regional myocardial function. A variety of approaches to strain imaging with CMR are clinically available, including use of line tags and spatial modulation of magnetization (SPAMM), use of radiofrequency pulses to conduct displacement encoding with stimulated echoes (DENSE), and use of through-plane tags by strain-encoding (SENC), to name a few (114–116), although only a subset have been reliably applied to a PH population. SENC is technique with low intra- and inter-observer variabilities (117), and is based on the acquisition of two images with different frequency modulation, or low-tuning (LT) and high-tuning (HT) images in the slice-selection direction representing static and contracting tissues, respectively. Fast-SENC RV longitudinal and circumferential strain has been utilized in PH patients allowing for characterization of RV regional function with a unique pattern of reduction in RV circumferential shortening (118). Reductions in longitudinal strain correlate with RVEF and NT-proBNP in PH (119) and have a higher sensitivity and specificity to detect low RVEF when compared to circumferential strain.

Similar to STE-derived strain, CMR strain can be measured using dedicated sequences such as SENC or post-processing of cine images using feature-tracking. While CMR-derived myocardial tissue tagging and SENC have quantitative value, these modalities have not gained widespread clinical use due to expertise needed in specific sequences, additional scanning time, and the required time and cost for complex post-processing analysis (120). Ohyama et al. recently employed an alternative method of CMR strain known as multimodality tissue tracking (MTT), which similar to STE, utilizes tissue patterns obtained from cine CMR images and automatically tracks them frame to frame using an automated matching software algorithm. Findings from 30 PH patients demonstrated close correlation between MTT and SENC with high reproducibility suggesting that quantification of regional cardiac deformation using CMR cine images is feasible without the additional limitations of other CMR strain techniques. CMR and STE-basesd longitudinal strain have good inter-modality agreement while both SENC- and FT-derived circumferential strain, especially in the presence of LGE, is better detected using CMR techniques (121).

CMR Flow and PA Vasoreactivity

2D and 4D flow characterization through the RV is a novel technique to investigate the hemodynamics of the RV and pulmonary artery. CINE phase-contrast MRI can be used to quantify blood's velocity. When velocity in one direction is measured through a 2D plane it is called 2D flow MRI. However, it can underestimate the peak velocity if it is not orthogonal to the flow of interest and it cannot measure complex flow patterns with direction change. 4D flow MRI (3D CINE phase-contrast MRI) can analyze this through *post-hoc* 3D flow analysis (122). Flow through the pulmonary artery has been found to be qualitatively and quantitatively different in PH. Patients with PH have been found to have a reduced velocity of blood flow through the pulmonary artery correlating with higher pulmonary vascular resistance (123–126). The pulmonary artery is also noted to be less distensible in patients with PH, which may predict mortality (127–129). There is a greater retrograde blood flow through the PA in patients with PH (130) thought to be secondary to a turbulent vortex. The length of time of which the vortex is present during the cardiac cycle correlates with mPAP (131–133).

Endothelial dysfunction of the pulmonary vasculature is thought to be the central underlying pathophysiologic mechanism of PH and results in decreased relaxation of the PA (134). PA endothelial function is typically measured by invasive assessment of changes in PA in cross-sectional area and flow in response to an endothelial-dependent stress (135, 136). Previous work from our group utilizing the novel combination of 3T MRI methods with isometric handgrip exercise (IHE), a well-established endothelial-dependent stressor, demonstrated a non-invasive method of measuring coronary endothelial dysfunction with high reproducibility (137, 138). In recent work from our group, we demonstrated the feasibility of the

TABLE 1 | Characteristic imaging findings are summarized across imaging modalities.

Imaging modality	Characteristic findings in pulmonary hypertension
Echocardiography	**Abnormal hemodynamics**
	Right ventricular systolic pressure > 40 mmHg and/or mean pulmonary arterial pressure > 20 mmHg
	Abnormal pulmonary vascular resistance > 2 Wood Units
	Dilated inferior vena cava with or without respirophasic variation: IVC diameter ≤ 2.1 cm that collapses >50% suggests normal RAP of 3 mmHg; IVC diameter >2.1 cm that collapses <50% equivalent to RAP of 15 mmHg. In indeterminant cases, an intermediate value of 8 mmHg may be used
	Systolic flow reversal in hepatic veins suggestive of elevated right ventricular end-diastolic pressure
	Abnormal right heart chamber size and function
	Distortion of interventricular septal morphology suggestive of pressure volume overload
	Enlargement of the right atrium in chronically elevated right ventricular filling pressures
	Abnormal TAPSE ≤ 1.7 cm, tissue Doppler S' < 9.5 cm/s, fractional area change <35%
	Presence of right ventricular hypertrophy
	Globally reduced right ventricular longitudinal strain with or without regional abnormalities
	Abnormal regurgitant lesions
	Presence of pulmonary and/or tricuspid regurgitation
Chest Computed Tomography Imaging	Enlargement of main pulmonary artery in comparison to ascending aorta at same level > 1
	Evaluation of lung parenchyma which may be abnormal in Group 3 pulmonary hypertension
	Assessment for acute pulmonary embolism using contrast imaging
	Assessment of chronic thromboembolic pulmonary hypertension in Group 4 disease
Scintigraphy and Nuclear Imaging	**Abnormal Ventilation-Perfusion (VQ) Scan**
	Presence of mismatched perfusion defects by VQ scan as well as signs of thromboembolism on CT and/or pulmonary angiography following three months of therapeutic anticoagulation
	Abnormal FDG-18 uptake
	Increased FDG-18 uptake in the right ventricle and pulmonary artery
Cardiac Magnetic Resonance Imaging	**Abnormal right heart chamber size and function**
	Increased right atrial and ventricular volumes
	Abnormal interventricular septal morphology suggestive of pressure/volume overload
	Presence of right ventricular hypertrophy
	Reflux of contrast into the hepatic veins
	Decreased right ventricular function
	Abnormal CMR-derived strain along both longitudinal and circumferential axis
	Abnormal tissue characterization
	Abnormal native T1 mapping and expanded extracellular volume suggestive of tissue inflammation seen in acute phase
	Presence of late Gadolinium enhancement which can be seen at insertion points of the right ventricle and within the right and left ventricles
	Suggestive of fibrosis and tissue remodeling
	Abnormal perfusion
	Reduced right and left ventricular perfusion is inversely correlated with pulmonary pressures, and right ventricular workload and ejection fraction
	Abnormal flow and pulmonary arterial vasoreactivity
	Reduced pulmonary arterial blood flow velocity correlates with increased pulmonary vascular resistance
	Decreased pulmonary arterial distensibility
	Abnormal pulmonary artery vasoreactivity suggestive of endothelial dysfunction

non-invasive measurement of PA vasoreactivity in HIV patients with pulmonary vascular disease (139, 140).

CONCLUSION

Echocardiography, CT, nuclear imaging, and CMR are useful for non-invasively screening, classifying, prognosticating, and monitoring effectiveness of therapy in PH. Characteristic findings for each modality are further summarized in **Table 1**. The standardized algorithm using echocardiogram, CT scan, and VQ scan in the initial diagnosis and classification in PH can also be supplemented by CMR methods. While multiple modalities exist and can complement each other in the investigation of PH, a well-designed clinical approach should

account for expertise and availability of necessary imaging equipment and analytic software in a value-based framework focused on patient-specific clinical needs and prioritizing the minimization of imaging redundancy. Novel imaging techniques such as strain imaging, 3D echo, DECT, FDG-PET, and 4D flow MRI can evaluate for the severity of PH and can be used in conjunction with standard imaging modalities to monitor for disease progression and response to therapy. While RHC is the gold standard in the diagnosis and monitoring of PH, it can be supplemented by these non-invasive imaging modalities to ensure that it is selectively and appropriately used. Earlier detection of PA and RV dysfunction using these common imaging modalities can lead to earlier diagnosis and treatment of PH which has been shown to improve clinical outcomes.

AUTHOR CONTRIBUTIONS

MM was the principal investigator, had access to all the data in the study, and takes full responsibility for the integrity and accuracy of the manuscript. All authors contributed equally to the design, drafting, and final approval of this manuscript.

FUNDING

Funding for this work was supported by the American Lung Association (AB), NIH/NHLBI R01HL147660-03 (AH), NIH/NHLBI R01-HL114910 (PH), NIH/NHLBI K23-HL146889 (SH), Jerome Green Foundation (SH), Scleroderma Foundation (MM and SM), Department of Defense W81XWH2010768 (SM), and Johns Hopkins Clinician Scientist Award (MM).

REFERENCES

1. Hoeper MM, Humbert M, Souza R, Idrees M, Kawut SM, Sliwa-Hahnle K, et al. A global view of pulmonary hypertension. *Lancet Respir Med.* (2016) 4:306–22. doi: 10.1016/S2213-2600(15)00543-3
2. Wijeratne DT, Lajkosz K, Brogly SB, Lougheed MD, Jiang L, Housin A, et al. Increasing incidence and prevalence of World Health Organization Groups 1 to 4 pulmonary hypertension: a population-based cohort study in Ontario, Canada. *Circ Cardiovasc Qual Outcomes.* (2018) 11:e003973. doi: 10.1161/CIRCOUTCOMES.117.003973
3. Gall H, Felix JF, Schneck FK, Milger K, Sommer N, Voswinckel R, et al. The Giessen Pulmonary Hypertension Registry: survival in pulmonary hypertension subgroups. *J Heart Lung Transplant.* (2017) 36:957–67. doi: 10.1016/j.healun.2017.02.016
4. Humbert M, Yaici A, de Groote P, Montani D, Sitbon O, Launay D, et al. Screening for pulmonary arterial hypertension in patients with systemic sclerosis: clinical characteristics at diagnosis and long-term survival. *Arthritis Rheum.* (2011) 63:3522–30. doi: 10.1002/art.30541
5. Deaño RC, Glassner-Kolmin C, Rubenfire M, Frost A, Visovatti S, McLaughlin VV, et al. Referral of patients with pulmonary hypertension diagnoses to tertiary pulmonary hypertension centers: the multicenter RePHerral study. *JAMA Intern Med.* (2013) 173:887–93. doi: 10.1001/jamainternmed.2013.319
6. Brown LM, Chen H, Halpern S, Taichman D, McGoon MD, Farber HW, et al. Delay in recognition of pulmonary arterial hypertension: factors identified from the REVEAL Registry. *Chest.* (2011) 140:19–26. doi: 10.1378/chest.10-1166
7. Simonneau G, Montani D, Celermajer DS, Denton CP, Gatzoulis MA, Krowka M, et al. Haemodynamic definitions and updated clinical classification of pulmonary hypertension. *Eur Respir J.* (2019) 53:1801913. doi: 10.1183/13993003.01913-2018
8. Simonneau G, Hoeper MM. The revised definition of pulmonary hypertension: exploring the impact on patient management. *Eur Heart J Suppl.* (2019) 21(Suppl K):K4–8. doi: 10.1093/eurheartj/suz211
9. Hoeper MM, Lee SH, Voswinckel R, Palazzini M, Jais X, Marinelli A, et al. Complications of right heart catheterization procedures in patients with pulmonary hypertension in experienced centers. *J Am Coll Cardiol.* (2006) 48:2546–52. doi: 10.1016/j.jacc.2006.07.061
10. Galiè N, Humbert M, Vachiery J-L, Gibbs S, Lang I, Torbicki A, et al. 2015 ESC/ERS Guidelines for the diagnosis and treatment of pulmonary hypertension: The Joint Task Force for the Diagnosis and Treatment of Pulmonary Hypertension of the European Society of Cardiology (ESC) and the European Respiratory Society (ERS): Endorsed by: Association for European Paediatric and Congenital Cardiology (AEPC), International Society for Heart and Lung Transplantation (ISHLT). *Eur Respir J.* (2015) 46:903–75. doi: 10.1183/13993003.01032-2015
11. Pearlman AS, Ryan T, Picard MH, Douglas PS. Evolving trends in the use of echocardiography: a study of Medicare beneficiaries. *J Am Coll Cardiol.* (2007) 49:2283–91. doi: 10.1016/j.jacc.2007.02.048
12. Berger M, Haimowitz A, Van Tosh A, Berdoff RL, Goldberg E. Quantitative assessment of pulmonary hypertension in patients with tricuspid regurgitation using continuous wave Doppler ultrasound. *J Am Coll Cardiol.* (1985) 6:359–65. doi: 10.1016/S0735-1097(85)80172-8
13. Rudski LG, Lai WW, Afilalo J, Hua L, Handschumacher MD, Chandrasekaran K, et al. Guidelines for the echocardiographic assessment of the right heart in adults: a report from the American Society of Echocardiography. *Journal of the American Society of Echocardiography.* (2010) 23:685–713. doi: 10.1016/j.echo.2010.05.010
14. Strange G, Playford D, Stewart S, Deague JA, Nelson H, Kent A, et al. Pulmonary hypertension: prevalence and mortality in the Armadale echocardiography cohort. *Heart.* (2012) 98:1805–11. doi: 10.1136/heartjnl-2012-301992
15. Fisher MR, Forfia PR, Chamera E, Housten-Harris T, Champion HC, Girgis RE, et al. Accuracy of Doppler echocardiography in the hemodynamic assessment of pulmonary hypertension. *Am J Respir Crit Care Med.* (2009) 179:615–21. doi: 10.1164/rccm.200811-1691OC
16. Yin D, Wang Y, Zheng M, Wei H, Li M, Lv T, et al. Comparison of pulmonary artery pressure measurement with Doppler echocardiography or with right heart catheterization in patients with congenital heart disease. *Front Pediatr.* (2019) 7:421. doi: 10.3389/fped.2019.00421
17. Nathan SD, Shlobin OA, Barnett SD, Saggar R, Belperio JA, Ross DJ, et al. Right ventricular systolic pressure by echocardiography as a predictor of pulmonary hypertension in idiopathic pulmonary fibrosis. *Respir Med.* (2008) 102:1305–10. doi: 10.1016/j.rmed.2008.03.022
18. Fisher MR, Criner GJ, Fishman AP, Hassoun PM, Minai OA, Scharf SM, et al. Estimating pulmonary artery pressures by echocardiography in patients with emphysema. *Eur Respir J.* (2007) 30:914–21. doi: 10.1183/09031936.00033007
19. Borgeson DD, Seward JB, Miller FA, Oh JK, Tajik AJ. Frequency of Doppler measurable pulmonary artery pressures. *J Am Soc Echocardiogr.* (1996) 9:832–7. doi: 10.1016/S0894-7317(96)90475-7
20. Coghlan JG, Denton CP, Grünig E, Bonderman D, Distler O, Khanna D, et al. Evidence-based detection of pulmonary arterial hypertension in systemic sclerosis: the DETECT study. *Ann Rheum Dis.* (2014) 73:1340–9. doi: 10.1136/annrheumdis-2013-203301
21. Takahama H, McCully RB, Frantz RP, Kane GC. Unraveling the RV ejection doppler envelope: insight into pulmonary artery hemodynamics and disease severity. *JACC Cardiovasc Imaging.* (2017) 10(10 Pt B):1268–77. doi: 10.1016/j.jcmg.2016.12.021
22. Do DH, Therrien J, Marelli A, Martucci G, Afilalo J, Sebag IA. Right atrial size relates to right ventricular end-diastolic pressure in an adult population with congenital heart disease. *Echocardiography.* (2011) 28:109–16. doi: 10.1111/j.1540-8175.2010.01277.x

23. Lai WW, Gauvreau K, Rivera ES, Saleeb S, Powell AJ, Geva T. Accuracy of guideline recommendations for two-dimensional quantification of the right ventricle by echocardiography. *Int J Cardiovasc Imaging.* (2008) 24:691–8. doi: 10.1007/s10554-008-9314-4
24. Lang RM, Badano LP, Mor-Avi V, Afilalo J, Armstrong A, Ernande L, et al. Recommendations for cardiac chamber quantification by echocardiography in adults: an update from the American Society of Echocardiography and the European Association of Cardiovascular Imaging. *J Am Soc Echocardiogr.* (2015) 28:1–39.e14. doi: 10.1016/j.echo.2014.10.003
25. Kossaify A. Echocardiographic assessment of the right ventricle, from the conventional approach to speckle tracking and three-dimensional imaging, and insights into the "right way" to explore the forgotten chamber. *Clin Med Insights Cardiol.* (2015) 9:65–75. doi: 10.4137/CMC.S27462
26. Li Y, Wang Y, Zhai Z, Guo X, Yang Y, Lu X. Real-time three-dimensional echocardiography to assess right ventricle function in patients with pulmonary hypertension. *PLoS ONE.* (2015) 10:e0129557. doi: 10.1371/journal.pone.0129557
27. Gripari P, Muratori M, Fusini L, Tamborini G, Ali SG, Brusoni D, et al. Right ventricular dimensions and function: why do we need a more accurate and quantitative imaging? *J Cardiovasc Echogr.* (2015) 25:19–25. doi: 10.4103/2211-4122.158420
28. Modin D, Møgelvang R, Andersen DM, Biering-Sørensen T. Right ventricular function evaluated by tricuspid annular plane systolic excursion predicts cardiovascular death in the general population. *J Am Heart Assoc.* (2019) 8:e012197. doi: 10.1161/JAHA.119.012197
29. Sato T, Tsujino I, Ohira H, Oyama-Manabe N, Yamada A, Ito YM, et al. Validation study on the accuracy of echocardiographic measurements of right ventricular systolic function in pulmonary hypertension. *J Am Soc Echocardiogr.* (2012) 25:280–6. doi: 10.1016/j.echo.2011.12.012
30. Hsiao S-H, Lin S-K, Wang W-C, Yang S-H, Gin P-L, Liu C-P. Severe tricuspid regurgitation shows significant impact in the relationship among peak systolic tricuspid annular velocity, tricuspid annular plane systolic excursion, and right ventricular ejection fraction. *J Am Soc Echocardiogr.* (2006) 19:902–10. doi: 10.1016/j.echo.2006.01.014
31. Tei C, Dujardin KS, Hodge DO, Bailey KR, McGoon MD, Tajik AJ, et al. Doppler echocardiographic index for assessment of global right ventricular function. *J Am Soc Echocardiogr.* (1996) 9:838–47. doi: 10.1016/S0894-7317(96)90476-9
32. Tei C, Nishimura RA, Seward JB, Tajik AJ. Noninvasive Doppler-derived myocardial performance index: Correlation with simultaneous measurements of cardiac catheterization measurements. *J Am Soc Echocardiogr.* (1997) 10:169–78. doi: 10.1016/S0894-7317(97)70090-7
33. Lindqvist P, Waldenström A, Henein M, Mörner S, Kazzam E. Regional and global right ventricular function in healthy individuals aged 20-90 years: a pulsed Doppler tissue imaging study: Umeå General Population Heart Study. *Echocardiography.* (2005) 22:305–14. doi: 10.1111/j.1540-8175.2005.04023.x
34. Kylhammar D, Kjellström B, Hjalmarsson C, Jansson K, Nisell M, Söderberg S, et al. A comprehensive risk stratification at early follow-up determines prognosis in pulmonary arterial hypertension. *Eur Heart J.* (2018) 39:4175–81. doi: 10.1093/eurheartj/ehx257
35. Grünig E, Tiede H, Enyimayew EO, Ehlken N, Seyfarth H-J, Bossone E, et al. Assessment and prognostic relevance of right ventricular contractile reserve in patients with severe pulmonary hypertension. *Circulation.* (2013) 128:2005–15. doi: 10.1161/CIRCULATIONAHA.113.001573
36. Kane GC, Maradit-Kremers H, Slusser JP, Scott CG, Frantz RP, McGoon MD. Integration of clinical and hemodynamic parameters in the prediction of long-term survival in patients with pulmonary arterial hypertension. *Chest.* (2011) 139:1285–93. doi: 10.1378/chest.10-1293
37. Benza RL, Gomberg-Maitland M, Elliott CG, Farber HW, Foreman AJ, Frost AE, et al. Predicting survival in patients with pulmonary arterial hypertension: the REVEAL Risk Score Calculator 2.0 and comparison with ESC/ERS-based risk assessment strategies. *Chest.* (2019) 156:323–37. doi: 10.1016/j.chest.2019.02.004
38. Batal O, Dardari Z, Costabile C, Gorcsan J, Arena VC, Mathier MA. Prognostic value of pericardial effusion on serial echocardiograms in pulmonary arterial hypertension. *Echocardiography.* (2015) 32:1471–6. doi: 10.1111/echo.12909
39. Mathai SC, Suber T, Khair RM, Kolb TM, Damico RL, Hassoun PM. Health-related quality of life and survival in pulmonary arterial hypertension. *Ann Am Thorac Soc.* (2016) 13:31–9. doi: 10.1513/AnnalsATS.201412-572OC
40. Forfia PR, Fisher MR, Mathai SC, Housten-Harris T, Hemnes AR, Borlaug BA, et al. Tricuspid annular displacement predicts survival in pulmonary hypertension. *Am J Respir Crit Care Med.* (2006) 174:1034–41. doi: 10.1164/rccm.200604-547OC
41. Sebbag I, Rudski LG, Therrien J, Hirsch A, Langleben D. Effect of chronic infusion of epoprostenol on echocardiographic right ventricular myocardial performance index and its relation to clinical outcome in patients with primary pulmonary hypertension. *Am J Cardiol.* (2001) 88:1060–3. doi: 10.1016/S0002-9149(01)01995-6
42. Lee J-H, Park J-H. Strain analysis of the right ventricle using two-dimensional echocardiography. *J Cardiovasc Imaging.* (2018) 26:111–24. doi: 10.4250/jcvi.2018.26.e11
43. Simon MA, Rajagopalan N, Mathier MA, Shroff SG, Pinsky MR, López-Candales A. Tissue Doppler imaging of right ventricular decompensation in pulmonary hypertension. *Congest Heart Fail.* (2009) 15:271–6. doi: 10.1111/j.1751-7133.2009.00113.x
44. Meris A, Faletra F, Conca C, Klersy C, Regoli F, Klimusina J, et al. Timing and magnitude of regional right ventricular function: a speckle tracking-derived strain study of normal subjects and patients with right ventricular dysfunction. *J Am Soc Echocardiogr.* (2010) 23:823–31. doi: 10.1016/j.echo.2010.05.009
45. Shukla M, Park J-H, Thomas JD, Delgado V, Bax JJ, Kane GC, et al. Prognostic value of right ventricular strain using speckle-tracking echocardiography in pulmonary hypertension: a systematic review and meta-analysis. *Can J Cardiol.* (2018) 34:1069–78. doi: 10.1016/j.cjca.2018.04.016
46. Haeck MLA, Scherptong RWC, Marsan NA, Holman ER, Schalij MJ, Bax JJ, et al. Prognostic value of right ventricular longitudinal peak systolic strain in patients with pulmonary hypertension. *Circ Cardiovasc Imaging.* (2012) 5:628–36. doi: 10.1161/CIRCIMAGING.111.971465
47. Fine NM, Chen L, Bastiansen PM, Frantz RP, Pellikka PA, Oh JK, et al. Outcome prediction by quantitative right ventricular function assessment in 575 subjects evaluated for pulmonary hypertension. *Circ Cardiovasc Imaging.* (2013) 6:711–21. doi: 10.1161/CIRCIMAGING.113.000640
48. Sachdev A, Villarraga HR, Frantz RP, McGoon MD, Hsiao J-F, Maalouf JF, et al. Right ventricular strain for prediction of survival in patients with pulmonary arterial hypertension. *Chest.* (2011) 139:1299–309. doi: 10.1378/chest.10-2015
49. Mukherjee M, Mercurio V, Tedford RJ, Shah AA, Hsu S, Mullin CJ, et al. Right ventricular longitudinal strain is diminished in systemic sclerosis compared with idiopathic pulmonary arterial hypertension. *Eur Resp J.* (2017) 50:1701436. doi: 10.1183/13993003.01436-2017
50. Mukherjee M, Chung S-E, Ton Von K, Tedford RJ, Hummers LK, Wigley FM, et al. Unique abnormalities in right ventricular longitudinal strain in systemic sclerosis patients. *Circul Cardiovasc Imaging.* (2016) 9:e003792. doi: 10.1161/CIRCIMAGING.115.003792
51. Chan J, Shiino K, Obonyo NG, Hanna J, Chamberlain R, Small A, et al. Left ventricular global strain analysis by two-dimensional speckle-tracking echocardiography: the learning curve. *J Am Soc Echocardiogr.* (2017) 30:1081–90. doi: 10.1016/j.echo.2017.06.010
52. Farsalinos KE, Daraban AM, Ünlü S, Thomas JD, Badano LP, Voigt J-U. Head-to-head comparison of global longitudinal strain measurements among nine different vendors: the EACVI/ASE inter-vendor comparison study. *J Am Soc Echocardiogr.* (2015) 28:1171–81.e2. doi: 10.1016/j.echo.2015.06.011
53. Tamborini G, Brusoni D, Torres Molina JE, Galli CA, Maltagliati A, Muratori M, et al. Feasibility of a new generation three-dimensional echocardiography for right ventricular volumetric and functional measurements. *Am J Cardiol.* (2008) 102:499–505. doi: 10.1016/j.amjcard.2008.03.084
54. Jenkins C, Chan J, Bricknell K, Strudwick M, Marwick TH. Reproducibility of right ventricular volumes and ejection fraction using real-time three-dimensional echocardiography: comparison with cardiac MRI. *Chest.* (2007) 131:1844–51. doi: 10.1378/chest.06-2143
55. Leibundgut G, Rohner A, Grize L, Bernheim A, Kessel-Schaefer A, Bremerich J, et al. Dynamic assessment of right ventricular volumes and function by real-time three-dimensional echocardiography: a comparison study with

magnetic resonance imaging in 100 adult patients. *J Am Soc Echocardiogr.* (2010) 23:116–26. doi: 10.1016/j.echo.2009.11.016
56. Shimada YJ, Shiota M, Siegel RJ, Shiota T. Accuracy of right ventricular volumes and function determined by three-dimensional echocardiography in comparison with magnetic resonance imaging: a meta-analysis study. *J Am Soc Echocardiogr.* (2010) 23:943–53. doi: 10.1016/j.echo.2010.06.029
57. Morikawa T, Murata M, Okuda S, Tsuruta H, Iwanaga S, Murata M, et al. Quantitative analysis of right ventricular function in patients with pulmonary hypertension using three-dimensional echocardiography and a two-dimensional summation method compared to magnetic resonance imaging. *Am J Cardiol.* (2011) 107:484–9. doi: 10.1016/j.amjcard.2010.09.047
58. Khoo NS, Young A, Occleshaw C, Cowan B, Zeng ISL, Gentles TL. Assessments of right ventricular volume and function using three-dimensional echocardiography in older children and adults with congenital heart disease: comparison with cardiac magnetic resonance imaging. *J Am Soc Echocardiogr.* (2009) 22:1279–88. doi: 10.1016/j.echo.2009.08.011
59. Smith BCF, Dobson G, Dawson D, Charalampopoulos A, Grapsa J, Nihoyannopoulos P. Three-dimensional speckle tracking of the right ventricle: toward optimal quantification of right ventricular dysfunction in pulmonary hypertension. *J Am Coll Cardiol.* (2014) 64:41–51. doi: 10.1016/j.jacc.2014.01.084
60. Otto CM, Nishimura RA, Bonow RO, Carabello BA, Erwin JP, Gentile F, et al. 2020 ACC/AHA guideline for the management of patients with valvular heart disease: executive summary: a report of the American College of Cardiology/American Heart Association Joint Committee on Clinical Practice Guidelines. *Circulation.* (2021) 143:e35–71. doi: 10.1161/CIR.0000000000000932
61. Truong QA, Massaro JM, Rogers IS, Mahabadi AA, Kriegel MF, Fox CS, et al. Reference values for normal pulmonary artery dimensions by noncontrast cardiac computed tomography: the Framingham Heart Study. *Circ Cardiovasc Imaging.* (2012) 5:147–54. doi: 10.1161/CIRCIMAGING.111.968610
62. Mahammedi A, Oshmyansky A, Hassoun PM, Thiemann DR, Siegelman SS. Pulmonary artery measurements in pulmonary hypertension: the role of computed tomography. *J Thorac Imaging.* (2013) 28:96–103. doi: 10.1097/RTI.0b013e318271c2eb
63. Kam JC, Pi J, Doraiswamy V, Elnahar Y, Abdul-Jawad S, DeBari VA, et al. CT scanning in the evaluation of pulmonary hypertension. *Lung.* (2013) 191:321–6. doi: 10.1007/s00408-013-9464-6
64. Chan AL, Juarez MM, Shelton DK, MacDonald T, Li C-S, Lin T-C, et al. Novel computed tomographic chest metrics to detect pulmonary hypertension. *BMC Med Imaging.* (2011) 11:7. doi: 10.1186/1471-2342-11-7
65. Shen Y, Wan C, Tian P, Wu Y, Li X, Yang T, et al. CT-base pulmonary artery measurement in the detection of pulmonary hypertension: a meta-analysis and systematic review. *Medicine.* (2014) 93:e256. doi: 10.1097/MD.0000000000000256
66. Tan RT, Kuzo R, Goodman LR, Siegel R, Haasler GB, Presberg KW. Utility of CT scan evaluation for predicting pulmonary hypertension in patients with parenchymal lung disease. Medical College of Wisconsin Lung Transplant Group. *Chest.* (1998) 113:1250–6. doi: 10.1378/chest.113.5.1250
67. Devaraj A, Wells AU, Meister MG, Corte TJ, Hansell DM. The effect of diffuse pulmonary fibrosis on the reliability of CT signs of pulmonary hypertension. *Radiology.* (2008) 249:1042–9. doi: 10.1148/radiol.2492080269
68. Rajaram S, Swift AJ, Capener D, Elliot CA, Condliffe R, Davies C, et al. Comparison of the diagnostic utility of cardiac magnetic resonance imaging, computed tomography, and echocardiography in assessment of suspected pulmonary arterial hypertension in patients with connective tissue disease. *J Rheumatol.* (2012) 39:1265–74. doi: 10.3899/jrheum.110987
69. Devaraj A, Wells AU, Meister MG, Corte TJ, Wort SJ, Hansell DM. Detection of pulmonary hypertension with multidetector CT and echocardiography alone and in combination. *Radiology.* (2010) 254:609–16. doi: 10.1148/radiol.09090548
70. Thieme SF, Johnson TRC, Reiser MF, Nikolaou K. Dual-energy lung perfusion computed tomography: a novel pulmonary functional imaging method. *Semin Ultrasound CT MR.* (2010) 31:301–8. doi: 10.1053/j.sult.2010.05.001
71. Dournes G, Verdier D, Montaudon M, Bullier E, Rivière A, Dromer C, et al. Dual-energy CT perfusion and angiography in chronic thromboembolic pulmonary hypertension: diagnostic accuracy and concordance with radionuclide scintigraphy. *Eur Radiol.* (2014) 24:42–51. doi: 10.1007/s00330-013-2975-y
72. Nakazawa T, Watanabe Y, Hori Y, Kiso K, Higashi M, Itoh T, et al. Lung perfused blood volume images with dual-energy computed tomography for chronic thromboembolic pulmonary hypertension: correlation to scintigraphy with single-photon emission computed tomography. *J Comput Assist Tomogr.* (2011) 35:590–5. doi: 10.1097/RCT.0b013e318224e227
73. Thieme SF, Becker CR, Hacker M, Nikolaou K, Reiser MF, Johnson TRC. Dual energy CT for the assessment of lung perfusion–correlation to scintigraphy. *Eur J Radiol.* (2008) 68:369–74. doi: 10.1016/j.ejrad.2008.07.031
74. Koike H, Sueyoshi E, Sakamoto I, Uetani M, Nakata T, Maemura K. Comparative clinical and predictive value of lung perfusion blood volume CT, lung perfusion SPECT and catheter pulmonary angiography images in patients with chronic thromboembolic pulmonary hypertension before and after balloon pulmonary angioplasty. *Eur Radiol.* (2018) 28:5091–9. doi: 10.1007/s00330-018-5501-4
75. Pitton MB, Kemmerich G, Herber S, Schweden F, Mayer E, Thelen M. Chronic thromboembolic pulmonary hypertension: diagnostic impact of Multislice-CT and selective Pulmonary-DSA. *Rofo.* (2002) 174:474–9. doi: 10.1055/s-2002-25117
76. Hoey ETD, Mirsadraee S, Pepke-Zaba J, Jenkins DP, Gopalan D, Screaton NJ. Dual-energy CT angiography for assessment of regional pulmonary perfusion in patients with chronic thromboembolic pulmonary hypertension: initial experience. *AJR Am J Roentgenol.* (2011) 196:524–32. doi: 10.2214/AJR.10.4842
77. Meinel FG, Graef A, Thierfelder KM, Armbruster M, Schild C, Neurohr C, et al. Automated quantification of pulmonary perfused blood volume by dual-energy CTPA in chronic thromboembolic pulmonary hypertension. *Rofo.* (2014) 186:151–6. doi: 10.1055/s-0033-1350412
78. Ameli-Renani S, Ramsay L, Bacon JL, Rahman F, Nair A, Smith V, et al. Dual-energy computed tomography in the assessment of vascular and parenchymal enhancement in suspected pulmonary hypertension. *J Thorac Imaging.* (2014) 29:98–106. doi: 10.1097/RTI.0000000000000061
79. Koike H, Sueyoshi E, Sakamoto I, Uetani M, Nakata T, Maemura K. Quantification of lung perfusion blood volume (lung PBV) by dual-energy CT in patients with chronic thromboembolic pulmonary hypertension (CTEPH) before and after balloon pulmonary angioplasty (BPA): Preliminary results. *Eur J Radiol.* (2016) 85:1607–12. doi: 10.1016/j.ejrad.2016.06.016
80. Tunariu N, Gibbs SJR, Win Z, Gin-Sing W, Graham A, Gishen P, et al. Ventilation-perfusion scintigraphy is more sensitive than multidetector CTPA in detecting chronic thromboembolic pulmonary disease as a treatable cause of pulmonary hypertension. *J Nucl Med.* (2007) 48:680–4. doi: 10.2967/jnumed.106.039438
81. He J, Fang W, Lv B, He J-G, Xiong C-M, Liu Z-H, et al. Diagnosis of chronic thromboembolic pulmonary hypertension: comparison of ventilation/perfusion scanning and multidetector computed tomography pulmonary angiography with pulmonary angiography. *Nucl Med Commun.* (2012) 33:459–63. doi: 10.1097/MNM.0b013e32835085d9
82. Furfaro D, Azadi J, Housten T, Kolb TM, Damico RL, Hassoun PM, et al. Discordance between imaging modalities in the evaluation of chronic thromboembolic pulmonary hypertension: a combined experience from two academic medical centers. *Ann ATS.* (2019) 16:277–80. doi: 10.1513/AnnalsATS.201809-588RL
83. Wang L, Li W, Yang Y, Wu W, Cai Q, Ma X, et al. Quantitative assessment of right ventricular glucose metabolism in idiopathic pulmonary arterial hypertension patients: a longitudinal study. *Eur Heart J Cardiovasc Imaging.* (2016) 17:1161–8. doi: 10.1093/ehjci/jev297
84. Oikawa M, Kagaya Y, Otani H, Sakuma M, Demachi J, Suzuki J, et al. Increased [18F]fluorodeoxyglucose accumulation in right ventricular free wall in patients with pulmonary hypertension and the effect of epoprostenol. *J Am Coll Cardiol.* (2005) 45:1849–55. doi: 10.1016/j.jacc.2005.02.065
85. Saygin D, Highland KB, Farha S, Park M, Sharp J, Roach EC, et al. Metabolic and functional evaluation of the heart and lungs in pulmonary hypertension by gated 2-[18F]-Fluoro-2-deoxy-D-glucose positron emission tomography. *Pulm Circ.* (2017) 7:428–38. doi: 10.1177/2045893217701917

86. Tatebe S, Fukumoto Y, Oikawa-Wakayama M, Sugimura K, Satoh K, Miura Y, et al. Enhanced [18F]fluorodeoxyglucose accumulation in the right ventricular free wall predicts long-term prognosis of patients with pulmonary hypertension: a preliminary observational study. *Eur Heart J Cardiovasc Imaging.* (2014) 15:666–72. doi: 10.1093/ehjci/jet276
87. Fang W, Zhao L, Xiong C-M, Ni X-H, He Z-X, He J-G, et al. Comparison of 18F-FDG uptake by right ventricular myocardium in idiopathic pulmonary arterial hypertension and pulmonary arterial hypertension associated with congenital heart disease. *Pulm Circ.* (2012) 2:365–72. doi: 10.4103/2045-8932.101651
88. Park J-B, Suh M, Park JY, Park JK, Kim Y, Kim H, et al. Assessment of inflammation in pulmonary artery hypertension by ^{68} Ga-Mannosylated human serum albumin. *Am J Respir Crit Care Med.* (2020) 201:95–106. doi: 10.1164/rccm.201903-0639OC
89. Kazimierczyk R, Szumowski P, Nekolla SG, Blaszczak P, Malek LA, Milosz-Wieczorek B, et al. Prognostic role of PET/MRI hybrid imaging in patients with pulmonary arterial hypertension. *Heart.* (2021) 107:54–60. doi: 10.1136/heartjnl-2020-316741
90. Mannting F, Zabrodina YV, Dass C. Significance of increased right ventricular uptake on 99mTc-Sestamibi SPECT in patients with coronary artery disease. *J Nuclear Med.* (1999) 40:889–94.
91. Mavrogeni S, Sfikakis PP, Gialafos E, Bratis K, Karabela G, Stavropoulos E, et al. Cardiac tissue characterization and the diagnostic value of cardiovascular magnetic resonance in systemic connective tissue diseases. *Arthritis Care Res.* (2014) 66:104–12. doi: 10.1002/acr.22181
92. Grothues F, Moon JC, Bellenger NG, Smith GS, Klein HU, Pennell DJ. Interstudy reproducibility of right ventricular volumes, function, and mass with cardiovascular magnetic resonance. *Am Heart J.* (2004) 147:218–23. doi: 10.1016/j.ahj.2003.10.005
93. Kawel-Boehm N, Maceira A, Valsangiacomo-Buechel ER, Vogel-Claussen J, Turkbey EB, Williams R, et al. Normal values for cardiovascular magnetic resonance in adults and children. *J Cardiovasc Magn Reson.* (2015) 17:29. doi: 10.1186/s12968-015-0111-7
94. Swift AJ, Rajaram S, Campbell MJ, Hurdman J, Thomas S, Capener D, et al. Prognostic value of cardiovascular magnetic resonance imaging measurements corrected for age and sex in idiopathic pulmonary arterial hypertension. *Circ Cardiovasc Imaging.* (2014) 7:100–6. doi: 10.1161/CIRCIMAGING.113.000338
95. Swift AJ, Capener D, Johns C, Hamilton N, Rothman A, Elliot C, et al. Magnetic resonance imaging in the prognostic evaluation of patients with pulmonary arterial hypertension. *Am J Respir Crit Care Med.* (2017) 196:228–39. doi: 10.1164/rccm.201611-2365OC
96. Baggen VJM, Leiner T, Post MC, van Dijk AP, Roos-Hesselink JW, Boersma E, et al. Cardiac magnetic resonance findings predicting mortality in patients with pulmonary arterial hypertension: a systematic review and meta-analysis. *Eur Radiol.* (2016) 26:3771–80. doi: 10.1007/s00330-016-4217-6
97. van Wolferen SA, Marcus JT, Boonstra A, Marques KMJ, Bronzwaer JGF, Spreeuwenberg MD, et al. Prognostic value of right ventricular mass, volume, and function in idiopathic pulmonary arterial hypertension. *Eur Heart J.* (2007) 28:1250–7. doi: 10.1093/eurheartj/ehl477
98. Peacock AJ, Crawley S, McLure L, Blyth KG, Vizza CD, Poscia R, et al. Changes in right ventricular function measured by cardiac magnetic resonance imaging in patients receiving pulmonary arterial hypertension-targeted therapy: the EURO-MR study. *Circ Cardiovasc Imaging.* (2014) 7:107–14. doi: 10.1161/CIRCIMAGING.113.000629
99. van Wolferen SA, van de Veerdonk MC, Mauritz G-J, Jacobs W, Marcus JT, Marques KMJ, et al. Clinically significant change in stroke volume in pulmonary hypertension. *Chest.* (2011) 139:1003–9. doi: 10.1378/chest.10-1066
100. Mavrogeni SI, Schwitter J, Gargani L, Pepe A, Monti L, Allanore Y, et al. Cardiovascular magnetic resonance in systemic sclerosis: "Pearls and pitfalls." Semin Arthritis Rheum (2017) 47(1):79–85. doi: 10.1016/j.semarthrit.2017.03.020
101. Mavrogeni S, Markousis-Mavrogenis G, Koutsogeorgopoulou L, Dimitroulas T, Bratis K, Kitas GD, et al. Cardiovascular magnetic resonance imaging pattern at the time of diagnosis of treatment naïve patients with connective tissue diseases. *Int J Cardiol.* (2017) 236:151–6. doi: 10.1016/j.ijcard.2017.01.104
102. Barison A, Gargani L, De Marchi D, Aquaro GD, Guiducci S, Picano E, et al. Early myocardial and skeletal muscle interstitial remodelling in systemic sclerosis: insights from extracellular volume quantification using cardiovascular magnetic resonance. *Eur Heart J Cardiovasc Imaging.* (2015) 16:74–80. doi: 10.1093/ehjci/jeu167
103. Ntusi NAB, Piechnik SK, Francis JM, Ferreira VM, Rai ABS, Matthews PM, et al. Subclinical myocardial inflammation and diffuse fibrosis are common in systemic sclerosis–a clinical study using myocardial T1-mapping and extracellular volume quantification. *J Cardiovasc Magn Reson.* (2014) 16:21. doi: 10.1186/1532-429X-16-21
104. Mayr A, Kitterer D, Latus J, Steubing H, Henes J, Vecchio F, et al. Evaluation of myocardial involvement in patients with connective tissue disorders: a multi-parametric cardiovascular magnetic resonance study. *J Cardiovasc Magn Reson.* (2016) 18:67. doi: 10.1186/s12968-016-0288-4
105. Bessa LGP, Junqueira FP, Bandeira ML da S, Garcia MI, Xavier SS, Lavall G, et al. Pulmonary arterial hypertension: use of delayed contrast-enhanced cardiovascular magnetic resonance in risk assessment. *Arq Bras Cardiol.* (2013) 101:336–43. doi: 10.5935/abc.20130168
106. Shehata ML, Lossnitzer D, Skrok J, Boyce D, Lechtzin N, Mathai SC, et al. Myocardial delayed enhancement in pulmonary hypertension: pulmonary hemodynamics, right ventricular function, and remodeling. *AJR Am J Roentgenol.* (2011) 196:87–94. doi: 10.2214/AJR.09.4114
107. Sanz J, Dellegrottaglie S, Kariisa M, Sulica R, Poon M, O'Donnell TP, et al. Prevalence and correlates of septal delayed contrast enhancement in patients with pulmonary hypertension. *Am J Cardiol.* (2007) 100:731–5. doi: 10.1016/j.amjcard.2007.03.094
108. Junqueira FP, Macedo R, Coutinho AC, Loureiro R, De Pontes PV, Domingues RC, et al. Myocardial delayed enhancement in patients with pulmonary hypertension and right ventricular failure: evaluation by cardiac MRI. *Br J Radiol.* (2009) 82:821–6. doi: 10.1259/bjr/28241773
109. Freed BH, Gomberg-Maitland M, Chandra S, Mor-Avi V, Rich S, Archer SL, et al. Late gadolinium enhancement cardiovascular magnetic resonance predicts clinical worsening in patients with pulmonary hypertension. *J Cardiovasc Magn Reson.* (2012) 14:11. doi: 10.1186/1532-429X-14-11
110. Swift AJ, Rajaram S, Capener D, Elliot C, Condliffe R, Wild JM, et al. LGE patterns in pulmonary hypertension do not impact overall mortality. *JACC Cardiovasc Imaging.* (2014) 7:1209–17. doi: 10.1016/j.jcmg.2014.08.014
111. Blyth KG, Groenning BA, Martin TN, Foster JE, Mark PB, Dargie HJ, et al. Contrast enhanced-cardiovascular magnetic resonance imaging in patients with pulmonary hypertension. *Eur Heart J.* (2005) 26:1993–9. doi: 10.1093/eurheartj/ehi328
112. McCann GP, Gan CT, Beek AM, Niessen HWM, Vonk Noordegraaf A, van Rossum AC. Extent of MRI delayed enhancement of myocardial mass is related to right ventricular dysfunction in pulmonary artery hypertension. *AJR Am J Roentgenol.* (2007) 188:349–55. doi: 10.2214/AJR.05.1259
113. Rodríguez-Reyna TS, Morelos-Guzman M, Hernández-Reyes P, Montero-Duarte K, Martínez-Reyes C, Reyes-Utrera C, et al. Assessment of myocardial fibrosis and microvascular damage in systemic sclerosis by magnetic resonance imaging and coronary angiotomography. *Rheumatology (Oxford).* (2015) 54:647–54. doi: 10.1093/rheumatology/keu350
114. Vogel-Claussen J, Skrok J, Shehata ML, Singh S, Sibley CT, Boyce DM, et al. Right and left ventricular myocardial perfusion reserves correlate with right ventricular function and pulmonary hemodynamics in patients with pulmonary arterial hypertension. *Radiology.* (2011) 258:119–27. doi: 10.1148/radiol.10100725
115. Scatteia A, Baritussio A, Bucciarelli-Ducci C. Strain imaging using cardiac magnetic resonance. *Heart Fail Rev.* (2017) 22:465–76. doi: 10.1007/s10741-017-9621-8
116. Ibrahim E-SH. Myocardial tagging by Cardiovascular Magnetic Resonance: evolution of techniques–pulse sequences, analysis algorithms, and applications. *J Cardiovasc Magn Reson.* (2011) 13:36. doi: 10.1186/1532-429X-13-36
117. Auger DA, Zhong X, Epstein FH, Spottiswoode BS. Mapping right ventricular myocardial mechanics using 3D cine DENSE cardiovascular magnetic resonance. *J Cardiovasc Magn Reson.* (2012) 14:4. doi: 10.1186/1532-429X-14-4
118. Youssef A, Ibrahim E-SH, Korosoglou G, Abraham MR, Weiss RG, Osman NF. Strain-encoding cardiovascular magnetic resonance for assessment

of right-ventricular regional function. *J Cardiovasc Magn Reson.* (2008) 10:33. doi: 10.1186/1532-429X-10-33
119. Shehata ML, Basha TA, Tantawy WH, Lima JA, Vogel-Claussen J, Bluemke DA, et al. Real-time single-heartbeat fast strain-encoded imaging of right ventricular regional function: normal versus chronic pulmonary hypertension. *Magn Reson Med.* (2010) 64:98–106. doi: 10.1002/mrm.22408
120. Oyama-Manabe N, Sato T, Tsujino I, Kudo K, Manabe O, Kato F, et al. The strain-encoded (SENC) MR imaging for detection of global right ventricular dysfunction in pulmonary hypertension. *Int J Cardiovasc Imaging.* (2013) 29:371–8. doi: 10.1007/s10554-012-0105-6
121. Ohyama Y, Ambale-Venkatesh B, Chamera E, Shehata ML, Corona-Villalobos CP, Zimmerman SL, et al. Comparison of strain measurement from multimodality tissue tracking with strain-encoding MRI and harmonic phase MRI in pulmonary hypertension. *Int J Cardiol.* (2015) 182:342–8. doi: 10.1016/j.ijcard.2015.01.016
122. Erley J, Genovese D, Tapaskar N, Alvi N, Rashedi N, Besser SA, et al. Echocardiography and cardiovascular magnetic resonance based evaluation of myocardial strain and relationship with late gadolinium enhancement. *J Cardiovasc Magn Reson.* (2019) 21:46. doi: 10.1186/s12968-019-0559-y
123. Bollache E, van Ooij P, Powell A, Carr J, Markl M, Barker AJ. Comparison of 4D flow and 2D velocity-encoded phase contrast MRI sequences for the evaluation of aortic hemodynamics. *Int J Cardiovasc Imaging.* (2016) 32:1529–41. doi: 10.1007/s10554-016-0938-5
124. Ley S, Mereles D, Puderbach M, Gruenig E, Schöck H, Eichinger M, et al. Value of MR phase-contrast flow measurements for functional assessment of pulmonary arterial hypertension. *Eur Radiol.* (2007) 17:1892–7. doi: 10.1007/s00330-006-0559-9
125. Mousseaux E, Tasu JP, Jolivet O, Simonneau G, Bittoun J, Gaux JC. Pulmonary arterial resistance: noninvasive measurement with indexes of pulmonary flow estimated at velocity-encoded MR imaging–preliminary experience. *Radiology.* (1999) 212:896–902. doi: 10.1148/radiology.212.3.r99au21896
126. Barker AJ, Roldán-Alzate A, Entezari P, Shah SJ, Chesler NC, Wieben O, et al. Four-dimensional flow assessment of pulmonary artery flow and wall shear stress in adult pulmonary arterial hypertension: results from two institutions. *Magn Reson Med.* (2015) 73:1904–13. doi: 10.1002/mrm.25326
127. Ohno Y, Hatabu H, Murase K, Higashino T, Nogami M, Yoshikawa T, et al. Primary pulmonary hypertension: 3D dynamic perfusion MRI for quantitative analysis of regional pulmonary perfusion. *AJR Am J Roentgenol.* (2007) 188:48–56. doi: 10.2214/AJR.05.0135
128. Sanz J, Kariisa M, Dellegrottaglie S, Prat-González S, Garcia MJ, Fuster V, et al. Evaluation of pulmonary artery stiffness in pulmonary hypertension with cardiac magnetic resonance. *JACC Cardiovasc Imaging.* (2009) 2:286–95. doi: 10.1016/j.jcmg.2008.08.007
129. Bogren HG, Klipstein RH, Mohiaddin RH, Firmin DN, Underwood SR, Rees RS, et al. Pulmonary artery distensibility and blood flow patterns: a magnetic resonance study of normal subjects and of patients with pulmonary arterial hypertension. *Am Heart J.* (1989) 118(5 Pt 1):990–9. doi: 10.1016/0002-8703(89)90235-4
130. Gan CT-J, Lankhaar J-W, Westerhof N, Marcus JT, Becker A, Twisk JWR, et al. Noninvasively assessed pulmonary artery stiffness predicts mortality in pulmonary arterial hypertension. *Chest.* (2007) 132:1906–12. doi: 10.1378/chest.07-1246
131. Kondo C, Caputo GR, Masui T, Foster E, O'Sullivan M, Stulbarg MS, et al. Pulmonary hypertension: pulmonary flow quantification and flow profile analysis with velocity-encoded cine MR imaging. *Radiology.* (1992) 183:751–8. doi: 10.1148/radiology.183.3.1584932
132. Reiter G, Reiter U, Kovacs G, Kainz B, Schmidt K, Maier R, et al. Magnetic resonance-derived 3-dimensional blood flow patterns in the main pulmonary artery as a marker of pulmonary hypertension and a measure of elevated mean pulmonary arterial pressure. *Circ Cardiovasc Imaging.* (2008) 1:23–30. doi: 10.1161/CIRCIMAGING.108.780247
133. Reiter U, Reiter G, Kovacs G, Stalder AF, Gulsun MA, Greiser A, et al. Evaluation of elevated mean pulmonary arterial pressure based on magnetic resonance 4D velocity mapping: comparison of visualization techniques. *PLoS ONE.* (2013) 8:e82212. doi: 10.1371/journal.pone.0082212
134. Reiter G, Reiter U, Kovacs G, Olschewski H, Fuchsjäger M. Blood flow vortices along the main pulmonary artery measured with MR imaging for diagnosis of pulmonary hypertension. *Radiology.* (2015) 275:71–9. doi: 10.1148/radiol.14140849
135. Budhiraja R, Tuder RM, Hassoun PM. Endothelial dysfunction in pulmonary hypertension. *Circulation.* (2004) 109:159–65. doi: 10.1161/01.CIR.0000102381.57477.50
136. Apitz C, Zimmermann R, Kreuder J, Jux C, Latus H, Pons-Kühnemann J, et al. Assessment of pulmonary endothelial function during invasive testing in children and adolescents with idiopathic pulmonary arterial hypertension. *J Am Coll Cardiol.* (2012) 60:157–64. doi: 10.1016/j.jacc.2012.04.010
137. Flammer AJ, Anderson T, Celermajer DS, Creager MA, Deanfield J, Ganz P, et al. The assessment of endothelial function: from research into clinical practice. *Circulation.* (2012) 126:753–67. doi: 10.1161/CIRCULATIONAHA.112.093245
138. Hays AG, Iantorno M, Soleimanifard S, Steinberg A, Schär M, Gerstenblith G, et al. Coronary vasomotor responses to isometric handgrip exercise are primarily mediated by nitric oxide: a noninvasive MRI test of coronary endothelial function. *Am J Physiol Heart Circ Physiol.* (2015) 308:H1343–1350. doi: 10.1152/ajpheart.00023.2015
139. Hays AG, Hirsch GA, Kelle S, Gerstenblith G, Weiss RG, Stuber M. Noninvasive visualization of coronary artery endothelial function in healthy subjects and in patients with coronary artery disease. *J Am Coll Cardiol.* (2010) 56:1657–65. doi: 10.1016/j.jacc.2010.06.036
140. Goerlich E, Mukherjee M, Schar M, Brown TT, Bonanno G, Weiss RG, et al. Noninvasive detection of impaired pulmonary artery endothelial function in people living with HIV. *AIDS.* (2020) 34:2231–8. doi: 10.1097/QAD.0000000000002671

Conflict of Interest: The authors declare that the research was conducted in the absence of any commercial or financial relationships that could be construed as a potential conflict of interest.

frontiers in Cardiovascular Medicine

MINI REVIEW
published: 26 January 2022
doi: 10.3389/fcvm.2021.811593

The Role of Multimodality Imaging in HIV-Associated Cardiomyopathy

*Ellise T. Gambahaya[1], Rimsha Rana[2], Shashwatee Bagchi[3], Garima Sharma[4,5], Sudipa Sarkar[6], Erin Goerlich[4], Blanche Cupido[1], Monica Mukherjee[4] and Allison G. Hays[4,5]**

[1] Division of Cardiology, Department of Medicine, University of Cape Town and Groote Schuur Hospital, Observatory, Cape Town, South Africa, [2] Department of Medicine, Georgetown University School of Medicine, Baltimore, MD, United States, [3] Division of Infectious Disease and Institute of Human Virology, University of Maryland School of Medicine, Baltimore, MD, United States, [4] Division of Cardiology, Department of Medicine, Johns Hopkins University School of Medicine, Baltimore, MD, United States, [5] Ciccarone Center for the Prevention of Cardiovascular Disease, Johns Hopkins University School of Medicine, Baltimore, MD, United States, [6] Division of Endocrinology, Department of Medicine, Johns Hopkins University School of Medicine, Baltimore, MD, United States

Despite marked advances in therapeutics, HIV infection remains a leading cause of morbidity and mortality worldwide. HIV infection is associated with cardiovascular complications including myocardial dysfunction. The description of HIV-associated cardiomyopathy (HIVAC) has evolved over time from a predominantly dilated cardiomyopathy with systolic dysfunction to one of subclinical diastolic dysfunction. Multimodality cardiovascular imaging plays an integral role in our understanding of the etiology and pathogenesis of HIVAC. Such imaging is also essential in the evaluation of individuals with chronic HIV disease who present with cardiac symptoms, especially of heart failure. In the present review, we will highlight current evidence for the role of multimodality imaging in establishing the diagnosis, etiology and pathophysiology of HIVAC as well as guiding treatment and assessing prognosis.

Keywords: human immunodeficiency virus, cardiomyopathy, echocardiography, cardiac magnetic resonance imaging, computed cardiac tomography

OPEN ACCESS

Edited by:
Juan Pablo Kaski, University College London, United Kingdom

Reviewed by:
Douglas Cannie, University College London, United Kingdom
Sarah Kraus, University of Oxford, United Kingdom
Edith Delewe Majonga, Biomedical Research and Training Institute, Zimbabwe

***Correspondence:**
Allison G. Hays
ahays2@jhmi.edu

Specialty section:
This article was submitted to Cardiovascular Imaging, a section of the journal Frontiers in Cardiovascular Medicine

Received: *09 November 2021*
Accepted: *30 December 2021*
Published: *26 January 2022*

Citation:
Gambahaya ET, Rana R, Bagchi S, Sharma G, Sarkar S, Goerlich E, Cupido B, Mukherjee M and Hays AG (2022) The Role of Multimodality Imaging in HIV-Associated Cardiomyopathy. Front. Cardiovasc. Med. 8:811593. doi: 10.3389/fcvm.2021.811593

INTRODUCTION

Human immunodeficiency virus (HIV) infection remains a leading cause of morbidity and mortality worldwide (1). Of the estimated 37.9 million people living with HIV (PWH) worldwide, 25.6 million live in sub-Saharan Africa (2). There are ∼1.2 million PWH in the United States (3). With the widespread advent of antiretroviral therapy (ART), HIV infection has largely become a chronic manageable condition. This is especially true in developed countries where ART is readily accessible. However, in some parts of the developing world, ART is not readily available and HIV remains an untreated and underrecognized condition characterized by progression to AIDS (acquired immune deficiency syndrome) and death.

HIV infection is associated with various cardiovascular manifestations. In settings where ART is readily accessible, PWH are living longer but continue to have chronic low-grade inflammation despite immunosuppression (4). In addition, as patients live longer traditional comorbidities such as hypertension, dyslipidaemia and diabetes with concomitant HIV infection contribute to accelerated atherosclerosis leading to vascular disease including coronary artery disease (CAD) (5). In fact, CAD has become the leading cause of cardiovascular mortality and morbidity in PWH (6). However, in resource limited settings where ART is not readily available, pericardial disease and myocardial disease in the form of myocarditis and cardiomyopathy are the leading causes of cardiac disease in PWH (7).

The presentation of myocardial disease in PWH ranges from incidental asymptomatic findings on autopsy or cardiovascular imaging to symptomatic heart failure. Decades after its recognition, the etiology and pathophysiology of HIV-associated cardiomyopathy (HIVAC) remains a topic of intense speculation with no consensus criteria for its definition. Nevertheless, its description has evolved from the pre-HAART era, when HIVAC was characterized by a dilated cardiomyopathy with systolic dysfunction associated with end-stage HIV disease and a poor prognosis. Morbidity and mortality occurred largely in the context of myocarditis, opportunistic infections, toxicity from medications, nutritional disorders, autoimmune mechanisms and inflammation. In more recent times, subclinical diastolic dysfunction has become the hallmark of HIVAC in individuals with treated HIV infection (8).

Cardiac imaging plays an integral role in the assessment of PWH who present with cardiac symptoms and signs especially those of heart failure. In the current review, we will highlight evidence for the role of multimodality imaging in establishing the diagnosis, etiology, and pathophysiology of HIVAC as well as guiding treatment and assessing prognosis.

EPIDEMIOLOGY AND PATHOGENESIS OF HIV ASSOCIATED CARDIOMYOPATHY

The epidemiology of HIVAC has changed over the course of time from its initial description characterized by left ventricular (LV) systolic dysfunction to its current description of varying levels of diastolic dysfunction. Data on the prevalence of HIVAC is largely from studies conducted in the United States and Europe despite the fact that more than two-thirds of PWH are found in Sub-Saharan Africa (9). With the advent of ART, contemporary studies show that the prevalence of diastolic dysfunction is relatively high, with lower prevalence of systolic dysfunction. In a recent metanalysis of 11 studies conducted in Europe and the United States which included 2,242 mildly symptomatic and asymptomatic patients with HIV, the prevalence of systolic dysfunction was 8.3% and diastolic dysfunction was 43.4% (10). The Heart of Soweto Study conducted in South Africa showed that out of 5,328 cases of newly diagnosed heart failure, 518 (9.7%) were HIV positive. Moreover, 148 patients (29%) had systolic dysfunction and 196 (38%) had both systolic and diastolic dysfunction regardless of whether they were symptomatic for heart failure (7).

The pathogenesis of HIVAC is unclear but is likely multifactorial. Prior to the widespread implementation of ART, systolic dysfunction was thought to be mainly due to direct viral invasion of the myocardium, with or without myocarditis by the HIV virus or secondary to opportunistic infections such as toxoplasmosis and cryptococcosis (11). However, with the advent of ART other mechanisms of myocardial involvement in HIV infection have emerged including CAD and drug toxicity (12). Other putative mechanisms include autoimmunity, nutritional deficiencies and inflammation.

ECHOCARDIOGRAPHY

Echocardiography remains the first line imaging modality in assessing myocardial function. It is readily available, cost effective and robust in detecting both systolic and diastolic dysfunction. Prior to HAART, HIVAC was recognized on transthoracic echocardiography (TTE) as systolic LV dysfunction with varying degrees of LV dilatation. However, with the onset of HAART, HIVAC is largely recognized on TTE as subclinical diastolic dysfunction.

A study by Hakim et al. based in Zimbabwe aimed to determine the prevalence and characteristics of myocardial dysfunction in acutely ill HIV positive patients admitted to hospital. Out of a total of 151 patients, 14 (9%) had a dilated cardiomyopathy, 33 (22%) had LV dysfunction and 9 (6%) had isolated right ventricular (RV) dysfunction (13). These results mirrored a similar study in the United Kingdom which showed a relatively high prevalence of myocardial dysfunction of 26/173 (15%) patients (14). Dilated cardiomyopathy was a feature of advanced HIV disease and mean CD4 count was 38 cells/mm^3 in these patients. The HIV-HEART study assessed the prevalence of abnormalities in cardiac structure and function in 803 PWH in the era of ART (15). The main findings of the study included LV dilatation in 10.1% of all PWH while 34 and 48% of patients had systolic and diastolic dysfunction, respectively. Severe forms of ventricular dysfunction were rare. In a large systematic review of 54 studies looking at cardiac dysfunction in ∼125,382 PWH, there were 12,655 cases of cardiac dysfunction (16). The authors also found that there was a lower prevalence of LV systolic dysfunction in those studies reporting a higher use of HAART. LV systolic dysfunction was higher in the African region possibly reflecting lower access to HAART. These studies highlight the shift of HIVAC from a predominant systolic dysfunction to one of predominant diastolic dysfunction in the post ART era.

Echocardiography has been shown to be instrumental in early detection of cardiovascular disease and has also been helpful for researchers to diagnose differences between heart disease in PWH and in people without HIV. One study analyzed 1,195 participants from the Multicenter AIDS Cohort (MACS) study who underwent TTE exams demonstrating that men with HIV had a larger LV mass index and right ventricular size compared to controls (17). In addition to the structural differences found between groups, this study demonstrated that men with HIV had higher rates of diastolic dysfunction and RV dysfunction compared to men without HIV after adjusting for cardiovascular comorbidities. These cardiac abnormalities were also seen in virally suppressed men with HIV. The study however did not find any association between left ventricular ejection fraction (LVEF) and HIV seropositivity. Overall, the MACS study concluded that structural changes in HIV-positive patients may predispose them to heart failure with preserved ejection fraction.

Other studies evaluated LV systolic function by tissue Doppler strain echocardiography in PWH and participants without HIV. One study demonstrated that while LVEF in PWH was slightly lower than in patients who were uninfected, the LVEF values were still within normal limits. However, PWH had subtle cardiac dysfunction, as evidenced by reduced LV strain (18). Subclinical

LV systolic dysfunction in HIV is further supported by other studies revealing no significant difference in conventional echocardiographic parameters including LVEF between PWH and people without HIV. However, the HIV population had significantly lower mean global longitudinal strain values (GLS). Furthermore, studies have shown that impaired GLS correlated with decreased CD4 counts (19, 20).

Right ventricular (RV) dysfunction is relatively common in PWH occurring largely in the setting of dilated cardiomyopathy or with varying degrees of HIV associated pulmonary hypertension (PH) (21). Isolated RV dysfunction has been documented in both the pre-ART and ART eras. RV dysfunction is associated with increased mortality in patients with PH and other forms of heart disease (22, 23). Therefore, understanding RV function in PWH is essential in determining the prognosis of patients with cardiac dysfunction and potentially guiding therapy. Prior to the widespread use of ART, smaller studies demonstrated isolated RV dilatation in PWH (13, 14, 24). In a more contemporary study, the prevalence of RV structural abnormalities and RV dysfunction was determined using echocardiography in 104 PWH on ART (25). RV dysfunction was common, but did not always correlate with elevated pulmonary artery systolic pressure (>35 mmHg) or LV systolic dysfunction, suggesting that RV dysfunction in PWH may occur independently of pulmonary hypertension or LV dysfunction.

The evidence highlights the value of echocardiography in the evaluation of myocardial function in PWH. Studies from the pre-HAART era demonstrate the pivotal role that echocardiography played in diagnosing systolic dysfunction in symptomatic patients often with advanced HIV disease. The same remains true today, and echocardiography remains an essential first line modality for assessing cardiac structure and function in PWH who present with heart failure symptoms. This non-invasive approach is important in characterizing biventricular function and cardiac structure as well as excluding other non-myocardial causes of symptoms. In the case of LV systolic dysfunction, evidence-based goal directed medical therapy should be considered per guideline recommendations (26). Although asymptomatic diastolic dysfunction is generally associated with an increased risk of symptomatic heart failure and death, screening echocardiography in asymptomatic PWH is not indicated although remains an area of active investigation. Rather the focus should be on aggressively managing comorbidities such as hypertension, obesity, or diabetes which may contribute to ventricular dysfunction.

CARDIAC MAGNETIC RESONANCE IMAGING

Cardiac magnetic resonance (CMR) has been used to detect subtle and subclinical myocardial abnormalities, contributing to the current understanding of the pathogenesis of HIVAC. Untreated HIV infection is characterized by an immunodeficient state. In contrast, patients with well-treated HIV infection are in a state of immune activation. Several studies have shown a correlation between elevated inflammatory biomarkers and cardiovascular events in PWH (27). This observation has led to the postulation that inflammation may play an important role in the pathogenesis of HIV associated cardiovascular disease including myocardial dysfunction. At a cellular level, immune activation and chronic inflammation leads to deposition of collagen and myocardial fibrosis which is associated with an increased incidence of both systolic and diastolic dysfunction (28).

CMR is a useful tool in assessing the role of inflammation and fibrosis in myocardial dysfunction in PWH. CMR can detect several components of inflammation, which include edema and fibrosis depending on the extent of cardiac involvement and stage of disease. **Figure 1** shows CMR findings demonstrating fibrosis by late gadolinium enhancement (LGE) in a patient with HIV as well as markedly elevated myocardial T1 consistent with diffuse myocardial fibrosis (29).

Several studies have looked at the role of CMR in detecting subclinical myocardial dysfunction and fibrosis in PWH. In a study by Holloway et al., a total of 129 asymptomatic PWH on ART underwent CMR to assess cardiac function and myocardial fibrosis (30). Seventy-six percent of PWH were observed to have myocardial fibrosis predominantly in the basal inferolateral wall as compared to 13% of control subjects. In addition, peak myocardial systolic and diastolic strain were significantly lower in PWH. An extension of this study demonstrated that treated HIV infection was associated with chronic subclinical myocardial edema and pericardial effusions (31). Another study by Leutkens et al. studied PWH who were virally suppressed and underwent CMR. Compared to controls, the investigators found that PWH had lower LV strain values and ejection fraction, and higher myocardial inflammation by T2 weighted images. Myocardial fibrosis on LGE was also significantly elevated in PWH compared to controls (82% vs. 27%, $p < 0.001$) (32). A more recent study in South Africa demonstrated that PWH who were virally suppressed had greater myocardial fibrosis by extracellular volume (ECV) fraction compared with age and sex matched HIV negative controls. In addition, an elevated NT-proBNP level was associated with higher ECV (3.4%; 85% CI 1.3–5.5) (33). CMR has also played a role in tissue characterization of the RV in PWH, by demonstrating the presence of RV fibrosis by LGE (34). However, the clinical significance of these findings is yet unknown.

CMR plays an important role in the evaluation of HIV associated myocarditis. Before the introduction of ART, an early autopsy study demonstrated myocarditis in 52% of patients who died of AIDS (35). However, with the widespread use of ART, the incidence of HIV associated myocarditis has declined and the condition occurs almost exclusively in those with advanced immunosuppression. The gold standard for diagnosing myocarditis is endomyocardial biopsy however this techniques is invasive and can have low diagnostic yield (36). CMR on the other hand is a non-invasive imaging technique that permits detection of various stages of myocarditis with excellent diagnostic performance (37).

Measures of tissue characterization using CMR also have prognostic value for PWH. In a recent study, CMR was used to quantify ECV, reflective of myocardial inflammation

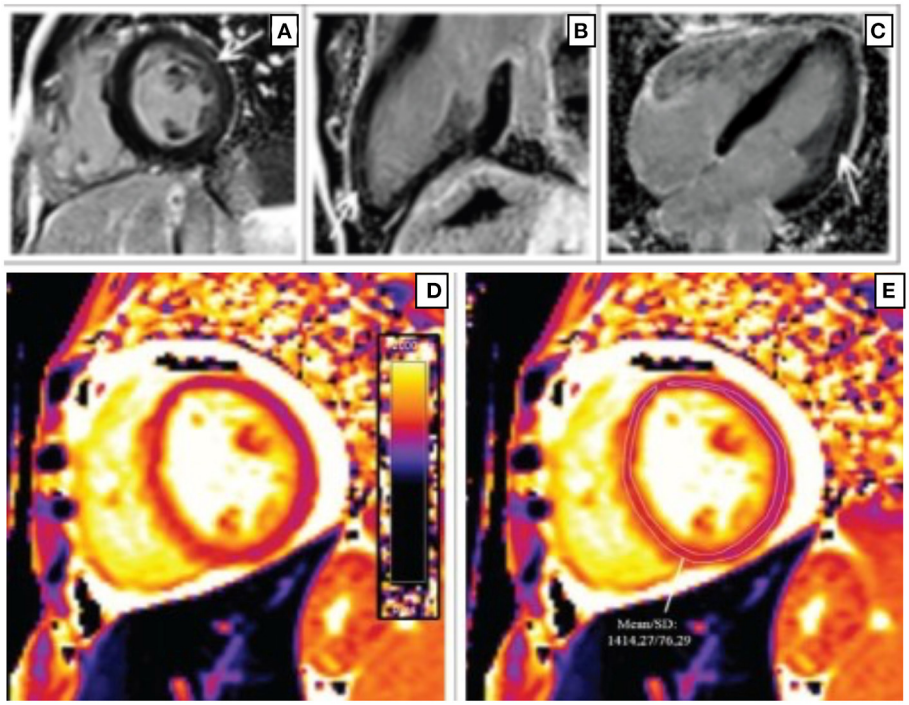

FIGURE 1 | Short-axis **(A)**, 2-chamber **(B)**, and 4-chamber **(C)** late gadolinium phase-sensitive inversion recovery images show linear mid-wall enhancement in the lateral wall of the LV (white arrows) in a patient with HIV. T1 map at the level of the mid-LV **(D)** shows a markedly elevated myocardial T1 time of 1,414 m/s (normal 1,052 m/s ± 23 m/s at 3 T) **(E)** consistent with diffuse myocardial fibrosis (29).

or fibrosis, and showed that PWH have significantly higher ECV fraction when compared to people without HIV. The higher ECV value corresponded to more diffuse fibrosis, and studies have also shown a link between higher ECV values and increased adverse cardiovascular events. A prospective observational study evaluated the prognostic association between CMR measures and cardiovascular outcomes including heart failure in PWH on HAART. It was found that patients with diffuse myocardial fibrosis on CMR had a higher rate of cardiovascular events (38).

Lastly, novel non-contrast CMR techniques have been developed that may help in the work up of PWH who are prone to developing early vascular disease and microvascular dysfunction that may contribute to the pathogenesis of cardiomyopathy (39). Impaired coronary endothelial function (CEF) provides a promising early indication of coronary vascular disease in PWH. Abnormal CEF plays a critical role in the development, progression and clinical manifestations of coronary artery disease (CAD), independently predicts cardiovascular (CV) events, and is a target for medical interventions (40, 41). Using CMR combined with isometric handgrip exercise, an endothelial dependent stressor, studies in PWH revealed depressed CEF (measured by stress-induced change in coronary artery area and blood flow) compared to HIV negative matched adults (42).

CARDIAC COMPUTED TOMOGRAPHY AND CORONARY COMPUTED TOMOGRAPHY ANGIOGRAPHY

Cardiac computed tomography (CT) and coronary CT Angiography (CCTA) have emerged as important imaging tools for evaluating both clinical and subclinical CAD in PWH. An analysis of the MACS cohort, a large cohort of HIV infected and matched uninfected men showed that after adjusting for known CVD risk factors, HIV infected men had an increased prevalence of non-calcified and mixed plaques compared to HIV uninfected men using CCTA (43). CCTA was also used to evaluate differences in the degree of coronary stenosis between the two groups. After adjustment for risk factors only a borderline association remained between HIV and increased degree of coronary artery stenosis.

Coronary artery calcification (CAC) is a highly specific marker of coronary atherosclerosis and is frequently employed to screen for CAD and assess risk for cardiovascular events (44). The MACS study showed that after adjustments for race, age, cohort and location, HIV infected men had a greater prevalence of CAC than HIV uninfected men (43). However, once adjustments for traditional CAD risk factors were made, the association between HIV and increased prevalence of CAC was borderline. Although coronary CT and CCTA are not indicated as screening tests in asymptomatic PWH, results from the MACS cohort and other

TABLE 1 | Clinical and investigational utility of cardiac imaging modalities in HIV associated cardiomyopathy.

	ECHO	CMR	CT SCAN	Nuclear Imaging
Chamber dimensions and volumes	***	****	*	*
Left ventricular systolic and diastolic function	***	****	–	*** (MUGA)
Mechanisms of ventricular dysfunction (ischemia vs. non ischemia)	**	***	*	****
Atherosclerosis	–	–	***	–
Myocardial tissue characterisation	**	****	–	–
Staging and monitoring disease progress	***	****	**	–
Limitations	Operator dependent and may be limited by acoustic windows Limited by geometric assumptions when assessing cardiac structure and function	Not widely available	Use of ionizing radiation, contrast (CTA)	Not widely available, patient preparation

*Echo, echocardiography; CMR, cardiac magnetic resonance; CT scan, computerized tomography; MUGA, multigated acquisition scan; *poor; **intermediate, ***good, ****excellent performance.*

studies emphasize the importance of evaluating and modifying traditional cardiovascular risk factors in this population.

PWH may present with symptomatic heart failure secondary to ischemic heart disease. In this setting CCTA is useful in the diagnostic workup of CAD. The utility of CT to establish the diagnosis of CAD as well as its value as a gatekeeper for invasive coronary angiography in patients with heart failure and LV systolic dysfunction was shown in a study of 93 patients with newly diagnosed heart failure of unknown etiology (45). If the CAC score was 0, the diagnosis of ischemic heart failure was ruled out; if the score was more than 0, CCTA was performed. Using this proposed algorithm, there was a sensitivity of 100%, with a specificity of 67% in the prediction of CAD.

NUCLEAR MEDICINE TECHNIQUES

Nuclear medicine-based techniques have the ability to identify vascular inflammation and can permit the early detection of vascular disease in PWH (46). The degree of uptake of Fluorodeoxyglucose (FDG) in the carotid arteries and aorta detected by positron emission tomography-computed tomography (PET-CT) imaging techniques is useful in characterizing vascular inflammation, early atheroma and atherosclerotic plaques that are prone to rupture. One study reported a higher uptake of FDG in the carotid arteries and aorta of HIV infected individuals as compared to non-infected individuals (47).The use of myocardial perfusion imaging (MPI) with single-photon emission computerized tomography (SPECT) and PET have been evaluated in patients with HIV and found to have a high sensitivity and specificity in diagnosing CAD. These nuclear imaging techniques shed light on the etiology of cardiomyopathy by detecting cardiac stunning, presence of scar and assessing viability in patients with HIV thereby directing further management. In addition, the prevalence of RV dysfunction in a population of PWH was also investigated by radionuclide ventriculography in 95 patients (48). Although there was no significant LV dysfunction, a small but significant proportion of the cohort had modestly reduced RV systolic function defined as an ejection fraction <44%.

A summary of multimodality cardiovascular imaging techniques used for HIV-related heart disease is shown in **Table 1**.

DISCUSSION: GAPS IN KNOWLEDGE AND FUTURE DIRECTIONS

The introduction of HAART has led to a paradigm shift in the presentation of cardiovascular disease in PWH including that of HIVAC. Although the etiopathogenesis of HIVAC remains unclear, multimodality imaging has played a role in defining various putative mechanisms including inflammation and myocardial fibrosis. Multimodality imaging is also crucial in establishing a diagnosis of HIVAC in symptomatic patients. Although many studies have established prognosis in HIV patients with cardiomyopathy and systolic dysfunction, the prognostic significance as well as progression of diastolic dysfunction in HIVAC remains largely unknown and further long-term studies are needed. In addition, the mechanism and significance of right ventricular dysfunction especially in the absence of PH and LV dysfunction should be explored further. In summary, an approach tailored to the clinical presentation of the patient should be used to guide the use of cardiovascular imaging to identify myocardial dysfunction, investigate the possible underlying causes and facilitate appropriate preventive and evidence-based treatment for this condition.

AUTHOR CONTRIBUTIONS

EG, RR, and AH drafted the manuscript. MM, GS, EG, SB, SS, and BC reviewed and edited the manuscript. All authors contributed to the article and approved the submitted version.

FUNDING

EG and AH received support from the Women as One Foundation. Further support was received from the National Institute of Health (R01HL147660) and the Johns Hopkins Center for AIDS Research (P30AI094189), Ruth L. Kirschstein Institutional National Research Service Award; T32HL007227-Pathophysiology of Myocardial Disease, the National Institute of Health.

REFERENCES

1. HIV/AIDS. Available online at: https://www.who.int/news-room/fact-sheets/detail/hiv-aids (accessed October 3, 2021).
2. So-Armah K, Benjamin LA, Bloomfield GS, Feinstein MJ, Hsue P, Njuguna B, et al. HIV and cardiovascular disease. *Lancet HIV*. (2020) 7:e279–93. doi: 10.1016/S2352-3018(20)30036-9
3. Statistics Overview | Statistics Center. *HIV/AIDS*. CDC (2021). Available online at: https://www.cdc.gov/hiv/statistics/overview/index.htmlhttps://www.cdc.gov/hiv/statistics/overview/index.html (accessed September 25, 2021).
4. Deeks SG, Tracy R, Douek DC. Systemic effects of inflammation on health during chronic HIV infection. *Immunity*. (2013) 39:633–45. doi: 10.1016/j.immuni.2013.10.001
5. Triant VA, Lee H, Hadigan C, Grinspoon SK. Increased acute myocardial infarction rates and cardiovascular risk factors among patients with human immunodeficiency virus disease. *J Clin Endocrinol Metab*. (2007) 92:2506–12. doi: 10.1210/jc.2006-2190
6. Dominick L, Midgley N, Swart L-M, Sprake D, Deshpande G, Laher I, et al. HIV-related cardiovascular diseases: the search for a unifying hypothesis. *Am J Physiol-Heart Circ Physiol*. (2020) 318:H731–46. doi: 10.1152/ajpheart.00549.2019
7. Sliwa K, Carrington MJ, Becker A, Thienemann F, Ntsekhe M, Stewart S. Contribution of the human immunodeficiency virus/acquired immunodeficiency syndrome epidemic to *de novo* presentations of heart disease in the Heart of Soweto Study cohort. *Eur Heart J*. (2012) 33:866–74. doi: 10.1093/eurheartj/ehr398
8. Remick J, Georgiopoulou V, Marti C, Ofotokun I, Kalogeropoulos A, Lewis W, et al. Heart failure in patients with human immunodeficiency virus infection. *Circulation*. (2014) 129:1781–9. doi: 10.1161/CIRCULATIONAHA.113.004574
9. Lumsden RH, Bloomfield GS. The causes of HIV-associated cardiomyopathy: a tale of two worlds. *BioMed Res Int*. (2016) 2016:e8196560. doi: 10.1155/2016/8196560
10. Cerrato E, D'Ascenzo F, Biondi-Zoccai G, Calcagno A, Frea S, Grosso Marra W, et al. Cardiac dysfunction in Pauci symptomatic human immunodeficiency virus patients: a meta-analysis in the highly active antiretroviral therapy era. *Eur Heart J*. (2013) 34:1432–6. doi: 10.1093/eurheartj/ehs471
11. Barbaro G, Di Lorenzo G, Grisorio B, Barbarini G. Cardiac involvement in the acquired immunodeficiency syndrome: a multicenter clinical-pathological study. *AIDS Res Hum Retroviruses*. (1998) 14:1071–7. doi: 10.1089/aid.1998.14.1071
12. Barbaro G. HIV-associated cardiomyopathy. *Herz Kardiovaskuläre Erkrank*. (2005) 30:486–92. doi: 10.1007/s00059-005-2728-z
13. Hakim JG, Matenga JA, Siziya S. Myocardial dysfunction in human immunodeficiency virus infection: an echocardiographic study of 157 patients in hospital in Zimbabwe. *Heart*. (1996) 76:161–5. doi: 10.1136/hrt.76.2.161
14. Jacob AJ, Sutherland GR, Bird AG, Brettle RP, Ludlam CA, McMillan A, et al. Myocardial dysfunction in patients infected with HIV: prevalence and risk factors. *Br Heart J*. (1992) 68:549–53. doi: 10.1136/hrt.68.12.549
15. Reinsch N, Kahlert P, Esser S, Sundermeyer A, Neuhaus K, Brockmeyer N, et al. Echocardiographic findings and abnormalities in HIV-infected patients: results from a large, prospective, multicenter HIV-heart study. *Am J Cardiovasc Dis*. (2011) 1:176–84.
16. Erqou S, Lodebo BT, Masri A, Altibi AM, Echouffo -Tcheugui Justin B, Dzudie A, et al. Cardiac dysfunction among people living with HIV. *JACC Heart Fail*. (2019) 7:98–108. doi: 10.1016/j.jchf.2018.10.006
17. Doria de Vasconcellos H, Post WS, Ervin A, Haberlen SA, Budoff M, Malvestutto C, et al. Associations between HIV serostatus and cardiac structure and function evaluated by 2-dimensional echocardiography in the multicenter AIDS cohort study. *J Am Heart Assoc*. (2021) 10:e019709. doi: 10.1161/JAHA.120.019709
18. Onur I, Ikitimur B, Oz F, Ekmekci A, Elitok A, Cagatay AA, et al. Evaluation of human immunodeficiency virus infection-related left ventricular systolic dysfunction by tissue Doppler strain echocardiography. *Echocardiography*. (2014) 31:1199–204. doi: 10.1111/echo.12569
19. Sherpa K, Sah RK, Maskey A, Malla R, Sharma D, Rajbhandari S, et al. Evaluation of left ventricular systolic function by Myocardial Deformation Imaging in asymptomatic HIV patients. *Nepal Heart J*. (2019) 16:11–5. doi: 10.3126/njh.v16i2.26310
20. Sims A, Frank L, Cross R, Clauss S, Dimock D, Purdy J, et al. Abnormal cardiac strain in children and young adults with HIV acquired in early life. *J Am Soc Echocardiogr*. (2012) 25:741–8. doi: 10.1016/j.echo.2012.04.004
21. Currie PF, Jacob AJ, Foreman AR, Elton RA, Brettle RP, Boon NA. Heart muscle disease related to HIV infection: prognostic implications. *BMJ*. (1994) 309:1605–7. doi: 10.1136/bmj.309.6969.1605
22. McLaughlin VV, Presberg KW, Doyle RL, Abman SH, McCrory DC, Fortin T, et al. Prognosis of pulmonary arterial hypertension*: ACCP evidence-based clinical practice guidelines. *Chest*. (2004) 126:78–92S. doi: 10.1378/chest.126.1_suppl.78S
23. de Groote P, Millaire A, Foucher-Hossein C, Nugue O, Marchandise X, Ducloux G, et al. Right ventricular ejection fraction is an independent predictor of survival in patients with moderate heart failure. *J Am Coll Cardiol*. (1998) 32:948–54. doi: 10.1016/S0735-1097(98)00337-4
24. Rangasetty UC, Rahman AM, Hussain N. Reversible right ventricular dysfunction in patients with HIV infection. *South Med J*. (2006) 99:274–8. doi: 10.1097/01.smj.0000202698.25909.97
25. Simon MA, Lacomis CD, George MP, Kessinger C, Weinman R, McMahon D, et al. Isolated right ventricular dysfunction in patients with human immunodeficiency virus. *J Card Fail*. (2014) 20:414–21. doi: 10.1016/j.cardfail.2014.03.009
26. McDonagh TA, Metra M, Adamo M, Gardner RS, Baumbach A, Böhm M, et al. 2021 ESC Guidelines for the diagnosis treatment of acute chronic heart failure: developed by the Task Force for the diagnosis treatment of acute chronic heart failure of the European Society of Cardiology (ESC) With the special contribution of the Heart Failure Association (HFA) of the ESC. *Eur Heart J*. (2021) 42:3599–726. doi: 10.1093/eurheartj/ehab368
27. Kuller LH, Tracy R, Belloso W, Wit SD, Drummond F, Lane HC, et al. Inflammatory and coagulation biomarkers and mortality in patients with HIV infection. *PLoS Med*. (2008) 5:e203. doi: 10.1371/journal.pmed.0050203
28. Thiara DK, Liu CY, Raman F, Mangat S, Purdy JB, Duarte HA, et al. Abnormal myocardial function is related to myocardial steatosis and diffuse myocardial fibrosis in HIV-Infected adults. *J Infect Dis*. (2015) 212:1544–51. doi: 10.1093/infdis/jiv274
29. Sood V, Jermy S, Saad H, Samuels P, Moosa S, Ntusi N. Review of cardiovascular magnetic resonance in human immunodeficiency virus-associated cardiovascular disease. *South Afr J Radiol*. (2017) 21:10. doi: 10.4102/sajr.v21i2.1248
30. Holloway CJ, Ntusi N, Suttie J, Mahmod M, Wainwright E, Clutton G, et al. Comprehensive cardiac magnetic resonance imaging and spectroscopy reveal a high burden of myocardial disease in HIV patients. *Circulation*. (2013) 128:814–22. doi: 10.1161/CIRCULATIONAHA.113.001719
31. Ntusi N, O'Dwyer E, Dorrell L, Wainwright E, Piechnik S, Clutton G, et al. HIV-1–related cardiovascular disease is associated with chronic inflammation, frequent pericardial effusions, and probable myocardial edema. *Circ Cardiovasc Imaging*. (2016) 9:e004430. doi: 10.1161/CIRCIMAGING.115.004430

32. Luetkens JA, Doerner J, Schwarze-Zander C, Wasmuth J-C, Boesecke C, Sprinkart AM, et al. Cardiac magnetic resonance reveals signs of subclinical myocardial inflammation in asymptomatic HIV-infected patients. *Circ Cardiovasc Imaging.* (2016) 9:e004091. doi: 10.1161/CIRCIMAGING.115.004091
33. Shuldiner SR, Wong L-Y, Peterson TE, Wolfson J, Jermy S, Saad H, et al. Myocardial fibrosis among antiretroviral therapy-treated persons with human immunodeficiency virus in South Africa. *Open Forum Infect Dis.* (2021) 8:ofaa600. doi: 10.1093/ofid/ofaa600
34. Kristoffersen US, Lebech A-M, Petersen CL, Gutte H, Gerstoft J, Kjaer A. Right and left sided cardiac function in HIV patients on anti-retroviral therapy: a cine magnetic resonance imaging study. *J Cardiovasc Magn Reson.* (2009) 11:P60. doi: 10.1186/1532-429X-11-S1-P60
35. Anderson DW, Virmani R, Reilly JM, O'Leary T, Cunnion RE, Robinowitz M, et al. Prevalent myocarditis at necropsy in the acquired immunodeficiency syndrome. *J Am Coll Cardiol.* (1988) 11:792–9. doi: 10.1016/0735-1097(88)90213-6
36. Bennett MK, Gilotra NA, Harrington C, Rao S, Dunn JM, Freitag TB, et al. Evaluation of the role of endomyocardial biopsy in 851 patients with unexplained heart failure from 2000–2009. *Circ Heart Fail.* (2013) 6:676–84. doi: 10.1161/CIRCHEARTFAILURE.112.000087
37. Luetkens JA, Faron A, Isaak A, Dabir D, Kuetting D, Feisst A, et al. Comparison of original and 2018 Lake Louise criteria for diagnosis of acute myocarditis: results of a validation cohort. *Radiol Cardiothorac Imaging.* (2019) 1:e190010. doi: 10.1148/ryct.2019190010
38. de LP, Arendt CT, Haberl AE, Froadinadl D, Kann G, Wolf T, et al. Myocardial fibrosis and inflammation by CMR predict cardiovascular outcome in people living with HIV. *JACC Cardiovasc Imaging.* (2021) 14:1548–57. doi: 10.1016/j.jcmg.2021.01.042
39. Iantorno M, Hays AG, Schär M, Krishnaswamy R, Soleimanifard S, Steinberg A, et al. Simultaneous noninvasive assessment of systemic and coronary endothelial function. *Circ Cardiovasc Imaging.* (2016) 9:e003954. doi: 10.1161/CIRCIMAGING.115.003954
40. Schächinger V, Britten MB, Zeiher AM. Prognostic impact of coronary vasodilator dysfunction on adverse long-term outcome of coronary heart disease. *Circulation.* (2000) 101:1899–906. doi: 10.1161/01.CIR.101.16.1899
41. Treasure CB, Klein JL, Weintraub WS, Talley JD, Stillabower ME, Kosinski AS, et al. Beneficial effects of cholesterol-lowering therapy on the coronary endothelium in patients with coronary artery disease. *N Engl J Med.* (1995) 332:481–7.
42. Iantorno M, Soleimanifard S, Schär M, Brown TT, Bonanno G, Barditch-Crovo P, et al. Regional coronary endothelial dysfunction is related to the degree of local epicardial fat in people with HIV. *Atherosclerosis.* (2018) 278:7–14. doi: 10.1016/j.atherosclerosis.2018.08.002
43. Post WS, Budoff M, Kingsley L, Palella FJ, Witt MD, Li X, et al. Associations between HIV infection and subclinical coronary atherosclerosis. *Ann Intern Med.* (2014) 160:458–67. doi: 10.7326/M13-1754
44. Greenland P, Blaha MJ, Budoff MJ, Erbel R, Watson KE. Coronary calcium score and cardiovascular risk. *J Am Coll Cardiol.* (2018) 72:434–47. doi: 10.1016/j.jacc.2018.05.027
45. ten Kate G-JR, Caliskan K, Dedic A, Meijboom WB, Neefjes LA, Manintveld OC, et al. Computed tomography coronary imaging as a gatekeeper for invasive coronary angiography in patients with newly diagnosed heart failure of unknown aetiology. *Eur J Heart Fail.* (2013) 15:1028–34. doi: 10.1093/eurjhf/hft090
46. Hyafil F, Vigne J. Nuclear imaging. *Arterioscler Thromb Vasc Biol.* (2019) 39:1369–78. doi: 10.1161/ATVBAHA.119.312586
47. Ankrah AO, Glaudemans AWJM, Klein HC, Dierckx RAJO, Sathekge M. The role of nuclear medicine in the staging and management of human immune deficiency virus infection and associated diseases. *Nucl Med Mol Imaging.* (2017) 51:127–39. doi: 10.1007/s13139-016-0422-0
48. Lebech A-M, Gerstoft J, Hesse B, Petersen CL, Kjaer A. Right and left ventricular cardiac function in a developed world population with human immunodeficiency virus studied with radionuclide ventriculography. *Am Heart J.* (2004) 147:482–8. doi: 10.1016/j.ahj.2003.09.009

Conflict of Interest: The authors declare that the research was conducted in the absence of any commercial or financial relationships that could be construed as a potential conflict of interest.

frontiers in Cardiovascular Medicine

REVIEW
published: 27 January 2022
doi: 10.3389/fcvm.2021.785279

Current State and Future Directions of Multimodality Imaging in Cardiac Sarcoidosis

Alison L. Wand[1], *Jonathan Chrispin*[1], *Elie Saad*[2], *Monica Mukherjee*[1], *Allison G. Hays*[1] *and Nisha A. Gilotra*[1]*

[1] Division of Cardiology, Department of Medicine, Johns Hopkins University School of Medicine, Baltimore, MD, United States, [2] Department of Radiology, Johns Hopkins University School of Medicine, Baltimore, MD, United States

Cardiac sarcoidosis (CS) is an increasingly recognized cause of heart failure and arrhythmia. Historically challenging to identify, particularly in the absence of extracardiac sarcoidosis, diagnosis of CS has improved with advancements in cardiac imaging. Recognition as well as management may require interpretation of multiple imaging modalities. Echocardiography may serve as an initial screening study for cardiac involvement in patients with systemic sarcoidosis. Cardiac magnetic resonance imaging (CMR) provides information on diagnosis as well as risk stratification, particularly for ventricular arrhythmia in the setting of late gadolinium enhancement. More recently, ^{18}F-fluorodeoxyglucose position emission tomography (FDG-PET) has assumed a valuable role in the diagnosis and longitudinal management of patients with CS, allowing for the assessment of response to treatment. Hybrid FDG-PET/CT may also be used in the evaluation of extracardiac inflammation, permitting the identification of biopsy sites for diagnostic confirmation. Herein we examine the approach to diagnosis and management of CS using multimodality imaging via a case-based review.

Keywords: cardiac sarcoidosis, sarcoid cardiomyopathy, multimodality imaging, inflammatory cardiomyopathy, echocardiography, cardiac PET, cardiac MRI (CMR)

OPEN ACCESS

Edited by:
Sanjeev Bhattacharyya, Barts Heart Centre, United Kingdom

Reviewed by:
Kevin Alexander, Stanford University, United States
Toral Patel, University of Virginia, United States

***Correspondence:**
Nisha A. Gilotra
naggarw2@jhmi.edu

Specialty section:
This article was submitted to Cardiovascular Imaging, a section of the journal Frontiers in Cardiovascular Medicine

Received: *29 September 2021*
Accepted: *31 December 2021*
Published: *27 January 2022*

Citation:
Wand AL, Chrispin J, Saad E, Mukherjee M, Hays AG and Gilotra NA (2022) Current State and Future Directions of Multimodality Imaging in Cardiac Sarcoidosis. Front. Cardiovasc. Med. 8:785279. doi: 10.3389/fcvm.2021.785279

INTRODUCTION

Sarcoidosis is a multiorgan system disease characterized by noncaseating granulomatous inflammation (1–3). Sarcoidosis most commonly involves the lungs or lymph nodes (2, 4). However cardiac sarcoidosis (CS) is increasingly recognized and may occur with extracardiac findings or, rarely, in isolation (4). Clinically, cardiac involvement may manifest with cardiomyopathy, arrhythmia, or atrioventricular conduction disease, or CS may remain relatively subclinical (2). While identifying CS has significant therapeutic and prognostic implications (5–7), diagnosis may be challenging, particularly in the absence of extracardiac disease.

Diagnosis of CS traditionally requires histopathologic evidence of sarcoidosis (i.e., noncaseating granulomas) either in the heart or another organ in addition to characteristic clinical and imaging findings. Several diagnostic criteria for CS have been proposed, including the Japanese Ministry of Health and Welfare (JMHW) criteria (8) and the Heart Rhythm Society (HRS) criteria (9). The widely used HRS criteria require confirmatory cardiac histopathology to make a "definite CS" diagnosis. When there is a histologic diagnosis of extracardiac sarcoidosis, a diagnosis of "probable CS" can be made with the following HRS imaging criteria: reduced left ventricular ejection fraction (LVEF) <40%, patchy uptake on dedicated ^{18}F-fluorodeoxyglucose position emission tomography

(FDG-PET) scan, and/or late gadolinium enhancement (LGE) on cardiac magnetic resonance imaging (CMR) (9). However, with advancements in cardiac imaging, and the limited diagnostic yield of biopsy (4, 10, 11), there has been increased reliance on imaging and clinical presentation for the diagnosis of CS (12). More recently, the revised Japanese Circulation Society updated criteria for CS to allow for a diagnosis of possible or isolated CS based on imaging characteristics, including cardiac FDG uptake, LGE on CMR, and abnormalities in ventricular wall anatomy and function (basal thinning of the interventricular septum, ventricular aneurysm, LVEF $< 50\%$) (12). Notably, while the updated Japanese criteria still include abnormal 12-lead electrocardiogram (ECG) findings (ventricular arrhythmias, bundle branch bock, axis deviation, pathologic Q waves) as minor criteria for CS diagnosis (12), ECG has low sensitivity and specificity for CS (7). HRS guidelines include ECG as a screening tool for cardiac involvement among patients with known extracardiac sarcoidosis, where it is best used for screening in conjunction with echocardiography to increase diagnostic yield (9).

Here we provide a case-based review of multimodality cardiac imaging, specifically echocardiography, CMR, and FDG-PET, in CS, with an emphasis on diagnostic and management strategies (**Figure 1**). We also highlight the current limitations and challenges as well as future directions of advanced cardiac imaging in CS.

ECHOCARDIOGRAPHY

A 42-year-old male with a history of previously treated, well controlled pulmonary sarcoidosis presents with 3 months of progressive dyspnea on exertion, weight gain and fatigue. Physical exam is notable for elevated jugular venous pressure, bilateral inspiratory rales and pitting pretibial edema. He is referred for an echocardiogram, which demonstrates low normal left ventricular systolic function with an LVEF of 50–55%, moderate concentric left ventricular (LV) hypertrophy, restrictive diastolic filling pattern (mitral inflow E/A ratio 2.2) and mild hypokinesis of the right ventricle. Global longitudinal strain (GLS) is reported at −6% (normal < −18%). Given concern for restrictive cardiomyopathy, he is referred for endomyocardial biopsy, which demonstrates fibrosis without active granulomatous inflammation. Ongoing suspicion for cardiac involvement of sarcoidosis prompts advanced cardiac imaging, ultimately confirming a diagnosis of CS. He is initiated on corticosteroids and mycophenolate mofetil.

Two-dimensional transthoracic echocardiography (TTE) remains a cornerstone in the investigation of patients with suspected CS (9). TTE is the only imaging modality recommended by HRS guidelines for the screening of patients with extracardiac sarcoidosis for cardiac involvement (9). Left ventricular systolic or diastolic dysfunction, ventricular dilatation, abnormal septal wall thickness, wall motion abnormalities in non-coronary distributions, ventricular aneurysms, and pericardial effusion are all findings that have been associated with CS (**Figure 2**) (2, 5, 7, 13, 14). Left ventricular hypertrophy and restrictive physiology may also be noted (2, 11, 15), with associated biatrial enlargement and restrictive diastolic filling pattern (as evidenced by mitral inflow pattern with E/A ratio ≥ 2 and findings consistent with increased left atrial pressure) (16). Several studies have identified thickening or thinning of the septal wall as a more specific finding for CS (17, 18). However, many patients with CS do not manifest any of these echocardiographic abnormalities, limiting the sensitivity of this modality for identifying CS (7, 19).

More recently, advanced techniques such as speckle tracking echocardiography (STE) have shown promise in identifying subclinical myocardial dysfunction in CS. The tracking of grayscale speckles within the myocardium over the cardiac cycle allows for assessment of myocardial deformation using measurements such as strain, or change in length compared to baseline length (20, 21). STE deformation parameters can assess mechanics at the level of the cardiomyocytes and are sensitive to histopathological changes in myocardial tissue (21). Thus, reductions in strain, globally or over a regional area of interest, can indicate underlying myocardial disease (20, 21).

CS is characterized by myocardial inflammation, fibrosis, and edema (22), pathologic changes that affect tissue function and, consequently, measures of strain before overt changes in LV function might be detected by TTE. Di Stefano and colleagues, for example, compared 23 patients with definite or probable CS and normal LV and RV systolic function with no baseline wall motion abnormalities to 97 healthy controls (23). The authors found a significant impairment in left ventricular global longitudinal strain, LVGLS (absolute LVGLS 15.9% ± 2.5 vs. 18.2% ± 2.7, $P = 0.001$) and right ventricular global longitudinal strain, RVGLS (absolute RVGLS 16.9% ± 4.5 vs. 24.1% ± 4.0, $P = 0.0001$) among those with CS (23). Notably, among the larger cohort of 83 patients with definite or probable CS in this study (including those with reduced LVEF), event rates for hospitalization or heart failure were higher in those patients with absolute LVGLS < 14% (23).

Additionally, multiple observational studies have demonstrated that reductions in GLS may be identified by STE in patients with sarcoidosis without known CS or apparent LV dysfunction, suggestive of early subclinical myocardial dysfunction (24–27). A recent meta-analysis of these studies found that LVGLS was significantly impaired in patients with extracardiac sarcoidosis and normal LV function compared with controls, and that among patients with sarcoidosis, LVGLS was significantly reduced in patients who experienced major cardiac events (28). These studies suggest a potential role for STE as a more sensitive screening tool than traditional echocardiography alone to identify patients with extracardiac sarcoidosis at increased risk for cardiac involvement.

Among patients with known CS, TTE and STE may have a role in longitudinal management. Recognition of LV dysfunction is important for implementing guideline-directed medical therapy (GDMT) for heart failure, while serial TTE may be used to monitor response to medications or potentially identify candidates for advanced heart failure therapies and devices (5, 10, 29). The role for neurohormonal blockade to prevent maladaptive LV remodeling is not well

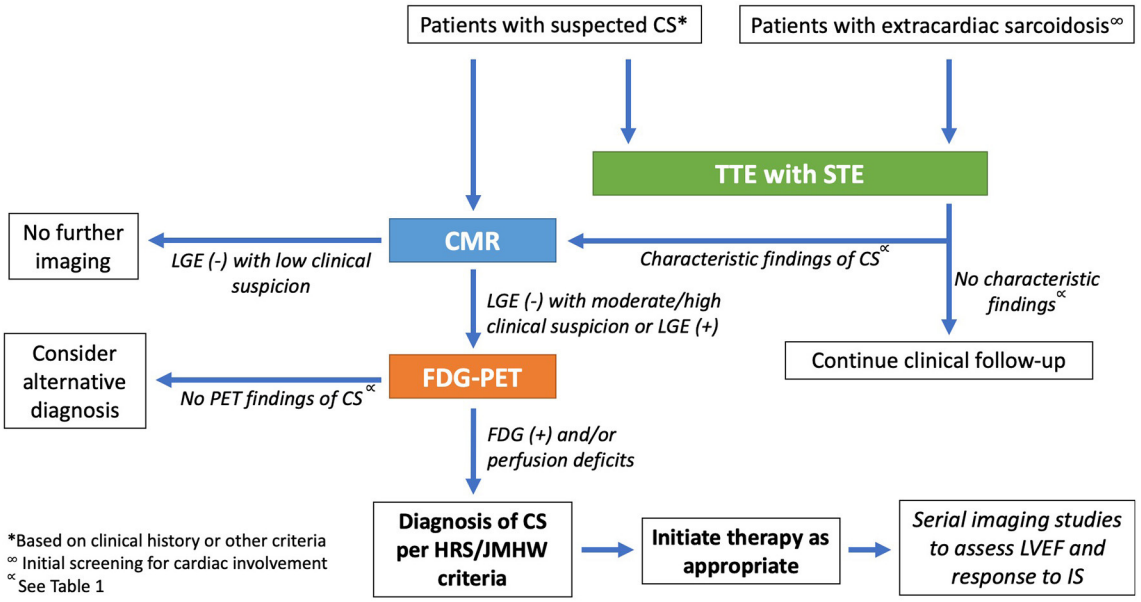

FIGURE 1 | Proposed algorithm for the multimodal imaging approach to diagnosis and management of CS.

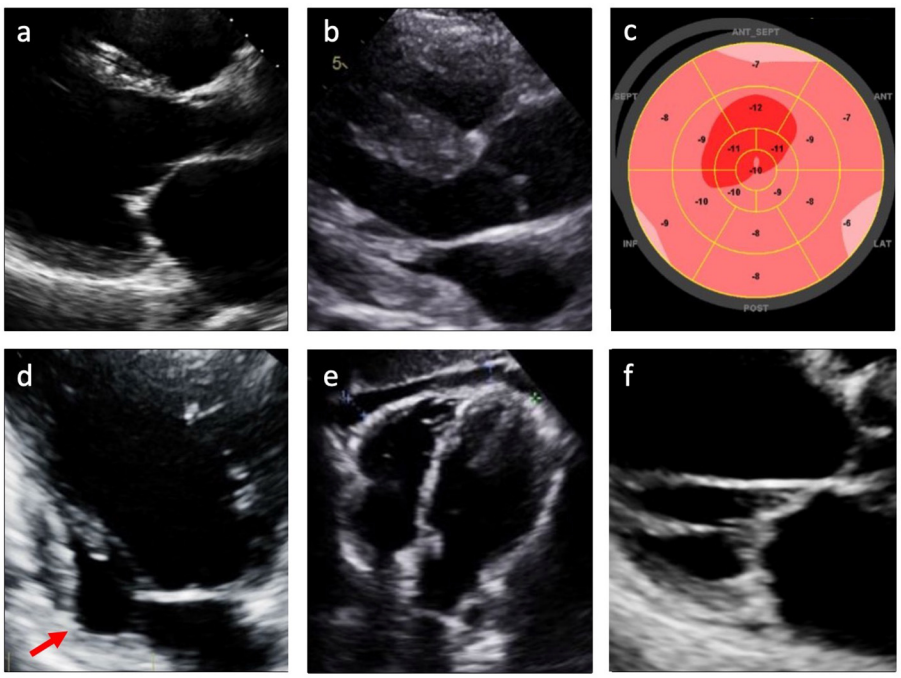

FIGURE 2 | Echocardiographic findings in cardiac sarcoidosis. **(a)** Left ventricular dilatation; **(b)** Left and/or right ventricular hypertrophy; **(c)** Reduced global longitudinal strain (GLS); **(d)** Left ventricular wall aneurysm (arrow); **(e)** Pericardial effusion; **(f)** Valvular thickening or dysfunction.

understood for patients with impaired GLS without overt LV dysfunction. The field of cardio-oncology, where preemptive use of cardioprotective medications in patients receiving cardiotoxic medications to prevent cancer treatment related cardiac dysfunction has been more extensively evaluated, may provide some insight (30, 31). For example, one study of 159 patients receiving potentially cardiotoxic chemotherapy (anthracyclines, trastuzumab, or both) showed that among patients with decreased absolute GLS by $\geq$ 11% relative to baseline, those who received beta blockers demonstrated

improvement in GLS on follow-up (32). Additional studies are needed to explore a similar role for cardioprotective medications among patients with CS, particularly those in whom subclinical LV dysfunction is identified early on cardiac imaging.

CARDIOVASCULAR MAGNETIC RESONANCE IMAGING

A 63-year-old African American female with a history of hypertension and dyslipidemia presents to the emergency department with 1 week of intermittent chest pressure and palpitations. ECG on arrival shows sinus rhythm with a nonspecific intraventricular conduction delay and occasional premature ventricular contractions. Serum troponin levels are undetectable. Chest x-ray is notable for an enlarged cardiac silhouette and hilar lymphadenopathy. Transthoracic echocardiogram reveals global LV systolic dysfunction with LVEF 40% and thinning of the basal septal wall. Coronary angiography shows non-obstructive coronary artery disease. She is referred for CMR, which shows midwall delayed gadolinium enhancement in the inferolateral basal septal LV, suspicious for CS. For further diagnostic evaluation, she undergoes bronchoscopy with endobronchial ultrasound-guided lymph node biopsy. Histopathology demonstrates macrophages and noncaseating granulomas. Given histologic confirmation of sarcoidosis, CMR findings and in context of borderline LV function, electrophysiology study is performed for further arrhythmic risk stratification and demonstrates inducible ventricular tachycardia. She undergoes implantable cardioverted-defibrillator (ICD) placement and initiation of immunosuppressive therapy for CS.

CMR has established a role as a highly sensitive tool with both diagnostic and prognostic value in the management of CS. CMR has wide application in the evaluation of nonischemic cardiomyopathies, in part owing to the ability to identify myocardial fibrosis by LGE (33). Midwall and subepicardial LGE, commonly involving the basal or mid-ventricular septum, are characteristic of CS, though other patterns have been noted (**Figure 3**) (34–39). Lesions detected by LGE-CMR may be too small to cause conduction disturbances or LV structural or functional changes that might be identified by ECG or TTE, but nonetheless may have clinical importance (33–35). LGE-CMR has demonstrated increased sensitivity for cardiac involvement among patients with sarcoidosis when compared with JMHW criteria alone (35). In another cohort of 321 sarcoidosis patients, among whom 96 (29.9%) met HRS criteria for CS, CMR demonstrated the highest sensitivity (96.9%), specificity (100%), and area under the curve (0.984) when compared to ECG, Holter monitoring, and TTE (40). CMR can also provide comprehensive assessment of cardiac morphology and function including left and right ventricular systolic function, ventricular dimensions, wall thickness, and wall motion abnormalities (41, 42). The emerging CMR technique of strain imaging may offer another means to assess the effect of CS on LV mechanics (43). Multiple authors have investigated the use of CMR strain imaging for diagnosis and prognostication (44–46). One recent study of 76 patients with CS who underwent CMR with both LGE and longitudinal strain imaging suggested that regional longitudinal strain was not well associated with either arrhythmic phenotype (atrioventricular block vs. ventricular arrhythmia) or future adverse events compared to LGE (46); however, more data are needed to understand the potential role of CMR strain imaging in CS.

In addition to its diagnostic utility, CMR has also demonstrated prognostic power (35, 47–50). In an early study by Patel and colleagues noted above, patients with LGE on CMR had higher rates of the composite endpoint of all-cause mortality or symptomatic arrhythmia as well as higher rates of cardiac death (35). Likewise, in a larger cohort of 155 patients with systemic sarcoidosis undergoing CMR for suspected cardiac involvement, LGE was associated with an increased risk of death, aborted sudden cardiac death, or appropriate ICD firing (HR 31.6, $P = 0.0014$) on multivariate analysis (48). The presence of LGE was found to be a better independent predictor of cardiac death than LVEF, which has previously been identified as a predictor of mortality among patients with CS (48, 51, 52). A recent meta-analysis including these and similar studies, including 694 subjects in total, found an increased risk of cardiovascular death (relative risk 10.7, 95% confidence interval [CI] 1.34–86.3, $P = 0.03$) and ventricular arrhythmia (relative risk 19.5, 95% CI 2.68–143, $P = 0.003$) in LGE-positive patients compared to LGE-negative patients (49). Notably, LGE-negative patients (495/694) had low rates of cardiovascular mortality and ventricular arrhythmias, suggesting that LGE-CMR also confers a high negative predictive value and that LGE-negative patients have a favorable prognosis (49). Similarly, it has been noted that inflammation on FDG-PET in the absence of LGE on CMR identifies lower risk group for ventricular arrhythmias compared to FDG positive patients with LGE (53).

LGE-CMR has a particularly nuanced role in the decision for ICD placement among patients with CS. Persistent LVEF $\leq$ 35% despite optimal medical therapy and immunosuppression (if indicated), sustained ventricular tachycardia, and aborted sudden cardiac arrest remain class I indications for an ICD by the most recent HRS guidelines (9, 54), while class IIa indications include patients with LVEF $\geq$ 35% and syncope, evidence of myocardial scar by CMR or FDG-PET, an indication for permanent pacing, or inducible sustained ventricular arrhythmia on electrophysiological study (54). LGE-CMR may identify additional patients at increased risk of sudden cardiac death in the absence of significantly reduced LV function (9). Interestingly, several studies have identified LGE regional variations in risk of ventricular arrhythmias and sudden cardiac death (46, 55). One study of 290 patients with biopsy-proven sarcoidosis undergoing CMR for suspected cardiac involvement found that LGE in the right ventricle was independently associated with the combined endpoint of sudden cardiac death or significant ventricular arrhythmia (HR 5.43, 95% CI 1.25–23.47, $P = 0.024$) (55). Thus, CMR may prompt referral for ICD for patients with higher risk LGE features. Conversely, the 2014 HRS consensus statement indicates that absence of LGE in patients without other class I indications identifies patients who should not receive ICD therapy (class III) (9).

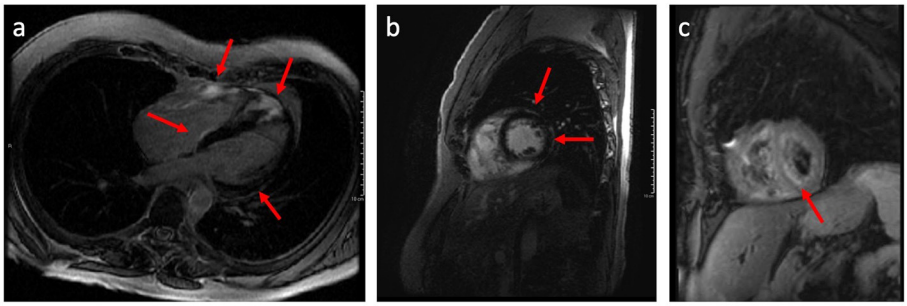

FIGURE 3 | Long axis **(a)** and short axis **(b)** CMR images demonstrating late gadolinium enhancement (LGE) having a patchy non-vascular midmyocardial and sub-epicardial pattern mainly involving the basal and apical septal wall, basal-mid lateral and anterior wall, and right ventricular wall; **(c)** Black blood T-2 weighted CMR images demonstrate patchy areas of predominantly midmyocardial increased signal intensity in the left and right ventricular myocardium denoting myocardial inflammation.

LGE-CMR is not without limitations. While sensitive to even small regions of fibrosis (34, 35), midwall enhancement is not specific to CS and can be seen in other nonischemic cardiomyopathies, including arrhythmogenic right ventricular cardiomyopathy (56). Though less common, transmural distribution or subepicardial and subendocardial distribution of LGE (with midwall sparing), as well as multifocal LGE may also indicate CS (5, 36). Additionally, LGE-CMR may be less sensitive in patients in earlier stages of CS, who have acute inflammation but have not yet developed myocardial fibrosis (33, 43). T2-weighted imaging may increase detection of acute inflammation, though more data are needed to understand the role of T2 mapping in CS (44, 57). CMR may be technically challenging in patients with permanent pacemakers or cardiac defibrillators (43, 58). Importantly, recent studies have demonstrated the safety of MRI in patients with non-MRI-conditional devices using safety protocols, which may mitigate this concern (59, 60). Finally, gadolinium is relatively contraindicated in patients with severe renal disease due to the risk of nephrogenic systemic fibrosis (43, 58).

^{18}F-FLUORODEOXYGLUCOSE POSITION EMISSION TOMOGRAPHY

A 49-year-old male with a history of biopsy-proven pulmonary sarcoidosis and recent complete heart block status post permanent pacemaker presents in clinic for further evaluation of possible cardiac involvement of sarcoidosis. ECG demonstrates sinus rhythm with right ventricular pacing. TTE shows normal biventricular size and function. CMR reveals LGE localized to the basal septum. He is referred for cardiac FDG-PET, which demonstrates patchy FDG uptake involving the basal septal and inferolateral LV wall with co-localized perfusion defects, concerning for active CS. A course of prednisone and methotrexate are initiated and 4 months later FDG-PET scan is repeated showing near resolution of cardiac FDG uptake. Pacemaker interrogation reveals recovery of AV node conduction.

FDG-PET with myocardial perfusion imaging has emerged as an important imaging modality in CS, combining assessment of active cardiac inflammation with evaluation of perfusion (**Figures 4**, **5**) (61, 62). ^{18}F-FDG is a glucose analog that is readily utilized by activated macrophages (61, 63). Accumulation of FDG by these highly metabolic inflammatory cells within active granulomas allows for visualization of active inflammation in CS (22, 64, 65). Patterns of FDG uptake associated with CS have been described as focal, focal on diffuse, or less commonly, diffuse, though diffuse FDG uptake may be difficult to interpret (9, 62). Hybrid PET/CT imaging facilitates identification of alternate sources of abnormal FDG uptake, such as malignant lesions or infections (62). Additionally, metrics to quantify FDG uptake, such as standardized uptake values (SUVs), may aid in interpretation and comparison of studies (62, 66, 67).

Importantly, whole-body PET can identify extracardiac inflammation and accessible biopsy sites to confirm histopathologic diagnosis of sarcoidosis (22, 67, 68). FDG-PET guidance can improve the diagnostic yield of noncardiac biopsy targets such as thoracic lymph nodes, which typically have higher yield than endomyocardial biopsy, especially when significantly FDG avid (67). Furthermore, assessment of the extent and activity of extracardiac involvement may have implications for treatment decisions (68).

It is recommended to combine ^{18}F-FDG metabolic imaging with myocardial perfusion imaging (MPI) using rubidium-82 or N-13-ammonia (62, 67). Perfusion defects, related to changes in coronary microcirculation caused by CS, typically occur in non-coronary distributions and may represent areas of inflammation or fibrosis (62, 69). Pairing FDG and MPI patterns can provide information regarding the activity and chronicity of cardiac involvement (62, 67, 70). Active inflammation may result in FDG uptake in an area of abnormal perfusion (mismatched segment), whereas fibrosis may cause a perfusion defect in the absence of FDG uptake (11, 67, 68).

The sensitivity of FDG-PET for the diagnosis of CS has been reported as 85–100% in various studies, with a specificity

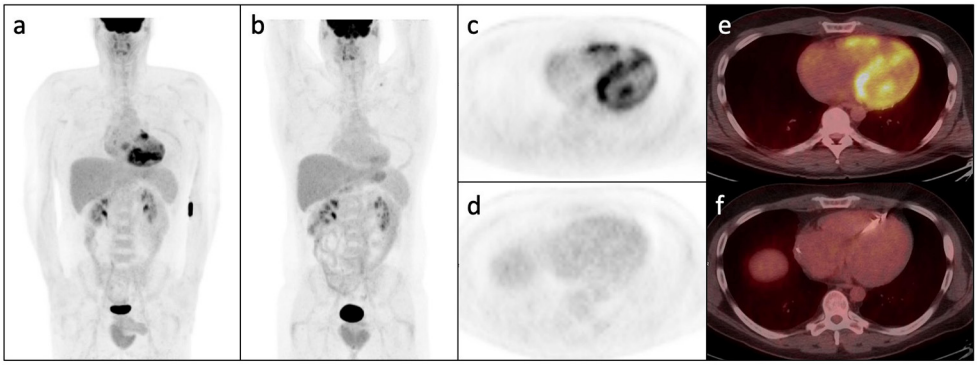

FIGURE 4 | Whole-body FDG PET **(a)** and axial PET and PET/CT images **(c,e)** following appropriate pre-test preparation demonstrating abnormal patchy increase in FDG avidity within the right and left ventricular myocardium with subtle increase in right atrial FDG uptake. **(b,d,f)** Show post-treatment FDG PET/CT images in the same patient demonstrating interval resolution of the previously seen abnormal myocardial FDG uptake. Note interval ICD placement.

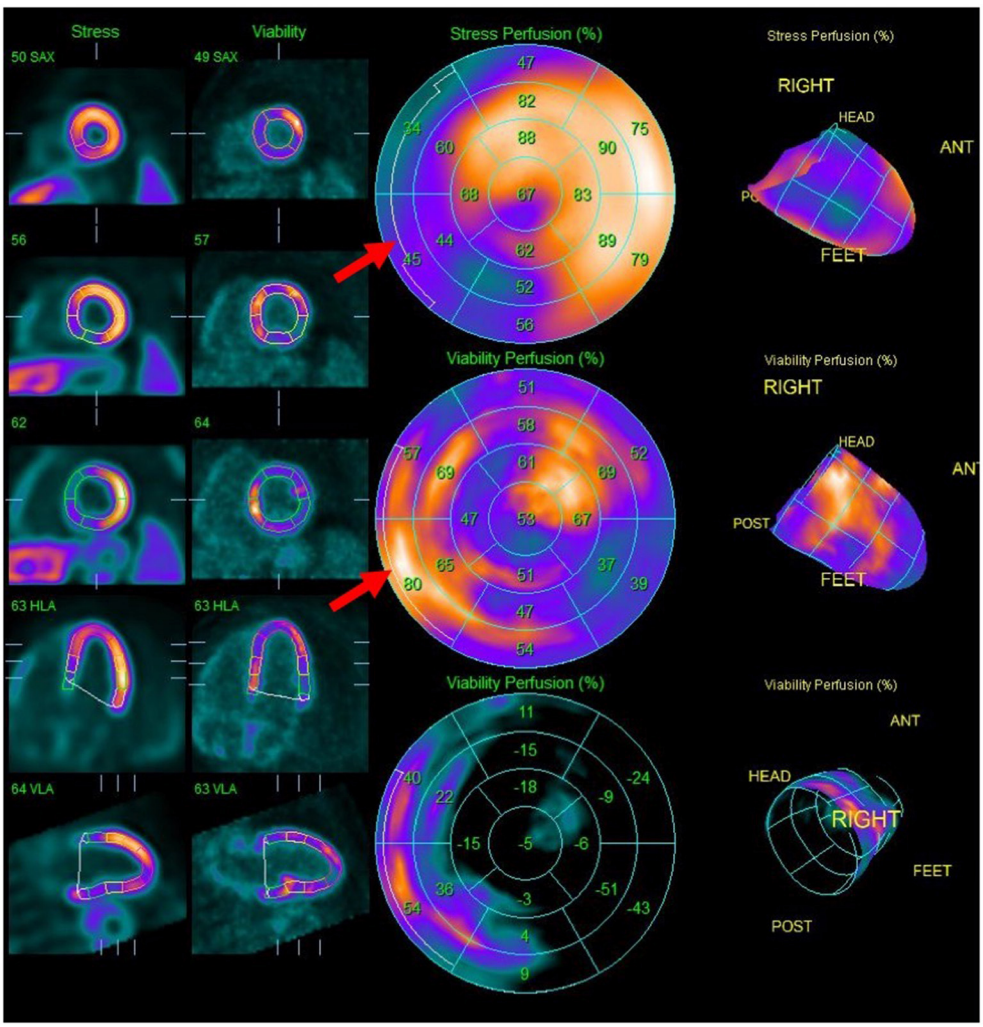

FIGURE 5 | Splash images demonstrating moderate to severe transmural perfusion abnormality mainly involving the mid-base septal and inferoseptal wall (upper row), corresponding to areas of increased FDG uptake (middle row), denoting significant inflammation causing decreased perfusion ("mismatch" pattern). Note additional sites of increased FDG uptake without corresponding decreased perfusion such as in the mid-apical anterolateral wall.

ranging from 39 to 100% (62, 67). One meta-analysis of 7 studies yielded a pooled sensitivity of 89% (95% CI 79–96%) and specificity of 78% (95% CI 68–86%) (61). However, multiple authors note that estimations of specificity may be limited by the use of JMHW criteria as the standard in multiple studies, which have lower sensitivity for CS than FDG-PET (62, 67). Other diagnoses to consider in the setting of positive FDG uptake include myocardial ischemia with hibernating myocardium, other forms of myocarditis or systemic rheumatologic diseases associated with myocardial inflammation, or some arrhythmogenic cardiomyopathies (67, 71, 72).

Important for ensuring high diagnostic accuracy of FDG-PET is effective suppression of physiologic myocardial glucose uptake by shifting cardiomyocytes preferentially to fatty acid metabolism (67). Suboptimal patient preparation may lead to diffuse FDG uptake, limiting visualization of active sarcoid lesions or leading to false positive results (61, 62, 73). The most recent joint SNMMI/ASNC expert consensus statement recommendations include two high-fat (>35 g), low carbohydrate (<3 g) meals the day prior to the study followed by a 4–12 period of fasting; an 18 hour fast is an alternative option (67). The adjunctive use of unfractionated heparin immediately prior to the scan has been described (74) but was not specifically recommended in the SNMMI/ASNC document (67). A recent study investigating the use of a structured preparation protocol adhering to the new SNMMI/ASNC guidelines compared to a former less-rigorous protocol showed that a strict high-fat, low-carbohydrate diet with prolonged fasting, compliance reinforcement, and detailed instructions was highly successful in suppressing physiologic ^{18}F-FDG uptake (91% among the structured protocol group vs. 78% in the standard protocol group, $P < 0.001$) (73).

Given the limitations posed by the use of ^{18}F-FDG in the setting of physiologic uptake by cardiac myocytes, alternative radiotracers have been explored to improve the specificity of PET imaging in CS (75–81). One novel radiotracer of particular interest is a radiolabeled somatostatin analog (^{68}Ga-somatostatin analog), which targets the somatostatin receptor (SSTR) 2 subtype that is highly expressed in sarcoid granulomas but not in normal cardiac myocytes (75). Early feasibility studies suggest somatostatin analogs may increase diagnostic accuracy compared to FDG-PET (77, 78); however, more data are needed to guide the use of this modality.

When high quality imaging can be obtained, serial FDG-PET imaging may be used to assess response to treatment and to guide management of CS. One single-center study of 32 patients with CS who underwent FDG-PET imaging before and after corticosteroid therapy demonstrated that 81% of patients had a decrease in the extent and 88% experienced a decrease in the intensity of FDG uptake on follow-up imaging (82). A separate study of 34 patients with CS who collectively underwent 128 FDG-PET scans per an institutional management protocol found that 94 (73%) of scans led to a change in therapy and 42 (33%) resulted in a decrease in prednisone dose (83). Several retrospective studies have now demonstrated the role of serial FDG-PET in guiding immunosuppression management, specifically the ability to taper corticosteroids while maintaining good cardiac disease control (83–85). While SNMMI/ASNC guidance recommends assessing change in intensity and extent of FDG uptake on follow-up studies (67), it is also worth noting that perfusion defects, which may be related to microvascular compression and local ischemia, may also resolve with treatment (62, 67). The ongoing CHASM-CS randomized clinical trial of combination prednisone/methotrexate compared to prednisone alone for initial treatment of active CS includes perfusion defects on 6-month PET scan as the primary endpoint (86). Experts recommend repeat FDG-PET imaging in a 3–6 month interval after initiation of immunosuppressive therapy to assess for improvement (which may guide tapering of corticosteroids and minimize drug related side effects) vs. stability to worsening of inflammation (possibly prompting escalation of therapy) (6, 11, 62, 68).

For patients with CS, FDG-PET imaging also conveys important prognostic information. Blankstein et al. found that among 118 patients referred for FDG-PET for evaluation of possible CS, the presence of both perfusion defects and FDG uptake was associated with increased incidence of death or sustained ventricular tachycardia (HR 3.94, 95% CI 1.50–10.31, $P < 0.01$) compared to patients with normal imaging (87). Notably, right ventricular FDG uptake was also associated with adverse events (HR 4.22, 95% CI 1.87–9.50, $P < 0.001$). Similarly, among 67 patients with CS who were referred for FDG-PET, intensity of FDG uptake (as quantified by standardized uptake values, SUV) was associated with increased incidence of cardiac events (88). Other studies have noted that decrease in inflammation on serial FDG-PET scans is associated with improvement in LVEF (89, 90). The longer-term implications however of mildly persistent FDG uptake or perfusion defects remain unknown in patients with otherwise clinically controlled CS.

IMAGING IN CS: A MULTIMODALITY APPROACH

The pathophysiology of CS lends itself to the complementary imaging modalities of echocardiography, CMR and FDG-PET for purposes of diagnosis, management, and prognostication. A proposed algorithm for imaging in CS is provided in **Figure 1**. Echocardiography is highly accessible and allows an initial, urgent assessment of ventricular function, valvular disease or pericardial effusion that may point toward specific immediate management approaches. Advanced cardiac imaging allows for more nuanced CS assessment. Focal inflammation identified and quantified by FDG uptake may be prominent in early stages of the disease, whereas fibrosis occurring later in the disease course may be better assessed by superior spatial resolution of CMR. Several studies have evaluated the utility of sequential (38, 91, 92) or hybrid (93–95) CMR/PET imaging for diagnosis of CS. In the largest of these studies, 107 patients underwent both CMR and FDG-PET for evaluation of known or suspected CS and imaging findings were integrated to determine the combined likelihood of CS (no CS, possible CS, probable CS, or highly probable CS) (38). When FDG-PET results were added to findings from CMR, 48 patients (45%) were reclassified as

TABLE 1 | Imaging modalities for the diagnosis and management of cardiac sarcoidosis.

Imaging modality	Techniques	Findings	Clinical role	Limitations
TTE	2D TTE STE	• Left or right ventricular systolic/diastolic dysfunction • Ventricular dilatation • Abnormal septal wall thickness • LVH • Wall motion abnormalities • Ventricular aneurysm • Pericardial effusion • Valvular dysfunction • Reduced GLS	• Initial screening of patients with ECS • Serial monitoring of LV function (for purpose of GDMT, ICD, AHF therapy) • Reduced GLS associated with adverse cardiac events	• Limited sensitivity/specificity
CMR	LGE T1/T2-mapping	• Midwall/ subepicardial LGE • Patchy, non-coronary distribution • Basal septum most commonly involved	• CS diagnosis (subacute/chronic) • Evaluation of LV morphology/function • Risk stratification (LGE associated with VA/SCD)	• May be less specific for CS • Limited sensitivity in early disease • Challenging in patients with devices • Gadolinium contraindicated in advanced CKD
FDG-PET	^{18}F-FDG MPI Hybrid PET/CT Whole body PET	• Focal or focal-on-diffuse FDG uptake • FDG-avid extracardiac lesions • Perfusion defects • FDG/perfusion mismatch	• CS diagnosis (acute/chronic) • Serial imaging to assess response to/titrate of IS • Assess ECS activity • Identify non-cardiac biopsy sites • Risk stratification (FDG uptake associated with death/VA)	• Patient preparation required for adequate glucose suppression • May be less specific for CS

AHF, advanced heart failure; CKD, chronic kidney disease; CMR, cardiac magnetic resonance imaging; ECS, extracardiac sarcoidosis; GDMT, guideline-directed medical therapy; GLS, global longitudinal strain; ICD, implantable cardioverter-defibrillator; IS, immunosuppression; LGE, late gadolinium enhancement; LVH, left ventricular hypertrophy; MPI, myocardial perfusion imaging; FDG-PET, ^{18}F-fluorodeoxyglucose position emission tomography; SCD, sudden cardiac death; STE, speckle-tracking echocardiography; TTE, transthoracic echocardiogram; VA, ventricular arrhythmia.

having a higher or lower probability of CS compared to results from a single imaging study (38). Similarly, a small study of patients undergoing hybrid CMR/PET imaging resulted in high quality ^{18}F-FDG and CMR images, demonstrating the value of this modality for diagnosis, prognosis, and potentially cost-saving (95). Notably, both FDG-PET and CMR are included among HRS criteria for diagnosis of CS and carry a class IIa recommendation for performing in patients with at least one abnormality detected on initial cardiac screening (history, ECG, and TTE) (9). However, given the high negative predictive value, CMR might serve as the best initial testing option—in many patients, a normal CMR might be sufficient to obviate the need for further testing (62, 68). By JMHW criteria, a clinical diagnosis of CS might be made with abnormalities on TTE and CMR in the presence of one major clinical criterion (advanced AV block, thinning of the basal interventricular septum, positive cardiac Gallium-67 uptake, or LVEF $<$ 50%) (8). Interstitial fibrosis or monocyte infiltration on endomyocardial biopsy may also comprise a minor criterion, with identification of noncaseating granulomas confirming a histological diagnosis; however, the yield of endomyocardial biopsy is often limited (9). FDG-PET is excluded from these guidelines, with potential implications for the sensitivity of JMHW criteria for diagnosing CS (62, 67). Importantly, advanced imaging modalities of CMR and FDG-PET are both incorporated into the more recent Japanese Circulation Society guidelines as major criteria for a diagnosis of CS (12), reflecting the value of these tests in evaluating patients with suspected CS.

Beyond confirming a diagnosis, the management of CS also relies heavily on multimodality imaging. As previously detailed, FDG-PET has shown to be an effective tool for monitoring response to and tailoring immunosuppression. Serial echocardiographic evaluation is invaluable for longitudinal assessment of LV function to guide GDMT and, if needed, identify candidates for advanced therapies including left ventricular assist devices and orthotopic heart transplant (4, 5, 11). Another important decision point pertains to ICD therapy and is again highly reliant on imaging findings to guide management. Echocardiography and CMR are essential for risk stratification of patients with CS to classify those at highest risk of sudden cardiac death (4, 9, 54).

CONCLUSIONS

CS is a disease of complex pathophysiology that is well-suited to a multimodality imaging approach for purposes of diagnosis, treatment, and prognostication. Together, TTE, CMR and FDG-PET provide complementary clinical information that allows for a comprehensive understanding of the extent of cardiac involvement for each individual patient (**Table 1**). Ongoing studies involving more advanced imaging techniques—including speckle-tracking echocardiography and hybrid CMR/PET imaging—may provide additional insights. Further studies are needed to best employ these more advanced modalities for optimal management of CS.

AUTHOR CONTRIBUTIONS

NG and AW conceived the design of the paper. AW completed the initial manuscript draft for review. ES assisted with design of figures and made critical revisions to the paper. NG, JC, MM, and AH made critical revisions to the intellectual content of the paper. All authors approved the final manuscript for publication.

REFERENCES

1. Iannuzzi MC, Rybicki BA, Teirstein AS. Sarcoidosis. *N Engl J Med.* (2007) 357:2153–65. doi: 10.1056/NEJMra071714
2. Aggarwal NR, Snipelisky D, Young PM, Gersh BJ, Cooper LT, Chareonthaitawee P. Advances in imaging for diagnosis and management of cardiac sarcoidosis. *Eur Heart J Cardiovasc Imaging.* (2015) 16:949–58. doi: 10.1093/ehjci/jev142
3. Drent M, Crouser ED, Grunewald J. Challenges of Sarcoidosis and Its Management. *Longo DL, ed N Engl J Med.* (2021) 385:1018–32. doi: 10.1056/NEJMra2101555
4. Birnie DH, Nery PB, Ha AC, Beanlands RSB. Cardiac Sarcoidosis. *J Am Coll Cardiol.* (2016) 68:411–21. doi: 10.1016/j.jacc.2016.03.605
5. Gilotra N, Okada D, Sharma A, Chrispin J. Management of Cardiac Sarcoidosis in 2020. *Arrhythm Electrophysiol Rev.* (2020) 9:182–8. doi: 10.15420/aer.2020.09
6. Trivieri MG, Spagnolo P, Birnie D, Liu P, Drake W, Kovacic JC, et al. Challenges in Cardiac and Pulmonary Sarcoidosis: JACC State-of-the-Art Review. *J Am Coll Cardiol.* (2020) 76:1878–901. doi: 10.1016/j.jacc.2020.08.042
7. Kim JS, Judson MA, Donnino R, Gold M, Cooper LT, Prystowsky EN, et al. Cardiac sarcoidosis. *Am Heart J.* (2009) 157:9–21. doi: 10.1016/j.ahj.2008.09.009
8. Hiraga H, Yuwai K, Hiroe M. Diagnostic standard and guidelines for sarcoidosis. *Jpn J Sarcoidosis Granulomatous Disord.* (2007) 27:102.
9. Birnie DH, Sauer WH, Bogun F, Cooper JM, Culver DA, Duvernoy CS, et al. HRS expert consensus statement on the diagnosis and management of arrhythmias associated with cardiac sarcoidosis. *Hear Rhythm.* (2014) 11:1304–23. doi: 10.1016/j.hrthm.2014.03.043
10. Birnie DH, Kandolin R, Nery PB, Kupari M. Cardiac manifestations of sarcoidosis: Diagnosis and management. *Eur Heart J.* (2017) 38:2663–70. doi: 10.1093/eurheartj/ehw328
11. Gilotra NA, Griffin JM, Pavlovic N, Houston BA, Chasler J, Goetz C, et al. Sarcoidosis-Related Cardiomyopathy: Current Knowledge, Challenges, and Future Perspectives State-of-the-Art Review. *J Card Fail.* (2021) 00:1–19. doi: 10.1016/j.cardfail.2021.06.016
12. Terasaki F, Yoshinaga K. New Guidelines for Diagnosis of Cardiac Sarcoidosis in Japan. *Ann Nucl Cardiol.* (2017) 3:42–5. doi: 10.17996/anc.17-00042
13. Burstow DJ, Tajik AJ, Bailey KR, DeRemee RA, Taliercio CP. Two-dimensional echocardiographic findings in systemic sarcoidosis. *Am J Cardiol.* (1989) 63:478–82. doi: 10.1016/0002-9149(89)90323-8
14. Skold CM, Larsen FF, Rasmussen E, Pehrsson SK, Eklund AG. Determination of cardiac involvement in sarcoidosis by magnetic resonance imaging and Doppler echocardiography. *J Intern Med.* (2002) 252:465–71. doi: 10.1046/j.1365-2796.2002.01058.x
15. Houston BA, Mukherjee M. Cardiac sarcoidosis: clinical manifestations, imaging characteristics, and therapeutic approach. *Clin Med Insights Cardiol.* (2014) 8s1:CMC.S15713. doi: 10.4137/CMC.S15713
16. Nagueh SF, Smiseth OA, Appleton CP, Byrd BF, Dokainish H, Edvardsen T, et al. Recommendations for the evaluation of left ventricular diastolic function by echocardiography: an update from the american society of echocardiography and the european association of cardiovascular imaging. *J Am Soc Echocardiogr.* (2016) 29:277–314. doi: 10.1016/j.echo.2016.01.011
17. Lewin RF, Mor R, Spitzer S, Arditti A, Hellman C, Agmon J. Echocardiographic evaluation of patients with systemic sarcoidosis. *Am Heart J.* (1985) 110:116–22. doi: 10.1016/0002-8703(85)90524-1
18. Yazaki Y, Isobe M, Hiramitsu S, Morimoto S, Hiroe M, Omichi C, et al. Comparison of clinical features and prognosis of cardiac sarcoidosis and idiopathic dilated cardiomyopathy. *Am J Cardiol.* (1998) 82:537–40. doi: 10.1016/S0002-9149(98)00377-4
19. Mehta D, Lubitz SA, Frankel Z, Wisnivesky JP, Einstein AJ, Goldman M, et al. Cardiac involvement in patients with sarcoidosis: Diagnostic and prognostic value of outpatient testing. *Chest.* (2008) 133:1426–35. doi: 10.1378/chest.07-2784
20. Collier P, Phelan D, Klein A, A. Test in Context: Myocardial Strain Measured by Speckle-Tracking Echocardiography. *J Am Coll Cardiol.* (2017) 69:1043–56. doi: 10.1016/j.jacc.2016.12.012
21. Moharram MA, Lamberts RR, Whalley G, Williams MJA, Coffey S. Myocardial tissue characterisation using echocardiographic deformation imaging. *Cardiovasc Ultrasound.* (2019) 17:1–11. doi: 10.1186/s12947-019-0176-9
22. Orii M, Imanishi T, Akasaka T. Assessment of cardiac sarcoidosis with advanced imaging modalities. *Biomed Res Int.* (2014) 2014:897956. doi: 10.1155/2014/897956
23. Di Stefano C, Bruno G, Arciniegas Calle MC, Acharya GA, Fussner LM, Ungprasert P, et al. Diagnostic and predictive value of speckle tracking echocardiography in cardiac sarcoidosis. *BMC Cardiovasc Disord.* (2020) 20:1–10. doi: 10.1186/s12872-019-01323-0
24. Joyce E, Ninaber MK, Katsanos S, Debonnaire P, Kamperidis V, Bax JJ, et al. Subclinical left ventricular dysfunction by echocardiographic speckle-tracking strain analysis relates to outcome in sarcoidosis. *Eur J Heart Fail.* (2015) 17:51–62. doi: 10.1002/ejhf.205
25. Bayat F, Fahimi A, Tavana S, Tabary M, Khaheshi I. Subclinical involvement of the heart and its associated factors in patients with sarcoidosis with normal systolic function using 2D speckle tracking. *Echocardiography.* (2020) 37:41–6. doi: 10.1111/echo.14572
26. Kusunose K, Fujiwara M, Yamada H, Nishio S, Saijo Y, Yamada N, et al. Deterioration of biventricular strain is an early marker of cardiac involvement in confirmed sarcoidosis. *Eur Heart J Cardiovasc Imaging.* (2020) 21:796–804. doi: 10.1093/ehjci/jez235
27. Schouver ED, Moceri P, Doyen D, Tieulie N, Queyrel V, Baudouy D, et al. Early detection of cardiac involvement in sarcoidosis with 2-dimensional speckle-tracking echocardiography. *Int J Cardiol.* (2017) 227:711–6. doi: 10.1016/j.ijcard.2016.10.073
28. Barssoum K, Altibi AM, Rai D, Kumar A, Kharsa A, Chowdhury M, et al. Speckle tracking echocardiography can predict subclinical myocardial involvement in patients with sarcoidosis: A meta-analysis. *Echocardiography.* (2020) 37:2061–70. doi: 10.1111/echo.14886
29. Yancy CW, Jessup M, Bozkurt B, Butler J, Casey DE, Colvin MM, et al. 2017 ACC/AHA/HFSA Focused Update of the 2013 ACCF/AHA Guideline for the Management of Heart Failure: A Report of the American College of Cardiology/American Heart Association Task Force on Clinical Practice Guidelines and the Heart Failure Society of Amer. *Circulation.* (2017) 136:e137–61. doi: 10.1161/CIR.0000000000000509
30. Liu JE, Barac A, Thavendiranathan P, Scherrer-Crosbie M. Strain Imaging in Cardio-Oncology. *JACC CardioOncol.* (2020) 2:677–89. doi: 10.1016/j.jaccao.2020.10.011
31. Kalam K, Marwick TH. Role of cardioprotective therapy for prevention of cardiotoxicity with chemotherapy: A systematic review and meta-analysis. *Eur J Cancer.* (2013) 49:2900–9. doi: 10.1016/j.ejca.2013.04.030
32. Negishi K, Negishi T, Haluska BA, Hare JL, Plana JC, Marwick TH. Use of speckle strain to assess left ventricular responses to cardiotoxic chemotherapy and cardioprotection. *Eur Hear J Cardiovasc Imaging.* (2014) 15:324–31. doi: 10.1093/ehjci/jet159
33. Patel AR, Kramer CM. Role of Cardiac Magnetic Resonance in the Diagnosis and Prognosis of Nonischemic Cardiomyopathy. *JACC Cardiovasc Imaging.* (2017) 10:1180–93. doi: 10.1016/j.jcmg.2017.08.005
34. Smedema JP, Snoep G, Van Kroonenburgh MP, Van Geuns RJ, Dassen WR, Gorgels AP, et al. Evaluation of the accuracy of gadolinium-enhanced

cardiovascular magnetic resonance in the diagnosis of cardiac sarcoidosis. *J Am Coll Cardiol.* (2005) 45:1683–90. doi: 10.1016/j.jacc.2005.01.047
35. Patel MR, Cawley PJ, Heitner JF, Klem I, Parker MA, Jaroudi WA, et al. Detection of Myocardial Damage in Patients With Sarcoidosis. *Circulation.* (2009) 120:1969–77. doi: 10.1161/CIRCULATIONAHA.109.851352
36. Sano M, Satoh H, Suwa K, Saotome M, Urushida T, Katoh H, et al. Intra-cardiac distribution of late gadolinium enhancement in cardiac sarcoidosis and dilated cardiomyopathy. *World J Cardiol.* (2016) 8:496. doi: 10.4330/wjc.v8.i9.496
37. Tezuka D, Terashima M, Kato Y, Toriihara A, Hirasawa K, Sasaoka T, et al. Clinical characteristics of definite or suspected isolated cardiac sarcoidosis: Application of cardiac magnetic resonance imaging and 18F-fluoro-2-deoxyglucose positron-emission tomography/computerized tomography. *J Card Fail.* (2015) 21:313–22. doi: 10.1016/j.cardfail.2014.12.004
38. Vita T, Okada DR, Veillet-Chowdhury M, Bravo PE, Mullins E, Hulten E, et al. Complementary value of cardiac magnetic resonance imaging and positron emission tomography/computed tomography in the assessment of cardiac sarcoidosis. *Circ Cardiovasc Imaging.* (2018) 11:e007030. doi: 10.1161/CIRCIMAGING.117.007030
39. Nagao S, Watanabe H, Sobue Y, Kodama M, Tanaka J, Tanabe N, et al. Electrocardiographic abnormalities and risk of developing cardiac events in extracardiac sarcoidosis. *Int J Cardiol.* (2015) 189:1–5. doi: 10.1016/j.ijcard.2015.03.175
40. Kouranos V, Tzelepis GE, Rapti A, Mavrogeni S, Aggeli K, Douskou M, et al. Complementary role of CMR to conventional screening in the diagnosis and prognosis of cardiac sarcoidosis. *JACC Cardiovasc Imaging.* (2017) 10:1437–47. doi: 10.1016/j.jcmg.2016.11.019
41. Hundley WG, Bluemke DA, Finn JP, Flamm SD, Fogel MA, Friedrich MG, et al. ACCF/ACR/AHA/NASCI/SCMR 2010 expert consensus document on cardiovascular magnetic resonance. A Report of the American College of Cardiology Foundation Task Force on Expert Consensus Documents. *J Am Coll Cardiol.* (2010) 55:2614–62. doi: 10.1016/j.jacc.2009.11.011
42. Hulten E, Aslam S, Osborne M, Abbasi S, Bittencourt MS, Blankstein R. Cardiac sarcoidosis-state of the art review. *Cardiovasc Diagn Ther.* (2016) 6:50–63. doi: 10.3978/j.issn.2223-3652.2015.12.13
43. Tadic M, Cuspidi C, Saeed S, Milojevic B, Milojevic IG. The role of cardiac magnetic resonance in diagnosis of cardiac sarcoidosis. *Heart Fail Rev.* (2021) 26:653–60. doi: 10.1007/s10741-020-10035-z
44. Puntmann VO, Isted A, Hinojar R, Foote L, Carr-White G, Nagel E. T1 and T2 Mapping in recognition of early cardiac involvement in systemic sarcoidosis. *Radiology.* (2017) 285:63–72. doi: 10.1148/radiol.2017162732
45. Dabir D, Meyer D, Kuetting D, Luetkens J, Homsi R, Pizarro C, et al. Diagnostic value of cardiac magnetic resonance strain analysis for detection of cardiac sarcoidosis. *RoFo Fortschritte auf dem Gebiet der Rontgenstrahlen und der Bildgeb Verfahren.* (2018) 190:712–21. doi: 10.1055/a-0598-5099
46. Okada DR, Xie E, Assis F, Smith J, Derakhshan A, Gowani Z, et al. Regional abnormalities on cardiac magnetic resonance imaging and arrhythmic events in patients with cardiac sarcoidosis. *J Cardiovasc Electrophysiol.* (2019) 30:1967–76. doi: 10.1111/jce.14082
47. Nadel J, Lancefield T, Voskoboinik A, Taylor AJ. Late gadolinium enhancement identified with cardiacmagnetic resonance imaging in sarcoidosis patients is associated with long-term ventricular arrhythmia and sudden cardiac death. *Eur Heart J Cardiovasc Imaging.* (2015) 16:634–41. doi: 10.1093/ehjci/jeu294
48. Greulich S, Deluigi CC, Gloekler S, Wahl A, Zürn C, Kramer U, et al. CMR imaging predicts death and other adverse events in suspected cardiac sarcoidosis. *JACC Cardiovasc Imaging.* (2013) 6:501–11. doi: 10.1016/j.jcmg.2012.10.021
49. Hulten E, Agarwal V, Cahill M, Cole G, Vita T, Parrish S, et al. Presence of late gadolinium enhancement by cardiac magnetic resonance among patients with suspected cardiac sarcoidosis is associated with adverse cardiovascular prognosis. *Circ Cardiovasc Imaging.* (2016) 9:e005001. doi: 10.1161/CIRCIMAGING.116.005001
50. Coleman GC, Shaw PW, Balfour PC, Gonzalez JA, Kramer CM, Patel AR, et al. Prognostic value of myocardial scarring on CMR in patients with cardiac sarcoidosis. *JACC Cardiovasc Imaging.* (2017) 10:411–20. doi: 10.1016/j.jcmg.2016.05.009
51. Chiu CZ, Nakatani S, Zhang G, Tachibana T, Ohmori F, Yamagishi M, et al. Prevention of left ventricular remodeling by long-term corticosteroid therapy in patients with cardiac sarcoidosis. *Am J Cardiol.* (2005) 95:143–6. doi: 10.1016/j.amjcard.2004.08.083
52. Kandolin R, Lehtonen J, Airaksinen J, Vihinen T, Miettinen H, Ylitalo K, et al. Cardiac Sarcoidosis. *Circulation.* (2015) 131:624–32. doi: 10.1161/CIRCULATIONAHA.114.011522
53. Gowani Z, Habibi M, Okada DR, Smith J, Derakhshan A, Zimmerman SL, et al. Utility of cardiac magnetic resonance imaging versus cardiac positron emission tomography for risk stratification for ventricular arrhythmias in patients with cardiac sarcoidosis. *Am J Cardiol.* (2020) 134:123–9. doi: 10.1016/j.amjcard.2020.08.007
54. Al-Khatib SM, Stevenson WG, Ackerman MJ, Bryant WJ, Callans DJ, Curtis AB, et al. 2017 AHA/ACC/HRS Guideline for management of patients with ventricular arrhythmias and the prevention of sudden cardiac death: a Report of the American College of Cardiology/American Heart Association Task Force on Clinical Practice Guidelines and the Heart Rhythm Society. *Heart Rhythm.* (2018) 15:e73–189. doi: 10.1016/j.hrthm.2017.10.036
55. Velangi PS, Chen KHA, Kazmirczak F, Okasha O, Von Wald L, Roukoz H, et al. Right ventricular abnormalities on cardiovascular magnetic resonance imaging in patients with sarcoidosis. *JACC Cardiovasc Imaging.* (2020) 13:1395–405. doi: 10.1016/j.jcmg.2019.12.011
56. Cipriani A, Bauce B, De Lazzari M, Rigato I, Bariani R, Meneghin S, et al. Arrhythmogenic right ventricular cardiomyopathy: Characterization of left ventricular phenotype and differential diagnosis with dilated cardiomyopathy. *J Am Heart Assoc.* (2020) 9:1–16. doi: 10.1161/JAHA.119.014628
57. Crouser ED, Ono C, Tran T, He X, Raman S V. Improved detection of cardiac sarcoidosis using magnetic resonance with myocardial T2 mapping. *Am J Respir Crit Care Med.* (2014) 189:109–12. doi: 10.1164/rccm.201309-1668LE
58. Zhang J, Li Y, Xu Q, Xu B, Wang H. Cardiac magnetic resonance imaging for diagnosis of cardiac sarcoidosis: a meta-analysis. *Can Respir J.* (2018) 2018:7457369. doi: 10.1155/2018/7457369
59. Nazarian S, Hansford R, Rahsepar AA, Weltin V, McVeigh D, Gucuk Ipek E, et al. Safety of magnetic resonance imaging in patients with cardiac devices. *N Engl J Med.* (2017) 377:2555–64. doi: 10.1056/NEJMoa1604267
60. Russo RJ, Costa HS, Silva PD, Anderson JL, Arshad A, Biederman RW, et al. Assessing the risks associated with mri in patients with a pacemaker or defibrillator. *N Engl J Med.* (2017) 376:755–64. doi: 10.1056/NEJMoa1603265
61. Youssef G, Leung E, Mylonas I, Nery P, Williams K, Wisenberg G, et al. The use of 18F-FDG PET in the diagnosis of cardiac sarcoidosis: a systematic review and metaanalysis including the Ontario experience. *J Nucl Med.* (2012) 53:241–8. doi: 10.2967/jnumed.111.090662
62. Slart RHJA, Glaudemans AWJM, Lancellotti P, Hyafil F, Blankstein R, Schwartz RG, et al. A joint procedural position statement on imaging in cardiac sarcoidosis: from the Cardiovascular and Inflammation & Infection Committees of the European Association of Nuclear Medicine, the European Association of Cardiovascular Imaging, and the American. *J Nucl Cardiol.* (2018) 25:298–319. doi: 10.1007/s12350-017-1043-4
63. Koiwa H, Tsujino I, Ohira H, Yoshinaga K, Otsuka N, Nishimura M. Imaging of cardiac sarcoid lesions using fasting cardiac 18F-fluorodeoxyglucose positron emission tomography: An autopsy case. *Circulation.* (2010) 122:535–6. doi: 10.1161/CIRCULATIONAHA.110.952184
64. Brudin LH, Valind S-O, Rhodes CG, Pantin CF, Sweatman M, Jones T, et al. Fluorine-18 deoxyglucose uptake in sarcoidosis measured with positron emission tomography. *Eur J Nucl Med.* (1994) 21:297–305. doi: 10.1007/BF00947964
65. Lewis PJ, Salama A. Uptake of fluorine-18-fluorodeoxyglucose in sarcoidosis. *J Nucl Med.* (1994) 35:1647–9. http://www.ncbi.nlm.nih.gov/pubmed/7931664
66. Ahmadian A, Brogan A, Berman J, Sverdlov AL, Mercier G, Mazzini M, et al. Quantitative interpretation of FDG PET/CT with myocardial perfusion imaging increases diagnostic information in the evaluation of cardiac sarcoidosis. *J Nucl Cardiol.* (2014) 21:925–39. doi: 10.1007/s12350-014-9901-9
67. Chareonthaitawee P, Beanlands RS, Chen W, Dorbala S, Miller EJ, Murthy VL, et al. Joint SNMMI-ASNC expert consensus document on the role of 18F-FDG PET/CT in carDiac sarcoid detection and therapy monitoring writing group. *J Nucl Med.* (2017) 58:1341–53. doi: 10.2967/jnumed.117.196287

68. Blankstein R, Waller AH. Evaluation of known or suspected cardiac sarcoidosis. *Circ Cardiovasc Imaging.* (2016) 9:e000867. doi: 10.1161/CIRCIMAGING.113.000867
69. Keijsers RGM, Grutters JC. In which patients with sarcoidosis is FDG PET/CT Indicated? *J Clin Med.* (2020) 9:890. doi: 10.3390/jcm9030890
70. Okumura W, Iwasaki T, Toyama T, Iso T, Arai M, Oriuchi N, et al. Usefulness of fasting 18F-FDG PET in identification of cardiac sarcoidosis. *J Nucl Med.* (2004) 45:1989–98. Available online at: http://jnm.snmjournals.org/cgi/reprint/45/12/1989%0Ahttp://ovidsp.ovid.com/ovidweb.cgi?T=JS&PAGE=reference&D=emed8&NEWS=N&AN=47611626
71. Protonotarios A, Wicks E, Ashworth M, Stephenson E, Guttmann O, Savvatis K, et al. Prevalence of 18F-fluorodeoxyglucose positron emission tomography abnormalities in patients with arrhythmogenic right ventricular cardiomyopathy. *Int J Cardiol.* (2019) 284:99–104. doi: 10.1016/j.ijcard.2018.10.083
72. Tung R, Bauer B, Schelbert H, Lynch JP, Auerbach M, Gupta P, et al. Incidence of abnormal positron emission tomography in patients with unexplained cardiomyopathy and ventricular arrhythmias: the potential role of occult inflammation in arrhythmogenesis. *Hear Rhythm.* (2015) 12:2488–98. doi: 10.1016/j.hrthm.2015.08.014
73. Christopoulos G, Jouni H, Acharya GA, Blauwet LA, Kapa S, Bois J, et al. Suppressing physiologic 18-fluorodeoxyglucose uptake in patients undergoing positron emission tomography for cardiac sarcoidosis: the effect of a structured patient preparation protocol. *J Nucl Cardiol.* (2021) 28:661–71. doi: 10.1007/s12350-019-01746-4
74. Masuda A, Naya M, Manabe O, Magota K, Yoshinaga K, Tsutsui H, et al. Administration of unfractionated heparin with prolonged fasting could reduce physiological 18F-fluorodeoxyglucose uptake in the heart. *Acta radiol.* (2016) 57:661–8. doi: 10.1177/0284185115600916
75. Saric P, Young K, Rodriguez-Porcel M, Chareonthaitawee P, PET. Imaging in cardiac sarcoidosis: a narrative review with focus on novel PET tracers. *Pharmaceuticals.* (2021) 14:1286. doi: 10.3390/ph14121286
76. Kircher M, Lapa C. Novel noninvasive nuclear medicine imaging techniques for cardiac inflammation. *Curr Cardiovasc Imaging Rep*. (2017) 10:6. doi: 10.1007/s12410-017-9400-x
77. Lapa C, Reiter T, Kircher M, Schirbel A, Werner RA, Pelzer T, et al. Somatostatin receptor based PET/CT in patients with the suspicion of cardiac sarcoidosis: an initial comparison to cardiac MRI. *Oncotarget*. 7:77807–14. doi: 10.18632/oncotarget.12799
78. Gormsen LC, Haraldsen A, Kramer S, Dias AH, Kim WY, Borghammer P. A dual tracer 68Ga-DOTANOC PET/CT and 18F-FDG PET/CT pilot study for detection of cardiac sarcoidosis. *EJNMMI Res.* (2016) 6:52. doi: 10.1186/s13550-016-0207-6
79. Reiter T, Werner RA, Bauer WR, Lapa C. Detection of cardiac sarcoidosis by macrophage-directed somatostatin receptor 2-based positron emission tomography/computed tomography. *Eur Heart J.* (2015) 36:2404. doi: 10.1093/eurheartj/ehv278
80. Manabe O, Hirata K, Shozo O, Shiga T, Uchiyama Y, Kobayashi K, et al. 18F-fluoromisonidazole (FMISO) PET may have the potential to detect cardiac sarcoidosis. *J Nucl Cardiol.* (2017) 24:329–31. doi: 10.1007/s12350-016-0495-2
81. Norikane T, Yamamoto Y, Maeda Y, Noma T, Nishiyama Y. 18F-FLT PET imaging in a patient with sarcoidosis with cardiac involvement. *Clin Nucl Med.* (2015) 40:433–4. doi: 10.1097/RLU.0000000000000653
82. Okada DR, Saad E, Wand AL, Griffin JM, Kasper EK, Chen EH, et al. Effect of Corticosteroid Dose and Duration on 18-Fluorodeoxyglucose Positron Emission Tomography in Cardiac Sarcoidosis. *JACC Cardiovasc Imaging.* (2020) 13:1280–2. doi: 10.1016/j.jcmg.2019.12.013
83. Ning N, Guo HH, Iagaru A, Mittra E, Fowler M, Witteles R. Serial cardiac FDG-PET for the diagnosis and therapeutic guidance of patients with cardiac sarcoidosis. *J Card Fail.* (2019) 25:307–11. doi: 10.1016/j.cardfail.2019.02.018
84. Griffin JM, Chasler J, Wand AL, Okada DR, Smith JN, Saad E, et al. Management of cardiac sarcoidosis using mycophenolate mofetil as a steroid-sparing agent. *J Card Fail.* (2021) 27:1348–58. doi: 10.1016/j.cardfail.2021.06.010
85. Gilotra NA, Wand AL, Pillarisetty A, Devraj M, Pavlovic N, Ahmed S, et al. Clinical and imaging response to tumor necrosis factor alpha inhibitors in treatment of cardiac sarcoidosis: a multicenter experience. *J Card Fail.* (2021) 27:83–91. doi: 10.1016/j.cardfail.2020.08.013
86. Birnie D, Beanlands RSB, Nery P, Aaron SD, Culver DA, DeKemp RA, et al. Cardiac Sarcoidosis multi-center randomized controlled trial (CHASM CS- RCT). *Am Heart J.* (2020) 220:246–52. doi: 10.1016/j.ahj.2019.10.003
87. Blankstein R, Osborne M, Naya M, Waller A, Kim CK, Murthy VL, et al. Cardiac positron emission tomography enhances prognostic assessments of patients with suspected cardiac sarcoidosis. *J Am Coll Cardiol.* (2014) 63:329–36. doi: 10.1016/j.jacc.2013.09.022
88. Flores RJ, Flaherty KR, Jin Z, Bokhari S. The prognostic value of quantitating and localizing F-18 FDG uptake in cardiac sarcoidosis. *J Nucl Cardiol.* (2020) 27:2003–10. doi: 10.1007/s12350-018-01504-y
89. Osborne MT, Hulten EA, Singh A, Waller AH, Bittencourt MS, Stewart GC, et al. Reduction in 18F-fluorodeoxyglucose uptake on serial cardiac positron emission tomography is associated with improved left ventricular ejection fraction in patients with cardiac sarcoidosis. *J Nucl Cardiol.* (2014) 21:166–74. doi: 10.1007/s12350-013-9828-6
90. Muser D, Santangeli P, Castro SA, Liang JJ, Enriquez A, Werner TJ, et al. Prognostic role of serial quantitative evaluation of 18F-fluorodeoxyglucose uptake by PET/CT in patients with cardiac sarcoidosis presenting with ventricular tachycardia. *Eur J Nucl Med Mol Imaging.* (2018) 45:1394–404. doi: 10.1007/s00259-018-4001-8
91. Bravo PE, Raghu G, Rosenthal DG, Elman S, Petek BJ, Soine LA, et al. Risk assessment of patients with clinical manifestations of cardiac sarcoidosis with positron emission tomography and magnetic resonance imaging. *Int J Cardiol.* (2017) 241:457–62. doi: 10.1016/j.ijcard.2017.03.033
92. Kebed KY, Carter S V, Flatley E, Ward RP, Moss JD, Appelbaum DE, et al. Prevalence of newly diagnosed sarcoidosis in patients with ventricular arrhythmias: a cardiac magnetic resonance and 18F-FDG cardiac PET study. *Int J Cardiovasc Imaging.* (2021) 37:1361–9. doi: 10.1007/s10554-020-02090-2
93. Wicks EC, Menezes LJ, Barnes A, Mohiddin SA, Sekhri N, Porter JC, et al. Diagnostic accuracy and prognostic value of simultaneous hybrid 18 F-fluorodeoxyglucose positron emission tomography/magnetic resonance imaging in cardiac sarcoidosis. *Eur Heart J Cardiovasc Imaging.* (2018) 19:757–67. doi: 10.1093/ehjci/jex340
94. Dweck MR, Abgral R, Trivieri MG, Robson PM, Karakatsanis N, Mani V, et al. Hybrid magnetic resonance imaging and positron emission tomography with fluorodeoxyglucose to diagnose active cardiac sarcoidosis. *JACC Cardiovasc Imaging.* (2018) 11:94–107. doi: 10.1016/j.jcmg.2017.02.021
95. Wisenberg G, Thiessen JD, Pavlovsky W, Butler J, Wilk B, Prato FS. Same day comparison of PET/CT and PET/MR in patients with cardiac sarcoidosis. *J Nucl Cardiol.* (2020) 27:2118–29. doi: 10.1007/s12350-018-01578-8

Conflict of Interest: The authors declare that the research was conducted in the absence of any commercial or financial relationships that could be construed as a potential conflict of interest.

frontiers in Cardiovascular Medicine

REVIEW
published: 28 January 2022
doi: 10.3389/fcvm.2021.799031

Cardiovascular Imaging in Stress Cardiomyopathy (Takotsubo Syndrome)

*Fawzi Zghyer[1], W. Savindu Pasan Botheju[2], Joshua E. Kiss[1], Erin D. Michos[1], Mary C. Corretti[1], Monica Mukherjee[1] and Allison G. Hays[1]**

[1] Division of Cardiology, School of Medicine, Johns Hopkins University, Baltimore, MD, United States, [2] Virginia Commonwealth University Medical Center, Richmond, VA, United States

Stress cardiomyopathy (Takotsubo syndrome) is a reversible syndrome stemming from myocardial injury leading to systolic dysfunction and is usually noted in the setting of a stressful event, be it an emotional or physical trigger. While the exact pathophysiology behind stress cardiomyopathy is yet unknown, there is ample evidence suggesting that neurocardiogenic mechanisms may play an important role. Although historically stress cardiomyopathy was generally thought to be a relatively benign condition, there is growing recognition of the cardiovascular complications associated with it despite its reversibility. Our review aims to shed light onto key cardiovascular imaging modalities used to diagnose stress cardiomyopathy while highlighting the role that imaging plays in assessing disease severity, identifying complications, dictating treatment approaches, and in short-term and long-term prognosis.

Keywords: cardiomyopathy, CMR (cardiovascular magnetic resonance), echocardiography, stress cardiomyopathy, imaging

OPEN ACCESS

Edited by:
Fabrizio Ricci,
University of Studies G. d'Annunzio Chieti and Pescara, Italy

Reviewed by:
Luca Arcari,
M.G. Ospedale Vannini, Italy
Anwar A. Chahal,
University of Pennsylvania, United States
Sylvia J. Buchmann,
Vivantes Klinikum Spandau, Germany

***Correspondence:**
Allison G. Hays
allison.hays@gmail.com

Specialty section:
This article was submitted to Cardiovascular Imaging, a section of the journal Frontiers in Cardiovascular Medicine

Received: *21 October 2021*
Accepted: *15 December 2021*
Published: *28 January 2022*

Citation:
Zghyer F, Botheju WSP, Kiss JE, Michos ED, Corretti MC, Mukherjee M and Hays AG (2022) Cardiovascular Imaging in Stress Cardiomyopathy (Takotsubo Syndrome). Front. Cardiovasc. Med. 8:799031. doi: 10.3389/fcvm.2021.799031

BACKGROUND

Takotsubo syndrome, also known as stress cardiomyopathy (stress CM), apical ballooning syndrome, or broken heart syndrome, is increasingly recognized as an important cause of acute reversible myocardial injury and acute systolic dysfunction (1). The origin of the name "takotsubo" refers to octopus traps used in Japan, which resemble the apical ballooning pattern often observed on fluoroscopic left ventriculogram in the classic presentation of stress CM (2). Previously thought to be a rare diagnosis, stress CM currently comprises around 2% of all the patients presenting with concern for acute coronary syndrome (ACS) (3).

Stress CM was initially thought to be a relatively benign, reversible condition, but as prevalence has increased it has become apparent that it is often associated with significant morbidity and mortality (1). There is increasing recognition of associated cardiovascular complications such as left ventricular (LV) outflow tract obstruction, mitral regurgitation, and heart failure which may all lead to cardiogenic shock (4).

In an era where the application of multimodality cardiovascular imaging has been increasing, our review will aim to highlight the diagnosis of stress CM with a particular focus on imaging.

DEFINITION AND DIAGNOSIS

Stress CM is defined as a syndrome of transient and acute LV systolic and diastolic dysfunction usually related to a profound emotional or physical stress within the prior 5 days (1, 5). The syndrome is suspected when observed regional wall motion abnormalities (RWMA) cannot be explained by corresponding coronary artery occlusions. The typical pattern of LV RWMA that is described includes apical hypokinesia, akinesia, or dyskinesia which gives the apical ballooning shape with relative basal hyperkinesis. Other forms of stress CM include "reverse Takotsubo" or "atypical Takotsubo" which are characterized by mid-ventricular or basal hypokinesis (6). Focal stress CM is another rare form described by its focal LV RWMA which makes it very hard to distinguish from myocarditis or myocardial infarction (7). Clinically, stress CM often presents with ST-segment changes on electrocardiography (ECG), elevation in troponins, a significant increase in serum natriuretic peptides, and characteristic imaging findings. However, coronary angiography remains an essential diagnostic modality to definitively exclude ischemic etiologies for RWMA (1).

Multiple diagnostic criteria have been proposed: the most commonly used are the Heart Failure Association of the European Society of Cardiology diagnostic criteria for Takotsubo Syndrome (8), the International Takotsubo Diagnostic Criteria (InterTAK) (9), and the Revised Mayo Clinic Criteria (10). The criteria are summarized in **Table 1**. The Japanese Society of Echocardiography (JSE) and the European Association of Cardiovascular Imaging (EACVI) published a joint consensus document in 2020 providing a comprehensive review of the various cardiovascular imaging modalities that can be utilized in diagnosing and prognosticating stress CM. They incorporated the InterTAK criteria into a simplified diagnostic algorithm that helps evaluate chest pain and/or dyspnea and rule out several cardiac causes before getting to stress CM (11).

TABLE 1 | The table below summarizes the diagnostic criteria for stress cardiomyopathy.

Heart Failure Association-European Society of Cardiology Criteria
• Transient RWMA in LV or RV which are frequently but not always accompanied by a stressor
• The RWMA usually extends beyond a single coronary artery with circumferential involvement of the segments involved
• The absence of acute coronary syndrome
• New and reversible electrocardiographic abnormalities
• Significantly elevated serum natriuretic peptides
• Mildly elevated cardiac enzymes
• Recovery of LV systolic function on cardiac imaging at follow-up (3–6 months)
International Takotsubo Diagnostic Criteria (InterTAK Diagnostic Criteria)
• Transient LV dysfunction presenting with apical ballooning or mid-ventricular, basal, or focal wall motion abnormalities. RV involvement can be present too. The regional wall motion abnormalities usually extend beyond a territory of a single coronary artery
• An emotional physical or combined trigger precedes the symptoms, however not obligatory
• Neurologic disorders as well as pheochromocytoma may serve as triggers for stress cardiomyopathy
• New ECG abnormalities are present
• Cardiac biomarkers are moderately elevated, but natriuretic peptides are significantly elevated
• Significant coronary artery disease is not a contradiction in Takotsubo syndrome
• Patients have no evidence of infectious myocarditis
• Postmenopausal women are predominantly affected
Revised Mayo Clinic Criteria
• Transient hypokinesis, akinesis, or dyskinesis of the LV with or without apical involvement, the RWMA extends beyond a single coronary artery distribution; a stressful trigger is often but not always present
• Absence of obstructive coronary artery disease or angiographic evidence of a plaque rupture
• New ECG abnormalities or moderate elevation in cardiac biomarkers
• Absence of pheochromocytoma or myocarditis

PATHOPHYSIOLOGY

The exact pathophysiology leading to stress CM still remains unknown. There is a known neuro-cardiovascular link that may contribute to stress CM, but recently neuroimaging studies have given us more insight (12). The central autonomic nervous system (CANS) is vital for cardiovascular regulation. Prior to adopting the terms Takotsubo and stress CM, clinicians have identified instances of transient systolic dysfunction as well as dynamic EKG changes in relation to intracranial pathology such as stroke or hemorrhages (12). This phenomenon has been later described as "neurogenic stunning" and was also seen in patients undergoing electroconvulsive therapy (ECT) (13). As described by de Chazal et al. in a recent review, in the acute phase, there is increased blood flow in the hippocampus, brainstem, and basal ganglia with return to normal upon resolution of the syndrome (1). However, it is still unknown why some emotional stressors cause myocardial dysfunction while other stressors do not. Stress induces activation of complex neocortical limbic pathways which leads to the activation of brainstem noradrenergic neurons and stress related neuropeptides (NPY) produced by the arcuate nucleus of the hypothalamus. Acute stressors induce brain activation, which increases the bioavailability of norepinephrine, cortisol, and NPY. Both circulating epinephrine and norepinephrine released from the medulla of the adrenal glands or locally from sympathetic nerve terminals are known to be significantly increased during the acute phase of stress CM. The catecholamine and NPY surge can lead to the apical ballooning physiology through multiple mechanisms including direct catecholamine toxicity, epicardial, and microvascular coronary spasm or vasoconstriction, and increased cardiac afterload (14). Experimental data have shown that β_2-adrenoceptors are more frequently expressed in an apical than the basal segment of the LV, while a reverse distribution is present for norepinephrine β_1-adrenoceptors and sympathetic and sympathetic nerve terminals of the neuro-cardiac axis, which are dense at the base but not the apex (15). Previously, it was widely thought that the catecholamine surge is solely responsible for the cardiomyopathy; however, it is increasingly recognized that alternate mechanisms may play more of a role. Catecholamine levels often increase in response to cardiac dysfunction and hypotension. It is not yet clear how norepinephrine and NPY contribute mechanistically to stress CM. One hypothesis maintains that the cardio-depressant effects

of catecholamines may lead to supply demand mismatch at the level of the myocardium and eventually myocardial stunning (1). Thus, it is plausible that in individuals with higher levels of NPY/norepinephrine, an intense stressor may predispose them to develop stress CM (1).

RISK FACTORS

Estrogen deficiency in post-menopausal women appears to be one of the strongest risk factors associated with stress CM. This is often superimposed on a background of anxiety or panic disorder (16). Diabetes has also been described as a risk factor, as 10–25% of all the patients presenting with stress CM have concomitant diabetes (17). One of the non-cardiac risk factors frequently associated with stress CM is asthma, particularly after the use of medical interventions such as beta-2 agonists, racemic epinephrine, and intubation. It is not fully understood whether it is the asthma itself or the treatment that triggers the syndrome (18). Marijuana use is also associated with stress CM with a subsequent higher mortality (19). Prior studies suggest that cannabinoids induce NPY expression from the arcuate nucleus of the hypothalamus which can lead to neurogenic myocardial stunning (20). Finally, as we continue to assimilate further data on the COVID-19 pandemic, there is increasing evidence of acute or chronic cardiac injury in the setting of a COVID-19 infection. Although stress CM has been reported in the setting of COVID-19, other pathologies as a cause of cardiac injury are more common including supply/demand mismatch ischemia, microvascular thromboses, myocarditis, or cytokine storm from a hyperinflammatory state (21–24).

ECHOCARDIOGRAPHIC FINDINGS

Left Ventricular Wall Motion and Systolic Function

In the acute phase of stress CM, an echocardiographic assessment is an essential first step toward the diagnosis. The typical echocardiographic findings are characterized by the presence of a large area of dysfunctional myocardium which extends beyond one coronary artery territory. In classic stress CM, symmetrical wall motion abnormalities are seen with akinesis or dyskinesis of the apical and mid-ventricular segments of the anterior, lateral, septal, and inferior walls with hyperdynamic function of the basal segments (25) (**Figure 1**). Other variants such as "mid-ventricular" or "inverted" stress cardiomyopathy can also be seen. The mid-ventricular variant is characterized by akinesis of the mid-ventricular segments with mild hypokinesis or normal contraction of the apical segments and hypercontractility of the base. The inverted variant has two different forms: the first manifests as preserved apical function and severe hypokinesis of the rest of the walls while the second form is characterized by hypokinesis only in the basal segments (often called "reverse Takotsubo") (25).

Echocardiography also demonstrates reduced LV ejection fraction (EF) with variable severity and in most cases recovers as the myocardial stunning resolves (2). The degree of the EF reduction varies depending on the level of myocardial impairment which can often correspond with pre-existing comorbidities, sex, and age. While the degree of myocardial impairment can sometimes be severe, this is not typically reflected by the degree of elevation of cardiac biomarkers, which may be only modestly elevated. The discrepancy between troponin levels and RWMAs can help clinicians to differentiate between ACS and stress CM. More recently, the product of Troponin I level and echocardiographic LVEF has been utilized as an index to differentiate stress CM from ST elevation myocardial infarction (STEMI). A value $\geq$250 is indicative of a STEMI, with a sensitivity and specificity of 95 and 87%, respectively (26).

Left ventricular EF has been found to be an independent predictor of major cardiovascular complications and can help identify stress CM patients at higher risk particularly in those aged >75 years (27). Elderly patients demonstrate significantly lower LV systolic function compared to younger patients (defined as <75 years) (25). If RWMAs persist, then it is reasonable to evaluate with a cardiac MRI to rule out necrosis or other pathologies.

Assessment of LV longitudinal strain may have an important prognostic value in the acute phases of stress CM. Decreased global longitudinal strain (GLS) in patients with stress CM was found to correlate with higher in-hospital mortality (28).

LV Diastolic Function

LV diastolic dysfunction is common in stress CM (29). Global diastolic dysfunction has been observed in some patients in the early phases of stress CM which is evident by impaired left ventricular relaxation and increased E/e' ratio, a non-invasive marker of LV filling pressures (30, 31). In the Takotsubo Italian Network (TIN) registry, E/e' ratios were higher in patients who went on to develop acute decompensated heart failure and was found to be an independent predictor of in-hospital mortality (32). Of all the complications associated with stress CM, acute decompensated heart failure is the most common early complication; thus, an early assessment of the E/e' ratio may allow for early identification of patients at higher risk of decompensation and could serve as a useful tool to guide management. As E/e' ratio elevations can be transient, the ratio itself could be used as a marker for functional recovery when followed serially across the course of the syndrome.

Mitral Regurgitation (MR)

The mechanism of MR in stress CM is not completely understood. Systolic anterior motion of the anterior mitral leaflet (SAM) has been reported in 40–50% of patients with stress CM and may be associated with significant MR (33) (**Figure 1**). MR in stress CM is typically described in cases where reduction in LVEF is severe and LV volume is high and likely represents functional MR due to papillary muscle displacement and tethering of the mitral leaflets in the setting of a dilated and dysfunctional LV (33). In the TIN registry, the presence of MR appeared to be a powerful prognostic marker associated with cardiogenic shock and in-hospital morbidity and mortality (32).

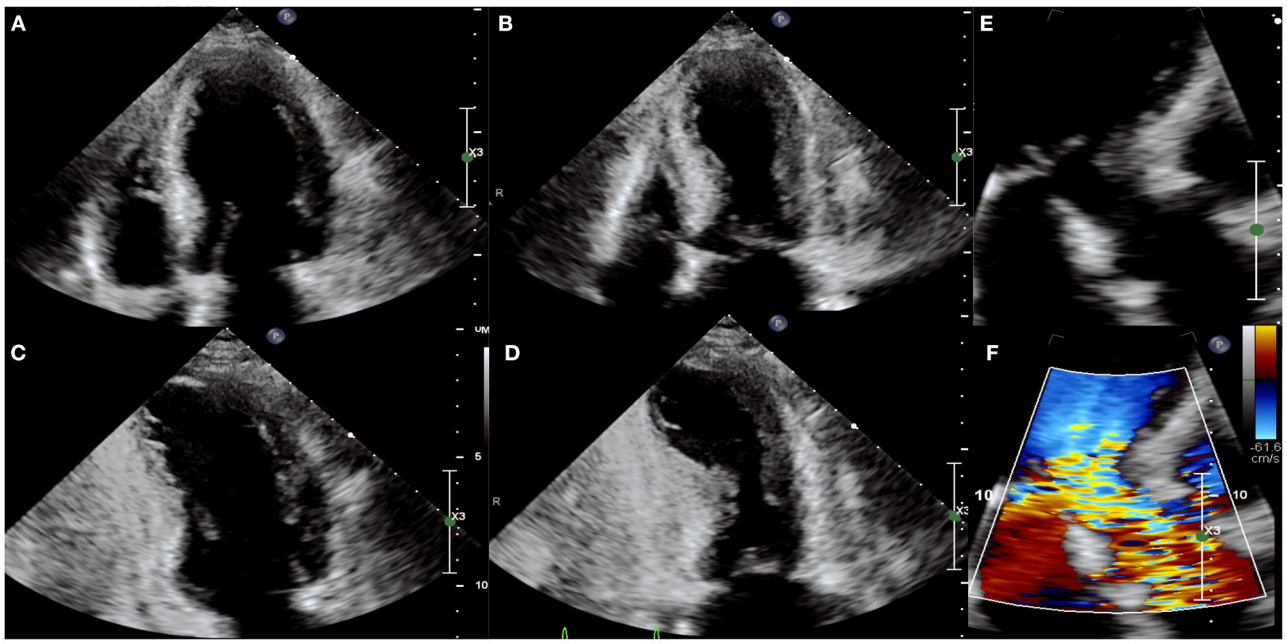

FIGURE 1 | Echocardiographic images of a person with stress cardiomyopathy with left ventricular outflow track obstruction (LVOT) and systolic anterior motion (SAM) of the mitral valve. The apical-4-chamber view in diastole **(A)** and systole **(B)** and 2-chamber view in diastole **(C)** and systole **(D)** showing classic apical ballooning with akinesis and hyperdynamic basal segments. **(E,F)** Illustrate SAM and turbulence across the LVOT indicative of LVOT obstruction.

LV Outflow Tract Obstruction (LVOTO)

LVOTO, diagnosed by echocardiogram, may result from basal hypercontractility with or without systolic anterior motion of the anterior mitral leaflet causing dynamic obstruction of the LV outflow tract (LVOT), and is seen in as many as 12.5–25% of cases (32, 34). Significant LVOTO is described as a peak instantaneous LVOT gradient $\geq$ 30 mmHg. The LVOT gradient has important clinical and therapeutic implications in patients with stress CM; in this cohort, inotropic agents and diuretics should be avoided as the basal hypercontractility induced by catecholamines and the reduction in preload can lead to an exacerbation in gradient with subsequent hemodynamic collapse and cardiogenic shock. LVOTO is associated with increased LV afterload and systolic wall tension which may lead to subendocardial ischemia. In this setting, beta blockade may be beneficial in reducing inotropy and reduced myocardial demand. Alpha-1 agonism with phenylephrine can increase systemic vascular resistance and thus help reduce the effect of dynamic LVOT obstruction, ultimately reducing LV afterload and wall stress (25). Patients with severe LVOTO and stress CM are at higher risk for free wall rupture and life-threatening arrhythmias.

Right Ventricular (RV) Function

Electrocardiographic signs of RV strain warrant special attention with regards to evaluation of RV function in stress CM.

The prevalence of RV involvement has been reported to be around 14% in one study; however, this may be an underestimation due to difficulty imaging the RV (25). In patients with biventricular ballooning, RV contraction often mirrors that of the LV (35). The pattern described is the opposite of the well-described McConnell's sign seen in massive pulmonary emboli which manifests itself as RV apical hyperkinesis and basal and mid hypokinesis to akinesis. The pattern of RV involvement was eventually called "reverse McConnell's sign" (36). There is conflicting evidence on whether RV involvement predicts worse outcomes. In the TIN registry, RV involvement was more prevalent in patients with major complications. No significant correlation has been found between tricuspid annular systolic excursion (TAPSE) and major adverse events (32).

Contrast Echocardiography

Per the updated American Society of Echocardiography guidelines (2018) and European Association of Cardiovascular Imaging (2017) guidelines, contrast echocardiography is a recommended tool to evaluate for the presence of an LV thrombus in situations where it is not detected on non-contrast echocardiography (37). However, if contrast echocardiography fails to detect a thrombus in cases with a high clinical suspicion for a thrombus, cardiac MRI would provide a higher sensitivity and specificity at detecting LV thrombi.

CARDIAC MAGNETIC RESONANCE IMAGING (CMR)

Cine CMR Sequence

Cine CMR sequences allow for more detailed assessment of LV and RV function, ventricular wall motion abnormalities, and possible complications of stress CM (38, 39). While the "apical ballooning" pattern of wall motion accounts for around 75–80% of patients, stress CM can also present in the form of other less common variants, namely the mid-ventricular variant or the inverted variant which are discussed earlier (40, 41) (**Figure 2**). The cine sequence can also be used to demonstrate LVOTO with or without systolic anterior motion of the mitral valve leaflet as well as functional mitral regurgitation (39). These complications can be further assessed with phase contrast velocity imaging in order to generate quantitative values such as LV outflow tract gradient.

Additionally, CMR allows for more quantitative assessment of RV function. RV involvement has been assessed by CMR in multiple studies: patients with RV dysfunction were older, had with longer hospital stays, had more frequent preceding stressful events, had significantly more pleural effusions, and had a lower LV EF compared to those that did not have RV involvement (41, 42).

Recently, CMR post-processing techniques called feature/tissue tracking CMR (FT-CMR) have been developed that enable strain analysis for the quantification of myocardial deformation. A study by Stiermaier et al. evaluated 141 patients with stress CM and found that reduced global circumferential (GCS) and global longitudinal strain (GLS) were associated with the apical ballooning variant while reduced global radial strain (GRS) was associated with the basal ballooning variant (43). Additionally, the study posited that GLS may be useful as a prognostic indicator as LV strain measures worse than −14.75% were associated with adverse outcomes (43).

Myocardial Edema

In the setting of myocardial injury, tissue inflammation may increase resulting in localized myocardial edema (41). Changes in the tissue water content can be evaluated via a CMR T2-weighted imaging protocol (**Figure 3**) which allows for assessment of the distribution of myocardial edema and can be helpful in differentiating between cardiac pathologies such as stress CM, ACS, and myocarditis.

By employing the black blood T2-weighted (fast spin echo) triple-inversion recovery (IR) sequence, fat, and flowing blood can be suppressed allowing the contrast signal to differentiate between normal myocardium and edematous tissue (44). This process can be quantified by calculating the ratio of the signal intensity (SI) between the myocardium and skeletal tissue, with a cut-off value of over 1.9 considered significant for edema.

The pattern of edema in stress CM classically overlaps with the dysfunctional ventricular regions noted on the cine CMR sequence and does not correspond to territories served by epicardial vessels that would generally be seen in ACS (41). The signal distribution tends to be transmural and circumferential over the affected area, unlike in myocarditis where it tends to be more diffuse and heterogenous with a propensity to have higher signal intensity in the sub-epicardial or mid-myocardial tissue.

It is important to note, however, that T2-weighted triple IR can be prone to artifacts from various factors such as arrhythmias, blood pooling, or breathing motion artifact. Therefore, studies investigating techniques that use motion correction algorithms such as extracellular volume (ECV) mapping and parametric T1 or T2 mapping have shown to improve diagnostic accuracy and provide further quantitative evidence in evaluating myocardial edema (15, 45–47). In patients with myocardial infarction, the intensity of T2 signaling tends to take months or even years to decline in the infarcted and surrounding tissue depending on the severity of the injury. In stress cardiomyopathy, there has been variable data with some studies showing a normalization of signaling as the myocardial function returns to normal, while other studies have shown a slower return to baseline, despite recovery in LV myocardial function (15, 45–48). These novel techniques could prove to be viable alternatives to evaluate myocardial inflammation and characterize disease severity without using gadolinium contrast and warrant further studies with larger patient cohorts.

Although the pathophysiology of myocardial inflammation in stress CM is not well-known, increased myocardial edema on imaging may indicate a direct inflammatory process from the syndrome, a secondary effect stemming from elevated sympathetic drive, or microvascular ischemia associated with stress CM (41, 48, 49).

Late Gadolinium Enhancement (LGE)

The use of gadolinium-mediated myocardial enhancement has been used to delineate areas of myocardial scarring or replacement fibrosis stemming from myocardial injury and inflammation. Conventionally, when using LGE to delineate areas of fibrosis in patients with a history of myocardial infarction or myocarditis, a threshold of 5 standard deviations (SDs) above the signal intensity seen in remote, unaffected tissue is used to define significant enhancement. In areas affected by myocardial infarction, the LGE pattern is generally predominant in the subendocardial tissue and can spread transmurally depending on the extent of injury, while in myocarditis the distribution tends to dominate in the sub-epicardial region (updated Lake Louise consensus criteria) (50). Previously, it was thought that the absence of LGE was a pathognomonic feature of stress CM that differentiated it from other pathologies such as myocardial infarctions or myocarditis; however, several studies have now shown that stress CM does present with a certain degree of LGE that is usually of reduced intensity compared to other conditions that cause fibrosis (41, 51, 52). Eitel et al. showed no evidence of LGE in any of the 239 patients assessed in one study, while lowering the threshold to 3 SD showed positive findings in 22 patients (9%) (41). These patients had higher troponin levels at presentation compared to those that had negative LGE but there were no differences in the LV ejection fraction, end-diastolic volume, or end-systolic volume. Another study similarly revealed that changing the SD threshold for LGE may yield different results (53).

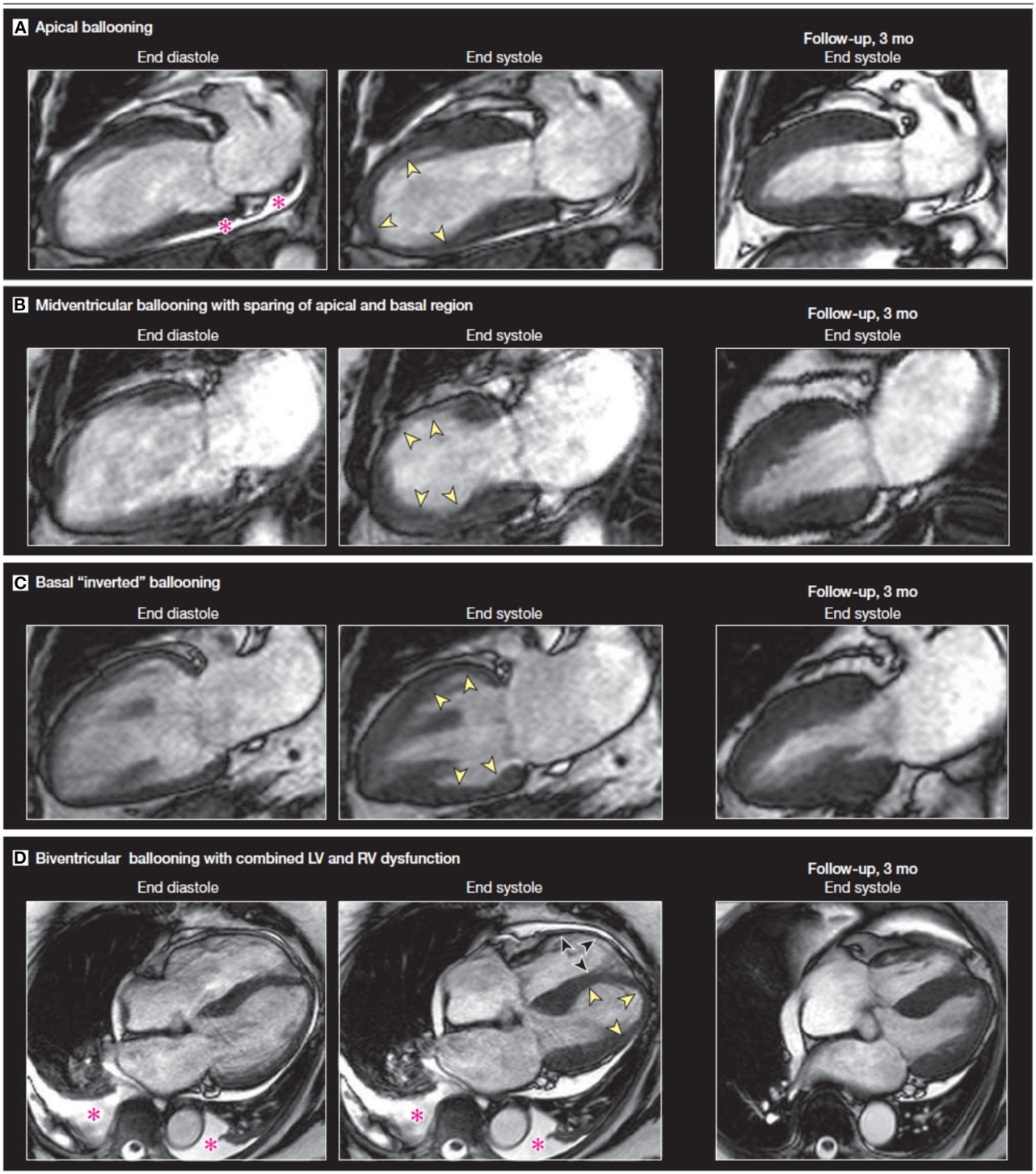

FIGURE 2 | A comparison of vertical long axis CMR cine sequence images on diagnosis and at 3-month follow-up showing a recovery of wall motion abnormalities. The four sets of images display four different variants associated with stress CM. The pink asterisk denotes a pericardial effusion. Yellow arrows indicate apical akinesis while the black arrows indicate RV apical akinesis in the biventricular ballooning variant. Figure adapted from Figure 2 on Clinical Characteristics and cardiovascular magnetic resonance findings in stress (Takotsubo) cardiomyopathy by Eitel et al. (41).

There are various theories as to what causes the delayed enhancement, with some studies suggesting a delayed washout of contrast due to the presence of myocardial inflammation and interstitial edema. Other studies have used immune-histological

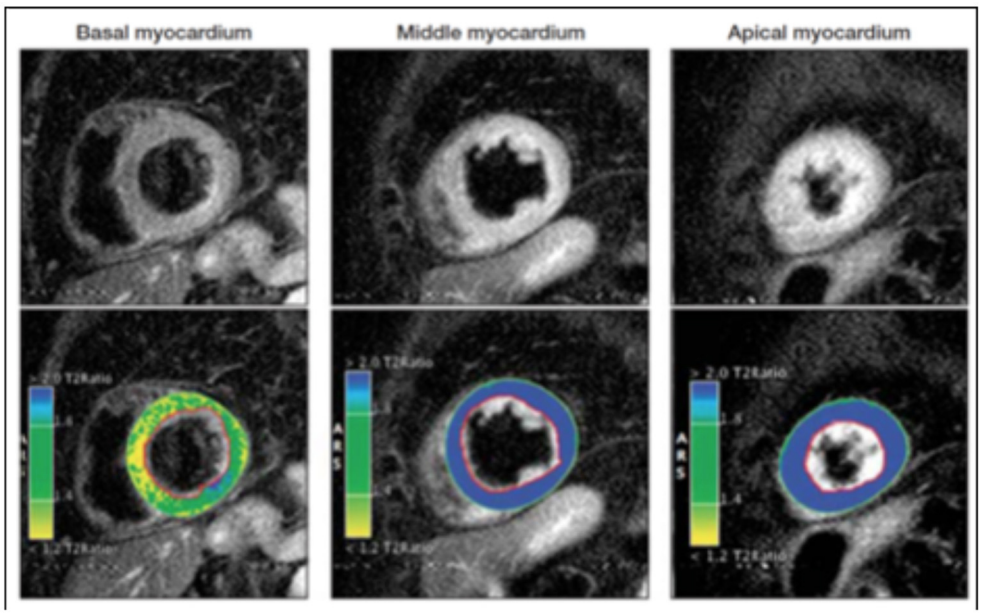

FIGURE 3 | T2-weighted sequences demonstrating variability in signal intensity based on the affected myocardial regions. The color coding resembles varying signal intensity ratios between myocardium and skeletal tissue with blue indicating a ratio ≥ 1.9 (indicating edema) while yellow/green indicates a ratio <1.9, indicative of normal myocardium. These images illustrate predominant myocardial edema in the mid-ventricular and apical segments. Adapted from Clinical Characteristics and cardiovascular magnetic resonance findings in stress (Takotsubo) cardiomyopathy by Eitel et al. (41).

evidence to show that affected areas in stress CM have increased collagen-1 which could be indicative of a fibrotic process (52, 53). Perhaps the low level of LGE reflects the reversibility of stress CM and near or complete resolution, which is an essential diagnostic component of this condition. In ischemic cardiomyopathies or non-ischemic cardiomyopathies such as sarcoidosis, higher degrees of LGE are often associated with poorer prognoses due to irreversible myocardial injury (54). In one study, stress CM patients with LGE had a higher frequency of cardiogenic shock and had a slower recovery of wall motion compared to those that did not display LGE (53). Therefore, extent of LGE on CMR may represent a useful prognostic marker in stress CM.

Early Gadolinium Enhancement (EGE)

Within 1–3 min of gadolinium administration, EGE can be accessed via a high T1 inversion time. This technique is essential for the identification of LV thrombus. Thrombi are characterized by having no gadolinium uptake and are seen as a hypodense mass (almost black) in contrast to the gray myocardium. Important CMR parameters are summarized in **Table 2**.

TABLE 2 | Important CMR parameters for the evaluation of stress CM.

Imaging sequence	Clinical significance
Cine CMR (balanced Steady State Free Precession/SSFP)	Assessing wall motion abnormalities
Feature/Tissue tracking CMR (FT-CMR)	Quantifying regional and global strain patterns
T2-weighted triple inversion recovery	Identifying areas with myocardial edema and distribution pattern
T1 or T2 mapping	Quantitative assessment of myocardial edema
First pass perfusion	Assessing perfusion defects
Early gadolinium enhancement	Ruling out LV thrombus
Late gadolinium enhancement	Assessing extent of regional inflammation and fibrosis

NUCLEAR IMAGING

Recent studies have reported a role for nuclear imaging findings in the diagnosis of stress CM. Single photon emission computed tomography can assess cardiac stunning using 201 Thallium or 99m Technetium-labeled radiopharmaceuticals and 123I-metalodobenzyl-guanidine (I-123 MIBG) (55). In addition, 18F-fluorodeoxyglucose (FDG) positron emission tomography can be used to detect myocardial glucose metabolism (56). In the acute and sub-acute phases of stress CM, the affected segments of the myocardium show defects in FDG and MIBG despite normal to slightly reduced perfusion (57). MIBG is a norepinephrine analog and uses the same mechanism of norepinephrine in the uptake and storage in presynaptic vesicles. After adrenergic stimulation, MIBG is released in the synaptic cleft but is not metabolized by monoamine oxidase (MOA) and catechol-O-methyltransferase (COMT) enzymes (58). MIBG is also labeled with iodine-123 (123I) as a radiotracer due to its suitability for imaging. With such properties, it is possible to evaluate the cardiac uptake of the MIBG and its distribution (59). Visually and quantitively, two

parameters are analyzed: heart to mediastinal ratio (H/MR) and myocardial washout rate (WR) (59).

The evaluation of stress CM by I-123 MIBG scintigraphy demonstrates a defect in MIBG uptake at the level of the apex. Semi-quantitative measures also demonstrate a reduction in H/MR and an increase in washout (59). The use of nuclear imaging for the diagnosis of stress CM is promising but given the presence of alternative more accessible modalities, it is not the first line imaging modality for diagnosis.

CARDIAC MULTI-DETECTOR COMPUTED TOMOGRAPHY

Cardiac multi-detector computed tomography (MDCT) is a comprehensive imaging modality that is used to assess cardiac function as well as coronary artery lesions (55). MDCT can provide valuable information regarding RWMA and can immediately rule out a coronary artery lesion with a high negative predictive value (60). In clinical practice, excluding the possibility of coronary obstruction or acute plaque rupture with MDCT still remains a challenge (55). Cardiac MDCT may be a promising imaging modality in the evaluation of suspected stress-induced cardiomyopathy. Cardiac MDCT may in particular be an appealing imaging modality when there is a clinical need to evaluate the coronary arteries at the same time or when there is a contraindication to MRI.

COMPLICATIONS

Although the hallmark of stress CM is that myocardial function returns to normal within weeks, many patients endure complications related directly to stress CM or comorbid medical conditions and can have significant morbidity and mortality in the inpatient setting (**Figure 4**).

Acute Heart Failure

Systolic heart failure is the most common complication encountered by these patients in the acute setting, with an incidence ranging between 3 and 46% (3, 32, 61, 62). This can occur as a result of depressed LV systolic function or secondary to other associated complications such as LVOTO or functional mitral regurgitation. Some patients have progression of heart failure to cardiogenic shock requiring inotropic or vasopressor support or even mechanical support via intra-aortic balloon pumps (IABP) or extracorporeal membrane oxygenation (ECMO), with a very small proportion of cases resulting in death. Biventricular involvement has a tendency to occur in the elderly population, is associated with lower LV ejection fraction, and is an independent predictor of adverse cardiovascular outcomes (41, 63). These patients tend to have longer and complicated hospital stays and have shown to have higher rates of in-hospital and long-term morbidity and mortality (64).

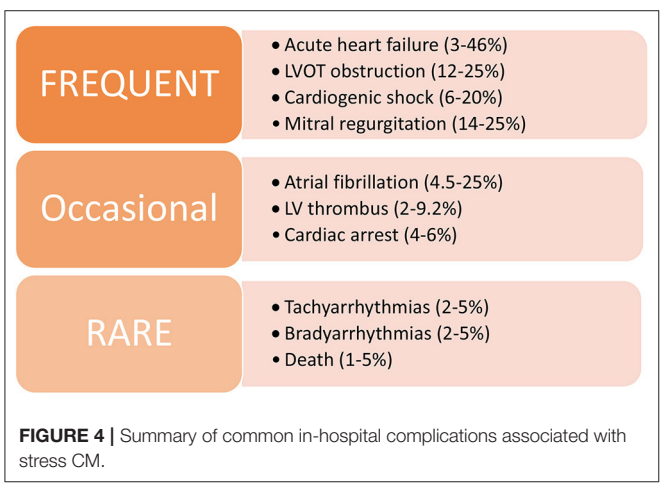

FIGURE 4 | Summary of common in-hospital complications associated with stress CM.

LV Thrombus and Systemic Emboli

Formation of an LV thrombus is a relatively rare but significant complication associated with stress CM, particularly with the apical ballooning variant. Studies have shown an incidence between 2 and 9.2% of patients (65–68). In these cases, likelihood of clot formation is increased due to blood stasis from apical hypokinesis/akinesis increased stasis; furthermore, the adrenergic surge that is often thought to be a contributing mechanism behind stress CM could potentially cause endocardial damage that may initiate a thrombotic process. Stress CM patients with LV thrombus are at increased risk for systemic emboli including cerebrovascular embolic events, which can occur in around 17–25% of cases (66, 68).

Arrhythmias

As cardiac arrhythmias are important potential complications of stress CM that could arise in the acute setting, patients need to be monitored closely via telemetry and serial ECGs in order to evaluate for abnormal rhythms and a prolonged QT interval. Atrial fibrillation can occur in ∼4.5–25% of patients and is the most common arrhythmia seen in stress CM patients (69–71). Rarely, patients may develop more dangerous cardiac arrhythmias such as ventricular tachycardia or torsades de pointes, especially if a prolonged QT interval >500 ms is present (72, 73). In one study, men were more likely to have cardiac arrhythmias and a higher incidence of cardiac arrest compared to women (69).

TREATMENT

Acute Heart Failure and Cardiogenic Shock

To date, there have been no large randomized controlled trials investigating various therapies that are commonly used for the treatment of acute heart failure in stress CM. The primary goal of therapy is to address any acute complications that arise, prophylactically treat to minimize risks of certain complications such as thromboembolism, and closely follow the patient throughout the course of the disease until full recovery and/or normalization of cardiac function. In determining the course of therapy, it is important to delineate the pattern of cardiomyopathy and identify certain features such as the

presence of LVOTO that may require adjustment in medication regimen (**Figure 5**).

In a patient with normal cardiac output, the standard of treatment involves use of diuretics in order to achieve euvolemia and afterload reduction with arterial vasodilators (e.g., ACE-inhibiters, angiotensin-receptor blockers, angiotensin receptor-neprilysin inhibitor, hydralazine) (1, 74). In patients who are hemodynamically stable with LVOTO, the use of beta-blockers has a negative inotropic effect on basal hypercontractility and reduces the obstruction. In the case of LVOTO, the use of nitrates in order to lower filling pressures may have negative effects by worsening the LVOT gradient and should be avoided (74).

When treating a patient with cardiogenic shock, the approach to therapy is heavily predicated on the presence or absence of LVOT obstruction. In the absence of LVOT obstruction, inotropic agents such as dobutamine or milrinone can be used to augment cardiac output. Vasopressors such as norepinephrine or vasopressin can be utilized as a second-line agent. There have been retrospective studies and case series suggesting the safety and feasibility of using levosimendan (a Ca^{2+} sensitizer) as a potential alternative inotropic agent (75, 76); however, clinical trials are needed to further study this agent before adoption in clinical practice. Several case reports have detailed complex stress CM cases requiring mechanical circulatory support via IABP or percutaneous left ventricular assist devices (such as Impella) until recovery (77, 78).

If LVOTO is present independent of concurrent mitral regurgitation, the use of inotropic support can increase basal hypercontractility and worsen the LVOTO, potentially worsening cardiogenic shock. These patients benefit from measures such as administration of IV fluids and/or the use of low-dose beta-adrenergic antagonists such as metoprolol or esmolol for the purpose of negative inotropy on the hyperdynamic basal myocardium which can reduce the LVOT obstruction. Extreme caution must be practiced with use of beta blockers, however, as despite their benefit in reducing LVOTO they can be potentially detrimental by reducing cardiac output further due to negative inotropy. Other therapeutic agents include vasopressors such as phenylephrine or vasopressin which can be administered to increase systemic vascular resistance and thereby reduce obstruction at the LVOT (1). In refractory cases, ECMO may be used to provide support (79).

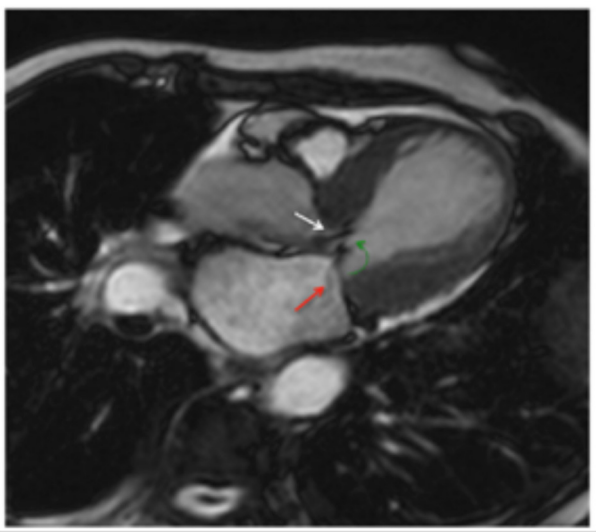

FIGURE 5 | Cine CMR horizontal long-axis view illustrating the systolic "jet" seen in LVOT (white arrow) with concurrent systolic anterior motion of the mitral leaflets (green arrow) and functional mitral regurgitation (red arrow). Adapted from Figure 6 in Plácido et al. (39).

Much like with acute management of stress CM, chronic management of stress CM has limited evidence with no official guidelines in place to date. There have been several studies ranging from case series to retrospective studies to meta-analyses investigating various heart failure drugs. Some studies favor ACE-inhibitors and angiotensin receptor blockers over beta blockers in terms of potential long-term mortality benefit while others have shown no significant findings (40, 80, 81). The general approach to chronic care of stress CM patients has been to initiate guideline-directed medical therapy as indicated in the care of the general cardiomyopathy patient. In patients with concurrent coronary artery disease, guideline-directed use of aspirin and statin therapies is likely beneficial as well (74).

Thromboembolism

In the 2013 ACCF/AHA guidelines for the management of STEMI, there is a Class IIb recommendation to consider prophylactic anticoagulation in patients with anterior wall myocardial infarctions resulting in hypokinetic or akinetic wall motion abnormalities that could pose a potential high risk of LV thrombus formation (82). In a review article by Heckle et al. (66), data compiled from four studies showed a prevalence of 9.2% for thromboembolic events in patients with stress CM. The study posited that an event rate of 9.2% would roughly equate to a score of at least 5 on the CHA2DS2-Vasc scoring system used to determine the need for anticoagulation in patients with atrial fibrillation; therefore, this could theoretically be extrapolated to initiate prophylactic anticoagulation in patients with stress CM (66). To date, there have not been any randomized clinical trials investigating the efficacy of anticoagulation and duration of therapy as a therapeutic or even prophylactic approach to patients with a LV thrombus in the setting of stress CM. Prior retrospective studies have suggested the use of systemic anticoagulation for at least 3 months in patients with a confirmed LV thrombus.

PROGNOSIS

A retrospective, international, multi-center study by Templin et al., utilized a database called the International Takotsubo Registry to identify risk factors for stress CM as well as and predictors of clinical outcomes in these patients (40). In the study, 21.8% of patients had in-hospital complications including death, which was similar when compared to those with ACS. A multivariate analysis in this study revealed that physical triggers, acute psychiatric disorders (including anxiety, adjustment disorder,

and severe stress), or neurologic disorders (including stroke/TIA, seizures, and headache disorders); a first troponin level >10 times the upper limit of normal; and an LVEF of <45% were all noted to be predictors of higher incidence of in-hospital complications and death. Conversely, older age (>70 years) and the presence of an emotional trigger were associated with a lower incidence of in-hospital complications and death; however, other studies have revealed higher rates of complications in older patients (27, 83).

In-hospital mortality rates for stress CM have ranged between 2 and 5% (32, 83–85). A study in Japan by Isogai et al. (86) compared patients with stress CM due to an out-of-hospital causative factor with those who developed stress CM during hospital admission and found that in-hospital stress CM patients had higher a proportions of co-morbidities along with higher in-hospital mortality (17.9 vs. 5.4%, $p < 0.001$). Presenting in an unstable condition (i.e., post-cardiac arrest or shock requiring pressor support) or having other non-cardiac acute co-morbidities were also associated with a higher risk of in-hospital mortality. In analyzing long-term outcomes, some studies have shown a higher mortality in patients with stress CM compared to a general age and gender-matched population while others have shown no differences in the long term (87, 88).

Data on recurrence have been limited but current evidence reports a recurrence rate of around 2–4% per year and up to as high as 20% in 10 years (40, 88, 89). There are reports of recurrence presenting with a different anatomical variant of stress CM. Some patients may continue to experience symptoms such as fatigue, shortness of breath, chest pain, and exercise intolerance even with recovery of LVEF (1). There is also evidence that patients can experience psychiatric consequences such as post-traumatic stress disorder as a long-term complication of stress CM (90).

CONCLUSION

As featured comprehensively in this review, cardiovascular imaging plays a vital role in stress CM and offers many facets of benefits ranging from the initial diagnosis to long-term outcomes. Echocardiography and certain sequences in CMR enable us to differentiate between variants of stress CM, characterize severity of left ventricular dysfunction and identify prognostic features such as LVOTO, mitral regurgitation and RV involvement that often drive our course of therapy. Additionally, several CMR sequences such as feature/tissue tracking, T1/T2 mapping are useful in providing qualitative and quantitative evidence of myocardial injury and degree of inflammation on a cellular and tissue level that can then be translated into prognostic information. As we begin to understand that stress CM is not a benign condition and can often have serious complications in the acute and chronic setting similar to more common cardiac pathologies such as ACS, there is a strong call for further large scale trials in order to investigate and refine our diagnostic and therapeutic approach to this disease.

AUTHOR CONTRIBUTIONS

All authors listed have made a substantial, direct, and intellectual contribution to the work and approved it for publication.

REFERENCES

1. Medina de Chazal H, Del Buono MG, Keyser-Marcus L, Ma L, Moeller FG, Berrocal D, et al. Stress Cardiomyopathy diagnosis and treatment: JACC state-of-the-art review. *J Am Coll Cardiol.* (2018) 72:1955–71. doi: 10.1016/j.jacc.2018.07.072
2. Kurisu S, Sato H, Kawagoe T, Ishihara M, Shimatani Y, Nishioka K, et al. Tako-tsubo-like left ventricular dysfunction with ST-segment elevation: a novel cardiac syndrome mimicking acute myocardial infarction. *Am Heart J.* (2002) 143:448–55. doi: 10.1067/mhj.2002.120403
3. Gianni M, Dentali F, Grandi AM, Sumner G, Hiralal R, Lonn E. Apical ballooning syndrome or takotsubo cardiomyopathy: a systematic review. *Eur Heart J.* (2006) 27:1523–9. doi: 10.1093/eurheartj/ehl032
4. Kurowski V, Kaiser A, Von Hof K, Killermann DP, Mayer B, Hartmann F, et al. Apical and midventricular transient left ventricular dysfunction syndrome (Tako-Tsubo cardiomyopathy): frequency, mechanisms, and prognosis. *Chest.* (2007) 132:809–16. doi: 10.1378/chest.07-0608
5. Wittstein IS, Thiemann DR, Lima JAC, Baughman KL, Schulman SP, Gerstenblith G, et al. Neurohumoral features of myocardial stunning due to sudden emotional stress. *N Engl J Med.* (2005) 352:539–48. doi: 10.1056/NEJMoa043046
6. Tsuchihashi K, Ueshima K, Uchida T, Oh-mura N, Kimura K, Owa M, et al. Transient left ventricular apical ballooning without coronary artery stenosis: a novel heart syndrome mimicking acute myocardial infarction. angina pectoris-myocardial infarction investigations in Japan. *J Am Coll Cardiol.* (2001) 38:11–8. doi: 10.1016/S0735-1097(01)01316-X
7. Tini G, Limite LR, Arcari L, Cacciotti L, Russo D, Sclafani M, et al. A systematic review on focal takotsubo syndrome: a not-so-small matter. *Heart Fail Rev*. (2020). doi: 10.1007/s10741-020-09988-y. [Epub ahead of print].
8. Lyon AR, Bossone E, Schneider B, Sechtem U, Citro R, Underwood SR, et al. Current state of knowledge on Takotsubo syndrome: a position statement from the taskforce on takotsubo syndrome of the heart failure association of the european society of cardiology. *Eur J Heart Fail.* (2016) 18:8–27. doi: 10.1002/ejhf.424
9. Ghadri JR, Cammann VL, Jurisic S, Seifert B, Napp LC, Diekmann J, et al. A novel clinical score (InterTAK Diagnostic Score) to differentiate takotsubo syndrome from acute coronary syndrome: results from the International Takotsubo Registry. *Eur J Heart Fail.* (2017) 19:1036–42. doi: 10.1002/ejhf.683
10. Madhavan M, Prasad A. Proposed Mayo Clinic criteria for the diagnosis of Tako-Tsubo cardiomyopathy and long-term prognosis. *Herz.* (2010) 35:240–3. doi: 10.1007/s00059-010-3339-x
11. Citro R, Okura H, Ghadri JR, Izumi C, Meimoun P, Izumo M, et al. Multimodality imaging in takotsubo syndrome: a joint consensus document of the European Association of Cardiovascular Imaging (EACVI) and the Japanese Society of Echocardiography (JSE). *Eur Hear J.* (2020) 21:1184–207. doi: 10.1093/ehjci/jeaa149
12. Pollick C, Cujec B, Parker S, Tator C. Left ventricular wall motion abnormalities in subarachnoid hemorrhage: an echocardiographic study. *J Am Coll Cardiol.* (1988) 12:600–5. doi: 10.1016/S0735-1097(88)80044-5
13. Biso S, Wongrakpanich S, Agrawal A, Yadlapati S, Kishlyansky M, Figueredo V. A review of neurogenic stunned myocardium. Nalivaiko E, ed. *Cardiovasc Psychiatry Neurol.* (2017) 2017:5842182. doi: 10.1155/2017/5842182
14. Pelliccia F, Kaski JC, Crea F, Camici PG. Pathophysiology of takotsubo syndrome. *Circulation.* (2017) 135:2426–41. doi: 10.1161/CIRCULATIONAHA.116.027121
15. Haaf P, Garg P, Messroghli DR, Broadbent DA, Greenwood JP, Plein S. Cardiac T1 Mapping and Extracellular Volume (ECV) in clinical practice: a comprehensive review. *J Cardiovasc Magn Reson.* (2016) 18:89. doi: 10.1186/s12968-016-0308-4

16. Sharkey SW, Windenburg DC, Lesser JR, Maron MS, Hauser RG, Lesser JN, et al. Natural history and expansive clinical profile of stress (Tako-Tsubo) cardiomyopathy. *J Am Coll Cardiol.* (2010) 55:333–41. doi: 10.1016/j.jacc.2009.08.057
17. Stiermaier T, Santoro F, El-Battrawy I, Möller C, Graf T, Novo G, et al. Prevalence and prognostic impact of diabetes in Takotsubo syndrome: insights from the international, multicenter GEIST registry. *Diabetes Care.* (2018) 41:1084–8. doi: 10.2337/dc17-2609
18. Pontillo D, Patruno N, Stefanoni R. The tako-tsubo syndrome and bronchial asthma: the chicken or the egg dilemma. *J Cardiovasc Med.* (2011) 12:149–50. doi: 10.2459/JCM.0b013e32833cdbb0
19. Pacher P, Bátkai S, Kunos G. Cardiovascular pharmacology of cannabinoids. *Handb Exp Pharmacol.* (2005) 168:599–625. doi: 10.1007/3-540-26573-2_20
20. Bakkali-Kassemi L, El Ouezzani S, Magoul R, Merroun I, Lopez-Jurado M, Errami M. Effects of cannabinoids on neuropeptide Y and β-endorphin expression in the rat hypothalamic arcuate nucleus. *Br J Nutr.* (2011) 105:654–60. doi: 10.1017/S0007114510004095
21. Siripanthong B, Nazarian S, Muser D, Deo R, Santangeli P, Khanji MY, et al. Recognizing COVID-19–related myocarditis: the possible pathophysiology and proposed guideline for diagnosis and management. *Hear Rhythm.* (2020) 17:1463. doi: 10.1016/j.hrthm.2020.05.001
22. Chung MK, Zidar DA, Bristow MR, Cameron SJ, Chan T, Harding C V., et al. COVID-19 and cardiovascular disease. *Circ Res.* (2021) 128:1214–36. doi: 10.1161/CIRCRESAHA.121.317997
23. Jabri A, Kalra A, Kumar A, Alameh A, Adroja S, Bashir H, et al. Incidence of stress cardiomyopathy during the coronavirus disease 2019 pandemic. *JAMA Netw Open.* (2020) 3:1–7. doi: 10.1001/jamanetworkopen.2020.14780
24. Minhas AS, Scheel P, Garibaldi B, Liu G, Horton M, Jennings M, et al. Takotsubo syndrome in the setting of COVID-19. *JACC Case Rep.* (2020) 2:1321–5. doi: 10.1016/j.jaccas.2020.04.023
25. Citro R, Lyon AR, Meimoun P, Omerovic E, Redfors B, Buck T, et al. Standard and advanced echocardiography in takotsubo (stress) cardiomyopathy: clinical and prognostic implications. *J Am Soc Echocardiogr.* (2015) 28:57–74. doi: 10.1016/j.echo.2014.08.020
26. Nascimento FO, Yang S, Larrauri-Reyes M, Pineda AM, Cornielle V, Santana O, et al. Usefulness of the troponin-ejection fraction product to differentiate stress cardiomyopathy from ST-segment elevation myocardial infarction. *Am J Cardiol.* (2014) 113:429–33. doi: 10.1016/j.amjcard.2013.10.013
27. Citro R, Rigo F, Previtali M, Ciampi Q, Canterin FA, Provenza G, et al. Differences in clinical features and in-hospital outcomes of older adults with tako-tsubo cardiomyopathy. *J Am Geriatr Soc.* (2012) 60:93–8. doi: 10.1111/j.1532-5415.2011.03730.x
28. Dias A, Franco E, Rubio M, Bhalla V, Pressman GS, Amanullah S, et al. Usefulness of left ventricular strain analysis in patients with takotsubo syndrome during acute phase. *Echocardiography.* (2018) 35:179–83. doi: 10.1111/echo.13762
29. Akashi YJ, Goldstein DS, Barbaro G, Ueyama T. Takotsubo cardiomyopathy: a new form of acute, reversible heart failure. *Circulation.* (2008) 118:2754–62. doi: 10.1161/CIRCULATIONAHA.108.767012
30. Nagueh SF, Smiseth OA, Appleton CP, Byrd BF 3rd, Dokainish H, Edvardsen T, et al. Recommendations for the evaluation of left ventricular diastolic function by echocardiography: an update from the American Society of Echocardiography and the European Association of Cardiovascular Imaging. *J Am Soc Echocardiogr.* (2016) 29:277–314. doi: 10.1016/j.echo.2016.01.011
31. Meimoun P, Passos P, Benali T, Boulanger J, Elmkies F, Zemir H, et al. Assessment of left ventricular twist mechanics in Tako-tsubo cardiomyopathy by two-dimensional speckle-tracking echocardiography. *Eur J Echocardiogr.* (2011) 12:931–9. doi: 10.1093/ejechocard/jer183
32. Citro R, Rigo F, D'Andrea A, Ciampi Q, Parodi G, Provenza G, et al. Echocardiographic correlates of acute heart failure, cardiogenic shock, and in-hospital mortality in tako-tsubo cardiomyopathy. *JACC Cardiovasc Imaging.* (2014) 7:119–29. doi: 10.1016/j.jcmg.2013.09.020
33. Izumo M, Nalawadi S, Shiota M, Das J, Dohad S, Kuwahara E, et al. Mechanisms of acute mitral regurgitation in patients with takotsubo cardiomyopathy an echocardiographic study. *Circ Cardiovasc Imaging.* (2011) 4:392–8. doi: 10.1161/CIRCIMAGING.110.962845
34. **El Mahmoud R**, Mansencal N, Pilliére R, Leyer F, Abbou N, Michaud P, et al. Prevalence and characteristics of left ventricular outflow tract obstruction in Tako-Tsubo syndrome. *Am Heart J.* (2008). 156:543-548. doi: 10.1016/j.ahj.2008.05.002
35. Citro R, Caso I, Provenza G, Santoro M, Gregorio G, Bossone E. Right ventricular involvement and pulmonary hypertension in an elderly woman with tako-tsubo cardiomyopathy. *Chest.* (2010) 137:973–5. doi: 10.1378/chest.09-0923
36. Liu K, Carhart R. "Reverse McConnell's sign?": A unique right ventricular feature of takotsubo cardiomyopathy. *Am J Cardiol.* (2013). 111:1232-1235. doi: 10.1016/j.amjcard.2012.12.007
37. Senior R, Becher H, Monaghan M, Agati L, Zamorano J, Vanoverschelde JL, et al. Clinical practice of contrast echocardiography: recommendation by the European Association of Cardiovascular Imaging (EACVI) (2017). *Eur Hear J - Cardiovasc Imaging.* (2017) 18:1205–1205af. doi: 10.1093/ehjci/jex182
38. Kohan AA, Yeyati EL, Stefano L De, Dragonetti L, Pietrani M, Arenaza DP de, et al. Usefulness of MRI in takotsubo cardiomyopathy: a review of the literature. *Cardiovasc Diagn Ther.* (2014) 4:138.
39. Plácido R, Cunha Lopes B, Almeida AG, Rochitte CE. The role of cardiovascular magnetic resonance in takotsubo syndrome. *J Cardiovasc Magn Reson.* (2016) 18:1–12. doi: 10.1186/s12968-016-0279-5
40. Templin C, Ghadri JR, Diekmann J, Napp LC, Bataiosu DR, Jaguszewski M, et al. Clinical features and outcomes of takotsubo (Stress) cardiomyopathy. *N Engl J Med.* (2015) 373:929–38. doi: 10.1056/NEJMoa1406761
41. Eitel I, Knobelsdorff-Brenkenhoff F von, Bernhardt P, Carbone I, Muellerleile K, Aldrovandi A, et al. Clinical characteristics and cardiovascular magnetic resonance findings in stress (Takotsubo) cardiomyopathy. *JAMA.* (2011) 306:277–86. doi: 10.1001/jama.2011.992
42. Haghi D, Athanasiadis A, Papavassiliu T, Suselbeck T, Fluechter S, Mahrholdt H, et al. Right ventricular involvement in Takotsubo cardiomyopathy. *Eur Heart J.* (2006) 27:2433–9. doi: 10.1093/eurheartj/ehl274
43. Stiermaier T, Lange T, Chiribiri A, Möller C, Graf T, Villnow C, et al. Left ventricular myocardial deformation in Takotsubo syndrome: a cardiovascular magnetic resonance myocardial feature tracking study. *Eur Radiol.* (2018) 28:5160–70. doi: 10.1007/s00330-018-5475-2
44. Eitel I, Friedrich MG. T2-weighted cardiovascular magnetic resonance in acute cardiac disease. *J Cardiovasc Magn Reson.* (2011) 13:13. doi: 10.1186/1532-429X-13-13
45. Thavendiranathan P, Walls M, Giri S, Verhaert D, Rajagopalan S, Moore S, et al. Improved detection of myocardial involvement in acute inflammatory cardiomyopathies using T2 mapping. *Circ Cardiovasc Imaging.* (2012) 5:102–10. doi: 10.1161/CIRCIMAGING.111.967836
46. Vermes E, Berradja N, Saab I, Genet T, Bertrand P, Pucheux J, et al. Cardiac magnetic resonance for assessment of cardiac involvement in Takotsubo syndrome: do we still need contrast administration? *Int J Cardiol.* (2020) 308:93–5. doi: 10.1016/j.ijcard.2020.03.039
47. Aikawa Y, Noguchi T, Morita Y, Tateishi E, Kono A, Miura H, et al. Clinical impact of native T1 mapping for detecting myocardial impairment in takotsubo cardiomyopathy. *Eur Hear J Cardiovasc Imaging.* (2019) 20:1147–55. doi: 10.1093/ehjci/jez034
48. Neil C, Nguyen TH, Kucia A, Crouch B, Sverdlov A, Chirkov Y, et al. Slowly resolving global myocardial inflammation/oedema in Tako-Tsubo cardiomyopathy: evidence from T2-weighted cardiac MRI. *Heart.* (2012) 98:1278–84. doi: 10.1136/heartjnl-2011-301481
49. Ojha V, Khurana R, Ganga KP, Kumar S. Advanced cardiac magnetic resonance imaging in takotsubo cardiomyopathy. *Br J Radiol.* (2020) 93:20200514. doi: 10.1259/bjr.20200514
50. Ferreira VM, Schulz-Menger J, Holmvang G, Kramer CM, Carbone I, Sechtem U, et al. Cardiovascular magnetic resonance in nonischemic myocardial inflammation: expert recommendations. *J Am Coll Cardiol.* (2018) 72:3158–76. doi: 10.1016/j.jacc.2018.09.072
51. Nakamori S, Matsuoka K, Onishi K, Kurita T, Ichikawa Y, Nakajima H, et al. Prevalence and signal characteristics of late gadolinium enhancement on contrast-enhanced magnetic resonance imaging in patients with takotsubo cardiomyopathy. *Circ J.* (2012) 76:914–21. doi: 10.1253/circj.CJ-11-1043
52. Rolf A, Nef HM, Möllmann H, Troidl C, Voss S, Conradi G, et al. Immunohistological basis of the late gadolinium enhancement phenomenon in tako-tsubo cardiomyopathy. *Eur Heart J.* (2009) 30:1635–42. doi: 10.1093/eurheartj/ehp140

53. Naruse Y, Sato A, Kasahara K, Makino K, Sano M, Takeuchi Y, et al. The clinical impact of late gadolinium enhancement in Takotsubo cardiomyopathy: serial analysis of cardiovascular magnetic resonance images. *J Cardiovasc Magn Reson.* (2011) 13:67. doi: 10.1186/1532-429X-13-67
54. Wu KC, Weiss RG, Thiemann DR, Kitagawa K, Schmidt A, Dalal D, et al. Late gadolinium enhancement by cardiovascular magnetic resonance heralds an adverse prognosis in nonischemic cardiomyopathy. *J Am Coll Cardiol.* (2008) 51:2414–21. doi: 10.1016/j.jacc.2008.03.018
55. Kang Y, Kim YK, Chun EJ, Chor S Il. Potential pathophysiology and clinical workflow of stress- induced cardiomyopathy. *Cardiovasc Imaging Asia*. (2018) 2:19–27. doi: 10.22468/cvia.2017.00157
56. Cimarelli S, Imperiale A, Ben-Sellem D, Rischner J, Detour J, Morel O, et al. Nuclear medicine imaging of takotsubo cardiomyopathy: typical form and midventricular ballooning syndrome. *J Nucl Cardiol.* (2008) 15:137–141. doi: 10.1007/BF02976903
57. Lancellotti P, Price S, Edvardsen T, Cosyns B, Neskovic AN, Dulgheru R, et al. The use of echocardiography in acute cardiovascular care: recommendations of the European Association of Cardiovascular Imaging and the Acute Cardiovascular Care Association. *Eur Hear J Cardiovasc Imaging.* (2015) 16:119–46. doi: 10.1093/ehjci/jeu210
58. Chirumamilla A, Travin MI. Cardiac applications of 123I-mIBG imaging. *Semin Nucl Med.* (2011) 41:374–87. doi: 10.1053/j.semnuclmed.2011.04.001
59. Squame F, Mansi L, Tinoco Mesquita C, Rezende MF. *Nuclear Cardiology Basic and Advanced Concepts in Clinical Practice*. Cham: Springer Nature Switzerland (2021).
60. Marano R, De Cobelli F, Floriani I, Becker C, Herzog C, Centonze M, et al. Italian multicenter, prospective study to evaluate the negative predictive value of 16- and 64-slice MDCT imaging in patients scheduled for coronary angiography (NIMISCAD-Non Invasive Multicenter Italian Study for Coronary Artery Disease). *Eur Radiol.* (2009) 19:1114–23. doi: 10.1007/s00330-008-1239-8
61. Stiermaier T, Moeller C, Oehler K, Desch S, Graf T, Eitel C, et al. Long-term excess mortality in takotsubo cardiomyopathy: predictors, causes and clinical consequences. *Eur J Heart Fail.* (2016) 18:650–6. doi: 10.1002/ejhf.494
62. Bybee KA, Kara T, Prasad A, Lerman A, Barsness GW, Wright; R Scott, et al. Systematic Review: transient left ventricular apical ballooning: a syndrome that mimics ST-segment elevation myocardial infarction. *Ann Intern Med.* (2004) 141:858–65. doi: 10.7326/0003-4819-141-11-200412070-00010
63. Citro R, Bossone E, Parodi G, Rigo F, Nardi F, Provenza G, et al. Independent impact of RV involvement on in-hospital outcome of patients with takotsubo syndrome. *JACC Cardiovasc Imaging.* (2016) 9:894–5. doi: 10.1016/j.jcmg.2015.06.005
64. Kagiyama N, Okura H, Tamada T, Imai K, Yamada R, Kume T, et al. Impact of right ventricular involvement on the prognosis of takotsubo cardiomyopathy. *Eur Heart J Cardiovasc Imaging.* (2016) 17:210. doi: 10.1093/ehjci/jev145
65. Haghi D, Papavassiliu T, Heggemann F, Kaden JJ, Borggrefe M, Suselbeck T. Incidence and clinical significance of left ventricular thrombus in tako-tsubo cardiomyopathy assessed with echocardiography. *QJM*. (2008) 101:381–6. doi: 10.1093/qjmed/hcn017
66. Heckle MR, McCoy CW, Akinseye OA, Khouzam RN. Stress-induced thrombus: prevalence of thromboembolic events and the role of anticoagulation in Takotsubo cardiomyopathy. *Ann Transl Med.* (2018) 6:4–4. doi: 10.21037/atm.2017.11.01
67. Kurisu S, Inoue I, Kawagoe T, Ishihara M, Shimatani Y, Nakama Y, et al. Incidence and treatment of left ventricular apical thrombosis in Tako-tsubo cardiomyopathy. *Int J Cardiol.* (2011) 146:e58–60. doi: 10.1016/j.ijcard.2008.12.208
68. Santoro F, Stiermaier T, Tarantino N, De Gennaro L, Moeller C, Guastafierro F, et al. Left ventricular Thrombi in Takotsubo syndrome: Incidence, predictors, and management: Results from the GEIST (German Italian stress cardiomyopathy) registry. *J Am Heart Assoc.* (2017) 6:e006990. doi: 10.1161/JAHA.117.006990
69. Pant S, Deshmukh A, Mehta K, Badheka AO, Tuliani T, Patel NJ, et al. Burden of arrhythmias in patients with Takotsubo Cardiomyopathy (Apical Ballooning Syndrome). *Int J Cardiol.* (2013) 170:64–8. doi: 10.1016/j.ijcard.2013.10.041
70. Syed FF, Asirvatham SJ, Francis J. Arrhythmia occurrence with takotsubo cardiomyopathy: a literature review. *EP Eur.* (2011) 13:780–8. doi: 10.1093/europace/euq435
71. Stiermaier T, Santoro F, Eitel C, Graf T, Möller C, Tarantino N, et al. Prevalence and prognostic relevance of atrial fibrillation in patients with Takotsubo syndrome. *Int J Cardiol.* (2017) 245:156–61. doi: 10.1016/j.ijcard.2017.07.053
72. Migliore F, Zorzi A, Peruzza F, Perazzolo Marra M, Tarantini G, Iliceto S, et al. Incidence and management of life-threatening arrhythmias in Takotsubo syndrome. *Int J Cardiol.* (2013) 166:261–3. doi: 10.1016/j.ijcard.2012.09.107
73. Madias C, Fitzgibbons TP, Alsheikh-Ali AA, Bouchard JL, Kalsmith B, Garlitski AC, et al. Acquired long QT syndrome from stress cardiomyopathy is associated with ventricular arrhythmias and torsades de pointes. *Hear Rhythm*. (2011) 8:555–61. doi: 10.1016/j.hrthm.2010.12.012
74. Ghadri J-R, Wittstein IS, Prasad A, Sharkey S, Dote K, Akashi YJ, et al. International expert consensus document on takotsubo syndrome (Part II): diagnostic workup, outcome, and management. *Eur Heart J.* (2018) 39:2047–62. doi: 10.1093/eurheartj/ehy077
75. Yaman M, Arslan U, Kaya A, Akyol A, Ozturk F, Okudan YE, et al. Levosimendan accelerates recovery in patients with takotsubo cardiomyopathy. *Cardiol J.* (2016) 23:610–5. doi: 10.5603/CJ.a2016.0100
76. Santoro F, Ieva R, Ferraretti A, Ienco V, Carpagnano G, Lodispoto M, et al. Safety and feasibility of levosimendan administration in takotsubo cardiomyopathy: a case series. *Cardiovasc Ther.* (2013) 31:e133–7. doi: 10.1111/1755-5922.12047
77. Lisi E, Guida V, Blengino S, Pedrazzi E, Ossoli D, Parati G. Intra-aortic balloon pump for treatment of refractory ventricular tachycardia in Tako-Tsubo cardiomyopathy: a case report. *Int J Cardiol.* (2014) 174:135–6. doi: 10.1016/j.ijcard.2014.03.102
78. Rashed A, Won S, Saad M, Schreiber T. Use of the Impella 2.5 left ventricular assist device in a patient with cardiogenic shock secondary to takotsubo cardiomyopathy. *BMJ Case Rep*. (2015) 2015:bcr2014208354. doi: 10.1136/bcr-2014-208354
79. Bonacchi M, Maiani M, Harmelin G, Sani G. Intractable cardiogenic shock in stress cardiomyopathy with left ventricular outflow tract obstruction: is extra-corporeal life support the best treatment? *Eur J Heart Fail*. (2009) 11:721–7. doi: 10.1093/eurjhf/hfp068
80. Singh K, Carson K, Shah R, Sawhney G, Singh B, Parsaik A, et al. Meta-analysis of clinical correlates of acute mortality in takotsubo cardiomyopathy. *Am J Cardiol*. (2014) 113:1420–8. doi: 10.1016/j.amjcard.2014.01.419
81. Santoro F, Ieva R, Musaico F, Ferraretti A, Triggiani G, Tarantino N, et al. Lack of efficacy of drug therapy in preventing takotsubo cardiomyopathy recurrence: a meta-analysis. *Clin Cardiol.* (2014) 37:434–9. doi: 10.1002/clc.22280
82. O'Gara PT, Kushner FG, Ascheim DD, Casey DE Jr, Chung MK, de Lemos JA, et al. 2013 ACCF/AHA guideline for the management of ST-elevation myocardial infarction. *Circulation*. (2013) 127:e362–425. doi: 10.1161/CIR.0b013e3182742cf6
83. Schneider B, Athanasiadis A, Schwab J, Pistner W, Gottwald U, Schoeller R, et al. Complications in the clinical course of tako-tsubo cardiomyopathy. *Int J Cardiol.* (2014) 176:199–205. doi: 10.1016/j.ijcard.2014.07.002
84. Deshmukh A, Kumar G, Pant S, Rihal C, Murugiah K, Mehta JL, et al. Prevalence of Takotsubo cardiomyopathy in the United States. *Am Heart J.* (2012) 164:66–71.e1. doi: 10.1016/j.ahj.2012.03.020
85. Brinjikji W, El-Sayed AM, Salka S. In-hospital mortality among patients with takotsubo cardiomyopathy: a study of the national inpatient sample 2008 to 2009. *Am Heart J.* (2012) 164:215–21. doi: 10.1016/j.ahj.2012.04.010
86. Isogai T, Yasunaga H, Matsui H, Tanaka H, Ueda T, Horiguchi H, et al. Out-of-hospital versus in-hospital Takotsubo cardiomyopathy: analysis of 3719 patients in the diagnosis procedure combination database in Japan. *Int J Cardiol.* (2014) 176:413–7. doi: 10.1016/j.ijcard.2014.07.110
87. Sharkey SW, Pink VR, Lesser JR, Garberich RF, Maron MS, Maron BJ. Clinical profile of patients with high-risk tako-tsubo cardiomyopathy. *Am J Cardiol*. (2015) 116:765–72. doi: 10.1016/j.amjcard.2015.05.054
88. Elesber AA, Prasad A, Lennon RJ, Wright RS, Lerman A, Rihal CS. Four-year recurrence rate and prognosis of the apical ballooning syndrome. *J Am Coll Cardiol*. (2007) 50:448–52. doi: 10.1016/j.jacc.2007.03.050

89. Schneider B, Athanasiadis A, Sechtem U. Gender-related differences in takotsubo cardiomyopathy. *Heart Fail Clin*. (2013) 9(2):137–46, vii. doi: 10.1016/j.hfc.2012.12.005
90. Salmoirago-Blotcher E, Rosman L, Wittstein IS, Dunsiger S, Swales HH, Aurigemma GP, et al. Psychiatric history, post-discharge distress, and personality characteristics among incident female cases of takotsubo cardiomyopathy: a case–control study. *Hear Lung J Cardiopulm Acute Care*. (2016) 45:503–9. doi: 10.1016/j.hrtlng.2016.07.008

Conflict of Interest: The authors declare that the research was conducted in the absence of any commercial or financial relationships that could be construed as a potential conflict of interest.

Publisher's Note: All claims expressed in this article are solely those of the authors and do not necessarily represent those of their affiliated organizations, or those of the publisher, the editors and the reviewers. Any product that may be evaluated in this article, or claim that may be made by its manufacturer, is not guaranteed or endorsed by the publisher.

frontiers in Cardiovascular Medicine

ORIGINAL RESEARCH
published: 16 March 2022
doi: 10.3389/fcvm.2022.830572

Diagnostic Value of ^{11}C-PIB PET/MR in Cardiac Amyloidosis

Xiao Bi[1†‡], Baixuan Xu[1‡], Jiajin Liu[1†], Guanyun Wang[1†], Jing An[2], Xiaojun Zhang[1], Ruimin Wang[1], Wei Dong[3*†] and Zhiwei Guan[1,4*]*

[1] Department of Nuclear Medicine, The First Medical Centre, Chinese PLA General Hospital, Beijing, China, [2] Siemens Healthcare Ltd., Guangdong, China, [3] Department of Cardiology, The Sixth Medical Centre, Chinese PLA General Hospital, Beijing, China, [4] National Clinical Research Center for Geriatric Diseases, Chinese PLA General Hospital, Beijing, China

OPEN ACCESS

Edited by:
Ali Yilmaz,
University Hospital Münster, Germany

Reviewed by:
Filippo Cademartiri,
Gabriele Monasterio Tuscany Foundation (CNR), Italy
Maria Concetta Pastore,
Università del Piemonte Orientale, Italy

***Correspondence:**
Zhiwei Guan
nmguan@139.com
Baixuan Xu
xbx301@163.com
Wei Dong
dongwei@301hospital.com.cn

[†]These authors have contributed equally to this work
[‡]These authors share first authorship

Specialty section:
This article was submitted to Cardiovascular Imaging, a section of the journal Frontiers in Cardiovascular Medicine

Received: *07 December 2021*
Accepted: *07 February 2022*
Published: *16 March 2022*

Citation:
Bi X, Xu B, Liu J, Wang G, An J, Zhang X, Wang R, Dong W and Guan Z (2022) Diagnostic Value of ^{11}C-PIB PET/MR in Cardiac Amyloidosis. Front. Cardiovasc. Med. 9:830572. doi: 10.3389/fcvm.2022.830572

Background: The thioflavin T derivative, ^{11}C-Pittsburgh-B (PIB), is used for Alzheimer's disease imaging because it specifically binds to β-amyloid protein deposits in the brain. The aim of this study was to estimate the diagnostic value of combined ^{11}C-PIB positron emission tomography/magnetic resonance (PET/MR) in cardiac amyloidosis (CA).

Methods: We enrolled 23 heart failure patients with suspected CA based on echocardiographic and electrocardiograph findings. All patients underwent cardiac ^{11}C-PIB PET/MR and non-cardiac biopsy within one week. We also enrolled eight healthy volunteers that underwent cardiac ^{11}C-PIB PET/MR as a control group. The cardiac magnetic resonance (CMR) protocol included cine imaging, late gadolinium enhancement (LGE), and native and post-contrast T1 mapping. Extracellular volume (ECV) was measured using pre- and post-contrast T1 mapping images. LVEF, IVSD, LVPW, LVmass, LVESV, LVEDV, native T1 value, ECV, and maximum uptake of myocardial tissue-to-blood background ratio (TBR) values were obtained from PET/MR images in all patients and healthy subjects.

Results: Thirteen out of twenty-three heart failure patients were clinically diagnosed with CA. The remaining 10 patients were CA-negative (non-CA patient group). Twelve of the thirteen CA patients showed diffuse transmural LGE patterns, whereas LGE was either absent or patchy in the non-CA patients. The diagnostic sensitivity and specificity of TBRmax were 92.3 and 100%, respectively, at a cut-off value of 1.09. Several CMR imaging parameters (LVEF, IVSD, LVmass, LVEDV, LVESV, LVPW, native T1 value and ECV) and TBR showed significant differences between CA patients, non-CA patients, and healthy controls ($P < 0.05$). Native T1 mapping values positively correlated with TBRmax values in CA and non-CA patients ($r = 0.38$, $P = 0.0004$).

Conclusions: ^{11}C-PIB PET/MRI is a valuable tool for the accurate and non-invasive diagnosis of CA because it distinguishes CA patients from non-CA patients and healthy subjects with high specificity and sensitivity. Moreover, native T1 mapping values positively correlated with TBRmax values in CA and non-CA patients. In the future, larger cohort studies are necessary to confirm our findings.

Keywords: ^{11}C-PIB, PET/MR, cardiac amyloidosis, non-invasive diagnosis, LGE, ECV, TBR

INTRODUCTION

Amyloidosis refers to a group of systemic diseases caused by extracellular and/or intracellular accumulation of insoluble misfolded amyloid protein fibrils, which progressively damage the structure and function of related organs (1). Cardiac amyloidosis (CA) is a type of restrictive cardiomyopathy caused by the accumulation of misfolded amyloid protein deposits in the myocardium (2). Heart failure is the main cause of death and morbidity in CA patients, which manifests either as a primary disease or as part of systemic amyloidosis (3). Endocardial biopsy (EB) is the current gold standard for the clinical diagnosis of myocardial amyloidosis (4). However, EB is an invasive procedure that cannot be performed routinely. EB is also associated with high false-negative biopsy interpretation rates. Moreover, it does not provide sufficient clinical information regarding the status of the disease and is not effective for determining prognosis or response to treatment.

Cardiovascular magnetic resonance (CMR) imaging with late gadolinium enhancement (LGE) is the most commonly performed non-invasive technique for characterizing myocardial tissue abnormalities in a wide spectrum of cardiomyopathies (5). Although multiple LGE distributions have been described for cardiac amyloidosis, sub-endocardial and transmural LGE patterns are most commonly observed in cardiac amyloidosis and serve as diagnostic markers (6). However, LGE-CMR is not amenable for the early recognition of mild myocardial amyloidosis during differential diagnosis (7, 8). LGE-CMR is also not suitable for suspected CA patients with severe renal impairment (9, 10). Non-contrast T1 mapping is performed before administering contrast agents to quantify the direct signal from the myocardium (11). Several studies have shown that native T1 values are slightly elevated in focal and diffuse fibrosis (12, 13), edema, and inflammation (14). Boomen et al. reported that myocardial T1 values were significantly higher for patients with amyloidosis, including those without any confirmed cardiac involvement through biopsy or decreased cardiac function (15). However, a major disadvantage of native T1 mapping is that the results can vary significantly based on the type of scanners and magnetic field intensities (1.5T vs. 3T) used for the analysis. ECV (extracellular volume) is another early marker of cardiac involvement in patients with amyloidosis (confirmed by biopsy) and is more reproducible than absolute T1 values (16). However, in the absence of biopsy confirmation, ECV values may overlap with other cardiomyopathy pathologies and limit the specificity of ECV in the early detection of amyloidosis (8).

The thioflavin-T derivate, ^{11}C-Pittsburgh B (PIB), is used for the diagnostic imaging of patients with Alzheimer's disease because it binds with high-affinity to fibrillar β-amyloid protein deposits in the brain (17). Amyloid positron emission tomography (PET) imaging can be used for quantitative analysis of cardiac amyloidosis because it shows high sensitivity and specificity for amyloid protein deposits (18). This feature can be useful for the early diagnosis of CA.

The aim of this study was to assess the diagnostic accuracy of combined ^{11}C-PIB positron emission tomography/magnetic resonance (PET/MR) in a cohort of patients with heart failure and suspected cardiac amyloidosis.

MATERIALS AND METHODS

Patients

Twenty-three patients with heart failure and suspected CA diagnosed with echocardiography and electrocardiograph were enrolled in this retrospective study at the First Medical Center of PLA General Hospital between May 1, 2017 and December 31, 2019. Diagnostic criteria included the thickening of the wall of the ventricular septum plus any two of the following criteria: (a) Ultrasound showed characteristic enhanced echo, such as Granular echo, Speckled echo or Ground glass echo; (b) Unexplained low voltage <0.5 mV in the limb leads of the 12-lead electrocardiogram; (c) Left ventricular diastolic function decreased; (d) or Left atrium enlarged. A series of ^{11}C-PIB PET/MR, echocardiography, extra-cardiac biopsy, and laboratory tests were performed. Eight healthy volunteers without any signs or symptoms of cardiac disease were also enrolled (5 males and 3 females; age range: 41–65 y). The non-CA patients and healthy subjects were considered as the control group. We compared ^{11}C-PIB uptake in the myocardium and the values of several CMR imaging parameters between the patients with CA and control subjects to establish cutoff values. Written informed consent was obtained from all patients prior to recruitment. This study was approved by the Human Ethics Committee of the Chinese PLA General Hospital.

^{11}C-PIB PET/MR Scanning Parameters

Simultaneous ^{11}C-PIB PET and CMR of the heart were performed using a 3T hybrid PET/MR system (Biograph mMR, Siemens Healthineers, Erlangen, Germany). All study subjects were injected with 555 MBq of 11C-PIB through the antecubital vein, and PET data was acquired in list mode using a 20 min table time. The acquisition was started 30 mins after the administration of ^{11}C-PIB. PET images were reconstructed with a 256 × 256 matrix with the ordered-subset expectation maximization method (4 iterations, 8 subsets), and post-smoothing was performed using a 4 mm Gaussian filter. PET images of 5 mm slice thicknesses were then displayed along the transversal, coronal, and sagittal planes. Attenuation correction was performed using the respiratory-gated 2-point Dixon sequence, which was acquired before injection of the gadolinium contrast medium. The Dixon imaging parameters were as follows: repetition time (TR) = 3.6 ms; echo time (TE)1 = 1.23 ms; TE2 = 2.46 ms; field-of-view = 500 × 500 mm; and flip angle (FA) = 10°.

Each CMR series was acquired during the expiratory phase with breath holding. The heart was localized by first acquiring two-dimensional (2D) scout images in the transversal, coronal, and sagittal planes. CMR cine images were acquired using ECG-gated 2D-segmented balanced steady-state free precession (bSSFP) sequence. Two-, three-, and four-chamber long-axis and 10–12 short-axis slices covering the LV were acquired to evaluate cardiac motion and function. The key parameters were as follows: TR/TE = 3.3/1.43; FA = 55°–70°; voxel size = 1.6 ×

$1.6 \times 6.0\ mm^3$; temporal resolution = 45.6 ms; bandwidth = 962 Hz/pixel. The 5(3)3 and 4(1)3(1)2 MOLLI sequence acquisition schemes were used for native T1 and post-contrast T1 mapping, respectively. Identical images were obtained from the basal, mid, and apical short axis slices of the ventricle and the 4-chamber long-axis slices (19, 20). The parameters were as follows: TR/TE = 2.7/1.12 ms; FA = 35°; voxel size = $1.4 \times 1.4 \times 8.0\ mm^3$. LGE images were generated using a 2D phase-sensitive inversion-recovery (PSIR) gradient-echo pulse sequence with the following parameters: TR/TE = 5.2/1.96 ms FA = 20°; voxel size = $1.4 \times 1.4 \times 8.03$ mm.

PET/MRI Analysis

PET activity was measured within the LV myocardium by analyzing fused and co-registered PET and LGE-MR images. Myocardial PET uptake was quantified using standard uptake values (SUV) and target-to-background ratio (TBR) after correcting for the blood-pool activity in the descending thoracic aorta. The standard uptake value (SUV) of the myocardium was measured by drawing the contour of the whole LV at an approximate thickness of 10 mm from base to apex. Maximal SUV (SUVmax) was defined as the voxel with the highest uptake among all the volumes of interest (VOIs) analyzed. Mean SUV (SUVmean) was defined as the average SUV of the total voxels in the VOI. The maximal myocardium to blood cavity ratio (TBRmax) was defined as the maximal SUV of the myocardial VOI divided by the mean SUV of the descending thoracic aorta VOI.

CMR functional parameters, native T1, and ECV were measured semi-automatically using a dedicated CMR software, cvi42 version 5.3 (Circle Cardiovascular Imaging, Calgary, Canada) (5). LV ejection fraction (LVEF) and standard parameters of the cardiac structure such as LV mass, ventricle volume, inter-ventricular septum thickness (IVSD), and left ventricular posterior wall thickness (LVPW) were measured by tracing the endocardial and epicardial borders in the long-axis and short axis cine images at the end-systolic and end-diastolic timepoints. T1 values of global LV were obtained by drawing contours around the endocardium and epicardium as well as indicating the inter-ventricular septum on pre-contrast T1 mapping images with indexing for the hematocrit. Native T1 and ECV of global LV were measured by drawing contours around the endocardium and epicardium as well as indicating the inter-ventricular septum on pre-contrast and post-contrast T1 mapping images with indexing for the hematocrit. Global LV native T1 and ECV values were used for further analyses. All ^{11}C-PIB PET/MR images were analyzed independently by two experienced investigators in nuclear medicine independently. All disagreements were resolved in consultation with a third investigator.

Statistical Analysis

The continuous variables are presented as means ± SD and compared between control and CA patient groups using the Mann–Whitney U test. Receiver operating characteristic (ROC) curves were used to determine the diagnostic TBRmax and native T1 values for CA. Spearman's correlation analysis was performed to determine the degree of association (Spearman's r value) between native T1 value and TBRmax. $P < 0.05$ was considered statistically significant. All statistical analyses were performed using the R 4.0.1 Statistical Package (the R foundation for Statistical Computing, Vienna, Austria) and SPSS software v.24.0 (Statistical Package for Social Science; IBM, Chicago, IL, USA).

RESULTS

Baseline Characteristics

Among the 23 enrolled patients with heart-failure suspected of having CA, thirteen patients were diagnosed with CA. Ten patients with CA were diagnosed by typical non-invasive detection of cardiac involvement by CMR LGEs and positive Congo-red staining of abdominal fat pad biopsies and bone marrow; 2 patients with CA were diagnosed by diffuse sub-endocardial or transmural LGEs and at least one of the monoclonal protein tests being reported as abnormal (21); 1 patient with CA was diagnosed by a positive abdominal fat pad biopsy, positive genetic test for amyloid, and typical echocardiography patterns, including >12 mm thick left ventricular wall and the appearance of grain scintillation in the myocardial wall. The remaining 10 cases were diagnosed as different types of cardiomyopathy: dilated cardiomyopathy (DCM, $n = 2$), rheumatic heart disease (RHD, $n = 1$), valvular heart disease (VHD, $n = 1$), hypertensive heart disease (HHD, $n = 3$), and hypertrophic cardiomyopathy (HCM, $n = 3$). The baseline characteristics of the enrolled patients are summarized in **Table 1**.

Comparison of Clinical and Biochemical Biomarkers Between CA and Non-CA Patients

We did not observe any significant differences in age between CA patients, non-CA patients, and healthy subjects ($P > 0.05$). The BMI values of non-CA patients were significantly higher compared with the CA patients and healthy subjects ($P = 0.033$). We also did not observe any significant differences in the serum cardiac troponin-I (cTnI), calcium, and creatinine values between CA patients and non-CA patients ($P > 0.05$). CA patients showed significantly higher levels of NT-proBNP (13011.46 ± 11726.99 pg/mL vs. 4709.30 ± 5428.82 pg/mL, $P = 0.036$) and blood-free light chain kappa/lambda (1.88 ± 5.77 vs. 0.85 ± 0.31 mg/dL, $P = 0.021$) compared with the non-CA patients. The 13 CA patients were classified under NYHA classification I ($n = 0$), II ($n = 2$), III ($n = 5$), and IV ($n = 6$), respectively (**Table 2**).

The Echocardiography Diagnositic Parameters and PET/MR Structural and Functional Parameters

The echocardiography data for CA patients and non-CA patients are summarized in **Table 3.** There were no differences in the echocardiographic parameters between the CA patients and the

TABLE 1 | Comparison of the baseline clinical data and ^{11}C-PIB PET/MR parameters between patients with and without cardiac amyloidosis (CA).

Patient no.	Age	Sex	Diagnosis	ECG low voltage	NYHA functional class	Urine IFE	Blood IFE	Biopsy (bone marrow)	Biopsy (abdominal wall)	^{11}C-PIB PET/MR			
										Visually PET positive	TBR	T1 native	ECV
1	68	M	CA	+	II	-	NA	NA	+	Yes	3.69	1,525	47
2	67	M	CA	+	IV	+	-	NA	+	Yes	8.08	1,487	52
3	64	M	CA	-	III	+	+	NA	+	Yes	1.77	1,496	50
4	64	F	CA	+	IV	+	+	+	+	Yes	1.30	1,503	51
5	61	F	CA	+	III	+	+	NA	+	Yes	1.82	1,506	61
6	76	F	CA	+	IV	NA	+	NA	-	Yes	5.11	1,432	45
7	51	M	CA	-	III	-	+	+	-	Yes	2.02	1,506	52
8	71	M	CA	+	III	-	-	+	+	Yes	1.21	1,507	65
9	63	M	CA	+	III	NA	-	+	+	Yes	2.44	1,456	51
10	61	M	CA	+	IV	-	-	+	+	Yes	2.24	1,601	54
11	67	F	CA	+	IV	+	-	+	+	Yes	2.75	1,537	56
12	44	F	CA	-	II	-	-	NA	-	No	1.29	1,433	52
13	60	M	CA	-	IV	-	-	NA	+	No	0.92	1,432	38
14	33	M	HHD	-	II	-	-	NA	+	No	0.91	1,419	NA
15	68	M	HHD	-	IV	-	-	NA	+	No	0.94	1,378	32
16	55	M	DCM	-	III	-	-	NA	-	No	0.89	1,315	37
17	70	F	RHD	+	III	-	-	NA	+	No	0.87	1,420	29
18	58	M	VHD	-	IV	NA	-	NA	+	No	0.79	1,349	27
19	73	F	HCM	-	I	-	-	NA	+	No	0.89	1,402	34
20	28	M	HCM	-	II	-	NA	NA	+	No	0.78	1,427	33
21	32	F	HCM	-	II	-	-	+	-	No	0.82	1,363	31
22	67	F	DCM	-	III	-	-	NA	-	No	0.91	1,363	40
23	56	F	HHD	+	III	-	-	+	-	No	0.94	1,467	NA

ECG, electrocardiograph; NYHA, new york heart association; IFE, immunofixation electrophoresis; PET, positron emission tomography; TBR, tissue-to-blood background ratio; ECV, extracellular volume; M, male; F, female; HHD, hypertensive heart disease; DCM, dilated cardiomyopathy; RHD, rheumatic heart disease; VHD, valvular heart disease; HCM, hypertrophic cardiomyopathy.

TABLE 2 | Baseline clinical characteristics of patients with cardiac amyloidosis (CA), those without CA (non-CA), and healthy control subjects.

Characteristics	CA (n:13)	Non-CA (n:10)	Controls (n:8)	*P*
General parameters				
Age (years)	62.9 ± 8.2	54.0 ± 17.0	47.9 ± 13.8	0.105
Female/Male	5/8	5/5	3/5	
BMI (kg/m^2)	22.30 ± 3.04	26.52 ± 4.28	23.84 ± 2.62	0.033
HTN/CHD/DM/Arrhythmia/AF	11/3/1/5/6	7/2/4/4/1	-	-
Biomarkers				
cTnI (ng/ml)	0.13 ± 0.14	0.07 ± 0.07	-	0.166*
NT-proBNP (pg/ml)	13011.46 ± 11726.99	4709.30 ± 5428.82	-	0.036*
Calcium (mg/ml)	2.17 ± 0.11	2.16 ± 0.15	-	0.879*
Creatinine (mg/ml)	117.16 ± 78.90	129.79 ± 70.43	-	0.605*
Blood free light chain Kap/Lam (mg/dl)	1.88 ± 5.77	0.85 ± 0.31	-	0.021*
CMR parameters				
LVEF (%)	48.1 ± 9.4	42.2 ± 15.1	65.2 ± 1.8	<0.001
LV mass (g)	164.3 ± 42.0	181.9 ± 70.1	94.2 ± 22.8	0.002
LVEDV (ml)	101.6 ± 28.2	180.8 ± 67.7	94.0 ± 16.7	0.001
LVESV (ml)	53.9 ± 22.9	108.8 ± 67.4	32.8 ± 8.7	<0.001
IVSD (cm)	15.0 ± 1.6	12.0 ± 2.9	9.0 ± 1.8	<0.001
LVPW (cm)	10.3 ± 2.2	9.8 ± 3.0	7.9 ± 0.9	0.030
Native T1 value (ms)	1493.9 ± 48.1	1390.3 ± 44.8	1264.6 ± 25.6	<0.001
ECV	51.9 ± 6.7	32.5 ± 3.8	-	<0.001
TBR	2.66 ± 1.99	0.85 ± 0.06	0.88 ± 0.07	<0.001

*BMI, body mass index; HTN, hypertension; CHD, coronary heart disease; DM, diabetic mellitus; AF, atrial fibrillation; cTnI, cardiac troponin; NT-proBNP, N-terminal pro-B-type natriuretic peptide; CMR, cardiac magnetic resonance; LVEF, left ventricular ejection fraction; LVEDV, left ventricle end-diastolic volume; LVESV, left ventricle end-systolic volume; IVSD, interventricular septal thickness at diastole; LVPW, left ventricular posterior wall thickness; ECV, extracellular volume; TBR, maximum target-to-background ratio. The symbol * represents the comparison between the two groups.*

TABLE 3 | Echocardiography data from CA patients and non-CA patients.

	Clinical diagnositic of cardiac amyloidosis		
	Yes ($n = 13$)	No ($n = 10$)	*P*
Ventricular septum wall thickness, mm	15.0 ± 2.4	13.4 ± 2.0	0.103
LV ejection fraction, %	47.0 ± 11.8	47.8 ± 14.9	0.887
LV end-diastolic volume, ml	83.2 ± 28.4	134.4 ± 44.0	0.003
Decrease of LV	9	7	-
Diastolic function			
Enlargement of LA	12	7	-
Granular echo	11	6	-
Speckled echo	1	-	-
Ground glass echo	1	-	-

LVEF, left ventricular ejection fraction.

non-CA patients, except for a significant difference in the LV end-diastolic volume (83.2 ± 28.4 vs. 134.4 ± 44.0 ml, $P < 0.05$). We observed significant differences among several CMR parameters (LVEF, IVSD, LVmass, LVEDV, LVESV, LVPW, native T1 value, and ECV) and TBR between CA patients, non-CA patients, and healthy subjects ($P < 0.05$; **Table 2**). PET data showed that the maximal myocardial ^{11}C-PiB uptake was significantly higher in the CA patients compared with the non-CA patients and healthy subjects (0.88 ± 0.07) (2.66 ± 1.99 vs. 0.85 ± 0.06 vs. 0.88 ± 0.07; $P < 0.05$; **Figure 1A**). The native T1 values were significantly higher in the CA patients compared with the non-CA and healthy subjects (1493.9 ± 48.1 vs. 1390.3 ± 44.8 vs. 1264.6 ± 25.6; $P < 0.05$; **Figure 1B**). The ECV values were significantly higher for the CA patients compared with the non-CA patients (51.9 ± 6.7 vs. 32.9 ± 4.2; $P < 0.05$; **Figure 1C**).

Twelve of the thirteen CA patients showed characteristic LGE patterns including diffuse transmural myocardial enhancement, typical subendocardial ring enhancement, and heterogeneous transmural LGE pattern. Only one patient did not show any characteristic LGE pattern. Gadolinium-enhanced CMR was not

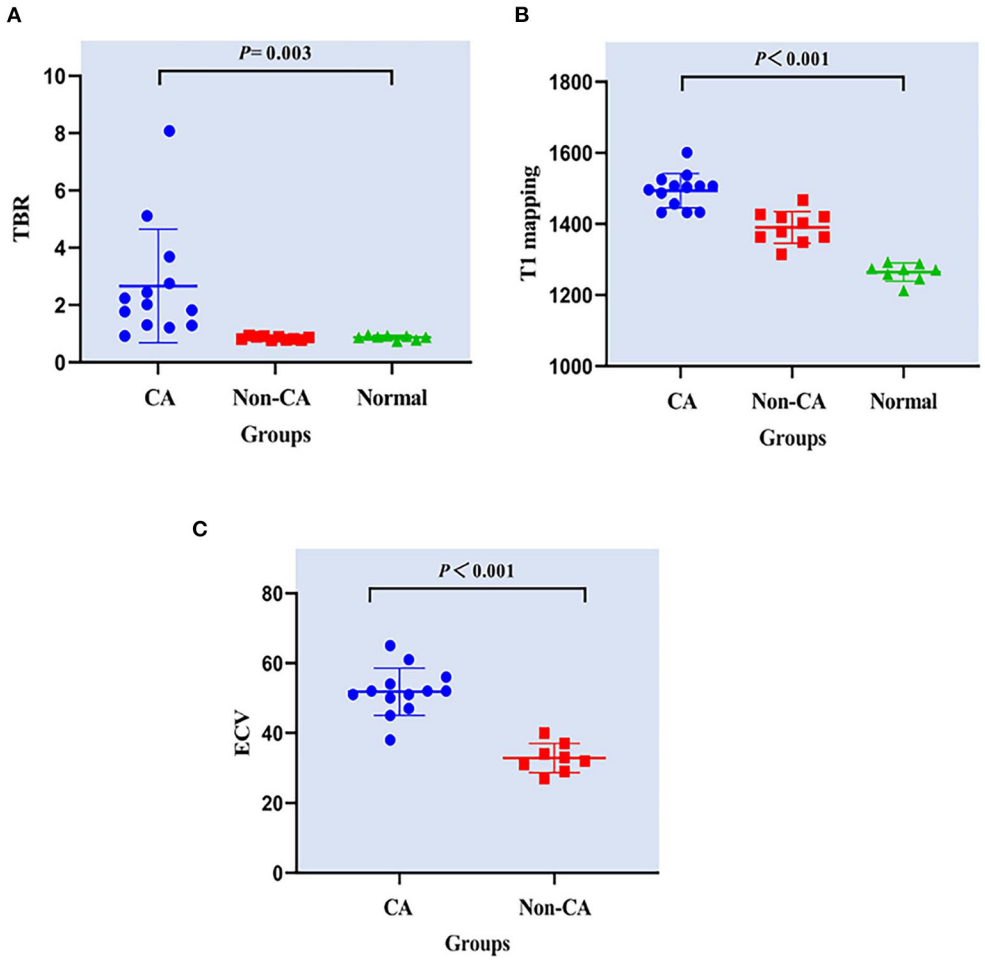

FIGURE 1 | Comparison of **(A)** TBR, **(B)** T1 mapping, and **(C)** ECV values between CA patients, non-CA patients, and healthy control subjects. CA, cardiac amyloidosis; TBR, maximum target-to-background ratio; ECV, extracellular volume. **(A)** PET data showed that the TBR was significantly higher in the CA patients compared with the non-CA patients and healthy subjects (2.66 ± 1.99 vs. 0.85 ± 0.06 vs. 0.88 ± 0.07; $P < 0.05$). **(B)** The native T1 values were significantly higher in the CA patients compared with the non-CA and healthy subjects (1493.9 ± 48.1 vs. 1390.3 ± 44.8 vs. 1264.6 ± 25.6; $P < 0.05$). **(C)** The ECV values were significantly higher for the CA patients compared with the non-CA patients (51.9 ± 6.7 vs. 32.9 ± 4.2; $P < 0.05$).

performed in 2 non-CA patients because of significant azotemia (creatinine clearance < 30 ml/kg/min). In the remaining 8 non-CA patients, we observed patchy LGE enhancement patterns including discrete areas of LGE or diffuse areas of LGE in less than half of the short axis images (**Table 4**). LGE patterns, T1 mapping, and PET images of a representative CA patient are shown in **Figure 2**. Visual inspection of PET images demonstrated positive ^{11}C-PIB uptake in 12 out of 13 CA patients. However, none of the non-CA patients and healthy subjects showed any visible ^{11}C-PIB uptake.

ROC curve analysis using a TBR cutoff value of 1.09 showed that the area under the curve (AUC) value for discriminating CA patients from the controls (10 non-CA patients and 8 healthy subjects) was 0.99 (95% CI: 0.96–1.00) with a sensitivity of 92% (95% CI: 62–100%) and specificity of 100% (95% CI: 78–100%) (**Table 4**). The positive predictive value (PPV) using a TBR cutoff value of 1.09 was 100% (95% CI: 70–100%) and the negative predictive value (NPV) was 95% (95% CI: 72–100%). The PPV, AUC, sensitivity, and specificity values for both ECV and TBR were similar at the ECV cutoff value of 42.5, but NPV [89% (95% CI: 51%–99%)] was lower than TBR. The AUC value for discriminating CA patients from controls using a T1 mapping cutoff value of 1,429.5 was 0.98 (95% CI: 0.96–1.00) with a sensitivity of 100% (95% CI: 72–100%) and specificity of 94% (95% CI: 71–100%). The positive predictive value with this cutoff was 93% (95% CI: 64–100%) and the negative predictive value was 100% (95% CI: 77–98%). The other CMR parameters are shown in **Table 5**.

False-positive ^{11}C-PIB PET/MR scan results were not observed in any of the non-CA patients and healthy subjects using a TBR cut-off value of 1.09. In contrast, one CA patient (Patient #13) showed a false-negative ^{11}C-PIB PET/MR result (maximal LV myocardium to blood cavity ratio of 0.92) (**Figure 3**). We observed positive ECV and native T1 mapping

TABLE 4 | Baseline late gadolinium enhancement (LGE) patterns for all cardiac amyloidosis (CA) and non-CA patients based on ^{11}C-PIB PET/MR data.

Patients	Diagnosis	^{11}C-PIB PET/MR	
		Uptake	LGE pattern
1	CA	Yes	Diffuse transmural myocardial enhancement
2	CA	Yes	Diffuse transmural myocardial enhancement
3	CA	Yes	Diffuse transmural myocardial enhancement
4	CA	Yes	Subendocardial ring enhancement
5	CA	Yes	Diffuse transmural myocardial enhancement
6	CA	Yes	Diffuse transmural myocardial enhancement
7	CA	Yes	Diffuse transmural myocardial enhancement
8	CA	Yes	Subendocardial ring enhancement
9	CA	Yes	Heterogeneous transmural enhancement
10	CA	Yes	Subendocardial ring enhancement
11	CA	Yes	Subendocardial ring enhancement
12	CA	No	Diffuse transmural myocardial enhancement
13	CA	No	Negative
14	HHD	No	Not done because of azotemia
15	HHD	No	Left ventricular apex subendocardium enhancement
16	DCM	No	Enhancement of the left ventricular septal middle layer
17	RHD	No	Negative
18	VHD	No	Enhancement of the left ventricular septal middle layer
19	HCM	No	Enhancement of the junction between interventricular septum and inferior wall
20	HCM	No	Negative
21	HCM	No	Enhancement of the medial anterior wall and inferior wall papillary muscle
22	DCM	No	Enhancement of apex, anterior wall papillary muscle, interwall and inferior wall subendocardium
23	HHD	No	Not done because of azotemia

LGE, late gadolinium enhanced.

values in a PET-negative CA patient who did not show a typical CMR LGE pattern for cardiac amyloidosis, thereby prompting false-positive diagnosis of CA. We did not observe any false positive cases in the non-CA and healthy control groups with a ECV cut-off value of 42.5, but the CA patient with false-negative ^{11}C-PIB (Patient #13) also showed false-negative ECV result. None of the CA patients were false-negative and none of the healthy subjects were false-positive when the cut-off value for native T1 mapping was 1,429.5 ms However, one non-CA patient showed false-positive result because the native T1 mapping value was 1467 ms. The ^{11}C-PIB PET result of this patient was negative, and MR LGE was not performed on this patient because of renal insufficiency. A positive correlation between native T1 mapping value and TBR in CA and non-CA patients was also observed ($r = 0.38$, $P = 0.0004$, **Figure 4**).

DISCUSSION

Our study demonstrated that ^{11}C-PIB PET/MR was a highly sensitive and accurate method to confirm cardiac amyloidosis. Moreover, we demonstrated that a combination of TBRmax values derived from ^{11}C-PIB PET scans, T1 mapping values, and ECV values derived from CMR can be used for accurate diagnosis of CA.

CA is caused by extracellular and intracellular accumulation of insoluble and misfolded fibrillar amyloid protein and shows clinical features resembling restrictive cardiomyopathy (2). Endomyocardial biopsy, the gold standard for diagnosis of CA, is invasive and cannot be performed routinely (22). Moreover, focal myocardial biopsy does not provide information regarding the overall myocardial amyloid load and active accumulation of the amyloid protein. Therefore, there is an urgent need for techniques that can accurately and non-invasively confirm cardiac amyloidosis in clinical settings. Previous studies (23, 24) have demonstrated that ^{11}C-PIB PET/CT is a valuable tool for the non-invasive diagnosis of CA with $\geq$ 95% sensitivity and specificity (18). Our study showed that ^{11}C-PIB PET distinguishes CA patients from both non-CA patients and healthy controls with 94% sensitivity and 100% specificity. Moreover, 11C-PIB-PET was 99% accurate in the positive diagnosis of CA. Rosengren et al. demonstrated that 11C-PIB-PET detected CA in different amyloid subtypes with 89 to 100% accuracy in a dual-center setting (25). Therefore, our results are consistent with these previous findings and suggest that 11C-PIB PET is an independent diagnostic indicator of CA.

LGE-CMR has shown great promise in clinical diagnosis and prognosis because it offers high spatial resolution and the ability to identify pathology in the extracellular space (26). CA patients show diverse patterns of late gadolinium enhancement,

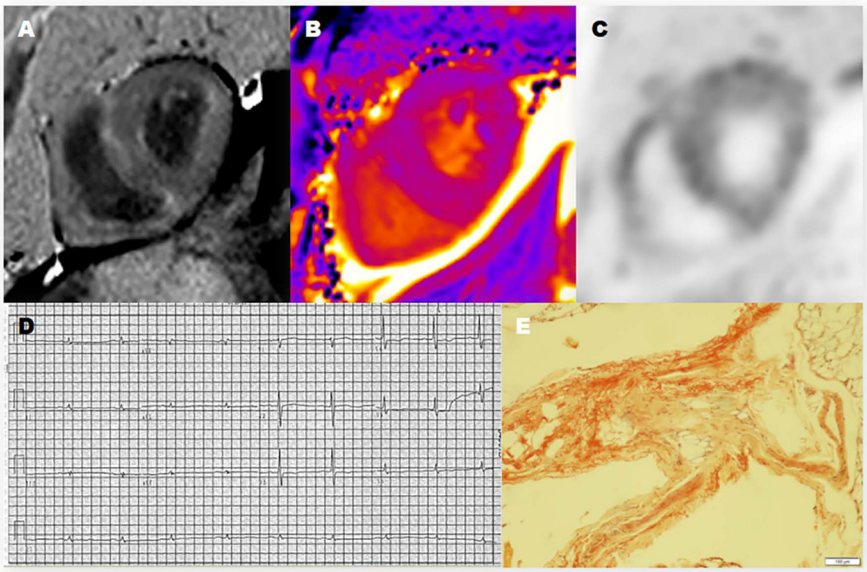

FIGURE 2 | Representative ^{11}C-PiB PET/MR, electrocardiogram, and histologic photomicrograph of one CA patient. **(A)** Late-gadolinium enhancement (LGE)-CMR image demonstrates a diffuse transmural enhancement pattern. **(B)** Native T1 mapping shows that the myocardial T1 value was 1,569 ms. **(C)** The PET/MR image of the myocardium shows strong uptake of ^{11}C-PIB in the left ventricle (LV) and right ventricle (RV). **(D)** The electrocardiogram (12-lead) shows low voltage in the limb leads. **(E)** Histopathologic examination shows positive Congo red staining and amyloid deposits in the adipose tissue.

TABLE 5 | Differential diagnostic efficiency of TBR and CMR parameters between cardiac amyloidosis (CA) patients and control subjects (non-CA patients' and healthy subjects).

	Cutoff	Sensitivity (%)	95% CI (%)	Specificity (%)	95% CI (%)	AUC	95% CI (%)
TBR	1.09	92	62–100	100	78–100	0.99	0.96–1.00
T1 mapping value	1,429.5	100	72–100	94	71–100	0.98	0.95–1.00
ECV	42.5	92	62–100	100	78–100	0.99	0.96–1.00
IVSD (cm)	13.4	100	71–100	83	57–96	0.91	0.79–1.00
LVPW (cm)	8.9	85	54–97	67	41–86	0.71	0.52–0.90
LVEF ()	51.4	77	46–94	72	46–89	0.66	0.46–0.86
LVESV (ml)	64.2	85	54–97	39	18–64	0.53	0.32–0.74
LVEDV (ml)	104.1	77	46–94	72	46–89	0.70	0.51–0.89
LV mass (g)	128.4	85	54–97	67	41–86	0.67	0.47–0.87

AUC, area under the curve; CI, confidence interval; TBR, maximum target-to-background ratio; ECV, extracellular volume; IVSD, interventricular septal thickness at diastole; LVPW, left ventricular posterior wall thickness; LVEF, left ventricular ejection fraction; LVESV, left ventricle end-systolic volume; LVEDV, Left ventricle end-diastolic volume.

such as global subendocardial enhancement, transmural LGE, and patchy focal LGE. In some CA cases, it is very difficult to quantify the degree of abnormality based on LGE-CMR. A recent meta-analysis of seven published studies showed that the accuracy of CMR-based LGE in the positive diagnosis of CA was high with 85% sensitivity and 92% specificity. In our study, 12 out of 13 CA patients showed global left ventricular LGE, a typical enhancement pattern of cardiac amyloidosis. In non-CA patients, we did not observe any typical CA enhancement. However, some patients showed patchy enhancement characteristics, which were indistinguishable from non-CA patients.

The native T1 value has been proposed as a quantitative parameter for evaluating CA with diffuse disease. Furthermore, native T1 mapping eliminates the need for gadolinium and can be used as an alternative method for assessing CA patients with renal insufficiency (27). ECV is more reproducible than absolute T1 mapping values. Moreover, ECV is more advantageous than LGE because it can quantify expansion of the extracellular space based on the region of interest drawn on the ECV maps. Our study showed that the diagnostic accuracy of native T1 values and ECV were significantly higher than the other CMR parameters, with the AUC value of ECV being the highest. However, at a molecular level, both native T1 mapping and ECV are not specific to amyloidosis (6, 28). In contrast, ^{11}C-PIB PET is a useful method for direct evaluation of overall myocardial amyloid load in cardiac amyloidosis. In our study, the diagnostic accuracy of both

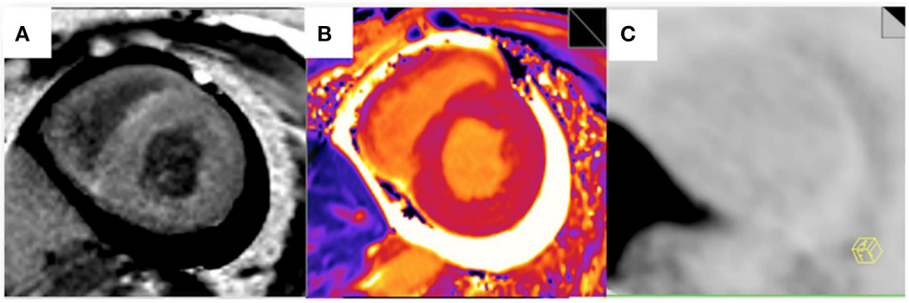

FIGURE 3 | Myocardial LGE, T1 mapping, and PET images from the false-negative CA patient. **(A)** A late gadolinium enhancement image shows a diffuse transmural delayed enhancement pattern in the myocardium. **(B)** The native T1 value was 1,401 ms. **(C)** 11C-PiB PET staining of the myocardium was negative.

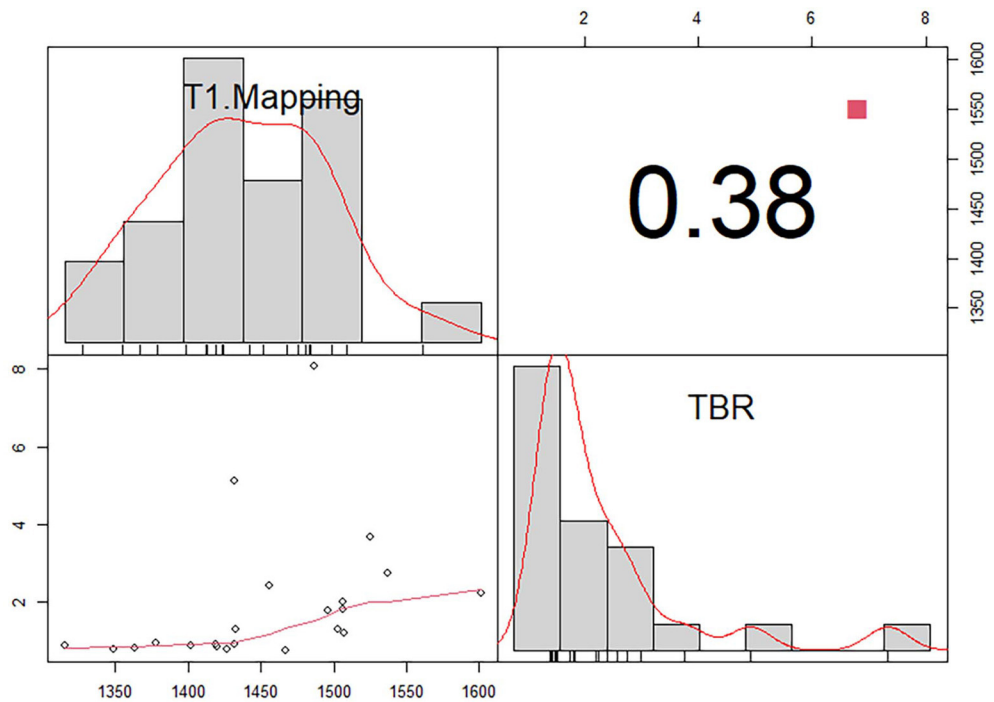

FIGURE 4 | Correlation between T1 mapping and maximum target-to-background ratio (TBR) in patients with (CA) and without cardiac amyloidosis (non-CA).There is a positive correlation between native T1 mapping value and TBR in CA and non-CA patients ($r = 0.38$, $P = 0.0004$).

TBR and ECV was 99%. Native T1 showed higher sensitivity (100 vs. 94%) and lower specificity (94 vs. 100%) than TBR and ECV. In our study, one CA patient (Patient #13) was false-negative for both ^{11}C-PIB PET and ECV. The CMR result of this patient did not show any LV LGE, but the nativeT1 mapping results were positive. Therefore, patient #13 was positively diagnosed as CA based on the native T1 mapping data. The cases of patients #14 and #23 demonstrated unique superiority of ^{11}C-PIB PET for differential diagnosis of cardiac amyloidosis from other cardiomyopathies in the setting of significant azotemia, a clinical condition that prevents contrast-enhanced CMR from being performed. Although the native T1 mapping results were positive for patient #23, the PET results were negative. Therefore, patient #23 was classified as non-CA based on the PET results.

We also analyzed the correlations between TBR values derived from ^{11}C-PIB PET and native T1. Our analysis showed that TBR and native T1 in PET/MR can be used to diagnose CA patients that cannot undergo delayed enhancement because of renal insufficiency. Hence, the combination of the 2 diagnostic indices played a complementary role and improved the diagnostic accuracy of CA. We did not obtain ECV values for some patients who did not undergo delayed enhancement. Both ECV and TBR showed the same AUC (0.99), sensitivity (92%), specificity (100%) and PPV (100%). However, ECV showed lower NPR compared with TBR (89 vs. 95%). This suggested that ECV can be used as an independent diagnostic index for CA.

There are several limitations to this study. Firstly, the sample size of study subjects was small. Therefore, our results need to be confirmed in large cohort studies. Secondly, we could

not complete typing of myocardial amyloidosis in this study because (1) endomyocardial biopsies were not performed for some patients; (2) bone marrow biopsies were performed for only a few patients; and (3) laboratory tests for urine and blood IFE were not performed for all patients. Fontana et al. (29) showed that native T1 values were relatively higher, and ECV values were lower patients with immunoglobulin light chain amyloidosis compared with those with transthyretin amyloidosis (ATTR). Ezawa and Katoh (24) showed that ^{11}C-PIB uptake was lower in patients with ATTR compared with the patients with AL. Therefore, the diagnostic value of ^{11}C-PIB PET/MR imaging for CA requires further evaluation according to the cardiac amyloidosis type because the underlying mechanisms are not completely known. Finally, normal ranges vary for different CMR systems and T1 mapping sequences (30). Normal T1 values are higher when measured at 3T with different sequences and typically with newer versions of mapping compared with older ones. This is a significant obstacle to using native T1 mapping in clinical practice. Therefore, uniform guidelines and normal ranges need to be established for different CMR techniques and sequences so that data can be compared between different patients that have undergone MRI scans at different facilities.

Although endomyocardial biopsy is the golden standard for diagnosis of CA, extrapolating the amyloid content in line with the biopsy sample to the entire heart may be inaccurate, especially in the early CA when the amyloid deposits may not be extensive or diffuse (31). Quantification of amyloid burden is currently based on assessment of wall thickness, LV mass, ECV, or semi-quantitative index on amyloid PET imaging (32). ^{11}C-PIB PET/MR offers substantial advantages. It is non-invasive, quantitative, fuses quantitative parameters of PET and MR to estimate whole-heart cardiac amyloid burden, and can be easily repeated to monitor response to therapy. For patients clinically suspected of CA with heart failure ^{11}C-PIB PET/MR is valuable in CA patients with contraindications to gadolinium (due to renal dysfunction). Our study confirms that ^{11}C-PIB PET/MR multi-parameter imaging provides additional evidence for the diagnosis of CA in the absence of LGE. Moreover, the high sensitivity and specificity of ^{11}C-PIB PET/MR make it possible to detect CA early.

CONCLUSIONS

In conclusion, this study showed that ^{11}C-PIB PET/MR accurately diagnosed cardiac amyloidosis with high sensitivity and specificity. ^{11}C-PIB PET/MR showed structural and functional changes in CA patients and helped to accurately determine the location and extent of amyloid protein deposition. Our study also demonstrated the advantages of using multiple parameters and multi-sequence imaging characteristics of CMR in combination with the high specificity of ^{11}C-PIB PET for the accurate diagnosis of CA.

DATA AVAILABILITY STATEMENT

The raw data supporting the conclusions of this article will be made available by the authors, without undue reservation.

ETHICS STATEMENT

The studies involving human participants were reviewed and approved by the Human Ethics Committee of the Chinese PLA General Hospital. The patients/participants provided their written informed consent to participate in this study. Written informed consent was obtained from the individual(s) for the publication of any potentially identifiable images or data included in this article.

AUTHOR CONTRIBUTIONS

XB, JL, WD, JA, RW, BX, and ZG: conception and design. XB, JL, XZ, and WD: data collation. XB, JL, and GW: statistical Analysis. XB and JL: article writing. GW, JA, WD, BX, and ZG: article revision. All authors contributed to the article and approved the submitted version.

FUNDING

Granting agencies: National Clinical Research Center for Geriatric Diseases, Chinese PLA General Hospital. Grant number: NCRCG-PLAGH-2019012.

ACKNOWLEDGMENTS

I would like to thank JL, ZG, WD, BX, JA, and RW for their guidance to me in the experimental design. I would also like to thank JL, XZ, and WD for their help in patient enrollment and data collection. Thanks to GW for his support in data processing. I would like to thank JL for guiding me in writing PET/MR related technologies. I would like to thank GW, ZG, WD, BX, and JA for carefully revisingmy article. Thanks to everyone's help and joint efforts, we have completed this meaningful article.

REFERENCES

1. Merlini G, Bellotti V. Molecular mechanisms of amyloidosis. *N Engl J Med.* (2003) 349:583–96. doi: 10.1056/NEJMra023144
2. Rapezzi C, Merlini G, Quarta CC, Riva L, Longhi S, Leone O, et al. Systemic cardiac amyloidoses: disease profiles and clinical courses of the 3 main types. *Circulation.* (2009) 120:1203–12. doi: 10.1161/CIRCULATIONAHA.108.843334
3. Yusuf SW, Solhpour A, Banchs J, Lopez-Mattei JC, Durand JB, Iliescu C, et al. Cardiac amyloidosis. *Expert Rev Cardiovasc Ther.* (2014) 12:265–77. doi: 10.1586/14779072.2014.876363
4. Bokhari S, Shahzad R, Castano A, Maurer MS. Nuclear imaging modalities for cardiac amyloidosis. *J Nucl Cardiol.* (2014) 21:175–84. doi: 10.1007/s12350-013-9803-2
5. Lin L, Li X, Feng J, Shen KN, Tian Z, Sun J, et al. The prognostic value of T1 mapping and late gadolinium enhancement cardiovascular magnetic

resonance imaging in patients with light chain amyloidosis. *J Cardiovasc Magn Reson.* (2018) 20:2. doi: 10.1186/s12968-017-0419-6
6. Syed IS, Glockner JF, Feng D, Araoz PA, Martinez MW, Edwards WD, et al. Role of cardiac magnetic resonance imaging in the detection of cardiac amyloidosis. *JACC Cardiovasc Imaging.* (2010) 3:155–64. doi: 10.1016/j.jcmg.2009.09.023
7. Barison A, Aquaro GD, Pugliese NR, Cappelli F, Chiappino S, Vergaro G, et al. Measurement of myocardial amyloid deposition in systemic amyloidosis: insights from cardiovascular magnetic resonance imaging. *J Intern Med.* (2015) 277:605–14. doi: 10.1111/joim.12324
8. Mongeon FP, Jerosch-Herold M, Coelho-Filho OR, Blankstein R, Falk RH, Kwong RY, et al. Quantification of extracellular matrix expansion by CMR in infiltrative heart disease. *JACC Cardiovasc Imaging.* (2012) 5:897–907. doi: 10.1016/j.jcmg.2012.04.006
9. Bollée G, Guery B, Joly D, Snanoudj R, Terrier B, Allouache M, et al. Presentation and outcome of patients with systemic amyloidosis undergoing dialysis. *Clin J Am Soc Nephrol.* (2008) 3:375–81. doi: 10.2215/CJN.02470607
10. Lachmann HJ, Gillmore JD. Renal amyloidosis. *Br J Hosp Med.* (2010) 71:83–6. doi: 10.12968/hmed.2010.71.2.46485
11. Muscogiuri G, Suranyi P, Schoepf UJ, De Cecco CN, Secinaro A, Wichmann JL, et al. Cardiac magnetic resonance T1-mapping of the myocardium: technical background and clinical relevance. *J Thorac Imaging.* (2018) 33:71–80. doi: 10.1097/RTI.0000000000000270
12. aus dem Siepen F, Buss SJ, Messroghli D, Andre F, L ossnitzer D, Seitz S, et al. T1 mapping in dilated cardiomyopathy with cardiac magnetic resonance: quantification of diffuse myocardial fibrosis and comparison with endomyocardial biopsy. *Eur Heart J Cardiovasc Imaging.* (2015) 16:210–6. doi: 10.1093/ehjci/jeu183
13. Ntusi NA, Piechnik SK, Francis JM, Ferreira VM, Rai AB, Matthews PM, et al. Subclinical myocardial inflammation and diffuse fibrosis are common in systemic sclerosis – a clinical study using myocardial T1-mapping and extracellular volume quantification. *J Cardiovasc Magn Reson.* (2014) 16:21–33. doi: 10.1186/1532-429X-16-21
14. Ferreira VM, Piechnik SK, Dall'Armellina E, Karamitsos TD, Francis JM, Ntusi N, et al. Native T1-mapping detects the location, extent and patterns of acute myocarditis without the need for gadolinium contrast agents. *J Cardiovasc Magn Reson.* (2014) 16:36–47. doi: 10.1186/1532-429X-16-36
15. Boomen MVD, Slart RHJA, Hulleman EV, Dierckx RAJO, Velthuis BK, van der Harst P, et al. Native T1 Reference Values for Nonischemic Cardiomyopathies and Populations With Increased Cardiovascular Risk: A Systematic Review and Meta- analysis. *JMRI.* (2017) 47:891–912. doi: 10.1002/jmri.25885
16. Fontana M, White SK, Banypersad SM, Sado DM, Maestrini V, Flett AS, et al. Comparison of T1 mapping techniques for ECV quantification. Histological validation and reproducibility of ShMOLLI versus multi breath-hold T1 quantification equilibrium contrast CMR. *J Cardiovasc Magn Res.* (2012) 14:88. doi: 10.1186/1532-429X-14-88
17. Nordberg A, Carter SF, Rinne J, Drzezga A, Brooks DJ, Vandenberghe R, et al. A European multicentre PET study of fibrillar amyloid in Alzheimer's disease. *Eur J Nucl Med Mol Imaging.* (2013) 40:104–14. doi: 10.1007/s00259-012-2237-2
18. Kim Y J, Ha S, Kim Y. Cardiac amyloidosis imaging with amyloid positron emission tomography: a systematic review and meta-analysis. *J Nucl Cardiol.* (2018) 27:123–32. doi: 10.1007/s12350-018-1365-x
19. Kellman P, Hansen MS. T1 mapping in the heart: accuracy and precision. *J Cardiovasc Magn Reson.* (2014) 16:20. doi: 10.1186/1532-429X-16-2
20. Kellman P, Bandettini WP, Hammer-Hansen S, Hansen MS, Arai AE. Characterization of myocardial T1- mapping bias caused by intramyocardial fat in inversion recovery and saturation recovery techniques. *J Cardiovasc Magn Reson.* (2015) 17:33. doi: 10.1186/s12968-015-0136-y
21. Garcia-Pavia P, Rapezzi C, Adler Y, Arad M. Linhart A. Diagnosis and treatment of cardiac amyloidosis: a position statement of the ESC Working Group on Myocardial and Pericardial Diseases. *Eur J Heart Failur.* (2021) 23:512–26. doi: 10.1093/eurheartj/ehab072
22. Gertz MA, Lacy MQ, Dispenzieri A, Hayman SR. Amyloidosis: diagnosis and management. *Clin LymphomaMyeloma.* (2005) 6:208–19. doi: 10.3816/CLM.2005.n.048
23. Lee SP, Lee ES, Choi H, Im HJ, Koh Y, Lee MH, et al. 11C-Pittsburgh B PET imaging in cardiac amyloidosis. *JACC Cardiovasc Imaging.* (2015) 8:50–9. doi: 10.1016/j.jcmg.2014.09.018
24. Ezawa N, Katoh N. Visualization of multiple organ amyloid involvement in systemic amyloidosis using 11C-PiB PET imaging. *Eur J Nucl Med Mol Imaging.* (2018) 45:452–61. doi: 10.1007/s00259-017-3814-1
25. Rosengren S, Clemmensen TS, Tolbod L, Granstam SO, Eiskjær H, Wikström G, et al. Diagnostic accuracy of [11C]PIB positron emission tomography for detection of cardiac amyloidosis. *J Am Coll Cardiol Imaging.* (2020) 13:1299–1460. doi: 10.1016/j.jcmg.2020.02.023
26. Bhatti S, Watts E, Syed F, Vallurupalli S, Pandey T, Jambekar K, et al. Clinical and prognostic utility of cardiovascular magnetic resonance imaging in myeloma patients with suspected cardiac amyloidosis. *Eur Heart J Cardiovasc Imaging.* (2016) 17:970–7. doi: 10.1093/ehjci/jew101
27. Baggiano A, Boldrini M, Martinez-Naharro A, Kotecha T, Petrie A, Rezket T, et al. Non-contrast magnetic resonance for the diagnosis of cardiac amyloidosis. *JACC: Cardiovascular Imaging.* (2020) 13:69–80. doi: 10.1016/j.jcmg.2019.03.026
28. Ruberg FL, Appelbaum E, Davidoff R, Ozonoff A, Kissinger KV, Harrigan C, et al. Diagnostic and prognostic utility of cardiovascular magnetic resonance imaging in light-chain cardiac amyloidosis. *Am J Cardiol.* (2009) 103:544–9. doi: 10.1016/j.amjcard.2008.09.105
29. Fontana M, Banypersad SM, Treibel TA, Abdel-Gadir A, Maestrini V, Lane T, et al. Differential myocyte responses in patients with cardiac transthyretin amyloidosis and light-chain amyloidosis: a cardiac MR imaging study. *Radiology.* (2015) 277:388–97. doi: 10.1148/radiol.2015141744
30. Roujol S, Weingärtner S, Foppa M, Chow K, Kawaji K, Ngo LH, et al. Accuracy, precision, and reproducibility of four T1 mapping sequences: a head-to-head comparison of MOLLI, ShMOLLI, SASHA, and SAPPHIRE. *Radiology.* (2014) 272:6. doi: 10.1148/radiol.14140296
31. Haq M, Pawar S, Berk JL. Miller EJ, Ruberg FL. Can (99m)Tc-Pyrophosphate aid in early detection of cardiac involvement in asymptomatic variant TTR amyloidosis? *JACC Cardiovasc Imaging.* (2017) 10:713–4. doi: 10.1016/j.jcmg.2016.06.003
32. Dorbala S, Cuddy S, Falk RH. How to image cardiac amyloidosis: a practical approach. *JACC Cardiovasc Imaging.* (2020) 13:1368–83. doi: 10.1016/j.jcmg.2019.07.015

Conflict of Interest: JA is employed at Siemens Healthcare Ltd.

The remaining authors declare that the research was conducted in the absence of any commercial or financial relationships that could be construed as a potential conflict of interest.

Publisher's Note: All claims expressed in this article are solely those of the authors and do not necessarily represent those of their affiliated organizations, or those of the publisher, the editors and the reviewers. Any product that may be evaluated in this article, or claim that may be made by its manufacturer, is not guaranteed or endorsed by the publisher.

frontiers in Cardiovascular Medicine

MINI REVIEW
published: 21 March 2022
doi: 10.3389/fcvm.2022.839400

Artificial Intelligence Advancements in the Cardiovascular Imaging of Coronary Atherosclerosis

*Pedro Covas[1], Eison De Guzman[2], Ian Barrows[1], Andrew J. Bradley[1], Brian G. Choi[1,3], Joseph M. Krepp[1], Jannet F. Lewis[1], Richard Katz[1], Cynthia M. Tracy[1], Robert K. Zeman[3], James P. Earls[3] and Andrew D. Choi[1,3]**

[1] Division of Cardiology, The George Washington University School of Medicine, Washington, DC, United States,
[2] Department of Internal Medicine, The George Washington University School of Medicine, Washington, DC, United States,
[3] Department of Radiology, The George Washington University School of Medicine, Washington, DC, United States

Coronary artery disease is a leading cause of death worldwide. There has been a myriad of advancements in the field of cardiovascular imaging to aid in diagnosis, treatment, and prevention of coronary artery disease. The application of artificial intelligence in medicine, particularly in cardiovascular medicine has erupted in the past decade. This article serves to highlight the highest yield articles within cardiovascular imaging with an emphasis on coronary CT angiography methods for % stenosis evaluation and atherosclerosis quantification for the general cardiologist. The paper finally discusses the evolving paradigm of implementation of artificial intelligence in real world practice.

Keywords: artificial intelligence, machine learning, coronary artery disease, cardiovascular imaging, atherosclerosis

OPEN ACCESS

Edited by:
Andrea Igoren Guaricci, Azienda Ospedaliero Universitaria Consorziale Policlinico di Bari, Italy

Reviewed by:
Fu-Zong Wu, Kaohsiung Veterans General Hospital, Taiwan

***Correspondence:**
Andrew D. Choi
adchoi@mfa.gwu.edu

Specialty section:
This article was submitted to Cardiovascular Imaging, a section of the journal Frontiers in Cardiovascular Medicine

Received: *19 December 2021*
Accepted: *03 February 2022*
Published: *21 March 2022*

Citation:
Covas P, De Guzman E, Barrows I, Bradley AJ, Choi BG, Krepp JM, Lewis JF, Katz R, Tracy CM, Zeman RK, Earls JP and Choi AD (2022) Artificial Intelligence Advancements in the Cardiovascular Imaging of Coronary Atherosclerosis. Front. Cardiovasc. Med. 9:839400. doi: 10.3389/fcvm.2022.839400

INTRODUCTION

Artificial intelligence (AI) is a broad term that refers to computing that can perform complex human-like tasks (1). Machine learning (ML) is a subset of AI which encompasses a growing collection of algorithms that is divided into supervised learning, unsupervised learning, semi supervised learning, and reinforcement learning (2, 3). Supervised learning refers to learning from labeled examples, while unsupervised and reinforcement learning performs unlabeled learning and learning from pattern recognition (4). Further subsets of ML include Deep Learning (DL), which uses complex data sets which mirror human neural networks (5). Human cognition is finite, but the use of AI may allow for improved discrimination and evaluation of these immense datasets (6). At the same time, the "black-box" nature of AI can lead to uncertainty in clinical practice in part due to the complexity of the algorithms, unrecognized bias and application to appropriate clinical needs (7).

The application of AI in cardiology has increased exponentially annually, specifically in the diagnosis of coronary artery disease (CAD). These novel approaches may enhance future implementation of the new 2021 American College of Cardiology/American Heart Association Chest Pain Guideline that elevate the role of imaging to Class I recommendation in both acute and stable chest pain in intermediate risk patients (8). Current investigations aim to augment and enhance current risk-based approaches through the analysis of multiomic data sets, while also recently showing promise in the direct image interpretation of cardiac and coronary structures through a myriad of approaches (9). Between 2001 and 2015 the proportion of AI/ML related articles in relevant journals per month was

0.1% in relation to the total number published in the journals. This increased to 16.2% per month by 2020 (1). Literature search was completed on PubMed and EMBASE databases by searching "artificial intelligence" or "machine learning" AND various terminology related to cardiology such as "cardiac," "cardio," "cardiology," "infarct," "valve," "cardiosurgical," etc. (1). Over the past 5 years there were over 3,000 papers published in Pubmed related to AI/ML learning in cardiovascular medicine (4). In cardiovascular imaging specifically, there's been increases in non-invasive coronary imaging including applications of coronary artery plaque, automated calcium scoring, perivascular fat attenuation and machine learning based image enhancement as well in the application of nuclear imaging, and myocardial perfusion to large data sets to improve risk enhancement. This review article serves to summarize the recent advancements (**Table 1**) of Artificial Intelligence in respect to coronary artery disease (CAD) and imaging.

CORONARY ARTERY DISEASE RISK PREDICTION

Current prevention guidelines incorporate the use of the pooled cohort equation for adults aged 40–75 with non-traditional cardiovascular risk factors to determine a 10 year risk of cardiac events (19). The pooled cohort equation creates a simplified risk score with a finite number of variables; however the simplification of the approach may overestimate cardiovascular risk in certain populations (20, 21). Multiple studies have sought to enhance the risk prediction model. AI has been particularly impactful in the area of improved cardiovascular risk prediction (16). Nakanishi et al. demonstrated that ML using logistic regression modeling that incorporate multiple clinical and cardiac computed tomography (CT) variables was superior in predicting 10 year coronary artery disease death [area under the curve (AUC) = 0.86] than clinical data alone (AUC = 0.835), coronary artery calcium (CAC) alone (AUC = 0.816), or ML CT (AUC = 0.827) (12). This model used a total of 77 variables [46 clinical such as atherosclerotic cardiovascular disease (ASCVD) risk score, sex, age] and 31 CT variables from CAC scan to train the machine learning algorithm. Similarly, Motwani et al. (22) demonstrated that ML incorporating 25 clinical and 44 coronary computed tomography angiography (CCTA) parameters better predicted 5 year mortality than current clinical or imaging metrics. This study involved 10,030 patients, and ML exhibited a higher AUC compared with Framingham Risk Score (FRS) (ML 0.79 vs. FRS 0.61) or CCTA severity scores such as segment stenosis score (SSS) (ML 0.79 vs. SSS 0.64) (22). Al'Aref studied 13,054 patients in The Coronary CT Angiography Evaluation For Clinical Outcomes (CONFIRM) registry. ML with CAC performed the best in predicting obstructive CAD on CCTA (AUC 0.881) compared to ML alone (AUC = 0.682) and CAD consortium clinic score +CACS (0.866) (3). These models demonstrate the potential to improve predictive models. By incorporating numerous variables, both clinical and imaging, these machine learning algorithms can better predict cardiovascular mortality. Therefore, in addition to current tools such as the 10-year ASCVD risk, CAC score, and CCTA, these models can prove to add invaluable information in assessing a patient's cardiovascular risk.

CORONARY STENOSIS

The recent 2021 American Heart Association/American College of Cardiology/Multisociety Guideline for the Evaluation and Diagnosis of Chest Pain redefines the presence of coronary artery disease as obstructive (≥50% stenosis) and non-obstructive (<50%) stenosis (23). In the realm of invasive and non-invasive coronary angiography (*via* CCTA), the evaluation of coronary artery stenosis requires visual analysis by a trained provider (18, 24). However, there can be inter-provider variability in interpretation of these studies in real world practice. Lu et al. (25) showed in the analysis of the Prospective Multicenter Imaging Study for Evaluation of Chest Pain (PROMISE) trial, coronary CTA scans read by both core laboratory and local site readers, 41% of the scans were in discordance regarding the presence of significant stenosis (defined as stenosis ≥50%). There remains great interest in identifying solutions that allow for improved reproducibility. AI has shown promising advancements in the detection of obstructive CAD. In 2015, Kang et al. (26) demonstrated that machine learning algorithms allowed for the detection of both obstructive (≥50% stenosis) and non-obstructive (<50% stenosis) lesions with an AUC of 0.94. In addition, Freiman et al. (27) used a deep sparse autoencoder—mixed structure regularization approach in 90 subjects and observed an AUC that ranged from 0.78 to 0.94 for discrimination of mild stenosis <30% to severe stenosis ≥70%.

More recently, the CT Evaluation by Artificial Intelligence for Atherosclerosis, Stenosis and Vascular Morphology (CLARIFY) multi-center study compared AI to level 3 (L3) readers in detecting coronary artery stenosis on CCTA (11). AI analysis (**Figure 1**) showed 99.7% accuracy in detecting >70% stenosis and 94.8% accuracy in detecting >50% stenosis. Among the vessels analyzed, the mean difference in maximal diameter stenosis between AI and L3 readers was minimal at −0.8 %. AI analysis to determine the Coronary Artery Disease Reporting and Data System (CAD-RADS) categorization compared to L3 readers was also examined. AI generated a CAD-RADS score that was in agreement with the readers in 78% of scans, and generated a score that was in agreement within 1 category in 98% of the scans. A subsequent analysis by Griffin et al. evaluated a multi-center cohort of patients undergoing core-lab quantitative invasive angiography (QCA) and found that AI CCTA had high diagnostic accuracy when compared to QCA in detecting >50% stenosis (AUC 0.88) and >70% stenosis (AUC 0.92) (10). The analysis time was approximately 10 mins, which represents an improvement over the several hours that previous methods have required. The deep convolutional neural network based approach utilized in these studies has been cleared by the Food and Drug Administration (FDA), and is clinically available and are expected to enable widespread generalizability of the studied approaches.

TABLE 1 | Summary of high-yield artificial intelligence/machine learning studies in coronary artery disease imaging.

Study	Population	Method	Application	AI method	Performance*
Griffin et al. (10)	Diverse stable chest pain patients from 23 global sites undergoing CCTA plus quantitative coronary angiography, stress testing and fractional flow reserve (CREDENCE study)	Direct image analysis using a series of validated convolutional neural networks for AI-guided evaluation of coronary segmentation, lumen wall evaluation and plaque characterization of CCTA images	Ground truth: Core-Lab quantitative coronary angiography and invasive fractional flow reserve for identification of % coronary stenosis and adverse plaque characteristics in comparison to in	Validated convolutional neural network models; Image analysis 10 mins	Accuracy, sensitivity, specificity of 86%, 94%, 82% for ≥70% stenosis. Intra-class correlation of 0.73; For false positive AI-CCTA (≥70% by AI-CCTA, QCA < 70%), 66% of vessels had FFR < 0.8
Choi et al. (11)	Acute and stable chest pain patients from 3 international centers undergoing CCTA (CLARIFY study)	Direct image analysis using a series of validated convolutional neural networks for AI-guided evaluation of coronary segmentation, lumen wall evaluation and plaque characterization of CCTA images.	Ground truth: Level 3 Expert consensus for identification of % coronary stenosis and adverse plaque characteristics	Validated convolutional neural network models; Image analysis 10 mins	Accuracy, sensitivity, specificity for ≥70% stenosis was 99.7, 90.9, 99.8%. Mean difference for maximal diameters stenosis −0.8% (95% CI 13.8% to −15.3%)
Nakanishi et al. (12)	Asymptomatic adults without known CHD, part of CAC Consortium, *n* = 66,636	Coronary artery calcium and clinical variables. 77 variables incorporated, including ASCVD risk score, age, sex, race, CACS, and the number, volume and density of CAC plaques	Risk prediction for ASCVD related death and CHD related death	ML using a 10-fold cross validation framework to train and evaluate the model, as well as information gain ratio and model building using an ensemble algorithm	AUC 0.845 and 0.860 for ML predicting CVD death and CHD death respectively, compared to 0.821 and 0.835 for clinical data alone, and 0.781 and 0.816 for CAC score alone
Al'Aref et al. (3)	Stable patients with suspected CAD, from CONFIRM registry, *n* = 13,054	Coronary artery calcium and clinical variables. 25 clinical variables used, including age, gender, diabetes mellitus, hypertension, cholesterol levels	Prediction of obstructive CAD on CCTA	ML using a gradient boosting algorithm. A ten-fold cross validation framework was used to train and evaluate the model	AUC 0.881 for ML + CACS, compared to ML alone (0.773), CAD consortium clinical score (0.734), and with CACS (0.866)
Hu et al. (13)	Stable patients with suspected CAD from the REFINE SPECT registry, *n* = 1980	Stress/rest ^{99m}Tc-sestamibi/tetrofosmin MPI with SPECT, followed by invasive coronary angiography within 6 months. 18 clinical, 9 stress test, and 28 imaging variables utilized	Early coronary revascularization (ECR) prediction for stable patients after stress testing	ML using a ten-fold cross validation framework to train and evaluate the model, as well as information gain ratio and model building using an ensemble LogitBoost algorithm	AUC of ECR prediction by ML (0.812)
Oikonomou et al. (14)	Patients with stable chest pain referred for CCTA, *n* = 1575	CCTA, including perivascular adipose tissue data, and clinical variables.	5-year MACE risk prediction (cardiac death, non-fatal MI, late revascularization, non-cardiac death)	ML using random forest algorithm and repeated five-fold cross-validation	MACE prediction with and without addition of perivascular adipose tissue data (AUC 0.880 vs. 0.754)

(Continued)

TABLE 1 | Continued

Study	Population	Method	Application	AI method	Performance*
Betancur et al. (15)	Patients who underwent clinically indicated exercise or pharmacologic stress myocardial perfusion SPECT imaging, $n = 2,619$	Rest/stress 1-day ^{99m}Tc-sestamibi imaging. 28 clinical variables, 17 stress test variables, and 25 imaging variables used.	3-year MACE risk prediction, including all-cause mortality, non-fatal myocardial infarction, unstable angina, or late coronary revascularization	ML using a ten-fold cross validation framework to train and evaluate the model, as well as information gain ratio and model building using an ensemble LogitBoost algorithm	MACE prediction by ML (AUC 0.81), vs. automated stress TPD (0.73) and physician interpretation (0.64)
Motwani et al. (16)	Stable patients with suspected CAD, from CONFIRM registry, $n =$ 10,030	Clinical and CCTA data. 25 clinical and 44 CCTA parameters evaluated, including segment stenosis score, segment involvement score, number of segments with non-calcified, mixed or calcified plaques, age, sex, gender, and FRS	Risk prediction of 5-year all-cause mortality of CAD	ML using a 10-fold cross validation framework to train and evaluate the model, as well as information gain ratio and model building using an ensemble algorithm	AUC 0.79 for ML predicting 5-year all cause mortality vs. FRS (0.61) and CCTA severity score (0.64 for SSS)
Arsanjani et al. (17)	Stable patients with suspected CAD, $n = 713$	Rest^{201}Thallium/stress ^{99m}Technetium with SPECT, followed by invasive coronary angiography within 3 months. 33 total clinical, stress test, and imaging variables utilized.	Early coronary revascularization prediction for stable patients after stress testing	ML with model building using an ensemble LogitBoost algorithm and a ten-fold cross validation framework to train and evaluate the model	Receiver operator characteristic AUC of 0.81 for ML, vs. 0.81 for reader 1, 0.72 for reader 2, and 0.77 for standalone measure of perfusion
Kang et al. (18)	Patients who underwent clinically indicated CCTA, $n = 42$	CCTA patient datasets, with visual identification of lesions with stenosis ≥25% by three expert readers, using consensus reading	Automated CCTA reading to detect both obstructive (stenosis ≥50%) and non-obstructive (stenosis 25–50%) CAD.	ML incorporating a learning-based method and an analytic method. A ten-fold cross validation framework was used to train and evaluate the model	Receiver operator characteristic AUC of 0.94 for detecting obstructive and non-obstructive lesions

**All values statistically significant, $p < 0.05$.*

ML, machine learning; AUC, area under curve; CACS, coronary artery calcium score, ASCVD, atherosclerotic cardiovascular disease; CHD, coronary heart disease; CCTA, coronary computed tomography angiography; CAD, coronary artery disease; FRS, Framingham risk score; SSS, segment stenosis score; FRP, fat radiomic profile; MPI, myocardial perfusion imaging; ECR, early coronary revascularization; TPD, total perfusion defect.

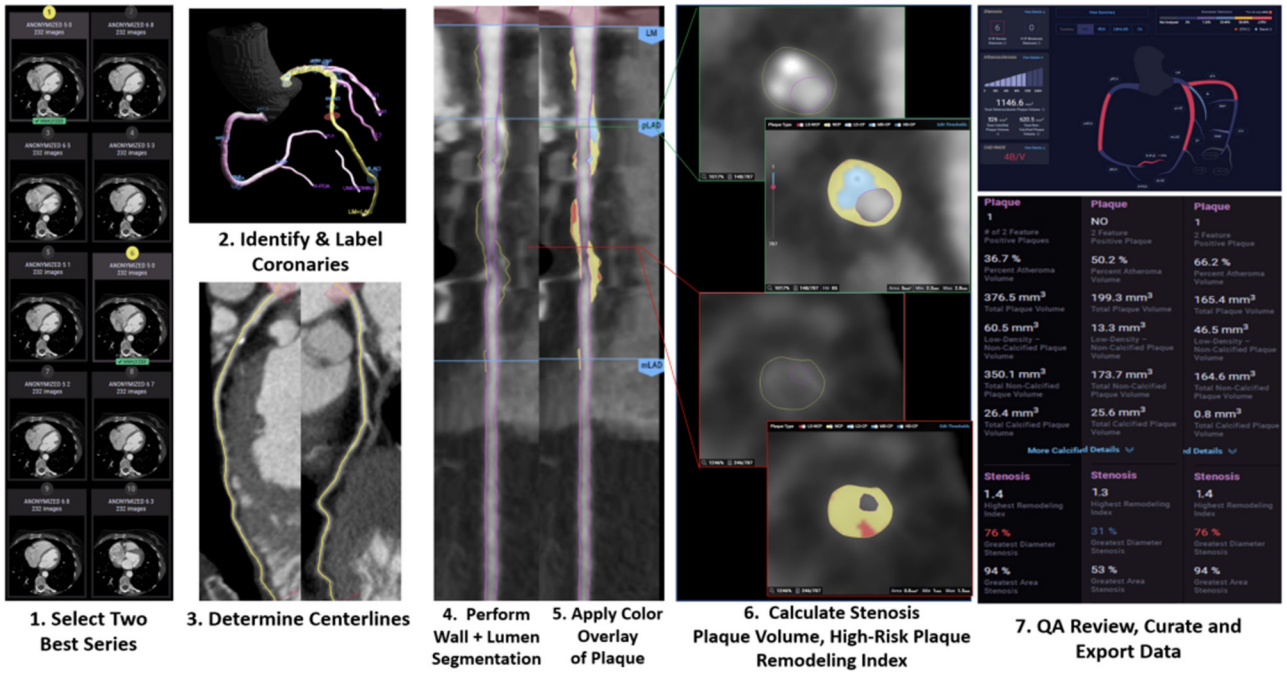

FIGURE 1 | Case example of AI-guided coronary computed tomography angiography. Using a series of validated convolutional neural network models (including VGG19 network, 3D U-Net, and VGG Network variant) for image quality assessment, the machine learning algorithm (Cleerly, New York, NY) selects the best series, identifies and labels all of the major epicardial coronaries and their side branches, determines centerlines, performs coronary segmentation and labeling and then performs a rapid assessment of % stenosis, plaque volume and of adverse plaque characteristics. The data is then displayed in a graphical output to allow for clinical review.

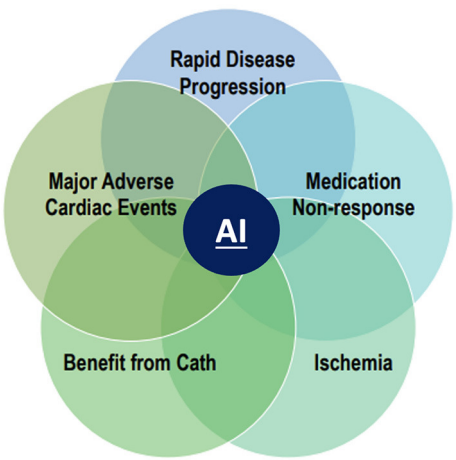

FIGURE 2 | New paradigm of AI guided coronary artery disease imaging. An artificial intelligence (AI) guided approach to coronary artery disease in CAD imaging opens several new frontiers in the evaluation and treatment of atherosclerosis. These include the evaluation of rapid disease progressors, accessing response or non-response to statin and other lipid lowering therapies, improved prediction of ischemia, enhanced selection for guideline based invasive angiography and prognostication of major adverse cardiovascular events.

CORONARY ATHEROSCLEROSIS QUANTIFICATION

Beyond coronary stenosis or coronary artery calcium contemporary evidence has shown that the quantification of adverse atherosclerotic plaque characteristics enhances prognostication of patients at elevated risk for acute coronary syndrome (ACS) (28). Rosendael et al. (29) showed that calcium density (calculated from semi-automated software) can be associated with ACS risk. In this study, patients with and without ACS had similar calcified plaque volume. However, those who experienced ACS had less highly dense plaque, termed by the authors as "1K plaque" (HU > 1,000) than ACS-free subjects, suggesting that 1K plaque has lower risk for acute plaque rupture. The SCOT-HEART trial showed that low-attenuation plaque (HU < 30) was associated with three times the risk of coronary heart disease death or nonfatal MI (30). Other features of plaques which contribute to the prognosis of CAD were studied by Yang et al. (31). The investigators used machine learning to analyze vessels in CCTA that had low fractional flow reserve (FFR) (≤0.80). In these vessels, adverse plaque features beyond lumen area which were found to be associated with low FFR vessels that included: percent atheroma volume, fibrofatty/necrotic core volume, plaque volume, proximal left anterior descending

coronary artery involvement, and remodeling index. Al' Aref et al. (32) trained a machine learning model to detect culprit lesions (which had been confirmed on invasive coronary angiography) by combining quantitative and qualitative plaque features on CCTA. The machine learning model yielded an area under the curve of 0.77 for identifying the culprit lesion, significantly outperforming other models that were based solely on diameter stenosis or high-risk plaque features.

Quantification of plaque and identifying high risk plaque features is time consuming, often taking several hours for a single study, and requires a high level of expertise in a dedicated research core lab limiting such application to real world practice (33). Machine learning offers tremendous potential to allow for interpretation of imaging matrices that encompass the millions of pixels required to fully quantify atherosclerotic plaque from CCTA data in the clinical world. The aforementioned CLARIFY study by Choi et al. and the subsequent evaluation by Griffin et al. has evaluated a broad range of atherosclerosis plaque features using AI analysis (11, 34). Subsequent initial analysis has further shown that AI detected high risk features, such as lumen volume and low-attenuation, more often than experienced level 3 readers as well as accuracy when compared to fractional flow reserve. Furthermore, the analysis was performed as little as under 10 mins.

There are a number of important ongoing applications of plaque quantification. Budoff et al. (35) demonstrated that in CAD patients with elevated triglyceride levels and already taking a statin, icosapent ethyl significantly decreased the volume of low-attenuation plaque compared to placebo over an 18 month period. The application of well-validated AI guided approach to atherosclerosis quantification may enable important advances in assessing the response to preventive therapies.

NUCLEAR MYOCARDIAL PERFUSION IMAGING

AI has also been applied to the field of nuclear medicine (36). Its utility has been demonstrated in the evaluation of coronary artery disease via single photon emission computed tomography (SPECT). Hu et al. studied 1980 patients with suspected CAD (37). Those patients underwent SPECT imaging and later invasive coronary angiography. ML utilized multiple clinical, imaging, and stress test variables to predict the need for early coronary revascularization (ECR). On a per vessel basis, ML better predicted the need for ECR (AUC = 0.79) vs. Regional Stress Tissue perfusion deficit (TPD) (AUC = 0.71), combined view TPD (AUC = 0.71), or ischemic TPD (AUC = 0.72). This was also true on a per patient basis (AUC = 0.81). Interestingly, ML also outperformed expert nuclear readers on the need for ECR in a per patient basis. Arsanjani et al. showed that machine learning can improve the accuracy of SPECT in identifying significant CAD (≥70% stenosis). AI performed with similar, if not better, accuracy (87%) in detecting these lesions compared to two expert readers (86 and 82%) (38). A similar study found that support vector machines algorithm was superior to two expert readers in detecting obstructive CAD (AUC 0.92 vs. 0.87 and 0.88) (39). Betancur et al. also showed that compared to current clinical method (total perfusion deficit), deep learning was able to predict obstructive CAD with more accuracy per patient (AUC 0.80 vs. 0.78) and also per vessel (AUC 0.76 vs. 0.73) (14). While identifying obstructive CAD is certainly important, what is of greater clinical value is predicting those patients who will go on to have adverse outcomes. In one study, machine learning demonstrated superiority to visual analysis by physicians in predicting 3-year major adverse cardiovascular events (MACE) (AUC 0.78 vs. 0.65). When incorporating clinical information (age, gender, risk factors, family history) into the algorithm, machine learning performed with even greater accuracy in predicting MACE (AUC 0.81) (40).

Furthermore, Alonso et al. showed that by analyzing SPECT data, a machine learning model outperformed logistic regression in predicting cardiac death (AUC 0.83 vs. 0.76) (13). In analyzing patients with obstructive CAD, AI has also proven its ability to predict those that may require intervention in the future. Arsanjani et al. (41) explored the utility of AI in predicting the need for revascularization. The researchers discovered that by incorporating clinical parameters such as age, smoking history, hypertension, diabetes, and family history, machine learning algorithm could predict the need for revascularization with similar or better accuracy compared to two expert readers (AUC 0.81 vs. 0.81 and 0.72). As AI interpretion of nuclear imaging continues to improve, its clinical value may increase the automated identification of ischemia beyond currently available perfusion mapping.

CORONARY FLOW

In 2011, the non-invasive evaluation of fractional flow reserve by computed tomography (FFRCT) was introduced into the field of cardiac imaging by the DISCOVER-FLOW trial (42). Machine learning has been subsequently applied to the analysis of non-invasive coronary flow (43). The MACHINE registry was the first study comparing CT FFR from machine learning algorithm vs. CT FFR from computational fluid dynamics (CFD) algorithm (15). The study demonstrated that machine learning CT FFR algorithm distinguished functionally significant obstructive CAD equally well as FFR derived from a hybrid CFD approach. Tesche et al. (44) found that machine learning CT FFR had a per-lesion sensitivity of 79% and specificity of 94% in detecting lesion-specific ischemia. The area under the curve for detecting lesion-specific ischemia was 0.89 for machine learning CT FFR, equal to CFD CT FFR (AUC 0.89) and significantly higher than CCTA (AUC 0.61) and quantitative coronary angiography (AUC 0.69). The diagnostic value of machine learning CT FFR was also studied by Dugua et al. (17), who retrospectively investigated patients with symptoms of ACS who were worked up with CCTA followed by invasive coronary angiography. The investigators identified non-culprit lesions (≥ 25% stenosis, not intervened on during invasive coronary angiography). In an average of 19.5 month follow-up period, 14 patients (29%) suffered a MACE due to these non-culprit lesions. The mean FFR CT for these non-culprit lesions was 0.78, therefore showing that FFR CT ≤

80% in patients with symptoms consistent with ACS can be a predictor of future MACE. These studies show the clinical utility of machine learning FFR CT, which also has the potential to be more efficient. Calculating FFR CT using computational flow dynamics is technologically demanding and can take up to 10 mins (15). On the other hand Itu et al. (45) demonstrated how machine learning models could generate FFR CT in as little as 2.4 s. Mannil et al. (46) conducted a proof-of-concept study showing that machine learning and texture analysis of low-dose cardiac CT was able to detect myocardial infarction that was not visible to radiologists.

PERIVASCULAR ADIPOSE INFLAMMATION BY CT

Vascular inflammation is a significant contributor to atherosclerosis and plaque destabilization (47). Perivascular Adipose Tissue (PVAT) can be monitored by CT fat attenuation to predict coronary artery disease due to the inflammatory effects from the vessels to the PVAT (48, 49). Higher fat attenuation index (FAI) is associated with increased cardiovascular mortality (50). One study found that there is higher FAI in culprit lesions compared to non-culprit lesions in ACS (51, 52). Oikonomou et al. (53) studied the use of ML in PVAT in three different studies/methodologies for enhanced cardiac risk prediction beyond looking at the coronary vessel anatomy and risk factors. The first study analyzed 167 patients undergoing cardiac surgery. PVAT was biopsied for transcriptional factors and CT scan to image the PVAT was performed. This demonstrated a non-invasive method of detecting and adipose tissue microvacuolar remodeling by correlation with increased levels of Collagen Type 1 Alpha 1 Chain (53). Study 2 analyzed the Fat Radiomic Profile (FRP) of 1,575 patients from the SCOT-HART trial and concluded that high FRP (designated as ≥ 0.63) was associated with a 10.8 fold increase of MACE after adjustment for risk factors (53). Lastly in study 3, 44 patients with acute myocardial infarctions (AMI) underwent CT scans on admission and 6 months later. The authors found that there were higher FRP values consistent with adverse PVAT remodeling with persistence at 6 months compared to perivascular Fat attenuation index (FAI) which was present at only with initial presentation of AMI (53).

EPICARDIAL FAT QUANTIFICATION

In multiple studies, the location of the epicardial fat, particularly in the left atrioventricular groove has been a modest predictor of obstructive CAD (54, 55). In a study by Commanduer et al. (56), deep learning to quantify epicardial adipose tissue (EAT) was compared to quantification from two expert readers. 70 patients underwent non-contrast calcium scans and correlation of EAT volumes with deep learning quantification highly correlated with expert readers $R = 0.973$ and $R = 0.979$; $p < 0.001$. Deep learning quantification was also associated with increased non-calcified plaque on subsequent CCTA (5.7 vs. 1.8%, $p = 0.026$). Deep learning quantification was performed with a mean of 1.57 s $\pm$ 0.49 s compared to 15 mins for expert readers.

CORONARY ARTERY CALCIUM

Increased coronary artery calcium has demonstrated to have important prognostic significance across age and diverse ethnic groups (57–59). In addition, CAC now has an important guideline-level role in risk-stratification and treatment decisions of CAD for patients at intermediate risk. For example, in non-diabetic adults aged 40–75 with LDL-C between 70 and 189 mg/dl and a 10-year ASCVD risk between 7.5 and 19.9%, current guidelines encourage the use of CAC score to guide clinicians on de-risking patients or initiating intensive lipid lowering therapy (60). Typically, calcium scores are obtained from regular dose, ECG-gated chest CT's and require some degree of manual input (the provider selecting/confirming areas of calcification and the software subsequently generating a calcium score).

There has been recent interest in using artificial intelligence/machine learning to allow for the automated quantification of coronary artery calcium as well as incorporating a calculated coronary artery calcium score to improve current risk prediction models. Isgum et al. (61) demonstrated that coronary artery calcium score can also be obtained from low-dose chest CT performed for lung cancer screening in the smoking population. Investigators identified CAC with a statistical pattern recognition system, and then utilized support vector machines to correctly classify cardiovascular risk category in 82% of the subjects based on Agatston score. The accuracy of fully automated calcium scores from low-dose CT has also been evaluated in other studies. Takx et al. (62), examined automatic calcium scores derived from low-dose CT. There was good reliability between fully automated calcium scores and reference scores set by human readers (kappa 0.85). Most of the discordance was due to the automated method failing to detect calcifications in the right coronary artery. Isgum et al. (63), also yielded similar results. The study showed agreement of CVD risk category (based on Agatston score) not only between fully automatic and manual calcium scores derived from low dose CT (kappa 0.89), but also between fully automatic calcium score from low dose CT and calcium score from dedicated calcium scoring CT (kappa 0.74). Winkel et al. (64) used deep-learning software to calculate vessel-specific CAC sub-scores (right coronary artery, left main, left main, left anterior descending, and circumflex). The risk class assignment determined by AI showed agreement with that of human readers (kappa = 0.91). Given the association of smoking history with cardiovascular disease, and the abundance of lung cancer screening CT scans, the ability to automatically estimate calcium scores from such scans could provide the added benefit of identifying patients at increased cardiovascular risk.

ETHICS, LIMITATIONS AND STANDARDS OF ARTIFICIAL INTELLIGENCE IN CAD IMAGING

The ease in which ML can acquire data can present ethical dilemmas. Big data can be analyzed in minutes (11) raising issues such as proper consent and safe storage of protected health information (PHI). The "black box" nature of AI may lead to uncertainty for physicians seeking to apply these

approaches to practice. Clinicians must be aware of the specific validation of AI (65) and the limitations to avoid unintended extrapolation and biased results. As automated analysis improves to better address gaps in expert level care, the field of cardiovascular imaging training may be inadvertently depleted of the "Human Neural Network" when there is overreliance on AI to create the foundations of analyzing images (66). The use of AI in cardiovascular medicine needs to be tailored to specific patient-centered goals to avoid unintended or false discoveries (9).

In the imaging of coronary artery disease, it is important to establish appropriate ground truth standards such as quantitative coronary angiography, fractional flow reserve and invasive ultrasound. In addition, new artificial intelligence and machine learning based approaches should be validated in randomized controlled trials (RCT). An RCT in which one arm receives usual care and the other arm receives AI assisted care can be extremely influential and may be a novel trial approach to further create an evidence base for the use AI in clinical practice. It is important that these tools are vetted by the Food and Drug Administration and similar regulatory bodies, through peer-reviewed studies as well as through the professional societies. The field will also need to further develop models for integration into clinical practice, its use as a clinical decision support tool as well as addressing scenarios in which the AI/ML tool disagrees with clinical readers. It is also expected there may be clinical scenarios in which the AI/ML has not been fully trained. For example, in an acute coronary syndrome, the AI/ML may be able to identify severity of stenosis and adverse plaque characteristics, but not recognize a coronary artery dissection. With its various application to cardiovascular medicine, there will be a continued and ongoing need to apply ethnical and scientific standards in AI/ML in coronary imaging.

CONCLUSIONS

The promise of artificial intelligence lies in leveraging modern algorithms to improve decision making and risk prediction beyond current models that are patient-centered (**Figure 2**) (11). In the opinion of this author group, the recently validated stenosis and atherosclerosis quantification methods discussed in this paper, with their FDA approval and clinical availability represent a practice ready approach. Application of an AI/ML guided CCTA approach opens several new frontiers in the assessment and treatment of atherosclerosis. Specific examples include the opportunity to evaluate rapid disease progressors and those that do not respond to lipid lowering therapies. AI/ML may also allow for non-invasive evaluation of those that demonstrate plaque regression after intensified, personalized medical therapies. AI/ML guided atherosclerosis evaluation may better predict ischemia as well as those patients that will require invasive angiography

A future paradigm includes utilization of AI so that the cardiologist may use the AI/ML guided information to make improved clinical decisions and enhance patient-centered outcomes. With continued research in the field and promising outcomes it is expected that the next decade will see AI applied broadly in clinical practice to allow improved outcomes while care remains led by the cardiovascular clinician.

AUTHOR CONTRIBUTIONS

PC and AC contributed to the conception and design of the manuscript. PC, ED, IB, and AC wrote the first draft of the manuscript. All authors provided important intellectual review, contributed to manuscript revision, read and approved the final version.

REFERENCES

1. Friedrich S. Applications of artificial intelligence/machine learning approaches in cardiovascular medicine: a systematic review with recommendations. In: Groß IRK, Engelhardt S, Bahls M, Heinz J, Huber C, Kaderali L, editor *European Heart Journal—Digital Health* (2021).
2. Singh G. Al'Aref SJ, Van Assen M, Kim TS, van Rosendael A, Kolli KK, et al. Machine learning in cardiac CT: basic concepts and contemporary data. *J Cardiovasc Comput Tomogr.* (2018) 12:192–201. doi: 10.1016/j.jcct.2018.04.010
3. Al'Aref SJ, Maliakal G, Singh G, van Rosendael AR, Ma X, Xu Z, et al. Machine learning of clinical variables and coronary artery calcium scoring for the prediction of obstructive coronary artery disease on coronary computed tomography angiography: analysis from the CONFIRM registry. *Eur Heart J.* (2020) 41:359–67. doi: 10.1093/eurheartj/ehz565
4. Quer G, Arnaout R, Henne M. Machine learning and the future of cardiovascular care: JACC state-of-the-art review. *J Am Coll Cardiol.* (2021) 77:300–13. doi: 10.1016/j.jacc.2020.11.030
5. Bizopoulos P, Koutsouris D. Deep learning in cardiology. *IEEE Rev Biomed Eng.* (2019) 12:168–93. doi: 10.1109/RBME.2018.2885714
6. Sengupta PP, Shrestha S. Machine learning for data-driven discovery: the rise and relevance. *JACC Cardiovasc Imaging.* (2019) 12:690–2. doi: 10.1016/j.jcmg.2018.06.030
7. Seetharam K, Shrestha S, Sengupta PP. Artificial intelligence in cardiovascular medicine. *Curr Treat Options Cardiovasc Med.* (2019) 21:25. doi: 10.1007/s11936-019-0728-1
8. Gulati M, Levy PD, Mukherjee D, Amsterdam E, Bhatt DL, Birtcher KK, et al. 2021 AHA/ACC/ASE/CHEST/SAEM/SCCT/SCMR guideline for the evaluation and diagnosis of chest pain: a report of the American College of Cardiology/American Heart Association Joint Committee on clinical practice guidelines. *Circulation.* (2021) 2021:CIR0000000000001029. doi: 10.1161/CIR.0000000000001029
9. Seetharam K, Brito D, Farjo PD, Sengupta PP. The role of artificial intelligence in cardiovascular imaging: state of the art review. *Front Cardiovasc Med.* (2020) 7:618849. doi: 10.3389/fcvm.2020.618849
10. Griffin W, Choi A, Earls J, Marques H, Barkovich E, Riess J, et al. Evaluation of coronary stenosis on CT coronary angiography, comparison with quantitative coronary angiography and fractional flow reserve; A CREDENCE trial sub-study. *JACC: Cardiovasc Imaging.* (2022) S1936-878X(22)00001-8. doi: 10.1016/j.jcmg.2021.10.020
11. Choi AD, Marques H, Kumar V, Griffin WF, Rahban H, Karlsberg RP, et al. CT EvaLuation by ARtificial Intelligence For Atherosclerosis, Stenosis and Vascular MorphologY (CLARIFY): a multi-center, international study. *J Cardiovasc Comput Tomogr.* (2021) 15:470–6. doi: 10.1016/j.jcct.2021.05.004
12. Nakanishi R, Slomka PJ, Rios R, Betancur J, Blaha MJ, Nasir K, et al. Machine learning adds to clinical and CAC assessments in predicting

10-year CHD and CVD deaths. *JACC Cardiovasc Imaging.* (2021) 14:615–25. doi: 10.1016/j.jcmg.2020.08.024
13. Haro Alonso D, Wernick MN, Yang Y, Germano G, Berman DS, Slomka P. Prediction of cardiac death after adenosine myocardial perfusion SPECT based on machine learning. *J Nucl Cardiol.* (2019) 26:1746–54. doi: 10.1007/s12350-018-1250-7
14. Betancur J, Commandeur F, Motlagh M, Sharir T, Einstein AJ, Bokhari S, et al. Deep learning for prediction of obstructive disease from fast myocardial perfusion SPECT: a multicenter study. *JACC Cardiovasc Imaging.* (2018) 11:1654–63. doi: 10.1016/j.jcmg.2018.01.020
15. Coenen A, Kim YH, Kruk M, Tesche C, De Geer J, Kurata A, et al. Diagnostic accuracy of a machine-learning approach to coronary computed tomographic angiography-based fractional flow reserve: result from the MACHINE Consortium. *Circ Cardiovasc Imaging.* (2018) 11:e007217. doi: 10.1161/CIRCIMAGING.117.007217
16. Shameer K, Johnson KW, Glicksberg BS, Dudley JT, Sengupta PP. Machine learning in cardiovascular medicine: are we there yet? *Heart.* (2018) 104:1156–64. doi: 10.1136/heartjnl-2017-311198
17. Duguay TM, Tesche C, Vliegenthart R, De Cecco CN, Lin H, Albrecht MH, et al. Coronary computed tomographic angiography-derived fractional flow reserve based on machine learning for risk stratification of non-culprit coronary narrowings in patients with acute coronary syndrome. *Am J Cardiol.* (2017) 120:1260–6. doi: 10.1016/j.amjcard.2017.07.008
18. Choi AD, Blankstein R. Becoming an expert practitioner: the lifelong journey of education in cardiovascular imaging. *JACC Cardiovasc Imaging.* (2021) 14:1594–7. doi: 10.1016/j.jcmg.2021.03.006
19. Arnett DK, Blumenthal RS, Albert MA, Buroker AB, Goldberger ZD, Hahn EJ, et al. 2019 ACC/AHA guideline on the primary prevention of cardiovascular disease: a report of the American College of Cardiology/American Heart Association Task Force on clinical practice guidelines. *J Am Coll Cardiol.* (2019) 74:e177–232. doi: 10.1161/CIR.0000000000000678
20. Rana JS, Tabada GH, Solomon MD, Lo JC, Jaffe MG, Sung SH, et al. Accuracy of the atherosclerotic cardiovascular risk equation in a large contemporary, multiethnic population. *J Am Coll Cardiol.* (2016) 67:2118–30. doi: 10.1016/j.jacc.2016.02.055
21. DeFilippis AP, Young R, McEvoy JW, Michos ED, Sandfort V, Kronmal RA, et al. Risk score overestimation: the impact of individual cardiovascular risk factors and preventive therapies on the performance of the American Heart Association-American College of Cardiology-Atherosclerotic Cardiovascular Disease risk score in a modern multi-ethnic cohort. *Eur Heart J.* (2017) 38:598–608. doi: 10.1093/eurheartj/ehw301
22. Motwani M, Dey D, Berman DS, Germano G, Achenbach S, Al-Mallah MH, et al. Machine learning for prediction of all-cause mortality in patients with suspected coronary artery disease: a 5-year multicentre prospective registry analysis. *Eur Heart J.* (2017) 38:500–7. doi: 10.1093/eurheartj/ehw188
23. Gulati M, Levy PD, Mukherjee D, Amsterdam E, Bhatt DL, Birtcher KK, et al. 2021 AHA/ACC/ASE/CHEST/SAEM/SCCT/SCMR guideline for the evaluation and diagnosis of chest pain: a report of the American College of Cardiology/American Heart Association Joint Committee on clinical practice guidelines. *J Am Coll Cardiol.* (2021) 78:e187–285. doi: 10.1016/j.jacc.2021.07.053
24. Choi AD, Thomas DM, Lee J, Abbara S, Cury RC, Leipsic JA, et al. 2020 SCCT guideline for training cardiology and radiology trainees as independent practitioners (Level II) and advanced practitioners (Level III) in cardiovascular computed tomography: a statement from the society of cardiovascular computed tomography. *J Cardiovasc Comput Tomogr.* (2021) 15:2–15. doi: 10.1016/j.jcct.2020.08.003
25. Lu MT, Meyersohn NM, Mayrhofer T, Bittner DO, Emami H, Puchner SB, et al. Central core laboratory versus site interpretation of coronary ct angiography: agreement and association with cardiovascular events in the PROMISE Trial. *Radiology.* (2018) 287:87–95. doi: 10.1148/radiol.2017172181
26. Kang D, Dey D, Slomka PJ, Arsanjani R, Nakazato R, Ko H, et al. Structured learning algorithm for detection of nonobstructive and obstructive coronary plaque lesions from computed tomography angiography. *J Med Imaging.* (2015) 2:014003. doi: 10.1117/1.JMI.2.1.014003
27. Freiman M, Manjeshwar R, Goshen L. Unsupervised abnormality detection through mixed structure regularization (MSR) in deep sparse autoencoders. *Med Phys.* (2019) 46:2223–31. doi: 10.1002/mp.13464
28. Shaw LJ, Blankstein R, Bax JJ, Ferencik M, Bittencourt MS, Min JK, et al. Society of Cardiovascular Computed Tomography/North American Society of cardiovascular imaging—expert consensus document on coronary CT imaging of atherosclerotic plaque. *J Cardiovasc Comput Tomogr.* (2021) 15:93–109. doi: 10.1016/j.jcct.2020.11.002
29. van Rosendael AR, Narula J, Lin FY, van den Hoogen IJ, Gianni U, Al Hussein Alawamlh O, et al. Association of high-density calcified 1K plaque with risk of acute coronary syndrome. *JAMA Cardiol.* (2020) 5:282–90. doi: 10.1001/jamacardio.2019.5315
30. Williams MC, Kwiecinski J, Doris M, McElhinney P, D'Souza MS, Cadet S, et al. Sex-specific computed tomography coronary plaque characterization and risk of myocardial infarction. *JACC Cardiovasc Imag.* (2021) 14:1804–14. doi: 10.1016/j.jcmg.2021.03.004
31. Yang S, Koo BK, Hoshino M, Lee JM, Murai T, Park J, et al. CT Angiographic and plaque predictors of functionally significant coronary disease and outcome using machine learning. *JACC Cardiovasc Imaging.* (2021) 14:629–41. doi: 10.1016/j.jcmg.2020.08.025
32. Al'Aref SJ, Singh G, Choi JW, Xu Z, Maliakal G, van Rosendael AR, et al. A boosted ensemble algorithm for determination of plaque stability in high-risk patients on coronary CTA. *JACC Cardiovasc Imaging.* (2020) 13:2162–73. doi: 10.1016/j.jcmg.2020.03.025
33. Williams MC, Newby DE. Understanding quantitative computed tomography coronary artery plaque assessment using machine learning. *JACC Cardiovasc Imaging.* (2020) 13:2174–6. doi: 10.1016/j.jcmg.2020.04.027
34. Griffin WF. AI vs. quantitative coronary angiography. *JACC Cardiovasc Imaging.* (2021).
35. Budoff MJ, Muhlestein JB, Bhatt DL, Le Pa VT, May HT, Shaikh K, et al. Effect of icosapent ethyl on progression of coronary atherosclerosis in patients with elevated triglycerides on statin therapy: a prospective, placebo-controlled randomized trial (EVAPORATE): interim results. *Cardiovasc Res.* (2021). 117:1070–7. doi: 10.1093/cvr/cvaa184
36. Currie G, Rohren E. Intelligent imaging in nuclear medicine: the principles of artificial intelligence, machine learning and deep learning. *Semin Nucl Med.* (2021) 51:102–11. doi: 10.1053/j.semnuclmed.2020.08.002
37. Hu LH, Betancur J, Sharir T, Einstein AJ, Bokhari S, Fish MB, et al. Machine learning predicts per-vessel early coronary revascularization after fast myocardial perfusion SPECT: results from multicentre REFINE SPECT registry. *Eur Heart J Cardiovasc Imaging.* (2020) 21:549–59. doi: 10.1093/ehjci/jez177
38. Arsanjani R, Xu Y, Dey D, Vahistha V, Shalev A, Nakanishi R, et al. Improved accuracy of myocardial perfusion SPECT for detection of coronary artery disease by machine learning in a large population. *J Nucl Cardiol.* (2013) 20:553–62. doi: 10.1007/s12350-013-9706-2
39. Arsanjani R, Xu Y, Dey D, Fish M, Dorbala S, Hayes S, et al. Improved accuracy of myocardial perfusion SPECT for the detection of coronary artery disease using a support vector machine algorithm. *J Nucl Med.* (2013) 54:549–55. doi: 10.2967/jnumed.112.111542
40. Betancur J, Otaki Y, Motwani M, Fish MB, Lemley M, Dey D, et al. Prognostic value of combined clinical and myocardial perfusion imaging data using machine learning. *JACC Cardiovasc Imaging.* (2018) 11:1000–9. doi: 10.1016/j.jcmg.2017.07.024
41. Arsanjani R, Dey D, Khachatryan T, Shalev A, Hayes SW, Fish M, et al. Prediction of revascularization after myocardial perfusion SPECT by machine learning in a large population. *J Nucl Cardiol.* (2015) 22:877–84. doi: 10.1007/s12350-014-0027-x
42. Koo BK, Erglis A, Doh JH, Daniels DV, Jegere S, Kim HS, et al. Diagnosis of ischemia-causing coronary stenoses by noninvasive fractional flow reserve computed from coronary computed tomographic angiograms. Results from the prospective multicenter DISCOVER-FLOW (Diagnosis of ischemia-causing stenoses obtained via noninvasive fractional flow reserve) study. *J Am Coll Cardiol.* (2011) 58:1989–97. doi: 10.1016/j.jacc.2011.06.066
43. Peper J, Suchá D, Swaans M, Leiner T. Functional cardiac CT-going beyond anatomical evaluation of coronary artery disease with Cine CT, CT-FFR, CT perfusion and machine learning. *Br J Radiol.* (2020) 93:20200349. doi: 10.1259/bjr.20200349
44. Tesche C, De Cecco CN, Baumann S, Renker M, McLaurin TW, Duguay TM, et al. Coronary CT angiography-derived fractional flow reserve: machine

learning algorithm versus computational fluid dynamics modeling. *Radiology.* (2018) 288:64–72. doi: 10.1148/radiol.2018171291
45. Itu L, Rapaka S, Passerini T, Georgescu B, Schwemmer C, Schoebinger M, et al. A machine-learning approach for computation of fractional flow reserve from coronary computed tomography. *J Appl Physiol.* (2016) 121:42–52. doi: 10.1152/japplphysiol.00752.2015
46. Mannil M, von Spiczak J, Manka R, Alkadhi H. Texture analysis and machine learning for detecting myocardial infarction in noncontrast low-dose computed tomography: unveiling the invisible. *Invest Radiol.* (2018) 53:338–43. doi: 10.1097/RLI.0000000000000448
47. Ridker PM, Libby P, MacFadyen JG, Thuren T, Ballantyne C, Fonseca F, et al. Modulation of the interleukin-6 signalling pathway and incidence rates of atherosclerotic events and all-cause mortality: analyses from the Canakinumab Anti-Inflammatory Thrombosis Outcomes Study (CANTOS). *Eur Heart J.* (2018) 39:3499–507. doi: 10.1093/eurheartj/ehy310
48. Antonopoulos AS, Sanna F, Sabharwal N, Thomas S, Oikonomou EK, Herdman L, et al. Detecting human coronary inflammation by imaging perivascular fat. *Sci Transl Med.* (2017) 9:398. doi: 10.1126/scitranslmed.aal2658
49. Margaritis M, Antonopoulos AS, Digby J, Lee R, Reilly S, Coutinho P, et al. Interactions between vascular wall and perivascular adipose tissue reveal novel roles for adiponectin in the regulation of endothelial nitric oxide synthase function in human vessels. *Circulation.* (2013) 127:2209–21. doi: 10.1161/CIRCULATIONAHA.112.001133
50. Oikonomou EK, Marwan M, Desai MY, Mancio J, Alashi A, Hutt Centeno E, et al. Non-invasive detection of coronary inflammation using computed tomography and prediction of residual cardiovascular risk (the CRISP CT study): a post-hoc analysis of prospective outcome data. *Lancet.* (2018) 392:929–39. doi: 10.1016/S0140-6736(18)31114-0
51. Goeller M, Achenbach S, Cadet S, Kwan AC, Commandeur F, Slomka PJ, et al. Pericoronary adipose tissue computed tomography attenuation and high-risk plaque characteristics in acute coronary syndrome compared with stable coronary artery disease. *JAMA Cardiol.* (2018) 3:858–63. doi: 10.1001/jamacardio.2018.1997
52. Yu M, Dai X, Deng J, Lu Z, Shen C, Zhang J. Diagnostic performance of perivascular fat attenuation index to predict hemodynamic significance of coronary stenosis: a preliminary coronary computed tomography angiography study. *Eur Radiol.* (2020) 30:673–81. doi: 10.1007/s00330-019-06400-8
53. Oikonomou EK, Williams MC, Kotanidis CP, Desai MY, Marwan M, Antonopoulos AS, et al. A novel machine learning-derived radiotranscriptomic signature of perivascular fat improves cardiac risk prediction using coronary CT angiography. *Eur Heart J.* (2019) 40:3529–43. doi: 10.1093/eurheartj/ehz592
54. Wu FZ, Chou KJ, Huang YL, Wu MT. The relation of location-specific epicardial adipose tissue thickness and obstructive coronary artery disease: systemic review and meta-analysis of observational studies. *BMC Cardiovasc Disord.* (2014) 14:62. doi: 10.1186/1471-2261-14-62
55. Wu FZ, Huang YL, Wang YC, Lin HS, Chen CS, Ju YJ, et al. Impact of location of epicardial adipose tissue, measured by coronary artery calcium-scoring computed tomography on obstructive coronary artery disease. *Am J Cardiol.* (2013) 112:943–9. doi: 10.1016/j.amjcard.2013.05.022
56. Commandeur F, Goeller M, Razipour A, Cadet S, Hell MM, Kwiecinski J, et al. Fully automated CT quantification of epicardial adipose tissue by deep learning: a multicenter study. *Radiol Artif Intell.* (2019) 1:e190045. doi: 10.1148/ryai.2019190045
57. Criqui MH, Denenberg JO, Ix JH, McClelland RL, Wassel CL, Rifkin DE, et al. Calcium density of coronary artery plaque and risk of incident cardiovascular events. *JAMA.* (2014) 311:271–8. doi: 10.1001/jama.2013.282535
58. Shen YW, Wu YJ, Hung YC, Hsiao CC, Chan SH, Mar GY, et al. Natural course of coronary artery calcium progression in Asian population with an initial score of zero. *BMC Cardiovasc Disord.* (2020) 20:212. doi: 10.1186/s12872-020-01498-x
59. Wu YJ, Mar GY, Wu MT, Wu FZ. A LASSO-derived risk model for subclinical CAC progression in Asian population with an initial score of zero. *Front Cardiovasc Med.* (2020) 7:619798. doi: 10.3389/fcvm.2020.619798
60. Grundy SM, Stone NJ, Bailey AL, Beam C, Birtcher KK, Blumenthal RS, et al. 2018 AHA/ACC/AACVPR/AAPA/ABC/ACPM/ADA/AGS/APhA/ASPC/NLA/PCNA guideline on the management of blood cholesterol: executive summary: a report of the American College of Cardiology/American Heart Association Task Force on Clinical Practice Guidelines. *J Am Coll Cardiol.* (2019) 73:3168–209. doi: 10.1016/j.jacc.2018.11.002
61. Isgum I, Prokop M, Niemeijer M, Viergever MA, van Ginneken B. Automatic coronary calcium scoring in low-dose chest computed tomography. *IEEE Trans Med Imaging.* (2012) 31:2322–34. doi: 10.1109/TMI.2012.2216889
62. Takx RA, de Jong PA, Leiner T, Oudkerk M, de Koning HJ, Mol CP, et al. Automated coronary artery calcification scoring in non-gated chest CT: agreement and reliability. *PLoS ONE.* (2014) 9:e91239. doi: 10.1371/journal.pone.0091239
63. Išgum I, de Vos BD, Wolterink JM, Dey D, Berman DS, Rubeaux M, et al. Automatic determination of cardiovascular risk by CT attenuation correction maps in Rb-82 PET/CT. *J Nucl Cardiol.* (2018) 25:2133–42. doi: 10.1007/s12350-017-0866-3
64. Winkel DJ, Suryanarayana VR, Ali AM, Görich J, Buß SJ, Mendoza A, et al. Deep learning for vessel-specific coronary artery calcium scoring: validation on a multi-centre dataset. *Eur Heart J Cardiovasc Imaging.* (2021) jeab119. doi: 10.1093/ehjci/jeab119
65. Sengupta PP, Shrestha S, Berthon B, Messas E, Donal E, Tison GH, et al. Proposed requirements for cardiovascular imaging-related machine learning evaluation (PRIME): a checklist: reviewed by the American College of Cardiology Healthcare Innovation Council. *JACC Cardiovasc Imaging.* (2020) 13:2017–35. doi: 10.1016/j.jcmg.2020.07.015
66. Dey D, Slomka PJ, Leeson P, Comaniciu D, Shrestha S, Sengupta PP, et al. Artificial intelligence in cardiovascular imaging: JACC state-of-the-art review. *J Am Coll Cardiol.* (2019) 73:1317–35. doi: 10.1016/j.jacc.2018.12.054

Conflict of Interest: JE is an employee and retains equity in Cleerly Inc. AC reports grant funding from GW Heart and Vascular Institute, and equity in Cleerly.

The remaining authors declare that the research was conducted in the absence of any commercial or financial relationships that could be construed as a potential conflict of interest.

Publisher's Note: All claims expressed in this article are solely those of the authors and do not necessarily represent those of their affiliated organizations, or those of the publisher, the editors and the reviewers. Any product that may be evaluated in this article, or claim that may be made by its manufacturer, is not guaranteed or endorsed by the publisher.

frontiers in Cardiovascular Medicine

ORIGINAL RESEARCH
published: 24 March 2022
doi: 10.3389/fcvm.2022.831231

Additive Effects of Obesity on Myocardial Microcirculation and Left Ventricular Deformation in Essential Hypertension: A Contrast-Enhanced Cardiac Magnetic Resonance Imaging Study

Pei-Lun Han[1], Xue-Ming Li[2], Li Jiang[2], Wei-Feng Yan[2], Ying-Kun Guo[3], Yuan Li[2], Kang Li[1†] and Zhi-Gang Yang[2*†]*

[1] West China Biomedical Big Data Center, West China Hospital, Sichuan University, Chengdu, China, [2] Department of Radiology, West China Hospital, Sichuan University, Chengdu, China, [3] Department of Radiology, West China Second University Hospital, Sichuan University, Chengdu, China

Objective: The combination of hypertension and obesity is a major cause of cardiovascular risk, and microvascular changes and subclinical dysfunction should be considered to illustrate the underlying mechanisms and early identification, thereby developing targeted therapies. This study aims to explore the effect of obesity on myocardial microcirculation and left ventricular (LV) deformation in hypertensive patients by cardiac magnetic resonance (CMR).

Methods: This study comprised 101 hypertensive patients, including 54 subjects with a body mass index (BMI) of 18.5–24.9 kg/m^2 and 47 subjects with a BMI ≥25 kg/m^2, as well as 55 age- and sex-matched controls with a BMI of 18.5–24.9 kg/m^2. Myocardial perfusion indicators [upslope, time to maximum signal intensity (TTM), maximum signal intensity (Max SI)] and LV strains [radial, circumferential, and longitudinal global peak strain (PS), peak systolic strain rate (PSSR), and peak diastolic strain rate (PDSR)] were measured.

Results: Upslope was numerically increased in obese patients but statistically decreased in non-obese patients compared with controls. Longitudinal PS deteriorated significantly and gradually from controls to non-obese and obese hypertensive patients. Longitudinal PSSR and PDSR were significantly decreased in obese hypertensive patients compared with the other two groups. BMI was associated with upslope ($\beta = -0.136$, $P < 0.001$), Max SI ($\beta = -0.922$, $P < 0.001$), longitudinal PSSR ($\beta = 0.018$, $P < 0.001$), and PDSR ($\beta = -0.024$, $P = 0.001$). Myocardial perfusion was independently associated with longitudinal PSSR (TTM: $\beta = 0.003$, $P = 0.017$) and longitudinal PDSR (upslope: $\beta = 0.067$, $P = 0.020$) in hypertension.

OPEN ACCESS

Edited by:
Monica Mukherjee, The Johns Hopkins Hospital, Johns Hopkins Medicine, United States

Reviewed by:
Filippo Cademartiri, Gabriele Monasterio Tuscany Foundation (CNR), Italy
Qin Shao, Shanghai Jiao Tong University, China

***Correspondence:**
Kang Li
likang@wchscu.cn
Zhi-Gang Yang
yangzg666@163.com

† These authors have contributed equally to this work and share last authorship

Specialty section:
This article was submitted to Cardiovascular Imaging, a section of the journal Frontiers in Cardiovascular Medicine

Received: *08 December 2021*
Accepted: *25 February 2022*
Published: *24 March 2022*

Citation:
Han P-L, Li X-M, Jiang L, Yan W-F, Guo Y-K, Li Y, Li K and Yang Z-G (2022) Additive Effects of Obesity on Myocardial Microcirculation and Left Ventricular Deformation in Essential Hypertension: A Contrast-Enhanced Cardiac Magnetic Resonance Imaging Study. Front. Cardiovasc. Med. 9:831231. doi: 10.3389/fcvm.2022.831231

Conclusion: Obesity had adverse effects on microvascular changes and subclinical LV dysfunction in hypertension, and BMI was independently associated with both myocardial perfusion and LV deformation. Impaired myocardial perfusion was independently associated with subclinical LV dysfunction in hypertension.

Keywords: hypertension, obesity, left ventricular deformation, myocardial perfusion, magnetic resonance imaging

INTRODUCTION

Hypertension and obesity are well-recognized global health concerns, and the two conditions often coexist (1–3). Both hypertension and obesity are associated with an increased risk of cardiovascular morbidity and mortality in isolation, and when combined the cardiovascular risk increases (4). Myocardial microcirculatory damage is an important mechanism of myocardial impairment (5) that is associated with cardiac dysfunction (6), poor prognosis (7), and adverse outcomes (8). Although abnormalities of myocardial perfusion and left ventricular (LV) function have been demonstrated separately in hypertension (9, 10) and obesity (11, 12) separately, their combined effects are still poorly investigated. Elucidation of the interaction between obesity and hypertension may provide insights into mechanisms underlying the impairment of myocardial microcirculation and cardiac function, and may help in identifying patient subgroups that could benefit from early prevention and treatment.

Cardiac magnetic resonance (CMR) imaging has been increasingly used to evaluate myocardial microcirculation and cardiac function with high reproducibility. First-pass CMR imaging allows non-invasive assessment of myocardial perfusion during the transit of contrast agent and has been increasingly used in recent years to detect microvascular dysfunction (13, 14). In addition, conventional functional parameters are not sensitive enough to detect minor abnormalities of LV function, such as left ventricular ejection fraction (LVEF), which may mask the impairment in the preclinical stage (15). CMR feature tracking (CMR-FT) can drive LV deformation indicators using only clinical routine cine images, and has been well established as a sensitive technique for evaluating subclinical LV dysfunction (16, 17).

Therefore, we aimed to evaluate myocardial microcirculation and LV function by CMR first-pass perfusion and CMR-FT imaging in hypertensive patients without or with obesity, as well as to explore the relationship between myocardial perfusion, LV strains and BMI.

MATERIALS AND METHODS

Ethical Considerations

This study was approved by the Biomedical Research Ethics Committee of the West China hospital of Sichuan University (Approval No. 2019-756) and was conducted in accordance with institutional guidelines. All patients gave their informed consent for contrast-enhanced CMR examination. All patient information was used only for research purposes.

Study Population

We retrospectively identified patients with essential hypertension from consecutive hospitalized subjects who underwent contrast-enhanced CMR for suspected cardiomyopathy at our hospital from January 2016 to May 2021. Hypertension was defined as clinical systolic blood pressure (SBP) $\geq$140 mmHg and/or diastolic blood pressure (DBP) $\geq$90 mmHg or a previous diagnosis of essential hypertension or usage of antihypertensive medication. The exclusion criteria included coronary artery disease, myocardial infarction, severe arrhythmias, symptoms of heart failure or LVEF <50%, cardiomyopathy, severe valvular disease, congenital heart disease, diabetes diseases, estimated glomerular filtration rate (e-GFR) <30 ml/min, severe hepatopulmonary dysfunction, underweight (BMI <18.5 kg/m^2), and poor image quality. Ultimately, 101 hypertensive patients (51 [50.49%] females; mean age, 54.56 $\pm$ 15.33 years) were included in the final analysis. Then, the hypertensive patients were categorized into two groups (without and with obesity) according to World Health Organization (WHO) BMI standards (18) for Asian populations. The hypertensive patients without obesity group comprised those with a BMI of 18.5 kg/m^2–24.9 kg/m^2 (n = 54), and the hypertensive patients with obesity group comprised those with a BMI $\geq$25.0 kg/m^2 (n = 47). For comparison, 55 age- and sex- matched controls (33 [60.0%] females; mean age, 53.54 $\pm$ 10.08 years) were identified though subjects who underwent contrast-enhanced CMR during the study period. All these individuals had BMIs of 18.5 kg/m^2–24.9 kg/m^2 and no evidence of hypertension. Moreover, the aforementioned exclusion criteria for the hypertensive group also applied to the control group. Demographic and clinical data within 1 month of the CMR examination were collected through a review of electronic medical charts.

Cardiac Magnetic Resonance Imaging Acquisition

Cardiac magnetic resonance scans were performed on a 3.0 T whole-body scanner MAGNETOM Trio Tim (Siemens Medical Solutions, Erlangen, Germany). Patients were placed in the supine position with a dedicated two-element cardiac-phased array coil attached.

A standard ECG-triggering device was simultaneously used. Localizers were used to determine the cardiac axes. To achieve complete and high-quality LV coverage, CMR images were

acquired from the base to the apex during multiple breath-holding periods. To analyze cardiac function and myocardial strain, a balanced steady-state free-precession (bSSFP) sequence (repetition time [TR]/echo time [TE]: 2.81/1.22 ms, flip angle: 40°, slice thickness: 8 mm, field of view [FOV]: 250 × 300 mm, matrix size: 208 × 139) was used to obtain 8–12 continuous cine images of the long-axis, short-axis, 2-chamber, and 4-chamber views. For perfusion imaging, a contrast dose of 0.2 ml/kg gadobenate dimeglumine (MultiHance 0.5 mmol/mL; Bracco, Milan, Italy) was injected into the right antecubital vein using an automated injector (Stellant, MEDRAD, Indianola, PA, United States) at a flow rate of 2.5–3.0 ml/s, followed by a 20 ml saline flush at a rate of 3.0 ml/s. Resting perfusion images were acquired concurrently with intravenous contrast agents in three stand- and short-axis slices (apical, middle, and basal) and in one 4-chamber view slice by inversion-recovery echo-planar sequence (TR/TE: 163/1.12 ms, flip angle: 10°, slice thickness: 8 mm, FOV: 360 × 270 mm, matrix size: 256 × 192). Each set of first-pass perfusion images was acquired in 80 cardiac cycles. To exclude myocardial infarction, late gadolinium enhancement (LGE) imaging was obtained at an average of 10–15 min after contrast injection by segmented-turbo-FLASH–phase-sensitive inversion recovery (PSIR) sequence (TR/TE: 750/1.18 ms, flip angle: 40°, slice thickness: 8 mm, FOV: 400 × 270 mm, matrix size: 256 × 148).

Cardiac Magnetic Resonance Imaging Analysis

All CMR data were transferred to a dedicated software program (CVI42 version 5.9.1, Circle Cardiovascular Imaging, Inc., Calgary, Canada) and measured by two experienced (at least 2 years of CMR experience) investigators blinded to the clinical profiles of the subjects. For measurement of left ventricular (LV) function parameters, we manually delineated the endocardial and epicardial contours in serial short-axis slices at the end-diastolic and end-systolic, and then left ventricular end diastolic volume (LVEDV), left ventricular end systolic volume (LVESV), left ventricular stroke volume (LVSV), LVEF and left ventricular mass (LVM) were calculated automatically. LVEDV, LVESV and LVM were indexed to body surface area (LVEDVI, LVESVI and LVMI, respectively). The LV remodeling index was calculated as LVM divided by LVEDV.

For semiquantitative analysis of LV myocardial perfusion, we manually delineated the endocardial contours, epicardial contours, and a region of interest drawn in the LV blood pool in all of the first-pass perfusion images of the basal, mid and apical short-axis slices. A 16-segment mode (Bull's eye plot) was constructed based on AHA standard segmentation recommendations, including six basal segments, six middle segments, and four apical segments (19). Subsequently, a myocardial signal intensity-time curve was generated, and the LV segmental perfusion parameters [upslope, max signal intensity (Max SI), and time to maximum signal intensity (TTM)] were obtained automatically.

Cardiac magnetic resonance feature tracking (CMR-FT) was used for the analysis of LV myocardial strain. We manually delineated the endocardial and epicardial contours in long-axis 2-chamber, 4-chamber, and serial short-axis slices at the end-diastole phase, which was the reference phase, in a 3-dimensional (3D) tissue tracking module. Then, the LV global myocardial strain parameters (radial, circumferential, and longitudinal global peak strain (PS), peak systolic strain rate (PSSR), and peak diastolic strain rate (PDSR)) were acquired automatically.

Reproducibility of Left Ventricular Strain and First-Pass Myocardial Perfusion Parameters

After 1 month, 30 patients (20 hypertensive subjects, 10 controls) were randomly selected and LV strain and first-pass myocardial perfusion parameters were measured again by the same radiologist to evaluate the intraobserver variability. The parameters were measured again as above by a second blinded investigator to determine the interobserver variability.

Statistical Analysis

All statistical analyses were performed with R version 3.6.3 (The R Foundation, Vienna, Austria). Continuous variables are presented as the mean ± standard deviation and categorical variables are presented as frequencies (%). The Kolmogorov–Smirnov test was used to assess the normality of the distribution of continuous variables. Normally distributed continuous variables among groups were compared by one-way analysis of variance (ANOVA) followed by the least-significant difference (LSD) test. Comparisons of non-normally distributed continuous variables among groups were performed by the Kruskal-Wallis rank test. Categorical variables were compared by the Chi-square test. Correlations between myocardial perfusion and LV strain parameters were analyzed by Pearson correlation analysis. Univariable linear regression analyses were performed to demonstrate the relationship between candidate factors and myocardial perfusion/LV strain parameters. Age, sex and variables with a P-value <0.1 in the univariable analyses were entered into a stepwise multivariable linear regression analysis. The inter- and intraobserver variabilities for reproducibility were evaluated using the intraclass correlation coefficient (ICC). For all statistical analyses, a P-value <0.05 was considered statistically significant.

RESULTS

Baseline Characteristics

Table 1 presents the demographic and clinical characteristics of the study population. BMI and BSA were significantly higher in hypertensive patients with obesity than in the other two groups (all $P < 0.05$). Office SBP and DBP were significantly higher in hypertensive patients with or without obesity than in controls (all $P < 0.05$); office

TABLE 1 | Baseline characteristics.

	Controls (*n* = 55)	Hypertensive patients without obesity (*n* = 54)	Hypertensive patients with obesity (*n* = 47)	P
Demographics				
Age, years	53.54 ± 10.08	54.15 ± 16.18	55.02 ± 14.46	0.862
Sex				0.288
Male, *n* (%)	22 (40.0%)	24 (44.4%)	26 (55.3%)	
Female, *n* (%)	33 (60.0%)	30 (55.6%)	21 (44.7%)	
BMI, kg/m^2	22.49 ± 1.75	22.70 ± 1.46	27.57 ± 2.20*§	<0.001
BSA, m^2	1.62 ± 0.13	1.59 ± 0.14	1.79 ± 0.18*§	<0.001
Hemodynamic variables				
Heart rate, bpm	71.03 ± 10.52	75.98 ± 16.46	77.02 ± 15.14	0.161
Office SBP, mmHg	114.55 ± 10.33	138.98 ± 23.57*	143.13 ± 17.78*	<0.001
Office DBP, mmHg	73.49 ± 10.98	82.54 ± 16.59*	91.34 ± 15.68*§	<0.001
Laboratory data				
TG, mmol/L	1.46 ± 0.81	1.61 ± 1.48	1.98 ± 1.77	0.156
TC, mmol/L	4.53 ± 1.08	4.36 ± 0.82	4.66 ± 1.08	0.301
HDL, mmol/L	1.37 ± 0.38	1.61 ± 1.42	1.25 ± 0.45*§	0.018
LDL, mmol/L	2.68 ± 1.00	2.41 ± 0.68	2.78 ± 0.86	0.082
eGFR, mL/min/1.73 m^2	90.62 ± 13.95	91.16 ± 24.70	91.98 ± 20.14	0.965
Medication usage				
ACEI, *n* (%)	–	4 (7.4%)	4 (8.5%)	1.000
ARB, *n* (%)	–	17 (31.5%)	14 (29.8%)	0.854
Beta-blockers, n (%)	–	18 (33.3%)	15 (31.9%)	0.880
CCB, *n* (%)	–	19 (35.2%)	28 (59.6%)§	0.014
Diuretics, n (%)	–	4 (7.4%)	4 (8.5%)	1.000
Duration of hypertension, years	–	5.88 ± 7.93	6.23 ± 5.35	0.124

BMI, body mass index; BSA, body surface area; SBP, systolic blood pressure; DBP, diastolic blood pressure; TG, plasma triglycerides; TC, total cholesterol; HDL, high-density lipoprotein; LDL, low-density lipoprotein; eGFR, estimated glomerular filtration rate; ACEI, angiotensin-converting enzyme inhibitors; ARB, angiotensin receptor blocker; CCB, Calcium channel blocker

**P < 0.05 versus controls.*

§P < 0.05 versus hypertensive patients without obesity.

DBP was significantly higher in hypertensive patients with obesity than in those without obesity (P = 0.003). High-density lipoprotein (HDL) was significantly increased in hypertensive patients without obesity compared with the other two groups. Calcium channel blocker use was more common in obese patients than in non-obese patients (P = 0.014). No significant differences were found in sex, age, heart rate or other laboratory data among the three groups. There were no significant differences in other medication usage or duration of hypertension between hypertensive patients with and without obesity.

Comparison of Cardiac Magnetic Resonance Findings Between Groups

As shown in **Table 2**, LVEDVI and LVESVI were significantly higher in hypertensive patients without obesity than in the other two groups (all $P < 0.05$). LVMI was significantly higher in hypertensive patients than in controls (both $P < 0.05$). The LV remodeling index was gradually increased in non-obese and obese hypertensive patients compared with controls (all $P < 0.005$).

Hypertensive patients without obesity had numerically higher upslope and Max SI values than controls (upslope: 2.83 ± 0.89 vs. 2.56 ± 0.86, P = 0.084; Max SI: 26.24 ± 7.96 vs. 23.26 ± 6.32, P = 0.073). Hypertensive patients with obesity had a significantly reduced upslope compared with the other two groups, and a significantly decreased Max SI compared with patients without obesity (all $P < 0.05$) (**Figures 1**, **2**).

Longitudinal PS significantly and gradually deteriorated from controls to patients without obesity to patients with obesity (all $P < 0.05$). Longitudinal PSSR and PDSR were significantly decreased in hypertensive patients with obesity compared with the other two groups (all $P < 0.05$). In addition, circumferential PDSR was significantly decreased in hypertensive patients with obesity compared with controls (P = 0.005). No significant differences were seen in other parameters among the three groups.

Associations Between Perfusion and Deformation Parameters in Non-obese and Obese Hypertensive Patients

Among hypertensive patients, TTM was correlated with all strain parameters (all $P < 0.05$) (**Supplementary Figure 1**). In addition, there were significant correlations between upslope and longitudinal PS, PSSR and PDSR (all $P < 0.05$). Univariable linear regression analyses between potential

TABLE 2 | Comparisons of CMR findings between controls, non-obese and obese patients.

	Controls (*n* = 55)	Hypertensive patients without obesity (*n* = 54)	Hypertensive patients with obesity (*n* = 47)	P
Conventional LV function				
LVEF,%	64.45 ± 5.08	62.57 ± 6.06	62.65 ± 7.10	0.239
LVEDVI, ml/m^2	74.51 ± 13.58	84.24 ± 19.66*	74.00 ± 19.47§	0.004
LVESVI, ml/m^2	26.83 ± 6.27	34.19 ± 11.06*	28.32 ± 10.03§	< 0.001
LVSV, ml	77.53 ± 15.96	81.56 ± 21.85	82.88 ± 24.26	0.757
LVMI, g/m^2	47.02 ± 14.26	61.00 ± 19.35*	62.06 ± 23.26*	< 0.001
LVremodeling index, g/mL	0.64 ± 0.18	0.73 ± 0.19*	0.85 ± 0.25*§	< 0.001
Myocardial perfusion				
Upslope	2.56 ± 0.86	2.83 ± 0.89	1.90 ± 0.60*§	< 0.001
TTM, s	26.94 ± 10.04	26.94 ± 12.53	32.05 ± 13.65	0.059
Max SI	23.26 ± 6.32	26.24 ± 7.96	20.61 ± 6.33§	0.001
LV strain				
PS,%				
Radial	35.81 ± 8.31	34.80 ± 9.14	33.17 ± 8.83	0.221
Circumferential	−20.58 ± 2.66	−20.20 ± 3.25	−20.31 ± 3.14	0.798
Longitudinal	−14.32 ± 2.28	−13.10 ± 3.12*	−11.72 ± 2.82*§	< 0.001
PSSR, 1/s				
Radial	1.92 ± 0.52	1.92 ± 0.63	1.81 ± 0.71	0.619
Circumferential	−1.00 ± 0.36	−1.04 ± 0.26	−1.06 ± 0.23	0.813
Longitudinal	−0.84 ± 0.20	−0.78 ± 0.22	−0.68 ± 0.17*§	< 0.001
PDSR, 1/s				
Radial	−2.40 ± 0.89	−2.17 ± 0.88	−2.00 ± 0.61	0.086
Circumferential	1.23 ± 0.25	1.15 ± 0.30	1.07 ± 0.26*	0.018
Longitudinal	0.91 ± 0.24	0.82 ± 0.22	0.67 ± 0.22*§	< 0.001

*LV, left ventricular; EF, ejection fraction; EDVI, end diastolic volume index; ESVI, end systolic volume index; SV, stroke volume; MI, mass index; TTM, time to maximum signal intensity; Max SI, maximum signal intensity; PS, peak strain; PSSR, peak systolic strain rate; PDSR, peak diastolic strain rate *P < 0.05 versus controls §P < 0.05 versus hypertensive patients without obesity.*

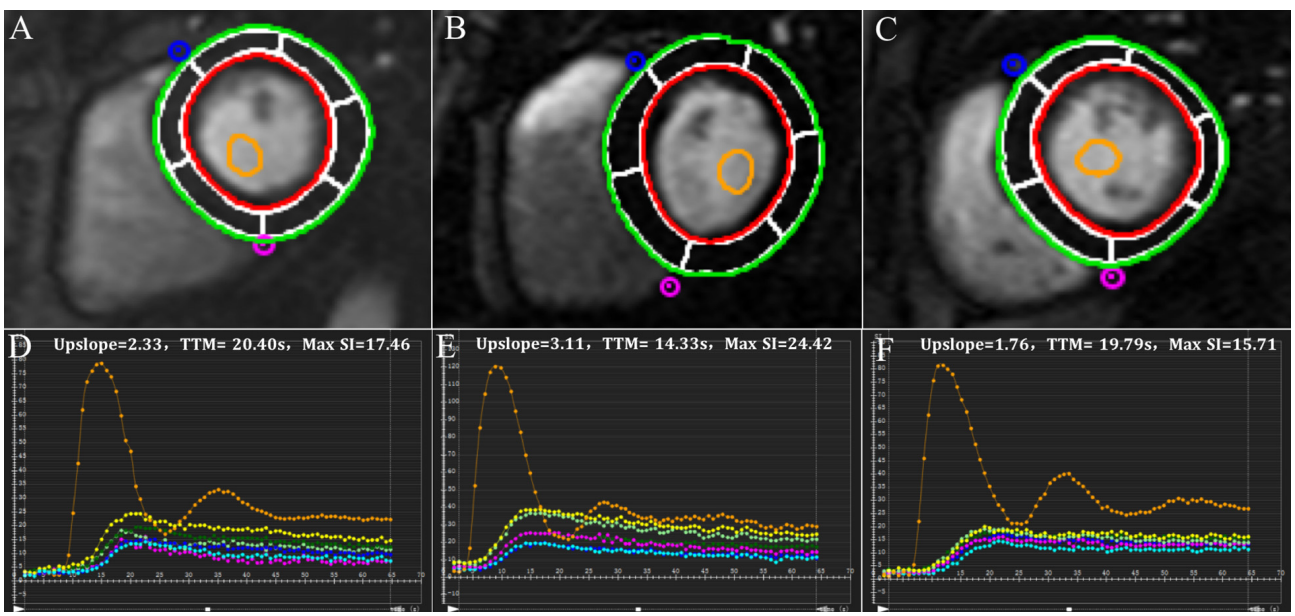

FIGURE 1 | Representative first-pass myocardial perfusion MR images and signal intensity-time curves of a control subject **(A,D)**, a hypertensive patient without obesity **(B,E)** and a hypertensive patient with obesity **(C,F)**.

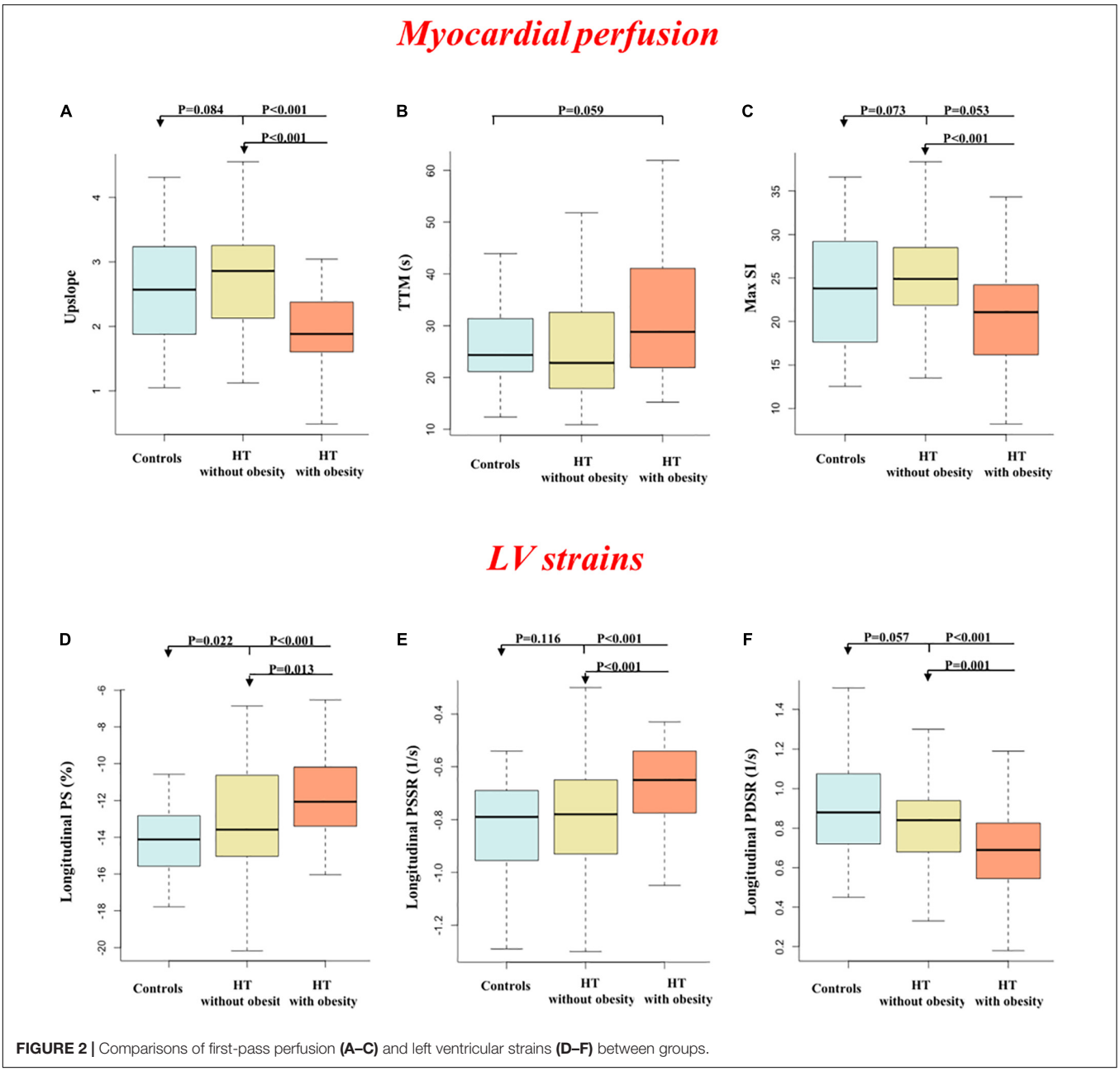

FIGURE 2 | Comparisons of first-pass perfusion **(A–C)** and left ventricular strains **(D–F)** between groups.

influencing factors and perfusion/strain parameters are shown in **Supplementary Table 1**.

looseness1 Multivariable linear regression analyses (**Table 3**) showed that BMI was significantly associated with myocardial perfusion (upslope: β = −0.136, $P < 0.001$, model $R^2 = 0.214$; Max SI: β = −0.922, $P < 0.001$, model $R^2 = 0.172$) and LV strains (longitudinal PSSR: β = 0.018, $P < 0.001$, model $R^2 = 0.245$; longitudinal PDSR: β = −0.024, $P = 0.001$, model $R^2 = 0.278$) in hypertensive patients (**Figure 3**). After adjustment for perfusion, there was a significant association between BMI and longitudinal PS after adjustment for perfusion (β = 0.493, $P = 0.022$, model $R^2 = 0.496$). The association between BMI and longitudinal PSSR remained significant (β = 0.016, $P = 0.009$, model $R^2 = 0.326$), while the association between BMI and PDSR was absent (β = −0.013, $P = 0.132$, model $R^2 = 0.385$). In addition, multivariable linear regression analyses including both BMI and all perfusion parameters revealed that myocardial perfusion was significantly associated with longitudinal PSSR (TTM: β = 0.003, $P = 0.017$) and longitudinal PSDR (upslope: β = 0.067, $P = 0.020$) in hypertension (**Figure 4**).

Intra- and Interobserver Variability

There was excellent intra- and interobserver variability for first-pass perfusion (ICC = 0.900–0.980) and LV deformation indicators (ICC = 0.850–0.977) (**Table 4**).

TABLE 3 | Multivariable linear regression analyses in hypertensive patients.

	Upslope			TTM			Max SI		
Model 1	**β (95% CI)**	**P**	**R^2**	**β**	**P**	**R^2**	**β**	**P**	**R^2**
BMI	−0.136 (−0.189, −0.084)	<0.001*	0.214	–	–	0.067	−0.922 (−1.385, −0.458)	<0.001*	0.172
	Longitudinal PS			**Longitudinal PSSR**			**Longitudinal PDSR**		
	β (95% CI)	***P***	***R^2***	**β**	***P***	***R^2***	**β**	***P***	***R^2***
Model 2									
BMI	–	–	0.385	0.018 (0.005–0.030)	<0.001*	0.245	−0.024 (−0.037, −0.010)	0.001*	0.278
Model 3									
BMI	0.493 (0.079, 0.906)	0.022*	0.496	0.016 (0.004, 0.028)	0.009*	0.326	−0.013 (−0.028, 0.002)	0.132	0.385
Upslope	–	–		–	–		0.067 (0.011, 0.124)	0.020*	
TTM	–	–		0.003 (0.000, 0.006)	0.017*		−0.002 (−0.006, 0.001)	0.156	
Max SI	0.184 (−0.035, 0.402)	0.095		–	–		–	–	

BMI, body mass index; PDSR, peak diastolic strain rate; PSSR, peak systolic strain rate; PS, peak strain; TTM, time to maximum signal intensity; Max SI, maximum signal intensity.
Age, sex, and factors with $p < 0.1$ in the univariable analysis were included in the multivariable analysis.
Model 1: Association between BMI and perfusion parameters in hypertension.
Model 2: Association between BMI and longitudinal strain/strain rates in hypertension.
Model 3: Association between perfusion parameters and longitudinal strain/strain rates in hypertension.
**P < 0.05.*
–Factors not incorporated into the final regression equation.

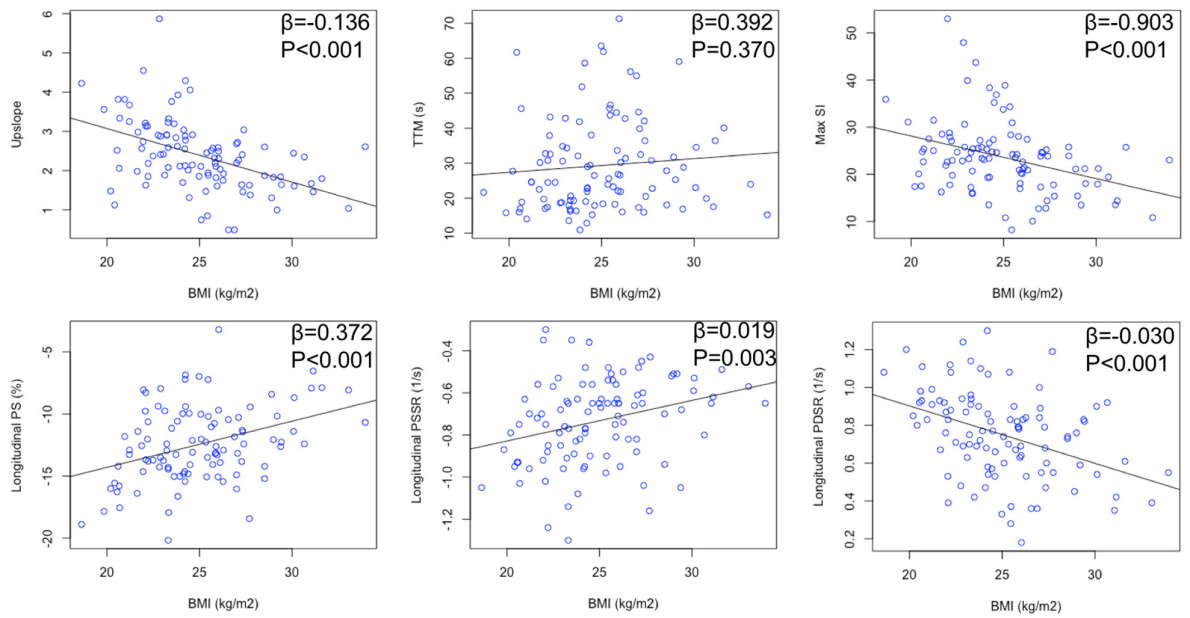

FIGURE 3 | Relationship between BMI and myocardial perfusion/LV deformation in hypertensive patients.

DISCUSSION

In this work, we used contrast-enhanced CMR and found that (1) myocardial perfusion was slightly increased in hypertensive patients without obesity but significantly decreased in hypertensive patients with obesity; (2) subclinical LV function gradually decreased from controls to hypertensive patients without and with coexisting obesity; and (3) myocardial microcirculatory damage was independently associated with subclinical LV dysfunction in hypertensive patients.

The Combined Effects of Obesity and Hypertension on Myocardial Microcirculatory Damage

The pathophysiology of cardiomyopathy related to obesity and hypertension is complex and multifactorial. Among these,

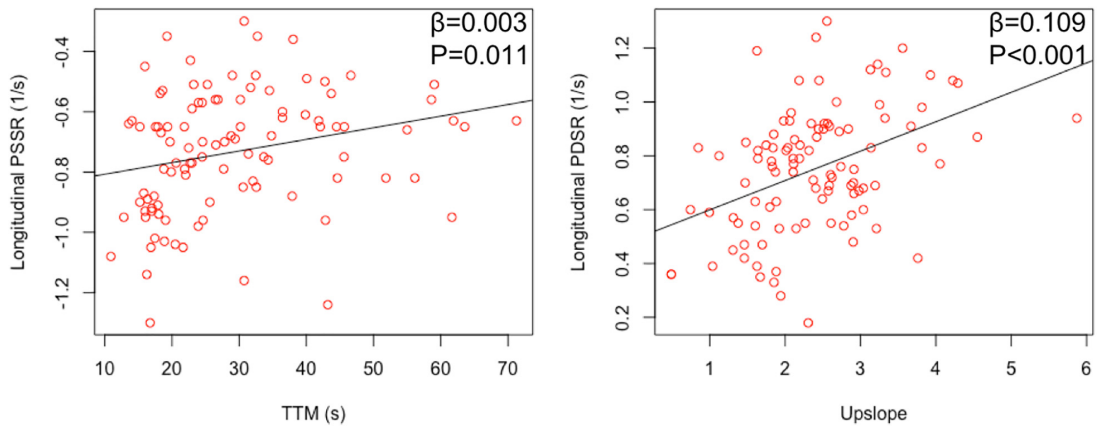

FIGURE 4 | Relationship between myocardial perfusion and LV deformation in hypertensive patients.

TABLE 4 | Inter- and intra-observer variability of CMR first-pass perfusion and LV strain parameters.

Variable	Intra-observer (*n* = 30)		Inter-observer (*n* = 30)	
	ICC	95%CI	ICC	95%CI
First-pass perfusion parameters				
Upslope	0.960	0.917–0.981	0.980	0.959–0.991
TTM	0.951	0.899–0.976	0.953	0.903–0.977
Max SI	0.900	0.801–0.951	0.973	0.944–0.987
Strain parameters				
PS,%				
Radial	0.950	0.899–0.976	0.930	0.858–0.966
Circumferential	0.924	0.847–0.917	0.854	0.716–0.928
Longitudinal	0.946	0.942–0.987	0.857	0.721–0.929
PSSR, 1/s				
Radial	0.887	0.777–0.945	0.879	0.762–0.941
Circumferential	0.938	0.874–0.970	0.842	0.694–0.921
Longitudinal	0.973	0.944–0.987	0.922	0.842–0.962
PDSR, 1/s				
Radial	0.977	0.952–0.989	0.850	0.709–0.926
Circumferential	0.889	0.780–0.945	0.877	0.757–0.939
Longitudinal	0.932	0.863–0.967	0.925	0.849–0.964

LV, left ventricular; EF, ejection fraction; EDVI, end diastolic volume index; ESVI, end systolic volume index; SV, stroke volume; MI, mass index; TTM, time to maximum signal intensity; Max SI, maximum signal intensity; PS, peak strain; PSSR, peak systolic strain rate; PDSR, peak diastolic strain rate.

microvascular abnormalities are an important disorder in both conditions with certain common pathological changes: endothelial dysfunction, microvascular remodeling and rarefaction (20). Some previous studies revealed no obvious difference in the resting myocardial perfusion between hypertensive and normotensive subjects (21, 22), while other studies reported significantly increased resting myocardial perfusion in hypertensive patients due to an adaptive mechanism (23, 24). Our results showed slightly increased resting myocardial perfusion in hypertensive patients without obesity compared with controls, but this difference did not reach statistical significance. Regarding the effects of obesity alone on myocardial microvascular damage, Bajaj et al. (11) reported that coronary microvascular dysfunction was independently associated with elevated BMI in patients with suspected coronary artery disease based on clinical symptoms. Such association was also confirmed in persons without traditional coronary artery disease risk factors (25). Considering the shared pathophysiology of obesity and hypertension above, we hypothesized that the obesity status contributes to the aggravation of the microcirculatory dysfunction by hypertension.

Although a combined effect of obesity and diabetes on damage to myocardial microcirculation has been reported (14), whether such an effect would be observed among obese individuals with hypertension is still unclear. Our findings demonstrated that hypertensive patients with obesity had significantly decreased perfusion compared with both controls and hypertensive patients without obesity even in the resting state, suggesting that the coexistence of obesity may amplify the microcirculatory damage in hypertension. This result may help to provide a better understanding of the possible mechanisms of the combined effect of hypertension and obesity on the myocardium. In addition, coronary microvascular dysfunction was reported to be a better risk marker of adverse outcomes than BMI and other traditional risk factors (11), which provides a direction for tailoring therapeutic strategies for hypertensive patients with obesity.

The Combined Effects of Obesity and Hypertension on Left Ventricular Deformation Deterioration

The results of our study showed that hypertensive patients without obesity had significantly decreased strain values but preserved LVEF compared with control subjects, which confirmed the value of CMR-FT based myocardial deformation analysis in the detection of early and subtle LV dysfunction with previous studies (26, 27). A previous CMR-FT study (10) demonstrated decreased global longitudinal, circumferential and

radial PS in essential hypertension. In the present study, the global strain decreased longitudinally but was preserved radially and circumferentially, consistent with an echocardiographic strain study by Sera (28). This difference suggests that longitudinal PS may be a more sensitive indicator than radial and circumferential PS for identifying the subclinical LV systolic dysfunction. This may be because the myocardium producing longitudinal stress mainly exists in the endocardium (29), which is generally reported to be the first site of myocardial ischemia (30).

Previous epidemiologic studies have provided substantial evidence that obesity could worsen cardiac function (31, 32). If there is hypertension at the same time, it also promotes the deterioration of cardiac function due to the chronic hemodynamic burden and central pressure overload (33). However, a previous study (34) showed that the presence of hypertension and obesity had no obvious effect on systolic function by LVEF. In this context, we have further examined the simultaneous presence of hypertension and obesity on the subclinical systolic function. Our results showed that in obese hypertensive patients, longitudinal PS was further decreased, and longitudinal PSSR began to be significantly impaired, despite comparable LVEF. These results suggest that subclinical systolic dysfunction caused by hypertension was further aggravated with obesity. This may be attributed to interrelated factors such as various neurohormonal and metabolic abnormalities, abnormalities in microvasculature and cardiac remodeling (4). In addition, these results also indicate that CMR-FT technique allows for early detection of subclinical systolic dysfunction, thus enabling timely intervention to prevent disease progression.

In addition, the occurrence of longitudinal and circumferential PDSR impairment in obese patients indicated an adverse effect of hypertension and combined obesity on subclinical diastolic dysfunction. Consistently, Kim et al. (34) demonstrated that obesity and hypertension intensified diastolic dysfunction by echocardiography. A previous study (35) showed that there was limited interaction on pathophysiological changes between obesity and hypertension in the development of diastolic function. Specifically, hypertension triggered apoptosis, inflammation and fibrosis, while obesity triggered oxidative stress and hypertrophic remodeling. The aggravation of subclinical LV diastolic dysfunction may provide a perspective in comorbidity-specific characterization.

Associations Between Myocardial Perfusion, Left Ventricular Deformation and Body Mass Index in Hypertensive Patients

Multivariable stepwise regression analysis revealed that BMI exerted negative impacts on both myocardial perfusion and LV function. The negative effect of BMI on longitudinal PSSR and PDSR indicated that BMI was an important factor influencing LV systolic and diastolic function. In addition, we found that BMI was significantly associated with longitudinal PS in model adjustment with perfusion with improved model fit. With the increase in BMI, LV hypertrophic remodeling was noticeably intensified in hypertensive patients. Although the association between BMI and longitudinal PDSR lost significance after correction for myocardial perfusion, we assume that BMI is more likely to be higher in patients with lower perfusion, which also shows more severe diastolic dysfunction. Considering that microcirculation damage and subclinical LV systolic and diastolic dysfunction are predecessors of poor outcomes, these results emphasize the clinical implications of the adverse effects of obesity and the importance of weight management for hypertensive patients.

The present study found an independent association between TTM and longitudinal PSSR in hypertension, which is in accordance with previous evidence regarding diabetes by Liu et al. (6). Consistently, Li et al. demonstrated a significant association between impaired myocardial perfusion and subclinical systolic function in hypertension (24). In addition, previous studies have indicated an association between resting regional perfusion abnormalities and impaired diastolic function in consecutive patients who underwent single-photon emission computed tomography (SPECT) (36, 37). Our study also analyzed possible associations between perfusion and diastolic function in hypertension and found a similar association between upslope and longitudinal PDSR. These findings might suggest a possible mechanistic link between myocardial perfusion impairment by hypertension and subclinical LV systolic and diastolic dysfunction. Further investigation into underlying mechanisms and optimal treatment are warranted to improve LV function and prognosis for patients with essential hypertension.

Limitations

There are several limitations of this study. First, this is a retrospective single-center study with inherent limitations. Therefore, further large-scale, multicenter, prospective research is needed to validate our results. Second, patient BMI was measured before CMR, and the predisease BMI and dynamic changes in BMI were not recorded and discussed in this study. Further studies are warranted to investigate the impact of dynamic changes in BMI on myocardial microcirculation and cardiac function. Third, the present study assessed only myocardial perfusion at rest, since stress perfusion has contraindications and potential risks. However, even in the resting state, the additive effect of hypertension and obesity on myocardial microcirculation has been proven.

CONCLUSION

Obesity had an additive deleterious effect on myocardial microcirculation and LV function in patients with hypertension, and BMI was associated with myocardial microcirculation and LV function. Impaired myocardial perfusion was associated with subclinical LV dysfunction in hypertensive patients. These results emphasize the adverse effects of obesity and the importance of weight management for hypertensive patients and may imply mechanistic perspectives that could help in early diagnosis

and the development of therapeutic strategies, thus improving prognosis for hypertensive patients.

DATA AVAILABILITY STATEMENT

The raw data supporting the conclusions of this article will be made available by the authors, without undue reservation.

ETHICS STATEMENT

The studies involving human participants were reviewed and approved by Ethics Committee on Biomedical Research, West China Hospital of Sichuan University. The patients/participants provided their written informed consent to participate in this study.

AUTHOR CONTRIBUTIONS

P-LH: conceptualization, and writing—original draft. P-LH, X-ML, and W-FY: data curation. LJ, Y-KG, and YL: writing—review and editing. Z-GY and KL: supervision and writing—review and editing. Z-GY: funding acquisition. All authors contributed to the article and approved the submitted version.

FUNDING

This work was supported by 1.3.5 project for disciplines of excellence, West China Hospital, Sichuan University (ZYGD 18013).

ACKNOWLEDGMENTS

We thank all the subjects, research coordinators, and investigators who participated in the trials.

SUPPLEMENTARY MATERIAL

The Supplementary Material for this article can be found online at: https://www.frontiersin.org/articles/10.3389/fcvm.2022.831231/full#supplementary-material

REFERENCES

1. Mills KT, Bundy JD, Kelly TN, Reed JE, Kearney PM, Reynolds K, et al. Global disparities of hypertension prevalence and control: a systematic analysis of population-based studies from 90 countries. *Circulation.* (2016) 134:441–50. doi: 10.1161/CIRCULATIONAHA.115.018912
2. Blüher M. Obesity: global epidemiology and pathogenesis. *Nat Rev Endocrinol.* (2019) 15:288–98. doi: 10.1038/s41574-019-0176-8
3. Hall JE, do Carmo JM, da Silva AA, Wang Z, Hall ME. Obesity, kidney dysfunction and hypertension: mechanistic links. *Nat Rev Nephrol.* (2019) 15:367–85. doi: 10.1038/s41581-019-0145-4
4. La Sala L, Tagliabue E, Vieira E, Pontiroli AE, Folli F. High plasma renin activity associates with obesity-related diabetes and arterial hypertension, and predicts persistent hypertension after bariatric surgery. *Cardiovasc Diabetol.* (2021) 20:118. doi: 10.1186/s12933-021-01310-w
5. Konst RE, Guzik TJ, Kaski JC, Maas AHEM, Elias-Smale SE. The pathogenic role of coronary microvascular dysfunction in the setting of other cardiac or systemic conditions. *Cardiovasc Res.* (2020) 116:817–28. doi: 10.1093/cvr/cvaa009
6. Liu X, Yang Z, Gao Y, Xie L, Jiang L, Hu B, et al. Left ventricular subclinical myocardial dysfunction in uncomplicated type 2 diabetes mellitus is associated with impaired myocardial perfusion: a contrast-enhanced cardiovascular magnetic resonance study. *Cardiovasc Diabetol.* (2018) 17:139. doi: 10.1186/s12933-018-0782-0
7. Zhou W, Brown JM, Bajaj NS, Chandra A, Divakaran S, Weber B, et al. Hypertensive coronary microvascular dysfunction: a subclinical marker of end organ damage and heart failure. *Eur Heart J.* (2020) 41:2366–75. doi: 10.1093/eurheartj/ehaa191
8. Vita T, Murphy DJ, Osborne MT, Bajaj NS, Keraliya A, Jacob S, et al. Association between nonalcoholic fatty liver disease at CT and coronary microvascular dysfunction at myocardial perfusion PET/CT. *Radiology.* (2019) 291:330–7. doi: 10.1148/radiol.2019181793
9. Laurent S, Agabiti-Rosei C, Bruno RM, Rizzoni D. Microcirculation and macrocirculation in hypertension: a dangerous cross-link? *Hypertension.* (2022) 79:479–90. doi: 10.1161/HYPERTENSIONAHA.121.17962
10. Liu H, Wang J, Pan Y, Ge Y, Guo Z, Zhao S. Early and quantitative assessment of myocardial deformation in essential hypertension patients by using cardiovascular magnetic resonance feature tracking. *Sci Rep.* (2020) 10:3582. doi: 10.1038/s41598-020-60537-x
11. Bajaj NS, Osborne MT, Gupta A, Tavakkoli A, Bravo PE, Vita T, et al. Coronary microvascular dysfunction and cardiovascular risk in obese patients. *J Am Coll Cardiol.* (2018) 72:707–17. doi: 10.1016/j.jacc.2018.05.049
12. Blomstrand P, Sjöblom P, Nilsson M, Wijkman M, Engvall M, Länne T, et al. Overweight and obesity impair left ventricular systolic function as measured by left ventricular ejection fraction and global longitudinal strain. *Cardiovasc Diabetol.* (2018) 17:113. doi: 10.1186/s12933-018-0756-2
13. Hendel RC, Friedrich MG, Schulz-Menger J, Zemmrich C, Bengel F, Berman DS, et al. CMR first-pass perfusion for suspected inducible myocardial ischemia. *JACC Cardiovasc Imaging.* (2016) 9:1338–48. doi: 10.1016/j.jcmg.2016.09.010
14. Jiang L, Shi K, Guo Y, Ren Y, Li Z, Xia C, et al. The additive effects of obesity on myocardial microcirculation in diabetic individuals: a cardiac magnetic resonance first-pass perfusion study. *Cardiovasc Diabetol.* (2020) 19:52. doi: 10.1186/s12933-020-01028-1
15. Jacobse JN, Steggink LC, Sonke GS, Schaapveld M, Hummel YM, Steenbruggen TG, et al. Myocardial dysfunction in long-term breast cancer survivors treated at ages 40–50 years. *Eur J Heart Fail.* (2020) 22:338–46. doi: 10.1002/ejhf.1610
16. Zhang Y, Yan WF, Jiang L, Shen MT, Li Y, Huang S, et al. Aggravation of functional mitral regurgitation on left ventricle stiffness in type 2 diabetes mellitus patients evaluated by CMR tissue tracking. *Cardiovasc Diabetol.* (2021) 20:158. doi: 10.1186/s12933-021-01354-y
17. Zhang Y, Wang J, Ren Y, Yan WF, Jiang L, Li Y, et al. The additive effects of kidney dysfunction on left ventricular function and strain in type 2 diabetes mellitus patients verified by cardiac magnetic resonance imaging. *Cardiovasc Diabetol.* (2021) 20:11. doi: 10.1186/s12933-020-01203-4
18. WHO Expert Consultation. Appropriate body-mass index for Asian populations and its implications for policy and intervention strategies. *Lancet.* (2004) 363:157–63. doi: 10.1016/S0140-6736(03)15268-3
19. Maron BJ, McKenna WJ, Danielson GK, Kappenberger LJ, Kuhn HJ, Seidman CE, et al. American college of cardiology/European society of cardiology clinical expert consensus document on hypertrophic cardiomyopathy. *J Am Coll Cardiol.* (2003) 42:1687–713. doi: 10.1016/S0735-1097(03)00941-0
20. Levy BI, Schiffrin EL, Mourad J-J, Agostini D, Vicaut E, Safar ME, et al. Impaired tissue perfusion: a pathology common to hypertension,

obesity, and diabetes mellitus. *Circulation.* (2008) 118:968–76. doi: 10.1161/CIRCULATIONAHA.107.763730
21. Schäfer S, Kelm M, Mingers S, Strauer BE. Left ventricular remodeling impairs coronary flow reserve in hypertensive patients. *J Hypertens.* (2002) 20:1431–7. doi: 10.1097/00004872-200207000-00031
22. Schwartzkopff B, Motz W, Frenzel H, Vogt M, Knauer S, Strauer BE. Structural and functional alterations of the intramyocardial coronary arterioles in patients with arterial hypertension. *Circulation.* (1993) 88:993–1003. doi: 10.1161/01.CIR.88.3.993
23. Kawecka-Jaszcz K, Czarnecka D, Olszanecka A, Klecha A, Kwiecień-Sobstel A, Stolarz-Skrzypek K, et al. Myocardial perfusion in hypertensive patients with normal coronary angiograms. *J Hypertens.* (2008) 26:1686–94. doi: 10.1097/HJH.0b013e328303df42
24. Li X-M, Jiang L, Guo Y-K, Ren Y, Han P-L, Peng L-Q, et al. The additive effects of type 2 diabetes mellitus on left ventricular deformation and myocardial perfusion in essential hypertension: a 3.0 T cardiac magnetic resonance study. *Cardiovasc Diabetol.* (2020) 19:161. doi: 10.1186/s12933-020-01138-w
25. Schindler TH, Cardenas J, Prior JO, Facta AD, Kreissl MC, Zhang XL, et al. Relationship between increasing body weight, insulin resistance, inflammation, adipocytokine leptin, and coronary circulatory function. *J Am Coll Cardiol.* (2006) 47:1188–95. doi: 10.1016/j.jacc.2005.10.062
26. Drazner MH. The progression of hypertensive heart disease. *Circulation.* (2011) 123:327–34. doi: 10.1161/CIRCULATIONAHA.108.845792
27. Wu L, Germans T, Güçlü A, Heymans MW, Allaart CP, van Rossum AC. Feature tracking compared with tissue tagging measurements of segmental strain by cardiovascular magnetic resonance. *J Cardiovasc Magn Reson.* (2014) 16:10. doi: 10.1186/1532-429X-16-10
28. Sera F, Jin Z, Russo C, Lee ES, Schwartz JE, Rundek T, et al. Relationship of office and ambulatory blood pressure with left ventricular global longitudinal strain. *Am J Hypertens.* (2016) 29:1261–7. doi: 10.1093/ajh/hpv188
29. Wang J, Khoury DS, Yue Y, Torre-Amione G, Nagueh SF. Preserved left ventricular twist and circumferential deformation, but depressed longitudinal and radial deformation in patients with diastolic heart failure. *Eur Heart J.* (2007) 29:1283–9. doi: 10.1093/eurheartj/ehn141
30. Vinereanu D, Lim PO, Frenneaux MP, Fraser AG. Reduced myocardial velocities of left ventricular long-axis contraction identify both systolic and diastolic heart failure-a comparison with brain natriuretic peptide. *Eur J Heart Fail.* (2005) 7:512–9. doi: 10.1016/j.ejheart.2004.07.014
31. Liu Y, Yan Y, Jiang T, Li S, Guo Y, Fernandez C, et al. Impact of long-term burden of body mass index and blood pressure from childhood on adult left ventricular structure and function. *J Am Heart Assoc.* (2020) 9:e016405. doi: 10.1161/JAHA.120.016405
32. Kishi S, Armstrong AC, Gidding SS, Colangelo LA, Venkatesh BA, Jacobs DR Jr., et al. Association of obesity in early adulthood and middle age with incipient left ventricular dysfunction and structural remodeling: the CARDIA study (Coronary Artery Risk Development in Young Adults). *JACC Heart Fail.* (2014) 2:500–8. doi: 10.1016/j.jchf.2014.03.001
33. Alpert MA, Omran J, Bostick BP. Effects of obesity on cardiovascular hemodynamics, cardiac morphology, and ventricular function. *Curr Obes Rep.* (2016) 5:424–34. doi: 10.1007/s13679-016-0235-6
34. Kim J, Kim MG, Kang S, Kim BR, Baek MY, Park YM, et al. Obesity and hypertension in association with diastolic dysfunction could reduce exercise capacity. *Korean Circ J.* (2016) 46:394–401. doi: 10.4070/kcj.2016.46.3.394
35. Brandt MM, Nguyen ITN, Krebber MM, Wouw J, Mokry M, Cramer MJ, et al. Limited synergy of obesity and hypertension, prevalent risk factors in onset and progression of heart failure with preserved ejection fraction. *J Cell Mol Med.* (2019) 23:6666–78. doi: 10.1111/jcmm.14542
36. Gimelli A, Liga R, Avogliero F, Coceani M, Marzullo P. Relationships between left ventricular sympathetic innervation and diastolic dysfunction: the role of myocardial innervation/perfusion mismatch. *J Nucl Cardiol.* (2018) 25:1101–9. doi: 10.1007/s12350-016-0753-3
37. Gimelli A, Liga R, Bottai M, Pasanisi EM, Giorgetti A, Fucci S, et al. Diastolic dysfunction assessed by ultra-fast cadmium-zinc-telluride cardiac imaging: impact on the evaluation of ischaemia. *Eur Heart J Cardiovasc Imaging.* (2015) 16:68–73. doi: 10.1093/ehjci/jeu16

Conflict of Interest: The authors declare that the research was conducted in the absence of any commercial or financial relationships that could be construed as a potential conflict of interest.

Publisher's Note: All claims expressed in this article are solely those of the authors and do not necessarily represent those of their affiliated organizations, or those of the publisher, the editors and the reviewers. Any product that may be evaluated in this article, or claim that may be made by its manufacturer, is not guaranteed or endorsed by the publisher.

frontiers in Cardiovascular Medicine

REVIEW
published: 24 March 2022
doi: 10.3389/fcvm.2022.787618

Multimodality Imaging in the Evaluation and Prognostication of Cardiac Amyloidosis

*Paul J. Scheel III, Monica Mukherjee, Allison G. Hays and Joban Vaishnav**

Division of Cardiology, Johns Hopkins University School of Medicine, Baltimore, MD, United States

Cardiac amyloidosis (CA) is an infiltrative cardiomyopathy resulting from deposition of misfolded immunoglobulin light chains (AL-CA) or transthyretin (ATTR-CA) proteins in the myocardium. Survival varies between the different subtypes of amyloidosis and degree of cardiac involvement, but accurate diagnosis is essential to ensure initiation of therapeutic interventions that may slow or potentially prevent morbidity and mortality in these patients. As there are now effective treatment options for CA, identifying underlying disease pathogenesis is crucial and can be guided by multimodality imaging techniques such as echocardiography, magnetic resonance imaging, and nuclear scanning modalities. However, as use of cardiac imaging is becoming more widespread, understanding optimal applications and potential shortcomings is increasingly important. Additionally, certain imaging modalities can provide prognostic information and may affect treatment planning. In patients whom imaging remains non-diagnostic, tissue biopsy, specifically endomyocardial biopsy, continues to play an essential role and can facilitate accurate and timely diagnosis such that appropriate treatment can be started. In this review, we examine the multimodality imaging approach to the diagnosis of CA with particular emphasis on the prognostic utility and limitations of each imaging modality. We also discuss how imaging can guide the decision to pursue tissue biopsy for timely diagnosis of CA.

Keywords: cardiac amyloidosis, echocardiography, cardiac magnetic resonance imaging (CMR), endomyocardial biopsy, cardiac scintigraphy, nuclear imaging

OPEN ACCESS

Edited by:
Grigorios Korosoglou, GRN Klinik Weinheim, Germany

Reviewed by:
Alberto Giannoni, Sant'Anna School of Advanced Studies, Italy
Concetta Zito, University of Messina, Italy
Filippo Cademartiri, Gabriele Monasterio Tuscany Foundation (CNR), Italy

****Correspondence:***
Joban Vaishnav
Jvaishn1@jhmi.edu

Specialty section:
This article was submitted to Cardiovascular Imaging, a section of the journal Frontiers in Cardiovascular Medicine

Received: *01 October 2021*
Accepted: *14 February 2022*
Published: *24 March 2022*

Citation:
Scheel PJ III, Mukherjee M, Hays AG and Vaishnav J (2022) Multimodality Imaging in the Evaluation and Prognostication of Cardiac Amyloidosis. Front. Cardiovasc. Med. 9:787618. doi: 10.3389/fcvm.2022.787618

INTRODUCTION

Systemic amyloidosis is terminology for a broad spectrum of diseases that result from the aggregation of misfolded proteins. Cardiac amyloidosis (CA) occurs when amyloid fibrils accumulate in the myocardium often resulting in a restrictive cardiomyopathy (1–3). The two most common proteins that lead to CA include monoclonal immunoglobulin light chains (AL-CA) and transthyretin (ATTR-CA). AL-CA is rare with an incidence of 10–12 per million person-years and a slight male predominance (4). ATTR-CA, on the other hand, has a significant male predominance and is likely more common than reported and as such, a true estimate of prevalence is difficult (2). An autopsy study of individuals greater than 80 years old found ATTR-CA in 25% of subjects, though only a subset of those were thought to be clinically relevant (5). The misfolded amyloid fibrils in ATTR-CA can either occur due to an age-related phenomenon, known as wild-type CA (wtATTR), or related to a genetic variant, known as hereditary CA (hATTR). There are more

than 130 TTR mutations identified, with the most common mutation in the United States being Val122Ile, present in 3–4% of African Americans (6). While the amyloid fibril deposition in AL and ATTR-CA can be systemic (it is the cardiac involvement that determines prognosis). Survival for treated AL-CA has improved with advances in chemotherapy (7). ATTR-CA survival varies between subtypes, but in general is 3–5 years without treatment (2). With the advancements in the treatment of both AL and ATTR-CA, there is a need for increased recognition of this condition. Additionally, the efficacy of available therapies for CA is far more favorable if instituted earlier in the disease course, highlighting the need for early diagnosis and treatment.

Although direct tissue characterization with organ biopsy had historically been the mainstay for diagnosis of CA, more recently non-invasive cardiac imaging algorithms have become the cornerstone of evaluation (8, 9). These algorithms are typically predicated on establishing suspicion for CA based on clinical factors and complementing that with imaging findings. If imaging affirms clinical suspicion, laboratory evaluation, and nuclear techniques or tissue biopsy are needed to determine specific amyloidosis subtype (8–10). However, the test performance characteristics and prognostic utility are evolving given more widespread application and treatment. In this review, we examine the multimodality imaging approach to the diagnosis of CA. We highlight the evolution in diagnostic performance, complementary information, and prognostic utility of each modality as well as emerging imaging techniques in the diagnosis and management of CA. Finally, we focus on how multimodality imaging can guide clinicians on when to pursue tissue biopsy in select cases.

CLINICAL RECOGNITION OF CARDIAC AMYLOIDOSIS

Cardiac amyloidosis is under-recognized and the diagnosis often delayed, with the majority of patients experiencing greater than 10 healthcare interactions in the 3 years before accurate diagnosis (2). CA should be suspected in any patient presenting with heart failure (HF), a non-dilated left ventricle (LV), and unexplained left ventricular hypertrophy (LVH). However, as disease prevalence may increase with age, particularly for wtATTR, patients may have co-morbid conditions such as hypertension, ischemic heart disease, or aortic stenosis that confound the diagnosis. Therefore, it is important to maintain a high index of suspicion and also screen for other cardiac clues that may suggest underlying ATTR-CA as the driver of HF (**Table 1**). Additionally, there are non-cardiac manifestations of CA that may precede overt cardiac symptoms and recognition of such clues may allow for an earlier diagnosis of ATTR-CA (**Table 1**). AL amyloidosis is a systemic condition, and may present with proteinuria, macroglossia, periorbital purpura, or neuropathy. Once AL-CA is suspected, clinicians should aim to confirm the diagnosis within 1–2 weeks, as AL-CA should be considered a diagnostic emergency due to the rapid progression of disease without treatment.

TABLE 1 | Cardiac and non-cardiac clinical clues for possible ATTR-CA.

Non-imaging cardiac red flags for ATTR-CA	Non-cardiac red flags for ATTR-CA
Intolerance of GDMT	Polyneuropathy
Persistent low-level troponin elevation	Autonomic dysfunction/Orthostatic hypotension
Unexplained AV block	Bilateral carpal tunnel syndrome
Family history of cardiomyopathy	Lumbar spine stenosis
HFpEF diagnosis in the absence of risk factors	Diarrhea alternating with constipation

GDMT, guideline directed medical therapy for heart failure; HFpEF, heart failure with preserved ejection fraction.

ECHOCARDIOGRAPHY

Transthoracic echocardiogram (TTE) is a mainstay of initial HF evaluation and a common imaging modality that will raise initial diagnostic suspicion of CA (**Table 2**). Patients undergoing echocardiography eventually diagnosed with CA will likely fall into two categories: (1) symptomatic, with clinical clues to suggest underlying CA as part of evaluation for congestive HF or (2) asymptomatic but at risk for CA because of known non-cardiac AL amyloid involvement or family history of hATTR with known genotype positivity (**Figure 1**). While TTE is a widely available and helpful diagnostic test that may raise the initial suspicion for CA, demonstration of tissue uptake of the specific type of abnormal protein, either with advanced imaging or biopsy, will always be needed to confirm a diagnosis of CA. Abnormal parameters commonly seen on echocardiography are summarized in **Figure 2**.

Morphologic Changes

LVH is the hallmark finding of CA on echocardiography and is generally considered a prerequisite to pursuing further investigation for CA in patients not otherwise at risk (**Figures 3A,B**). LVH is defined as septal or posterior LV wall thickness greater than 1.1 cm in men and greater than 1.0 cm in women (11). LVH represents either increased muscle mass (true hypertrophy) or increased presence of a non-muscle substance like amyloid fibrils (pseudohypertrophy). LVH in CA is typically concentric and symmetric but asymmetric hypertrophy can also be seen (12, 13). A normal wall thickness in a patient with known AL amyloidosis traditionally signified a lack of cardiac involvement but very early involvement of disease is also possible in this circumstance (14, 15).

Typically, LVH in ATTR-CA is slowly progressive, allowing for early detection of disease prior to significant symptom onset. In a study by Itzhaki Ben Zadok et al., echocardiograms in AL and ATTR-CA patients analyzed in the years prior to a formal diagnosis found LVH $\geq$ 12 mm in 79% of patients more than 3 years prior to diagnosis (16). Additionally, ATTR-CA patients developed LVH earlier than AL-CA patients prior to their formal diagnosis, possibly related to the rapid disease progression seen with AL-CA as compared to ATTR-CA (12). LVH, especially mild LVH (wall thickness $<$ 1.5 cm), can have many causes including hypertensive heart disease (HHD), hypertrophic cardiomyopathy

TABLE 2 | Comparison of each imaging modality with their specific findings in cardiac amyloidosis as well as their relative strengths and weakness.

Imaging modality	Findings in cardiac amyloidosis	Strengths	Limitations
Echocardiography	LVH	Readily available	No differentiation between CA subtypes
	Small LV cavity	Cheap	Variable image quality
	Large atria	High temporal resolution	Early findings in CA non-specific
	RV/LV systolic dysfunction	Identify other causes of LVH (AS, HCM, etc.)	
	Abnormal LV diastolic function	No radiation	
	Abnormal strain	Patient ease	
	Pericardial/pleural effusion		
Magnetic resonance imaging (MRI)	Similar morphologic findings to echocardiography (**Figure 2**)	Reproducible	Expensive
	Late gadolinium enhancement in atria and ventricles	Direct tissue characterization	Limited availability
	Pericardial/pleural effusion	No radiation	Special expertise required
	Atria dysfunction	Identify other causes of LVH (HCM, infiltrating disease)	Multiple patient specific exclusions (implants, claustrophobia, etc.)
	Interatrial septum thickening	Higher spatial resolution and multi-dimensional strain	
	Abnormal strain		
Cardiac scintigraphy (PYP, DPD, and HDMP)	Increased radiotracer uptake	Cheap	Radiation
	Increased H/CL ratio	Widely available	Mostly qualitative
		Ease of interpretation	Genetic variant uptake variability
		Differentiate amyloid subtype	
PET imaging	Increased radiotracer uptake	Quantitative assessment	Radiation
		Differentiate amyloid subtype	Expensive

AS, aortic stenosis; H/CL, heart/contralateral; HCM, hypertrophic cardiomyopathy; LV, left ventricle; LVH, left ventricular hypertrophy; PET, positron-emission tomography.

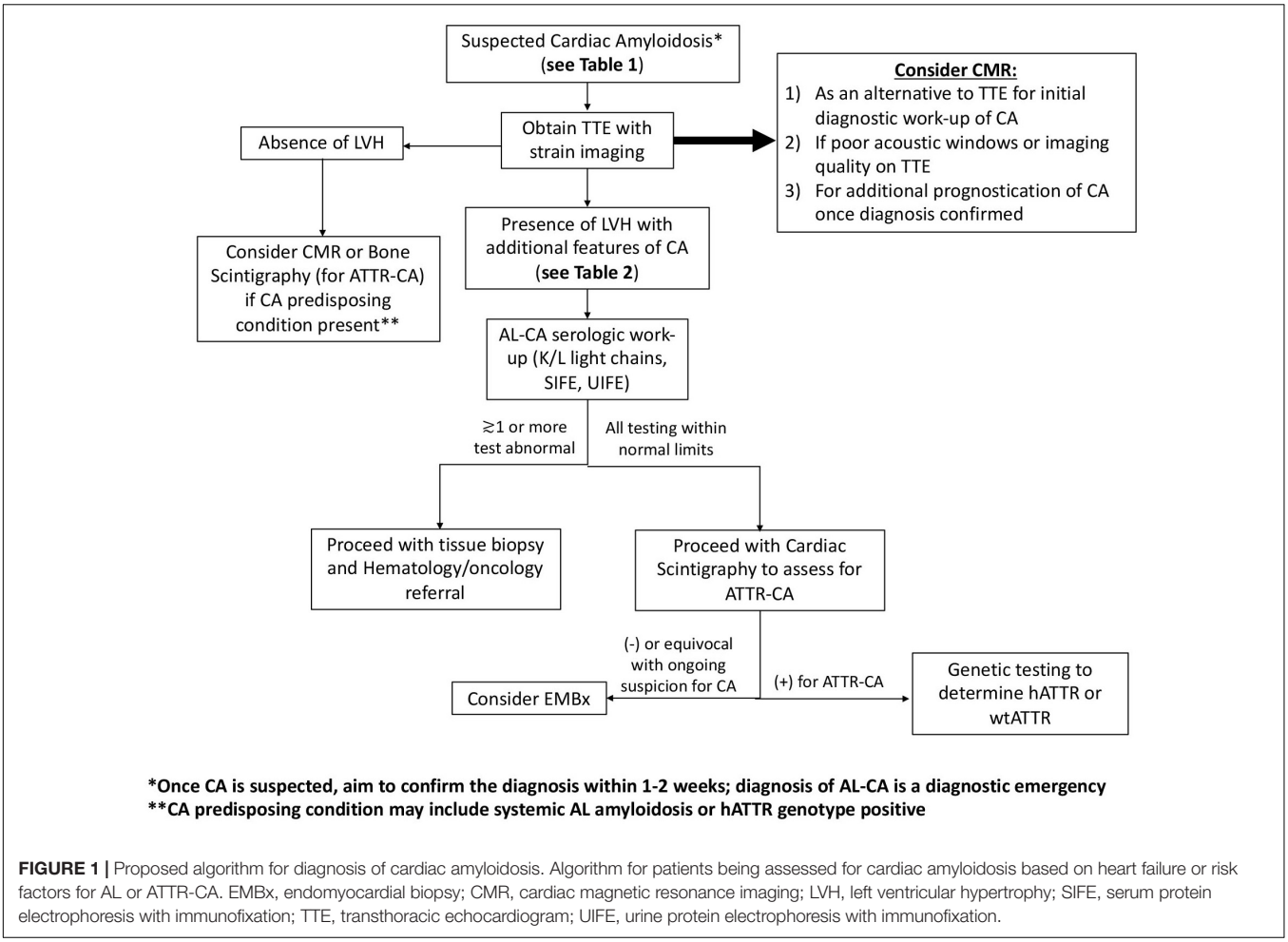

FIGURE 1 | Proposed algorithm for diagnosis of cardiac amyloidosis. Algorithm for patients being assessed for cardiac amyloidosis based on heart failure or risk factors for AL or ATTR-CA. EMBx, endomyocardial biopsy; CMR, cardiac magnetic resonance imaging; LVH, left ventricular hypertrophy; SIFE, serum protein electrophoresis with immunofixation; TTE, transthoracic echocardiogram; UIFE, urine protein electrophoresis with immunofixation.

(HCM), aortic stenosis, or other infiltrative cardiomyopathies but if additional clinical or morphologic features consistent with CA are present (**Table 1**), further testing for CA should be pursued. Characteristic echocardiographic findings combined with epidemiologic and clinical clues frequently differentiates between other causes of LVH but overlap can still exist and may requiring additional diagnostics, such as cardiac magnetic resonance imaging (CMR) or genetic testing, to aid diagnosis (**Table 3**). Of note, low voltage on electrocardiogram (ECG) especially in the setting of LVH on imaging was once considered a hallmark sign of CA but many studies demonstrate this only occurs in a minority of CA patients and may be a finding suggestive of advanced disease (17–19). Sensitivity of low voltage on ECG for CA can be increased by using a Sokolow-Lyon index of $\leq$ 15 mm (sum of S wave in V1 plus R wave in either V5 or V6, whichever is larger; >35 mm indicates true LV hypertrophy) or combining objective measures of ECG voltage and LV mass based on imaging (17, 20).

While LVH is universal in the current diagnostic paradigm for CA, other morphologic changes occur with variable frequencies in CA (**Figure 2**). LV cavity size is generally normal or decreased (15, 21), except in the rare circumstance where CA develops after development of an unrelated dilated cardiomyopathy. Compared to other causes of LVH, a small LV cavity size may point more toward CA (7). LV mass index (LVMI), a specific measure of LVH utilizing LV wall thickness and cavity dimension, also tends to be higher in CA compared to other causes of LVH (18). More so, right ventricular hypertrophy (RVH) and significant left atrial enlargement (left atrial volume index, LAVI $\geq$ 47 mL/m^2) may be a more specific sign for CA in those patients with LVH (18, 22, 23). Thickened cardiac valve leaflets related to amyloid deposition have been observed in some patients, but is subjective given lack of defined parameters. Pericardial or pleural effusion is also common, and has been described in up to 50% of patients with CA (24, 25).

Many studies initially described increased echogenicity or "sparkling" of the myocardium on TTE in patients with CA (25–28). Advances in image processing has made this feature less pronounced. Contemporary studies have also shown that this is fairly subjective between readers and less common than previously reported (18).

Diastolic Function

Aberrations in Doppler based diastolic parameters in CA was recognized soon after this technology was developed (29). These abnormal parameters include shorter deceleration time (DT),

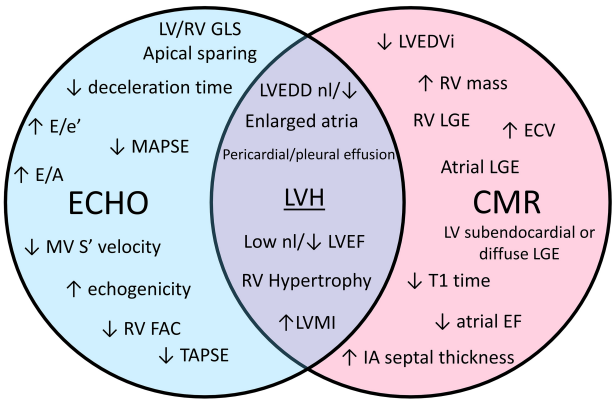

FIGURE 2 | A Venn diagram comparing echocardiogram (echo) and cardiac magnetic resonance (CMR) characteristics seen in cardiac amyloidosis. ECV, extra cellular volume; EF, ejection fraction; FAC, fractional area change; GLS, global longitudinal strain; LGE, late gadolinium enhancement; LV, left ventricle; LVEDD, left ventricular end diastolic diameter; LVEDVi, left ventricular end diastolic volume index; LVH, left ventricular hypertrophy; LVMI, left ventricle mass index; MAPSE, mitral annular plane systolic excursion; MV, mitral valve; nl, normal; RV, right ventricle; TAPSE, tricuspid annular plane systolic excursion.

higher E/A, and higher E/e′ (**Figure 4**). A limitation for diastolic assessment in CA is atrial fibrillation, a common comorbidity in this condition (30). CA typically leads to more severe diastolic dysfunction compared to other causes of LVH (18, 21, 23) and diastolic parameters may worsen with disease progression (10, 15, 31). Chacko et al. (32) showed that a spectrum of diastolic function exists even within ATTR-CA and depending on the underlying genetic variant, if present. Despite having similar wall thickness, wtATTR patients had worse diastolic function compared to Thr60Ala hATTR patients, though both had better diastolic function than Val122Ile hATTR patients (32). The variations in diastolic function based on genetic subtype correlated with differences in symptoms, biomarkers, and mortality (32).

Systolic Function

Early models classified CA as a "diastolic heart failure" with systolic dysfunction being a later manifestation of disease (15). However, even early CA may have subtle abnormalities in systolic function. Left ventricular ejection fraction (LVEF) in CA can be normal or low-normal, though typically lower as compared to other causes of LVH (18, 21–23). Mitral annular plane systolic excursion (MAPSE) is frequently abnormal in CA especially as HF develops but this is not performed on routine TTEs and may be a late manifestation of disease (33). Tissue Doppler measuring mitral annular velocity (S′) is another marker of systolic function and a cutoff $\leq$ 6 cm/s performed well as a screening test for possible CA in a population of patients with severe aortic stenosis (34). The presence of RV systolic dysfunction in CA, which may occur due to direct amyloid infiltration or related to left heart disease in CA, is currently an area of active investigation. Both AL and ATTR-CA patients have been shown to have lower RV fractional shortening and tricuspid annular plane systolic excursion (TAPSE) compared to patients with alternative causes of LVH (35, 36). Licordari et al. examined 37 patients with a known pathogenic TTR variant with no or minimal symptoms and found that in those with CA, echocardiographic markers of RV function were already impaired in this early stage of disease (37). RV dilation is non-specific and can be seen later in the disease course as well (38).

Strain Imaging

Left ventricular strain imaging using speckle tracking echocardiographic techniques measures the regional and global deformation of the myocardium (19, 39). The reduction in strain and strain rate occurs before overt myocardial dysfunction allowing for earlier detection of systolic dysfunction (14). Initial studies of strain in CA demonstrated clear differences between patients without CA and those with CA even in the absence of

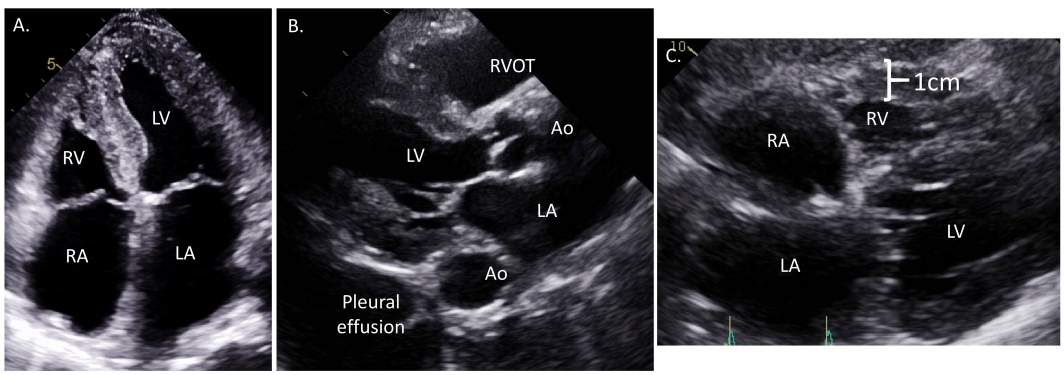

FIGURE 3 | Representative echocardiographic images from a patient with cardiac amyloidosis. **(A)** Apical 4-chamber view showing moderate concentric left ventricular hypertrophy with more prominent proximal septal hypertrophy, significant bi-atrial enlargement, and diffusely thickened atrioventricular valves. **(B)** Parasternal long axis view showing large pleural effusion, moderate concentric hypertrophy, small left ventricular end diastolic diameter (LVEDD), and right ventricle outflow track dilation. **(C)** Subcostal view demonstrating significant right ventricular hypertrophy, biatrial enlargement, and interatrial septal thickening.

TABLE 3 | Clinical and echocardiographic characteristics of alternative causes of left ventricular hypertrophy beyond cardiac amyloidosis.

Hypertrophic disease	Clinical clues	Echocardiographic clues
Fabry disease	Childhood to adulthood	Concentric/symmetric LVH
	X-linked inheritance	Papillary hypertrophy
	Abdominal pain	Papillary position variants
	Angiokeratomas	RV hypertrophy
	Kidney abnormalities	Regional strain abnormalities
	Hypohidrosis	Occasional areas of LV thinning
	Conduction disease	
Hypertrophic cardiomyopathy	Childhood to adulthood	Most commonly asymmetric LVH
	Sudden cardiac death	Apical/mid-cavity variants
	Often inherited	Apical aneurysm
	ECG pattern often	Papillary position variants
	characteristic	MV abnormalities
		Mitral regurgitation
Hypertensive heart disease (HHD)	Long-standing documented HTN	Non-specific
	Strong family history HTN	
	Multiple anti-hypertensives	
Athlete's heart	Endurance/high-intensity exercise	Eccentric hypertrophy (LV dilation)
	Resting bradycardia	RV dilation/hypertrophy
		Atrial dilation
		Non-compaction sometimes seen
Friedreich ataxia	Usually childhood/adolescent	Asymmetric or concentric LVH
	Autosomal recessive	Dilated variants
	Gait ataxia	
	Vision/hearing problems	
	Nystagmus	
Danon disease	Childhood/adolescent	Non-compaction
	X-linked inheritance	
	Skeletal myopathy	
	Cognitive impairment	
	Pre-excitation on ECG	
Left ventricular non-compaction (LVNC)	Childhood to adulthood	Non-compaction
	Thromboembolic events	Colour Doppler of hypertrophy for flow
	Malignant arrhythmias	Contrast usage may help
Hypereosinophilic cardiomyopathy	Hypereosinophilic state	Restrictive
	Thromboembolic events	Endomyocardial thickening
	Fulminant to indolent	LV/RV thrombi
		MV/TV entrapment
Mitochondrial cardiomyopathies	Childhood	Non-compaction
	Often maternal inheritance	
	Multiple distinct syndromes	
	Myopathy	
	Stressors worsen symptoms	
RASopathies (Noonan, etc.)	Childhood	Other heart defects
	Myopathy	
	Developmental delay	
	Often characteristic appearance	

HTN, hypertension; LV, left ventricle; LVH, left ventricular hypertrophy; MV, mitral valve; RV, right ventricle; TV, tricuspid valve.

overt HF (15). Furthermore, CA patients with HF have worse strain compared to those who were asymptomatic, suggesting that abnormal strain may occur as a continuum related to disease severity (15).

As strain imaging was increasingly used in CA, a distinct pattern of "relative apical sparing," referring to a reduced longitudinal strain (LS) rate in the basal to mid-ventricular segments of the LV compared to the apical segments, was recognized (**Figure 3C**). While strain was already shown to be reduced in CA compared to other causes of LVH (21), this pattern may be of additive diagnostic value for CA. Relative apical longitudinal strain (RALS; = [average apical LS]/[average basal LS + average mid LS]) is an objective measure of the apical sparing pattern. Using a cutoff off of RALS > 1, CA could be differentiated from other causes of LVH with a sensitivity $> 90\%$ and specificity $>80\%$ in 55 AL and ATTR-CA patients (19). However, a slightly larger study that included AL-CA, wtATTR, and hATTR demonstrated apical sparing in a minority (48%) of patients (39). This may be due to early studies on LS in CA including predominantly AL-CA patients since this phenomenon is less common in ATTR-CA (19). Another explanation for these differences is that apical sparing may vary based on disease stage. Therefore, while an apical sparing pattern can certainly be seen in CA and may enhance the likelihood of diagnosis, the absence of this pattern should not eliminate the possibility of a CA diagnosis. Additional novel echocardiographic markers have been derived from strain imaging to help differentiate CA from other causes of LVH including the LVEF to global longitudinal strain (GLS) ratio (EFSR). A study comparing CA to HHD and HCM patients showed an EFSR > 4.1 had sensitivity and specificity of 90% for detecting CA in this population (18).

Right ventricular strain can also be measured on echocardiogram; however, this technique is not used in widespread clinical practice. Palomero and colleagues (40) evaluated RV strain in a group of AL and ATTR-CA patients ($n = 78$) compared to controls. All patients had reduced biventricular function and LV apical sparing. Notably an RV apical sparing pattern was only seen in AL-CA patients. AL-CA patients also had worse RV function measured by traditional parameters, which could support worsening RV function existing on a continuum of disease severity (40).

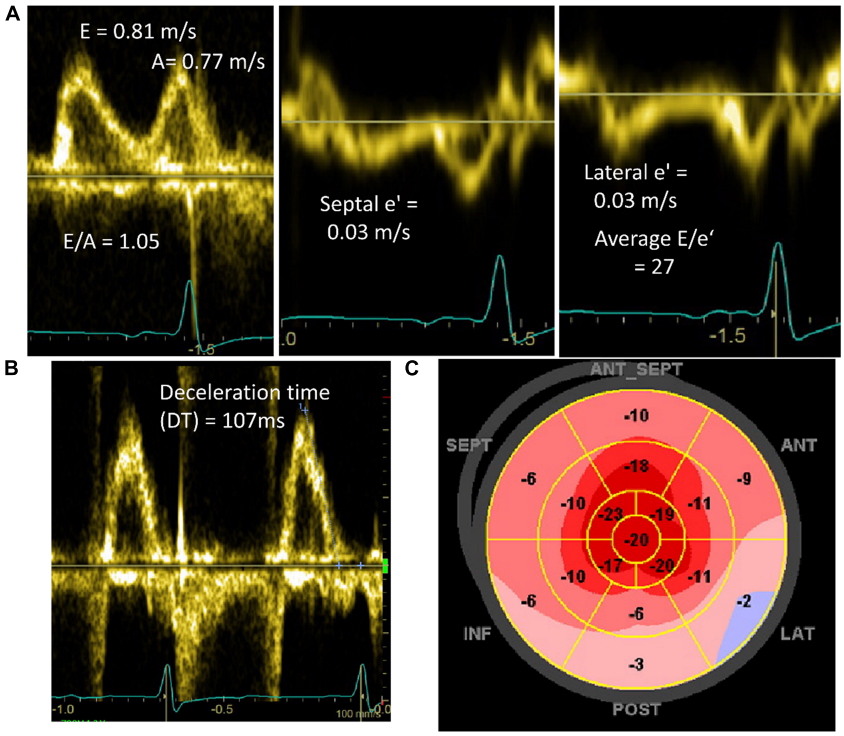

FIGURE 4 | Doppler and longitudinal strain abnormalities in patients diagnosed with cardiac amyloidosis. **(A)** Mitral inflow and mitral annular tissue Doppler showing pseudonormal diastolic filling (Grade 2) and high E/e′ signaling elevated left atrial pressures. **(B)** Mitral inflow pulse wave Doppler of patient in atrial fibrillation demonstrating short deceleration time (DT) (normal 130–220 ms). **(C)** Peak systolic longitudinal strain map demonstrating reduced longitudinal strain in basal and mid ventricular segments with relative apical sparing.

In addition to the atrial morphologic changes that can be seen as a secondary hemodynamic consequence from any cause of ventricular impairment, there is increasing evidence to suggest CA can also impair atrial function as measured by atrial strain. Diagnostically, left atrial strain can help differentiate CA from other causes of LVH (41–43). Multiple studies have demonstrated significant reduction in left atrial strain parameters in both AL and ATTR-CA compared to HHD despite similar degrees of LV wall thickness. Left atrial strain outperformed LV RALS in discriminating between disease states (41, 43). Another study also showed that while both ATTR-CA and HCM patients have reduced peak LA strain compared to controls, the degree of reduction was greater in ATTR-CA patients providing another potential discriminatory variable (42). Atrial strain correlates with other echocardiographic markers of disease burden (41). Furthermore, both LA and right atrial (RA) strain have prognostic value for CA patients and independently predict mortality (44). Atrial strain techniques are mostly isolated to research protocols but with a growing body of evidence demonstrating diagnostic and prognostic utility, clinical application will likely increase in the coming years.

Multi-Parametric Scores

The multitude of abnormal echocardiographic parameters seen in CA has led to the development of multi-parametric scores for the diagnosis of CA. These may be particular importance in early disease when the echocardiographic changes are subtle and less specific (10, 45). Boldrini et al. (22) studied >1,000 patients who either had proven systemic AL amyloidosis or LVH suspicious for possible CA who then underwent subsequent work-up with myocardial or non-myocardial biopsy. Patients with suspected ATTR-CA underwent bone scintigraphy and 85% of patients also underwent CMR. For patients with AL amyloidosis, there was higher specificity for cardiac involvement, with more points using relative wall thickness (RWT = 2 × PWd/LVEDD, >0.52, two points), E/e′ (>10, two points), TAPSE (≤19 mm, one point), and LS (≥−14%, one point). For patients referred with LVH and possible CA, more points increased specificity for CA using RWT (>0.6, three points), E/e′ (>11, one point), TAPSE (≤19 mm, two points), LS (≥−13%, one points), and septal longitudinal systolic apex-to-base ratio (SAB, >2.9, three points). SAB is a measure similar to RALS as a measure of apical sparing (22).

Aimo and colleagues developed a simpler echocardiographic score to maximize specificity of the diagnosis. The Amyloidosis Index (AMYLI) score equals RWT × E/e′, with its main limitation being the exclusion of patients in atrial fibrillation during echocardiogram. A cutoff < 2.36 in patients with systemic AL amyloidosis and <2.22 in unexplained LVH excluded CA (22). The AMYLI score was compared to the two scoring systems developed by Boldrini et al. and demonstrated non-inferiority for the exclusion of CA (23). CA is primed for the use of multi-parametric echocardiography scores and we suspect the

applicability of such scores will continue to increase. These scores help to objectify the echocardiographic parameters many clinicians may notice by clinical gestalt but can be overlooked in combination. More widespread use could decrease delays in diagnosis and treatment.

Prognosis

The prognostic significance of echocardiographic findings in CA has been long recognized (31). In early studies, the most useful echocardiogram predictor of mortality was E/A closely followed by shorter DT and lower fractional shortening (15, 31). These same parameters correlate with HF severity and mortality. Contemporary studies added apical LS and lower LVEF as an independent predictor of major adverse cardiac events (MACE) in patients with CA (39). RV function in CA has also been shown to predict mortality with lower TAPSE and RV strain correlating with MACE in some studies (36). A recent study consisting predominantly of AL-CA patients demonstrated the prognostic significance of both RA and LA strain (44). It remains to be seen how these prognostic echocardiographic measures are affected by CA treatment and specifically if these parameters may be helpful in predicting treatment response.

Emerging Techniques

Despite increasing knowledge about numerous echocardiographic changes in CA, final diagnosis is contingent on further testing based on level of suspicion, which may vary from clinician to clinician. Multiparametric scores can help streamline this diagnostic assessment, but may not be readily applied in clinical practice, and still relies on maintaining an underlying diagnostic suspicion for CA (2). Machine learning (ML) provides the potential to bridge this important diagnostic pitfall. ML methodology refers to a computational approach that incorporates a multitude of complex data structures to agnostically identify relationships commonly seen in disease patterns without explicit instruction. The variable and diverse echocardiographic changes seen in CA, even in early disease, could potentially be detected by ML and signal to clinicians to consider further testing. Goto et al. (46) performed a large multicenter study using ML techniques of both ECG and echocardiograms in CA. They used a video-based model for echocardiography using a single apical 4-chamber view. Their model was able to detect CA by echocardiography with a C-statistic $\geq$ 0.85 at each site up to 1 year prior to diagnosis. Additionally, their model was able to discriminate CA from other diseases causing LVH including HCM, HHD, and end-stage renal disease with C-statistic $\geq$ 0.90 at each site. Their model outperformed two expert echocardiography readers in diagnostic accuracy. The area under the curve (AUC) for differentiating between causes of LVH ranged between 0.87 and 0.96 at each institution which is comparable or higher than the AUC for similar populations using the multiparametric scores developed by Boldrini and Aimo (22, 23). The ECG model also performed well on its own across sites. When combining ECG and echocardiography in a step-wise fashion, they demonstrated a positive predictive value (PPV) of nearly 75% across two sites (46). A layered testing and referral algorithm using ML on initial ECG and subsequent echocardiography holds promise in detecting more CA cases and earlier in the disease course. However, as with all testing modalities, the impact on performance with more widespread use will need to be examined.

MAGNETIC RESONANCE IMAGING

Magnetic resonance imaging (MRI) utilizes strong magnetic fields in different orientations to excite hydrogen atoms then measures the emitted signal as they relax. Hydrogen atoms in different tissues have distinct excitation and relaxation properties based on their surrounding structure making it possible to characterize tissue properties. CMR was first employed over 3 decades ago and has been used for diagnosis and prognostication with increasing frequency in multiple cardiac conditions. Given the high chamber fidelity, it is considered the gold standard for chamber size quantification and EF measurement. CMR is less subject to limitations in image quality compared to echocardiogram, but requires a higher level of expertise, is costlier, and is not as widely available (**Table 2**). The main patient-related limitations to CMR are body habitus, claustrophobia, non-MRI compatible metallic implants, and severe renal dysfunction if gadolinium-based contrast agents are to be used.

Cardiac magnetic resonance may be utilized in the initial evaluation of CA or to supplement initial diagnostic suspicion of CA based on echocardiogram in select patients (**Figure 1**). Acquisition of CMR should ideally not delay diagnosis of CA, as additional modalities are typically necessary to confirm a diagnosis of CA prior to initiating treatment. CMR is excellent at demonstrating morphologic changes in CA, similar to echocardiogram and therefore, is very beneficial in patients with poor acoustic windows on echocardiogram. CMR adds significant information on tissue characterization of the myocardium compared to echocardiogram (**Figure 2**), which is enhanced with the use of gadolinium-based contrast agents. Additionally, improved tagging and strain techniques in CMR allow for more detailed myocardial deformation analysis than currently provided by echocardiography. CMR technology is continually improving as novel techniques and applications are being developed. Representative CMR images for a patient with CA are shown in **Figure 5**.

Morphologic Changes

As with echocardiogram, LVH is the hallmark finding of CA on CMR regardless of the underlying type of CA. In studies comparing findings on CMR in patients with CA to those of healthy volunteers, patients with CA had higher LVMI, lower LV end diastolic volume index (LVEDVI), and lower LVEF (47). However, in one study of 36 patients with HF and either myocardial biopsy or autopsy evidence of CA (n = 11) or extra cardiac biopsy plus LVH on echocardiogram, nearly one-third of patients had normal LVMI by CMR (47). This suggests that CA may be present to some extent without frank hypertrophy as measured by LVMI on CMR. There may also be differences in the degree of LVH on CMR between the types of CA, with wtATTR

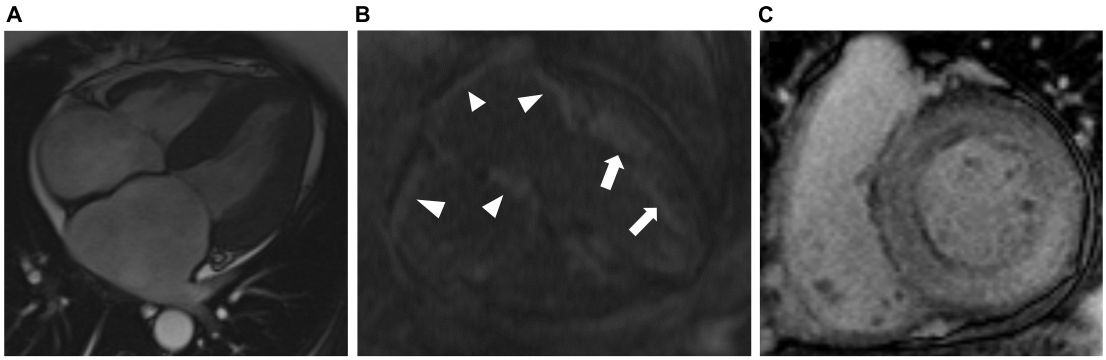

FIGURE 5 | Representative cardiac magnetic resonance images (CMR) from patients with cardiac amyloidosis. **(A)** T2 TRUFI 4-chamber view showing biventricular hypertrophy, biatrial enlargement, and pericardial effusion. **(B)** T1 4-chamber view late post-contrast image in a patient with ATTR-CA showing diffuse atrial LGE (arrowheads) and left ventricular subendocardial LGE (arrows). **(C)** T1 short-axis late post-contrast image in a patient with AL-CA showing diffuse LGE of the left ventricle.

generally having higher LVMI, possibly related to the elderly demographic and longer asymptomatic disease state compared to AL-CA (48). CMR can help differentiate between CA and other diseases that cause LVH. Specifically, compared to HHD controls, patients with CA have been shown to have lower LVEF and right ventricular ejection fraction (RVEF), higher LVMI, higher RV mass, and greater degree of RVH on CMR (49–52). Differences in degree of RVH may also exist between types of CA, occurring less commonly in AL-CA (53).

While both right and left ventricular changes can be seen on echocardiogram, CMR outperforms echocardiogram at assessment of atrial abnormalities. Increased interatrial (IA) septum thickness originally had promise as a fairly specific finding in CA compared to other causes of LVH (49, 50, 54). Proposed IA thickness cutoffs ranged from greater than 5 to 6 mm. Contemporary studies do not show this finding with as high of frequency possibly because of earlier CA diagnosis (47). Additionally, there may be differences in frequency of increased IA thickness based on type of CA, with this being more common in wtATTR (48). Kwong and colleagues recently demonstrated lower total LA emptying in the setting of higher LA volumes in CA compared to those with HHD and non-ischemic cardiomyopathy (55). This, in addition to other LA parameters, had high likelihood ratios in differentiating CA from other disease states. Given the unique atrial abnormalities that may be present in CA, imaging of the atria should be given special attention in patients undergoing evaluation for CA.

Echocardiography, as compared to CMR, remains the preferred modality for examination of diastolic filling patterns. Rubinshtein et al. (56) compared diastolic function in patients with CA utilizing echocardiography and CMR. In general, E/A was lower by CMR compared to echocardiography but DT correlated well across both imaging modalities. However, there was a subset of patients in whom diastolic dysfunction assessment significantly differed across the imaging modalities, with the more severe pattern identified by echocardiogram (56). Without significant leaps in CMR technology and given the improvements in time resolution on echocardiogram, echocardiogram will likely remain as the preferred modality for assessment of diastolic dysfunction in CA and other disease states.

Tissue Characterization

The major strength of CMR as compared to echocardiogram in evaluation of CA lies in the superior detection of myocardial tissue properties. A typical CMR sequence for CA will start with cine images in various orientations to assess function and other static measurements. After these are obtained, most of the remaining sequences are designed to assess various properties of tissue. Amyloid fibril deposition in the myocardium alters the myocardial tissue and therefore CMR characteristics such as T1 relaxation and T2 decay. T1 relaxation varies between tissues based on the time it takes for hydrogen atom spin to reorient in the direction of applied magnetic field after it was altered with a perpendicular radiofrequency pulsation. In the heart, fat and gadolinium (Gd), if used, have short T1 and will appear bright in these sequences. Tissue T2 decay is based on the time it takes for a hydrogen atom to spin out of phase. Fat and water have long T2 and will appear bright on these sequences. The addition of Gd based contrast agents enhances tissue characterization. Traditionally, Gd contrast was used to detect areas of increased extracellular space that may be caused by fibrosis or ischemic scar. These areas had delayed wash-out of contrast, known as late gadolinium enhancement (LGE). In CA, this likely works in a similar manner, but there also appears to be altered Gd kinetics caused by the amyloid fibrils (50). However, the early work on CMR in CA was marked by inconsistencies leading to disparate conclusions for LGE assessment. Additionally, there are a number of operator-dependent factors in CMR imaging such as amount of time delay from injection to imaging and the selection of time intervals based on initial images. Over time, more standardized CMR imaging protocols were developed for CA that have allowed for more uniform interpretation of the results.

The extracellular localization of Gd-based contrast agents made contrast-enhanced CMR the initial technique of interest in CA. Early (<5 mins) after contrast injection, patients affected by CA frequently (60–90%) have abnormal enhancement of the

myocardium (47, 50). Maceira et al. (50) noted shorter T1 times of the myocardium with a cut-off of 535 ms having a sensitivity and specificity of 86% and 75%, respectively, for distinguishing CA from HHD controls. However, they also noticed increased contrast clearance from the blood pool leading to higher T1 times. By taking the difference between the subendocardial T1 (smaller in CA) and blood T1 (higher in CA) sensitivity and specificity for detection of CA compared to controls increased to 90% and 87%, respectively (50). Initial studies examining LGE in CA found this phenomenon in a majority (>70%) of CA patients (50, 54). However, the reported patterns of LGE differed possibly due to varying patient populations and technical differences in image acquisition, including in myocardial nulling. In traditional CMR imaging, "nulling" is an operator dependent process where an inversion time is selected to "null" or "make black" normal myocardium. Incorrect selection can actually reverse signals which confounds interpretation. Therefore "nulling" can be different in a diffuse myocardial process where there may be no normal myocardium. Multiple studies have noted more difficulty with this process for CA patients (54, 57). Phase-sensitive inversion recovery (PSIR) is a newer CMR sequence that negates this issue of improper nulling and can allow for more consistency. Fontana et al. showed traditional techniques using operator nulling were discordant from T1 maps the majority of the time whereas PSIR was fully concordant (58). These issues stress the importance of experienced CMR operators as well as the use of operator independent CMR protocols for accurate detection of CA.

With time and newer techniques, two predominant patterns of LGE in CA emerged including a global subendocardial pattern and a diffuse transmural pattern. These likely exist on a continuum from subendocardial to transmural enhancement as the disease progresses (59). Global subendocardial enhancement differs from subendocardial enhancement seen in aborted myocardial infarction as the latter correlates with vascular territories of the infarcted vessel. One study evaluating use of CMR for work-up of restrictive cardiomyopathy with associated LVH demonstrated a sensitivity of 80% and specificity of 94% for a global subendocardial LGE pattern compared to the gold-standard of endomyocardial biopsy in diagnosing CA (57). Similar performance in detecting cardiac involvement was seen for any LGE pattern in a group of systemic AL patients (48). Different subtypes of CA are known to demonstrate LGE patterns with varying frequencies. Dungu et al. (53) examined 100 patients with CA, with all but 1 having LGE. The "classic" subendocardial pattern was seen in 39% of AL-CA and 12% of ATTR-CA whereas a transmural involvement of affected segments occurred in 37% of AL-CA and 90% ATTR-CA and. A global LGE pattern was seen in 4% of AL-CA patients and 22% ATTR-CA (53). Similar frequencies and distributions were seen in other studies (58, 60). Additionally, a greater degree of LGE was present in ATTR-CA compared to AL-CA.

Based on this, the Query Amyloid Late Enhancement (QALE) tool, a semi-quantitative way to assess degree of LGE, was developed. In short axis, the LV is divided into three segments (base, mid, and apex) and each segment is scored from 0 to 4 (0 = no LGE, 1 = non-circumferential subendocardial OR patchy LGE, 2 = circumferential subendocardial LGE, 3 = any transmural LGE, and 4 = circumferential transmural LGE). An additional six points is added if RV LGE is present, which is more common in ATTR-CA (48, 60). A QALE $\geq$ 13 predicted ATTR-CA over AL-CA with a sensitivity of 82% and specificity of 76%. Combining QALE with age and interventricular septal wall thickness in a logistic probability unit increased sensitivity and specificity to 87 and 96%, respectively (53). In addition to being able to distinguish between ATTR-CA and AL-CA LGE patterns may vary between wtATTR and hATTR (48, 60).

Atrial LGE may also be a useful diagnostic marker in CA. Kwong et al. found left atrial LGE in 78% of CA patients compared to 14% of HHD patients and 9% of patients with non-ischemic cardiomyopathy (55). This study also demonstrated increased discriminatory power of having multiple LA segments with LGE in CA compared to non-amyloid HF. More so, interatrial LGE may be more common in ATTR-CA compared to AL-CA (55). While CMR can be suggestive of a specific subtype of CA, further testing is needed to definitively identify causative protein (**Figure 1**).

While use of Gd contrast is preferred in the CMR evaluation of CA, severe renal dysfunction, a common co-morbidity in CA, may preclude use. However, novel T1 mapping sequencing techniques that do not utilize contrast have shown to be useful in identifying CA compared to other forms of HF. In one particular study, the T1 signal was higher in a cohort of AL-CA patients compared to healthy volunteers and in patients with aortic stenosis (61). Other studies have shown consistently higher global T1 values in ATTR-CA as compared to non-CA controls (62). While global T1 values are beneficial, regional T1 variations in CA are also seen. Similar to the pattern seen with other imaging parameters, higher T1 in basilar segments compared to apical segments is commonly seen and can help differentiate CA from other disease states where T1 may be increased (63, 64). Regional areas of higher T1 correlates with lower strain in the same segment as well as extracellular volume (ECV) and LGE (63, 65). Incremental increases in basal and mid T1 correlates with higher mortality as well (64). Acquiring T1 mapping signals to detect CA is not usually standard CMR protocol so referring physicians would need to specify CMR indication and potentially discuss with the radiologist about required sequences to aid in diagnosis.

Emerging Techniques

Quantification of myocardial ECV, a marker of myocardial tissue remodeling, is a relatively novel technique that is becoming more widespread in diagnosis and prognostication of CA. ECV is similar to T1 but the latter incorporates extracellular and intracellular factors and is heavily influenced by water content like in edema. CA is a complex interplay between amyloid fibrils, cardiomyocytes, and edema, which all affect T1 signal. Therefore, ECV is likely superior in providing a true quantification of amyloid burden (66). CA patients have consistently elevated ECV compared to healthy and other disease state controls. In a study by Kim et al. (67), the degree and relative distribution of increased ECV varied by LGE pattern. In patients with diffuse transmural LGE, the basal segments had higher ECV compared to the apex. The opposite was seen in healthy controls who tended to have a

higher ECV at the apex. Conversely, patients with subendocardial or other patterns of LGE had no base-apex variation in ECV, despite having higher absolute values of ECV in all segments compared to healthy controls, likely indicating diffuse amyloid deposition but to a lesser degree than in individuals with diffuse transmural LGE (67). Finally, elevated ECV was detected in patients with a high probability of CA in the absence of LGE likely indicating early disease (66).

Strain imaging using CMR is evolving and may overcome the technical challenges of echocardiographic strain. Contrary to echocardiography, strain analysis with CMR is not reliant on imaging plane and therefore can be evaluated in multiple dimensions with greater certainty providing a more complete picture of myocardial function. Kim and colleagues (67) demonstrated worse peak strain in all dimensions (circumferential, radial, and longitudinal) in patients with CA compared to healthy controls. Additionally, a continuum of worsening strain was demonstrated from focal or patchy LGE to diffuse LGE. There was also a correlation between basal peak circumferential strain and basal ECV supporting the theory that amyloid burden is the primary driver of abnormal strain (67). These techniques also allow for strain analysis in the more complex geometry of the right ventricle.

In addition to multi-dimensional strain analysis, CMR strain techniques have higher spatial resolution than echocardiography thereby providing information on complex strain relationships, like twisting and shearing, throughout the entire thickness of the myocardium. Early CMR strain techniques used deformable registration algorithms (DRAs) that relied on the routinely obtained cine images. Newer techniques utilize changing magnetic fields and radiofrequency (RF) pulses along with time delays between generation and detection to measure deformation. Some of these create local alternations in tissue signal with magnetic fields and RF pulses creating an array over the myocardium. Through the cardiac cycle, movement of each part of the array can then be tracked and deformation parameters determined. The strain of myocardium can also be encoded in the detected signal after excitation either using stimulated echo (DENSE) or unbalanced gradient pulse during excitation and again prior to detection (strain-encoded, SENC). These latter techniques have higher spatial resolution than tagged techniques as each pixel is "encoded" with strain data instead of artificially creating a strain array (68). All of these techniques require special imaging protocols and therefore expertise in performing them. These special protocols will also add imaging time which could affect patient comfort. As advanced CMR strain techniques become more widely used in CA, the impact of specific strain patterns on symptoms and prognosis should become more evident and may eventually help guide treatment.

Prognosis

Many morphologic and tissue characteristics seen on CMR have prognostic significance. Understanding prognosis based on these findings may inform treatment decisions while framing expectations for patients and families. It remains to be seen how pre-treatment imaging characteristics may guide prognosis in the era of contemporary therapy for CA.

Like echocardiography, static dimensions and function parameters on CMR have been shown to correlate with mortality in CA. Abnormal LVEF or RVEF generally indicates worse prognosis with degree of systolic dysfunction correlating with increased morbidity and mortality (47, 52). Lower indexed RV volumes (RVESVi or RVEDVi) were also associated with worse survival in CA and can be consistently measured with CMR (51, 52). The prognostic significance of LGE is mixed in the literature, likely related to inconsistencies in imaging protocol as well as variable follow-up lengths across studies. In general, the presence of LGE predicts a worse prognosis in CA compared to the absence of LGE (51, 58). Fontana et al. showed a clear relationship with mortality at 24 months in a large study of both AL and ATTR-CA based on LGE pattern including 92% survival in those without LGE, 81% survival with subendocardial LGE, and 61% survival with transmural LGE (51, 58, 60). Conversely, RV LGE was a consistent predictor of worse prognosis (47, 51, 52, 69). More so, higher mortality rates have been demonstrated in individuals with higher ECV, again reflecting disease burden (60). Early studies showed reduced ECV in response to treatment, suggesting this could be a marker of treatment efficacy (66, 70). Overall, the prognostic significance of LGE and ECV is not surprising as they function as surrogate markers of total amyloid burden within a progressive disease process.

NUCLEAR IMAGING

In medicine, nuclear imaging techniques are ubiquitous with diverse indications. The fundamental principle involves radioactive labeling of a tracer that has affinity for a specific organ or disease process. Use of nuclear imaging in CA provides certain advantages over echocardiography and CMR including: (1) diagnostic specificity for type of amyloid fibril uptake and (2) detection of early or subclinical disease which may allow for earlier treatment. Additionally, nuclear techniques, and particularly positron emission tomography (PET), in additional to CMR, incorporate semi-quantitative measurements, which may be followed for treatment response in AL-CA and the now more readily treatable ATTR-CA. The main nuclear imaging technique being used in the diagnosis of CA is cardiac scintigraphy using labeled phosphonate tracers; however, PET imaging is emerging with growing interest.

Cardiac Scintigraphy

Phosphonate molecules labeled with a radioactive tracer, usually technetium-99m (^{99m}Tc), combined with a nuclear detector, was originally developed for bone imaging. Increased uptake represented areas of higher bone turnover in fractures, metastases, and osteomyelitis. Affinity of phosphonate tracers for amyloid deposition in soft tissue has been recognized for more than 3 decades (71). The exact mechanism of this affinity is unclear, but is thought to result from calcium deposition within amyloid fibrils (72).

Similar to early CA research in echocardiography and CMR, initial studies examining cardiac scintigraphy in CA

were limited due to a low number of patients and ill-defined patient populations that leaned heavily toward AL-CA. Additionally, despite consistent demonstration of deposition in other organs affected by amyloidosis with multiple different phosphonate tracers, cardiac uptake was inconsistent (71, 73). Despite these early limitations, with improved patient selection, the usefulness of cardiac scintigraphy for diagnosis of ATTR-CA became evident.

Three main phosphonate tracers are labeled with ^{99m}Tc in routine clinical practice for CA: 3,3-diphosphono-1,2-propanodicarboxylic acid (DPD), hydroxymethylene diphosphonate (HMDP), and pyrophosphate (PYP). The selection of radiotracer type is generally based on availability although research continues on inter-radiotracer performance. DPD is most commonly used in Europe whereas PYP is generally used in the United States (74). HMDP is less studied than the other two radiotracers and therefore the performance characteristics are considered less refined. Cardiac or chest single-photon emitted computed tomography (SPECT) and planar images are typically obtained 1 hour after radiotracer injection. Imaging can be delayed to 3 hours if persistent blood pool activity is noted, however. Planar imaging is rapid, and allows for visual interpretation and quantification of the degree of myocardial uptake. SPECT imaging is necessary to simultaneously perform to confirm uptake is seen in the myocardium and not in the blood pool or an extra cardiac focus (75, 76).

The major breakthrough in cardiac scintigraphy imaging for CA came from the hypothesis that variable uptake in earlier studies resulted from different amyloid protein composition (77). In 2005, Perugini and colleagues were the first to demonstrate this in a study of 25 patients (15 ATTR-CA) where sensitivity and specificity of 100 and 100%, respectively, was shown for distinguishing ATTR-CA from AL-CA (77). Genotyping and immunohistochemistry served as the gold standard and scan positivity was based on qualitative analysis of uptake using a scoring system that is still applied in clinical practice: grade 0 = no cardiac uptake and normal bone uptake; grade 1 = cardiac uptake intensity less than bone uptake; grade 2 = cardiac uptake intensity similar to bone uptake; and grade 3 = cardiac uptake intensity greater than bone uptake or even absent bone signal (72). In their initial study, a scan was considered positive if above a grade 0. Examples of scan results in ATTR-CA are shown in **Figure 6**.

To limit inter-observer variability and provide more quantitative rigor, ratios of heart to other body part uptake are also used, with the most common in modern practice being heart-to-contralateral chest ratio (H/CL) (**Figures 6B,D**) (78, 79). The initial study had excellent differentiation of AL-CA from ATTR-CA (78) using a cutoff of H/CL $\geq$ 1.5, but subsequent studies fall short on sensitivity while maintaining high specificity (79). Per current guidelines, H/CL $\geq$ 1.5 is positive, $<$ 1.0 is negative, and in between is equivocal (75). Some physicians use a cutoff of H/CL $\geq$ 1.3 to increase sensitivity (80). Other signal ratios are scattered throughout the literature including heart to whole body (H/WBR) and heart to skull (H/S).

The high sensitivity and specificity of DPD seen in the initial study is stunning and ultimately was not nearly as stark for larger DPD studies or the other radiotracers. In other studies, a subset of patients with AL-CA ranging from 32% to 41%, had myocardial uptake with DPD on cardiac scintigraphy (81–83). With PYP, one study showed 17% of AL-CA patients had grade $\geq$ 2 uptake (78). HMDP use may lead to less uptake for AL-CA, but this is at the cost of lower sensitivity for diagnosis of ATTR-CA (72, 83). Larger studies pooling the main radiotracers demonstrate that $\geq$grade 1 on bone scintigraphy has a sensitivity $>$ 99% and specificity 68% for diagnosis of ATTR-CA (74). Using grade 2/3 increases specificity to 87% at the cost of lower sensitivity to 91% (74). A meta-analysis pooling 529 patients across 6 studies found similar sensitivity and specificity of 92% and 95%, respectively (72). All patients in the large study by Gillmore et al. (74) underwent appropriate screening for AL-CA, but the methods in each study included in the meta-analysis are less clear. Treglia et al. also pooled the cohorts based on radiotracer used with grade 2/3 considered positive: DPD (sensitivity 95%, specificity 88%), PYP (sensitivity 87%, specificity 75%), HMDP (sensitivity 86%, specificity 98%) (72). In current clinical practice, grade 2/3 is considered positive, grade 0 is negative and grade 1 is equivocal and needs to be interpreted within the specific clinical context (**Figure 6A**).

Fortunately, the diagnostic accuracy of cardiac scintigraphy can be greatly enhanced with the addition of appropriate serologic work-up to rule out systemic AL amyloidosis. This includes serum free light chain measurement and ratio along with serum and urine electrophoresis with immunofixation. If these tests are normal, abnormal cardiac scintigraphy with grade of 2 or 3 uptake has a specificity of 100% for ATTR-CA (74). This stresses the importance of appropriate serologic work-up before pursuing and certainly before interpreting cardiac scintigraphy for possible ATTR-CA (**Figure 1**).

While specificity in this scenario approaches 100%, the sensitivity is $<$100%, highlighting the possibility of missing a diagnosis of ATTR-CA. Reasons why certain patients may have a false negative scan are under active investigation. One obvious reason is the increased recognition of CA leading to earlier diagnostic work-up. Degree of amyloid deposition along with clinical and biomarker characteristics correlate with Perugini grade (74, 83). These characteristics also correlate with degree of amyloid deposition on CMR (58). The initial use in more advanced disease led to high sensitivity and specificity but more contemporary ordering practices aimed at early diagnosis may have less uptake which may not be detectable below a certain amount of total amyloid deposition (74, 80–82). However, the lower sensitivity is not entirely explained by early disease as some patients with advanced disease by symptoms and other imaging have grade 0/1 uptake (83, 84).

There is building evidence that different ATTR genetic variants may lead to more or less radiotracer uptake. Therefore, some variants may lead to grade 0/1 uptake despite a heavy burden of disease. Musumeci and colleagues (84) retrospectively examined 19 DPD and HMDP scans over nearly 2 decades in hATTR patients with a Phe64Leu variant. Seventeen (85%) of these patients had grade 0/1 uptake (84). Alternatively, patients with Val122Ile, in a different study had grade 3 uptake (83). Ser77Tyr also seems to have reduced frequency of high-grade

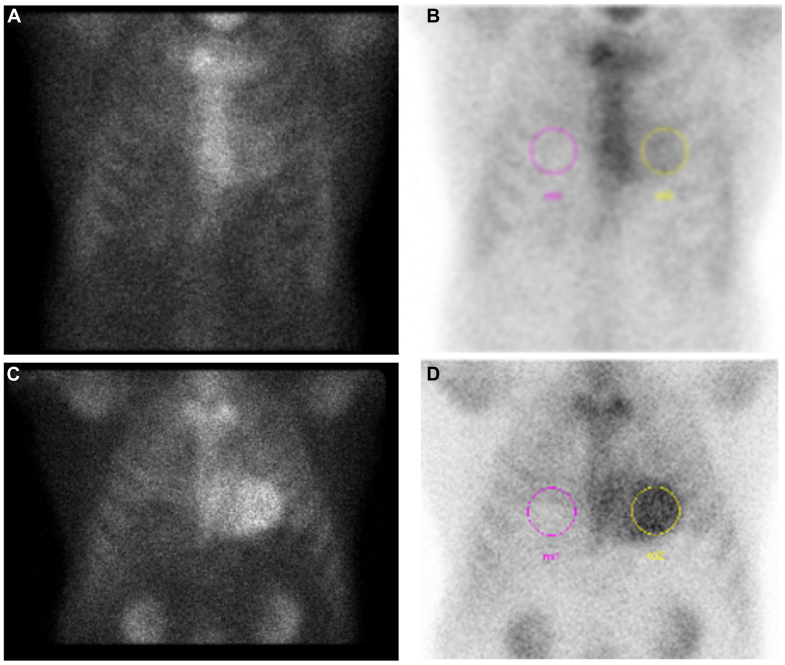

FIGURE 6 | Example results of pyrophosphate (PYP) scan in two patients diagnosed with ATTR-CA. **(A)** Grade 1 (negative) scan with **(B)** H/CL = 1.4 in a patient later diagnosed by endomyocardial biopsy. **(C)** Grade 3 (positive) PYP scan with **(D)** H/CL = 2.26.

uptake but the data are limited (60). Genotyping is often performed after clinical and imaging diagnosis so a "negative" cardiac scintigraphy is not likely to trigger genetic testing (85). It is incumbent on the physician to pursue additional testing in those patients whom clinical suspicion remains even if cardiac scintigraphy is negative or equivocal.

Alternatively, some patients without suspicion of CA may undergoing cardiac scintigraphy for another indication and be found to have positive myocardial uptake. Two recent studies have examined the frequency of grade 2/3 cardiac uptake on patient scans performed for indications other than evaluation of CA. Soumalainen et al. (80) looked at 2,000 patients undergoing HMDP scans mostly for prostate and breast cancer. They found grade 1 in 16.7%, grade 2 in 2.7%, and grade 3 in 0.8% of this cohort. Additionally, 2.4% of patients had an H/CL $\geq$ 1.3 suggestive of ATTR-CA. Notably, of those with suspected ATTR-CA (grade 2/3), 41% had a history of HF prior to scan (80). Bianco et al. found a prevalence of 0.54% grade 2/3 uptake on 3,228 scans performed over 5 years using DPD or HDMP at their center (86). With higher clinical suspicion, ATTR-CA may have been suspected in some of these patients as 48% had prior HF, 34.8% had known neuropathy, and 21.7% had carpal tunnel syndrome. However, 21.7% were entirely asymptomatic highlighting the existence of an asymptomatic disease state during which treatment could prevent disease progression (86).

Prognosis

The prognostic significance of cardiac scintigraphy ordered for assessment of CA is limited by the qualitative nature of the grading system although semi-quantitative results provide more granularity. Using semi-quantitative analysis, generally higher heart to other structure ratios is associated with a worse prognosis. Galat and colleagues found a H/S (heart to skull) ratio $\geq$ 1.94 had a higher chance of major cardiovascular event (MACE) along with NYHA III or IV symptoms (83). Another early study found that H/WB (heart to whole body) ratio $>$ 7.5 was associated with worse prognosis (81).

For incidentally discovered myocardial uptake, the presence of myocardial uptake still portends a worse prognosis. In one study, 51% of patients died over a mean 4 years of follow-up, 9% of which were classified as related to a cardiac cause. Grade 3 uptake and H/CL $\geq$ 1.3 were predictors of mortality on univariate analysis and grade 3 uptake remained a mortality predictor on multivariate analysis (80). These patients likely had undiagnosed ATTR-CA which progressed in follow-up ultimately leading to death. If myocardial uptake is incidentally found, complete work-up including serologic screening for AL disease and genetic testing should be facilitated.

Currently there is no known utility of repeating scans for assessment of disease burden, but this is not yet studied in the current era of ATTR-CA treatment. One potential scenario for a repeat scan may be if a prior scan was negative despite a known ATTR genotype positivity and a repeat scan is done after some interval to assess for CA; though the optimal time frame is unknown and likely depends on the age of the patient as well as specific family history (81).

Positron Emission Tomography

Positron emission tomography (PET) imaging has many established cardiovascular disease indications, but use in CA is

emerging. Like cardiac scintigraphy, the goal of PET is to have high fidelity to identify the type of amyloid fibril protein but also to have a more quantitative method to assess amyloid burden and response to treatment. Prior to determining its role in the latter, optimally performing radiotracers for AL and ATTR-CA amyloidosis need to be identified.

Multiple pilot studies using different radiotracers have been studied using either fluorine-18 (^{18}F) or carbon-11 (^{11}C), with ^{18}F being more common (87–90). Fludeoxyglucose (FDG) is a commonly encountered compound in oncology but its use in CA is not established (91). In contrast to bone scintigraphy, some PET radiotracers like ^{18}F-florbetaben may have more affinity for AL-CA compared to ATTR-CA. Myocardial tracer retention (MTR) is calculated using standardized uptake value (SUV) in the early time frame (0–5 mins) and a delayed time frame (15–20 mins) then expressed as a percentage. In a small study inclusive of 22 patients with CA, eight patients with AL-CA had a median MTR of 66% compared to 42% in the five patients with ATTR-CA ($p < 0.01$). In non-CA patients, median MTR was 27% (91). A sensitivity and specificity of 100% and 100%, respectively, for ruling out amyloidosis was achieved with MTR $\leq$ 36%. An MTR cutoff $\leq$ 52% could differentiate ATTR-CA from AL-CA with a sensitivity of 100% and specificity of 89% (91). Another study by Genovesi et al. (92) performed dynamic and static imaging at various time points after injection. All patients (AL, ATTR, other) had early uptake but AL-CA patients had a higher degree of early uptake. AL-CA patients then had much more retention of radiotracer throughout the imaging time compared to ATTR-CA which washed out much quicker (92). Larger confirmatory studies are needed but PET imaging has the potential to serve as the first non-invasive modality of diagnosing AL-CA and may decrease the need for biopsy in some patients.

Simultaneous imaging of patients using PET and CMR has also been under investigation in CA. Albuizi and colleagues used PET and CMR technology in 27 patients with strong suspicion of CA using ^{18}F-NaF after a promising proof of concept study. Though qualitative measures were unreliable to distinguish CA subtypes, with semi-quantification comparing the myocardium to blood pool (M/B ratio), there was increased relative uptake in ATTR-CA patients compared to AL-CA and non-CA patients. An M/B $\geq$ 0.90 was able to differentiate ATTR from AL-CA with a sensitivity and specificity of 81% and 100%, respectively (93). The simultaneous use of PET and CMR could allow for identification of morphologic and tissue characteristic changes supporting the presence of CA, then utilizing PET to identify the CA subtype.

PET results have been shown to correlate to findings on other imaging modalities including echocardiography, CMR, and cardiac scintigraphy. MTR had a positive correlation with apical sparing, E/e′, and wall thickness along with a negative correlation with TAPSE and LVEDV on echocardiography (91). PET had 94% concordance regarding extent of affected myocardium on CMR. Interestingly, in one patient, a positive PET study did not have any CMR abnormalities, which may point to a role in earlier diagnosis. Cardiac scintigraphy (DPD) matched PET results in 81% of patients. Notably all ATTR-CA patients in this study had grade 3 uptake (91).

Follow-up PET scans do not have a defined role in clinical practice, but this remains a promising avenue of future study. In the study by Kircher et al. (91), four patients had repeat PETs either for treatment follow-up or restaging. In all cases, imaging findings correlated with clinical status. One patient had a repeat scan after approximately 1 year of treatment with ATTR stabilizer, Tafamidis, showing stable MTR and correlating with stable HF symptoms as well. One patient had improvement in biomarkers but worsening clinical status which correlated with a higher MTR on follow-up scan; this patient went on to receive a heart transplant (91). Repeat PET scans may serve as a way to assess response to treatment and decide if escalation or alternatives are needed. The main limitation to PET in this context will be cost, availability, and radiation exposure. As experience accumulates, the impact of genetic variant on radiotracer uptake will also need to be investigated given the emerging data seen with cardiac scintigraphy. Finally, the prognostic implications of PET imaging in CA have not been investigated beyond anecdotal reports.

ROLE OF ENDOMYOCARDIAL BIOPSY IN CARDIAC AMYLOIDOSIS DIAGNOSIS

Once a clinical suspicion of CA is established, further testing focuses on culprit protein identification. All patients need a serologic assessment of AL amyloidosis consisting of serum light chain measurement and ratio (kappa/lambda ratio), and urine and serum electrophoresis with immunofixation (**Figure 1**). If any of these tests are abnormal, AL amyloidosis must be expeditiously evaluated with tissue biopsy and referral to hematologic oncologist. An abnormal kappa/lambda ratio (>1.65–3.1) in the absence of a monoclonal gammopathy on protein electrophoresis may create a diagnostic dilemma in those with renal dysfunction, as the kidneys are responsible for clearing light chains. In this setting, clinical correlation

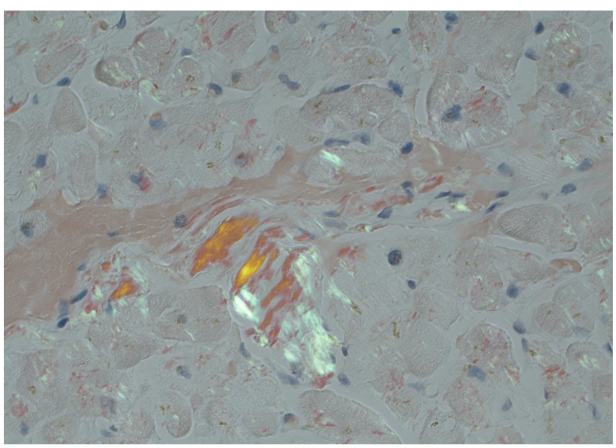

FIGURE 7 | Endomyocardial biopsy pathology in a patient with cardiac amyloidosis. Congo red stain at 10×× magnification showing apple-green birefringence under polarized light consistent with amyloid deposition.

is recommended to determine suspicion for AL amyloidosis, which can then guide further diagnostic testing (76). If serologic testing for AL amyloidosis is all within normal limits, AL-CA is effectively ruled out and cardiac scintigraphy can be performed to assess for ATTR-CA (**Figure 1**). If this is positive (grade 2/3), a diagnosis of ATTR-CA can be made without further testing. If cardiac scintigraphy is negative or equivocal, echocardiography, CMR, and patient history needs to be reviewed and referral for tissue biopsy should be considered for patients with ongoing clinical suspicion for CA. While rare, endomyocardial biopsy may also detect dual pathology of AL and ATTR-CA, further highlighting the importance of pursuing biopsy in the appropriate clinical context.

The site chosen for tissue biopsy varies by center. Abdominal fat pad biopsy may be first pursued as this is a minimally invasive and well-tolerated procedure. However, sensitivity is very poor for ATTR-CA and ranges considerably for AL-CA (94–96). Therefore, if negative, endomyocardial biopsy ought to be pursued for definitive diagnosis. In modern practice, most endomyocardial biopsies are performed on the RV septum through venous access. The major complication of RV biopsy is cardiac perforation leading to tamponade. Minor complications of biopsy include ventricular arrhythmias, access site bleeding, arterial injury, pericardial effusion, and conduction disturbances. Major complications occur on <1% of RV biopsies and minor complications occur in 2–5% of cases (97). CA is a diffuse process so diagnostic yield is greater than patchier myocardial processes and with adequate samples, the sensitivity and specificity approach 100% and 100%, respectively. In very early disease, amyloid deposition may be patchy thereby decreasing yield but these situations are likely rare. CA will classically have the appearance of Congo red staining on histology, with an apple-green birefringence appearance under polarized light (**Figure 7**). Once amyloidosis is identified on tissue biopsy, the tissue should be then be typed with either mass spectrometry or immunohistochemistry to further determine subtype (96).

All patients diagnosed with ATTR-CA, whether non-invasively or with biopsy, must undergo genetic testing to establish a diagnosis of either hATTR or wtATTR. Genetic testing is typically performed with salivary kit testing and in conjunction with genetic counseling. Identification of hATTR can trigger cascade screening in family members.

CONCLUSION

CA is underdiagnosed but improved treatment options have created a diagnostic imperative for earlier and more widespread recognition. Non-invasive evaluation is the backbone of this process and multiple imaging modalities are integral to this process including echocardiography, CMR, and nuclear techniques. CA must first be recognized based on clinical clues and supportive echocardiogram or CMR features. Once CA is suspected based on these imaging modalities, serologic markers, nuclear imaging, and in some cases tissue biopsy allow for on culprit protein identification. Specificity for subtype of CA is high using this algorithm but sensitivity falls short for multiple reasons still being investigated. Endomyocardial biopsy continues to play a pivotal role in CA work-up for a subset of patients in whom CA subtype is unclear or high suspicion remains despite negative or equivocal serologic and imaging work-up. Recognizing when biopsy should be pursued can decrease treatment delays and ultimately increase life expectancy in CA patients.

AUTHOR CONTRIBUTIONS

PS and JV conceptualized the content of the article, drafted the manuscript, and obtained appropriate images. MM and AH conceptualized the content of the article, provided extensive critical review, and edited the manuscript. All authors contributed to the article and approved the submitted version.

REFERENCES

1. Falk RH, Alexander KM, Liao R, Dorbala SAL. (Light-chain) cardiac amyloidosis: a review of diagnosis and therapy. *J Am Coll Cardiol.* (2016) 68:1323–41. doi: 10.1016/j.jacc.2016.06.053
2. Lane T, Fontana M, Martinez-Naharro A, Quarta CC, Whelan CJ, Petrie A, et al. Natural history, quality of life, and outcome in cardiac transthyretin amyloidosis. *Circulation.* (2019) 140:16–26.
3. Stern LK, Kittleson MM. Updates in cardiac amyloidosis diagnosis and treatment. *Curr Oncol Rep.* (2021) 23:47. doi: 10.1007/s11912-021-01028-8
4. Kyle RA, Larson DR, Kurtin PJ, Kumar S, Cerhan JR, Therneau TM, et al. Incidence of AL amyloidosis in Olmsted county, Minnesota, 1990 through 2015. *Mayo Clin Proc.* (2019) 94:465–71. doi: 10.1016/j.mayocp.2018.08.041
5. Tanskanen M, Peuralinna T, Polvikoski T, Notkola I, Sulkava R, Hardy J, et al. Senile systemic amyloidosis affects 25% of the very aged and associates with genetic variation inalpha2-macroglobulinandtau: a population-based autopsy study. *Ann Med.* (2008) 40:232–9. doi: 10.1080/07853890701842988
6. Jacobson DR, Alexander AA, Tagoe C, Buxbaum JN. Prevalence of the amyloidogenic transthyretin (TTR) V122I allele in 14333 African–Americans. *Amyloid.* (2015) 22:171–4. doi: 10.3109/13506129.2015.1051219
7. Lilleness B, Ruberg FL, Mussinelli R, Doros G, Sanchorawala V. Development and validation of a survival staging system incorporating BNP in patients with light chain amyloidosis. *Blood.* (2019) 133:215–23. doi: 10.1182/blood-2018-06-858951
8. Jurcut R, Onciul S, Adam R, Stan C, Coriu D, Rapezzi C, et al. Multimodality imaging in cardiac amyloidosis: a primer for cardiologists. *Eur Heart J Cardiovasc Imaging.* (2020) 21:833–44. doi: 10.1093/ehjci/jeaa063
9. Korosoglou G, Giusca S, Andre F, Aus dem Siepen F, Nunninger P, Kristen AV, et al. Diagnostic work-up of cardiac amyloidosis using cardiovascular imaging: current standards and practical algorithms. *Vasc Health Risk Manag.* (2012) 17:661–73. doi: 10.2147/VHRM.S295376
10. Di Bella G, Pizzino F, Minutoli F, Zito C, Donato R, Dattilo G, et al. The mosaic of the cardiac amyloidosis diagnosis: role of imaging in subtypes and stages of the disease. *Eur Heart J Cardvasc Imging.* (2014) 15:1307–15. doi: 10.1093/ehjci/jeu158
11. Marwick TH, Gillebert TC, Aurigemma G, Chirinos J, Derumeaux G, Galderisi M, et al. Recommendations on the use of echocardiography in adult hypertension: a report from the european association of cardiovascular imaging (EACVI) and the American society of echocardiography (ASE). *J Am Soc Echocardiogr.* (2015) 28:727–54.

12. Gonzalez-Lopez E, Gagliardi C, Dominguez F, Quarta CC, de Haro-del Moral FJ, Milandri A, et al. Clinical characteristics of wild-type transthyretin cardiac amyloidosis: disproving myths. *Eur Heart J.* (2017) 38:1895–904. doi: 10.1093/eurheartj/ehx043
13. Yamamoto H, Hashimoto T, Kawamura S, Hiroe M, Yamashita T, Ando Y, et al. Hereditary cardiac amyloidosis associated with Pro24Ser transthyretin mutation: a case report. *J Med Case Rep.* (2018) 12:370. doi: 10.1186/s13256-018-1931-5
14. Bellavia D, Abraham TP, Pellikka PA, Al-Zahrani GB, Dispenzieri A, Oh JK, et al. Detection of left ventricular systolic dysfunction in cardiac amyloidosis with strain rate echocardiography. *J Am Soc Echocardiogr.* (2007) 20:1194–202. doi: 10.1016/j.echo.2007.02.025
15. Koyama J, Ray-Sequin PA, Falk RH. Longitudinal myocardial function assessed by tissue velocity, strain, and strain rate tissue Doppler echocardiography in patients with AL (primary) cardiac amyloidosis. *Circulation.* (2003) 107:2446–52. doi: 10.1161/01.CIR.0000068313.67758.4F
16. Itzhaki Ben Zadok O, Eisen A, Shapira Y, Monakier D, Iakobishvili Z, Schwartzenberg S, et al. Natural history and disease progression of early cardiac amyloidosis evaluated by echocardiography. *Am J Cardiol.* (2020) 133:126–33. doi: 10.1016/j.amjcard.2020.07.050
17. Cyrille NB, Goldsmith J, Alvarez J, Maurer MS. Prevalence and prognostic significance of low QRS voltage among the three main types of cardiac amyloidosis. *Am J Cardiol.* (2014) 114:1089–93. doi: 10.1016/j.amjcard.2014.07.026
18. Pagourelias ED, Mirea O, Duchenne J, Van Cleemput J, Delforge M, Bogaert J, et al. Echo parameters for differential diagnosis in cardiac amyloidosis: a head-to-head comparison of deformation and nondeformation parameters. *Circ Cardiovasc Imaging.* (2017) 10:e005588. doi: 10.1161/CIRCIMAGING.116.005588
19. Phelan D, Collier P, Thavendiranathan P, Popoviæ ZB, Hanna M, Plana JC, et al. Relative apical sparing of longitudinal strain using two-dimensional speckle-tracking echocardiography is both sensitive and specific for the diagnosis of cardiac amyloidosis. *Heart.* (2012) 98:1442–8. doi: 10.1136/heartjnl-2012-302353
20. Ton V, Bhonsale A, Gilotra NA, Halushka MK, Steenbergen C, Almansa J, et al. Baseline characteristics predict the presence of amyloid on endomyocardial biopsy. *J Card Fail.* (2017) 23:340–4. doi: 10.1016/j.cardfail.2016.12.006
21. Sun JP, Stewart WJ, Yang XS, Donnell RO, Leon AR, Felner JM, et al. Differentiation of hypertrophic cardiomyopathy and cardiac amyloidosis from other causes of ventricular wall thickening by two-dimensional strain imaging echocardiography. *Am J Cardiol.* (2009) 103:411–5. doi: 10.1016/j.amjcard.2008.09.102
22. Boldrini M, Cappelli F, Chacko L, Restrepo-Cordoba MA, Lopez-Sainz A, Giannoni A, et al. Multiparametric echocardiography scores for the diagnosis of cardiac amyloidosis. *JACC Cardiovasc Imaging.* (2020) 13:909–20. doi: 10.1016/j.jcmg.2019.10.011
23. Aimo A, Chubuchny V, Vergaro G, Barison A, Nicol M, Cohen-Solal A, et al. A simple echocardiographic score to rule out cardiac amyloidosis. *Eur J Clin Invest.* (2020) 51:e13449. doi: 10.1111/eci.13449
24. Binder C, Duca F, Binder T, Rettl R, Dachs TM, Seirer B, et al. Prognostic implications of pericardial and pleural effusion in patients with cardiac amyloidosis. *Clin Res Cardiol.* (2021) 110:532–43. doi: 10.1007/s00392-020-01698-7
25. Siqueira-Filho AG, Cunha CL, Tajik AJ, Seward JB, Schattenberg TT, Giuliani ER. M-mode and two-dimensional echocardiographic features in cardiac amyloidosis. *Circulation.* (1981) 63:188–96. doi: 10.1161/01.cir.63.1.188
26. Belkin RN, Kupersmith AC, Khalique O, Aronow WS, Chilappa K, Palaniswamy C, et al. A novel two-dimensional echocardiographic finding in cardiac amyloidosis. *Echocardiography.* (2010) 27:1171–6. doi: 10.1111/j.1540-8175.2010.01238.x
27. Falk RH, Plehn JF, Deering T, Schick EC Jr, Boinay P, Rubinow A, et al. Sensitivity and specificity of the echocardiographic features of cardiac amyloidosis. *Am J Cardiol.* (1987) 59:418–22. doi: 10.1016/0002-9149(87)90948-9
28. Hamer J, Janssen S, Van Ruswuk MH, Lie KI. Amyloid cardiomyopathy in systemic non-hereditary amyloidosis. Clinical, echocardiographic and electrocardiographic findings in 30 patients with AA and 24 patients with AL amyloidosis. *Eur Heart J.* (1992) 13:623–7. doi: 10.1093/oxfordjournals.eurheartj.a060225
29. Klein AL, Hatle LK, Burstow DJ, Seward JB, Kyle RA, Bailey KR, et al. Doppler characterization of left ventricular diastolic function in cardiac amyloidosis. *J Am Coll Cardiol.* (1989) 13:1017–26. doi: 10.1016/0735-1097(89)90254-4
30. Longhi S, Quarta CC, Milandri A, Lorenzini M, Gagliardi C, Manuzzi L, et al. Atrial fibrillation in amyloidotic cardiomyopathy: prevalence, incidence, risk factors and prognostic role. *Amyloid.* (2015) 22:147–55. doi: 10.3109/13506129.2015.1028616
31. Klein AL, Hatle LK, Taliercio CP, Oh JK, Kyle RA, Gertz MA, et al. Prognostic significance of Doppler measures of diastolic function in cardiac amyloidosis. A Doppler echocardiography study. *Circulation.* (1991) 83:808–16. doi: 10.1161/01.cir.83.3.808
32. Chacko L, Martone R, Bandera F, Lane T, Martinez-Naharro A, Boldrini M, et al. Echocardiographic phenotype and prognosis in transthyretin cardiac amyloidosis. *Eur Heart J.* (2020) 41:1439–47. doi: 10.1093/eurheartj/ehz905
33. Siepen FAD, Bauer RR, Voss AA, Hein SS, Aurich MM, Riffel JJ, et al. Predictors of survival stratification in patients with wild-type cardiac amyloidosis. *Clin Res Cardiol.* (2018) 107:158–69. doi: 10.1007/s00392-017-1167-1
34. Castaño A, Narotsky DL, Hamid N, Khalique OK, Morgenstern R, Deluca A, et al. Unveiling transthyretin cardiac amyloidosis and its predictors among elderly patients with severe aortic stenosis undergoing transcatheter aortic valve replacement. *Eur Heart J.* (2017) 38:2879–87. doi: 10.1093/eurheartj/ehx350
35. Bellavia D, Pellikka PA, Dispenzieri A, Scott CG, Al-Zahrani GB, Grogan M, et al. Comparison of right ventricular longitudinal strain imaging, tricuspid annular plane systolic excursion, and cardiac biomarkers for early diagnosis of cardiac involvement and risk stratification in primary systematic (AL) amyloidosis: a 5-year cohort study. *Eur Heart J Cardiovasc.* (2012) 13:680–9.
36. Bodez D, Ternacle J, Guellich A, Galat A, Lim P, Radu C, et al. Prognostic value of right ventricular systolic function in cardiac amyloidosis. *Amyloid.* (2016) 23:158–67. doi: 10.1080/13506129.2016.1194264
37. Licordari R, Minutoli F, Recupero A, Campisi M, Donato R, Mazzeo A, et al. Early impairment of right ventricular morphology and function in transthyretin-related cardiac amyloidosis. *J Cardiovasc Echogr.* (2021) 31:17–22. doi: 10.4103/jcecho.jcecho_112_20
38. Patel AR, Dubrey SW, Mendes LA, Skinner M, Cupples A, Falk RH, et al. Right ventricular dilation in primary amyloidosis. *Am J Cardiol.* (1997) 80:486–92. doi: 10.1016/s0002-9149(97)00400-1
39. Ternacle J, Bodez D, Guellich A, Audureau E, Rappeneau S, Lim P, et al. Causes and consequences of longitudinal LV dysfunction assessed by 2D strain echocardiography in cardiac amyloidosis. *JACC Cardiovasc Imaging.* (2016) 9:126–38. doi: 10.1016/j.jcmg.2015.05.014
40. Moñivas Palomero V, Durante-Lopez A, Sanabria MT, Cubero JS, González-Mirelis J, Lopez-Ibor JV, et al. Role of right ventricular strain measured by two-dimensional echocardiography in the diagnosis of cardiac amyloidosis. *J Am Soc Echocardiogr.* (2019) 32:845–53. doi: 10.1016/j.echo.2019.03.005
41. Brand A, Frumkin D, Hubscher A, Dreger H, Stangl K, Baldenhofer G, et al. Phasic left atrial strain analysis to discriminate cardiac amyloidosis in patients with unclear thick heart pathology. *Eur Heart J Cardiovasc Imging.* (2021) 22:680–7. doi: 10.1093/ehjci/jeaa043
42. de Gregorio C, Dattilo G, Casale M, Terrizzi A, Donato R, Di Bella G. Left atrial morphology, size and function in patients with transthyretin cardiac amyloidosis and primary hypertrophic cardiomyopathy; comparative strain imaging study. *Circ J.* (2016) 80:1830–7. doi: 10.1253/circj.CJ-16-0364
43. Rausch K, Scalia GM, Sato K, Edwards N, Lam AK, Platts DG, et al. Left atrial strain imaging differentiates cardiac amyloidosis and hypertensive heart disease. *Int J Cardiovasc Imaging.* (2021) 37:81–90. doi: 10.1007/s10554-020-01948-9
44. Huntjens PR, Zhang KW, Soyama Y, Karmpalioti M, Lenihan DJ, Gorcsan J. Prognostic utility of echocardiographic atrial and ventricular strain imaging in patients with cardiac amyloidosis. *JACC Cardiovasc Imaging.* (2021) 14:1508–19. doi: 10.1016/j.jcmg.2021.01.016
45. Di Nunzio D, Recupero A, de Gregorio C, Zito C, Carerj S, Di Bella G. Echocardiographic findings in cardiac amyloidosis: inside two dimensional, Doppler, and strain imaging. *Curr Cardiol Rep.* (2019) 21:7. doi: 10.1007/s11886-019-1094-z

46. Goto S, Mahara K, Beussink-Nelson L, Ikura H, Katsumata Y, Endo J, et al. Artificial intelligence-enabled fully automated detection of cardiac amyloidosis using electrocardiograms and echocardiograms. *Nat Commun.* (2021) 12:2726. doi: 10.1038/s41467-021-22877-8
47. Wassmuth R, Abdel-Aty H, Bohl S, Schulz-Menger J. Prognostic impact of T2-weighted CMR imaging for cardiac amyloidosis. *Eur Radiol.* (2011) 21:1643–50. doi: 10.1007/s00330-011-2109-3
48. Kristen AV, Aus dem Siepen F, Scherer K, Kammerer R, Andre F, Buss SJ, et al. Comparison of different types of cardiac amyloidosis by cardiac magnetic resonance imaging. *Amyloid.* (2015) 22:132–41. doi: 10.3109/13506129.2015.1020153
49. Fattori R, Rocchi G, Celletti F, Bertaccini P, Rapezzi C, Gavelli G. Contribution of magnetic resonance imaging in the differential diagnosis of cardiac amyloidosis and symmetric hypertrophic cardiomyopathy. *Am Heart J.* (1998) 136:824–30. doi: 10.1016/s0002-8703(98)70127-9
50. Maceira AM, Joshi J, Prasad SK, Moon JC, Perugini E, Harding I, et al. Cardiovascular magnetic resonance in cardiac amyloidosis. *Circulation.* (2005) 111:186–93.
51. Ruberg FL, Appelbaum E, Davidoff R, Ozonoff A, Kissinger KV, Harrigan C, et al. Diagnostic and prognostic utility of cardiovascular magnetic resonance imaging in light-chain cardiac amyloidosis. *Am J Cardiol.* (2009) 103:544–9. doi: 10.1016/j.amjcard.2008.09.105
52. Wan K, Sun J, Han Y, Luo Y, Liu H, Yang D, et al. Right ventricular involvement evaluated by cardiac magnetic resonance imaging predicts mortality in patients with light chain amyloidosis. *Heart Vessels.* (2018) 33:170–9. doi: 10.1007/s00380-017-1043-y
53. Dungu JN, Valencia O, Pinney JH, Gibbs SD, Rowczenio D, Gilbertson JA, et al. CMR-based differentiation of AL and ATTR cardiac amyloidosis. *JACC Cardiovasc Imaging.* (2014) 7:133–42. doi: 10.1016/j.jcmg.2013.08.015
54. Perugini E, Rapezzi C, Piva T, Leone O, Bacchi-Reggiani L, Riva L, et al. Non-invasive evaluation of the myocardial substrate of cardiac amyloidosis by gadolinium cardiac magnetic resonance. *Heart.* (2005) 92:343–9. doi: 10.1136/hrt.2005.061911
55. Kwong RY, Heydari B, Abbasi S, Steel K, Al-Mallah M, Wu H, et al. Characterization of cardiac amyloidosis by atrial late gadolinium enhancement using contrast-enhanced cardiac magnetic resonance imaging and correlation with left atrial conduit and contractile function. *Am J Cardiol.* (2015) 116:622–9. doi: 10.1016/j.amjcard.2015.05.021
56. Rubinshtein R, Glockner JF, Feng D, Araoz PA, Kirsch J, Syed IS, et al. Comparison of magnetic resonance imaging versus doppler echocardiography for the evaluation of left ventricular diastolic function in patients with cardiac amyloidosis. *Am J Cardiol.* (2009) 103:718–23. doi: 10.1016/j.amjcard.2008.10.039
57. Vogelsberg H, Mahrholdt H, Deluigi CC, Yilmaz A, Kispert EM, Greulich S, et al. Cardiovascular magnetic resonance in clinically suspected cardiac amyloidosis. *J Am Coll Cardiol.* (2008) 51:1022–30.
58. Fontana M, Pica S, Reant P, Abdel-Gadir A, Treibel TA, Banypersad SM, et al. Prognostic value of late gadolinium enhancement cardiovascular magnetic resonance in cardiac amyloidosis. *Circulation.* (2015) 132:1570–9.
59. Hosch W, Kristen AV, Libicher M, Dengler TJ, Aulmann S, Heye T, et al. Late enhancement in cardiac amyloidosis: correlation of MRI enhancement pattern with histopathological findings. *Amyloid.* (2008) 15:196–204. doi: 10.1080/13506120802193233
60. Martinez-Naharro A, Treibel TA, Abdel-Gadir A, Bulluck H, Zumbo G, Knight DS, et al. Magnetic resonance in transthyretin cardiac amyloidosis. *J Am Coll Cardiol.* (2017) 70:466–77.
61. Karamitsos TD, Piechnik SK, Banypersad SM, Fontana M, Ntusi NB, Ferreira VM, et al. Noncontrast T1 mapping for the diagnosis of cardiac amyloidosis. *JACC Cardiovasc Imaging.* (2013) 6:488–97. doi: 10.1016/j.jcmg.2012.11.013
62. Pan JA, Kerwin MJ, Salerno M. Native T1 mapping, extracellular volume mapping, and late gadolinium enhancement in cardiac amyloidosis: a meta-analysis. *JACC Cardiovasc Imaging.* (2020) 13:1299–310. doi: 10.1016/j.jcmg.2020.03.010
63. Korthals D, Chatzantonis G, Bietenbeck M, Meier C, Stalling P, Yilmaz A. CMR-based T1-mapping offers superior diagnostic value compared to longitudinal strain-based assessment of relative apical sparing in cardiac amyloidosis. *Sci Rep.* (2021) 11:15521. doi: 10.1038/s41598-021-94650-2
64. Wan K, Li W, Sun J, Xu Y, Wang J, Liu H, et al. Regional amyloid distribution and impact on mortality in light-chain amyloidosis: a T1 mapping cardiac magnetic resonance study. *Amyloid.* (2019) 25:45–51. doi: 10.1080/13506129.2019.1578742
65. Avitzur N, Satriano A, Afzal M, Narous M, Mikami Y, Hansen R, et al. 3D myocardial deformation analysis from cine MRI as a marker of amyloid protein burden in cardiac amyloidosis: validation versus T1 mapping. *Int J Cardiovasc Imaging.* (2018) 34:1937–46. doi: 10.1007/s10554-018-1410-5
66. Martinez-Naharro A, Baksi AJ, Hawkins PN, Fontana M. Diagnostic imaging of cardiac amyloidosis. *Nat Rev Cardiol.* (2020) 17:413–26.
67. Kim JY, Hong YJ, Han K, Lee HJ, Hur J, Kim YJ, et al. Regional Amyloid burden differences evaluated using quantitative cardiac MRI in patients with cardiac amyloidosis. *Korean J Radiol.* (2021) 22:880–9. doi: 10.3348/kjr.2020.0579
68. Chitiboi T, Axel L. Magnetic resonance imaging of myocardial strain: a review of current approaches. *J Magn Reson Imaging.* (2017) 46:1263–80. doi: 10.1002/jmri.25718
69. Austin BA, Tang WH, Rodriguez ER, Tan C, Flamm SD, Taylor DO, et al. Delayed hyper-enhancement magnetic resonance imaging provides incremental diagnostic and prognostic utility in suspected cardiac amyloidosis. *JACC Cardiovasc Imaging.* (2009) 2:1369–77. doi: 10.1016/j.jcmg.2009.08.008
70. Martinez-Naharro A, Abdel-Gadir A, Treibel TA, Knight DS, Rosmini S, Lane T, et al. CMR-verified regression of cardiac AL amyloid after chemotherapy. *J Am Coll Cardiol Cardiovasc Imaging.* (2018) 11:152–4. doi: 10.1016/j.jcmg.2017.02.012
71. Janssen S, Piers DA, Van Rijswijk MH, Meijer S, Mandema E. Soft-tissue uptake of 99mTc-diphosphonate and 99mTc-pyrophosphate in amyloidosis. *Eur J Nucl Med.* (1990) 16:663–70. doi: 10.1007/BF00998166
72. Treglia G, Glaudemans AWJM, Bertagna F, Hazenberg BPC, Erba PA, Giubbini R, et al. Diagnostic accuracy of bone scintigraphy in the assessment of cardiac transthyretin-related amyloidosis: a bivariate meta-analysis. *Eur J Nucl Med Mol Imaging.* (2018) 45:1945–55. doi: 10.1007/s00259-018-4013-4
73. Puille M, Altland K, Linke RP, Steen-Müller MK, Klett R, Steiner D, et al. 99mTc-DPD scintigraphy in transthyretin-related familial amyloidotic polyneuropathy. *Eur J Nucl Med.* (2002) 29:376–9. doi: 10.1007/s00259-001-0730-0
74. Gillmore JD, Maurer MS, Falk RH, Merlini G, Damy T, Dispenzieri A, et al. Nonbiopsy diagnosis of cardiac transthyretin amyloidosis. *Circulation.* (2016) 133:2404–12. doi: 10.1161/CIRCULATIONAHA.116.021612
75. Dorbala S, Bokhari S, Miller E, Bullock-Palmer R, Soman P, Thompson R. *99mTechntium-Pyrophosphate Imaging for Transthyretin Cardiac Amyloidosis. ASNC Cardiac Amyloidosis Practice Points*. Fairfax, VA: The American Society of Nuclear Cardiology (2019). p. 1–5.
76. Hanna M, Ruberg FL, Maurer MS, Dispenzieri A, Dorbala S, Falk RH, et al. Cardiac scintigraphy with technetium-99m-labeled bone-seeking tracers for suspected amyloidosis. *J Am Coll Cardiol.* (2020) 75:2851–62. doi: 10.1016/j.jacc.2020.04.022
77. Perugini E, Guidalotti PL, Salvi F, Cooke RMT, Pettinato C, Riva L, et al. Noninvasive etiologic diagnosis of cardiac amyloidosis using 99mTc-3,3-diphosphono-1,2-propanodicarboxylic acid scintigraphy. *J Am Coll Cardiol.* (2005) 46:1076–84. doi: 10.1016/j.jacc.2005.05.073
78. Bokhari S, Castaño A, Pozniakoff T, Deslisle S, Latif F, Maurer MS. 99m Tc-pyrophosphate scintigraphy for differentiating light-chain cardiac amyloidosis from the transthyretin-related familial and senile cardiac amyloidoses. *Circ Cardiovasc.* (2013) 6:195–201. doi: 10.1161/CIRCIMAGING.112.000132
79. Régis C, Harel F, Martineau P, Grégoire J, Abikhzer G, Juneau D, et al. Tc-99m-pyrophosphate scintigraphy for the diagnosis of ATTR cardiac amyloidosis: comparison of quantitative and semi– quantitative approaches. *J Nucl Cardiol.* (2020) 27:1808–15. doi: 10.1007/s12350-020-02205-1
80. Soumalainen O, Pilv J, Loimaala A, Mätzke S, Heliö T, Uusitalo V. Prognostic significance of incidental suspected transthyretin amyloidosis on routine bone scintigraphy. *J Nucl Cardiol.* (2020). doi: 10.1007/s12350-020-02396-7 [Epub ahead of print].
81. Rapezzi C, Quarta CC, Guidalotti PL, Pettinato C, Fanti S, Leone O, et al. Role of (99m)Tc-DPD scintigraphy in diagnosis and prognosis of hereditary transthyretin-related cardiac amyloidosis. *JACC Cardiovasc Imaging.* (2011) 4:659–70. doi: 10.1016/j.jcmg.2011.03.016

82. Hutt DF, Quigley A, Page J, Hall ML, Burniston M, Gopaul D, et al. Utility and limitations of 3,3-diphosphono-1,2-propanodicarboxylic acid scintigraphy in systemic amyloidosis. *Eur Heart J Cardiovasc.* (2014) 15:1289–98. doi: 10.1093/ehjci/jeu107
83. Galat A, Rosso J, Guellich A, Van Der Gucht A, Rappeneau S, Bodez D, et al. Usefulness of99mTc-HMDP scintigraphy for the etiologic diagnosis and prognosis of cardiac amyloidosis. *Amyloid.* (2015) 22:210–20. doi: 10.3109/13506129.2015.1072089
84. Musumeci MB, Cappelli F, Russo D, Tini G, Canepa M, Milandri A, et al. Low sensitivity of bone scintigraphy in detecting Phe64Leu mutation-related transthyretin cardiac amyloidosis. *JACC Cardiovasc Imaging.* (2020) 13:1314–21. doi: 10.1016/j.jcmg.2019.10.015
85. Maurer MS, Bokhari S, Damy T, Dorbala S, Drachman BM, Fontana M, et al. Expert consensus recommendations for the suspicion and diagnosis of transthyretin cardiac amyloidosis. *Circ Heart Fail.* (2019) 12:e006075. doi: 10.1161/CIRCHEARTFAILURE.119.006075
86. Bianco M, Parente A, Biolè C, Righetti C, Spirito A, Luciano A, et al. BRIEF REPORT The prevalence of TTR cardiac amyloidosis among patients undergoing bone scintigraphy. *J Nucl Cardiol.* (2021) 28:825–30. doi: 10.1007/s12350-021-02575-0
87. Antoni G, Lubberink M, Estrada S, Axelsson J, Carlson K, Lindsjö L, et al. In vivo visualization of amyloid deposits in the heart with 11C-PIB and PET. *J Nucl Med.* (2012) 54:213–20. doi: 10.2967/jnumed.111.102053
88. Dietemann S, Nkoulou R. Amyloid PET imaging in cardiac amyloidosis: a pilot study using 18F-flutemetamol positron emission tomography. *Ann Nucl Med.* (2019) 33:624–8. doi: 10.1007/s12149-019-01372-7
89. Dorbala S, Vangala D, Semer J, Strader C, Bruyere JR, Di Carli MF, et al. Imaging cardiac amyloidosis: a pilot study using 18F-florbetapir positron emission tomography. *Eur J Nucl Med Mol Imaging.* (2014) 41:1652–62. doi: 10.1007/s00259-014-2787-6
90. Law WP, Wang WYS, Moore PT, Mollee PN, Ng ACT. Cardiac amyloid imaging with 18F-florbetaben PET: a pilot study. *J Nucl Med.* (2016) 57:1733–9. doi: 10.2967/jnumed.115.169870
91. Kircher M, Ihne S, Brumberg J, Morbach C, Knop S, Kortüm KM, et al. Detection of cardiac amyloidosis with 18 F-Florbetaben-PET/CT in comparison to echocardiography, cardiac MRI and DPD-scintigraphy. *Eur J Nucl Med Mol Imaging.* (2019) 46:1407–16. doi: 10.1007/s00259-019-04290-y
92. Genovesi D, Vergaro G, Giorgetti A, Marzullo P, Scipioni M, Santarelli MF, et al. [18F]-florbetaben PET/CT for differential diagnosis among cardiac immunoglobulin light chain, transthyretin amyloidosis, and mimicking conditions. *JACC Cardiovasc Imaging.* (2021) 14:246–55. doi: 10.1016/j.jcmg.2020.05.031
93. Abulizi M, Sifaoui I, Wuliya-Gariepy M, Kharoubi M, Israël J, Emsen B, et al. F-sodium fluoride PET/MRI myocardial imaging in patients with suspected cardiac amyloidosis. *J Nucl Cardiol.* (2019) 28:1586–95. doi: 10.1007/s12350-019-01885-8
94. Aimo A, Emdin M, Musetti V, Pucci A, Vergaro G. Abdominal fat biopsy for the diagnosis of cardiac amyloidosis. *JACC Case Rep.* (2020) 2:1182–5. doi: 10.1016/j.jaccas.2020.05.062
95. Garcia Y, Collins AB, Stone JR. Abdominal fat pad excisional biopsy for the diagnosis and typing of systemic amyloidosis. *Hum Pathol.* (2018) 72:71–9. doi: 10.1016/j.humpath.2017.11.001
96. Kittleson MM, Maurer MS, Ambardekar AV, Bullock-Palmer RP, Chang PP, Eisen HJ, et al. Cardiac amyloidosis: evolving diagnosis and management: a scientific statement from the American heart association. *Circulation.* (2020) 142:e7–22.
97. Yilmaz A, Kindermann I, Kindermann M, Mahfoud F, Ukena C, Athanasiadis A, et al. Comparative evaluation of left and right ventricular endomyocardial biopsy: differences in complication rate and diagnostic performance. *Circulation.* (2010) 122:900–9. doi: 10.1161/CIRCULATIONAHA.109.924167

Conflict of Interest: The authors declare that the research was conducted in the absence of any commercial or financial relationships that could be construed as a potential conflict of interest.

frontiers in Cardiovascular Medicine

REVIEW
published: 31 March 2022
doi: 10.3389/fcvm.2022.846213

Cardiovascular Imaging for Systemic Sclerosis Monitoring and Management

Peter Glynn[1†], Sarah Hale[1†], Tasmeen Hussain[2†] and Benjamin H. Freed[1]*

[1] Division of Cardiology, Department of Medicine, Northwestern University Feinberg School of Medicine, Chicago, IL, United States, [2] Division of Hospital Medicine, Department of Medicine, Northwestern University Feinberg School of Medicine, Chicago, IL, United States

Systemic sclerosis (SSc) is a complex connective tissue disease with multiple clinical and subclinical cardiac manifestations. SSc can affect most structural components of the heart, including the pericardium, myocardium, valves, and conduction system through a damaging cycle of inflammation, ischemia, and fibrosis. While cardiac involvement is the second leading SSc-related cause of death, it is frequently clinically silent in early disease and often missed with routine screening. To facilitate identification of cardiac disease in this susceptible population, we present here a review of cardiac imaging modalities and potential uses in the SSc patient population. We describe well-characterized techniques including electrocardiography and 2D echocardiography with Doppler, but also discuss more advanced imaging approaches, such as speckle-tracking echocardiography, cardiovascular magnetic resonance imaging (CMR), and stress imaging, among others. We also suggest an algorithm for the appropriate application of these modalities in the workup and management of patients with SSc. Finally, we discuss future opportunities for cardiac imaging in SSc research to achieve early detection and to optimize treatment.

Keywords: cardiovascular imaging, systemic sclerosis (scleroderma), echocardiography, cardiovascular magnetic resonanace, scleroderma heart disease

OPEN ACCESS

Edited by:
Monica Mukherjee, The Johns Hopkins Hospital, Johns Hopkins Medicine, United States

Reviewed by:
Valentina Mercurio, University of Naples Federico II, Italy
Luna Gargani, University of Pisa, Italy

***Correspondence:**
Benjamin H. Freed
benjamin.freed@northwestern.edu

[†] These authors have contributed equally to this work and share first authorship

Specialty section:
This article was submitted to Cardiovascular Imaging, a section of the journal Frontiers in Cardiovascular Medicine

Received: *30 December 2021*
Accepted: *08 March 2022*
Published: *31 March 2022*

Citation:
Glynn P, Hale S, Hussain T and Freed BH (2022) Cardiovascular Imaging for Systemic Sclerosis Monitoring and Management. Front. Cardiovasc. Med. 9:846213. doi: 10.3389/fcvm.2022.846213

INTRODUCTION

Cardiac complications from systemic sclerosis (SSc) are numerous and often underdiagnosed. These complications are either a direct result of SSc on the myocardium, or indirect effects of other organ involvement [pulmonary arterial hypertension (PAH), interstitial lung disease (ILD), or renal crisis, etc.) (1). Direct myocardial manifestations of SSc include microvascular coronary artery disease, cardiac fibrosis, myocarditis, left and right ventricular systolic and diastolic dysfunction, pericardial disease, and conduction abnormalities (**Figure 1**) (2). When present, cardiac involvement predicts worse survival (3). In two meta-analyses of observational studies, cardiac deaths represented the most frequent cause of death in SSc, accounting for 20–29% of all deaths (4, 5). Early screening and detection of cardiac abnormalities is thus vitally important in SSc. Cardiac imaging is utilized extensively for that purpose.

As cardiac imaging techniques have progressed, they have allowed for new insights into the pathophysiology, diagnosis, and treatment of SSc. While two-dimensional echocardiography (2DE) remains the most utilized modality, tissue doppler imaging (TDI), speckle-tracking imaging (STE), and cardiac magnetic resonance imaging (CMR) all have growing importance. In the

present review, we will discuss the most recent data regarding the epidemiology, diagnosis, and management of cardiac complications of SSC, highlighting the evolving role that cardiac imaging plays in diagnosis and management.

EPIDEMIOLOGY

The prevalence of cardiac involvement in SSc is difficult to define for a number of reasons – rates vary depending on the methods used, signs and symptoms of cardiac disease can be subtle leading to underestimation, and symptoms of cardiac involvement are often attributed to pulmonary, musculoskeletal, or esophageal involvement. Rates of cardiac involvement vary depending on which manifestation is being considered. Broadly speaking, rates range from as low as 7% to as high as 44% depending on the study (6, 7). Major risk factors for cardiac involvement include male sex, African-American ethnicity, diffuse cutaneous SSc, older age at disease onset, tendon friction rubs, abnormal nail-fold capillaroscopy, and worse quality-of-life scores (6).

RIGHT VENTRICULAR DYSFUNCTION AND PULMONARY HYPERTENSION

In patients with SSc, right ventricular (RV) dysfunction is more common than left ventricular (LV) dysfunction and may exist due to primary myocardial involvement, increased pulmonary vascular resistance (PVR), or a mixture of both (2, 8, 9). RV function may occur early in the disease course (2, 9, 10) and myocardial fibrosis may be responsible for both diastolic and systolic dysfunction (2, 8, 11). While RV dysfunction is often associated with abnormal pulmonary artery (PA) pressures and PAH, myocardial fibrosis may directly lead to RV dysfunction and elevated right atrial pressure (RAP) even in the absence of elevated PA pressures (11).

In patients with SSc, pulmonary hypertension (PH) may manifest through various pathologic mechanisms, and can be categorized into one or more of the five WHO Groups of PH. SSc associated-PAH (SSc-PAH) is considered WHO Group 1 PH and may be the result of direct remodeling of the pre-capillary pulmonary arterioles, or rarely be attributable to pulmonary veno-occlusive disease/pulmonary capillary hemangiomatosis (PVOD/PCH). It is a leading cause of mortality in SSc patients, with an incidence of 8–13% (12, 13) and is more commonly associated with limited cutaneous systemic sclerosis (lcSSc) (14), Patients with SSc-PAH have a poor prognosis in comparison to SSc patients without PAH, with 3 year survival of only 52% (14–16). Several studies have demonstrated that the intrinsic RV dysfunction in SSc patients leads to worse outcomes in SSc-PAH in comparison to idiopathic PAH (2, 13, 17). One year mortality for SSc-PAH has been found to be 30%, while one year mortality for those with idiopathic PAH is 15% (17). Mortality rates remain high despite therapy (14).

Systemic sclerosis associated PH can also occur in the setting of capillary loss and hypoxemic respiratory failure as a result of ILD, categorized as WHO Group 3 PH. PH due to ILD is more common in patients with diffuse cutaneous systemic sclerosis (dcSSc) (18). In addition, patients with SSc may have evidence of left ventricular systolic and diastolic dysfunction, leading to WHO Group 2 PH. Rarely, patients with SSc may develop chronic thromboembolic pulmonary hypertension (CTEPH) and be classified as WHO Group 4 PH. Distinguishing among the different mechanisms of SSc associated PH is important as treatment and prognosis are impacted by a timely and accurate diagnosis (14, 19, 20).

In recent years, there has been a greater focus on understanding the pathophysiologic mechanisms driving RV dysfunction and PH associated with SSc patients, as well as the poor outcomes linked to the presence of PH in this patient population. Essential to this focus is the thorough investigation of the etiology of PH in patients with SSc, which often includes diagnostic tests such as full pulmonary function testing, including diffusion capacity for carbon monoxide (DLCO) for PH-ILD, ventilation perfusion scanning (V/Q scan) for CTEPH, and computed tomography scanning for radiographic correlates of PVOD/PCH (19). Cardiac imaging is frequently used for this purpose as well as diagnosing and monitoring disease status. 2DE and cardiovascular magnetic resonance (CMR) are the most common imaging modalities used. Notably, STE is a novel way to detect RV dysfunction earlier and its role in SSc associated RV dysfunction and PH is currently being studied. It is important to screen patients for PH and RV dysfunction early, as studies have demonstrated improved survival and improved treatment response in SSc-PAH patients with mild hemodynamics and symptoms (14, 21).

Evaluation

Given the high prevalence of RV dysfunction and PH in patients with SSc, current guidelines recommend echocardiographic screening of all SSc patients in order to detect and implement PH therapy as early as possible (22). In select patients, further imaging with CT or CMR may be helpful.

Echocardiography

Transthoracic echocardiography (TTE) is widely available and accessible to patients, making it an optimal screening tool for RV dysfunction and PH. Evidence of RV dysfunction on 2DE include RV dilation, flattening of interventricular septum (D-Sign) suggestive of RV pressure or volume overload, and reduced semi quantitative measures of RV function [i.e., tricuspid annular systolic planar excursion (TAPSE) and fractional area of change (FAC)]. Significant RV dysfunction has been defined as TAPSE less than 1.7 cm and FAC less than 35% (10).

Transthoracic echocardiography can also be used to distinguish WHO Group 1 PH from WHO Group 2 PH in patients with SSc. For example, echocardiographic findings suggestive of left heart disease, such as left atrial dilatation, abnormal markers of diastolic dysfunction (i.e., elevated E/e' ratio, reduced mitral annular tissue doppler velocities), or evidence of LV dysfunction, may be indicative of post-capillary PH (WHO Group 2 PH). On the other hand, echocardiographic markers demonstrating elevated PA pressures, RV dilation, and/or RV dysfunction, in the absence of left heart disease,

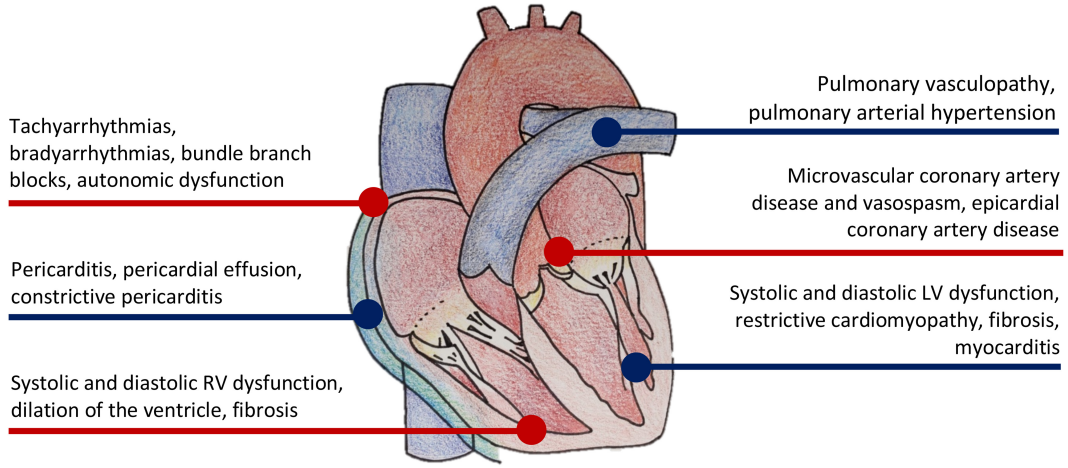

FIGURE 1 | Manifestations of cardiovascular disease in systemic sclerosis.

is more suggestive of pre-capillary PH (WHO Group 1 PH). Additional measures such as RV outflow tract (RVOT) systolic doppler flow velocity notching and RVOT acceleration time may also be useful in differentiating pre- versus post-capillary PH (23).

Right atrial and RV chamber enlargement in SSc are directly related to onset of heart failure symptoms as well as mortality (10). In addition, measurements of RV systolic function such as TAPSE, tissue Doppler of the tricuspid annulus S', RV FAC, and Tei index all correlate with decreased survival (10). Argula et al. demonstrated an improvement in TAPSE after medical therapy in patients with IPAH, while patients with SSc-PAH had worsening tricuspid regurgitant jet velocity and larger right heart chamber size after therapy (24). The attenuated response to PH therapy in the SSc population, demonstrated through echocardiographic markers, may signal the presence of intrinsic RV dysfunction in SSc-PAH patients in comparison to IPAH patients (13, 25).

Both RV systolic and diastolic dysfunction are prevalent in SSc patients (8). When compared to controls, Muene et al. showed that SSc patients had significantly reduced RV contractility ($p < 0.001$) and larger RA area. In addition, 25% of SSc patients had abnormal RV diastolic dysfunction compared to 0% in controls, as measured by trans-tricuspid E/A ratio (8). Although patients with SSc-PAH demonstrate greater prevalence of reduced RV contractility and diastolic dysfunction, patients with SSc who did not meet diagnostic criteria for PAH still had abnormalities in both RV systolic and diastolic dysfunction (8).

Abnormal echocardiographic findings can also be demonstrated early in the disease course, even before signs or symptoms manifest themselves (26). In a study by Pigatto et al., 45 SSc patients without any signs or symptoms of heart disease or PH were compared to 43 healthy controls, using both 2DE and three-dimensional echocardiography (3DE). The SSc patients were found to have a significant increase in RV volume and reduced RV ejection fraction as determined by 3DE. Doppler measurements demonstrated an increased systolic pulmonary artery pressure (sPAP) in SSc patients in comparison to the control group. In addition, the changes were more pronounced in patients with lcSSc than dcSSc (26). This study underscores the need for screening for RV dysfunction and PH in this patient population even in the absence of symptoms.

Speckle Tracking Echocardiography

Although RV dysfunction and PH in SSc is common and is a large determinant of long term prognosis, it often remains undetectable despite the use of 2D echocardiography. Most 2DE measures of RV function are limited by the complex shape of the RV, load dependency, and suboptimal reproducibility. STE avoids some of these pitfalls and can be used to detect subtle changes in global and regional RV systolic function that may be undetectable by conventional echocardiographic measures (10).

RV longitudinal systolic strain (RVLSS) has been shown to be more abnormal in SSc when compared to controls, despite comparable traditional echocardiographic parameters of RV function between groups (**Figure 2**) (27). For example, a study by Zairi et al. revealed a 3.3 fold increased risk of subclinical RV systolic impairment in SSc patients, manifested by more abnormal RVLSS, in comparison to controls (-18.2 vs. 22.3%; $p = 0.012$) (27). Meanwhile, multiple authors have illustrated a regional pattern of abnormal RVLSS seen in SSc patients (10, 28, 29). In a study by Mukherjee et al., 138 SSc patients were compared to 40 healthy non-SSc controls. While both TAPSE and RV FAC were normal in both groups, RVLSS was found to be abnormal in SSc patients, independent of PH and SSc phenotype. Specifically, a regional pattern of abnormal strain was seen in SSc patients, with increased strain in the basal segment and decreased strain in the apical and mid segments. Some hypothesize that the basal segment is hyperkinetic early in the disease course, and as PH develops, the ability of the basal segment to compensate decreases and RV failure ensues, suggesting a "two hit" hypothesis in which pre-existing RV contractile dysfunction may predispose to further dysfunction after PH occurs (28). While STE is a promising technique for detecting unique patterns of early, subclinical RV dysfunction in SSc patients, more evidence is needed to discern its role in this population.

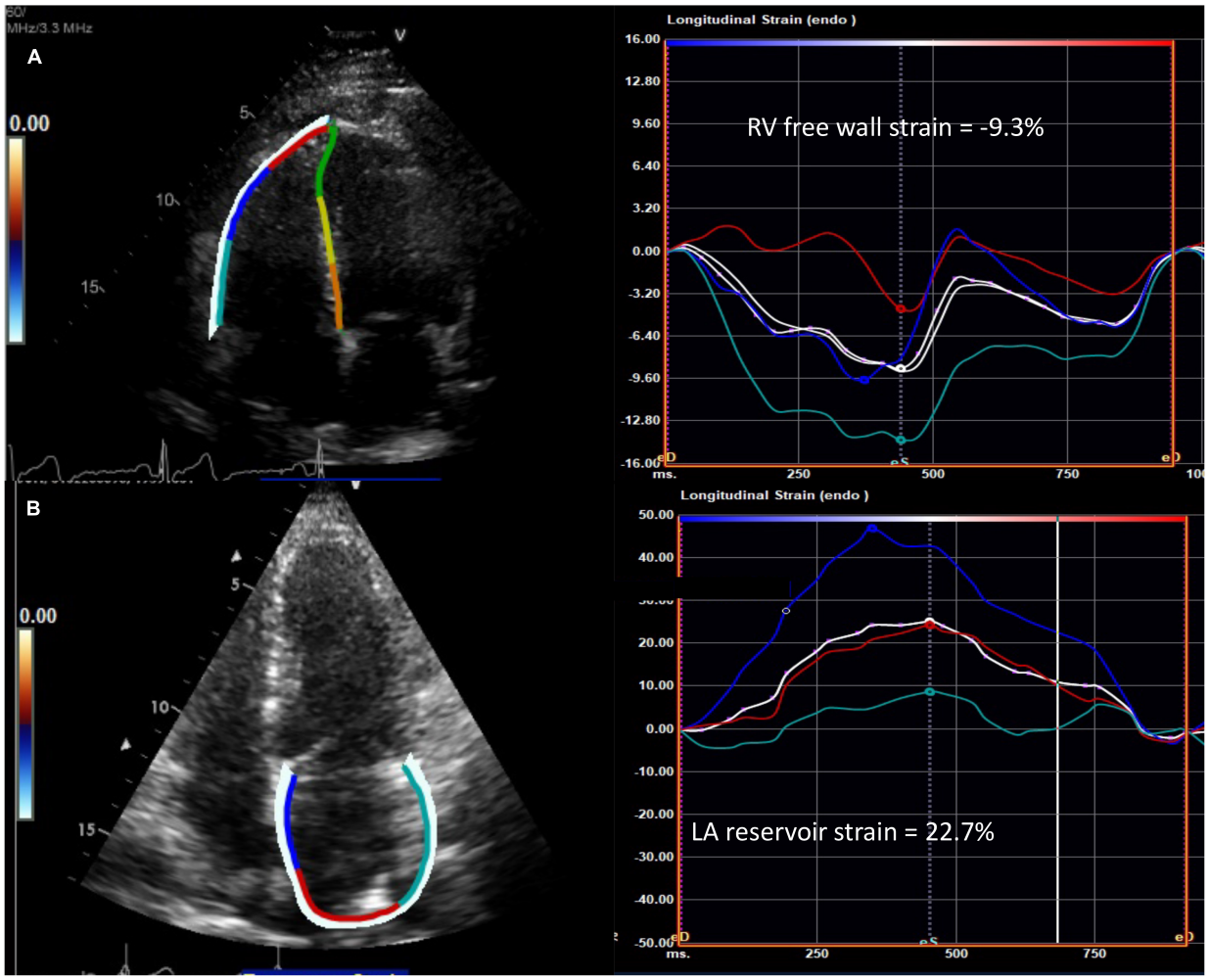

FIGURE 2 | Abnormal speckle tracking strain in diffuse cutaneous systemic sclerosis. **(A)** Example of reduced right ventricular free wall strain (normal <-20%) and **(B)** reduced left atrial reservoir strain (normal >39%) from the apical four chamber view in patients with systemic sclerosis. The white curve represents the average of the peak systolic strain curves. RV, right ventricle; LA, left atrium.

Exercise Echocardiography

Recent studies have investigated whether exercise echocardiography can unmask PH in SSc patients potentially leading to earlier diagnosis and therapy for patients with SSc-associated PH. A study by Rallidis et al. investigated 49 patients with SSc undergoing exercise stress echocardiography, and found that post-exercise TR velocity > 3.4 m/s had a sensitivity of 90.5% and a specificity of 80% in detecting PH, as confirmed with right heart catheterization (RHC) (30). In addition, a study by Mukherjee et al. used STE to demonstrate that SSc-PAH patients had diminished RV contractile reserve in response to exercise (29). The authors demonstrated that all patients with SSc had regional abnormalities in RVLSS at rest, but patients with elevated RV systolic pressure (defined by RV systolic pressure ≥35 mmHg) lacked an ability to increase both global and regional strain with exercise. This finding suggests a lack of RV contractile reserve in these patients likely due to intrinsic myocardial dysfunction (29).

Although exercise-induced PH has clinical and prognostic significance in patients with cardiopulmonary conditions, there remains a lack of standard definition for exercise-induced PH and a lack of standard measures for how the RV and pulmonary vasculature respond to exercise (14). Further study is needed to determine the utility of exercise echocardiography in unmasking PH, as well as the use of exercise echocardiography in assessing RV and PV contractile reserve.

Cardiovascular Magnetic Resonance

Cardiovascular magnetic resonance is the gold standard for measuring RV size and function and is superior in terms of reproducibility to 2DE in that it does not require a suitable acoustic window for measuring RV size, geometry, and function. CMR cine imaging provides excellent spatial resolution and free breathing sequences provides real-time physiologic assessment of the interventricular septal dynamics. While some interventricular septal flattening is expected

during inspiration to accommodate the increased volume of blood, significant interventricular septal flattening is indicative of a dysfunctional RV. Although evaluation of myocardial fibrosis with late gadolinium enhancement (LGE) is useful for the LV, it is challenging with the RV due to the RV's thin myocardium. Therefore, high resolution T1 mapping and myocardial extracellular volume (ECV) have emerged as useful techniques in detecting diffuse RV fibrosis, even in the absence of PH. CMR measures of myocardial fibrosis, such as T1 mapping and ECV, are valuable to detect fibrosis early in the disease course, which can potentially alter therapy and prevent worsening RV dysfunction (**Figure 3**) (2, 11, 31–36). A study by Chaosuwannakit et al. found that 21% of patients with SSc who underwent CMR had RV dilation despite not meeting criteria for PH suggesting the presence of intrinsic RV dysfunction – perhaps due to fibrosis – in these patients (37). It is hypothesized that myocardial fibrosis reflects a cellular response to increased RV afterload, but more investigation is needed to understand if myocardial fibrosis on CMR signals an adaptive or maladaptive response (35).

While STE is shown to be beneficial in assessing subclinical RV dysfunction in SSc-associated PH, CMR-derived strain has also exhibited utility in assessing patients' response to PH therapy (38). Measurements of strain and strain rate can be obtained using tissue-tracking CMR. In the ATPAHSS-O trial, 21 treatment naïve patients with SSc were analyzed using pre and post-treatment CMR examinations. The study found a significant improvement in measures of RVLSS, RV peak systolic longitudinal strain rate, RV peak longitudinal atrial-diastolic strain rate, and RV peak circumferential early diastolic strain rate after 36 weeks of treatment. Notably, improvements in RV and LV strain also correlated with improvements in clinical outcomes (38).

Computed Tomography

When evaluating a SSc patient using CT, increased PA diameter (>29 mm), septal flattening, and increased RV-LV ratio suggest elevated pulmonary artery pressures (2, 22). High resolution CT (HRCT) is used to assess for interstitial lung disease and for signs of PVOD that can complicate SSc-PH diagnosis and therapy (2, 39). Interstitial changes are visible on HRCT in up to 80% of SSc patients, while ILD is clinically apparent in up to 40% of patients (14). While ILD is common in SSc, there is no validated definition of the optimal threshold of lung involvement to differentiate SSc-PH associated with ILD from SSc-PAH (14). It has been demonstrated that combined fibrosis and emphysema is associated with an increased risk of PH (14, 39–41), and several studies have demonstrated poorer survival with SSc-PH associated with ILD compared to SSc-PAH, making an accurate diagnosis important (42, 43).

Right Heart Catheterization

Right heart catheterization remains the gold standard for hemodynamic assessment of PH (2). Per the 2015 ESC/ERS Guidelines for the diagnosis and treatment of pulmonary hypertension (22), the decision to pursue a RHC depends on three scores which include (1) peak tricuspid regurgitation velocity; (2) the presence of at least 2 PH signs on TTE [from two different categories among (a) the ventricles, (b) the pulmonary artery, and (c) the inferior vena cava and right atrium]; and (3) the presence of CTEPH or PAH risk factors or associated conditions. For patients with high echocardiographic probability of PH based on echo criteria (1 and 2 above), RHC is recommended. When the probability of PH is intermediate by echo but CTEPH or PAH risk factors are present, RHC should be considered. In patients with symptoms such as exertional dyspnea, angina, syncope, and exercise intolerance that remain unexplained after initial cardiopulmonary evaluation, RHC should be considered, especially when SSc is suspected or confirmed.

Patients are often first screened with echocardiography, and recommendations suggest referral for RHC if the tricuspid regurgitant velocity is more than 2.8 m/s, or more than 2.5 m/s if signs or symptoms of PH are present (2, 44). Because patients with SSc can develop PH through a variety of pathophysiologic mechanisms, RHC is recommended for confirmation of elevated PA pressures on 2DE and to differentiate between different mechanisms of PH (2, 22).

LEFT VENTRICULAR DYSFUNCTION

Left ventricular dysfunction in systemic sclerosis is most likely a result of microvascular disease and inflammation. Most patients do not have appreciable CAD (45). Autopsies of myocardial tissue from SSc patients show focal areas of pathology, ranging from contraction band necrosis to replacement fibrosis in the tissue (45). Early detection of fibrosis may assist clinicians in identifying those SSc patients at risk of arrythmia, rehospitalization, and cardiovascular mortality (46).

Left ventricular involvement in SSc includes primarily diastolic dysfunction, and, in some cases, restrictive cardiomyopathy. Several studies show that overtly decreased left ventricular ejection fraction (LVEF) is a relatively uncommon feature of SSc (7, 47–50). Non-invasive identification of LV abnormalities through imaging may have substantial diagnostic as well as prognostic benefits to clinicians and patients, as further elucidated below.

Evaluation

Echocardiography in SSc remains the best initial tool for the evaluation of LV disease, due to its low cost, lack of radiation, and extensive evidence base, as noted below. Tissue Doppler and STE, specifically, are sensitive tests for uncovering subclinical LV dysfunction, which may be suggestive of microvascular disease. Guidelines recommend asymptomatic patients with SSc receive yearly echocardiography by trained sonographers following a standardized Scleroderma Doppler Echocardiography Protocol, which includes multiple standardized 2D echo and Doppler images (51). In select patients, further imaging with CT or cardiac MRI may be helpful, though the literature is less clear on specific recommendations regarding these modalities.

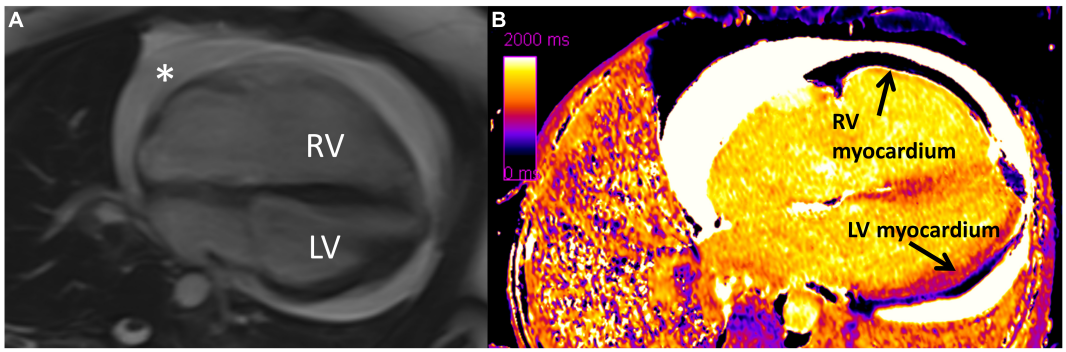

FIGURE 3 | Diffuse interstitial fibrosis of the right ventricle using cardiovascular magenetic resonance imaging. **(A)** Four chamber cine showing enlarged right ventricle and circumferential pericardial effusion (*). **(B)** Native T1 map showing increased T1 time (diffuse fibrosis) in right ventricular myocardium compared to left ventricular myocardium. RV, right ventricle; LV, left ventricle. Note: this image is reproduced with permission from Belin et al. (11).

Echocardiography

Compared to healthy patients, patients with SSc undergoing echocardiography show impaired LV diastolic function noted by multiple measures. Structurally, LV hypertrophy appears more common in SSc than controls (52). Patients with SSc also have higher E/e' ratios (53) (representing higher LV filling pressures) and increased isovolumetric relaxation times compared to controls (48). Interestingly, abnormal E/e' ratio [defined as transmitral to mitral annular early diastolic velocity ratio (54)] was also associated with duration of recognized SSc disease in months, as well as mean duration of Raynaud's phenomenon, suggesting temporal relation in SSc-related fibrotic disease of different organs (49). Additionally, certain measurements may also predict mortality in SSc patients. One study utilizing lateral tissue Doppler early mitral annular (e') velocity found that each standard deviation decrease in e' (suggesting impaired LV relaxation) was associated with increased risk of death in SSc patients at 1.9 $\pm$ 1.3 years (55). Thus, 2DE with tissue Doppler analysis can provide important structural clues that can correlate to disease progression as well as provide important prognostic information.

Speckle Tracking Echocardiography

Systemic sclerosis patients also show differences in strain imaging via echocardiography as compared to controls. Studies have shown both regional and global LV longitudinal systolic strain (LVLSS) is significantly lower in SSc patients than controls and is most pronounced in the endocardial layer of the LV (56, 57). Furthermore, SSc patients with lower global LVLSS were more likely to have elevated C-reactive protein values suggesting greater inflammation. LVLSS also appears to worsen in SSc patients over time (56, 58).

Lindholm et al. showed that SSc patients with PAH had the lowest LVLSS when compared to both SSc patients without PAH as well as controls, suggesting that PAH may be a co-contributor to apparent LV disease in this population (59). Similarly, SSc patients with hypertension had a higher prevalence of diastolic dysfunction and worse LVLSS when compared to SSc patients without hypertension and controls with and without hypertension (60). Thus, STE can help identify subclinical cardiac disease in SSc, and can also be used to show the incremental effects of other medical conditions on an already vulnerable myocardium.

Cardiovascular Magnetic Resonance

Similar to RV pathology, CMR provides information on LV dysfunction beyond echocardiography in patients with SSc. In a study evaluating 41 patients with SSc, Tzelepis et al. identified mesocardial LGE in a linear pattern located in the basal and midcavity segments of the LV. Patients with a greater than 15-year duration of Raynaud's phenomenon had a greater number of enhancing segments than those with a shorter duration of Raynaud's. Furthermore, those with abnormal Holter monitor results [defined as conduction delay or block, intermittent bundle branch block, ventricular arrythmias (mono- or polymorphic, or >100/day premature ventricular contractions {PVCs}), or ventricular tachycardias] over 24 h also had a greater number of enhancing segments suggesting an association between degree of fibrosis and arrhythmias (61).

As mentioned earlier, ECV can identify diffuse fibrosis even in patients with normal echocardiograms and without any evidence of LGE on CMR. Thuny et al. showed that SSc patients with normal echocardiograms had significantly higher global LV ECV than age matched healthy controls and that global LV ECV significantly correlated with the grade of diastolic dysfunction (62). Another study found that, in addition to higher ECV, SSc patients also had less myocardial blood flow augmentation (measured by CMR perfusion imaging) when experiencing a cold pressor test (hand immersion in cold water) compared to healthy controls. This muted vasodilatory response was favored to represent microvascular dysfunction in this population (63). Higher baseline ECV also correlates to risk of cardiovascular events among SSc patients with normal echocardiograms who are monitored over time. In a study of 50 patients with dcSSc, Markousis-Mavrogenis et al. found that baseline LGE, LV mass, T2 mapping (a measure of edema) and ECV values were all significant predictors of CV complications (arrythmia, heart failure, pulmonary hypertension, and/or sudden cardiac death)

over 1.2 years, including when data were controlled for sex, age, and duration of disease (64).

Similar to stress echocardiography, stress CMR may be more sensitive than rest CMR in detecting subclinical disease. Asymptomatic patients with SSc show evidence of significantly decreased myocardial perfusion on adenosine stress CMR when compared to controls, even when there is no difference on rest CMR (65). An additional study found that, of those patients with stress CMR perfusion defects, none had correlating stenotic lesions on coronary CT, suggesting that microvascular disease, rather than epicardial CAD, may be the primary driver of hypoperfusion in SSc (66).

PERICARDIAL DISEASE

Pericardial disease is a common feature of scleroderma, with manifestations including pericardial inflammation, effusion, fibrinous pericarditis, pericardial adhesions, and rarely constrictive pericarditis or tamponade (1, 67). The prevalence of clinically apparent pericardial disease is 5–16%, but autopsy studies suggest the incidence of asymptomatic involvement may be higher (1). Contemporary imaging studies suggest the incidence of pericardial effusion is between 15 and 19% (68, 69). Large effusions and those complicated by tamponade are rare but associated with poor outcomes (70). Drainage of these effusions or creation of a pericardial window in the context of associated PAH is associated with significant mortality (70, 71). Constrictive pericarditis represents a challenging diagnosis in this population as clinical symptoms may not be present until right-heart failure develops, and symptoms may overlap with signs of PAH and SSc-associated cardiomyopathy. For this reason, among others, a multimodality imaging approach is important in the assessment of pericardial disease (72).

Evaluation

The diagnostic approach for patients with pericardial disease and SSc is the same for those without associated SSc. All patients should receive an electrocardiogram and transthoracic echocardiogram. In select patients, further imaging with CT or CMR may be helpful.

Electrocardiography

In acute pericarditis, the EKG may demonstrate classic findings such as diffuse ST segment elevations and PR segment depressions, but up to 40% present with atypical and non-diagnostic findings (73). For those with small to moderate pericardial effusions, there may be no EKG changes. In large pericardial effusions, low voltage and electrical alternans may be present (74).

Echocardiography

2DE is considered the first line imaging modality in almost all types of pericardial disease because it is safe, readily available, and quick to perform (74). 2DE allows for detection of pericardial effusion and assessment of effusion size. It also can assess for hemodynamic features of tamponade, including diastolic collapse of right-sided chambers, significant respirophasic changes across the mitral and tricuspid valves, and ventricular interdependence with abnormal septal bounce during inspiration (75). Tissue Doppler imaging is especially helpful in the diagnosis of constrictive pericarditis. A high early (E) velocity, shortened deceleration time, and reduced atrial (A) wave are characteristic. With inspiration, mitral inflow velocity typically falls by 25–40%, while tricuspid velocity increases by 40–60% (75). STE may also be useful in this assessment, with reduced circumferential strain and preserved global longitudinal strain consistent with constriction (75). In addition, 3DE is useful in better delineating the extent of pericardial thickening and the exact size, location, and extent of stranding within the pericardial effusion (76). Because many patients with acute pericarditis may have a normal 2DE (75), additional imaging modalities such as CMR or CT may be helpful if clinical suspicion is high.

Computed Tomography

Computed tomography attenuation of the pericardium is similar to the myocardium so visualization of the pericardium can be challenging on CT. However, pericardial calcifications are well visualized on CT. CT density measurements facilitate the characterization of pericardial fluid; low density fluid [0–20 Hounsfield Units (HU)] is typical, while hemorrhagic effusions or those associated with bacterial infections may have densities of 50 HU or more (74). Because of the similar attenuation of myocardium and pericardium on CT, echocardiography and CMR are typically preferred.

Cardiovascular Magnetic Resonance

Due to its high inherent tissue contrast, excellent spatial and temporal resolution, and ability to reconstruct in multiple planes, CMR is well-suited for the evaluation of pericardial disease (77). While not necessary for the diagnosis of acute pericarditis, CMR can be helpful for those with incessant (ongoing symptoms >4–6 weeks, but <3 months), recurrent, or chronic (>3 months) of symptoms, or those in which clinical suspicion is high but initial evaluation (EKG, echo) has been negative. Pericardial thickening is readily viewed, and pericardial edema and inflammation can be evaluated by both T2-weighted LGE imaging (77). Fat suppression can increase the specificity of these findings. CMR has been used to guide steroid therapy in recurrent pericarditis, leading to lower overall steroid doses without an increased risk of constrictive pericarditis or need for pericardial window, and with lower rates of recurrence (78).

Constrictive pericarditis typically presents with thickening of the pericardium, which is best appreciated on T1-weighted imaging. However up to 18% of patients may have normal pericardial thickness (79). Pericardial fusion in the absence of active inflammation and parietal-visceral adherence are indicative of constrictive pericarditis (80, 81). Hemodynamic indicators of constriction are also well visualized on CMR; respiratory flow variation across the mitral valve greater than 25% is sensitive and specific for constriction, as is increased relative septal excursion (82, 83). While echocardiography remains the standard, consider CMR imaging when concern for pericarditis

TABLE 1 | Applications, strengths, and weaknesses of common diagnostic modalities in scleroderma heart disease.

	Imaging Modalities			Adjunctive Modalities	
SSc Disease Process	**Echo**	**CT**	**CMR**	**EKG**	**RHC**
RV Dysfunction	Initial screening tool. Assesses for: • chamber enlargement • diastolic dysfunction (TV E/A) • systolic function (TAPSE, FAC, RVEF by 3DE) • RV hemodynamics (RVSP) • subclinical disease (strain, exercise stress echo)	Often in conjunction with pulmonary imaging. Assesses for: • Chamber size, hypertrophy • RVEF • RV pressure and volume overload (septal flattening, increased RV-LV ratio)	Gold standard for assessing RV given complicated 3D geometry. Assesses for: • chamber enlargement • diastolic dysfunction (RV mass, hypertrophy) • systolic function (RVEF) • RV hemodynamics (RVSP) • subclinical disease (strain) • fibrosis and edema (T1 mapping, T2 mapping, ECV)	Signs of RVH, RV strain	Direct measurement of RV systolic and diastolic pressure, assessment of cardiac output
PAH	Initial screening tool. Provides estimates of PASP based on TV regurgitant jet velocity.	Cannot directly estimate pressure but may demonstrate increased PA diameter and signs of RV strain.	Like echo, provides estimates of PASP using estimates of TV regurgitant jet velocity.	Signs of RVH, RV strain	Gold standard for hemodynamic assessment of PH. Allows for differentiation among WHO groups
LV Dysfunction	Initial screening tool. Assesses for: • chamber enlargement • diastolic dysfunction (MV E/A) • systolic function (LVEF by 3DE) • subclinical disease (strain) • contractility via stress echo	Adjunct tool in selected cases. Assesses for: • chamber enlargement • systolic function (LVEF) • epicardial coronary disease (coronary CT)	Adjunct tool in selected cases. Assesses for: • chamber enlargement • diastolic dysfunction (LV mass, LV hypertrophy, LA size) • systolic function (LVEF) • subclinical disease (strain) • fibrosis and edema (LGE, T1 mapping, T2 mapping, ECV) • perfusion via stress cMR	Signs of LVH	Assessment of cardiac output and wedge pressure, which can reveal elevated LV filling pressures in diastolic dysfunction and PVH due to left heart disease
Pericardial Disease	Initial screening tool. Assesses for: • effusion • tamponade (diastolic collapse of RV, respirophasic changes across MV and TV, ventricular interdependence) • constriction (high E velocity, reduced A wave, decreased MV inflow velocity, increased TV velocity)	Pericardial calcifications, density assessment of fluid	Adjunct tool in selected cases. Assesses for: • effusion • pericardial thickening • pericardial edema and inflammation (T2 images, LGE) • constriction (respiratory flow variation across the mitral valve, septal excursion)	Diffuse ST segment elevations and PR segment depressions, electrical alternans and low voltage in large effusions	End-diastolic equalization of pressures across cardiac chambers in constriction; the stiffened pericardium limits expansion and exerts equal pressure on all chambers (requires concurrent R + LHC)
Arrhythmia	Provides initial assessment of cardiac structure and function in the setting of arrhythmia	N/A	Edema (T2 ratio) and fibrosis (%LGE) may predict ventricular arrhythmias	PVCs, conduction disease, atrial and ventricular arrhythmias	N/A
Strengths	Cheap, widely available. No radiation	Evaluation of underlying etiology of RV dysfunction/PAH (ILD, CTEPH). Not reliant on acoustic windows	Not reliant on acoustic windows. No radiation. Images can be reconstructed in any plane	Cheap, widely available	Gold standard assessment for PH
Limitations	Complex geometry of RV limits evaluation. Operator dependent. Requires adequate acoustic windows. Novel techniques such as STE require additional time, resources, and expertise	Radiation exposure. Limited assessment of hemodynamics. Motion artifact particularly at high heart rates	Limited availability. Expensive. Significant expertise required in acquisition and interpretation. Long examination time. Requires frequent breath holding. Sensitive, but findings often non-specific for SSc and require careful clinical correlation	Not highly sensitive or specific for any disease	Provides no information about morphology. Invasive

SSc, systemic sclerosis; echo: echocardiography; CT, computed tomography; cMR, cardiovascular magnetic resonance; EKG, electrocardiography; RHC, right heart catheterization; RV, right ventricle; TV, tricuspid valve; E/A; peak velocity in early diastole (E wave) to peak velocity flow in late diastole (atrial contraction, A wave); TAPSE, tricuspid annular plane systolic excursion; FAC, fractional area change; EF, ejection fraction; 3DE, three-dimensional echocardiography; RVSP, right ventricular systolic pressure; LV, left ventricle; ECV, extracellular volume; RVH, right ventricular hypertrophy; PAH, pulmonary arterial hypertension; PASP, pulmonary artery systolic pressure; PA, pulmonary artery; WHO, World Health Organization; MV; mitral valve; LVEF, left ventricular ejection fraction; LGE, late gadolinium enhancement; LVH, left ventricular hypertrophy; PVH, pulmonary venous hypertension; PVC, premature ventricular contractions; ILD, interstitial lung disease; CTEPH, chronic thromboembolic pulmonary hypertension; PH, pulmonary hypertension; STE, speckle-tracking echocardiography.

is high but echocardiography is unrevealing, or when symptoms of pericarditis persist or recur over months.

Catheterization

Invasive hemodynamic measurement of right and left ventricular pressure measurement is also important in the assessment of constriction. The "dip and plateau" sign (end-diastolic equalization of pressures), while not specific to constriction, can help confirm the diagnosis in the right clinical context (74).

ARRHYTHMIA

Electrophysiologic studies of patients with SSc report conduction defects, arrhythmia, and autonomic dysfunction in up to 51% of patients (6). Atrial and ventricular ectopy, atrial fibrillation and flutter, supraventricular tachycardia, ventricular tachycardia, and atrioventricular block have all been associated (6). In a recent study from a Danish cohort, there was a nearly two-fold relative risk increase for incident atrial fibrillation and flutter as well as pacemaker or ICD placement in patients with SSc compared to age-matched controls (84). In the EUSTAR database, arrhythmias caused 6% of SSc-related deaths, behind only pulmonary fibrosis and PAH (85). The mechanism of this is thought to be multifold- the direct consequences of microvascular injury, the effects of fibrosis in the conduction system and myocardium, and autonomic dysfunction (51, 86). Importantly, autonomic dysfunction occurs early in the disease course, even before the development of fibrosis or other visceral manifestations. Low heart rate variability is a marker of autonomic dysfunction and is correlated with pre-clinical cardiac involvement (86).

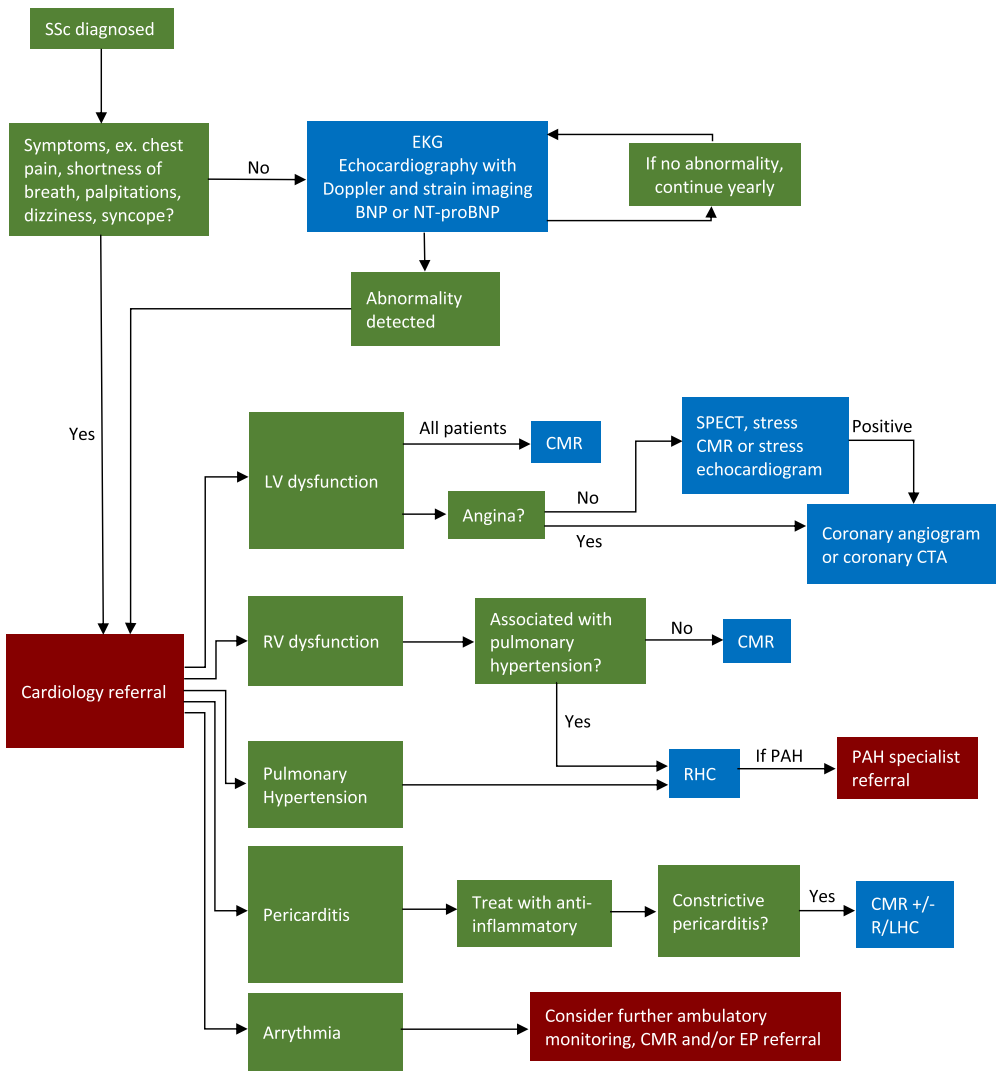

FIGURE 4 | Algorithm for screening and workup of cardiovascular disease in SSc patients. CMR, cardiovascular magnetic resonance; SSc, systemic sclerosis; EKG, electrocardiogram; LV, left ventricle; RV, right ventricle; RHC, right heart catheterization; LHC, left heart catheterization; EP, electrophysiology; CTA, computed tomography angiography; PAH, pulmonary arterial hypertension; SPECT, single photon emission computed tomography.

Evaluation

Arrhythmia is assessed by EKG and cardiac monitoring as indicated. 2DE and CMR can be useful adjuncts to detect structural or functional disease that may contribute to the arrhythmia.

Electrocardiography

Screening EKG should be performed in all patients with SSc (51). While not a particularly sensitive test, this can help identify both conduction abnormalities and signs of hypertrophy as well as chamber enlargement. Right bundle branch block has been associated with a greater than five-fold increase in mortality risk, thought to be reflective of either underlying lung pathology or cardiac involvement (87). In a study of 100 SSc patients investigated with new onset heart failure, 56% had EKG abnormalities and 24% had PVCs. The PVC burden corresponded positively with high-sensitivity troponin and negatively with LV ejection fraction. Seven patients in this study either suffered sudden cardiac death or required ICD placement; the presence of more than 1190 PVCs/day identified these patients with a sensitivity of 100% and specificity of 83% (88). Prolonged QTc interval and QT dispersion may also predict ventricular arrhythmias, as might an abnormal signal-averaged EKG (SAE) (89, 90). Holter monitoring should be utilized if there is any clinical concern for conduction abnormality, and there should be a low threshold for implantable loop recorder placement in the appropriate clinical context (51).

Echocardiography and Cardiovascular Magnetic Resonance

All patients with scleroderma should receive a routine screening echo, regardless of the presence or absence of arrhythmia. The recently published Scleroderma Arrhythmia Clinical Utility Study (SAnCtUS) evaluated 150 consecutive SSc patients assessed with 24-h Holter and CMR, looking at markers of LV function, edema (T2 mapping) and fibrosis (LGE). T2 mapping and LGE were significant predictors for ventricular arrhythmias, but not supraventricular arrhythmias. Using these CMR variables, the study developed the SAnCtUS score to predict risk of ventricular arrhythmia. The authors found that those with the highest score, independent of ejection fraction or the presence of ventricular tachycardia on baseline Holter, were 3.86 times more likely to have sustained ventricular tachycardia or sudden cardiac death at one year compared to those with lower scores (91). These data suggest a possible role for CMR to risk stratify patients for life threatening arrhythmias in the future, but this requires further evaluation and prior to incorporation into routine clinical care.

As evident in the discussion above, cardiac imaging modalities offer different but often complementary data in the evaluation of the SSc patient. Understanding the strengths and weaknesses of each diagnostic test is necessary when deciding how best to manage a particular symptom or abnormal finding. We have summarized the utility of each modality, along with their strengths and weaknesses, for the most common cardiac complications of SSc in **Table 1**.

Given the abundance of diagnostic options, some nuance is required when approaching a patient with newly diagnosed with SSc. Due to the high prevalence of subclinical cardiac disease in SSc and the low risk and relatively low cost of EKG, BNP or NT-proBNP, and echocardiography, it is reasonable to perform these tests annually. Echocardiography should be performed with Doppler and STE when possible. If further imaging is needed, patients with SSc should be referred to a cardiologist, preferably one with expertise in SSc cardiac disease, who can help guide appropriate and cost-effective management. With that in mind, it is worth noting that that CMR must be interpreted with care. CMR is highly sensitive, but abnormalities found in SSc such as LGE, elevated ECV, and abnormal strain, are not specific for SSc and can be found in a number of diseases (92). Imaging findings must be interpreted while considering the entirety of the clinical context to ensure accurate diagnosis. For this, among other reasons, referral to a cardiologist with SSc experience is ideal.

Of course, the approach will depend on which signs and symptoms are present, as well as the resources and expertise of a given center. With those caveats, we have outlined our approach to cardiac evaluation of the SSc patient in **Figure 4**. While this approach is based on the current literature, further studies are needed to determine whether this strategy is one that is centered on improvement in patient outcomes.

FUTURE DIRECTIONS

There are many novel therapeutics under investigation for use in scleroderma. While none appear specifically targeted toward myocardial involvement, they may impact cardiac disease through anti-inflammatory, anti-fibrotic, vascular/endothelial pathways (93, 94). Cardiovascular imaging has the potential to play an important role in the evaluation of these agents.

Cardiovascular imaging is increasingly being considered as an adjunct to clinical trials. Imaging can help improve patient selection by identifying those with the therapeutic target (i.e., pericardial inflammation or RV systolic dysfunction). It can help determine the baseline distribution of prognostic factors (such as myocardial fibrosis) in treatment and control arms and help shed light on mechanism of disease or response to therapy (95, 96). It can also serve as a measure of efficacy in phase II or phase III trials, helping inform larger randomized controlled trials of hard clinical outcomes. For all these reasons, imaging may play an increasingly important role in the evaluation of therapeutics for SSc.

As an example, a recent meta-analysis identified reduced RV ejection fraction and increased RV volumes as markers of risk for clinical worsening and mortality in patients with PAH; markers that could potentially be used as end points in clinical trials (97). In patients with SSc-PAH, Sato et al. showed that upfront combination therapy with tadalafil and ambrisentan improved CMR-derived LV and RV strain and this correlated with improvement in clinical outcomes, including WHO functional class, 6MWD, NT-proBNP, and invasive hemodynamic markers (38). However, these data were all collected as small case-control, case series, or single-arm studies. Incorporating CMR data into

randomized, double-blind, placebo-controlled trials of SSc-PAH therapies with both imaging and clinical outcomes may yield vital information. First, it would help definitively establish the relationship between imaging markers of disease and clinical endpoints. Second, as discussed above, it may help establish meaningful thresholds in CMR markers for clinical monitoring or future trials, as well as mechanistic insights into PAH pathophysiology.

While PAH has served a model for this discussion, one can imagine CMR being incorporated into randomized controlled trials of other SSc-related cardiac pathology. For instance, randomized controlled trials examining treatment effects of novel anti-inflammatories in SSc-related pericarditis may measure recurrence rates and persistence of symptoms as well as CMR markers of pericardial inflammation on follow-up. Trials of novel anti-fibrotics such as pirfenidone in SSc-related cardiac fibrosis may assess arrhythmia burden as well as CMR measures of fibrosis. By including these imaging endpoints, trials can help definitively connect imaging to outcomes, enabling confident use of surrogate endpoints going forward and facilitating clinical monitoring of disease.

Use of artificial intelligence continues to proliferate in imaging generally and it will undoubtedly impact SSc care. Already deep learning techniques are being used to aid in tissue segmentation and identification of fibrosis (98). Given the prominent role fibrosis plays in SSc and particularly arrhythmia risk, automated techniques may allow for earlier identification of at risk individuals. Algorithms are being developed to aid in motion and deformation pattern analysis (98), which may allow for earlier detection of subtle abnormalities, especially in the geometrically complex RV. Finally, learning algorithms combining both clinical and imaging may be helpful in guiding treatment selection and predicting response (98). Given the complexity of the disease and its multiple treatment options, SSc may prove a fertile ground for these types of studies.

CONCLUSION

Cardiac complications of SSc are common, varied, and impact heavily on patient outcomes. We have reviewed the evidence supporting the use of cardiac imaging in the evaluation and management of SSc heart disease and have offered our own approach to caring for the SSc patient based on current literature. While cardiac imaging is already foundational in that evaluation, we anticipate it will assume growing importance in the years to come.

AUTHOR CONTRIBUTIONS

PG, SH, and TH contributed to the literature review and drafting the manuscript and figures. BF provided editorial revision. All authors contributed to the article and approved the submitted version.

REFERENCES

1. Champion HC. The heart in scleroderma. *Rheum Dis Clin North Am.* (2008) 34:181–viii.
2. Rangarajan V, Matiasz R, Freed BH. Cardiac complications of systemic sclerosis and management: recent progress. *Curr Opin Rheumatol.* (2017) 29:574–84. doi: 10.1097/BOR.0000000000000439
3. Nihtyanova SI, Schreiber BE, Ong VH, Rosenberg D, Moinzadeh P, Coghlan JG, et al. Prediction of pulmonary complications and long-term survival in systemic sclerosis. *Arthritis Rheumatol.* (2014) 66:1625–35. doi: 10.1002/art.38390
4. Komócsi A, Vorobcsuk A, Faludi R, Pintér T, Lenkey Z, Költo G, et al. The impact of cardiopulmonary manifestations on the mortality of SSc: a systematic review and meta-analysis of observational studies. *Rheumatology (Oxford).* (2012) 51:1027–36. doi: 10.1093/rheumatology/ker357
5. Elhai M, Meune C, Avouac J, Kahan A, Allanore Y. Trends in mortality in patients with systemic sclerosis over 40 years: a systematic review and meta-analysis of cohort studies. *Rheumatology.* (2011) 51:1017–26. doi: 10.1093/rheumatology/ker269
6. Bissell LA, Md Yusof MY, Buch MH. Primary myocardial disease in scleroderma-a comprehensive review of the literature to inform the UK systemic sclerosis study group cardiac working group. *Rheumatology (Oxford).* (2017) 56:882–95. doi: 10.1093/rheumatology/kew364
7. Fernández-Codina A, Simeón-Aznar CP, Pinal-Fernandez I, Rodríguez-Palomares J, Pizzi MN, Hidalgo CE, et al. Cardiac involvement in systemic sclerosis: differences between clinical subsets and influence on survival. *Rheumatol Int.* (2017) 37:75–84. doi: 10.1007/s00296-015-3382-2
8. Meune C, Khanna D, Aboulhosn J, Avouac J, Kahan A, Furst DE, et al. A right ventricular diastolic impairment is common in systemic sclerosis and is associated with other target-organ damage. *Semin Arthritis Rheum.* (2016) 45:439–45. doi: 10.1016/j.semarthrit.2015.07.002
9. Meune C, Allanore Y, Devaux JY, Dessault O, Duboc D, Weber S, et al. High prevalence of right ventricular systolic dysfunction in early systemic sclerosis. *J Rheumatol.* (2004) 31:1941–5.
10. Mukherjee M, Chung SE, Ton VK, Tedford RJ, Hummers LK, Wigley FM, et al. Unique abnormalities in right ventricular longitudinal strain in systemic sclerosis patients. *Circ Cardiovasc Imaging.* (2016) 9:e003792. doi: 10.1161/CIRCIMAGING.115.003792
11. Belin RJ, Varga J, Collins JD, Freed BH. Right ventricular cardiomyopathy in systemic sclerosis. *Rheumatology (Oxford).* (2017) 56:1045–7. doi: 10.1093/rheumatology/kew494
12. Steen VD, Medsger TA. Changes in causes of death in systemic sclerosis, 1972-2002. *Ann Rheum Dis.* (2007) 66:940–4. doi: 10.1136/ard.2006.066068
13. Tedford RJ, Mudd JO, Girgis RE, Mathai SC, Zaiman AL, Housten-Harris T, et al. Right ventricular dysfunction in systemic sclerosis-associated pulmonary arterial hypertension. *Circ Heart Fail.* (2013) 6:953–63. doi: 10.1161/CIRCHEARTFAILURE.112.000008
14. Haque A, Kiely DG, Kovacs G, Thompson AAR, Condliffe R. Pulmonary hypertension phenotypes in patients with systemic sclerosis. *Eur Respir Rev.* (2021) 30:210053. doi: 10.1183/16000617.0053-2021
15. Kylhammar D, Persson L, Hesselstrand R, Radegran G. Prognosis and response to first-line single and combination therapy in pulmonary arterial hypertension. *Scand Cardiovasc J.* (2014) 48:223–33. doi: 10.3109/14017431.2014.931595
16. Benza RL, Miller DP, Gomberg-Maitland M, Frantz RP, Foreman AJ, Coffey CS, et al. Predicting survival in pulmonary arterial hypertension: insights from the registry to evaluate early and long-term pulmonary arterial hypertension disease management (REVEAL). *Circulation.* (2010) 122:164–72. doi: 10.1161/CIRCULATIONAHA.109.898122
17. Cucuruzac R, Muntean I, Benedek I, Mester A, Rat N, Mitre A, et al. Right ventricle remodeling and function in scleroderma patients. *Biomed Res Int.* (2018) 2018:4528148. doi: 10.1155/2018/4528148

18. Badesch DB, Tapson VF, McGoon MD, Brundage BH, Rubin LJ, Wigley FM, et al. Continuous intravenous epoprostenol for pulmonary hypertension due to the scleroderma spectrum of disease. A randomized, controlled trial. *Ann Intern Med.* (2000) 132:425–34. doi: 10.7326/0003-4819-132-6-200003210-00002
19. Attanasio U, Cuomo A, Pirozzi F, Loffredo S, Abete P, Petretta M, et al. Pulmonary hypertension phenotypes in systemic sclerosis: the right diagnosis for the right treatment. *Int J Mol Sci.* (2020) 21:4430. doi: 10.3390/ijms21124430
20. Bourji KI, Kelemen BW, Mathai SC, Damico RL, Kolb TM, Mercurio V, et al. Poor survival in patients with scleroderma and pulmonary hypertension due to heart failure with preserved ejection fraction. *Pulm Circ.* (2017) 7:409–20. doi: 10.1177/2045893217700438
21. Humbert M, Yaici A, de Groote P, Montani D, Sitbon O, Launay D, et al. Screening for pulmonary arterial hypertension in patients with systemic sclerosis: clinical characteristics at diagnosis and long-term survival. *Arthritis Rheum.* (2011) 63:3522–30. doi: 10.1002/art.30541
22. Galie N, Humbert M, Vachiery JL, Gibbs S, Lang I, Torbicki A, et al. 2015 ESC/ERS guidelines for the diagnosis and treatment of pulmonary hypertension: the joint task force for the diagnosis and treatment of pulmonary hypertension of the European society of cardiology (ESC) and the European respiratory society (ERS): endorsed by: association for European paediatric and congenital cardiology (AEPC), international society for heart and lung transplantation (ISHLT). *Eur Heart J.* (2016) 37:67–119. doi: 10.1093/eurheartj/ehv317
23. Takahama H, McCully RB, Frantz RP, Kane GC. Unraveling the RV ejection Doppler envelope: insight into pulmonary artery hemodynamics and disease Severity. *JACC Cardiovasc Imaging.* (2017) 10(10 Pt B):1268–77. doi: 10.1016/j.jcmg.2016.12.021
24. Argula RG, Karwa A, Lauer A, Gregg D, Silver RM, Feghali-Bostwick C, et al. Differences in right ventricular functional changes during treatment between systemic sclerosis-associated pulmonary arterial hypertension and idiopathic pulmonary arterial hypertension. *Ann Am Thorac Soc.* (2017) 14:682–9. doi: 10.1513/AnnalsATS.201608-655OC
25. French S, Amsallem M, Ouazani N, Li S, Kudelko K, Zamanian RT, et al. Non-invasive right ventricular load adaptability indices in patients with scleroderma-associated pulmonary arterial hypertension. *Pulm Circ.* (2018) 8:2045894018788268. doi: 10.1177/2045894018788268
26. Pigatto E, Peluso D, Zanatta E, Polito P, Miatton P, Bourji K, et al. Evaluation of right ventricular function performed by 3D-echocardiography in scleroderma patients. *Reumatismo.* (2015) 66:259–63. doi: 10.4081/reumatismo.2014.773
27. Zairi I, Mzoughi K, Jnifene Z, Kamoun S, Jabeur M, Ben Moussa F, et al. Speckle tracking echocardiography in systemic sclerosis: a useful method for detection of myocardial involvement. *Ann Cardiol Angeiol (Paris).* (2019) 68:226–31. doi: 10.1016/j.ancard.2018.08.027
28. Mercurio V, Mukherjee M, Tedford RJ, Zamanian RT, Khair RM, Sato T, et al. Improvement in right ventricular strain with ambrisentan and tadalafil upfront therapy in scleroderma-associated pulmonary arterial hypertension. *Am J Respir Crit Care Med.* (2018) 197:388–91. doi: 10.1164/rccm.201704-0789LE
29. Mukherjee M, Mercurio V, Hsu S, Mayer SA, Mathai SC, Hummers LK, et al. Assessment of right ventricular reserve utilizing exercise provocation in systemic sclerosis. *Int J Cardiovasc Imaging.* (2021) 37:2137–47. doi: 10.1007/s10554-021-02237-9
30. Rallidis LS, Papangelopoulou K, Anthi A, Tsangaris I, Varounis C, Makavos G, et al. The role of exercise Doppler echocardiography to unmask pulmonary arterial hypertension in selected patients with systemic sclerosis and equivocal baseline echocardiographic values for pulmonary hypertension. *Diagnostics (Basel).* (2021) 11:1200. doi: 10.3390/diagnostics11071200
31. Barison A, Gargani L, De Marchi D, Aquaro GD, Guiducci S, Picano E, et al. Early myocardial and skeletal muscle interstitial remodelling in systemic sclerosis: insights from extracellular volume quantification using cardiovascular magnetic resonance. *Eur Heart J Cardiovasc Imaging.* (2015) 16:74–80. doi: 10.1093/ehjci/jeu167
32. Hromadka M, Seidlerova J, Suchy D, Rajdl D, Lhotsky J, Ludvik J, et al. Myocardial fibrosis detected by magnetic resonance in systemic sclerosis patients – relationship with biochemical and echocardiography parameters. *Int J Cardiol.* (2017) 249:448–53. doi: 10.1016/j.ijcard.2017.08.072
33. Jankowich M, Abbasi SA, Vang A, Choudhary G. Right ventricular fibrosis is related to pulmonary artery stiffness in pulmonary hypertension: a cardiac magnetic resonance imaging study. *Am J Respir Crit Care Med.* (2019) 200:776–9. doi: 10.1164/rccm.201903-0580LE
34. Ntusi NA, Piechnik SK, Francis JM, Ferreira VM, Rai AB, Matthews PM, et al. Subclinical myocardial inflammation and diffuse fibrosis are common in systemic sclerosis–a clinical study using myocardial T1-mapping and extracellular volume quantification. *J Cardiovasc Magn Reson.* (2014) 16:21. doi: 10.1186/1532-429X-16-21
35. Simpson CE, Hassoun PM. Myocardial fibrosis as a potential maladaptive feature of right ventricle remodeling in pulmonary hypertension. *Am J Respir Crit Care Med.* (2019) 200:662–3. doi: 10.1164/rccm.201906-1154ED
36. Terrier B, Dechartres A, Gouya H, Ben Arfi M, Berezne A, Regent A, et al. Cardiac intravoxel incoherent motion diffusion-weighted magnetic resonance imaging with T1 mapping to assess myocardial perfusion and fibrosis in systemic sclerosis: association with cardiac events from a prospective Cohort study. *Arthritis Rheumatol.* (2020) 72:1571–80. doi: 10.1002/art.41308
37. Chaosuwannakit N, Makarawate P. Value of cardiac magnetic resonance imaging in systemic sclerosis. *Reumatologia.* (2018) 56:92–8. doi: 10.5114/reum.2018.75520
38. Sato T, Ambale-Venkatesh B, Lima JAC, Zimmerman SL, Tedford RJ, Fujii T, et al. The impact of ambrisentan and tadalafil upfront combination therapy on cardiac function in scleroderma associated pulmonary arterial hypertension patients: cardiac magnetic resonance feature tracking study. *Pulm Circ.* (2018) 8:2045893217748307. doi: 10.1177/2045893217748307
39. Gunther S, Jais X, Maitre S, Berezne A, Dorfmuller P, Seferian A, et al. Computed tomography findings of pulmonary venoocclusive disease in scleroderma patients presenting with precapillary pulmonary hypertension. *Arthritis Rheum.* (2012) 64:2995–3005. doi: 10.1002/art.34501
40. Antoniou KM, Margaritopoulos GA, Goh NS, Karagiannis K, Desai SR, Nicholson AG, et al. Combined pulmonary fibrosis and emphysema in scleroderma-related lung disease has a major confounding effect on lung physiology and screening for pulmonary hypertension. *Arthritis Rheumatol.* (2016) 68:1004–12. doi: 10.1002/art.39528
41. Cottin V, Nunes H, Brillet PY, Delaval P, Devouassoux G, Tillie-Leblond I, et al. Combined pulmonary fibrosis and emphysema: a distinct underrecognised entity. *Eur Respir J.* (2005) 26:586–93. doi: 10.1183/09031936.05.00021005
42. Launay D, Humbert M, Berezne A, Cottin V, Allanore Y, Couderc LJ, et al. Clinical characteristics and survival in systemic sclerosis-related pulmonary hypertension associated with interstitial lung disease. *Chest.* (2011) 140:1016–24. doi: 10.1378/chest.10-2473
43. Mathai SC, Hummers LK, Champion HC, Wigley FM, Zaiman A, Hassoun PM, et al. Survival in pulmonary hypertension associated with the scleroderma spectrum of diseases: impact of interstitial lung disease. *Arthritis Rheum.* (2009) 60:569–77. doi: 10.1002/art.24267
44. Khanna D, Zhao C, Saggar R, Mathai SC, Chung L, Coghlan JG, et al. Long-term outcomes in patients with connective tissue disease-associated pulmonary arterial hypertension in the modern treatment era: meta-analyses of randomized, controlled trials and observational registries. *Arthritis Rheumatol.* (2021) 73:837–47. doi: 10.1002/art.41669
45. Bulkley BH, Ridolfi RL, Salyer WR, Hutchins GM. Myocardial lesions of progressive systemic sclerosis. A cause of cardiac dysfunction. *Circulation.* (1976) 53:483–90. doi: 10.1161/01.cir.53.3.483
46. Mueller KA, Mueller II, Eppler D, Zuern CS, Seizer P, Kramer U, et al. Clinical and histopathological features of patients with systemic sclerosis undergoing endomyocardial biopsy. *PLoS One.* (2015) 10:e0126707. doi: 10.1371/journal.pone.0126707
47. Guerra F, Stronati G, Fischietti C, Ferrarini A, Zuliani L, Pomponio G, et al. Global longitudinal strain measured by speckle tracking identifies subclinical heart involvement in patients with systemic sclerosis. *Eur J Prev Cardiol.* (2018) 25:1598–606. doi: 10.1177/2047487318786315
48. Kepez A, Akdogan A, Sade LE, Deniz A, Kalyoncu U, Karadag O, et al. Detection of subclinical cardiac involvement in systemic sclerosis by echocardiographic strain imaging. *Echocardiography.* (2008) 25:191–7. doi: 10.1111/j.1540-8175.2007.00582.x
49. Poanta L, Dadu R, Tiboc C, Rednic S, Dumitrascu D. Systolic and diastolic function in patients with systemic sclerosis. *Eur J Intern Med.* (2009) 20:378–82. doi: 10.1016/j.ejim.2008.10.011

50. Wranicz J, Zielinska M, Cygankiewicz I, Dziankowska-Bartkowiak B, Sysa-Jedrzejowska A. Early cardiovascular involvement in patients with systemic sclerosis (SSc). *Med Sci Monit.* (2002) 8:CR78–82.
51. Bissell LA, Anderson M, Burgess M, Chakravarty K, Coghlan G, Dumitru RB, et al. Consensus best practice pathway of the UK systemic sclerosis study group: management of cardiac disease in systemic sclerosis. *Rheumatology (Oxford).* (2017) 56:912–21. doi: 10.1093/rheumatology/kew488
52. Papagoras C, Achenbach K, Tsifetaki N, Tsiouris S, Fotopoulos A, Drosos AA. Heart involvement in systemic sclerosis: a combined echocardiographic and scintigraphic study. *Clin Rheumatol.* (2014) 33:1105–11. doi: 10.1007/s10067-014-2666-3
53. Cadeddu C, Deidda M, Giau G, Lilliu M, Cadeddu F, Binaghi G, et al. Contractile reserve in systemic sclerosis patients as a major predictor of global cardiac impairment and exercise tolerance. *Int J Cardiovasc Imaging.* (2015) 31:529–36. doi: 10.1007/s10554-014-0583-9
54. Santas E, Garcia-Blas S, Minana G, Sanchis J, Bodi V, Escribano D, et al. Prognostic implications of tissue Doppler imaging-derived e/ea ratio in acute heart failure patients. *Echocardiography.* (2015) 32:213–20. doi: 10.1111/echo.12617
55. Hinchcliff M, Desai CS, Varga J, Shah SJ. Prevalence, prognosis, and factors associated with left ventricular diastolic dysfunction in systemic sclerosis. *Clin Exp Rheumatol.* (2012) 30(2 Suppl. 71):S30–7.
56. Stronati G, Manfredi L, Ferrarini A, Zuliani L, Fogante M, Schicchi N, et al. Subclinical progression of systemic sclerosis-related cardiomyopathy. *Eur J Prev Cardiol.* (2020) 27:1876–86. doi: 10.1177/2047487320916591
57. Karadag DT, Sahin T, Tekeoglu S, Isik OO, Yazici A, Eraldemir FC, et al. Evaluation of left and right ventricle by two-dimensional speckle tracking echocardiography in systemic sclerosis patients without overt cardiac disease. *Clin Rheumatol.* (2020) 39:37–48. doi: 10.1007/s10067-019-04604-3
58. Spethmann S, Rieper K, Riemekasten G, Borges AC, Schattke S, Burmester GR, et al. Echocardiographic follow-up of patients with systemic sclerosis by 2D speckle tracking echocardiography of the left ventricle. *Cardiovasc Ultrasound.* (2014) 12:13. doi: 10.1186/1476-7120-12-13
59. Lindholm A, Hesselstrand R, Radegran G, Arheden H, Ostenfeld E. Decreased biventricular longitudinal strain in patients with systemic sclerosis is mainly caused by pulmonary hypertension and not by systemic sclerosis per se. *Clin Physiol Funct Imaging.* (2019) 39:215–25. doi: 10.1111/cpf.12561
60. Mercurio V, Hinze AM, Hummers LK, Wigley FM, Shah AA, Mukherjee M. Essential hypertension worsens left ventricular contractility in systemic sclerosis. *J Rheumatol.* (2021) 48:1299–306. doi: 10.3899/jrheum.200873
61. Tzelepis GE, Kelekis NL, Plastiras SC, Mitseas P, Economopoulos N, Kampolis C, et al. Pattern and distribution of myocardial fibrosis in systemic sclerosis: a delayed enhanced magnetic resonance imaging study. *Arthritis Rheum.* (2007) 56:3827–36. doi: 10.1002/art.22971
62. Thuny F, Lovric D, Schnell F, Bergerot C, Ernande L, Cottin V, et al. Quantification of myocardial extracellular volume fraction with cardiac MR imaging for early detection of left ventricle involvement in systemic sclerosis. *Radiology.* (2014) 271:373–80. doi: 10.1148/radiol.13131280
63. Galea N, Rosato E, Gigante A, Borrazzo C, Fiorelli A, Barchetti G, et al. Early myocardial damage and microvascular dysfunction in asymptomatic patients with systemic sclerosis: a cardiovascular magnetic resonance study with cold pressor test. *PLoS One.* (2020) 15:e0244282. doi: 10.1371/journal.pone.0244282
64. Markousis-Mavrogenis G, Bournia VK, Panopoulos S, Koutsogeorgopoulou L, Kanoupakis G, Apostolou D, et al. Cardiovascular magnetic resonance identifies high-risk systemic sclerosis patients with normal echocardiograms and provides incremental prognostic value. *Diagnostics (Basel).* (2019) 9:220. doi: 10.3390/diagnostics9040220
65. Gyllenhammar T, Kanski M, Engblom H, Wuttge DM, Carlsson M, Hesselstrand R, et al. Decreased global myocardial perfusion at adenosine stress as a potential new biomarker for microvascular disease in systemic sclerosis: a magnetic resonance study. *BMC Cardiovasc Disord.* (2018) 18:16. doi: 10.1186/s12872-018-0756-x
66. Giacomelli R, Di Cesare E, Cipriani P, Ruscitti P, Di Sibio A, Liakouli V, et al. Pharmacological stress, rest perfusion and delayed enhancement cardiac magnetic resonance identifies very early cardiac involvement in systemic sclerosis patients of recent onset. *Int J Rheum Dis.* (2017) 20:1247–60. doi: 10.1111/1756-185X.13107
67. Lambova S. Cardiac manifestations in systemic sclerosis. *World J Cardiol.* (2014) 6:993–1005. doi: 10.4330/wjc.v6.i9.993
68. Meune C, Avouac J, Wahbi K, Cabanes L, Wipff J, Mouthon L, et al. Cardiac involvement in systemic sclerosis assessed by tissue-doppler echocardiography during routine care: a controlled study of 100 consecutive patients. *Arthritis Rheum.* (2008) 58:1803–9. doi: 10.1002/art.23463
69. Hachulla AL, Launay D, Gaxotte V, de Groote P, Lamblin N, Devos P, et al. Cardiac magnetic resonance imaging in systemic sclerosis: a cross-sectional observational study of 52 patients. *Ann Rheum Dis.* (2009) 68:1878–84. doi: 10.1136/ard.2008.095836
70. Dunne JV, Chou JP, Viswanathan M, Wilcox P, Huang SH. Cardiac tamponade and large pericardial effusions in systemic sclerosis. *Clin Rheumatol.* (2011) 30:433–8. doi: 10.1007/s10067-010-1667-0
71. Hemnes AR, Gaine SP, Wiener CM. Poor outcomes associated with drainage of pericardial effusions in patients with pulmonary arterial hypertension. *South Med J.* (2008) 101:490–4. doi: 10.1097/SMJ.0b013e31816c0169
72. Verhaert D, Gabriel RS, Johnston D, Lytle BW, Desai MY, Klein AL. The role of multimodality imaging in the management of pericardial disease. *Circ Cardiovasc Imaging.* (2010) 3:333–43. doi: 10.1161/CIRCIMAGING.109.921791
73. Chiabrando JG, Bonaventura A, Vecchié A, Wohlford GF, Mauro AG, Jordan JH, et al. Management of acute and recurrent pericarditis: JACC state-of-the-art review. *J Am Coll Cardiol.* (2020) 75:76–92. doi: 10.1016/j.jacc.2019.11.021
74. Cosyns B, Plein S, Nihoyanopoulos P, Smiseth O, Achenbach S, Andrade MJ, et al. European association of cardiovascular imaging (EACVI) position paper: multimodality imaging in pericardial disease. *Eur Heart J Cardiovasc Imaging.* (2014) 16:12–31. doi: 10.1093/ehjci/jeu128
75. Klein AL, Abbara S, Agler DA, Appleton CP, Asher CR, Hoit B, et al. American society of echocardiography clinical recommendations for multimodality cardiovascular imaging of patients with pericardial disease: endorsed by the society for cardiovascular magnetic resonance and society of cardiovascular computed tomography. *J Am Soc Echocardiogr.* (2013) 26:965–1012.e15. doi: 10.1016/j.echo.2013.06.023
76. Veress G, Feng D, Oh JK. Echocardiography in pericardial diseases: new developments. *Heart Fail Rev.* (2013) 18:267–75. doi: 10.1007/s10741-012-9325-z
77. Ho N, Nesbitt G, Hanneman K, Thavendiranathan P. Assessment of pericardial disease with cardiovascular MRI. *Heart Fail Clin.* (2021) 17:109–20. doi: 10.1016/j.hfc.2020.08.008
78. Alraies MC, AlJaroudi W, Yarmohammadi H, Yingchoncharoen T, Schuster A, Senapati A, et al. Usefulness of cardiac magnetic resonance-guided management in patients with recurrent pericarditis. *Am J Cardiol.* (2015) 115:542–7. doi: 10.1016/j.amjcard.2014.11.041
79. Talreja DR, Edwards WD, Danielson GK, Schaff HV, Tajik AJ, Tazelaar HD, et al. Constrictive pericarditis in 26 patients with histologically normal pericardial thickness. *Circulation.* (2003) 108:1852–7. doi: 10.1161/01.CIR.0000087606.18453.FD
80. Aquaro GD, Barison A, Cagnolo A, Todiere G, Lombardi M, Emdin M. Role of tissue characterization by cardiac magnetic resonance in the diagnosis of constrictive pericarditis. *Int J Cardiovasc Imaging.* (2015) 31:1021–31. doi: 10.1007/s10554-015-0648-4
81. Power JA, Thompson DV, Rayarao G, Doyle M, Biederman RW. Cardiac magnetic resonance radiofrequency tissue tagging for diagnosis of constrictive pericarditis: a proof of concept study. *J Thorac Cardiovasc Surg.* (2016) 151:1348–55. doi: 10.1016/j.jtcvs.2015.12.035
82. Thavendiranathan P, Verhaert D, Walls MC, Bender JA, Rajagopalan S, Chung YC, et al. Simultaneous right and left heart real-time, free-breathing CMR flow quantification identifies constrictive physiology. *JACC Cardiovasc Imaging.* (2012) 5:15–24. doi: 10.1016/j.jcmg.2011.07.010
83. Bolen MA, Rajiah P, Kusunose K, Collier P, Klein A, Popović ZB, et al. Cardiac MR imaging in constrictive pericarditis: multiparametric assessment in patients with surgically proven constriction. *Int J Cardiovasc Imaging.* (2015) 31:859–66. doi: 10.1007/s10554-015-0616-z
84. Butt SA, Jeppesen JL, Torp-Pedersen C, Sam F, Gislason GH, Jacobsen S, et al. Cardiovascular manifestations of systemic sclerosis: a Danish nationwide cohort study. *J Am Heart Assoc.* (2019) 8:e013405. doi: 10.1161/JAHA.119.013405

85. Tyndall AJ, Bannert B, Vonk M, Airò P, Cozzi F, Carreira PE, et al. Causes and risk factors for death in systemic sclerosis: a study from the EULAR scleroderma trials and research (EUSTAR) database. *Ann Rheumat Dis.* (2010) 69:1809–15. doi: 10.1136/ard.2009.114264
86. Othman KM, Assaf NY, Farouk HM, Aly Hassan IM. Autonomic dysfunction predicts early cardiac affection in patients with systemic sclerosis. *Clin Med Insights Arthritis Musculoskelet Disord.* (2010) 3:43–54. doi: 10.4137/cmamd.s4940
87. Draeger HT, Assassi S, Sharif R, Gonzalez EB, Harper BE, Arnett FC, et al. Right bundle branch block: a predictor of mortality in early systemic sclerosis. *PLoS One.* (2013) 8:e78808. doi: 10.1371/journal.pone.0078808
88. De Luca G, Bosello SL, Gabrielli FA, Berardi G, Parisi F, Rucco M, et al. Prognostic role of ventricular ectopic beats in systemic sclerosis: a prospective cohort study shows ECG indexes predicting the worse outcome. *PLoS One.* (2016) 11:e0153012. doi: 10.1371/journal.pone.0153012
89. Sebestyén V, Szűcs G, Páll D, Ujvárosy D, Ötvös T, Csige I, et al. Electrocardiographic markers for the prediction of ventricular arrhythmias in patients with systemic sclerosis. *Rheumatology.* (2020) 59:478–86. doi: 10.1093/rheumatology/kez644
90. Bissell L-A, Dumitru RB, Erhayiem B, Abignano G, Fent G, Kidambi A, et al. Abnormal electrophysiological testing associates with future incidental significant arrhythmia in scleroderma. *Rheumatology.* (2019) 59:899–900. doi: 10.1093/rheumatology/kez434
91. Mavrogeni S, Gargani L, Pepe A, Monti L, Markousis-Mavrogenis G, De Santis M, et al. Cardiac magnetic resonance predicts ventricular arrhythmias in scleroderma: the scleroderma arrhythmia clinical utility study (SAnCtUS). *Rheumatology (Oxford).* (2020) 59:1938–48. doi: 10.1093/rheumatology/kez494
92. Krumm P, Mueller KAL, Klingel K, Kramer U, Horger MS, Zitzelsberger T, et al. Cardiovascular magnetic resonance patterns of biopsy proven cardiac involvement in systemic sclerosis. *J Cardiovasc Magn Reson.* (2016) 18:70. doi: 10.1186/s12968-016-0289-3
93. McMahan ZH, Volkmann ER. An update on the pharmacotherapeutic options and treatment strategies for systemic sclerosis. *Expert Opin Pharmacother.* (2020) 21:2041–56. doi: 10.1080/14656566.2020.1793960
94. Campochiaro C, Allanore Y. An update on targeted therapies in systemic sclerosis based on a systematic review from the last 3 years. *Arthritis Res Ther.* (2021) 23:155. doi: 10.1186/s13075-021-02536-5
95. Pitcher A, Ashby D, Elliott P, Petersen SE. Cardiovascular MRI in clinical trials: expanded applications through novel surrogate endpoints. *Heart.* (2011) 97:1286–92. doi: 10.1136/hrt.2011.225904
96. Di Carli MF, Geva T, Davidoff R. The future of cardiovascular imaging. *Circulation.* (2016) 133:2640–61.
97. Alabed S, Shahin Y, Garg P, Alandejani F, Johns CS, Lewis RA, et al. Cardiac-MRI predicts clinical worsening and mortality in pulmonary arterial hypertension: a systematic review and meta-analysis. *JACC Cardiovasc Imaging.* (2021) 14:931–42. doi: 10.1016/j.jcmg.2020.08.013
98. Lekadir K, Leiner T, Young AA, Petersen SE. Editorial: current and future role of artificial intelligence in cardiac imaging. *Front Cardiovasc Med.* (2020) 7:137. doi: 10.3389/fcvm.2020.00137

Conflict of Interest: The authors declare that the research was conducted in the absence of any commercial or financial relationships that could be construed as a potential conflict of interest.

Publisher's Note: All claims expressed in this article are solely those of the authors and do not necessarily represent those of their affiliated organizations, or those of the publisher, the editors and the reviewers. Any product that may be evaluated in this article, or claim that may be made by its manufacturer, is not guaranteed or endorsed by the publisher.

frontiers | Frontiers in Cardiovascular Medicine

CASE REPORT
published: 29 April 2022
doi: 10.3389/fcvm.2022.845973

A Rare Case of Isolated Right Ventricular Non-compaction With the Novel *TTN* Mutation

*Piao-piao Huang†, Ya-xin Tang† and Xian-sheng Huang**

Department of Cardiovascular Medicine, The Second Xiangya Hospital, Central South University, Changsha, China

Isolated right ventricular non-compaction (RVNC) is rare yet life-threatening if left untreated, especially when accompanied by ventricular tachycardia. We describe a rare case of isolated RVNC, presenting as a prominent and excessive trabeculation of the right ventricle (RV), with an abnormal electrocardiogram. The transthoracic echocardiography, computed tomography, and ventricular angiography results clearly demonstrated an isolated spongy RV, both anatomically and functionally. Genetic testing identified a missense mutation of *TTN*. Combined, the diagnosis of RVNC was established. The subsequent combination of heart failure therapy, antiarrhythmic, and anticoagulation therapy were effective with a favorable outcome. This case report describes the possible etiology, manifestation, characteristic images, and problematic diagnostic criteria of the isolated RVNC. This case also emphasizes the necessity for comprehensive cardiac screening in familial cardiomyopathy.

Keywords: non-compaction, ventricular tachycardia, *TTN*, spongy heart, trabeculae

OPEN ACCESS

Edited by:
Andrew D. Choi,
George Washington University,
United States

Reviewed by:
Valeria Pergola,
University Hospital of Padua, Italy
Claudia Stöllberger,
Rudolfstiftung Hospital, Austria

****Correspondence:***
Xian-sheng Huang
huangxiansheng@csu.edu.cn

† These authors have contributed equally to this work and share first authorship

Specialty section:
This article was submitted to Cardiovascular Imaging, a section of the journal Frontiers in Cardiovascular Medicine

Received: *30 December 2021*
Accepted: *08 April 2022*
Published: *29 April 2022*

Citation:
Huang P-p, Tang Y-x and Huang X-s (2022) A Rare Case of Isolated Right Ventricular Non-compaction With the Novel TTN Mutation. Front. Cardiovasc. Med. 9:845973. doi: 10.3389/fcvm.2022.845973

INTRODUCTION

Ventricular non-compaction remains a genetically and phenotypically heterogeneous myocardial disorder with multiple possible concomitant phenotypes (1). Pathologically, it is characterized by excessive trabeculae and deep intertrabecular recesses in the ventricle. Non-compaction refers to the cessation of compaction of the loosely interwoven meshwork of myocardial fibers during intrauterine life, typically occurring in the left ventricle or bi-ventricle, and isolated RVNC is rare. The pathogenesis of ventricular non-compaction remains unclear. Genetics is believed to play an important role since genetic defects account for almost 40% of patients with ventricular non-compaction. However, studies have demonstrated that acquired causes are also expected, specifically in sporadic adults (2). Symptomatic individuals with ventricular non-compaction present varying degrees of heart failure, systemic thromboembolism, arrhythmia, or sudden cardiac death (SCD). Here, we present a case of an isolated RVNC, in which the first manifestation was syncope caused by VT.

CASE DESCRIPTION

A 61-year-old female patient was admitted to our hospital with exertional dyspnea and lower-extremity edema for 3 months. The patient's past medical history revealed hypertension for over

20 years, treated with oral nifedipine. Six years ago, the patient was admitted to a local hospital with several episodes of syncope. The patient noted feeling palpitation accompanied by perspiration and chest tightness; the symptoms had been recurrent. After admission to the local hospital, the patient underwent electrocardiogram (ECG) examination, echocardiography, and ventricle angiography. The ECG suggested VT and the ventricle angiography showed dilated right ventricle (LV) (**Figure 1**). Echocardiography revealed normal LV size and function. The initial diagnoses made by the local hospital were cardiomyopathy (undefined class) with VT. To reduce the risk of SCD, the patient received a single-chamber implantable cardioverter-defibrillator (ICD) at the local hospital. A single lead was also implanted in the RV (**Supplementary Figure 1**). Four years after the ICD implantation, the patient felt palpitations accompanied by discomfort in the precordial area. The ICD program recorded an attack of VT, which was terminated by ICD shock. The patient had no recurrence of such symptoms before admission to our hospital since then.

After admission to our hospital, physical examination showed severe pitting lower extremity edema. The laboratory test results were as follows: NT-proBNP, 1930.84 pg/ml (limit of reference, 0–125 pg/ml); troponin I, 472 ng/L (0–30.9 ng/L); fibrin degradation products, 49.33 μg/ml; and D-dimer, 17.23 ug/ml (0–0.5 μg/ml). Transthoracic echocardiography (TTE) revealed enlarged RV (RA, 36 mm; RV, 46 mm), right heart failure (tricuspid annular plane systolic excursion 9 mm, Tei index 0.27, RV-fractional area changes 22%), and typical features of spongy heart in the RV, including protruding trabecular muscles and deep intertrabecular recesses communicated with the RV cavity. Furthermore, the measured ratio of non-compacted to compacted myocardium (NC/C) was 2.7:1 (**Figure 2**). These findings suggested non-compaction in the RV. Furthermore, there were systolic blue regurgitation signals detected at the tricuspid orifice with a Vmax of 2.7 m/s, indicating tricuspid insufficiency (TI).

Ensuing, we reviewed the videos of coronary angiography from the local hospital, which demonstrated a smooth intima and no stenosis, excluding the possibility of obstructive coronary artery disease (**Supplementary Figure 2**). Ventricular angiography revealed a dilated RV, excessive trabeculae, and deep recesses with the feather-like retention of the contrast agent at the apex and outflow tract of RV. No abnormality was observed in the LV (**Figure 3**). However, the characteristic features of RVNC failed to attract the attention of the local doctors.

Due to the ICD, cardiac magnetic resonance (CMR) was not feasible; it was then substituted by Contrast Computed tomography (CT). The Contrast CT revealed multiple, protruding, low-density intracardiac trabeculae, high-density contrast agent in the intertrabecular recesses and RV cavity. The LV myocardium is slightly thickened, and the trabeculae is normal (**Figure 4**). Genetic testing identified a novel mutation (c.16799T > C/p.L5525S) in the exon 58 of titin gene (*TTN*, Ref Seq NM_001256850), which was predicted to be probably damaging by *in silico* prediction tools Polyphen2. The genetic implications further established the diagnosis of RVNC. Finally, isolated RVNC was diagnosed correctly by imaging and genetic testing results.

Subsequently, the patient was treated with loop diuretics for volume management, oral sacubitril/valsartan sodium for ventricular remodeling, amiodarone and metoprolol for arrhythmia and ICD shock prevention, and warfarin for embolism prevention. The patient's clinical symptoms markedly improved during hospitalization and within the 6 months of follow-up. The detailed timeline of this patient from symptom onset to follow-up is illustrated in **Figure 5**.

DISCUSSION

Isolated RVNC is not commonly reported. Ventricular non-compaction is associated with life-threatening complications, such as VT and systemic thromboembolism. The diagnosis of ventricular non-compaction was not considered by the local hospital when the patient manifested several episodes of syncope. Fortunately, the patient was treated in time and an ICD implantation was conducted to reduce the risk of SCD. The diagnostic criteria for ventricular non-compaction rely on non-invasive imaging examinations, such as TTE and CMR, which focus on the trabecular in the ventricle and the ratio of NC/C. At present, there are no diagnostic criteria for RVNC, and the diagnostic criteria for left ventricular non-compaction (LVNC) are mostly adopted clinically. Even so, overdiagnosis and overtreatment cannot be avoided. The prevalence rates in healthy populations who fulfill diagnostic criteria for LV non-compaction, proposed by Petersen et al. (3) (a ratio of NC/C greater than 2.3 at end-diastole) is up to 43%, raising concern about its disease status and the potential for overdiagnosis (4). Thus, population screening is generally ineffective. During the patient's hospitalization, a final diagnosis of isolated RVNC was made by a combined examination of ventricular angiography, TTE, and CT. For the differential diagnosis, it is necessary to distinguish RVNC from arrhythmogenic right ventricular cardiomyopathy (ARVC). ARVC mainly involves the RV and is characterized by gradual replacement of myocardial tissue by fibrous fat. In our case, the imaging results indicated the structure of the RV was excessive trabeculae and deep recesses, which did not conform to the pathological changes of ARVC. CMR could visualize ventricular structure and the tissue characterization clearly enough to distinguish between the two diseases. However, CMR was not performed in our hospital because of the non-diamagnetic model of the patient's ICD, and discontinuation of ICD during CMR scanning would put the patient at risk of ventricular tachycardia/fibrillation. A lack of CMR results is indeed a limitation of our case report. This case illustrates the crucial role of combined imaging examinations in the diagnosis of rare cardiomyopathy.

As the proband, the patient declared no history of syncope or SCD in her family. TTE screening was performed and no characteristic excessive trabeculae and deep intertrabecular recesses were found in any of the first-degree family members. Despite this, genetic testing in the setting of pathological

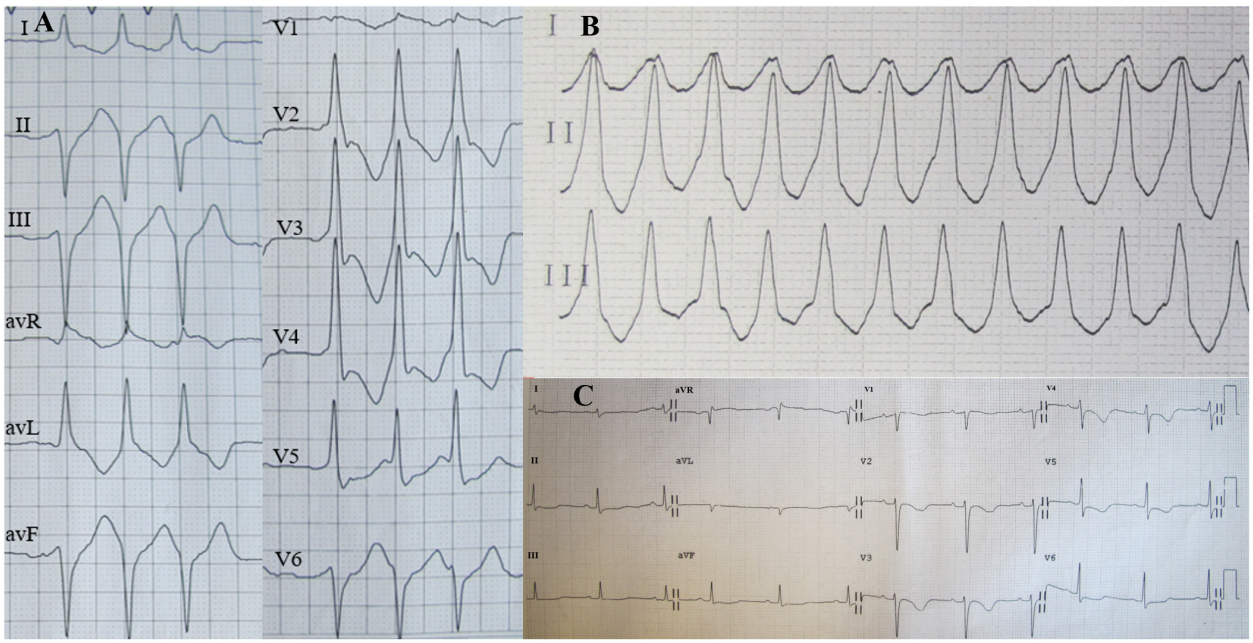

FIGURE 1 | Holter electrocardiogram (ECG) on admission showed three consecutive episodes of ventricular premature beats **(A)** and ventricular tachycardia (VT) **(B)**; Twelve-lead ECG after VT termination indicated sinus rhythm **(C)**.

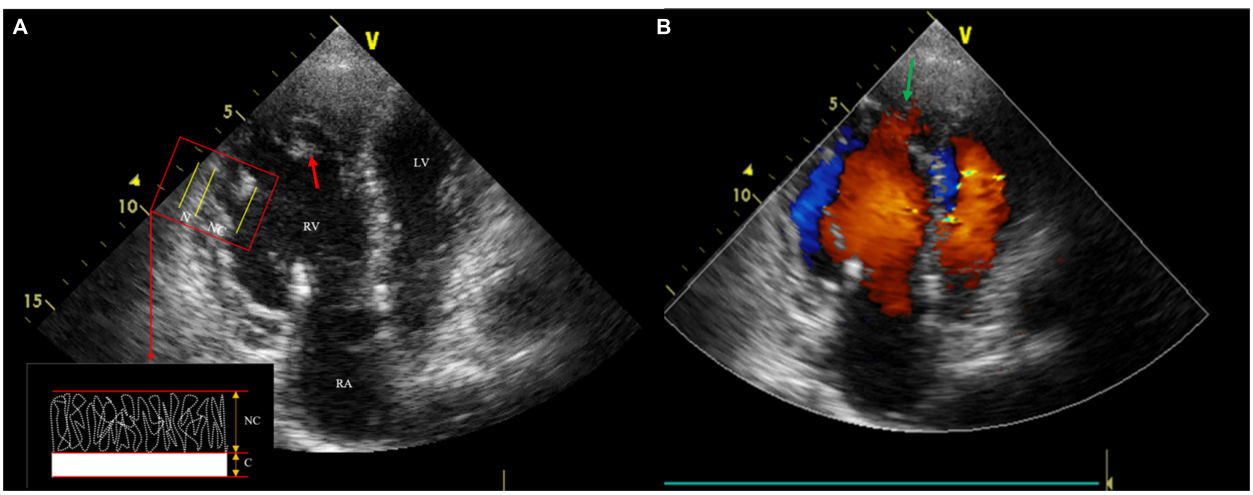

FIGURE 2 | Transthoracic echocardiography (TTE) shows three anatomical components, including thin compacted layer, prominent intracardiac trabeculae (the red arrow) and deep intertrabecular recesses. The measured ratio of non-compacted to compacted myocardium was 2.7:1 **(A)**; Color Doppler echocardiography reveals deep recesses communicated with the Right ventricle (RV) cavity (the green arrow) **(B)**.

non-compaction may contribute to the exact diagnosis and identification of at-risk relatives. Recently, accumulating studies have reported the genotype-phenotype correlations in patients with LVNC (2, 5). Ventricular non-compaction phenotype has been associated with more than 70 genes, such as *MYH7, ACTC1, MYBPC3, TNNT2, TPM1,* and *TTN* (6, 7). Among them, sarcomere genes, relevant for the structure of contractile and non-contractile elements with single missense mutations, are most commonly detected, accounting for the majority of genetic etiology of ventricle non-compaction (2, 8). The sarcomere gene consists of *MYH7, MYBPC3, TTN, ACTC1,* and so on (9). A meta-analysis indicated that the most frequently mutated genes in patients with LV non-compaction were *TTN* (11%), showing a pooled frequency of 11% (95% CI 4–29%) (10). In addition, sporadic cases of LVNC are prevalent in adults, indicating the contribution of acquired causes (2). Hence, the presumed mechanism of right heart failure in our patient is that the *TTN* gene

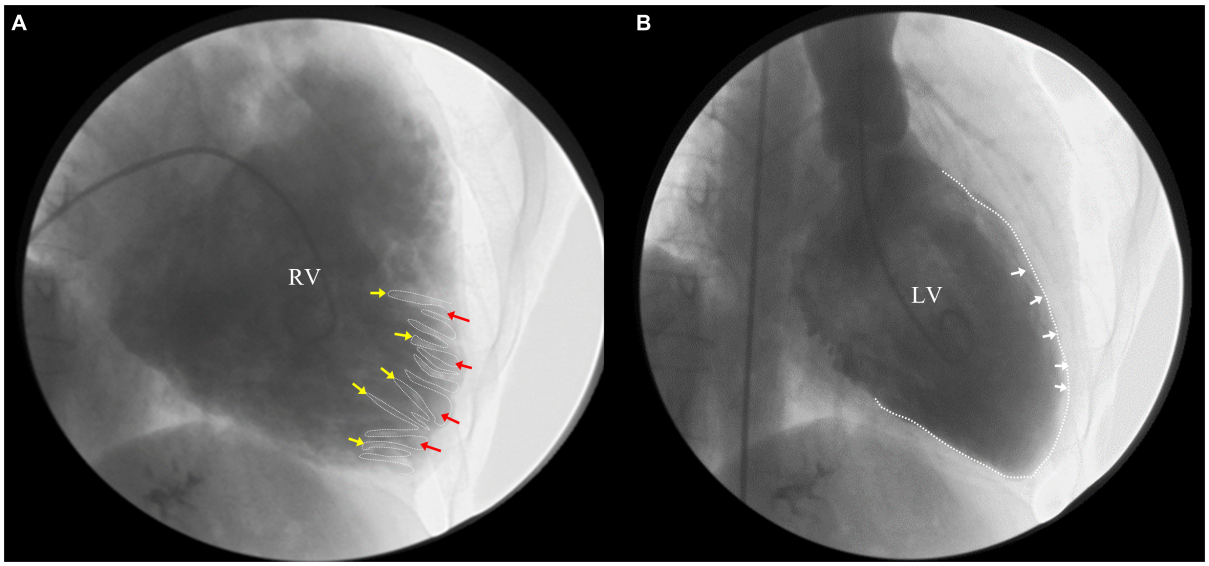

FIGURE 3 | Right ventricle (RV) angiography revealed a dilated RV, excessive trabeculae and deep recesses with the retention of contrast agent at the apex and outflow tract of RV **(A)** (yellow arrow: trabeculae; red arrow: deep intertrabecular recesses), while no abnormality in left ventricle (LV) **(B)**.

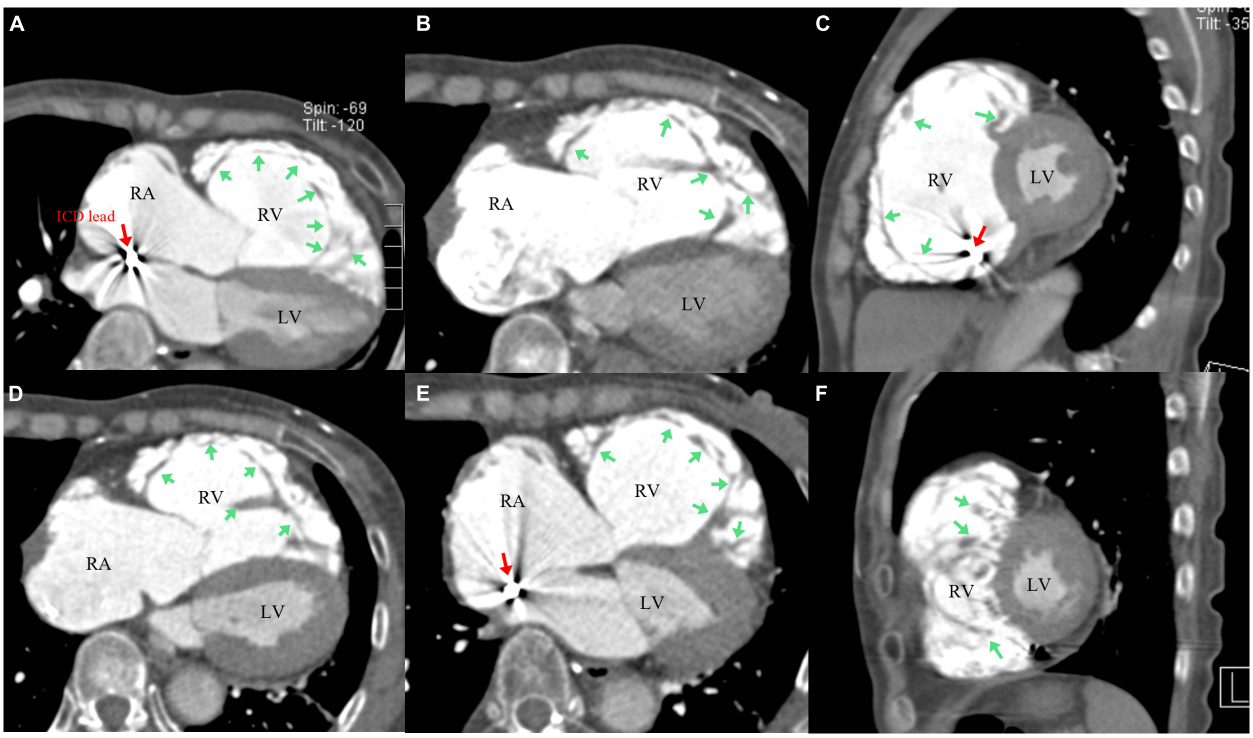

FIGURE 4 | Contrast Computed tomography (CT) revealed abnormally dilated right ventricle (RV) and right atrium (RA), multiple protruding low-density intracardiac trabeculae attached to wall of the RV, and the high-density contrast agent in intertrabecular recesses and RV cavity **(A–F)** [green arrow: trabeculae **(A–F)**; red arrow: ICD lead **(A,C,E)**]; The left ventricle (LV) myocardium is thickened, and the trabeculae is normal **(A–F)**.

missense mutation may terminate the compaction process of endocardial muscle trabecular muscle and result in non-compaction in RV, leading to reduced RV systolic function and severe right heart failure.

At present, the association between the clinical prognosis and genetics of non-compaction in adults remains controversial. Previous follow-up data on individuals with LVNC suggested no correlation between increased trabeculation and the development

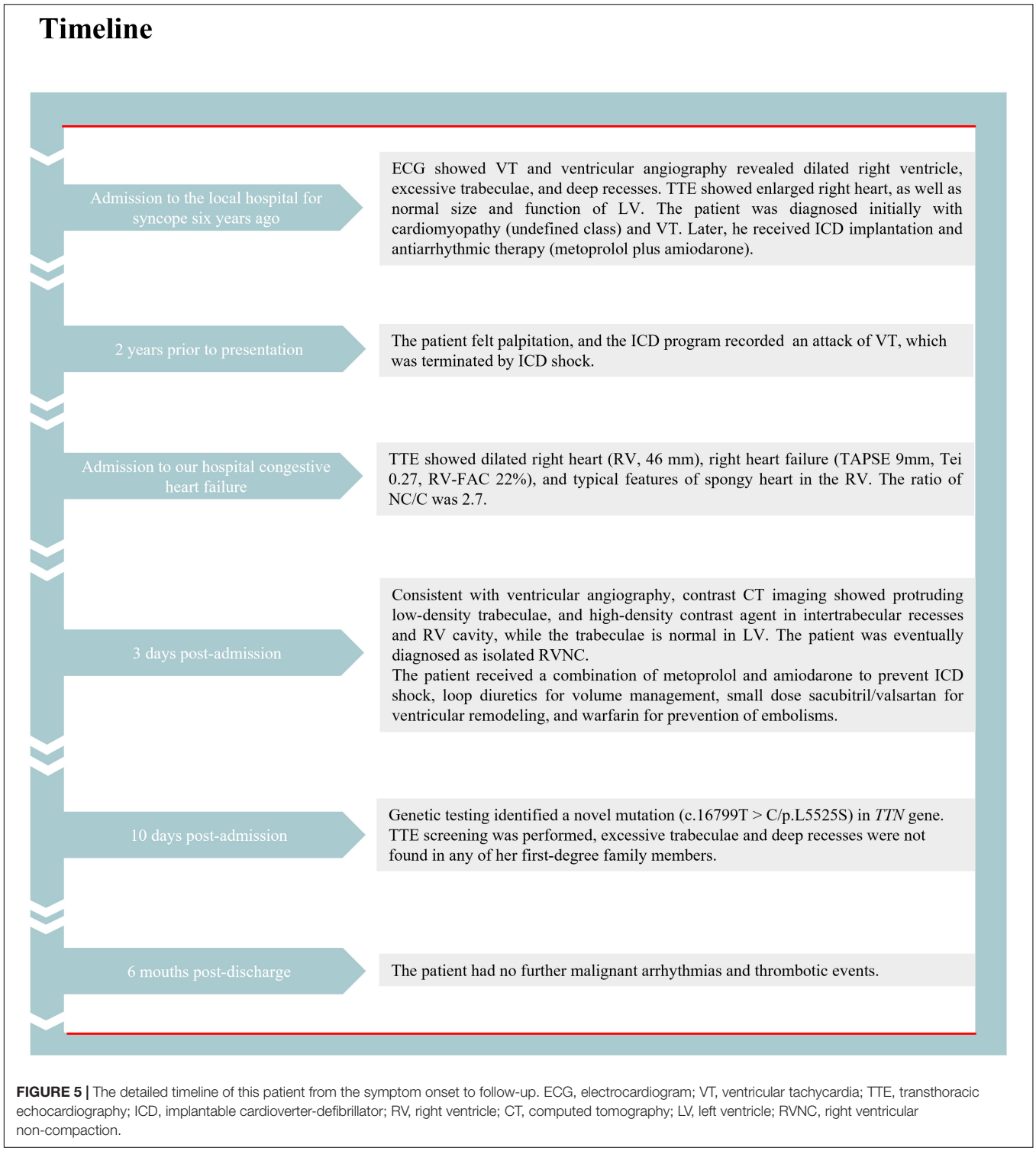

FIGURE 5 | The detailed timeline of this patient from the symptom onset to follow-up. ECG, electrocardiogram; VT, ventricular tachycardia; TTE, transthoracic echocardiography; ICD, implantable cardioverter-defibrillator; RV, right ventricle; CT, computed tomography; LV, left ventricle; RVNC, right ventricular non-compaction.

of diseases or adverse events (2, 11, 12). However, other evidence indicated carriers of pathogenic variants were more likely to develop adverse outcomes compared with non-carriers (58.5% vs. 25.8%; $P < 0.01$), and close follow-up for carriers was beneficial (1). Differences in screening genes and end points might partially explain the difference in these controversial results between these studies. Determining whether gene testing in adults with non-compaction can contribute to diagnostic issues and whether it benefits clinical treatment remains to be a major challenge for cardiologists.

Currently, there is no effective treatment for ventricular non-compaction. Strategies of therapy for confirmed patients are

mainly targeted at the three major complications: heart failure, arrhythmia, and thromboembolism. After ICD implantation and pharmaceutical treatment as previously discussed, the symptoms of our patient improved significantly, with a good prognosis.

CONCLUSION

We report a rare case of isolated RVNC that survived several episodes of syncope caused by VT. The patient was treated in time and correctly diagnosed through multi-imaging examinations and genetic testing. We recommended comprehensive cardiac screening for family members for earlier diagnosis and identification of at-risk relatives.

Isolated RVNC is rarely reported in current literature, causing possible underestimation of the incidence and severity of RVNC. Therefore, it is essential to identify and diagnose RVNC in clinical work.

DATA AVAILABILITY STATEMENT

The original contributions presented in the study are included in the article/**Supplementary Material**, further inquiries can be directed to the corresponding author/s.

ETHICS STATEMENT

Written informed consent was obtained from the patient for the publication of any potentially identifiable images or data included in this article.

AUTHOR CONTRIBUTIONS

All authors listed have made a substantial, direct, and intellectual contribution to the work, and approved it for publication.

FUNDING

This work was supported by the National Natural Science Foundation (81974281 and 81700999), the Natural Science Foundation of Hunan Province (2020JJ2052), and Chinese Cardiovascular Association-Access fund (2019-CCA-ACCESS-2020JJ2052).

SUPPLEMENTARY MATERIAL

The Supplementary Material for this article can be found online at: https://www.frontiersin.org/articles/10.3389/fcvm.2022.845973/full#supplementary-material

REFERENCES

1. Li S, Zhang C, Liu N, Bai H, Hou C, Wang J, et al. Genotype-positive status is associated with poor prognoses in patients with left ventricular noncompaction cardiomyopathy. *J Am Heart Assoc.* (2018) 7:e009910. doi: 10.1161/JAHA.118.009910
2. van Waning JI, Caliskan K, Hoedemaekers YM, van Spaendonck-Zwarts KY, Baas AF, Boekholdt SM, et al. Genetics, clinical features, and long-term outcome of noncompaction cardiomyopathy. *J Am Coll Cardiol.* (2018) 71:711–22.
3. Petersen SE, Selvanayagam JB, Wiesmann F, Robson MD, Francis JM, Anderson RH, et al. Left ventricular non-compaction: insights from cardiovascular magnetic resonance imaging. *J Am Coll Cardiol.* (2005) 46:101–5. doi: 10.1016/j.jacc.2005.03.045
4. Kawel N, Nacif M, Arai AE, Gomes AS, Hundley WG, Johnson WC, et al. Trabeculated (noncompacted) and compact myocardium in adults: the multi-ethnic study of atherosclerosis. *Circ Cardiovasc Imaging.* (2012) 5:357–66. doi: 10.1161/CIRCIMAGING.111.971713
5. Miszalski-Jamka K, Jefferies JL, Mazur W, Głowacki J, Hu J, Lazar M, et al. Novel genetic triggers and genotype-phenotype correlations in patients with left ventricular noncompaction. *Circ Cardiovasc Genet.* (2017) 10:e001763. doi: 10.1161/CIRCGENETICS.117.001763
6. Ross SB, Semsarian C. Clinical and genetic complexities of left ventricular noncompaction: preventing overdiagnosis in a disease we do not understand. *JAMA Cardiol.* (2018) 3:1033–4. doi: 10.1001/jamacardio.2018.2465
7. Sedaghat-Hamedani F, Haas J, Zhu F, Geier C, Kayvanpour E, Liss M, et al. Clinical genetics and outcome of left ventricular non-compaction cardiomyopathy. *Eur Heart J.* (2017) 38:3449–60. doi: 10.1093/eurheartj/ehx545
8. van Waning JI, Caliskan K, Michels M, Schinkel AFL, Hirsch A, Dalinghaus M, et al. Cardiac phenotypes, genetics, and risks in familial noncompaction cardiomyopathy. *J Am Coll Cardiol.* (2019) 73:1601–11. doi: 10.1016/j.jacc.2018.12.085
9. Klaassen S, Probst S, Oechslin E, Gerull B, Krings G, Schuler P, et al. Mutations in sarcomere protein genes in left ventricular noncompaction. *Circulation.* (2008) 117:2893–901. doi: 10.1161/CIRCULATIONAHA.107.746164
10. Kayvanpour E, Sedaghat-Hamedani F, Gi WT, Tugrul OF, Amr A, Haas J, et al. Clinical and genetic insights into non-compaction: a meta-analysis and systematic review on 7598 individuals. *Clin Res Cardiol.* (2019) 108:1297–308. doi: 10.1007/s00392-019-01465-3
11. Zemrak F, Ahlman MA, Captur G, Mohiddin SA, Kawel-Boehm N, Prince MR, et al. The relationship of left ventricular trabeculation to ventricular function and structure over a 9.5-year follow-up: the MESA study. *J Am Coll Cardiol.* (2014) 64:1971–80. doi: 10.1016/j.jacc.2014.08.035
12. Probst S, Oechslin E, Schuler P, Greutmann M, Boyé P, Knirsch W, et al. Sarcomere gene mutations in isolated left ventricular noncompaction cardiomyopathy do not predict clinical phenotype. *Circ Cardiovasc Genet.* (2011) 4:367–74. doi: 10.1161/CIRCGENETICS.110.959270

Conflict of Interest: The authors declare that the research was conducted in the absence of any commercial or financial relationships that could be construed as a potential conflict of interest.

Publisher's Note: All claims expressed in this article are solely those of the authors and do not necessarily represent those of their affiliated organizations, or those of the publisher, the editors and the reviewers. Any product that may be evaluated in this article, or claim that may be made by its manufacturer, is not guaranteed or endorsed by the publisher.

frontiers | Frontiers in Cardiovascular Medicine

ORIGINAL RESEARCH
published: 25 May 2022
doi: 10.3389/fcvm.2022.765191

Evaluation of Right Ventricular Myocardial Mechanics by 2- and 3-Dimensional Speckle-Tracking Echocardiography in Patients With an Ischemic or Non-ischemic Etiology of End-Stage Heart Failure

Fangyan Tian[1,2,3,4†], Ying Gu[4†], Yanting Zhang[1,2,3†], Bei Zhang[4], Yuji Xie[1,2,3], Shaomei Yu[4], Shuangshuang Zhu[1,2,3], Wei Sun[1,2,3], Shan Cheng[4], Mingzu Qian[1,2,3], Yixia Lin[1,2,3], Wenqian Wu[1,2,3], Yali Yang[1,2,3], Qing Lv[1,2,3], Jing Wang[1,2,3], Li Zhang[1,2,3], Yuman Li[1,2,3]* and Mingxing Xie[1,2,3]**

[1] Department of Ultrasound, Union Hospital, Tongji Medical College, Huazhong University of Science and Technology, Wuhan, China, [2] Clinical Research Center for Medical Imaging in Hubei Province, Wuhan, China, [3] Hubei Province Key Laboratory of Molecular Imaging, Wuhan, China, [4] Department of Ultrasound Medicine, The Affiliated Hospital of Guizhou Medical University, Guiyang, China

Background: The aims of our study were (1) to assess the right ventricular (RV) myocardial mechanics by two-dimensional (2D) and three-dimensional (3D) speckle-tracking echocardiography (STE) in patients with an ischemic or non-ischemic etiology of end-stage heart failure (HF) and (2) to explore which RV index evaluated by 2D- and 3D-STE was the most powerful indicator for identifying the ischemic and non-ischemic etiologies of end-stage HF.

Methods: A total of 96 patients with left ventricular ejection fraction (LVEF) < 30% were enrolled in our study: 42 patients (mean age, 52 ± 10 years; 9.5% female) with ischemic cardiomyopathy and 54 patients (mean age, 46 ± 14 years; 16.7% female) with non-ischemic cardiomyopathy. A total of 45 healthy subjects (mean age, 46 ± 13 years; 24.4% female) served as controls. The longitudinal strain of the RV free wall (RVFWLS) was determined by both 2D- and 3D-STE.

Results: Compared to controls, patients with an ischemic or non-ischemic etiology of end-stage HF had lower 2D-RVFWLS, 3D-RVFWLS and RV ejection fraction (RVEF) values ($P < 0.05$). Patients with non-ischemic cardiomyopathies (NICMs) had significantly lower 3D-RVFWLS and RVEF values than in those with ischemic cardiomyopathies (ICMs), whereas 2D-RVFWLS and conventional RV function parameters did not differ between the two subgroups. RVEF was highly related to 3D-RVFWLS ($r = 0.72$, $P < 0.001$), modestly related to 2D-RVFWLS ($r = 0.51$, $P < 0.001$), and weakly related to conventional RV function indices ($r = –0.26$ to 0.46, $P < 0.05$).

OPEN ACCESS

Edited by:
Allison G. Hays,
Johns Hopkins University,
United States

Reviewed by:
Maria Concetta Pastore,
Università del Piemonte Orientale, Italy
Chunyan Ma,
The First Affiliated Hospital of China Medical University, China
Valeria Pergola,
University Hospital of Padua, Italy

***Correspondence:**
Li Zhang
zli429@hust.edu.cn
Yuman Li
liym@hust.edu.cn
Mingxing Xie
xiemx@hust.edu.cn

† These authors have contributed equally to this work and share first authorship

Specialty section:
This article was submitted to Cardiovascular Imaging, a section of the journal Frontiers in Cardiovascular Medicine

Received: 26 August 2021
Accepted: 28 March 2022
Published: 25 May 2022

Citation:
Tian F, Gu Y, Zhang Y, Zhang B, Xie Y, Yu S, Zhu S, Sun W, Cheng S, Qian M, Lin Y, Wu W, Yang Y, Lv Q, Wang J, Zhang L, Li Y and Xie M (2022) Evaluation of Right Ventricular Myocardial Mechanics by 2- and 3-Dimensional Speckle-Tracking Echocardiography in Patients With an Ischemic or Non-ischemic Etiology of End-Stage Heart Failure. Front. Cardiovasc. Med. 9:765191. doi: 10.3389/fcvm.2022.765191

Receiver operating characteristic curve analysis revealed that the optimal 3D-RVFWLS cut-off value to distinguish NICM from ICM patients was –14.78% (area under the curve: 0.73, $P < 0.001$), while 2D-RVFWLS and conventional RV echocardiographic parameters did not.

Conclusion: Our study demonstrated the superiority of 3D-RVFWLS over 2D-RVFWLS and conventional RV function indices in identifying the ischemic and non-ischemic etiologies of end-stage HF. These findings support the idea that 3D-RVFWLS may be a promising non-invasive imaging marker for distinguishing NICM from ICM.

Keywords: three-dimensional, two-dimensional, speckle tracking echocardiography, right ventricular function, strain, heart failure

INTRODUCTION

Right ventricular (RV) function has a powerful capability for risk-stratifying patients with heart failure (HF) (1–3). In these patients, indeed, the presence of RV dysfunction is associated with adverse outcomes (4, 5). Non-ischemic cardiomyopathies (NICMs) are the most frequent cause of HF and death, and patients with NICMs have a poorer outcome than those with ischemic cardiomyopathies (ICMs) (6). For this reason, accurately distinguishing the non-ischemic and ischemic etiologies of HF is of great clinical significance. Coronary angiography, as the gold-standard modality for diagnosing ICM, is not used in every case due to its invasiveness, requirement of ionizing radiation, and high cost (7). Therefore, it is crucial to explore other non-invasive parameters to discern between the ischemic and non-ischemic etiologies of HF.

Echocardiography, which is readily available and relatively inexpensive, is considered a first-line modality for assessing ventricular performance. Nevertheless, completing an accurate assessment of RV function by traditional echocardiography is challenging because of its complex structure, contraction pattern, and response to overload. Two-dimensional (2D) speckle-tracking echocardiography (STE) is an angle-independent, less load-dependent technique that allows for the earlier identification of subtle RV dysfunction. It has been demonstrated to be a more reliable and accurate tool for RV function assessment than conventional RV function indices (8–10). However, this algorithm, based on the 2D plane, has limitations, which lead to the loss of a portion of the real motion due to out-of-plane motion (11). Recently, three-dimensional (3D) STE has emerged to overcome these limitations (12). Its accuracy and reproducibility in quantifying RV function have been verified in patients with pulmonary hypertension, transplanted hearts, and hypoplastic left heart syndrome after Fontan palliation (13–15). However, the possibility of interrogating RV mechanics in patients with end-stage HF using 3D-STE has hitherto not been explored.

Thus, the purposes of our study were (1) to assess RV myocardial mechanics using 2D- and 3D-STE in subjects with an ischemic or non-ischemic etiology of end-stage HF and (2) to explore which RV index evaluated by 2D- and 3D-STE has the potential to differentiate between the ischemic and non-ischemic etiologies of end-stage HF.

MATERIALS AND METHODS

Study Subjects

This was a prospective study of 109 consecutive patients with end-stage HF who required heart transplantation (HT) and were enrolled in this study at the Wuhan Union Hospital from June 2018 to July 2021. All patients had severely impaired left ventricular (LV) function [LV ejection fraction (LVEF) < 30%] (16), and their New York Heart Association (NYHA) functional class was III or IV. Patients were assigned to the ICM group if they had a prior history of myocardial infarction/revascularization and/or if they had significant coronary artery stenosis (≥50%) in ≥ 1 epicardial coronary vessel on angiography. Patients were classified as having NICM if they had none of these features (17). Exclusion criteria included an anomalous origin of the coronary artery, cardiac arrhythmia, and poor echocardiographic image quality.

Separately, we enrolled a control group of 45 healthy volunteers with a similar age and sex breakdown with no cardiovascular disease on the basis of clinical examination, electrocardiography, echocardiography, and chest X-ray imaging. This study was approved by the ethics committee of Tongji Medical College, Huazhong University of Science and Technology, and written informed consent was obtained from all participants.

Standard Echocardiography

All patients underwent transthoracic echocardiograms using the Philips EPIQ7C ultrasound machine (Philips Medical Systems, Andover, MA, United States). LV and RV parameters were measured according to the guidelines of the American Society of Echocardiography (18). The RV base diameter (RVD1), mid-diameter (RVD2), and length diameters (RVD3) were acquired from the RV-focused apical 4-chamber view. The RV fractional area change (FAC) was defined as the RV end-diastolic area – RV end-systolic area)/end-diastolic area × 100%. The tricuspid annular peak systolic excursion (TAPSE) was measured using M-mode echocardiography. The right-side index of myocardial performance (RIMP) was determined using tissue Doppler imaging. Peak systolic (s') tricuspid lateral annular velocities were also assessed by tissue Doppler imaging. The apical 4-chamber view

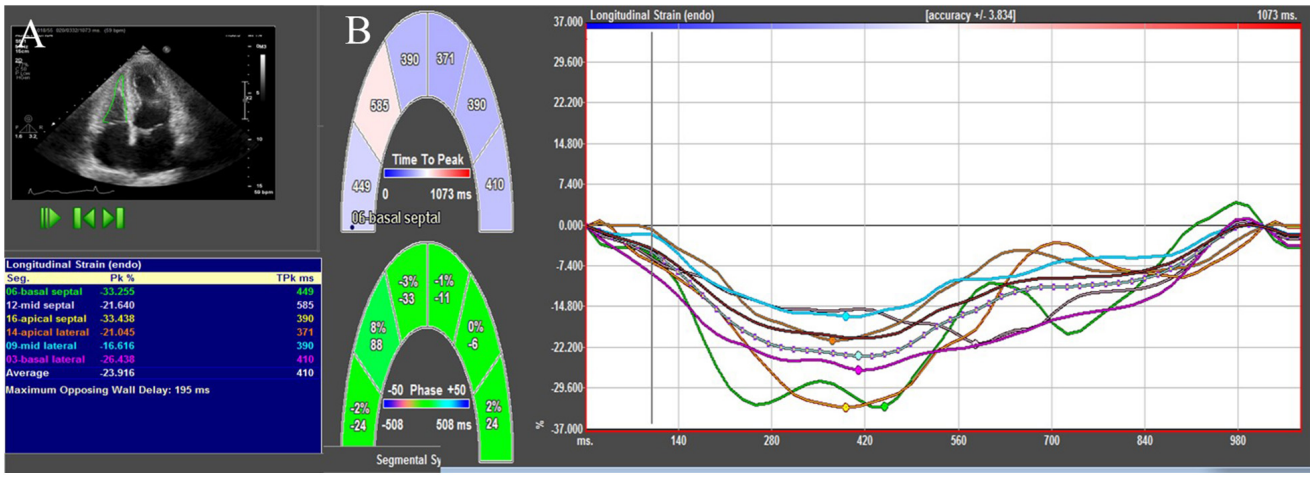

FIGURE 1 | 2D-STE showing RV endocardial border and the longitudinal strain values **(A)** and longitudinal strain curves **(B)**.

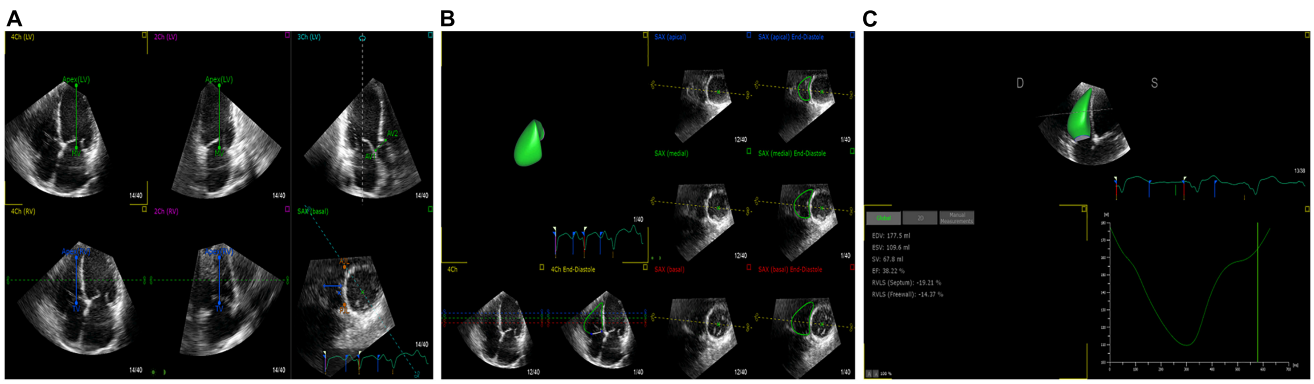

FIGURE 2 | 3D-STE offline analysis. **(A)** Setting reference points. **(B)** RV endocardial border identification and tracking. **(C)** Generating longitudinal strain of the RV free wall and RV volume curve.

was used for 2D-STE analysis, and 3D full-volume data were obtained from the apical 4-chamber view with four consecutive cardiac cycles.

Speckle-Tracking Echocardiography

2D-STE and 3D-STE analyses were performed using commercial software (4D-RV Function Analysis and 4D-LV Analysis version 3.1 software for 3D-STE and 2D Cardiac Performance Analysis for 2D-STE; Tom Tec Imaging Systems, Munich, Germany). For 2D-STE analysis, RV endocardial tracings were manually performed in the apical 4-chamber view. The software automatically tracked the speckle patterns in the myocardium. The endocardial border could be manually modified if necessary. Ultimately, the software generated the longitudinal strain curves and longitudinal peak systolic strain values of 6 segments of the RV. The 2D longitudinal strain of the RV free wall (2D-RVFWLS) was defined as the mean value of three segments of the RV free wall (**Figure 1**). For 3D-STE analysis, the operator set reference points (i.e., the center of the mitral annular line to the apex of the LV, the center of the tricuspid annular line to the apex of the RV, landmarks corresponding to the aortic annulus diameter, and the anterior and posterior junctions of the RV free wall with the interventricular septum and the septum-to-RV free wall) in 6 planes. Subsequently, the RV endocardial border was automatically identified by the software. Then, the software automatically tracked the RV endocardial border throughout the cardiac cycle, although the operator could manually adjust the RV contours if necessary. Finally, the software produced the RV end-diastolic volume (RVEDV), RV end-systolic volume (RVESV), RV stroke volume (RVSV), RV ejection fraction (RVEF), and 3D longitudinal strain values of the RV free wall (3D-RVFWLS) (**Figure 2**). We determined the RVEDV index (RVEDVI), RVESV index (RVESVI) normalized to BSA. Similarly, the operator set reference points (the center of the mitral annular line to the apex of the LV) in the apical 4-, 2-, and 3-chamber views. Then, the LV endocardial border was automatically identified by the software, and a manual adjustment was performed if necessary. Finally, the LVEDVI (ml/m^2 = LVEDV/BSA), LVESVI (ml/m^2 = LVESV/BSA), LV mass index (LVMI)

(g/m^2 = LVM/BSA), and LV global longitudinal strain (LVGLS) were obtained. The frame rate range of the 3D STE images was set at approximately 20 Hz or more.

Cardiac Magnetic Resonance Imaging Analysis

A total of 28 patients underwent cardiac magnetic resonance (CMR) examinations to assess RVEF within 1 day of echocardiography since CMR was regarded as the gold standard for RV systolic function. CMR imaging was analyzed using conventional CMR software (Argus; Siemens Medical Solutions, Erlangen, Germany). RV endocardial contours were manually traced on all short-axis slices on the end-diastolic and end-systolic frames by an experienced operator who was blinded to echocardiographic measurements. Finally, the software automatically obtained the CMR-RVEF.

Right Heart Catheterization

All patients underwent right heart catheterization before HT. A Swan-Ganz catheter were used to acquire cardiac hemodynamic data. Right atrial pressure and pulmonary artery pressure were obtained from right heart catheterization.

Statistical Analysis

Continuous variables are expressed as mean ± standard deviation values, non-normal distribution of continuous data are expressed as median (IQR),and categorical variables are expressed using frequency (percentage) values. Statistical significance was assessed by 1-way ANOVA followed by the Bonferroni *post hoc* test or by Student's t-test when only two groups were compared. For non-normally distributed data, Man-Whitney U test and Kruskal-Wallis test were used. Logistic regression analysis was used to evaluate the effect of explanatory variables. To calculate the sensitivity and specificity at various cutoff levels for the selected parameters, receiver operating characteristic (ROC) curves were used. Pearson's correlation coefficient was used for the assessment of correlations. Bland–Altman analysis and the intraclass correlation coefficient (ICC) to assess the consistency between 2D- and 3D-STE parameters were applied (19). The SPSS version 22.0 software (IBM Corporation, Armonk, NY, United States) and MedCalc version 19.0.4 software (MedCalc Software, Ostend, Belgium) were used for statistical analyses. A P value of < 0.05 in a two-sided test was considered to be statistically significant.

Reproducibility Analysis

The intra- and inter-observer variability of 2D- and 3D-STE parameters were evaluated by Bland–Altman analysis and the ICC. To assess the reproducibility, 20 patients were randomly selected from our study. For the assessment of intra-observer variability, the data were re-analyzed by the same investigator after 1 month. For the evaluation of inter-observer variability, the second investigator re-analyzed the data while blinded to the values obtained by the first investigator.

RESULTS

Clinical and Echocardiographic Characteristics

Following the exclusion of five patients with poor image quality, two with one-vessel coronary artery disease, and six with cardiac arrhythmias, 96 patients were included in our analysis. Of these 96 patients, 42 had ICM and 54 had NICM. The mean age of patients with end-stage HF was 48 ± 13 years, and 83 (86.5%) were men. Eighty (83.8%) patients had NYHA functional class IV. Tricuspid regurgitation (TR) was absent in 22 (22.9%), mild in 29 (30.2%), moderate in 17 (17.7%), and severe in 28 (29.2%) patients with end-stage HF, respectively. The clinical and echocardiographic data of the study participants are listed in **Table 1**. Sex, age, body surface area, prevalence of hypertension and diabetes, NYHA functional class, medical therapy, proportion of implantable cardioverter-defibrillator/cardiac resynchronization therapy-defibrillator (ICD/CRT-D) and laboratory data were not statistically different among the three groups. Patients with NICM had lower systolic and diastolic blood pressure values compared to the ICM and controls ($P < 0.001$), although they remained within the normal ranges. Compared to the controls, patients with ICM and NICM had increased RVEDVI, RVESVI, RVD1, RVD2, RVD3, RIMP, LVEDVI, LVESVI and LVMI values ($P < 0.05$), and decreased LVEF, LVGLS, TAPSE, RVFAC, tricuspid s', RVEF, 2D-RVFWLS, and 3D-RVFWLS values ($P < 0.05$). Patients with NICM had decreased 3D-RVFWLS and RVEF values, and increased RVEDVI and RVESVI compared to those with ICM ($P < 0.05$); however, no significant differences in LVEDVI, LVESVI, LVMI, LVEF, RVD1, RVD2, RVD3, conventional RV function parameters (TAPSE, RVFAC, tricuspid s', and RIMP), LVGLS and 2D-RVFWLS between the two subgroups were identified in our study. The severity of TR was similar between the ICM and NICM subgroups. CMR and right heart catheterization data were not significantly different between the groups (**Table 2**). In addition, we compared RVFWLS between patients with and without ICD/CRT-D, and our results revealed that 3D-RVFWLS and 2D-RVFWLS values did not differ between patients with and without ICD/CRT-D.

After adjustment for age, systolic and diastolic blood pressure, RVEDVI, RVESVI, RVEF, only 3D-RVFWLS remained significantly associated with NICM (odds ratio: 0.79; 95%CI:0.684–0.912; $P = 0.001$). 3D-RVFWLS, 2D-RVFWLS, LVGLS, and conventional RV function echocardiographic parameters were entered into ROC analysis to distinguish NICM and ICM patients from each other. ROC analysis revealed that the optimal cutoff value of 3D-RVFWLS was –14.78%, with a sensitivity of 85.2% and a specificity of 50.5%, for distinguishing between the ischemic and non-ischemic etiologies of end-stage HF (area under the ROC curve, 0.73; 95% confidence interval, 0.63–0.82; $P < 0.001$) (**Figure 3**). 2D-RVFWLS, LVGLS, and conventional RV echocardiographic parameters failed to distinguish NICM patients from ICM patients.

Figure 4 presents Bland–Altman analysis and correlation plots for RVFWLS as measured by 2D- and 3D-STE. 3D-RVFWLS

TABLE 1 | Clinical and echocardiographic characteristics of patients and normal controls.

Variables	Controls (*n* = 45)	ICM(*n* = 42)	NICM (*n* = 54)	*p*
Female (%)	11 (24.4%)	4 (9.5%)	9 (16.7%)	0.141
Age (years)	46 ± 13	52 ± 10	46 ± 14	0.052
Body surface area (m^2)	1.64 ± 0.40	1.73 ± 0.19	1.66 ± 0.33	0.582
Systolic blood pressure (mmHg)	116 ± 7	116 ± 21	101 ± 19*†	<0.001
Diastolic blood pressure (mmHg)	75 ± 8	74 ± 18	66 ± 12*†	<0.001
Hypertension		19 (45.2%)	15 (27.8%)	0.076
Diabetes mellitus		14 (33.3%)	9 (16.7%)	0.058
NYHA functional class, *n* (%)				0.581
III		6 (14.3%)	10 (18.5%)	
IV		36 (85.7%)	44 (81.5%)	
Medical therapy (*n*, %)				
Beta-blockers		42 (100%)	54 (100%)	
ACE inhibitors/ARBs		42 (100%)	54 (100%)	
Loop diuretics		41 (97.6%)	52 (96.3%)	>0.999
Aldosterone antagonists		40 (95.2%)	51 (94.4%)	>0.999
ICD/CRT-D		3 (7.1%)	9 (16.7%)	>0.999
Laboratory data				
Hemoglobin (g/L)		124.00 ± 17.78	133.46 ± 23.25	0.085
Total cholesterol (mmol/L)		3.03 (2.19, 3.52)	3.12 (2.63, 3.86)	0.357
Triglyceride (mmol/L)		1.37 (1.02, 2.13)	1.07 (0.81, 1.84)	0.715
Creatinine (μmol/L)		88 (78.2, 103.6)	85.8 (70.4, 105.85)	0.380
Echocardiography				
LVEDVI (ml/m^2)	48 (40, 56)^†	124 (91,141)	143 (120, 167)	<0.001
LVESVI (ml/m^2)	15 (12,19)^†	95 (77, 108)	105 (84, 135)	<0.001
LVEF (%)	67.51 ± 4.41^†	25.19 ± 6.39	24.54 ± 6.06	<0.001
LVMI (g/m^2)	86 (73, 92)^†	177 (169, 216)	203 (185, 249)	<0.001
LVGLS (%)	–21.92 ± 2.59^†	–6.16 ± 2.05	–7.46 ± 2.17	<0.001
RVD1 (mm)	27.51 ± 4.32^†	36.24 ± 6.83	36.94 ± 9.60	<0.001
RVD2 (mm)	27.93 ± 4.05^†	32.69 ± 8.17	32.66 ± 9.60	<0.001
RVD3 (mm)	66.76 ± 8.04^†	76.48 ± 9.76	80.91 ± 12.27	<0.001
Mild TR (*n*, %)		15 (33.3%)	14 (25.5%)	0.388
Moderate TR (*n*, %)		5 (11.1%)	12 (21.8%)	0.156
Severe TR (*n*, %)		9 (20%)	19 (35.2%)	0.095
TAPSE (mm)	21.48 ± 2.76^†	12.76 ± 2.46	11.99 ± 2.40	<0.001
RVFAC (%)	46.87 ± 4.67^†	27.25 ± 5.79	25.03 ± 5.63	<0.001
RIMP	0.36 ± 0.03^†	0.59 ± 0.05	0.67 ± 0.03	<0.001
Tricuspid s' (cm/s)	12.84 ± 1.98^†	9.05 ± 2.74	9.90 ± 2.66	<0.001
2D-RVFWLS (%)	–23.38 ± 8.90^†	–14.29 ± 4.90	–13.24 ± 3.49	<0.001
RVEDVI (ml/m^2)	47 (39,57)^†	65 (50,76)	76 (53,100) *	<0.001
RVESVI (ml/m^2)	26 (21,29)^†	46 (32,53)	53 (38,72) *	<0.001
RVSV (ml)	44 (33,55)^†	38 (24,45)	34 (24,42)	0.002
RVEF (%)	53.14 ± 4.49^†	31.87 ± 9.68	28.09 ± 6.87*	<0.001
3D-RVFWLS (%)	–23.78 ± 2.15^†	–15.36 ± 4.76	–11.92 ± 2.81*	<0.001

Data are mean ± SD, n (%), or median (IQR).
**P < 0.05 for ICM vs. NICM.*
^ P < 0.05 for ICM vs. controls.
†P < 0.05 for NICM vs. controls.
ACE, angiotensin-converting enzyme; ARB, angiotensin receptor blocker; ICD, Implantable cardioverter defibrillator; CRT-D, cardiac resynchronization therapy-defibrillation; RV, right ventricular; LV, left ventricular; MI, mass index; EDVI, end-diastolic volume index; ESVI, end-systolic volume index; SV, stroke volume; EF, ejection fraction; RVD1, right ventricular basal diameter; RVD2, right ventricular mid diameter; RVD3, right ventricular longitudinal dimension; TR, tricuspid regurgitation; TAPSE, tricuspid annular plane systolic excursion; FAC, fractional area change; RIMP, right-side index of myocardial performance; Tricuspid s', tricuspid annulus systolic velocity; 3D, three dimensional; 2D, two dimensional; RVFWLS, right ventricular free wall longitudinal strain.

TABLE 2 | Cardiac magnetic resonance and right heart catheterization characteristics of patients.

Variables	ICM (*n* = 42)	NICM (*n* = 54)	*p*
Cardiac magnetic resonance			
CMR-RVEF (%) (*n*)	14 (11,31) (8)	15 (11,22) (20)	0.739
Right heart catheterization			
Systolic PAP (mmHg)	45 ± 16	42 ± 15	0.313
Diastolic PAP (mmHg)	75 ± 18	66 ± 12	0.852
Mean PAP (mmHg)	30 ± 11	28 ± 12	0.591
RAP (mmHg)	10 (7,13)	9 (7,12)	0.780

Data are mean ± SD or median (IQR). CMR-RVEF, cardiac magnetic resonance-right ventricular ejection fraction; PAP, pulmonary arterial pressure; RAP, right atrial pressure.

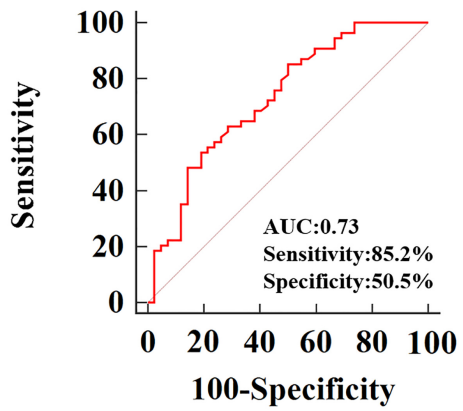

FIGURE 3 | Receiver operating characteristic curves of 3D-RVFWLS for distinguishing NICM from ICM.

was strongly related to 2D-RVFWLS (r = 0.70, P < 0.001). Good consistency for RVFWLS as assessed by 2D- and 3D-STE, respectively, was noted (ICC, 0.70; 95% CI, 0.59–0.79).

Relationships Between RV Ejection Fraction, Two-Dimensional- and Three-Dimensional-Speckle-Tracking Echocardiography, and Conventional RV Echocardiographic Indices

The relationships between RVEF, 2D- and 3D-STE, and conventional RV echocardiographic parameters are shown in **Figure 5**. RVEF was highly correlated with 3D-RVFWLS (r = 0.72, P < 0.001), modestly correlated with 2D-RVFWLS (r = 0.51, P < 0.001); and weakly associated with RVFAC (r = 0.46, P < 0.001), TAPSE (r = 0.37, P < 0.001), RVEDVI (r = –0.26, P = 0.017), RVESVI (r = –0.45, P < 0.001), and RVSV (r = 0.38, P < 0.001). Meanwhile, RVEF was not associated with RVD1, RVD2, RVD3, RIMP, or tricuspid s'. Moreover, 3D-RVFWLS correlated better with RVEF than 2D-RVFWLS and the conventional RV indices with RVEF (r = 0.72 vs. –0.26 to 0.51, P < 0.05). In addition, we found that CMR-RVEF was modestly correlated with 3D-RVFWLS (r = 0.53, P = 0.004),

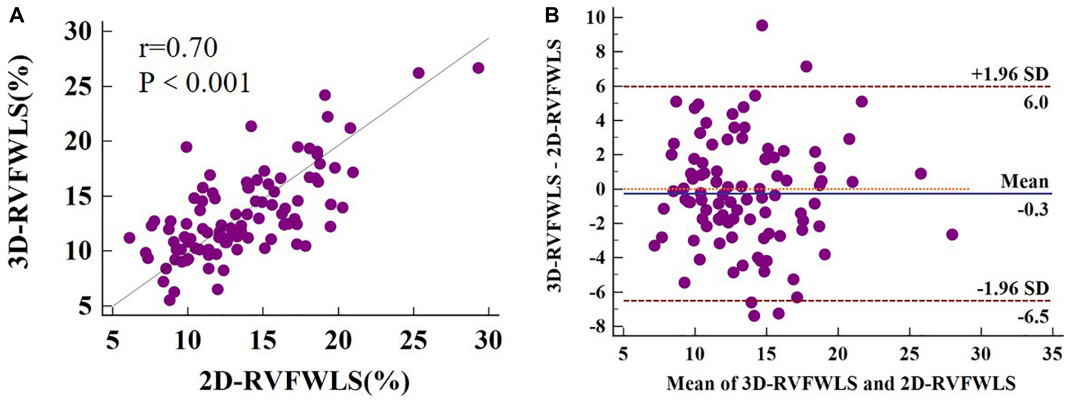

FIGURE 4 | 2D-3D longitudinal strain of RV free wall correlation plots **(A)** and Bland–Altman plots **(B)**. 3D-RVFWLS and 2D-RVFWLS values are absolute values.

and weakly associated with 2D-RVFWLS (r = 0.49, P = 0.008) (**Supplementary Figure 1**).

Reproducibility

The reproducibility of 2D- and 3D-STE parameters is shown in **Table 3**. 2D- and 3D-STE parameters had good intra- and inter-observer reproducibility, as evidenced by a higher ICC, small bias, and limits of agreement.

DISCUSSION

To our knowledge, this may be the first investigation to comprehensively assess RV function in patients with ischemic and non-ischemic etiologies of end-stage HF using 2D- and 3D-STE and conventional echocardiographic parameters. The main findings of our study were as follows: (1) patients with ischemic or non-ischemic etiology of end-stage HF had diminished 2D- and 3D-RVFWLS compared to healthy controls; (2) patients with NICM had lower 3D-RVFWLS compared to ICM patients, although no significant difference in 2D-RVFWLS between these two subgroups was noted in our study; and (3) more importantly, ROC analysis revealed that 3D-RVFWLS displayed the potential for distinguishing NICM patients from ICM patients, while 2D-RVFWLS and conventional RV echocardiographic parameters did not. Therefore, 3D-STE may be superior to 2D-STE for distinguishing between the non-ischemic and ischemic etiologies of end-stage HF.

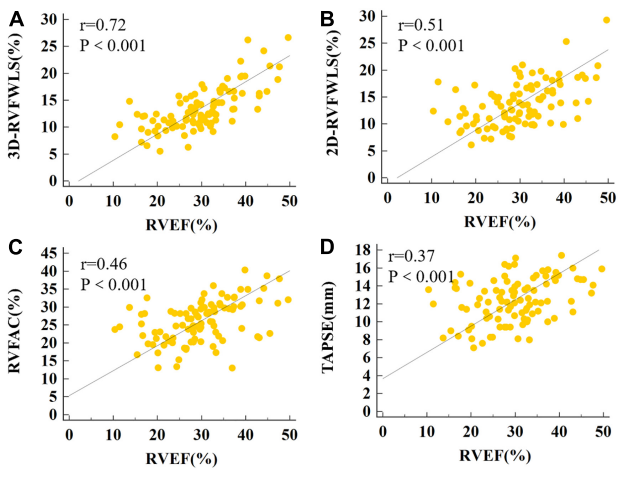

FIGURE 5 | The correlations of RVEF with 3D-RVFWLS, 2D-RVFWLS and conventional echocardiographic parameters. The association between the 3D-RVFWLS **(A)**, 2D-RVFWLS **(B)**, RVFAC **(C)**, TAPSE **(D)**, and RVEF. 3D-RVFWLS and 2D-RVFWLS values are absolute values.

RV Strain in Patients With End-Stage Heart Failure

Our results showed that 2D- and 3D-STE parameters were reduced in patients with ischemic or non-ischemic etiology of end-stage HF compared to healthy controls. These results are consistent with prior findings gathered using 2D-STE (20, 21). Our results have, for the first time, demonstrated that patients

TABLE 3 | Intraobserver and interobserver reproducibility.

Variables	ICC (95% CI)	Bias	Limits of agreement
Intraobserver			
RVEDV	0.98 (0.94–0.99)	4.2	–17.5, 25.9
RVESV	0.97 (0.93–0.99)	3.2	–14.7, 23.1
RVSV	0.93 (0.83–0.97)	–0.03	–12.2, 12.1
RVEF	0.89 (0.74–0.96)	–0.7	–7.8, 6.4
3D-RVFWLS	0.94 (0.84–0.97)	0.4	–1.8, 2.54
2D-RVFWLS	0.95 (0.88–0.98)	0.9	–0.9, 2.7
Interobserver			
RVEDV	0.94 (0.87–0.98)	6.8	–25.6, 39.2
RVESV	0.93 (0.84–0.97)	5.9	–21.9, 33.7
RVSV	0.92 (0.82–0.97)	0.8	–11.8, 13.5
RVEF	0.86 (0.68–0.94)	–0.6	–7.7, 6.6
3D-RVFWLS	0.91 (0.79–0.96)	0.5	–2.0, 3.0
2D- RVFWLS	0.90 (0.76–0.96)	0.8	–1.8, 3.3

*Abbreviations as in **Table 1**.*

with end-stage HF have diminished 3D-RVFWLS. Several mechanisms may contribute to RV dysfunction in end-stage HF patients, including impaired LV function, elevated pulmonary arterial pressure, RV myocardial ischemia, and neurohormonal interactions (22). Patients with end-stage HF present with depressed LV function. Ventricular interaction could influence RV strain through the interventricular septum. RV failure in terms of histology includes rarefaction of myocardial capillaries and myocardial fibrosis (23, 24). Myocardial fibrosis results in myocardial remodeling and stiffness elevation, presenting with ventricular chamber enlargement and systolic dysfunction.

RV Mechanics in Patients With Ischemic and Non-ischemic Etiologies of End-Stage Heart Failure

Differentiating NICM patients from ICM patients is essential on account of the different prognoses and treatment strategies for each group (18). Although the diagnosis is generally made by computed tomography angiography or coronary angiography, it is not practical for every patient to undergo an imaging study using angiography because of its radioactivity, invasiveness, and other contraindications. Therefore, it is critical to identify non-invasive parameters to distinguish between NICM and ICM. In our study, both algorithms provided substantially different results for patients with NICM and those with ICM, respectively. For example, we found that 3D-RVFWLS was lower in patients with NICM than those with ICM, but no difference in 2D-RVFWLS between the two subgroups was observed. With the use of 2D-STE algorithms, where speckles are only tracked in 2D planes, only a portion of the real myocardial motion is tracked. Thorstensen et al. reported 3D strain of left ventricle did not show incremental diagnostic value to the other modalities in patients with recent myocardial infarction, but patients with poor echocardiographic image quality were not excluded in their study and their study did not compare RV strain (25). A recent observation suggested that NICM exists as an intrinsic injury of the RV myocardium (21), and this proposal is compatible with our study findings revealed by 3D-STE. In contrast, in a small observational cohort of 40 patients with HF (including 20 with ICM and 20 with NICM), no significant difference in LVGLS obtained by 3D-STE between the ICM and NICM subgroups was noted (26). Another study, by Shanbhag et al., that followed a community-based sample of older adults for a median of 5.8 years showed that patients with NICM had a worse prognosis than those with ICM (6). Likewise, Meng et al. also demonstrated that patients with HF with poor clinical outcomes displayed impaired 3D-RVFWLS and RVEF compared to those without clinical events (27). Our findings provide direct evidence to support the aforementioned results. The fact that patients with NICM exhibited a poorer prognosis than those with ICM may be the reason why they also presented with more severely impaired 3D-RVFWLS. Moreover, ROC analysis revealed that the 3D-RVFWLS parameters had a good capacity for distinguishing NICM patients from ICM patients, while 2D-RVFWLS and conventional RV echocardiographic parameters failed to differentiate NICM patients from ICM patients. Therefore, 3D-RVFWLS may be a useful alternative to coronary angiography for distinguishing NICM from ICM, particularly among patients with end-stage HF who cannot undergo coronary angiography.

Comparisons of Three-Dimensional-Speckle-Tracking Echocardiography and Two-Dimensional-Speckle-Tracking Strain Parameters

Owing to the complex geometry of the RV, 3D-STE has no geometric assumptions or out-of-plane motion of speckles, allowing for a more accurate assessment of myocardial performance by overcoming the limitations of 2D-STE. There were significant correlations between the RVFWLS values obtained by the 2D and 3D modalities. These findings were consistent with those of previous studies in patients with pulmonary hypertension (28). RV contraction occurs primarily in the form of longitudinal shortening (29). The longitudinal shortening of the RV free wall contributes to 80% of the RV stroke volume and may indicate the global RV function (30, 31). 2D-RVFWLS has been reported to exhibit prognostic value in various diseases, including HF (32–34). The good correlation and consistency of RVFWLS obtained by 2D- and 3D-STE suggest that 3D-STE may be a choice for RV function quantification and prognostic stratification.

Correlations of RV Strain Parameters With RV Ejection Fraction

Our findings showed that there was a significant correlation between CMR-RVEF and 2D- and 3D-RVFWLS. This is compatible with findings of previous research, which demonstrated that CMR-RVEF was strongly related to 2D-RVFWLS (35). 3D echocardiography has been demonstrated to be more accurate than 2D echocardiography in the evaluation of RV function in patients with HF (36). RVEF as measured by 3D echocardiography has a great correlation with CMR-RVEF values (37) and has been considered a major determinant of RV systolic function in the updated 2015 recommendations (38). In this study, we also demonstrated that 3D-RVFWLS had a better association with RVEF than 2D-RVFWLS and conventional RV echocardiographic parameters.

Clinical Implications

Unlike structurally normal hearts, patients with end-stage HF present with marked ventricular remodeling that may be better served by the 3D algorithm. Although 3D-STE has a theoretical superiority over 2D-STE for RV quantification, head-to-head comparisons between 3D-STE and 2D-STE for assessing RV strain in patients with end-stage HF have not yet been performed. Our results demonstrated the superiority of 3D-STE over 2D-STE and conventional RV echocardiographic indices in reflecting the RV myocardial pathophysiology in relation to the ischemic and non-ischemic etiologies of end-stage HF. Considering that

3D-STE better detects the changes in RV strain compared to 2D-STE in patients with ischemic and non-ischemic etiologies of end-stage HF, it should be the optimal choice for the assessment of RV strain in patients with end-stage HF. Additionally, we noted that 3D-RVFWLS was significantly related to 2D-RVFWLS and RVEF, and there were good consistency for RVFWLS as assessed by 2D- and 3D-STE, only 3D-RVFWLS can distinguish NICM patients from ICM patients, while 2D-RVFWLS and RVEF failed to distinguish these. Therefore, we suggest that 2D-STE and 3D-STE values should not be used interchangeably in patients with end-stage HF.

Limitations

The present study had several limitations. First, 3D-STE analysis requires better image quality and experienced operators, and the technique is in its infancy and not yet widely validated for clinical use. Second, 3D-STE is hindered by low frame rates, which may have an effect on strain values. Third, we enrolled only patients with end-stage HF in this study, which may have led to a selection bias and an inability to generalize our findings to all patients with HF. Fourth, some patients with end-stage HF who were RV-paced or in a clinically critical state were not deemed suitable to undergo CMR examinations, so we could not obtain CMR data from all included patients. Fifth, although 3D-RVFWLS can distinguish NICM patients from ICM patients, while specificity of 50.5% is not so good. Sixth, 3D-STE parameters have vendor dependency (39); thus, our findings may not apply when using technology from other vendors. Ultimately, our study is a single-center observation with a relatively small number of patients. Future multicenter investigations with larger study populations are needed to confirm the superiority of 3D-STE over 2D-STE in quantifying RV performance in patients with end-stage HF.

CONCLUSION

Our study demonstrated the superiority of 3D-RVFWLS over 2D-RVFWLS and conventional RV echocardiographic indices in identifying the ischemic and non-ischemic etiologies of end-stage HF. These findings indicate that 3D-RVFWLS may be a promising non-invasive imaging marker for distinguishing NICM from ICM.

DATA AVAILABILITY STATEMENT

The original contributions presented in the study are included in the article/**Supplementary Material**, further inquiries can be directed to the corresponding author/s.

ETHICS STATEMENT

The studies involving human participants were reviewed and approved by the Ethics Committee of Tongji Medical College, Huazhong University of Science and Technology. The patients/participants provided their written informed consent to participate in this study.

AUTHOR CONTRIBUTIONS

FT, YG, YZ, BZ, YX, SY, JW, YY, QL, LZ, YML, and MX: conception and design of the study. FT, YG, YZ, YML, and MX: acquisition of data. MQ, YXL, SZ, YX, WW, SC, LZ, YML, and MX: analysis and interpretation of data. YML and MX: drafting the article. All authors contributed to the article and approved the submitted version.

FUNDING

This work was supported by the National Natural Science Foundation of China (Grant Nos. 81727805 and 81922033), the Key Research and Development Program of Hubei (Grant Nos. 2020DCD015 and 2021BCA138), the Fundamental Research Funds for the Central Universities (Grant No. 5003530082), and the Shenzhen Science and Technology (Grant no. SGDX20190917094601717).

SUPPLEMENTARY MATERIAL

The Supplementary Material for this article can be found online at: https://www.frontiersin.org/articles/10.3389/fcvm.2022.765191/full#supplementary-material

Supplementary Figure 1 | The Correlations of CMR-RVEF with RVFWLS. The association between the 2D-RVFWLS **(A)**, 3D-RVFWLS **(B)**, and CMR-RVEF.

REFERENCES

1. De Groote P, Millaire A, Foucher-Hossein C, Nugue O, Marchandise X, Ducloux G, et al. Right ventricular ejection fraction is an independent predictor of survival in patients with moderate heart failure. *J Am Coll Cardiol.* (1998) 32:948–54. doi: 10.1016/S0735-1097(98)00337-4
2. Meyer P, Filippatos GS, Ahmed MI, Iskandrian AE, Bittner V, Perry GJ, et al. Effects of right ventricular ejection fraction on outcomes in chronic systolic heart failure. *Circulation.* (2010) 121:252–8. doi: 10.1161/Circulationaha.109.887570
3. Field ME, Solomon SD, Lewis EF, Kramer DB, Baughman KL, Stevenson LW, et al. Right ventricular dysfunction and adverse outcome in patients with advanced heart failure. *J Cardiac Fail.* (2006) 12:616–20. doi: 10.1016/j.cardfail.2006.06.472
4. Zornoff LA, Skali H, Pfeffer MA, St John Sutton M, Rouleau JL, Lamas GA, et al. Right ventricular dysfunction and risk of heart failure and mortality after myocardial infarction. *J Am Coll Cardiol.* (2002) 39:1450–5. doi: 10.1016/s0735-1097(02)01804-1
5. Meluzin J, Spinarova L, Hude P, Krejci J, Dusek L, Vitovec J, et al. Combined right ventricular systolic and diastolic dysfunction represents a strong determinant of poor prognosis in patients with symptomatic heart failure. *Int J Cardiol.* (2005) 105:164–73. doi: 10.1016/j.ijcard.2004.12.031
6. Shanbhag SM, Greve AM, Aspelund T, Schelbert EB, Cao JJ, Danielsen R, et al. Prevalence and prognosis of ischaemic and non-ischaemic myocardial fibrosis

in older adults. *Eur Heart J.* (2019) 40:529–38. doi: 10.1093/eurheartj/ehy 713
7. Wielopolski PA, van Geuns RJ, de Feyter PJ, Oudkerk M. Coronary arteries. *Eur Radiol.* (2000) 10:12–35. doi: 10.1007/s00330005 0004
8. Collier P, Phelan D, Klein AA. Test in context: myocardial strain measured by speckle-tracking echocardiography. *J Am Coll Cardiol.* (2017) 69:1043–56. doi: 10.1016/j.jacc.2016.12.012
9. Longobardo L, Suma V, Jain R, Carerj S, Zito C, Zwicke DL, et al. Role of two-dimensional speckle-tracking echocardiography strain in the assessment of right ventricular systolic function and comparison with conventional parameters. *J Am Soc Echocardiogr.* (2017) 30:937–46.e6. doi: 10.1016/j.echo. 2017.06.016
10. Liou K, Negishi K, Ho S, Russell EA, Cranney G, Ooi SY. Detection of obstructive coronary artery disease using peak systolic global longitudinal strain derived by two-dimensional speckle-tracking: a systematic review and meta-analysis. *J Am Soc Echocardiogr.* (2016) 29:724–35.e4. doi: 10.1016/j. echo.2016.03.002
11. Cheung YF. The role of 3D wall motion tracking in heart failure. *Nat Rev Cardiol.* (2012) 9:644–57. doi: 10.1038/nrcardio.2012.128
12. Muraru D, Niero A, Rodriguez-zanella H, Cherata D, Badano L. Three-dimensional speckle-tracking echocardiography: benefits and limitations of integrating myocardial mechanics with three-dimensional imaging. *Cardiovasc Diagn Ther.* (2018) 8:101–17. doi: 10.21037/cdt.2017. 06.01
13. Li YM, Wang T, Haines P, Li MM, Wu WQ, Liu MW, et al. Prognostic value of right ventricular two-dimensional and three-dimensional speckle-tracking strain in pulmonary arterial hypertension: superiority of longitudinal strain over circumferential and radial strain. *J Am Soc Echocardiog.* (2020) 33:985–94. doi: 10.1016/j.echo.2020.03.015
14. Lv Q, Sun W, Wang J, Wu C, Li H, Shen XH, et al. Evaluation of biventricular functions in transplanted hearts Using 3-dimensional speckle-tracking echocardiography. *J Am Heart Assoc.* (2020) 9:e015742. doi: 10.1161/ JAHA.119.015742
15. Sato T, Calderon RJC, Klas B, Pedrizzetti G, Banerjee A. Simultaneous volumetric and functional assessment of the right ventricle in hypoplastic left heart syndrome after fontan palliation, Utilizing 3-dimensional speckle-tracking echocardiography. *Circ J.* (2020) 84:235–44. doi: 10.1253/circj.CJ-19-0926
16. McDonagh TA, Metra M, Adamo M, Gardner RS, Baumbach A, Bohm M, et al. ESC Guidelines for the diagnosis and treatment of acute and chronic heart failure. *Eur Heart J.* (2021) 42:3599–726. doi: 10.1093/eurheartj/ehab 368
17. Kusunose K, Kwon DH, Motoki H, Flamm SD, Marwick TH. Comparison of three-dimensional echocardiographic findings to those of magnetic resonance imaging for determination of left ventricular mass in patients with ischemic and non-ischemic cardiomyopathy. *Am J Cardiol.* (2013) 112:604–11. doi: 10.1016/j.amjcard.2013.04.028
18. Rudski LG, Lai WW, Afilalo J, Hua LQ, Handschumacher MD, Chandrasekaran K etal. Guidelines for the echocardiographic assessment of the right heart in adults: a report from the American Society of Echocardiography Endorsed by the European Association of Echocardiography, a registered branch of the European Society of Cardiology, and the Canadian Society of Echocardiography. *J Am Soc Echocardiog.* (2010) 23:685–13. doi: 10.1016/j.echo.2010.05.010
19. Bland JM, Altman DG. Statistical methods for assessing agreement between two methods of clinical measurement. *Lancet.* (1986) 1:307–10. doi: 10.1016/ s0140-6736(86)90837-8
20. Lisi M, Cameli M, Righini FM, Malandrino A, Tacchini D, Focardi M, et al. RV longitudinal deformation correlates with myocardial fibrosis in patients with end-stage heart failure. *JACC Cardiovasc Imaging.* (2015) 8:514–22. doi: 10.1016/j.jcmg.2014.12.026
21. Mouton S, Ridon H, Fertin M, Pentiah AD, Goemine C, Petyt G, et al. 2D-speckle tracking right ventricular strain to assess right ventricular systolic function in systolic heart failure. Analysis of the right ventricular free and posterolateral walls. *Int J Cardiol.* (2017) 245:190–5. doi: 10.1016/j.ijcard.2017. 07.077
22. Hamada-Harimura Y, Seo Y, Ishizu T, Nishi I, Machino-Ohtsuka T, Yamamoto M, et al. Incremental prognostic value of right ventricular strain in patients with acute decompensated heart failure. *Circ Cardiovasc Imaging.* (2018) 11:e007249. doi: 10.1161/CIRCIMAGING.117.0 07249
23. Drake JI, Bogaard HJ, Mizuno S, Clifton B, Xie B, Gao Y, et al. Molecular signature of a right heart failure program in chronic severe pulmonary hypertension. *Am J Resp Cell Mol.* (2011) 45:1239–47. doi: 10.1165/rcmb.2010-0412OC
24. Rain S, Handoko ML, Noordegraaf AV, Bogaard HJ, van der Velden J, de Man FS. Pressure-overload-induced right heart failure. *Pflug Arch Eur J Phy.* (2014) 466:1055–63. doi: 10.1007/s00424-014-1450-1
25. Thorstensen A, Dalen H, Hala P, Kiss M, D'hooge M, Torp M, et al. Three-dimensional echocardiography in the evaluation of global and regional function in patients with recent myocardial infarction: a comparison with magnetic resonance imaging. *Echocardiography.* (2013) 30:682–92. doi: 10. 1111/echo.12115
26. Vachalcova M, Valocik G, Kurecko M, Grapsa J, Taha VA, Michalek P, et al. The three-dimensional speckle tracking echocardiography in distinguishing between ischaemic and non-ischaemic aetiology of heart failure. *ESC Heart Fail.* (2020) 7:2297–304. doi: 10.1002/ehf2. 12766
27. Meng Y, Zhu S, Xie Y, Zhang Y, Qian M, Gao L, et al. Prognostic value of right ventricular 3D speckle-tracking strain and ejection fraction in patients with HFpEF. *Front Cardiovasc Med.* (2021) 8:694365. doi: 10.3389/fcvm.2021. 694365
28. Vitarelli A, Mangieri E, Terzano C, Gaudio C, Salsano F, Rosato E, et al. Three dimensional echocardiography and 2d-3d speckletracking imaging in chronic pulmonary hypertension: diagnostic accuracy in detecting hemodynamic signs of right ventricular (RV) failure. *J Am Heart Assoc.* (2015) 4:e001584. doi: 10.1161/JAHA.114.001584
29. Leather HA, Ama R, Missant C, Rex S, Rademakers FE, Wouters PF. Longitudinal but not circumferential deformation reflects global contractile function in the right ventricle with open pericardium. *Am J Physiol Heart Circ Physiol.* (2006) 290:H2369–75. doi: 10.1152/ajpheart.0121 1.2004
30. Haddad F, Hunt SA, Rosenthal DN, Murphy DJ. Right ventricular function in cardiovascular disease, part I: anatomy, physiology, aging, and functional assessment of the right ventricle. *Circulation.* (2008) 117:1436–48. doi: 10. 1161/CIRCULATIONAHA.107.653576
31. Sato T, Tsujino I, Ohira H, Oyama-Manabe N, Yamada A, Ito YM, et al. Validation study on the accuracy of echocardiographic measurements of right ventricular systolic function in pulmonary hypertension. *J Am Soc Echocardiogr.* (2012) 25:280–6. doi: 10.1016/j.echo.2011. 12.012
32. Carluccio E, Biagioli P, Lauciello R, Zuchi C, Mengoni A, Bardelli G, et al. Superior prognostic value of right ventricular free wall compared to global longitudinal strain in patients with heart failure. *J Am Soc Echocardiogr.* (2019) 32:836–44.e1. doi: 10.1016/j.echo.2019.0 2.011
33. Verhaert D, Mullens W, Borowski A, Popovic ZB, Curtin RJ, Thomas JD, et al. Right ventricular response to intensive medical therapy in advanced decompensated heart failure. *Circ Heart Fail.* (2010) 3:340–6. doi: 10.1161/ CIRCHEARTFAILURE.109.900134
34. Guendouz S, Rappeneau S, Nahum J, Dubois-Rande JL, Gueret P, Monin JL, et al. Prognostic significance and normal values of 2D strain to assess right ventricular systolic function in chronic heart failure. *Circ J.* (2012) 76:127–36. doi: 10.1253/circj.cj-11-0778
35. Focardi M, Cameli M, Carbone SF, Massoni A, De Vito R, Lisi M, et al. Traditional and innovative echocardiographic parameters for the analysis of right ventricular performance in comparison with cardiac magnetic resonance. *Eur Heart J Cardiovasc Imaging.* (2015) 16:47–52. doi: 10.1093/ ehjci/jeu156
36. Kim J, Cohen SB, Atalay MK, Maslow AD, Poppas A. Quantitative assessment of right ventricular volumes and ejection fraction in patients with left ventricular systolic dysfunction by real time three-dimensional echocardiography versus cardiac magnetic resonance

imaging. *Echocardiography*. (2015) 32:805–12. doi: 10.1111/echo.12715

37. Park JB, Lee SP, Lee JH, Yoon YE, Park EA, Kim HK, et al. Quantification of right ventricular volume and function using single-beat three-dimensional echocardiography: a validation study with cardiac magnetic resonance. *J Am Soc Echocardiog.* (2016) 29:392–401. doi: 10.1016/j.echo.2016.01.010
38. Lang RM, Badano LP, Mor-Avi V, Afilalo J, Armstrong A, Ernande L, et al. Recommendations for cardiac chamber quantification by echocardiography in adults: an update from the american society of echocardiography and the european association of cardiovascular imaging. *J Am Soc Echocardiog.* (2015) 28:1–39. doi: 10.1016/j.echo.2014.10.003
39. Farsalinos KE, Daraban AM, Unlu S, Thomas JD, Badano LP, Voigt JU. Head-to-head comparison of global longitudinal strain measurements among nine different vendors: the EACVI/ASE inter-vendor comparison study. *J Am Soc Echocardiog.* (2015). 28:1171–81.

Conflict of Interest: The authors declare that the research was conducted in the absence of any commercial or financial relationships that could be construed as a potential conflict of interest.

frontiers | Frontiers in Cardiovascular Medicine

REVIEW
published: 03 August 2022
doi: 10.3389/fcvm.2022.834738

Cardiovascular Imaging in Pregnancy: Valvulopathy, Hypertrophic Cardiomyopathy, and Aortopathy

*Haneen Ismail, Andrew J. Bradley and Jannet F. Lewis**

Division of Cardiology, Department of Medicine, George Washington University School of Medicine and Health Sciences, Washington, DC, United States

Pregnancy is associated with profound hemodynamic changes that are particularly impactful in patients with underlying cardiovascular disease. Management of pregnant women with cardiovascular disease requires careful evaluation that considers the well-being of both the woman and the developing fetus. Clinical assessment begins before pregnancy and continues throughout gestation into the post-partum period and is supplemented by cardiac imaging. This review discusses the role of imaging, specifically echocardiography, cardiac MRI, and cardiac CT, in pregnant women with valvular diseases, hypertrophic cardiomyopathy, and aortic pathology.

Keywords: cardiac MRI (CMR), cardiac CT, pregnancy, hypertrophic cardiomyopathy, valvulopathy, aortopathy, echocardiography, peripartum

OPEN ACCESS

Edited by:
Monica Mukherjee, Johns Hopkins Medicine, United States

Reviewed by:
Olga Vriz, King Faisal Specialist Hospital & Research Center, Saudi Arabia
Akshay Goel, Westchester Medical Center, United States

***Correspondence:**
Jannet F. Lewis
jlewis@mfa.gwu.edu

Specialty section:
This article was submitted to Cardiovascular Imaging, a section of the journal Frontiers in Cardiovascular Medicine

Received: *13 December 2021*
Accepted: *20 June 2022*
Published: *03 August 2022*

Citation:
Ismail H, Bradley AJ and Lewis JF (2022) Cardiovascular Imaging in Pregnancy: Valvulopathy, Hypertrophic Cardiomyopathy, and Aortopathy. Front. Cardiovasc. Med. 9:834738. doi: 10.3389/fcvm.2022.834738

INTRODUCTION

Pregnancy is associated with profound hemodynamic changes that significantly impact the cardiovascular system. These changes are particularly impactful in women with underlying heart disease. Management of pregnant women with cardiovascular abnormalities requires consideration of the well-being of both the woman and the developing fetus. Clinical evaluation, starting before and then continuing throughout pregnancy, is the foundation of this management with imaging playing a key role in patient risk stratification and monitoring. This review discusses the role of imaging for pregnant women with valvular diseases, hypertrophic cardiomyopathy, and aortic pathology. We will begin with a brief overview of general patient assessment and discussion of the value added by different imaging modalities.

A BASIC APPROACH TO PATIENT MANAGEMENT AND IMAGING SELECTION

Preconception evaluation of possible maternal and fetal risks during pregnancy is important to help tailor plans for maternal and fetal monitoring and identify the level of care needed during labor and in the post-delivery period. Maternal cardiac risk can be assessed using three main models including the World Health Organization (WHO) risk model, the Cardiac Disease in Pregnancy (CARPREG) risk score and the Zwangerschap bij Aangeboren HARtAfwijkingen I (ZAHARA) risk score (1–3). The three models share common features, such as incorporating lesion-specific predictors, but differ in a few key areas (1, 2). The World Health Organization (WHO) classification categorizes women into four different classes based on specific congenital and acquired heart disease, with

WHO Class IV being the highest risk for mortality where pregnancy is contraindicated. The CARPREG risk score emphasizes left-sided cardiac obstruction in stratifying pregnant women for adverse cardiac and fetal outcomes. The ZAHARA risk score includes all moderate and severe valvular lesions and mechanical valves in the risk prediction model (1). Assessment of risk is of course based on careful clinical assessment, but necessarily includes non-invasive imaging.

The choice of imaging modality first depends on the pathology or pathophysiology to be evaluated. Echocardiography remains the mainstay for assessment of valvular disease and non-ischemic cardiomyopathies but is less comprehensive for assessment of aortopathy (4). Advanced imaging modalities including contrast-enhanced computed tomography (CT) and magnetic resonance imaging (MRI) provide important corroborating and incremental information, particularly in patients with suspected or known aortopathy. MRI and CT provide primarily anatomic information, although cardiac MRI can provide valuable physiologic information as well. **Table 1** summarizes the advantages and disadvantages of imaging modalities.

The choice of imaging modality is therefore based on the reliability and accuracy of the modality for evaluation of the pathology in question, as well as safety for the mother and fetus. Echocardiography has essentially no safety concerns for the mother or fetus during pregnancy and remains the fundamental imaging modality for assessment of myocardial and valvular disease. However, imaging may be limited due to patient positioning and the gravid uterus (4). In particular, echocardiographic visualization of the aorta is often limited to the aortic root and proximal ascending aorta (**Figure 1**). Although echocardiography offers the greatest safety from a procedural standpoint, this must be weighed against the risk of missed or inadequately-characterized aortic pathology. We briefly review the existing data regarding use of CT and MRI in pregnancy.

Clinical MRI at 1.5 T has not been proven to confer any significant risk on the fetus. Studies performed at 3 T are considered safe at up to 30 min of scan time (5). A non-contrast cardiac MRI can provide a significant amount of clinically important information: accurate evaluation of cardiac chamber sizes, quantification of flows and regurgitant volumes, and delineation of aortic anatomy. The risk-benefit ratio for gadolinium-based contrast agents, on the other hand, is less clearly defined. One study found that gadolinium exposure during gestation was associated with an increased risk of stillbirth, neonatal death, and certain rheumatologic, dermatologic, and inflammatory conditions, therefore, guidelines recommend avoiding routine administration of GBCAs to pregnant patients (5, 6).

Cardiac CT uses ECG-gating to obtain high quality images of the heart and surrounding vasculature. Prospective gating provides a "freeze frame" evaluation of the heart and dramatically reduces radiation doses - approximately 1 milligray (mGy) to the fetus. Retrospective gating allows for evaluation of cardiac wall and valve motion but at approximately 3 mGy to the fetus (7). In general, the risk of malignancy due to radiation depends both on dose and life expectancy after radiation. Thus, for a given dose of radiation, a young woman of child-bearing age is at higher risk of eventually developing malignancy from medical radiation than an older, post-menopausal woman. When radiologic studies are necessary, the goal is to follow the ALARA (as low as reasonably achievable) principle, minimizing radiation dose as much as possible while still obtaining diagnostic images. The risks of ionizing radiation to a fetus vary with gestational age and dose. In general, doses of < 50 mGy pose insignificant risk to the fetus (8).

For conditions discussed in this review, CT scanning must be performed with contrast agents to provide diagnostically meaningful images. Iodinated contrast media can cross the placenta but there have been no proven adverse effects on fetal development. Therefore, contrast-enhanced CT scanning should not be withheld from a patient due to pregnancy (7). Rather, risk-benefit discussions should be held, comparing the theoretical risks to the fetus against the risks to both the patient and fetus if a crucial diagnosis is missed.

With an understanding of the value added by different imaging modalities, we will next discuss the management of specific conditions.

AORTIC VALVE DISORDERS

Aortic Valve Stenosis

Cardiac output and stroke volume increase during pregnancy and reach their peak during the second to third trimester. Output and stroke volume may be increased up to 45% in a normal pregnancy and an estimated additional 15% higher in twin pregnancy (9, 10). These hemodynamic changes lead to increases in valvular gradients (11). Women with severe aortic stenosis (AS) are more likely to develop heart failure and adverse fetal outcomes including preterm birth and low birth weight (12). As hemodynamics change during pregnancy, so too does the risk of heart failure, particularly during the period from the second trimester through the first 24–72 h postpartum (13).

Congenital aortic stenosis can be seen from bicuspid aortic valve, subvalvular, and supravalvular stenosis, but overall is well-tolerated during pregnancy (14). Additionally, bicuspid aortic valve and associated aortopathy or coarctation of the aorta may be seen together in women with Turner's syndrome (15).

Preconception Planning

The diagnosis of severe AS is made by echocardiography using standard methods to determine aortic valve gradients. Symptomatic severe aortic stenosis is a particularly high-risk condition (12). For example, the estimated risk of primary cardiac events in a woman with severe, symptomatic aortic stenosis using the CARPREG II score is 10%. In circumstances where pregnancy is deemed high risk for maternal and or fetal mortality, a collaborative approach with obstetric and cardiovascular specialists should include discussion of non-surgical or surgical intervention (16). Contraceptive approaches should also be discussed for high-risk women of child-bearing age (17).

Asymptomatic women with severe aortic stenosis are also not without significant risk. Although data are limited, evaluation with exercise echocardiography or cardiopulmonary exercise testing is recommended to evaluate the hemodynamic response

TABLE 1 | The advantages and the disadvantages of each imaging modality in pregnancy.

Modality	Echocardiography	Contrast-enhanced CT	MRI without contrast
Pathology evaluated	• Valve stenosis • Valvular regurgitation • Proximal aortopathy • Ventricular function	• Aortopathy (full visualization)	• Ventricular function and specific cardiomyopathies • Aortopathy (full visualization) • Valve dysfunction
Advantages	• Easily available • No ionizing radiation • No gadolinium-based contrast	• Excellent resolution • Complete visualization of aorta	• Excellent resolution • No ionizing radiation • Complete visualization of aorta
Disadvantages	• Acoustic windows may be compromised during pregnancy • Limited visualization of thoracic aorta	• Ionizing radiation • Intravenous contrast for assessment of aorta	• Relatively long scan times • Image quality adversely affected by arrhythmias

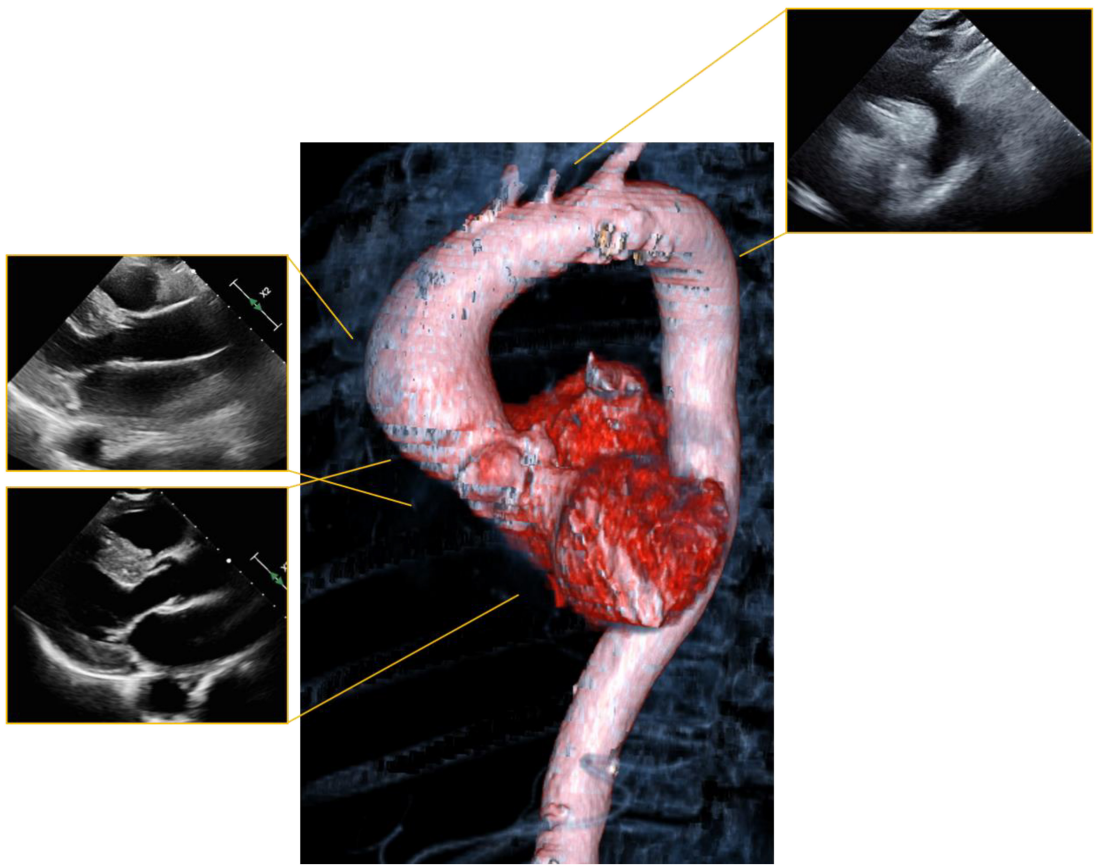

FIGURE 1 | Visualization of the aorta with echocardiography. Standard parasternal and suprasternal notch views (periphery) leave a significant portion of the aorta unvisualized. Computer tomography (CT) or magnetic resonance imaging (MRI) can visualize the aorta in three dimensions (center) and allows for comprehensive evaluation of anatomy.

to increased demand. Women with bicuspid aortic valve, without or without significant aortic stenosis, should have careful assessment of the thoracic aorta before pregnancy (16).

During Pregnancy

Given the dynamic physiological changes throughout pregnancy, clinical monitoring and serial echocardiography are appropriate. Clinical evaluation should assess for development of AS symptoms such as fatigue, shortness of breath, syncope, presyncope, or other heart failure symptoms (18).

Echocardiography once every trimester is generally adequate and most importantly, is recommended at the time of peak hemodynamic load estimated to be at about 32 weeks gestation (13). Congenital bicuspid aortic valve is associated with coarctation of the aorta in about 10% of patients and aortopathy is common. Therefore, the aorta should be carefully examined by echocardiography as well. Transesophageal echocardiography is safe in pregnancy but the aspiration risk is somewhat elevated compared to normal due to an increase in intra-abdominal pressure (19).

Cardiac CT is usually not necessary for diagnosis or planning management of AS but can be considered in women with bicuspid aortic valve when evaluation for aortopathy is indicated. A low radiation CT with a fetal dose of 0.01–0.66 mGy can be used to evaluate for aortic diameters before and during pregnancy (20). MRI generally does not add significantly to diagnosis or management of AS during pregnancy, and usually is not required or advised unless other diagnostic imaging are insufficient. Cardiac catheterization is rarely needed for diagnosis, but necessary if intervention must be performed for severe symptomatic AS in pregnancy. Fetal exposure to radiation from cardiac catheterization is low – the abdomen, if unshielded, receives 1.5 mGy on average with less than 20% reaching the fetus (21).

Management

Increased blood volume in pregnancy causes elevated gradients across the stenosed aortic valve and may result in development of decompensated heart failure (HF). Management includes use of loop diuretics for relief of vascular congestion, but they should be used with caution to avoid hypoperfusion of the placenta. According to the ACC/AHA guidelines, women with valvular disease undergoing uncomplicated vaginal delivery or Cesarean section do not require prophylactic antibiotics (16).

In severely symptomatic women with aortic stenosis who do not respond to medical management, aortic balloon valvuloplasty or transcatheter valve replacement can be considered in patients with favorable anatomy (11, 22). If aortic valvuloplasty is determined to be the best management approach, the best timing is after organogenesis is complete which is after the 4^{th} month of pregnancy (21). There are limited data on these interventional approaches, but case reports suggest their feasibility. Berry et al. reported a case of a 33 year-old woman at 22 weeks gestation with a 21-mm Carpentier Edwards Magna valve bioprosthetic aortic valve who developed progressive symptomatic AS during her pregnancy and a mean aortic valve gradient of 61 mmHg. She successfully underwent a valve-in-valve transcutaneous aortic valve replacement using a 20-mm Edwards Sapien 3 valve with significant improvement in clinical symptoms and reduction of the mean aortic valve gradient to 23 mmHg. At 37 weeks gestation, she delivered a healthy baby by Cesarean section (11). Orwat et al. reported a successful aortic balloon valvulotomy in a woman with severe AS at 20 weeks of gestation leading to symptomatic systolic heart failure. Pregnancy was subsequently uneventful though she required aortic valve replacement 1 month after delivery for recurrent symptoms (12). Surgical aortic valve replacement during pregnancy is exceptionally rare because of the reported risk of fetal mortality associated with cardiopulmonary bypass but has also been reported with success (23).

Labor and Delivery

The hemodynamic changes of pregnancy peak during labor and delivery with an increase in stroke volume and cardiac output up to 80% immediately following delivery in response to pain, bleeding, uterine contraction, and anxiety (10, 24). It is estimated that uterine contraction leads to approximately 300–500 ml of placental blood autotransfusion to the systemic circulation which contributes to the increase in both systolic and diastolic blood pressure (10).

In general, vaginal delivery is preferred and Cesarean delivery is not generally recommended unless there is severe aortic stenosis (21, 24). Compared to women with moderate valve disease, those with severe AS have a higher rate of Cesarean section (75.0 vs. 48.3%). Lower birth weight infants were more common in severe AS (35 vs. 6%), believed to be related to the hemodynamic compromise in severe AS that leads to decreased utero-placental blood flow. These infants usually have a lower Apgar score (< 7) (12).

Post-Partum Period

In patients with severe AS or symptomatic moderate AS, a 31% increase in complications has been reported in the early post-partum period (i.e., within 24–72 h of delivery) secondary to fluid shifts. These complications include arrhythmia, pulmonary congestion, death, or need for cardiac intervention. There is also an increased chance of deterioration of the diseased aortic valve weeks or months after delivery (25).

Aortic Valve Regurgitation

Pregnant women with aortic regurgitation are at low risk for cardiac complications and generally tolerate pregnancy, likely due to a decrease in afterload that reduces regurgitant volume (24). Nonetheless, data suggest that a dilated left ventricle with depressed function may predict an increased likelihood of adverse events (26). Aortic regurgitation may be secondary to bicuspid aortic valve with associated aortopathy which are discussed elsewhere in this review.

MITRAL VALVE DISORDERS

Mitral Valve Stenosis

Mitral stenosis most commonly occurs because of rheumatic heart disease, uncommon in developed countries but an important cause in developing nations and in major cities with significant immigrant populations (**Figure 2**). Congenital mitral stenosis due to parachute mitral valve is rare, and uncommonly seen in adult patients without prior repair. Heart failure symptoms related to mitral stenosis may appear when the mitral valve orifice area is reduced to < 2 cm^2 (27). The increased stroke volume and cardiac output of pregnancy may unmask previously asymptomatic mitral valve disease (24, 28). The increasing transmitral valve gradient during pregnancy may lead to pulmonary vascular congestion and pulmonary hypertension. Moreover, the increased heart rate associated with pregnancy limits diastolic filling which further worsens pulmonary edema (29).

Preconception Planning

A multidisciplinary team consisting of an obstetrician (preferably a high-risk specialist), cardiologist, and anesthesiologist should be involved in the initial evaluation of women with mitral valve stenosis and should follow her closely throughout

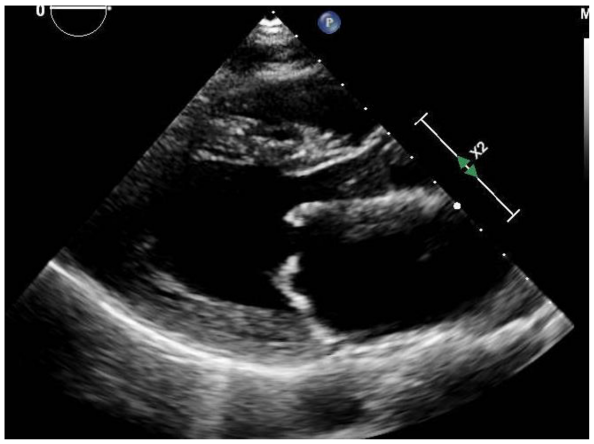

FIGURE 2 | Mitral stenosis: Representative parasternal long axis view during showing mitral stenosis in a woman with rheumatic heart disease. Both leaflets are affected with thickening and also restriction of their movement.

pregnancy and the post-partum period. The clinical evaluation should include an echocardiogram ideally performed at 6 to 12 months prior to pregnancy. Exercise stress echocardiography may provide additional hemodynamic information in patients without significant symptoms or questionable severity of mitral stenosis (16, 21).

Women should be counseled on the maternal and fetal adverse outcomes associated with mitral stenosis. Left heart obstruction that results from severe mitral stenosis results in uteroplacental insufficiency which consequently leads to increased fetal morbidity and mortality including intrauterine growth retardation (IUGR), low birth weight, preterm delivery and fetal death (30).

The adverse effects in women with mitral stenosis are related to the severity of mitral stenosis and the patient's NYHA class (27). Increased cardiovascular demand during pregnancy is very poorly tolerated in women with severe mitral stenosis and may result in rapid deterioration of NYHA class (31). More severe stenosis, NYHA III-IV symptoms, LVEF $<$ 40%, and prior cardiac all events are all predictors of adverse cardiac events during pregnancy (28). According to The American College of Cardiology/American Heart Association (ACC/AHA) guidelines, pregnant women who have symptomatic moderate to severe mitral stenosis defined as mitral valve area (MVA) $\leq$ 1.5 cm^2 or mean gradient $\geq$ 5 mmHg are advised to undergo percutaneous balloon mitral valvuloplasty prior to planning conception (16). Women with mitral stenosis on anticoagulation present significant issues during pregnancy. Pregnancy is associated with hypercoagulability and therfore increases the risk of thrombosis which persists up to 12 weeks into the postpartum period. Therefore, it is strongly advised that anticoagulation with heparin bridge to warfarin be resumed in the immediate postpartum period after assessment of bleeding risk and it can be generally started at 6–8 h after uncomplicated vaginal delivery and at 24–36 h after a Cesarean section (32, 33).

During Pregnancy

Valve gradients in mitral stenosis increase with increased stroke volume and cardiac output. Thus, for any severity of mitral stenosis, the increased cardiac output occurring during pregnancy results in increased gradients and may cause the severity of mitral stenosis to be overestimated. Therefore, mitral valve assessment should include measurement of mitral valve area, preferably using a method that involves measuring the increased stroke volume (28, 34). Echocardiography once every trimester is generally adequate although consideration must be given to changes in clinical status or symptoms (13). The role of MRI and CT is limited. Mitral valve area can also be obtained by planimetry on cardiac MR or CT, but in general these modalities have limited utility for valve assessment in pregnancy.

Management

Pregnancy is generally well tolerated in women with mild or moderate mitral valve stenosis. Women with severe MS should decrease their physical activity and are advised to bedrest during the latter stages of pregnancy (35). Heart failure and pulmonary edema tend to appear during the second or third trimester at the peak increase in cardiac output. In addition to bedrest, management of symptomatic patients should always start with conventional medical therapy for mitral stenosis, including diuretics for volume management and beta-blockade to decrease heart rate and improve diastolic filling. Beta blockers that are safe in pregnancy include propranolol and metoprolol as they do not pose significant fetal adverse effects (36) while atenolol is associated with more fetal growth retardation (28). Diuretics should be used with caution to avoid placental hypoperfusion. All women with mitral stenosis, regardless of severity, should be evaluated for atrial fibrillation. Cardioversion of atrial fibrillation is safe in pregnancy if needed to prevent systemic embolization and to improve left ventricular filling (29). Either warfarin $\leq$ 5 mg daily and/or low molecular weight heparin can be used for anticoagulation (37).

If intervention is deemed necessary in women with refractory symptoms, the second trimester is the preferred timing. In women without significant mitral regurgitation, percutaneous balloon mitral valvuloplasty results in substantial decrease in valve gradient and increased valve area (38). Open commissurotomy has similar success rate to percutaneous balloon valvuloplasty but poses a high, 8 times greater, risk of fetal loss. Mitral valve replacement is usually the last resort in severe cases in which the valve is not amenable to percutaneous intervention due to heavy calcification or if a mural thrombus is present. Surgical mitral valve replacement carries 1.5–5% risk of maternal mortality and 16–33% risk of fetal loss (29).

Labor and Delivery

Vaginal delivery under epidural anesthesia is generally recommended unless otherwise obstetrically contraindicated. Epidural anesthesia reduces tachycardia secondary to labor pain and therefore reduces left atrial pressure and the risk of pulmonary edema during labor. For women in NYHA classes III or IV, invasive hemodynamic monitoring during labor and delivery is helpful in guiding fluid and drug therapy (29).

The goal is to allow for uterine contraction while minimizing maternal Valsalva maneuver during expulsive effort. The use of epidural boluses in incremental doses allows for supplemental instrumentation in the second stage of labor to shorten this stage, and most importantly, the slow anesthetic onset allows for maternal compensation to prevent profound hypotension (39). In addition, epidural anesthesia provides segmental blockade which preserves the lower extremity muscle tone, decreasing the incidence of deep venous thrombosis (40).

Post-Partum Period

There is a sudden increase in preload during and immediately after delivery due both to relief of pressure of the uterus on the venous circulation and to autotransfusion from the placenta to the maternal central circulation. This may lead to severe pulmonary edema in women with mitral stenosis, and consequently the risk of maternal death is highest during labor and the immediate post-partum period. The increased risk may persist for 24–72 h after delivery until stabilization of the maternal hemodynamic shift (29).

Mitral Valve Regurgitation

Mitral regurgitation is most commonly due to mitral valve prolapse (**Figure 3**). Indeed, primary mitral valve prolapse (MVP) due to myxomatous valve disease is the most common valvular disease in pregnancy (41). MVP is usually suspected or diagnosed with clinical findings of systolic click and mitral regurgitant murmur, but these findings may not be classical in pregnancy because of the volume increases and lower systemic resistance that occur in pregnancy (42, 43). The diagnosis is confirmed and the severity of mitral regurgitation ascertained by echocardiography (**Figure 3**).

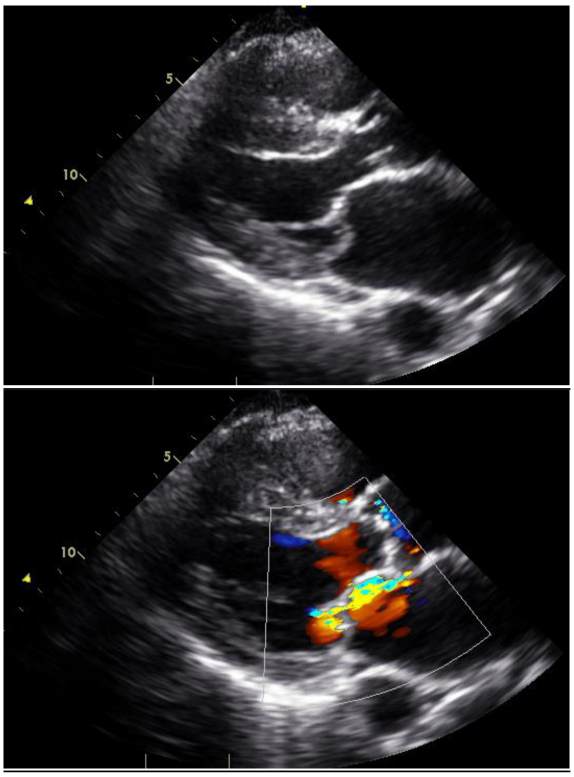

FIGURE 3 | Mitral valve prolapse: Still images with and without color Doppler in a woman with mitral valve prolapse affecting the posterior leaflet. The posterior leaflet bows beyond the mitral annular plane and produces an anteriorly-directed jet of mitral regurgitation.

In the absence of other cardiovascular pathology, the majority of pregnant women with MVP and mild or moderate mitral regurgitation have an uneventful pregnancy. Asymptomatic women with mitral valve prolapse and chronic, severe regurgitation usually tolerate pregnancy without significant complication although the increased cardiac volume may be associated with signs and symptoms of volume overload and atrial fibrillation. This can generally be managed with careful diuresis and beta blockers (16, 42, 44). Metoprolol can be safely used in pregnancy but may be associated with fetal bradycardia so should be used judiciously.

Women with mitral regurgitation, depressed LV function, and pulmonary hypertension with pulmonary artery systolic pressure $>$ 50 mm Hg are at high risk for development of heart failure during pregnancy. It is highly recommended that those patients be referred to a specialized valve center for consideration of surgical intervention. Similarly, patients with severe regurgitation and refractory heart failure should also be referred to a specialized valve center (16).

Right-Sided Valvular Heart Disease

Disease affecting the right-sided cardiac valves occurs much less commonly than left-sided cardiac valves. Involvement of the tricuspid and pulmonic valves in complex congenital heart disease is beyond the scope of this review. Acquired forms of tricuspid valve disease include tricuspid stenosis, a rare complication of rheumatic heart disease, and nearly always occurs with mitral and/or aortic valve involvement. Tricuspid stenosis is usually well tolerated in pregnancy, and the coexistent left sided disease (most commonly mitral stenosis) presents the major issues as discussed above (45). Significant tricuspid regurgitation is also quite uncommon in the absence of congenital heart disease or pulmonary hypertension. The latter poses a particularly high risk to the mother and fetus, and severe pulmonary hypertension should be considered a contraindication to pregnancy. In general, isolated tricuspid regurgitation does not impose clinically significant hemodynamic burden during pregnancy (24).

Isolated pulmonic stenosis is rare and if present is it usually due to branch pulmonary artery stenosis which in turn increases pressure gradient across the pulmonic valve (46). Pulmonic stenosis of mild or even moderate severity may be undetected until adulthood. Severe pulmonic stenosis most commonly occurs in the setting of complex congenital heart disease, typically Tetralogy of Fallot and is beyond the scope of this paper. Pulmonic valve regurgitation without coexistent complex congenital heart disease or pulmonary hypertension is also very uncommon. In general, pulmonic regurgitation with normal

right ventricular function is also very well tolerated in pregnancy but is largely influenced by coexistent structural disease (47).

Mechanical Heart Valves

Mechanical heart valves that necessitate the use of anticoagulation present additional challenges in managing valvular disease in pregnant women. The hypercoagulability associated with pregnancy poses added risk of valve thrombosis. The goal of adequate anticoagulation to prevent valve thrombosis must be balanced with avoiding fetal adverse outcomes. Echocardiography provides important information about prosthetic valve anatomy and function (21). As previously discussed, the increased stroke volume and cardiac output associated with pregnancy can be expected to cause increased transvalvular gradients that should not be misinterpreted as valve dysfunction. Cardiac CT, when performed with retrospective gating, can be used to assess valve motion, though at the cost of radiation (48). Fluoroscopy is another tool for assessment of mechanical valve motion (21). Cardiac MRI has limited use for valve assessment due to magnetic artifact (49).

Warfarin continued throughout pregnancy provides the best protection to the pregnant woman but carries a risk of fetal teratogenicity demonstrated by studies showing that warfarin leads to fetal birth defects if used in the first trimester particularly between weeks 6–12 (50). Current American College of Cardiology/American Heart Association (ACC/AHA) valvular heart disease guidelines recommend the use of warfarin at a daily dose of $\leq$ 5 mg/day throughout pregnancy, provided adequate anticoagulation is achieved (16). Warfarin at this low dose has been associated with better fetal outcomes and is comparable to low molecular weight heparin (LMWH) (32). Pregnant women who require higher warfarin dosage to maintain a therapeutic anticoagulation are recommended to be switched to low molecular weight heparin given subcutaneously every 12 h, and Anti-Xa levels monitored 4–6 h after a dose (goal range: 0.8–1.2 U/ml) (33). In women on anticoagulation, Cesarean delivery is recommended due to increased risks of neonatal intracranial bleeding during vaginal delivery (21).

In women with mechanical valves, combined hormonal contraception such as pills, patches and vaginal rings carry an increased risk of thrombosis and their use should be discouraged. In contrast, copper intrauterine devices and subcutaneous implants which contain single etonogestrel hormone are safe and are long acting to prevent unintended pregnancy for cardiac patients (51).

Hypertrophic Cardiomyopathy

Preconception Planning

Women with hypertrophic cardiomyopathy should be carefully counseled regarding the risk of HCM in the baby. Nonetheless, pregnancy is generally well-tolerated in patients with hypertrophic cardiomyopathy (52). One study evaluating a cohort of 100 women noted two deaths during pregnancy, both of whom were known to be high risk. One woman had sudden death four days post-partum and was known to have massive left ventricular hypertrophy (i.e., wall thickness 30 mm) with a resting left ventricular outflow gradient of 115 mmHg. The other patient with a particularly malignant family history with eight deaths in young relatives died of ventricular arrhythmia during pregnancy (53). This study illustrates the importance of risk stratification of women with HCM before pregnancy to identify features such as extreme left ventricular hypertrophy, strong family or personal history of sudden cardiac death, syncope, or identified arrhythmias on cardiac monitoring. Echocardiography is recommended in the current guidelines for managing HCM, particularly when new symptoms develop during pregnancy. Patients known to be high risk should also undergo regular echocardiograms while pregnant to assess for significant changes in outflow gradients or left ventricular function (21, 54).

Cardiac MR is not specifically recommended by current HCM guidelines for pregnant women or women who may become pregnant. However, CMR does offer advantages over echocardiography, for example by visualizing maximal wall thickness, detection of apical aneurysms, and identification of late gadolinium enhancement (**Figure 4**) (55). Each of these features has been associated with adverse outcomes in the general HCM population and may plausibly be associated with higher risk during pregnancy. CT has limited recommendations in the guidelines and essentially is considered appropriate for patients who cannot undergo CMR but require imaging beyond echocardiography (56).

During Pregnancy, Labor, Delivery, and Post-Partum Period

The increased blood volume occurring in pregnancy is often associated with reduced left ventricular outflow gradient. On the other hand, the increased volume may also result in heart failure in women with severe diastolic dysfunction (57). Diuretics can be used judiciously in women with evidence of vascular congestion (58). Echocardiography may be helpful in management to distinguish symptoms occurring as a normal consequence of pregnancy (for example, dyspnea) and those occurring due to HCM. Thus, evaluation of left ventricular outflow gradient and detection of mitral regurgitation due to systolic anterior motion of the mitral leaflet provide important management adjuncts (59). Most women can undergo uncomplicated vaginal delivery and Cesarean section is reserved for high-risk patients (54).

Aortopathy

Aortopathy is common in women with bicuspid aortic valve, Marfan's syndrome, Ehlers–Danlos type IV, Loeys–Dietz syndrome and Turner's syndrome. The risk of aortic dissection may be significant and related to the degree of aortic dilation (60–62). The risk of dissection appears to be highest during the third trimester, labor and delivery and during the early postpartum period (63). Cardiovascular imaging screening plays a particularly important role in management of these women to assure early identification, need for elective treatment, and avoidance of complications (**Figure 1**) (64).

Preconception Planning

Identification of aortopathy and assessment of severity of aortic dilation is crucial in preconception planning. Bicuspid aortic valve is the most common congenital heart disease (aside

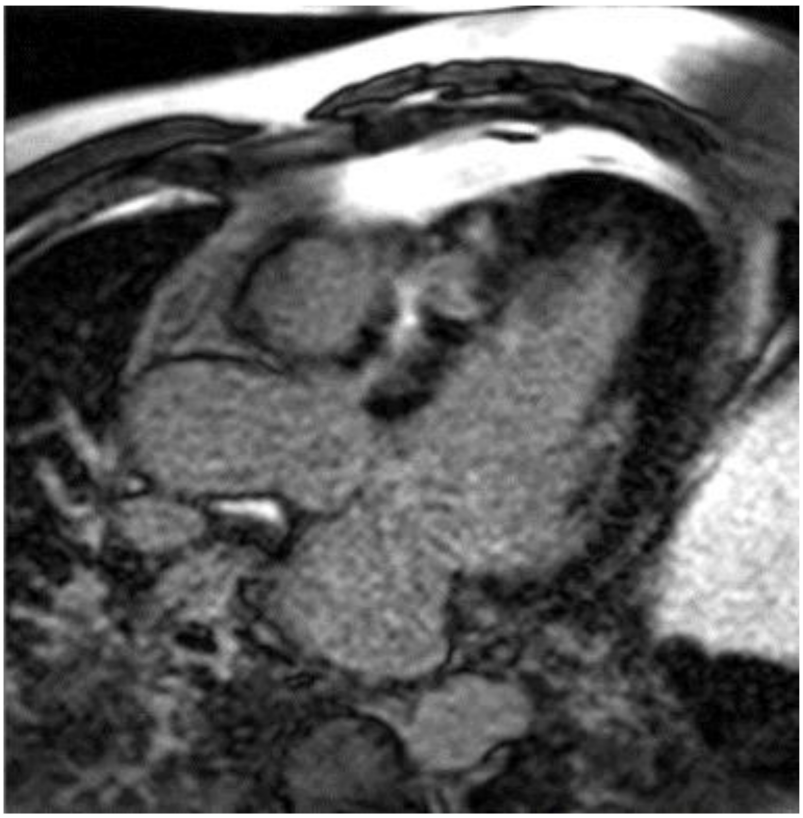

FIGURE 4 | Late gadolinium enhancement (LGE) image from a cardiac magnetic resonance image in the three-chamber view showing significant fibrosis in the anteroseptum of a patient with hypertrophic cardiomyopathy. Image courtesy Arlene Sirajuddin, MD.

from mitral valve prolapse) observed in adults, occurring in 1–2% of the population. BAV can be associated with coarctation of the aorta and aortic dilatation, even with normal valve function. Less common abnormalities such as Marfan's syndrome, Ehlers–Danlos type IV, Loeys–Dietz syndrome and Turner's syndrome, are also associated with aortic aneurysm and risk of dissection (63). Echocardiography is recommended for evaluation of the aortic root and proximal ascending aorta. Aortic dilatation involving the distal ascending aorta, arch and descending thoracic is often not well visualized by echocardiography. Therefore, a thorough evaluation of the aorta with CT or MRI in patients with possible aortopathy is strongly recommended for appropriate pre-conception counseling (21). Imaging and prophylactic aortic surgery for an aortic aneurysm can lead to better outcomes and reduce the risk of aortic dissection later in pregnancy. Pregnancy is not recommended in patients with severe dilatation of the aorta in heritable thoracic aortic disease such as Marfan syndrome $\geq$45 mm, bicuspid aortic valve > 50 mm or > 27 mm/m^2 BSA, or Turner syndrome ASI > 25 mm/m^2 BSA (21).

During Pregnancy

Women with aortic size < 4.0 cm are generally at low risk, but body surface area must be considered (21). Given the morbidity and possible mortality associated with aortic dilation and dissection, radiation concerns should not deter clinicians from proceeding with CT angiography. MRI with or without contrast is also an option based on local availability and expertise.

Pregnant women with aortopathy should undergo serial echocardiography. Echocardiography should be performed monthly in women with significant aortic dilatation (4–4.5 cm for Marfan's syndrome, 4.5–5.0 cm for bicuspid aortic valve), but is reasonable to be performed every 12 weeks in women with mild aortic dilation. If necessary, because of poor visualization by echocardiography (**Figure 1**), location of the aortic dilation, or suspected progression, cardiac MRI without contrast can be used for further assessment and follow up (21, 64).

Management

Close monitoring, strict blood pressure control, and beta blockers are highly advised throughout pregnancy, particularly among patients with high risk aortopathy (21, 65).

Surgical management is considered when progressive dilatation is observed and in type A aortic dissection and should be planned before fetal viability in the second trimester (62). In cases when progressive dilatation is seen after fetal viability, Cesarean section is recommended followed by aortic reconstructive surgery (63).

Labor and Delivery/Post-Partum Period

The goal is to minimize cardiovascular stress, therefore women are advised to continue beta blocker therapy in the peripartum period. Vaginal delivery with expedited second-stage using epidural anesthesia and instrumental delivery is advised in cases with an ascending aorta diameter between 4.0–4.5 cm to prevent abrupt increases in blood pressure and hence reduce risk of dissection. On the other hand, Cesarean delivery is strongly advocated when the aortic diameter exceeds 4.5 cm or in patients with Ehlers–Danlos syndrome type IV due to the high risk of dissection. The increased risk of dissection persists in the postpartum period, and women are recommended to be followed by echocardiography in the immediate post-partum period and 6 months after delivery (21).

CONCLUSION

Women with significant valvular heart disease, hypertrophic cardiomyopathy, and aortopathy require careful monitoring that becomes even more important during pregnancy. Careful clinical and appropriate imaging are relevant for risk stratification and surveillance during pregnancy and in the post-partum period.

Echocardiography is the foundation of cardiac imaging during pregnancy. In the conditions described in this review, echocardiography offers safe, readily-available, and diagnostic information to aid in patient management. However, echocardiography may be limited due to acoustic windows and image quality. MRI, including cardiac MRI, performed without gadolinium, can safely offer important diagnostic information, particularly in patients with aortopathy. Cardiac MRI may aid in preconception management of patients with HCM by clarifying anatomy and assisting with risk stratification. Finally, CT with intravenous contrast can provide accurate evaluation of the entire aorta, particularly when performed in an ECG-gated manner. CT is ideally performed prior to conception for assessment of risk in patients with known or suspected aortic disease. If deemed necessary during pregnancy, prospective ECG-gating can dramatically reduce the amount of radiation delivered to the patient and fetus.

AUTHOR CONTRIBUTIONS

HI drafted portions of the manuscript and revised the manuscript. AB drafted portions of the manuscript, revised the manuscript, and prepared images. JL outlined and revised the manuscript. All authors contributed to the article and approved the submitted version.

FUNDING

This manuscript was provided by the George Washington Heart and Vascular Institute.

REFERENCES

1. Balci A, Sollie-Szarynska KM, van der Bijl AG, Ruys TPE, Mulder BJM, Roos-Hesselink JW, et al. Prospective validation and assessment of cardiovascular and offspring risk models for pregnant women with congenital heart disease. *Heart.* (2014) 100:1373–81. doi: 10.1136/heartjnl-2014-305597
2. Drenthen W, Boersma E, Balci A, Moons P, Roos-Hesselink JW, Mulder BJ, et al. Predictors of pregnancy complications in women with congenital heart disease. *Eur Heart J.* (2010) 31:2124–32. doi: 10.1093/eurheartj/ehq200
3. Silversides CK, Grewal J, Mason J, Sermer M, Kiess M, Rychel V, et al. Pregnancy outcomes in women with heart disease: the CARPREG II Study. *J Am Coll Cardiol.* (2018) 71:2419–30. doi: 10.1016/j.jacc.2018.02.076
4. Prokšelj K, Brida M. Cardiovascular imaging in pregnancy. *Int J Cardiol Congenit Heart Dis.* (2021) 5:100235. doi: 10.1016/j.ijcchd.2021.100235
5. Kanal E, Greenberg T, Hoff M, Gilk T, Jackson E, McKinney A, et al. *ACR Manual on MR Safety*. Virginia, VA: American College of Radiology (2020).
6. Ray JG, Vermeulen MJ, Bharatha A, Montanera WJ, Park AL. Association between MRI exposure during pregnancy and fetal and childhood outcomes. *JAMA.* (2016) 316:952–61. doi: 10.1001/jama.2016.12126
7. Colletti PM, Lee KH, Elkayam U. Cardiovascular imaging of the pregnant patient. *Am. J Roentgenol.* (2013) 200:515–21. doi: 10.2214/AJR.12.9864
8. Hirshfeld J, John W, Ferrari VA, Bengel FM, Bergersen L, Chambers CE, et al. 2018 ACC/HRS/NASCI/SCAI/SCCT expert consensus document on optimal use of ionizing radiation in cardiovascular imaging: best practices for safety and effectiveness: a report of the American college of cardiology task force on expert consensus decision pathways. *J Am Coll Cardiol.* (2018) 71:e283–351. doi: 10.1016/j.jacc.2018.02.016
9. Reimold SC, Rutherford JD. Valvular heart disease in pregnancy. *N Engl J Med.* (2003) 349:52–9. doi: 10.1056/NEJMcp021265
10. Sanghavi M, Rutherford J. Cardiovascular physiology of pregnancy. *Circulation.* (2014) 130:1003–8. doi: 10.1161/CIRCULATIONAHA.114.009029
11. Berry N, Sawlani N, Economy K, Shook D, Nyman C, Singh MN, et al. Transcatheter aortic valve replacement for bioprosthetic aortic stenosis in pregnancy. *JACC Cardiovasc Interv.* (2018) 11:e161–2. doi: 10.1016/j.jcin.2018.07.046
12. Orwat S, Diller G, van Hagen IM, Schmidt R, Tobler D, Greutmann M, et al. Risk of pregnancy in moderate and severe aortic stenosis: from the multinational ROPAC registry. *J Am Coll Cardiol.* (2016) 68:1727–37. doi: 10.1016/j.jacc.2016.07.750
13. Lindley K, Williams D. *Valvular Heart Disease in Pregnancy*. (2018). Available online at: https://www.acc.org/latest-in-cardiology/articles/2018/02/12/07/29/valvular-heart-disease-in-pregnancy (accessed June 2, 2022).
14. Yap S, Drnthen W, Pieper PG, Moons P, Mulder BJM, Mostert B. Risk of complications during pregnancy in women with congenital aortic stenosis. *Int J Cardiol.* (2008) 126:240–6.
15. Prandstraller D, Mazzanti L, Picchio FM, Magnani C, Bergamaschi R, Perri A, et al. Turner's syndrome: cardiologic profile according to the different chromosomal patterns and long-term clinical follow-up of 136 nonpreselected patients. *Pediatr Cardiol.* (1999) 20:108–12. doi: 10.1007/s002469900416
16. Otto CM, Nishimura RA, Bonow RO, Carabello BA, Erwin JP III, Gentile F. 2020 ACC/AHA guideline for the management of patients with valvular heart disease: a report of the American college of cardiology/American heart association joint committee on clinical practice guidelines. *J Am Coll Cardiol.* (2021) 77:e25–197. doi: 10.1016/j.jacc.2020.11.018
17. Silversides CK, Sermer M, Siu SC. Choosing the best contraceptive method for the adult with congenital heart disease. *Curr Cardiol Rep.* (2009) 11:298–305. doi: 10.1007/s11886-009-0043-7
18. Davis MB, Arendt K, Bello NA, Brown H, Briller J, Epps K, et al. Team-based care of women with cardiovascular disease from pre-conception through pregnancy and postpartum: JACC focus seminar 1/5. *J Am Coll Cardiol.* (2021) 77:1763–77. doi: 10.1016/j.jacc.2021.02.033
19. Afari HA, Davis EF, Sarma AA. Echocardiography for the Pregnant Heart. *Curr Treat Options Cardio Med.* (2021) 23:55. doi: 10.1007/s11936-021-00930-5

20. American College of Obstetricians and Gynecologists' Committee on Obstetric Practice. Summary: guidelines for diagnostic imaging during pregnancy and lactation. *Obstet Gynecol.* (2016) 127:e75–80. doi: 10.1097/AOG.0000000000001316
21. Regitz-Zagrosek V, Blomstrom Lundqvist C, Borghi CB, Pasquet A. ESC guidelines on the management of cardiovascular diseases during pregnancy : the task force on the management of cardiovascular diseases during pregnancy of the European society of cardiology (ESC). *Eur Heart J.* (2011) 32:3147–97. doi: 10.1093/eurheartj/ehr218
22. McIvor RA. Percutaneous balloon aortic valvuloplasty during pregnancy. *Int J Cardiol.* (1991) 32:1–3. doi: 10.1016/0167-5273(91)90037-P
23. Arnoni RT, Arnoni AS, Bonini RCA, de Almeida AFS, Neto CA, Dinkhuysen JJ, et al. Risk factors associated with cardiac surgery during pregnancy. *Ann Thorac Surg.* (2003) 76:1605–8. doi: 10.1016/S0003-4975(03)01188-3
24. Nanna M, Stergiopoulos K. Pregnancy complicated by valvular heart disease: an update. *J Am Heart Assoc.* (2014) 3:e000712. doi: 10.1161/JAHA.113.000712
25. Hameed AB, Rahimtoola SH. Congenital aortic stenosis: pregnancy is another dimension. *J Am Coll Cardiol.* (2016) 68:1738–40. doi: 10.1016/j.jacc.2016.08.004
26. Leśniak-Sobelga A, Tracz W, KostKiewicz M, Podolec P, Pasowicz M. Clinical and echocardiographic assessment of pregnant women with valvular heart diseases—maternal and fetal outcome. *Int J Cardiol.* (2004) 94:15–23. doi: 10.1016/j.ijcard.2003.03.017
27. Saxena K, Wadhwa B, Mishra D. Anesthetic management of cesarean section in parturients with severe mitral stenosis: a case series. *J Obstet Anaesth Crit Care.* (2019) 9:46–9. doi: 10.4103/joacc.JOACC_6_18
28. Tsiaras S, Poppas A. Mitral valve disease in pregnancy: outcomes and management. *Obstet Med.* (2009) 2:6–10. doi: 10.1258/om.2008.080002
29. Kannan M, Vijayanand G. Mitral stenosis and pregnancy: current concepts in anaesthetic practice. *Indian J Anaesth.* (2010) 54:439–44. doi: 10.4103/0019-5049.71043
30. Siu SC, Sermer M, Colman JM. Prospective multicenter study of pregnancy outcomes in women with heart disease. *ACC Curr J Rev.* (2002) 11:87. doi: 10.1016/S1062-1458(01)00599-2
31. Bonow R, Mann D, Zipes D, Libby P. *Braunwald's Heart Disease: A Textbook of Cardiovascular Medicine*. Amsterdam: Elsevier (2012).
32. Chan WS, Anand S, Ginsberg JS. Anticoagulation of pregnant women with mechanical heart valves: a systematic review of the literature. *Arch Intern Med.* (2000) 160:191–6. doi: 10.1001/archinte.160.2.191
33. Bauersachs R, Lindhoff-Last E. Anticoagulation of pregnant women with mechanical heart valves using low-molecular-weight heparin. *Arch Intern Med.* (2003) 163:2788–9. doi: 10.1001/archinte.163.22.2788-a
34. Rokey R, Hsu Hw, Moise KJ, Adam K, Wasserstrum N. Inaccurate noninvasive mitral valve area calculation during pregnancy. *Obstet Gynecol.* (1994) 84:950–5. doi: 10.1016/0029-7844(94)P2321-Y
35. Norrad RS, Salehian O. Management of severe mitral stenosis during pregnancy. *Circulation.* (2011) 124:2756–60. doi: 10.1161/CIRCULATIONAHA.111.030601
36. Al Kasab SM, Sabag T, Al Zaibag M, Awaad M, Al Bitar I, Halim MA, et al. β-Adrenergic receptor blockade in the management of pregnant women with mitral stenosis. *Am J Obstet Gynecol.* (1990) 163:37–40. doi: 10.1016/S0002-9378(11)90661-9
37. Aggarwal S, Economy K, Valente A. State of the art management of mechanical heart valves during pregnancy. *Curr Treat Options Cardio Med.* (2018) 20:102. doi: 10.1007/s11936-018-0702-3
38. Fawzy ME, Kinsara AJ, Stefadouros M, Hegazy H, Kattan H, Chaudhary A, et al. Long-Term outcome of mitral balloon valvotomy in pregnant women. *J Heart Valve Dis.* (2001) 10:153–7.
39. Ngan KEEWD, Shen J, Chiu ATO, Lok I, Khaw KS. Combined spinal-epidural analgesia in the management of labouring parturients with mitral stenosis. *Anaesth Intens Care.* (1999) 27:523–6. doi: 10.1177/0310057X9902700516
40. Langesaeter E, Dragsund M, Rosseland LA. Regional anesthesia for a cesarean section in women with cardiac disease: a prospective study. *Obstet Anesth Dig.* (2010) 30:242. doi: 10.1097/01.aoa.0000389622.88166.29
41. Gelson E, Johnson M, Gatzoulis M, Abselm U. Cardiac disease in pregnancy. Part 2: acquired heart disease. *Obstet Gynaecol.* (2007) 9:83–7. doi: 10.1576/toag.9.2.083.27308
42. Yuan S, Yan S. Mitral valve prolapse in pregnancy. *Braz J Cardiovasc Surg.* (2016) 31:158–62. doi: 10.5935/1678-9741.20160034
43. Hass JM. The effect of pregnancy on the midsystolic click and murmur of the prolapsing posterior leaflet of the mitral valve. *Am Heart J.* (1976) 92:407–8. doi: 10.1016/s0002-8703(76)80125-1
44. Dill-Russell P, Jones LSJ. Anaesthesia for caesarean section in a patient with Ehlers-Danlos syndrome and mitral valve prolapse. *Int J Obstet Anesth.* (2001) 10:192–7. doi: 10.1054/ijoa.2000.0833
45. Roguin A, Rinkevich D, Milo S, Markiewicz W, Reisner SA. Long-term follow-up of patients with severe rheumatic tricuspid stenosis. *Am Heart J.* (1998) 136:103–8. doi: 10.1016/S0002-8703(98)70189-9
46. Hameed AB, Goodwin TM, Elkayam U. Effect of pulmonary stenosis on pregnancy outcomes—A case-control study. *Am Heart J.* (2007) 154:852–4. doi: 10.1016/j.ahj.2007.07.016
47. Khairy P, Ouyang DW, Fernandes SM, Lee-Parritz A, Economy KE, Landzberg MJ. Pregnancy outcomes in women with congenital heart disease. *Circulation.* (2006) 113:517–24. doi: 10.1161/CIRCULATIONAHA.105.589655
48. Gündüz S, Özkan M, Kalçik M, Gürsoy OM, Astarcioğlu MA, Karakoyun S, et al. Sixty-four-section cardiac computed tomography in mechanical prosthetic heart valve dysfunction: thrombus or pannus. *Circ Cardiovasc Imaging.* (2015) 8:e003246. doi: 10.1161/CIRCIMAGING.115.003246
49. Masci PG, Dymarkowski S, Bogaert J. Valvular heart disease: what does cardiovascular MRI add?. *Eur Radiol.* (2007) 18:197–208. doi: 10.1007/s00330-007-0731-x
50. Xu Z, Fan J, Luo X, Zhang WB, Ma J, Lin YB, et al. Anticoagulation regimens during pregnancy in patients with mechanical heart valves: a systematic review and meta-analysis. *Can J Cardiol.* (2016) 32:1248.e1–1248.e9. doi: 10.1016/j.cjca.2015.11.005
51. Anonymous Bahamondes L, Brache V, Meirik O, Ali M, Habib N, Landoulsi S, et al. A 3-year multicentre randomized controlled trial of etonogestrel- and levonorgestrel-releasing contraceptive implants, with non-randomized matched copper-intrauterine device controls. *Hum Reprod.* (2015) 30:2527–38. doi: 10.1093/humrep/dev221
52. Thaman R, Varnava A, Hamid MS, Firoozi S, Sachdev B, Condon M, et al. Pregnancy related complications in women with hypertrophic cardiomyopathy. *Br Heart J.* (2003) 89:752–6. doi: 10.1136/heart.89.7.752
53. Autore C, Conte MR, Piccininno M, Bernabò P, Bonfiglio G, Bruzzi P, et al. Risk associated with pregnancy in hypertrophic cardiomyopathy. *J Am Coll Cardiol.* (2002) 40:1864–9. doi: 10.1016/S0735-1097(02)02495-6
54. Goland S, van Hagen I, Elbaz-Greener G, Elkayam U, Shotan A, Merz WM, et al. Pregnancy in women with hypertrophic cardiomyopathy: data from the European society of cardiology initiated registry of pregnancy and cardiac disease (ROPAC). *Eur Heart J.* (2017) 38:2683–90. doi: 10.1093/eurheartj/ehx189
55. Hindieh W, Chan R, Rakowski H. Complementary role of echocardiography and cardiac magnetic resonance in hypertrophic cardiomyopathy. *Curr Cardiol Rep.* (2017) 19:81. doi: 10.1007/s11886-017-0897-z
56. Ommen S, Mital S, Burke M, Day S, Deswal A, Elliott P, et al. 2020 AHA/ACC Guideline for the diagnosis and treatment of patients with hypertrophic cardiomyopathy: executive summary: a report of the American college of cardiology/American heart association joint committee on clinical practice guidelines. *Circulation.* (2020) 142:e533–57. doi: 10.1161/CIR.0000000000000938
57. Saberi S. Hypertrophic cardiomyopathy in pregnancy. *Cardiol Clin.* (2021) 39:143–50. doi: 10.1016/j.ccl.2020.09.009
58. Pieper PG, Walker F. Pregnancy in women with hypertrophic cardiomyopathy. *Neth Heart J.* (2013) 21:14–8. doi: 10.1007/s12471-012-0358-7
59. Elliott PM, Anastasakis A, Borger MA, Borggrefe M, Cecchi F, Charron P, et al. 2014 ESC Guidelines on diagnosis and management of hypertrophic cardiomyopathy The Task Force for the Diagnosis and Management of Hypertrophic Cardiomyopathy of the European Society of Cardiology (ESC). *Eur Heart J.* (2014) 35:2733–79. doi: 10.1093/eurheartj/ehu284
60. Cheulot P, Saucedo M, Bouvier-Colle MH, Deneux Tharaux C, Kayem G. Maternal mortality among women with Marfan syndrome or vascular Ehlers-Danlos syndrome in France, 2001-2012. *Gynecol Obstet Fertil Senol.* (2019) 47:30–5. doi: 10.1016/j.gofs.2018.11.003

61. Donnelly RT, Pinto NM, Kocolas I, Yetman AT. The immediate and long-term impact of pregnancy on aortic growth rate and mortality in women with marfan syndrome. *J Am Coll Cardiol.* (2012) 60:224–9. doi: 10.1016/j.jacc.2012.03.051
62. Yates MT, Soppa G, Smelt J, Fletcher N, van Besouw JP, Thilaganathan B, et al. Perioperative management and outcomes of aortic surgery during pregnancy. *J Thorac Cardiovasc Surg.* (2015) 149:607–10. doi: 10.1016/j.jtcvs.2014.10.038
63. Stewart FM. Marfan's syndrome and other aortopathies in pregnancy. *Obstet Med.* (2013) 6:112–9. doi: 10.1177/1753495X13496237
64. Westerland O, Frigiola A, Robert L, Shaw A, Blakeway L, Katsanos K, et al. Vascular manifestations of syndromic aortopathies: role of current and emerging imaging techniques. *Clin Radiol.* (2015) 70:1344–54. doi: 10.1016/j.crad.2015.08.008
65. Ong K, Perdu J, De Backer J, Bozec E, Collignon P, Emmerich J, et al. Effect of celiprolol on prevention of cardiovascular events in vascular Ehlers-Danlos syndrome: a prospective randomised, open, blinded-endpoints trial. *Lancet.* (2010) 376:1476–84. doi: 10.1016/S0140-6736(10)60960-9

Conflict of Interest: The authors declare that the research was conducted in the absence of any commercial or financial relationships that could be construed as a potential conflict of interest.

Frontiers in
Cardiovascular Medicine

Innovations and improvements in cardiovascular treatment and practice

Focuses on research that challenges the status quo of cardiovascular care, or facilitates the translation of advances into new therapies and diagnostic tools.

Discover the latest Research Topics

See more →

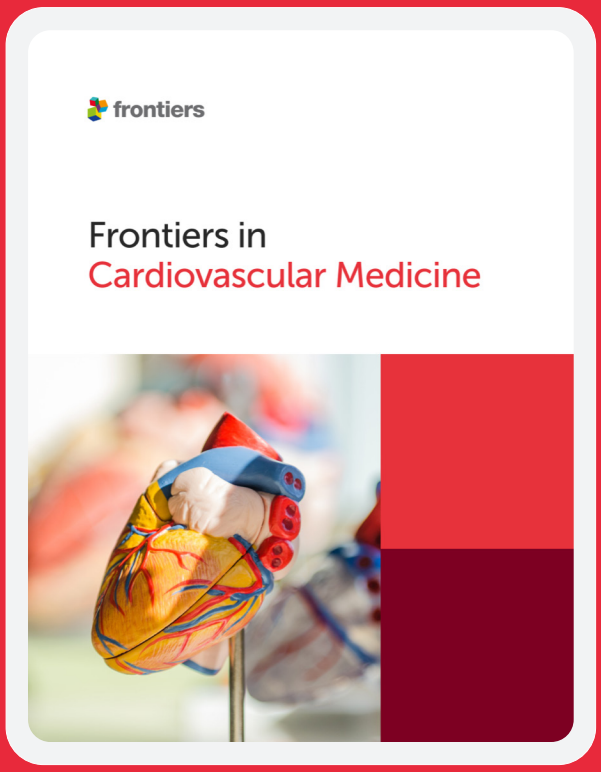

Frontiers

Avenue du Tribunal-Fédéral 34
1005 Lausanne, Switzerland
frontiersin.org

Contact us

+41 (0)21 510 17 00
frontiersin.org/about/contact